THE SEDIMENTOLOGY, MINERALOGY, AND GEOCHEMISTRY OF THE FRODINGHAM IRONSTONE FORMATION: IMPLICATIONS FOR THE GENESIS OF OOIDAL IRONSTONES.

A thesis submitted to the University of Manchester for the degree of

Doctor of Philosophy in the Faculty of Science, Department of Geology.

By

JOHN AGGETT

October 1990.

ProQuest LLC.
789 East Eisenhower Parkway
P.O. Box 1346
Ann Arbor, MI 48106 – 1346

This thesis is dedicated to my parents.

"Stand up to the blow, that fate has struck upon you,
Make the most of all, you still have coming to you..."

Genesis.

LIST OF CONTENTS.

LIST OF FIGURES.

PAGE

CHAPTER 4.

APPENDICES.

LIST OF TABLES.

PAGE

APPENDICES.

LIST OF PLATES.

ABSTRACT.

The Frodingham Ironstone Formation (L. Lias, Sinemurian) of Scunthorpe, was chosen to test the hypothesis that ooidal ironstone mineralogy results from post-oxic diagenetic processes (iron and manganese reduction) dominating over sulphate reduction during diagenesis.

Initial sedimentological studies of outcrop and borehole core provided a framework on which to base detailed petrographic and geochemical analyses. Thin-section petrography using transmitted and reflected light, with Cathodoluminescence and Ultra-Violet Fluorescence, was followed by Electron Probe Micro-Analysis, Scanning Electron Microscopy, X-Ray techniques, and Stable Isotopic Analysis of C and O in the carbonates.

The ironstone-formation consists of bioclastic ooidal grain-ironstones, pack/wacke-ironstones and subordinate mud-ironstones. Small scale fining sequences with basal coquinas are common. The ironstone-formation is typical of "Minette" type ironstones having been deposited under dominantly high energy conditions, here associated with storm activity, in a shallow marine environment. The ooids are generally composed of goethite (FeOOH) with small amounts of admixed berthierine in the cortex. They possess an oblate ellipsoidal shape that results from a specific three stage accretion process rather than compaction, and a micro-concretion origin is suggested for the goethitic, and also berthierine, ooids.

Berthierine, a ferrous aluminous 1:1 layer silicate, occurs as ooids, a replacement of detrital clay, and as isopachous cements, where it was usually the first formed authigenic phase. Its composition varies little from:

$(Ca_{0.073}Na_{0.095}K_{0.009})(Fe_{3.857}Mg_{0.871}Mn_{0.005}Ti_{0.004}Al_{0.992})(Si_{3.291}Al_{0.709})O_{10}(OH)_8$

Of the authigenic carbonates, ferroan/manganoan calcite (1-4% $FeCO_3$ and $MnCO_3$) is abundant and cements most grain-ironstones, often with more than one cement generation. Highly manganoan cements (up to 27% $MnCO_3$) are also present, but are uncommon. Siderite forms preferentially where berthierine is abundant, commonly replacing it. It is always calcian, manganoan and magnesian (up to 14% $CaCO_3$, 8% $MnCO_3$, and 20% $MgCO_3$), postdating berthierine cements, but often predating a final ferroan calcite cement. Stable isotope analysis has shown the calcites to have values of $\partial^{13}C_{PDB}$ from -3.6 to -22.1‰, which is consistent with mixing of HCO_3^- from the marine environment and from organic matter oxidation. A $\partial^{18}O_{PDB}$ of -6.0 to -9.43‰ suggests a meteoric groundwater source. Pyrite is uncommon, and has been seen replacing marcasite. Authigenic phosphatic cements are present in some samples, but are localised.

The mineral assemblage of the Frodingham Ironstone is consistent with post-oxic processes having acted within the sediment in shallow marine conditions in an iron-rich environment. Pyrite formation was limited, due to continued biodegradation of organic matter in the oxic zone, to levels unable to support sulphate reduction. Cementation was early (pre-compaction) and possibly dominated in the later stages by meteoric water. Examination of other British Jurassic ooidal ironstones suggests that similar processes of formation to those proposed for the Frodingham Ironstone Formation occurred during the genesis of many ooidal ironstones. This work has wider implications in delineating the role of iron in early diagenetic systems, and for the precipitation of early iron-rich minerals.

No portion of the work in this thesis has been submitted in support of an application for another degree or qualification of this or any other university or other institute of learning.

Research Experience.

This PhD research was initiated at the Department of Geology, Sheffield University in September 1987. Following the appointment of Professor C.D. Curtis as Head of Department to the Department of Geology at Manchester University, this research was continued at Manchester from August 1988.

ACKNOWLEDGEMENTS.

This project was funded by a N.E.R.C. research grant as a C.A.S.E. award with British Petroleum Plc. The project was supervised by Professors C.D. Curtis (Manchester), and M.L. Coleman (B.P.), whose guidance and help is acknowledged.

For sample material I wish to thank; Appleby Slag Reduction Co. and British Steel Plc. for access to Yarborough Pit, Scunthorpe; the Director of the British Geological Survey (Dragonby 31 borehole core); Dr. P. Turner, Birmingham University (Y138 borehole core); and Dr. T. Young, Cardiff University (Staithes samples).

I would like to thank all staff and research students of the Departments of Geology at the Universities of Sheffield and Manchester, who offered technical support, help and advice during the course of this research. Dr. T. Young is specifically mentioned for his continued support and interest in my work.

To the many friends I have made at Sheffield and Manchester, too numerous to mention individually, I offer my sincere thanks and wish them well. In particular, Alistair Gray and Fiona White are thanked for help and support, and for putting up with me during the less than perfect times of thesis writing. A special thankyou to Fiona for proof-reading and page-numbering this thesis, and for constant encouragement during the past two years.

STRUCTURE OF THE THESIS.

This thesis begins with a review of relevant literature on ooidal ironstones to outline their characteristics, complexity and problems associated with their genesis (chapter 1). The aims and methodology of the research is given, based upon this published research and recent developments in sedimentary geochemistry. The Frodingham Ironstone Formation was examined to test the hypothesis that post-oxic diagenetic reactions (iron and manganese reduction) dominated during the early diagenesis of the ironstones, resulting in the formation of iron silicates, carbonates and oxides, but not sulphides.

Chapter 2 provides a background to the ironstone-formation, and the sedimentology is described from field and core studies. Chapter 3 describes the detailed petrography of the ironstone components, with particular emphasis placed upon the iron-ooids that characterise these deposits. Berthierine petrography and composition is described in chapter 4, in order that all occurrences and compositions of this iron-silicate may be compared together, and with published analyses. The origin of this mineral is discussed with regard to new evidence obtained in this research.

Non-silicate mineralogy (excluding the oxides, which are present as ooids) is described in chapter 5, with the majority of the chapter devoted to carbonate petrography and composition, reflecting the dominance of carbonates over other non-silicates in the Formation. Chapter 6 concludes the discussion on the Frodingham Ironstone Formation by discussing models for the sedimentological and diagenetic evolution of this ironstone-formation, and subsequently tests the applicability of hypotheses for ooidal ironstone genesis based on this Formation, to ooidal ironstones in general by comparison with other British Jurassic ooidal ironstones examined during the course of this research.

Details of the techniques employed during this research and a full data and reference set, are given in the appendices at the end of this thesis.

ABBREVIATIONS USED IN THIS THESIS.

S.I. units have been used in all cases throughout this work, and original imperial units as quoted in older literature, are given in parentheses after the S.I. value. All abbreviations are given in full at their first usage in the text, but for reference purposes, the following list is collated:

Abbreviation.	Full Name.
[A.] T.E.M.	[Analytical] Transmission Electron Microscopy.
C.L.	Cathodoluminescence.
E.D.	Energy Dispersive (Microprobe analysis).
E.P.M.A.	Electron Probe Micro-Analysis.
H.M.C.	High Magnesian Calcite.
L.M.C.	Low Magnesian Calcite.
M.C.P.	Minus Cement Porosity.
O.M.	Organic Matter.
p.p.m.	Element concentration expressed in parts per million.
S.E.M.	Scanning Electron Microscopy.
T.O.C.	Total Organic Carbon.
U.V.	Ultra-Violet.
W.D.	Wavelength Dispersive (Microprobe analysis).
wt%	Weight percent of an element.
X.R.D.	X-Ray Diffraction.

Sample Numbers.	
ABB.	Abbotsbury Ironstone, various localities.
DRAG. 31.	Dragonby 31 borehole core, Frodingham Ironstone Formation.
HRT.	Hornton Quarry, Banbury Ironstone.
RSY.	Ironstone Mines, Raasay Ironstone.
STH.	Staithes coastal section, Cleveland Ironstone Formation.
Y183.	Y183 borehole core, Frodingham Ironstone Formation.
YAR.	Yarborough pit, Frodingham Ironstone Formation.

For abbreviations used within data tables see appendix D.
All values of °2θ in X.R.D studies are quoted for Cukα radiation.

CHAPTER 1: OOIDAL IRONSTONES AND DIAGENETIC MODELLING: A REVIEW.

1.1) Introduction.

A review of the literature on ironstones is presented in this section, and forms the background to this research. Initially, the rock type is defined by the use of specific terminology, and expanded so that the full suite of features characteristic of these unusual deposits are described. The literature relevant to ironstones is vast, for there are few sedimentologists who have not encountered an ironstone of some type, and derived their own interpretation for these enigmatic rocks.

1.2) Nomenclatural Problems.

1.2.1) Iron-rich sediments.

The terminology applied to iron-rich sedimentary rocks has been, until recently, largely of an informal nature, with individual researchers using their own preferences within their work. Even the addition of a hyphen to iron(-)formation may change the emphasis! James (1966 p. 1) defined iron-rich sedimentary rocks as those "...containing 15 percent or more of iron of depositional or diagenetic origin." Five types were recognised: the non-cherty 'ironstones' of post-Precambrian age; the laminated and cherty 'iron-formations' largely of Precambrian age, (also known as 'Banded Iron Formations', 'Itabirite', 'Taconite', and even 'Banded Ironstone'); the 'bog iron ores' in lakes/bogs of high latitudes; the 'blackband' and 'clayband' ores; and surficial accumulations (canga). Gross (1965) had also subdivided the 'ironstones' into 'Clinton' and 'Minette' types, to distinguish the dominantly Palaeozoic, hematite-rich, marine ooidal ironstones, from the dominantly Mesozoic and Tertiary, hematite-poor types respectively.

Kimberley (1978) addressed the problem of 'ironstone' and 'iron-formation' terminology, and defined 'ironstone' as a "...chemical sedimentary rock which contains over 15 percent Fe" (i.e. 'iron-rich sedimentary rock *sensu* James 1966), and 'iron formation' for "...a mappable rock unit composed mainly of ironstone, with the uppermost and lowermost

beds being ironstone." His classification is shown in table 1.1, and remains the only complete subdivision of iron formations (*sensu* Kimberley 1978) in a scheme not based on similarities to a well described type deposit. The classification is however far from ideal because it is based upon an interpretation of the physical characteristics of ironstones, and is hence open to debate.

The Geological Society International Symposium on "Phanerozoic Ironstones" at Sheffield in April 1987, discussed the question of 'ironstone' nomenclature, and is reviewed by Young (1989a). The symposium reaffirmed Kimberley's (1978) definition of 'ironstone' but proposed that the term 'iron-formation' should be replaced by 'ironstone-formation'. The terminology used by the symposium will be followed here, and it is suggested that the formalisation of the 'Cleveland Ironstone' to 'Cleveland Ironstone Formation', should be expanded to all 'ironstone-formations', so that for example the 'Frodingham Ironstone' should be renamed the 'Frodingham Ironstone Formation'. Where a unit is not in itself mappable, or the boundaries have not been strictly defined, the commonly used name is used rather than a stricter definition (for example,'Banbury Ironstone' is used as opposed to 'Banbury ironstone' or 'Banbury Ironstone Member'). In summary, the following terminology is used here:

ironstone : Chemical sedimentary rock which contains over 15 % Fe (Kimberley 1978)

ironstone-formation : A mappable rock unit composed mainly of ironstone, with the uppermost and lowermost beds being ironstone (Kimberley 1978 *emend* Young 1989a).

Ironstone Formation : (Prefixed by a name). Formal lithostratigraphical classification of a an ironstone-formation.

Note that under this scheme 'Frodingham ironstone' is still valid for describing ironstone obtained from Frodingham.

1.2.2) Coated Grains.

Various terms have been employed in the description of both coated grains, and the rocks in which they are found. For example 'Oolite', 'ooid', and 'oolith' have all been used

TABLE 1.1

PALAEOENVIRONMENTAL TYPES OF IRON FORMATIONS (From Kimberley (1978 p216)

Acronym	Full name	General features
SVOP-IF	Shallow-volcanic-platform iron formation	Cherty, mostly Archean and Paleozoic
MECS-IF	Metazoan-poor, extensive, chemical-sediment-rich,shallow-sea iron formation	Cherty, banded, most abundant Early Proterozoic (Precambrian X) type
SCOS-IF	Sandy, clayey, and oolitic, shallow-sea inland-sea iron formation	Chert-poor, most abundant Phanerozoic type
DWAT-IF	Deep-water iron formation	Cherty, mostly Archean
SOPS-IF	Sandy, oolite-poor, shallow-sea iron formation	Chert-poor, glauconite-rich, Phanerozoic only
COSP-IF	Coal-swamp iron formation	Chert-poor, non-oolitic, Phanerozoic only

to describe the same type of nearly spherical particle possessing a concentric structure, and 'oolite' has been further used as a descripition of the rock. Young (1989a) has standardised these terms which will be used in this thesis, and are given in table 1.2 However, it should be realised that the term 'spastolith' has been widely misused (see section 3.2.7). The iron-ooid classification of Kearsley (1989) is an excellent attempt to categorise the complexity of the ooids, but it is thought that 15 subclasses with infinite variation between, cannot be usefully employed in a single ironstone study, and cannot compare to petrographic description. It also suffers in that a considerable degree of interpretation is invoked once a classification has been assigned. However, for comparison between numerous examples, it may prove useful for computer correlation. The classification of coated grains used by Dahanayake and Krumbein (1986) is not recommended as it combines shape and origin, hence introducing a degree of interpretation into a descriptive classification.

1.2.3) Ironstone Texture

Where an ironstone consists of coarse iron particles (for example ooids), with bioclastic debris and carbonate cement, Folk's (1959, 1962) classification for carbonate sediments may be employed, but is not universally applicable. A more useful classification is a modified Dunham (1962) system as suggested by Young (1989a), with the replacement of '...stone' by '...-ironstone'. Taylors (1949) nomenclature that uses adjectival prefixes for groundmass mineralogy, and substantive prefixes for ooid mineralogy, has been used by many workers. It is believed here however that it is better and more scientific, to use a full textural and mineralogical description, rather than deciphering a 'chloritic sideritic cherty quartzose chlorite siderite quartz kaolinite magnetite oolite'!

1.3) General Characteristics of Ooidal Ironstone-Formations.

The S.C.O.S.-I.F.(*sensu* Kimberley 1978), 'Minette' type ironstones that this research is concerned with, have been extensively documented in Britain, Europe (including the type locality in Lorraine, France), and to a lesser extent, worldwide. This documentation has revealed many features that are common to many or most of these deposits, and serve to differentiate them from other ironstones. These shared characteristics are of importance in

TABLE 1.2. RECOMMENDED TERMINOLOGY FOR ALLOCHEMS IN IRONSTONES. (AFTER YOUNG 1989a).

	Less than 2mm.	Above 2mm.
	Concentrically structured grains.	
Grain	ooid	pisoid
Adjective	ooidal	pisoidal
Rock unit	oolite	pisolite
	Plastically deformed concentrically structured grains.[1]	
Grain	spastolith	
Adjective	spastolithic	
Rock unit	(no term)	
	Grains without concentric structure.	
Grain	peloid	peloid
Adjective	peloidal	peloidal
Rock unit	(no term)	
	Grains of faecal origin.	
Grain	pellet	pellet
Adjective	pelletal	pelletal
Rock unit	(no term)	
	Grains of probable cyanobacterial origin.[2]	
Grain	microoncoid	oncoid
Adjective	microoncoidal	oncoidal
Rock unit	microoncolite	oncolite

N.B.

1) These terms should only be used where plastic deformation of ooids is clearly demonstrated.

2) The term vadoid is used in this research to describe coated grains (pisoids and ooids) whose texture resembles oncoids, but which are interpreted to be inorganic precipitates as opposed to a cyanobacterial origin.

Commonly used petrographic terms whose use is not recommended:

oolith
oolitoid
ooloid (+ ooloid rock)
oncolith
oncoloid (+ oncoloid rock, microoncoloid, microoncoloid rock)
pisolith
pisoloid (+ pisoloid rock)

determining 'Minette' ooidal ironstone origin, and allow extension of hypotheses based on a single example, on a wider scale. These characteristics include:

1) Occurrence in the Mesozoic (mostly Jurassic) and early Tertiary.

2) A condensed and usually thin nature, often associated with disconformities.

3) Occurrence at the top of coarsening-upward sequences.

4) Local extent, with a lateral equivalent of 'normal' marine shales.

5) A marine fauna (though some cases of a restricted nature have been reported), with extensive bioturbation.

6) Indications of shallow marine, high-energy deposition.

7) Lack of terrigenous clastic material.

8) Ooids of a ferruginous mineralogy, usually berthierine and/or goethite, forming a significant proportion of the rock.

9) The presence of a matrix and/or cement consisting totally, or in part, of iron-rich minerals, commonly berthierine, ferroan calcite and siderite.

These characteristics are now described in more detail, with the emphasis placed on the three major areas of research; the sedimentological aspects, the origin of the iron-ooids, and the mineral assemblage.

1.4) Sedimentological and Palaeoenvironmental Aspects of Ooidal Ironstones.

1.4.1) Introduction.

High-energy conditions of deposition are indicated for most ironstone-formations. This is indicated by the presence of cross-lamination, lack of mud in some deposits, shell hashes and broken bioclastic debris. However, finer grained beds are also often present, and may be related to fining sequences. Many ooidal ironstones are clearly reworked accumulations of ferruginous debris, especially ooids, concentrated perhaps by tidal activity (Teyssen 1984), storms (Dreeson 1989, Gygi 1981), or by winnowing of finer material (Knox 1970). Reworking is indicated by the presence of intraclasts in ironstones (for example see Cayeux 1922, Davies and Dixie 1951, Hallimond 1925 page 10, Taylor 1949 page 23). Though most are clearly marine, Davidson (1961), reporting the work of Yanitsky (1960), describes ooidal ironstones in fluvial, deltaic, and lacustrine facies of Kazakhstan, U.S.S.R.

1.4.2) Depletion of terrigenous clastic material.

The lack of detrital quartz sand and silt within ooidal ironstones relative to associated deposits has been well documented. To explain this, the concept of a 'clastic trap' is implied by some authors (Cayeux 1922, Whitehead *et al.* 1952 page 150, Huber and Garrels 1953). The clastic trap is interpreted to be a feature such as a ridge or shallow basin which trapped the clastic influx before it reached the site of ironstone accumulation. Brookfield (1971) argues that the differing hydrodynamic behavoir of quartz and iron-ooids causes separation, with the iron-ooids being transported further by rolling. Knox (1971) disputes this interpretation on a number of points, specifically that the oblate spheroidal shape of many iron-ooids is unsuited to rolling. Hemingway (1951) and Hallam (1963) favour a simpler idea of a lower total clastic input due to subdued erosion of a peneplaned landmass, particularly when associated with a marine transgression (Hallam 1963). Hallam and Bradshaw (1979) have disputed the application of clastic trap models for the Marlstone Rock Bed and Northampton Sand Ironstones as they show a different facies relationship (figure 1.1).

1.4.3) Stratigraphic Relationships.

1.4.3.1) Vertical Sequence.

The stratigraphic sequence in which ooidal ironstones are found is variable, although the occurrence in or at the top of a coarsening upward, regressive sequence is common (see reviews in Van Houten and Bhattacharyya 1982, Maynard 1983, Van Houten and Purucker 1984, and recent papers by Teyssen 1989, Guerrak 1989, and Young 1989b). Of particular interest to this research is the work of Hallam and Bradshaw (1979) who showed that for British ooidal ironstones, the Marlstone Rock Bed, Westbury (Talbot 1974), and Abbotsbury (Brookfield 1973) Ironstones followed the trend clearly, and that the Frodingham (Hallam 1963) and Raasay (MacGreggor *et al.* 1920) Ironstones could be correlated with regressive sequences elsewhere. The Cleveland Ironstone Formation shows well defined regressive sequences beneath each ironstone seam, and the formation as a whole forms the second of three major regressive cycles in the Lias (Hemingway 1951, cycle 1b of Maynard 1983).

FIGURE 1.1. DEPOSITIONAL MODELS OF OOIDAL IRONSTONE FORMATION TO EXPLAIN THE LACK OF TERRIGENOUS CLASTIC MATERIAL.

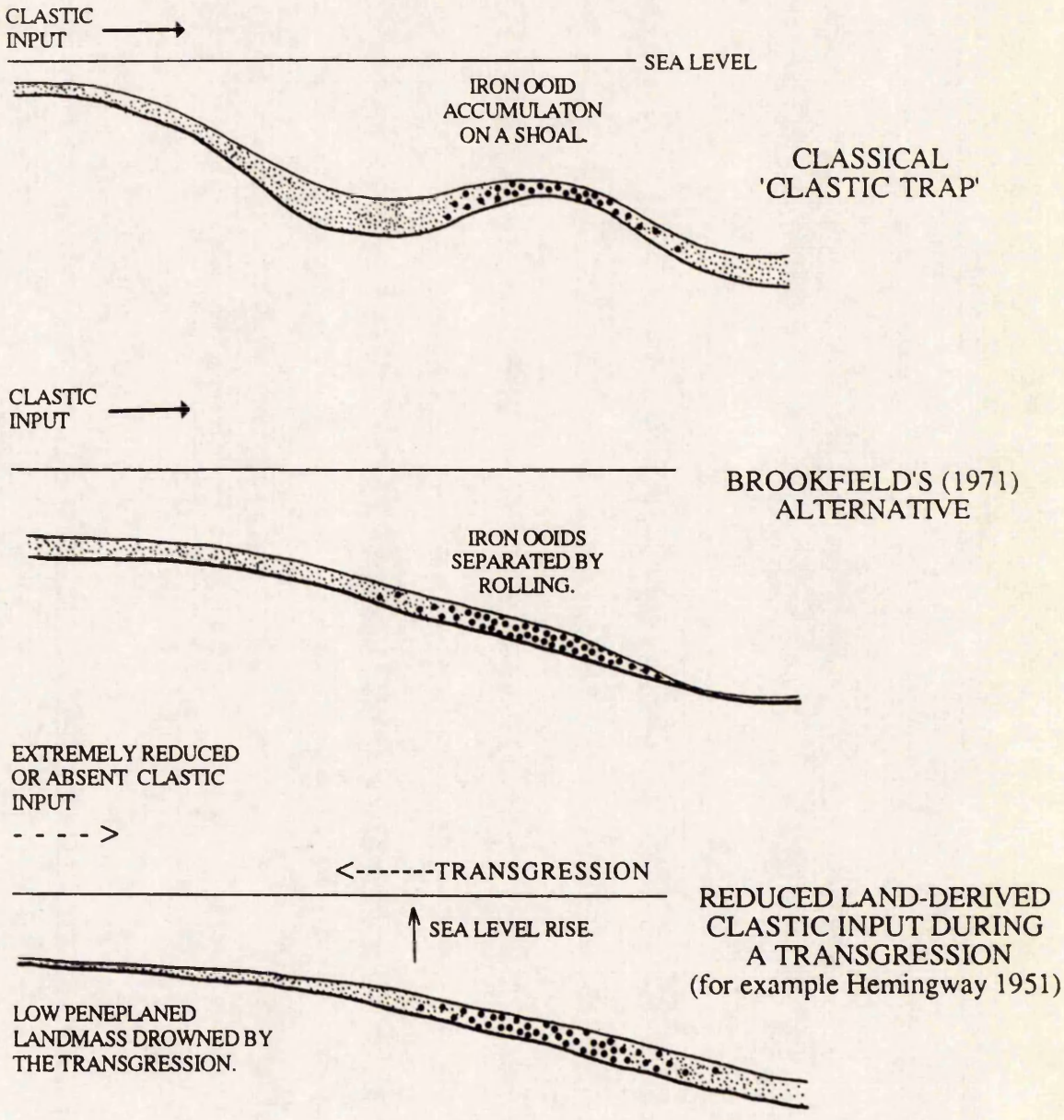

FACIES RELATIONSHIPS OF THE MARLSTONE ROCK BED AND NORTHAMPTON SAND IRONSTONE WHICH DO NOT FIT WITH THE ABOVE MODELS (From Hallam and Bradshaw 1979).

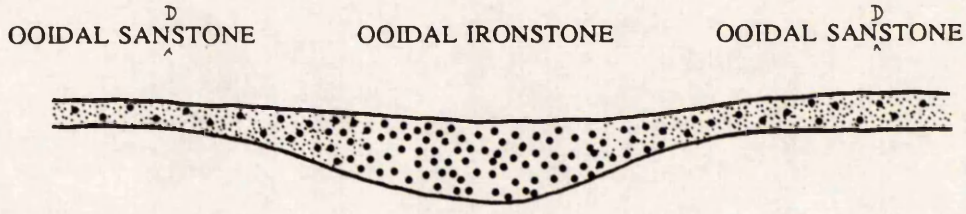

The regressive/transgressive association of ironstones is debated, and apparently variable. The occurrence at the top of regressive sequences suggested to Hemingway (1951) and Hallam and Bradshaw (1979) that the ironstones represented a simple continuation of the regression at the time of lowest sea level. Other ironstones have however been interpreted as transgressive, for example the Winter Gill (Knox 1970) and Agbaja Ironstones (Umeorah 1987). Young (1989b) has correlated ironstones of south-west Europe with periods of major global eustatic sea-level rise, whereas Teyssen (1989) suggests that the ooids of the Minette Ironstone formed during sea-level lowstands. Van Houten and Purucker (1984), Van Houten (1985), and Van Houten and Arthur (1989) suggest that the condensed nature of ooidal ironstones with extensive bioturbation, reworking, and reduced sediment influx, indicate relatively long periods of stillstand, after briefer intervals of progradation or shoaling. Young *et al.* (1990) suggest that the interpreted regressive ironstone seams of the Cleveland Ironstone Formation, are in fact associated with the drowning phase.

1.4.3.2) Lateral Facies Relationships.

Brookfield (1971) summarised the overall lateral facies scheme of 'Minette' ironstones as "...nearshore quartz sandstone facies, passing successively into sandy or silty shales and ironstone, finally basinal shales." Transitions between facies can be sharp, with ooidal ironstone passing into sparsely ooidal sandstone in less than 150m (Brockamp 1942, reported by Brookfield 1971). The above lateral facies change can be found in all British Mesozoic ooidal ironstones except the Abbotsbury (Brookfield 1971). Most workers agree that ironstones formed relatively near to a coastline, or isolated on a shoal or barrier bar system, so that lateral facies variation is therefore dependent on coastal processes acting outside the area of ironstone accumulation (see figure 1.2). The condensed nature of ooidal ironstones means that sediment thickness usually increases greatly into the basin. The Frodingham Ironstone Formation for example, has time equivalents of shale many times its thickness (Cope *et al.* 1980). The Abbotsbury Ironstone and Marlstone Rock Bed have however been shown to pass laterally into condensed phosphatic clays (Brookfield 1971).

Figure 1.2. Facies of Iron Deposition in Jurassic Ooidal Ironstones of Great Britain, With the Relationship of Ironstone Facies to Current Activity and Clastic Supply. Taken From Hallam (1975, figures 3-9 and 3-5).

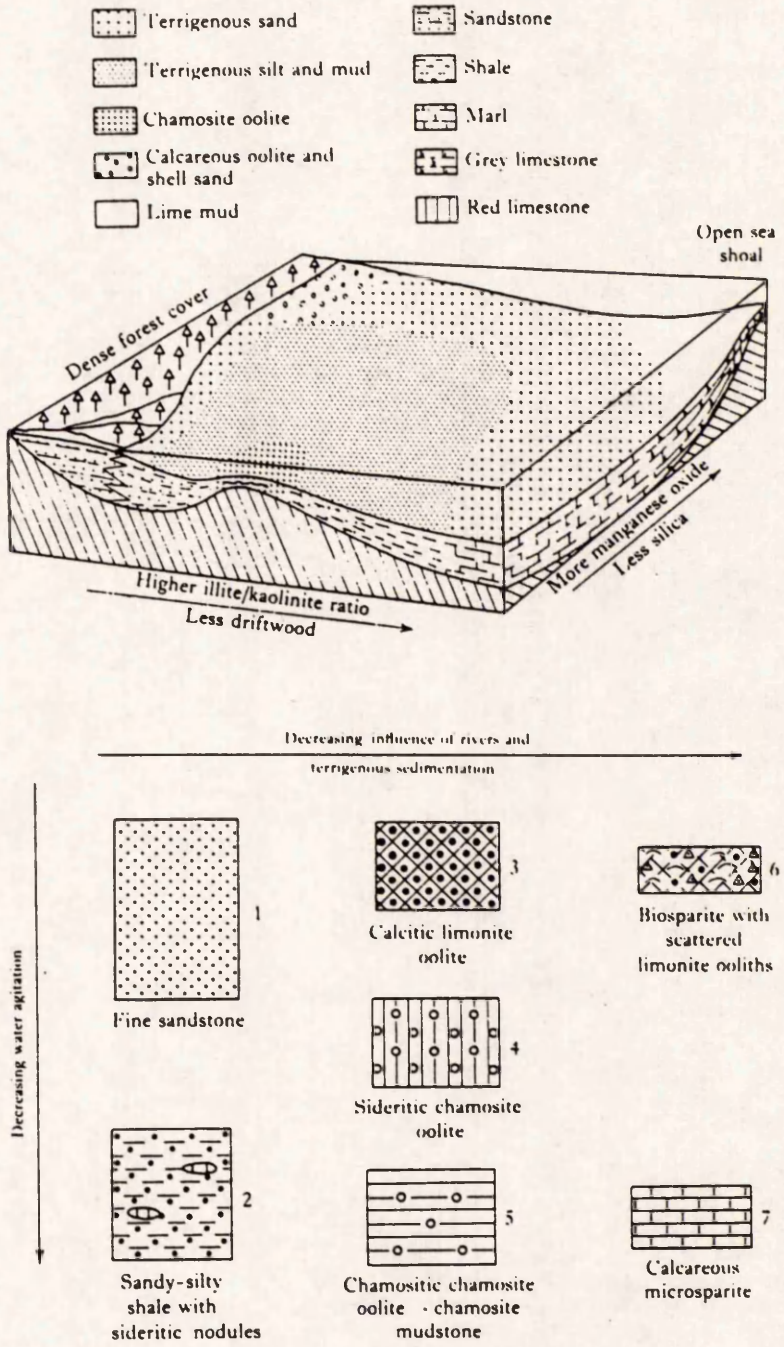

Facies models based on ironstone-formation mineralogy, such as those for 'iron-formations' with oxide, silicate carbonate facies etc.(see James 1954, 1966, Maynard 1983) are largely invalid for ironstones, since ironstone mineralogy often reflects mainly sediment diagenetic rather than primary (depth related) processes (see also Chauvel and Dimroth 1974). However, some diagenetic processes may be controlled by the distance from shore, due to other factors such as oxygen availability, meteoric water fluxes and detrital mineralogy (the presence of bioclasts for example).

1.4.4) Fauna and Palaeoecology.

Much information on the origin of ooidal ironstones can be obtained from an examination of the fauna it contains, but full palaeoecological studies such as Brookfield (1973) and Hallam (1963) are uncommon. A palaeoecological study of the Frodingham Ironstone Formation is presently in preparation by D. Parsons.(see section 2.5). Most ooidal ironstones support a full and varied marine fauna of ammonites belemnites, bivalves, brachiopods and echinoderms, at least in part (see Taylor 1951, Hallam 1963, Van Houten and Karasek 1981). A typical faunal community of ooidal ironstones based on British examples, has been described by McKerrow (1978), and is shown in figure 1.3. A freshwater fauna has however reported by Davidson (1961). Some ooidal ironstones are unfossiliferous, such as the Lokoja Ironstone, Nigeria (Jones 1965).

Descriptions of specialised and restricted faunas have been reported, but are debated. Arkell (1936) claimed the Abbotsbury Ironstone had a specialised fauna, but Brookfield (1973) did not find support for this. Alling (1947) showed a 20% reduction in bryozoan size relative to the surrounding sediments in the Silurian Clinton Ironstone, U.S.A., though Kimberley (1979b) assigns this to better sorting. The Cleveland Ironstone Formation shows a normal marine macrofauna, but Catt *et al.* (1971) found that the microfauna reflected conditions unfavourable to ostracods and foraminifera.

Figure 1.3. Ironstone Faunal Community. Taken From McKerrow (1978, figure 69 p. 222).

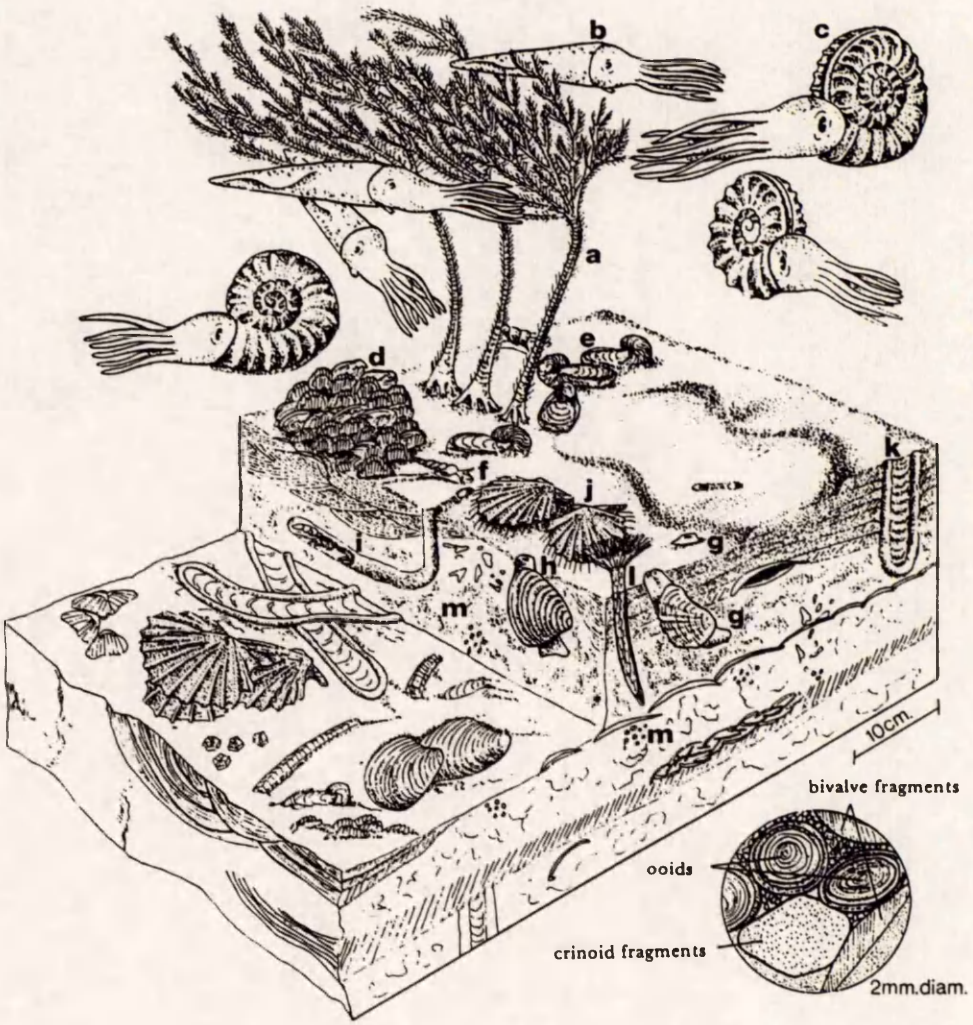

Ironstone Community

a *Pentacrinus* (Echinodermata: Crinozoa)
b belemnite (Mollusca: Cephalopoda: Coleoidea)
c *Asteroceras* (Mollusca: Cephalopoda: Ammonoidea)
d rhynchonellids (Brachiopoda: Articulata: Rhynchonellida)
e *Gryphaea* (Mollusca: Bivalvia: Pterioida-oyster)
f *Procerithium* (Mollusca: Gastropoda: Mesogastropoda)
g *Pholadomya* (Mollusca: Bivalvia: Anomalodesmata)
h *Cardinia* (Mollusca: Bivalvia: Veneroida)
i *Rhizocorallium* (trace-fossil – crustacean)
j *Pseudopecten* (Mollusca: Bivalvia: Pterioida – pectinid)
k *Diplocraterion* (trace-fossil – annelid or crustacean)
l terebellid (Annelida)
m *Chondrites* (trace-fossil – annelid)

1.4.5) Palaeoenvironmental Models of Ooidal Ironstone Formation.

It is commonly interpreted that Jurassic ooidal ironstones formed in shallow marine waters bordering an assumed low-lying well-vegetated landmass that was undergoing subdued, possibly lateritic weathering, in a warm humid climate (Hallam 1975). Ooidal ironstones are however not environmentally diagnostic (Talbot 1974), as many ironstones are clearly accumulations of iron-rich components that have been considerably reworked. Ooidal ironstone deposits have been assigned to various environments, though Strakhov (1967) suggests that gulfs, bays and insular seas with intricately indented shorelines are the favoured sites. More specifically, environments postulated include amongst others; fluvial, deltaic, and lacustrine (Davidson 1961); shallow inland sea (Kimberley 1978, Paz de Rio Ironstone); offshore barrier bar (Brookfield 1973, Abbotsbury Ironstone Formation); slightly hyposaline lagoon (Talbot 1974, Upper Oxfordian ironstones); shallow water estuarine conditions (Umeorah 1987, Agbaja Ironstone, Nigeria); shoal isolated from the land (Hallam 1963, Knox and Fletcher 1987a, Frodingham Ironstone Formation); and conditions similar to the carbonate flats of the Trucial coastline (Adeleye 1973, Middle Niger Valley, Nigeria).

The palaeoenvironment of ironstone deposition is hence variable, but is commonly associated with a coastline. Given that most ironstones represent accumulations of ferruginous and bioclastic debris, the formation of this type of ironstone is largely controlled by the supply of this material. The answer to ooidal ironstone formation may therefore be linked to the origin of the iron-ooids that characterise this type of deposit. Many ironstones would be 'normal' sedimentary rocks if the ooids were removed. Proposed mechanisms of iron-ooid formation are now discussed.

1.5) Modes of Iron-Ooid Formation.

The question of iron-ooid formation is an integral part of all studies of ooidal ironstones, and many papers have been devoted to the subject. Iron-ooid origin appears to hold a vital link in the genesis of these deposits, with theories for their formation becoming more complex and unusual through time as various hypotheses are debated. There is also a lack

of cited examples for ooids formed *in situ* within an ironstone (for example Bhattacharyya 1989), with most examples clearly of a reworked nature. Without recognition of modern ooids of the same mineralogy and texture, the debate is set to continue for some time yet. Modes of formation for iron-ooids suggested so far, are outlined below.

1.5.1) Replacement of Calcareous Ooids.

The replacement of original calcareous oolite by iron leached from surrounding muds, was originally proposed by Sorby (1857, 1906) as the origin of the Cleveland Ironstone Formation. Cayeux (1922) later supported this mechanism, but the main adherent to this model has been Kimberley (1974, 1975, 1979a, 1979b, 1980, 1983). The main arguments are set out in his 1979a paper, based on the Eocene Paz de Rio S.C.O.S.-I.F. of Columbia, S.America, but his ideas have not been generally accepted. Evidence against such a model is outlined in Binda and Moltzer (1979), Adeleye (1980) and Bradshaw *et al.* (1980). Hallam and Bradshaw (1979) state that Kimberley ignored the "...overwhelming petrographic evidence... that the ooids in question were originally chamositic...". Ferruginisation of calcareous particles within ironstones is common (for example Dreesen 1989), and can be readily demonstrated in the present day (for example Ferguson *et al.* 1983), but the model is poorly supported for the genesis of all ooidal ironstones.

1.5.2) Growth on the Sea Floor.

The formation of ooids on the sea floor has been well supported, though some authors have been imprecise about the exact mechanism of formation, other than stating that agitated water was involved (Rastall and Hemingway 1940, Taylor 1951, Dunham 1960, Van Houten and Karasek 1981). Hallimond (1925 page 10) is more specific and proposed that "chamosite" was precipitated on the ooid. Umeorah (1987) supports a direct precipitation mechanism, but for the formation of primary goethitic ooids. Davies and Dixie (1951) appear to support the alternative of mechanical accretion of previously formed material, a view also held by Bhattacharyya and Kakimoto (1982), and Bhattacharryya (1989). They argue for ooid formation by mechanical accretion of suspended particulate matter, in waters of sufficient agitation to mobilise the ooid. Knox (1970) adheres to a mechanical accretion

model and suggests that the oblate shape of the ooids within the Winter Gill Ironstone was dictated by the movement, concentration, and upper limit of suspension of the suspended material. "Eccentric" ooids (those with offset nuclei), he argued, are formed due to the particle being immobile during growth. Gehring (1989) recently suggested a model of ooid formation during reworking, whereby particulate matter (goethite, clay minerals, and apatite) was adsorped onto the ooid surface.

1.5.3) Growth Within the Sediment or a Gel.

Intrasedimentary growth as microconcretions, has been postulated as the method of iron-ooid genesis by some authors (for example Pulfrey 1933, Carozzi 1961, Jones 1965). Hallimond (1951) suggests that a single layer of "chamosite" is added within the sediment, and that repeated exposure and re-sedimentation produces successive layering. As pointed out by Hemingway (1974), laminae formation around several nuclei, and compound ooids of several bonded ooids, are unlikely to have occurred during agitation. James and Van Houten (1979) proposed that "chamosite" ooids probably formed within sediment but that goethitic ooids may be indicative of a higher energy of formation. Intrasedimentary growth has recently been proposed as the favoured mechanism for ooid formation in Algeria (Guerrak and Chauvel 1985, Guerrak 1987).

Ooid formation within or from a detrital gel composed essentially of $Fe(OH)_3$, $Al(OH)_3$ and SiO_2 that was later modified to "chamosite" during diagenesis, has been postulated by Caillere and Kraut (1953). Other workers (Curtis and Spears 1968, Harder 1978) have supported "chamosite" formation from a mixed gel of this nature, but have not applied this specifically to ooid genesis.

1.5.4) Formation Within Soils.

Iron-rich pisoids are commonly found within lateritic soil profiles of the present day (see for example McFarlane 1976), and this has led many authors to suggest they represent a modern analogue to ancient ooid formation. A pedogenic origin for iron-ooids was proposed by Nahon *et al.* (1980) based on examination of ferricretes in West Africa. They

suggested that the ooids grow within the soil profile by centripetal concentration and reorganisation of the iron oxides and hydroxides, especially aluminous goethite. Siehl and Thien (1986, 1989) support redeposition of soil-derived ooids as the major process generating "Minette-type" ironstones, where uncoated ferricrete clasts of the same grain size are always present. Jones (1965) has reported ironstones associated with laterites in the Cretaceous of Nigeria, indicating a clear link between ironstones and lateritic soils. The presence of desiccation cracks in ooids (Adeleye 1975) may support a pedogenic origin, as wetting and drying of the soil profile causes fracturing in modern soil pisoids. Bhattacharyya and Kakimoto (1982) have however argued that the tangential accretion fabric of iron-ooid cortices cannot be compared with the radial (precipitation) fabric of lateritic pisoids.

1.5.5) Other Modes of Formation.

Jones (1965) agrees with an accretionary mode of origin for most iron-ooids, but suggests that textures similar to the complex internal accretionary structures seen in many ooids, can be formed during weathering. This occurs by the centripetal diffusion of ferric hydroxides in the ooid, similar to the formation of Liesegang rings. He argues that such a mechanism formed concentric zoning in shale pellets within the Lower Limestone Shales of Skrinkle Haven, South Wales.

Dahanayake and Krumbein (1986) have concluded that ferriferous ooids are authigenically formed biogenic grains formed within microbial mat environments. The evidence for this is rather inadequate, and the suggested 'ooid-precursors' appear to be simply fungal shell borings.

Champetier *et al.* (1987) believe that many iron-ooids in the Lorraine (France) and Gara Djebilet (Algeria) ironstones are metasomatic replacements of Nubeculariidea foraminifera. This theory has not been widely accepted, and Chauvel and Guerrak (1989) have shown that the foraminiferid described predates the oldest known nubeculariid occurrence.

1.6) Temporal Patterns of Ooidal Ironstone Formation.

Large scale cyclicity of ooidal ironstone occurrence in the geological record associated with eustatic sea level changes, has been postulated by Hallam and Bradshaw (1979). The restricted abundance of ooidal ironstones to essentially the Jurassic and Ordovician Peroids is reviewed by Van Houten (1985) and related to two episodes of continent dispersal and sea-level highstands. Recently, Van Houten and Arthur (1989) have reviewed earlier work (for example Van Houten 1986 a,b) on the temporal patterns of ooidal ironstones and show that they developed most readily in an Ordovician to Devonian, and Jurassic to Palaeogene 150-170Ma interval controlled by plate-tectonics. Rapid sea floor spreading led to CO_2 mantle degassing, and formation of a warmer climate with higher precipitation. This resulted in intensified chemical weathering, allowing ironstone formation. Within these two major periods, cyclicity on a ≈32Ma secular cycle can be seen, and may also be linked to black shale formation.

1.7) Mineralogy of the Mesozoic/Cenozoic Ironstones.

Ooidal ironstones of the 'Minette' type have a mineral assemblage dominated by iron-rich varieties of silicates, oxides/hydroxides and carbonates. The main mineral species present are berthierine, goethite, siderite and calcite. Occurrences of these and other minor minerals are reviewed by James (1966 pp 2-11). The major species are briefly reviewed here for reference purposes.

1.7.1) Oxides/Hydroxides.

Goethite (α-FeOOH), is the most common oxide of iron, and occurs extensively as ooids in most 'Minette'-type ironstones. The name "limonite" has been widely used as a mineralogical term for a mixture of iron (and possibly aluminium) oxides/hydroxides, aluminosilicates, and other species, that is dominantly composed of goethite. However, this term should not be used as it does not constitute a distinct mineral species. Goethite is also commonly found as an oxidation product of berthierine, siderite, and other iron-bearing phases. Hematite (α-Fe_2O_3) is relatively uncommon in the Mesozoic 'Minette' ironstones, but is characteristic of the 'Clinton' type. The hematite in these older ores probably results

from geological ageing of an original goethite (James 1966). Magnetite is also uncommon, particularly in the 'Minette'-type ironstones. The Rosedale Ironstone (Rastall and Hemingway 1949) is unusual in that it contains magnetite ooids which form a significant proportion of the rock.

1.7.2) Carbonates.

Calcite ($CaCO_3$) is abundant as bioclastic debris in most ironstones. This calcite is Low Magnesian Calcite (see definitions in section **5**.5), with aragonitic debris having been dissolved or replaced. Calcite also occurs extensively as a cement, which may be highly ferroan and manganoan (this report), but precise compositional data are lacking from most deposits. Siderite ($FeCO_3$) is also abundant, and is well documented as both a cement and as a replacement of berthierine or less commonly goethite. Compositional data of Ca, Mg, and Mn substitution in these siderites that would allow more precise classification, are however poorly cited. Ankerite ($Ca(Fe,Mg)(CO_3)_2$) occurs sparsely (for example Garzanti *et al.* 1989), but dolomite ($CaMg(CO_3)_2$) has not been recorded.

1.7.3) Sulphides.

Sulphides are not common in Mesozoic ooidal ironstones. Pyrite (FeS_2), the common sulphide in most marine sediments, is present usually as only a minor constituent, and its dimorph marcasite has not been recorded. In some beds however, such as the "Snap Band" of the Frodingham Ironstone Formation, and the "Sulphur Bed" of the Cleveland Ironstone Formation, pyrite is abundant. Sphalerite (ZnS) has also been identified in the top bed of the latter ironstone.

1.7.4) Phosphates.

Occasional occurrences of reworked phosphatic nodules occur within ooidal ironstones, some of which contain ooidal debris. Authigenic phosphatic cements have also been reported but are not widely found, and never extensive. Phosphatic ooids (francolite) have been described from the Upper Lias of central England (Horton *et al.* 1980, Harrison *et al.* 1983), and the Abbotsbury Ironstone Formation has been correlated laterally with

condensed phosphorite (Brookfield 1971). Compositions of the phosphates have rarely been obtained.

1.7.5) Silicates.

Occurrences of silicates other than berthierine (see below) have been largely described as being of detrital origin. Quartz and felspar are found in low abundance within true ironstones, and are usually accompanied by a detrital clay of variable mineralogy (usually reported as kaolinite or illite). Authigenic kaolinite, and minor 'opal' have been described replacing ooids of the Cleveland Ironstone Formation (Whitehead *et al.* 1952), and the former also replaces ooids of the Yorkshire Dogger (Rastall and Hemingway 1940). Berthierine is very common in ooidal ironstones of the Mesozoic as both ooids and an authigenic cement, and is discussed separately in detail in section 1.9 below.

1.8) The Geochemistry of Iron and Manganese, and the Formation of Sedimentary Iron Minerals

The sedimentary geochemistry of Fe and Mn has been studied in detail by many workers, and their relative abundance within sediments allows detailed geochemical analysis of the environment of sediment accumulation. Fe and Mn occur ubiquitously together, due to their similar ionic size and overall geochemical behaviour. However at a more detailed level, geochemical differences that may lead to the separation of the two elements are apparent (see Krauskopf 1957). Both Fe and Mn form oxides, carbonates and sulphides, and may become incorporated within silicates. The occurrence of these different minerals can be linked with specific environments and processes, that allow the sediment geochemistry to be elucidated.

The distribution of Fe and Mn minerals has been shown to be sensitive to variations in pH and Eh, hence the common use of pH/Eh diagrams (Huber and Garrels 1953, Garrels and Christ 1965). The diagrams describe mineral species formation relative to the oxidising/reducing nature of the environment (oxidation potential measured as Eh), and its acidity/alkalinity (measured by pH). The concentrations of dissolved anionic species are

assumed for the calculations. Full details and methods for calculation of these diagrams are given in Garrels and Christ (1965). Examples of such diagrams for Fe and Mn are given in figures 1.4, 1.5, 1.8, and 1.9, all of which have been calculated for normal marine waters at near surface conditions. Actual environments encountered in nature do not cover the full field shown (see Baas-Becking *et al.* 1960), and most fall in the range of pH 4-9 (Krauskopf 1979).

Eh and pH alone are however insufficient to explain the behavior of Fe and Mn. Curtis and Spears (1968) addressed the problems of sedimentary iron mineral formation, and calculated stability diagrams based on Eh and dissolved anionic species concentration (figure 1.6). Similarly Maynard (1983) presents iron mineral stability as a function of oxygen and carbonate availability (figure 1.7). Construction and interpretation of such diagrams lead to important conclusions to the geochemical behavior of Fe and Mn. The geochemistry of Fe is discussed first , as this is the more common element.

Only hematite (Fe_2O_3), and other iron oxides/hydroxides are stable in depositional waters. This is shown in figures 1.4 and 1.5, where Fe_2O_3 has a large stability field for most values of Eh>0 within the pH range commonly found in nature. A pH<4 is rarely attained, and the solubility of Fe^{2+} is extremely low in such a situation. Relative to both $^aHS^-$ and $^aHCO_3^-$ (figure 1.6, a and b), hematite covers the entire range of positive Eh for all values given. Any ferrous species (siderite, pyrite, iron-silicate) will therefore oxidise readily at any pH to iron oxide, if conditions change from reducing to oxidising (Eh<0 to Eh>0).

Pyrite (FeS_2) is a very stable phase within the sediment under reducing conditions. This is best indicated in figure 1.6(a) that shows a large stability field for pyrite that covers most values of Eh below that of hematite even at low sulphide concentrations. This stability of pyrite is emphasised in figure 1.6(b) in which a very low sulphide activity ($^aHS^- = 10^{-7}$) has had to be assumed in order to plot the occurrence of other iron minerals. Even here however, the pyrite field is still considerable, and demonstrates how Fe^{2+} will be

Figure 1.4. Eh-pH Diagram Constructed for Iron Oxides, Sulphides, and Carbonates, in water at 25°C and 1 atmosphere. Total Dissolved Sulphur = 10^{-6}. Total Dissolved Carbonate = 10^{0}. Taken From Garrels and Christ (1965, figure 7.21 p. 224).

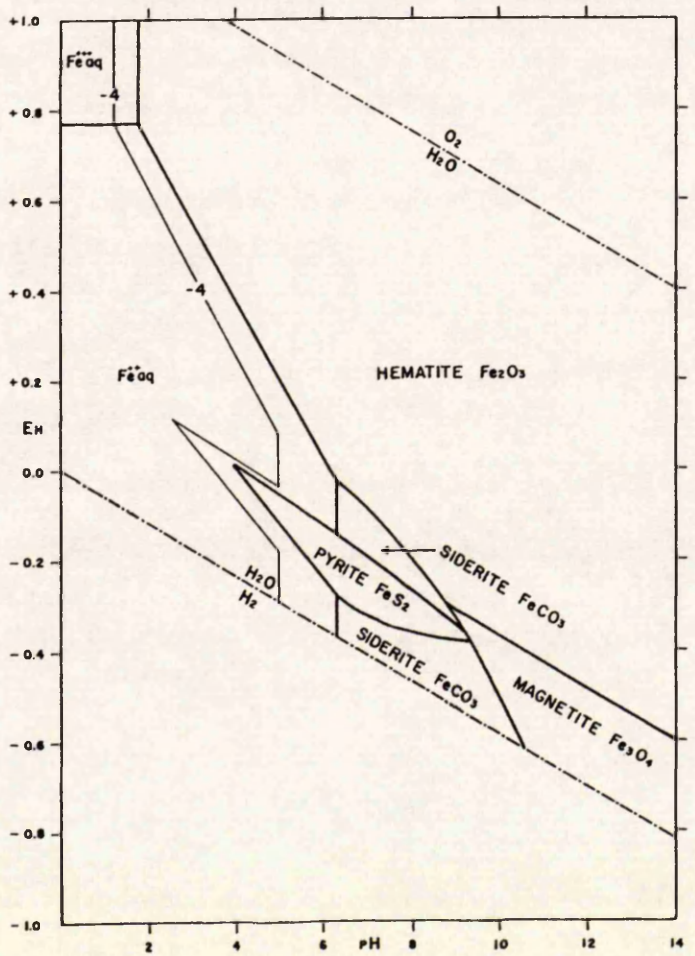

Figure 1.5. Eh-pH Diagram Constructed for Iron Oxides, Sulphides, and Carbonates, in water at 25°C and 1 atmosphere. Total Dissolved Sulphur = 10^{-6}. Total Dissolved Carbonate = 10^{0}. Amorphous Silica is Present. Taken From Garrels and Christ (1965, figure 7.23 p. 228).

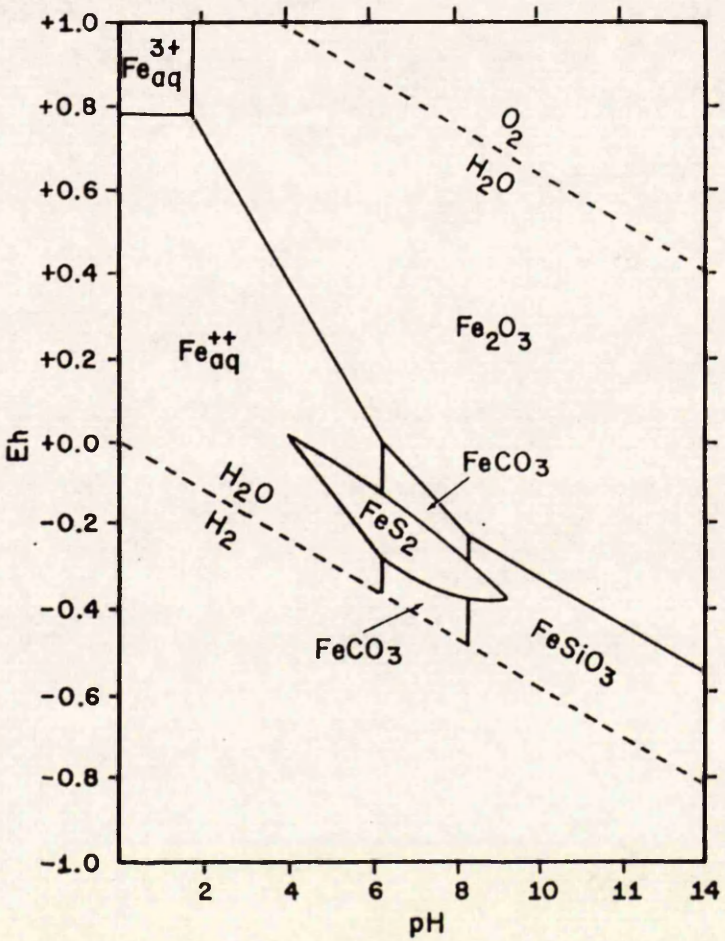

Figure 1.6. Iron Mineral Stability as a Function of Eh, $^aHS^-$ (or SO_4^{2-}) and $aHCO_3^-$ (After Curtis and Spears 1968. Diagram Taken From Leeder 1982). a) pH=8, $^aHCO_3^- = 10^{-3.5}$, $^aFe^{2+} < 10^{-6}$.
b) pH=8, $^aHS^- = 10^{-7}$, $^aFe^{2+} < 10^{-6}$.

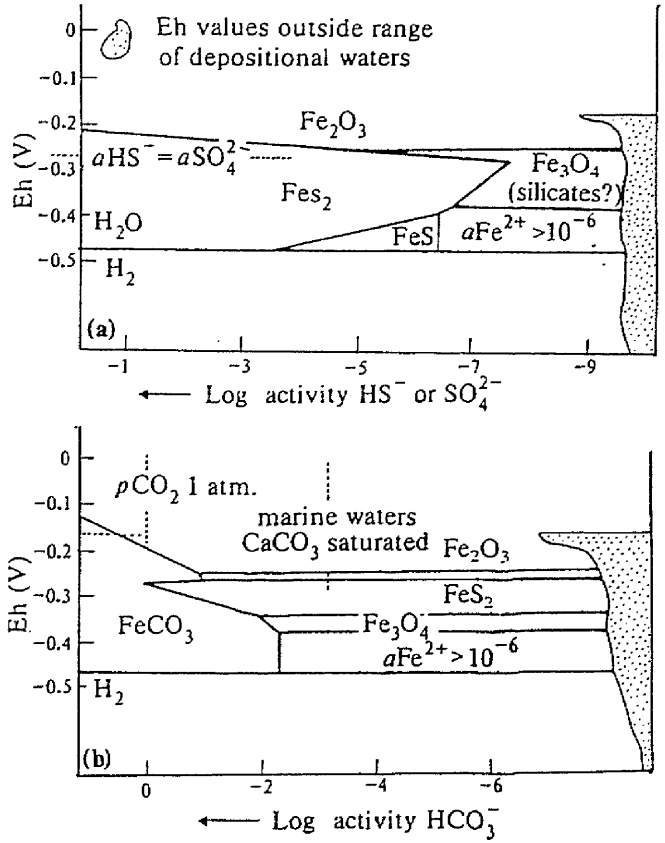

Figure 1.7. Iron Mineral Stability as a Function of Log P_{O2}, and Log P_{CO2}. Equilibrium With Kaolinite is Assumed. pH=8, Dissolved $S=10^{-6}$. Taken From Maynard (1983, figure 2.15 p. 45).

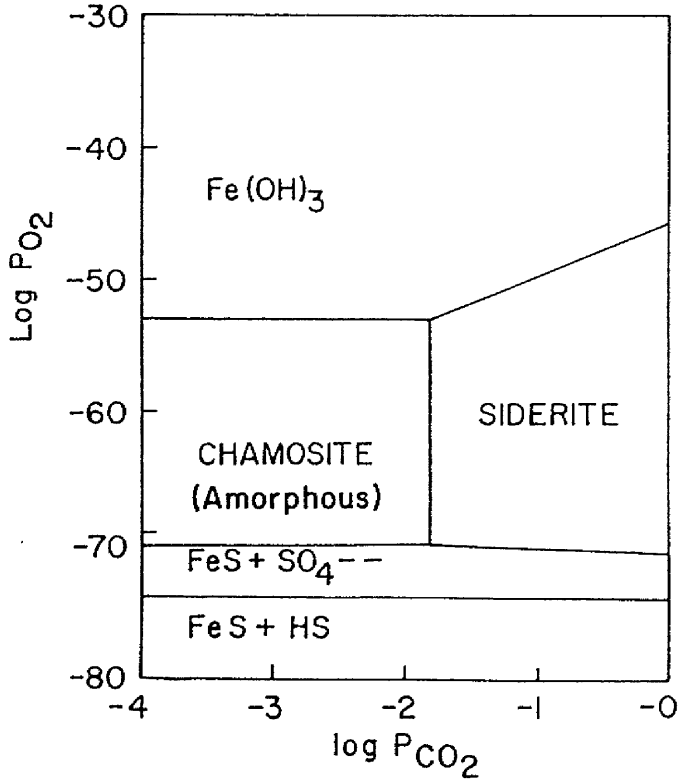

preferentially incorporated into pyrite under reducing conditions, if there is even a trace of dissolved sulphide.

The stability field of siderite ($FeCO_3$) overlaps that of pyrite (figures 1.4 and 1.5), indicating that they may form under the same conditions of Eh and pH. From the discussion on pyrite (above), it is evident that siderite will only form at very low sulphide levels. Figure 1.6(b) demonstrates how a high $^aHCO_3^-$ is also required if Fe^{2+} is not to be incorporated within silicates or magnetite.

Iron silicates cannot be studied as easily in a similar context, as their free energies of formation cannot be experimentally derived to any degree of certainty. Estimates therefore have to be used, based on more simple structures than the complex aluminosilicates commonly formed. The simple silicate $FeSiO_3$ was used by Garrels and Christ (1965) in their calculations. Figure 1.4 is modified in figure 1.5 to include the presence of silica, allowing the formation of the silicate $FeSiO_3$ which replaces the stability field of magnetite. Therefore $FeSiO_3$ and magnetite cannot coexist within normal sediments where silica is present. Figure 1.6(a) shows that pyrite will form in preference to silicates unless the $^aHS^-$ is low, and figure 1.6(b) indicates that silicates may form if both the Eh and carbonate/sulphide activities are low. Maynard (1983) addressed silicate formation in more detail using a "chamosite" formula (figure 1.7), and shows that this iron silicate follows the Eh-pH relationships described for the simpler silicate composition assumed by Garrels and Christ (1965). This diagram shows the relationship between iron silicates and the minerals described above, with oxygen availability strongly influencing hematite, iron silicate, or pyrite formation, and carbonate availability determining iron silicate or carbonate formation.

The geochemistry of Mn can be delineated in a similar way to that of iron. Figures 1.8 and 1.9 are Eh-pH diagrams calculated for Mn minerals by the same method as used for iron. In comparison to Fe, Mn has a larger stability field for the divalent ionic species (Mn^{2+}), and a very pronounced carbonate stability field ($MnCO_3$). This implies that Mn is more mobile than Fe, and has a stronger tendency to form carbonates. Therefore, whereas

Figure 1.8. Eh-pH Diagram Constructed for Manganese Oxides and Carbonates, in water at 25°C and 1 atmosphere. Total Dissolved Carbonate = $10^{-1.4}$. Taken From Garrels and Christ (1965, figure 7.28a p. 242).

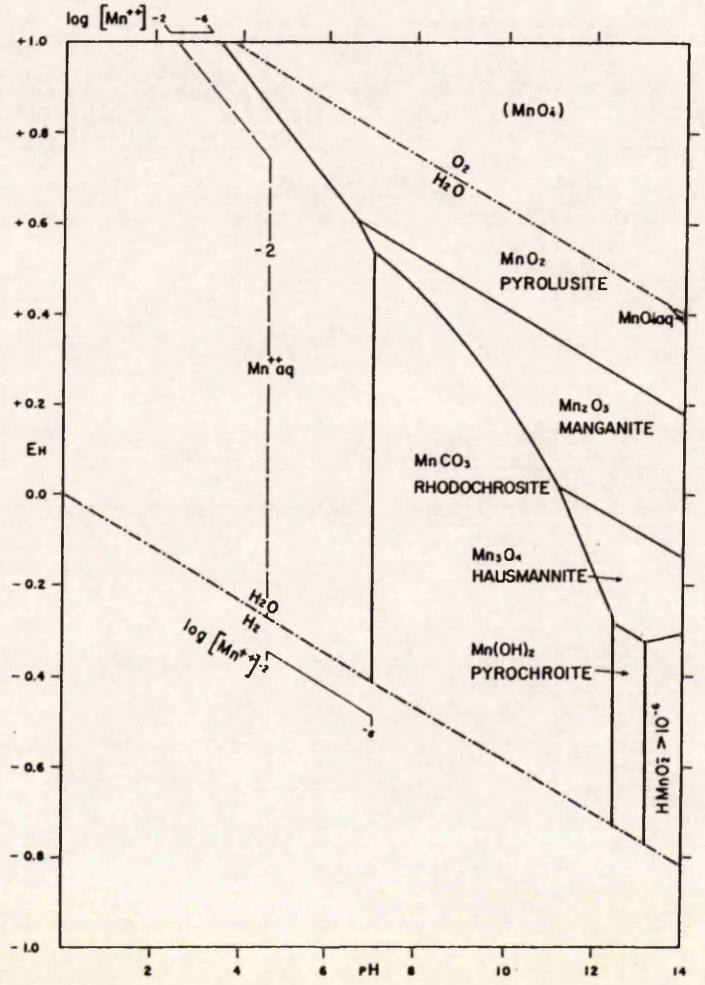

Figure 1.9. Eh-pH Diagram Constructed for Manganese Oxides Carbonates, and Sulphides, in water at 25°C and 1 atmosphere. Total Dissolved Sulphur = 10^{-1}, $P_{CO_2}=10^{-4}$. Taken From Garrels and Christ (1965, figure 7.28b p. 243).

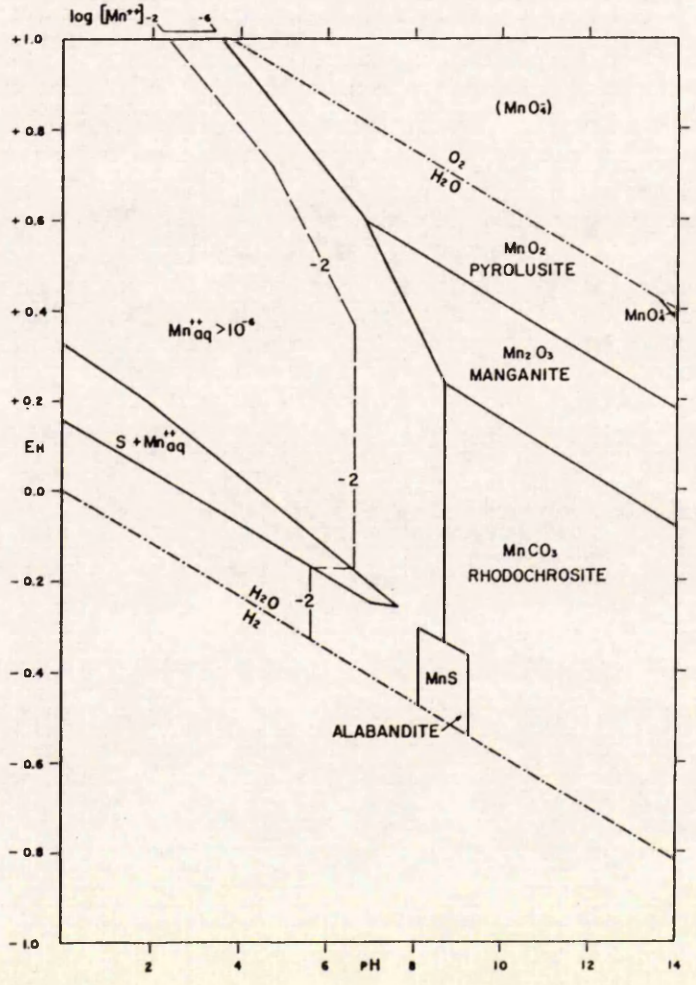

Fe is preferentially incorporated into pyrite, Mn will be preferentially sited within any carbonate being precipitated given similar metal concentrations. This carbonate will be very stable, as can be seen by the large area of the field that it covers, and even extends into the area of positive Eh. Of the oxides, pyrolusite (MnO_2), manganite (Mn_2O_3) and hausmannite (Mn_3O_4) form in sequence from highly oxidising to reducing conditions, reflecting the valency of the Mn species. The stability of the sulphide alabandite (MnS) is extremely small, and explains why this mineral is so uncommon in sediments. It should be noted that Mn does not readily form a simple silicate, but may be incorporated along with Fe into a precipitating mineral.

1.9) Berthierine Mineralogy, Composition, and Origin.

Berthierine is a ferrous, aluminous, 1:1 type layer silicate, with a structural composition of $(R^{2+}_a,R^{3+}_b,\square_c)(Si_{2-x}Al_x)O_5(OH)_4$ where R^{2+} and R^{3+} are cations, $\square$ represents vacant octahedral positions, and a+b+c = 3 (Brindley 1982). More specifically, Brindley and Brown (1980) gave the composition as $(Fe^{2+},Mn^{2+},Mg^{2+})_{3-x}(Fe^{3+},Al)_x(Si_{2-x}Al_x)O_5(OH)_4$. Berthierine classification is discussed further in section 4.7.

Berthierine, formerley known as "chamosite" is now recognised as a distinct mineral species. Though of a similar composition, the two minerals are differentiated by their structure, berthierine has a ≈7Å basal spacing whereas chamosite has a chlorite type ≈14Å spacing. Berthierine is hence structurally and compositionally similar to the serpentine group of minerals, and structurally similar to kaolinite. Where it is differentiated in the literature from chamosite and other chlorites, berthierine has also been termed 'septechlorite' and 'septechamosite', but these terms are now redundant. Berthierine has two structural types within this framework, described as 1T (tetragonal) and 1M (monoclinic) based on the symmetry of layer stacking. It possesses a green colour, low birefringence, and usually forms a platy morphology of very fine crystals similar to the chlorites (see plate 8d).

The origin of berthierine is widely debated in the literature as to its primary or diagenetic origin. There is a general concensus that berthierine is unstable in the presence of free

oxygen (Curtis and Spears 1968), so that precipitation in waters under reducing conditions was held to be the mechanism of berthierine formation by earlier workers (Hallimond 1925 p. 92, Taylor 1951, Davies and Dixie 1951, Dunham 1960). The possibility that precipitation may have occurred within a gel was briefly discussed by Hallimond (1925 p. 96), and mentioned as a possibility by Dunham (1960). Curtis and Spears (1968) suggested a mixed $Al(OH)_3$, $Fe(OH)_3$, $SiO_2.nH_2O$ gel, stable at positive Eh, with a diagenetic modification to form berthierine (also favoured by Talbot 1974).

A diagenetic (i.e. formation within the sediment) origin for berthierine is now favoured by most authors, but the primary source of cations for the authigenic berthierine precipitation varies. Bubenicek (1967) suggests formation of berthierine in the Lorraine ores (France) by the reaction:

6.05 "limonite" + 1 quartz = 4.72 siderite + 4.26 "chlorite" (berthierine)

Harder (1978) agrees that iron oxides/hydroxides in the form of detrital lateritic particles provided the source of iron, and suggests that these were reduced within the sediment. Iijima and Matsumoto (1982) state that the formation of berthierine in the coal measures of Japan occurred by the reaction of kaolinite and siderite:

$$Al_2Si_2O_5(OH)_4 + 2FeCO_3 = Fe_2Al_2Si_2O_5(OH)_4 + SiO_2 + CO_2.$$

kaolinite siderite berthierine quartz

Bhattacharyya (1983) suggests that a diagenetic transformation of kaolinite occurs by the introduction of Fe. This is represented schematically as:

1) $Al_4Si_4O_{10}(OH)_8 + 3Fe^{2+} = Fe^{2+}{}_3Al_2Si_4O_{10}(OH)_8 + 2Al^{3+}$

kaolinite "protoberthierine"

2) $Fe^{2+}{}_3Al_2Si_4O_{10}(OH)_8 + Fe^{2+} + 2Fe^{3+} = Fe^{2+}{}_4Fe^{3+}{}_2Al_2Si_2O_{10}(OH)_8 + 2Si^{4+}.$

"protoberthierine" berthierine

Curtis (1985) proposes the following reaction for the formation of berthierine from an assemblage typical of lateritic soils and sediments derived from them:

$$Al_4Si_4O_{10}(OH)_8 + 4H_2O + 2SiO_2 + 5Fe_2O_3 + 2.5[C] = 2Fe_5Al_2Si_3O_{10}(OH)_8 + 2.5CO_2$$

kaolinite quartz hematite O.M. berthierine

This schematic equation represents a detrital assemblage of kaolinite, quartz, and iron oxide (hematite) undergoing dissolution, and iron-reduction by bacterially induced oxidation of organic matter (O.M., simplified to pure carbon), with subsequent berthierine formation.

Though specific reaction pathways are not inferred due to the sheer complexities involved, the overall scenario implied by the model is becoming widely accepted, and is largely being tested in this thesis.

A model for berthierine formation from kaolinite has also been supported by Maynard (1983), who uses a standard Si - Al - (Fe+Mg) plot to show that berthierine (or "chamosite") formation is consistent with a derivation from kaolinite by the addition of Fe and Mg (figure 1.10). Using stability calculations, he suggests that greenalite is the iron silicate expected to precipitate directly from sea water, and that "chamosite" requires additional Al. He also shows that "chamosite" occupies a lower pH field than that of glauconite (figure 1.11), which may explain why these two minerals have a common lateral association. This diagram also shows that a detrital assemblage of $Fe(OH)_3$ and illite could become unstable and form "chamosite" or glauconite, simply by lowering the Eh, as occurs by the formation of reducing conditions within the sediment.

Experimental work on the formation of berthierine and other iron-rich silicates, has been largely undertaken by Harder (1978 ,1980, 1989). Solutions of Fe, Si, Al, and Mg, were prepared under reducing conditions, and iron hydroxides were allowed to precipitate by changing the Eh or pH. Silica was fixed into the hydroxides during the reaction between the colloids and ions in solution due to their charge differences. The precipitates were variably aged and initial composition changed, to produce the different clay minerals. Harder (1989) concludes from experiments to produce berthierine, nontronite and glauconite, that:

1) The precipitate composition must be similar to that of the appropriate clay mineral.
2) Di or Tri-octahedral, 2 or 3 layer iron clay minerals form only under reducing conditions.
3) A higher pH (8-9) and low Eh favours fuller and faster crystallisation.
4) 300 ppm KCl was necessary in initial solutions in order to produce glauconite.
5) In the Fe^{2+}-SiO_2 system, silica concentration controls the mineral formed;

SiO_2 Concentration in Initial Solution.	Mineral Formed.
<5ppm	Quartz (+iron oxide)
5-9ppm	Berthierine
>10ppm	Nontronite, Glauconite

Figure 1.10. Compositions of Iron-Ooids of Newfoundland, Great Britain, France and China, Determined by E.P.M.A., Plotted on a Si - Al - (Fe+Mg) Ternary Plot. Taken From Maynard (1983, figure 2.16 p. 46).

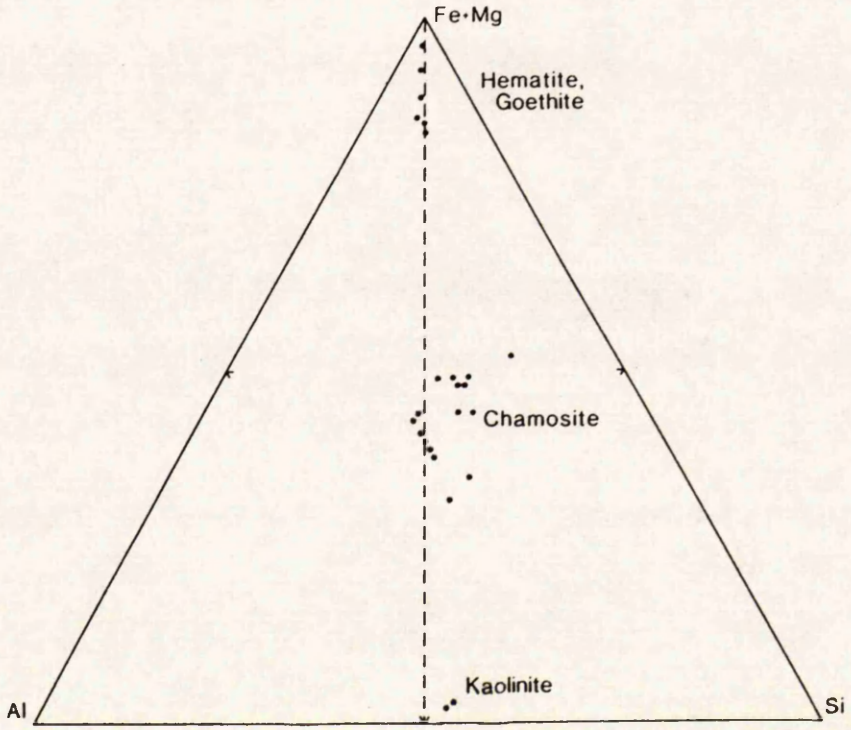

Figure 1.11. Eh-pH Diagram Constructed to Show The Stability Relationship Between 'Chamosite' and Glauconite, for Seawater Activities of K = $10^{-2.2}$, Al = $10^{-6.8}$, and Si = $10^{-2.7}$. Taken From Maynard (1983, figure 2.17 p. 47).

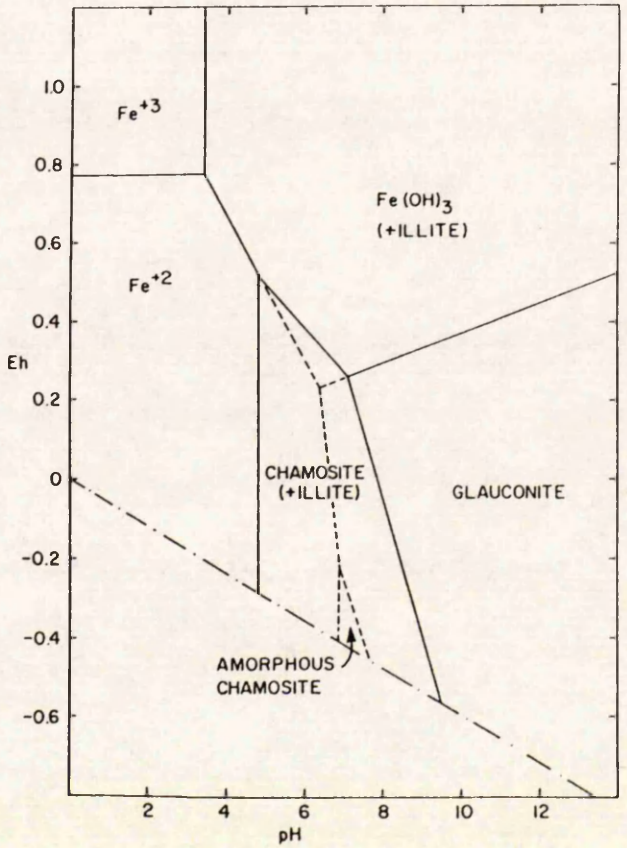

Green clays may be found within modern sediments, and have been studied by many workers (for example Von Gaertner and Schellman (1965), Coast of Guinea; Giresse and Odin (1973), Giresse *et al.* (1988), Coast of Gabon; Porrenga (1965,1967), Niger and Orinoco Deltas; Rohrlich *et al.* (1969), Loch Etive, Scotland; Lemoalle and Dupont (1973), Pedro *et al.* (1978), Lake Chad; Muller and Forstner (1973), Lake Malawi). However, none of these occurrences are true berthierines in composition (Odin 1988), and the textures of particles produced on formation of the clays are unlike those of ironstones. The occurrences, mineralogy and composition of these phases have been recently reviewed by Odin (1988), and the reader is referred to this text for detailed description and discussion. Odin (1988) concludes that modern marine green clay minerals fall into three distinct facies;

i) Verdine Facies. This is characterised by precipitation of various specific marine clays including phyllite V and phyllite C (Odin 1988) in microtest chambers, faecal pellets or pore space. Clay mineral precipitation proceeds via the interaction of sea water and sediment near a source of abundant iron in depths of 20-60m in tropical areas.

ii) Glaucony Facies. This differs from the verdine facies in that the minerals formed are 2:1-type clay minerals (glauconites), and form at greater depth >60m, well removed from continental detrital input.

iii) Celadonite Facies. A much more restricted facies characterised by the presence of the mineral celadonite, whose origin is associated with volcanic sediments.

The fourth facies that Odin describes to encompass all ancient and modern occurrences is that of the 'oolitic ironstone' facies, that is not represented in modern sediments.

Odin (1988 p. 216) discusses the similarity between the mineralogy of the verdine facies (7Å phyllite V, 14Å phyllite V) and that of ironstones (7Å berthierine, 14Å chamosite), and suggests there may be a possible genetic link between the two. Though the verdine facies is non-ooidal, it may be that this facies represents the modern day equivalent to that of the ancient ironstones, that are absent within modern sediments. Much more work is however required on these clays before an actual link between modern and ancient green clay formation is proven, particularly on the actual mode of mineral authigenesis.

1.10) Early Diagenetic Processes in Modern Sediments.

In most modern marine sediments, an ecological succession may be recognised in the uppermost few to tens of metres. This succession is identified from the variation of element concentrations within pore water profiles (for example, Nissenbaum *et al.* (1972), Claypool and Kaplan 1974, Goldhaber *et al.* 1977, Froelich *et al.* 1979, Aller *et al.* 1986, Jørgensen 1983, see also figures 1.12 and 1.13), that reflects microbial processes acting at various depths within the sediment. The diagenetic zonal scheme that results, and the mechanisms that control the formation of these zones, has been excellently reviewed in a number of publications including Claypool and Kaplan (1974), Berner (1980, 1981), Maynard (1982), Curtis (1977, 1983, 1985, 1987a,b), Coleman (1985), and Gautier (1985). The topic will hence only be discussed briefly here, with the following review based upon a synthesis of the above papers which should be referred to for greater detail.

In a normal oxic water column, and within the uppermost portion of the sediment, aerobic respiration is the principle metabolic pathway by which living organisms oxidise organic matter (O.M.) to obtain energy. This may be represented in the following reaction in which O.M. is represented by an average carbohydrate CH_2O:

$$CH_2O + O_2 \text{ -----> } H_2O + CO_2 \qquad \text{Oxidation (Ox)}$$

This reaction is depth limited within the sediment by the availability of free oxygen that diffuses downwards from the overlying sea water, its increased introduction by bioturbation, and by its rapid removal from pore water due to this organic matter oxidation.

Sulphate is abundant in sea water (0.028M), and below the aerobic (Ox) zone, sulphate reduction becomes the dominant reaction by which anaerobic bacteria derive oxygen for O.M. breakdown:

$$2CH_2O + SO_4^{2-} \text{ -----> } HS^- + HCO_3^- + H_2O + CO_2 \qquad \text{Sulphate Reduction (SR)}$$

The onset of this zone is marked in pore water profiles by a decrease in the concentration of SO_4^{2-} at the point where oxygen is depleted (figure 1.12). As with the Ox process, the thickness of this zone in the sediment is constrained by the diffusive recharge from sea water of the oxidant, which in this case is SO_4^{2-}.

Figure 1.12. Expected Variation in Selected Parameters with Sediment Depth, as Indicated From Pore Water profiles, With Reference to the Diagenetic Zonation Formed.

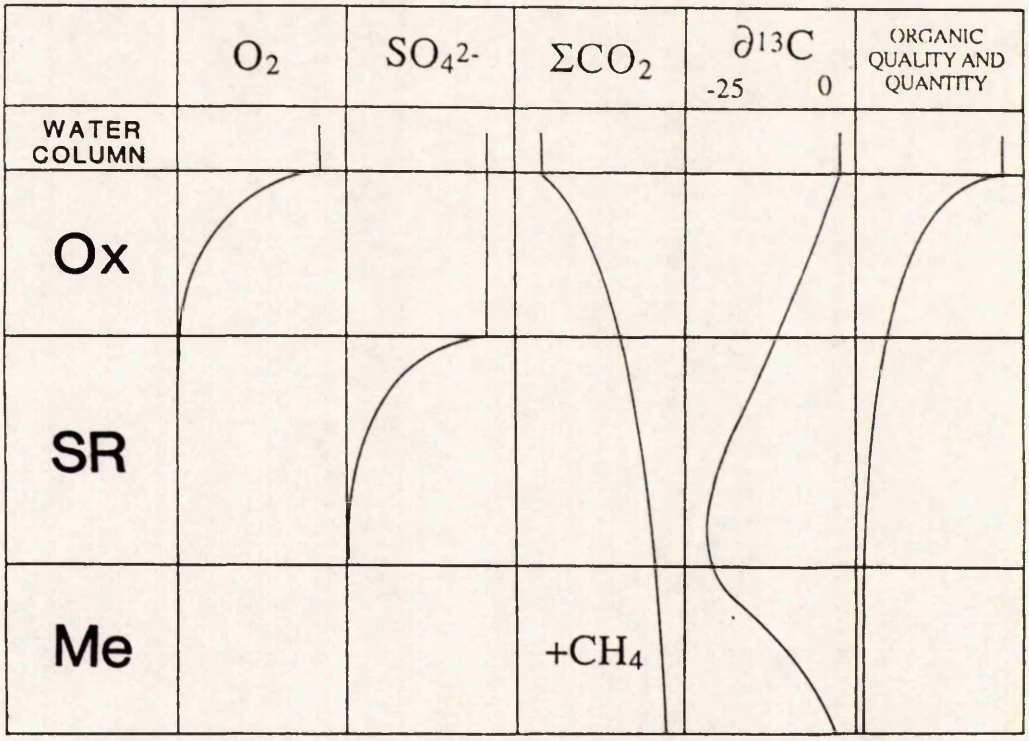

Figure 1.13. Expected Variation in Oxygen, Nitrate, Iron and Manganese Concentrations With Sediment Depth, as Indicated From Pore Water Profiles of Post-Oxic Sediments.

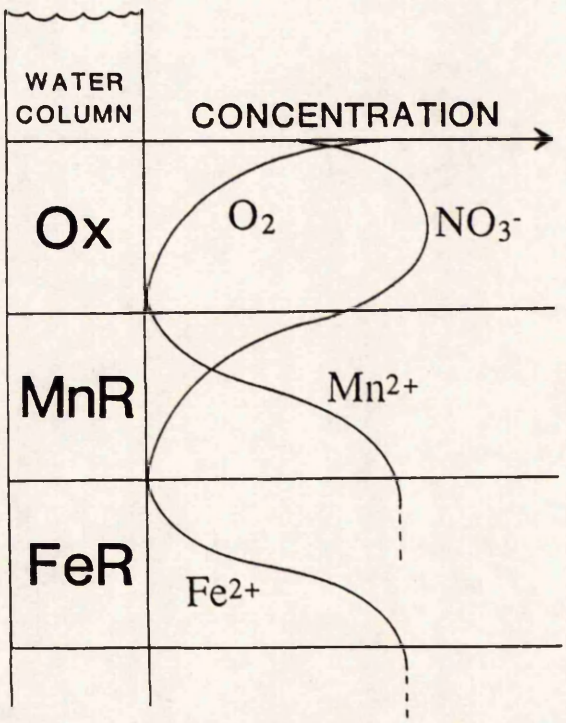

Beneath the zone of sulphate diffusion from sea water when SR effectively ceases, relying only on trapped marine pore waters, methane is found. This zone has hence been termed the Methanogenesis (Me) zone and is discussed in detail within Claypool and Kaplan (1974), who concluded that CO_2 reduction was important in its formation. Relatively little is still known about the organisms operating within this zone, but the overall effect is that O.M. is broken down, with two important products CH_4 and CO_2. This can be represented thus, but it must be emphasised that more than one process almost certainly operates, and the stochiometry of the reaction is unknown:

$$2CH_2O \text{ -----> } CH_4 + CO_2 \qquad \text{Methanogenesis (Me)}$$

The three zones described above form the commonly observed diagenetic zonal scheme of Ox --> SR --> Me (figure 1.14, columns A and B). Microbial reactions present during later burial will not be considered here.

The presence of Fe and Mn in pore water profiles and within early authigenic minerals, show that Fe^{III} and Mn^{IV} have been reduced within the sediment. These elements were present initially in the sediment as detrital oxides, and were subsequently reduced in a microbial process similar to those described above, represented as:

$$CH_2O + 2MnO_2 + H_2O \text{ -----> } 2Mn^{2+} + HCO_3^- + 3OH^- \qquad \text{Manganese Reduction (MnR)}$$

$$CH_2O + 2Fe_2O_3 + 3H_2O \text{ -----> } 4Fe^{2+} + HCO_3^- + 7OH^- \qquad \text{Iron Reduction (FeR)}$$

In most modern sediments these processes coincide with SR, leading to the formation of pyrite, so ubiquitous in ancient mudrock sequences. Both MnR and FeR increase alkalinity and generate HCO_3^- so would also be expected to favour carbonate precipitation. The onset of MnR prior to FeR, allows the recognition of early and later precipitated carbonates by the Mn/Fe ratio (for example Curtis *et al.* 1986).

Under conditions of slow sedimentation with moderate organic input, distinct zones of MnR, FeR and nitrate reduction (NR) develop, the nitrate having formed by oxidation of organic nitrogen. A sequence containing all the diagenetic zones results, and was recognised by Froelich *et al.* (1979) in pelagic sediments of the Atlantic. They showed that the order in which these zones occurred (Ox --> MnR --> NR --> FeR --> SR --> Me) coincide with a

FIGURE 1.14.

DIAGENETIC ZONES IN MODERN SEDIMENTS

MODIFIED FROM A PERS. COMM. C.D.CURTIS

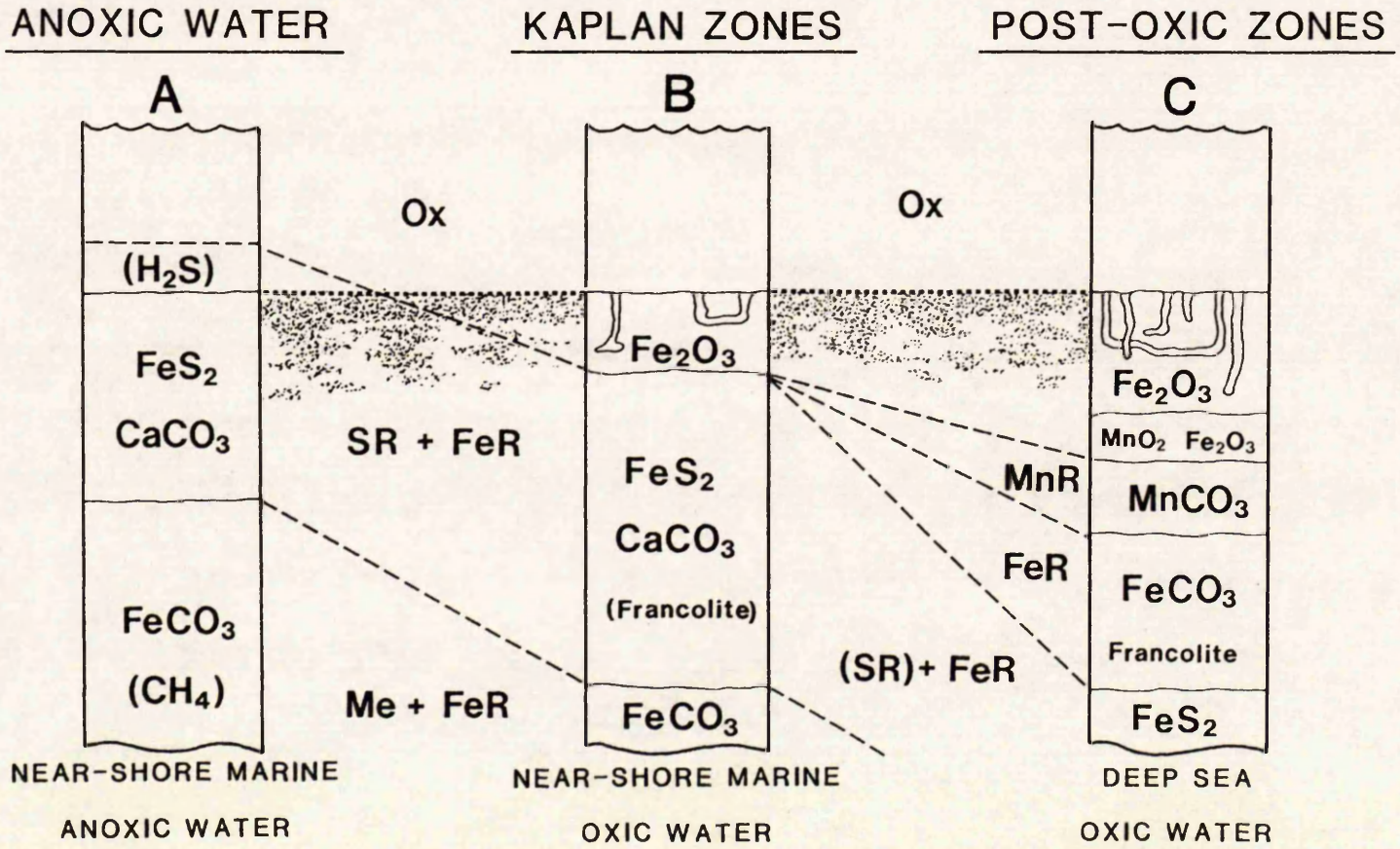

progressive sequence of calculated Gibbs free energy of release for reactions similar to those given above. Similar calculated values were produced by Coleman (1985) and are given in table 1.3. SR within these sediments had clearly been supressed despite the presence of abundant sulphate in the pore waters, so that the strong overprint of SR was therefore not present allowing the FeR and MnR zones to be delineated. The environment of MnR-NR-FeR was termed suboxic by Froelich *et al.* (1979) due to its intermediate nature between fully oxic and anoxic conditions, and later also called post-oxic (Berner 1981). FeR and MnR are therefore termed post-oxic reactions and result in post-oxic diagenesis. NR degrades organic matter in much the same way as Ox, and thus also contributes to the early production of CO_2. It seems that this full diagenetic zonation is only able to form when the O.M. that has passed through the Ox zone is of a refractory or degraded nature. The effect of this is that microbes must obtain the maximum energy release from oxidation of the available O.M., and hence utilise oxidants in the sequence described in order to facilitate the most efficient use of the degraded O.M.

1.10.1) Precipitation of Authigenic Minerals.

The presence of a diagenetic zonation in modern sediments is demonstrated by steady-state pore water solute profiles, but recognition of these zones in ancient sediments requires an examination of the authigenic mineralogy, i.e.the consequences of the former presence of zones. The oxidation of O.M. liberates CO_2 that acidifies pore waters, but if the pH can be raised, then authigenic carbonate can precipitate. In particular, FeR and MnR generate large quantities of OH^- that significantly increases the alkalinity, allowing their respective carbonates to form. In addition to carbonates, iron sulphides and silicates, may also form, depending on many factors including element concentrations, Eh and pH as discussed above in section 1.8. Berner (1981) addressed the relationship between diagenetic processes and authigenic mineralogy, and classified modern sedimentary environments with respect to authigenic minerals whose presence could indicate formation within a particular zone (figure 1.15). Maynard (1982) later extended this classification to include ancient sediments (figure 1.16). Reactions specific to particular diagenetic zones are now discussed.

TABLE 1.3

DIAGENETIC ZONAL SCHEME, INCLUDING ENERGY RELEASE AND MASS BALANCE FOR ONE MOLE ORGANIC CARBON, WITH $\delta^{13}C$ OF CARBONATE PRODUCED. TABULATED FROM DATA IN COLEMAN (1985).

	DIAGENETIC ZONE	ZONE CODE	$-\Delta G$ $KJ(_{MOL}C)^{-1}$	OXIDANT	PRODUCTS (EXCLUDING HCO_3^- & H_2O)			CARBONATE FORMED $\delta^{13}C_{PDB}‰$ -20 -10 0 +10 +20
OXIC	AEROBIC OXIDATION	Ox	530	O_2	—	—	H^+	INORGANIC
SUB-OXIC (POST-OXIC)	MANGANESE REDUCTION	MnR	485-515	$2MnO_2$	$2Mn^{2+}$	$3OH^-$	—	
	NITRATE REDUCTION	NR	460-505	NO_3^-	N_2/NH_3	OH^-	—	
	FERRIC IRON REDUCTION	FeR	220-235	$2Fe_2O_3$	$4Fe^{2+}$	$7OH^-$	—	
ANOXIC	SULPHATE REDUCTION	SR	65	$½SO_4^{2-}$	$½S^{2-}$	—	H^+	
	METHANOGENESIS	Me	60	—	$½CH_4$	—	$½H^+$	
	DECARBOXYLATION	D	≤60	—	$R-CH_3$	—	H^+	

Figure 1.15. Geochemical Classification for Sedimentary Environments. After Berner (1981)

ENVIRONMENT			CHARACTERISTIC PHASES
OXIC $C(O_2) \geq 10^{-6}$			Hematite, goethite, MnO_2 - type minerals. No organic matter
ANOXIC $C(O_2) < 10^{-6}$	SULPHIDIC $C(H_2S) \geq 10^{-6}$		Pyrite, marcasite, rhodochrosite, alabandite. Organic matter.
	NON-SULPHIDIC $C(H_2S) < 10^{-6}$	POST-OXIC	Glauconite, and other Fe^{2+} - Fe^{3+} silicates (also siderite, vivianite, rhodochrosite) No sulphide minerals; minor organic matter.
		METHANIC	Siderite, vivianite, rhodochrosite. Earlier formed sulphide minerals. Organic matter.

Figure 1.16. a) Maynard's (1983) Modification of Berner's Geochemical Classification, in terms of Oxygenation and Sulphate Supply. b) Stable Isotopic Relations of Sedimentary Environments - Boundaries Undetermined. (Both Diagrams Redrawn From Maynard 1983 p. 1327).

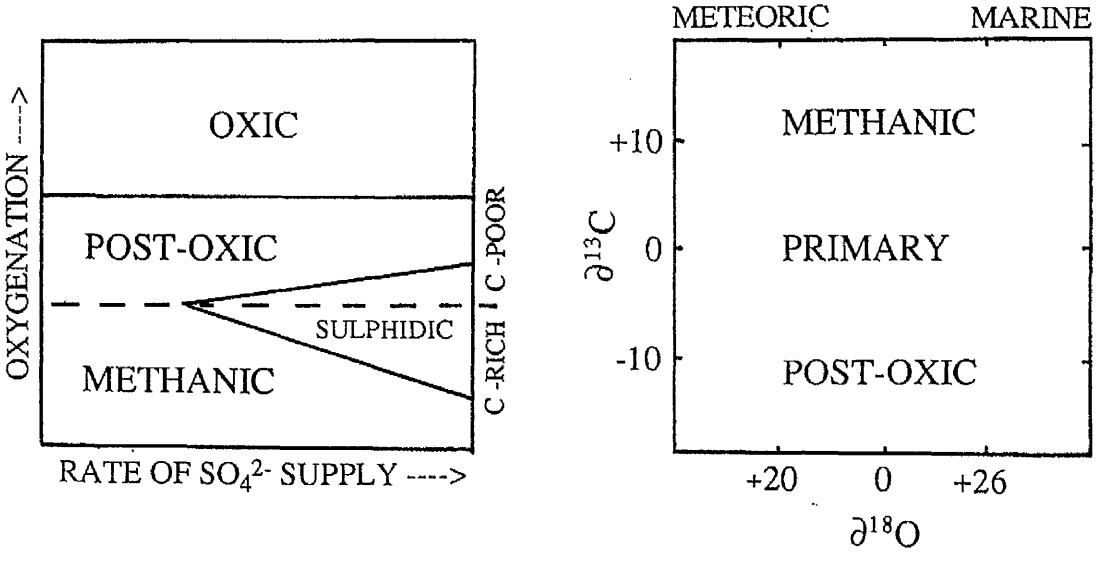

In the Ox zone, Fe and Mn are present in an oxidised form and hence largely unreactive. Diffusion upwards of Fe^{2+} and Mn^{2+} from post-oxic reactions may lead to the precipitation of Fe and Mn oxides at the redox boundary. Any detrital or authigenic carbonate is likely to undergo dissolution due to O.M. oxidation (see above) or oxidation of HS^- that has diffused upwards from the SR zone and acidifies pore waters:

$$HS^- + 2O_2 \text{ -----> } SO_4^{2-} + H^+$$

A similar effect is also produced on the oxidation of authigenic pyrite or iron monosulphides.

For the reasons given above, pyrite is likely to dominate the mineral assemblage of the SR zone, assuming that FeR is also taking place. Pyrite probably forms from a precurser iron monosulphide, but may be represented in a complete reaction by combining the FeR and SR reactions to:

$$15CH_2O + 2Fe_2O_3 + 8SO_4^{2-} \text{ -----> } 4FeS_2 + 7H_2O + 15HCO_3^- + OH^-$$

The formation of pyrite hence also increases alkalinity and generates large quantities of HCO_3^- leading to carbonate precipitation. The actual carbonate produced depends on the relative roles of SR and FeR. Where the former dominates, calcite and dolomite are expected, but if FeR predominates, ferroan calcites, siderite and ankerite may form. Large quantities of pyrite within a sediment are therefore likely to be associated with non-ferroan carbonates.

As mentioned, MnR and FeR are themselves likely to lead to the generation of their respective carbonates, rhodochrosite and siderite, if Ca concentrations are low. Using the reaction described above for iron reduction, siderite precipitation may be demonstrated:

$$CH_2O + 2Fe_2O_3 + 3H_2O \text{ -----> } FeCO_3 + 3Fe(OH)_2 + H_2O$$

The component $Fe(OH)_2$ represents the belief that under such a reaction scheme, Fe (in the reduced state) could be precipitated as a low temperature phyllosilicate, perhaps berthierine (Curtis 1987a).

Direct authigenic mineral precipitation by the Me process alone is unlikely, as the generation of CO_2 into pore fluid generates both HCO_3^- and H^+, the net effect of which is to cause carbonate dissolution:

$$2CH_2O + H_2O \text{ -----> } H^+ + HCO_3^- + CH_4.$$

However, if FeR accompanies Me, then the vastly increased alkalinity generated during FeR can lead to siderite formation. The relative roles of Me and FeR in authigenic mineral precipitation are described by Curtis (1987a), who showed that FeR and minor Me would tend to produce siderite with possible iron phyllosilicate formation, but that when both are important or Me dominates, siderite alone would be expected.

1.10.2) Controls on Early Diagenesis.

1.10.2.1) Organic Matter (O.M.).

O.M. is present in most marine sediments and comprises photosynthesised O.M. in surface waters which becomes degraded after the death of the organism, and terrigenous input which is already degraded before entering the basin. O.M. is the only significant reducing agent within sediments (some reduction by H_2S produced by SR may occur), and is essential for all of the diagenetic reactions given. The quantity of O.M. controls the extent by which diagenetic processes may operate, and ultimately the quantity of authigenic minerals produced. The quality of O.M. is equally important, as refractory terrigenous woody material (vitrinite) will not act as such a good reducing agent as marine-derived algal material (alginite).

1.10.2.2) Sedimentation Rate.

The net rate of sedimentation is a critical factor in the preservation of O.M. and the residence time that a sediment layer remains within any one diagenetic zone. The relationship between rate of burial and end mineralogy of the sediment is summarised in figure 1.17 from Curtis (1977). Extremely low sedimentation rates result in the available O.M. being oxidised within a few centimetres or even millimetres below the sediment water interface. No subsequent redox reactions are possible on burial, resulting in the formation of red/brown clays as often found within pelagic deposits.

Figure 1.17. Links Between Burial (Sedimentation) Rate and Sediment Mineralogy. Taken From Curtis (1977).

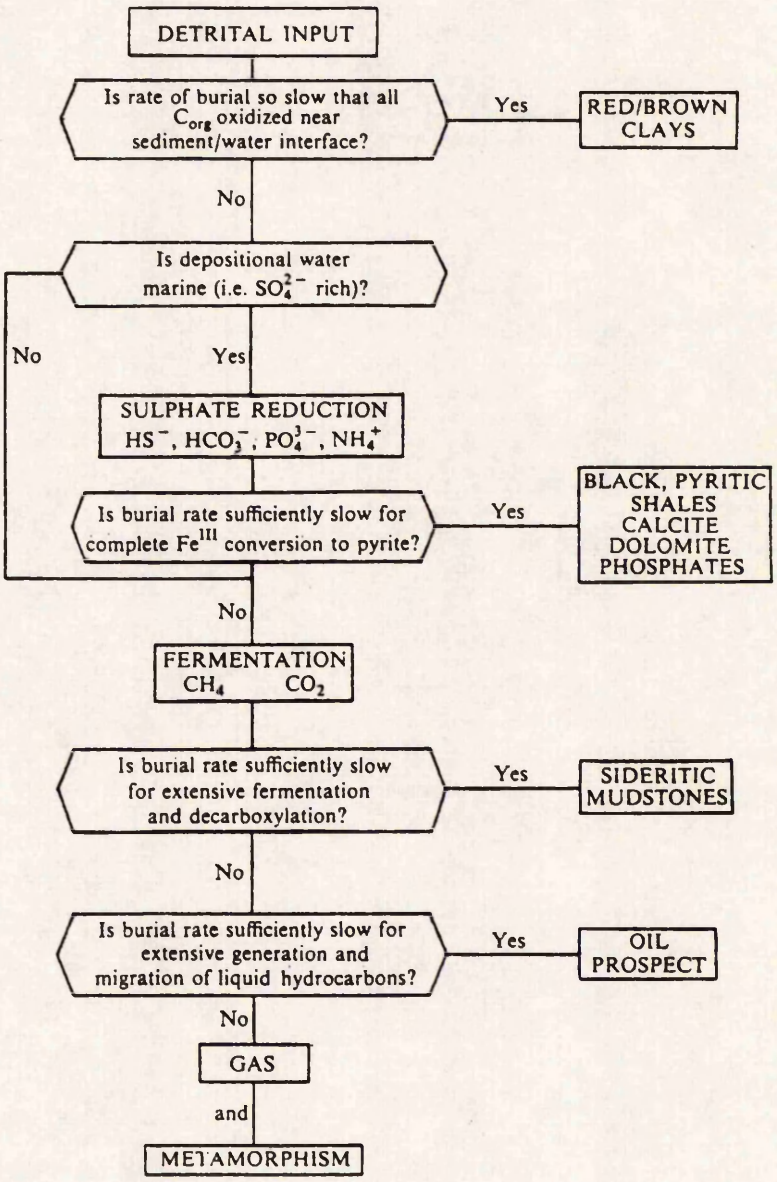

In most sediments, some organic matter survives degradation within the Ox zone, allowing subsequent microbial reactions. Sedimentation rate controls the length of time that SR can occur, before the sediment is buried below the depth that sulphate can diffuse from overlying sea water. Slow burial rates allow a long residence time of a sediment layer within the SR and FeR zones, and result in the complete conversion of all available potentially reactive Fe to pyrite. Faster burial rates result in the sediment moving rapidly through the Ox and SR zones, into the Me zone, where extensive siderite may form.

Residence time of a sediment within a diagenetic zone is also controlled by the thickness of that zone (Ox - a few centimetres, SR - a few metres, Me - many tens of metres). However, the rapidity of reaction, and organic quality is highest in the earliest zones, and hence a short residence time in the Ox zone has much more impact on the sediment diagenesis than a long period in the Me zone. Zone thickness also varies with sedimentation rate, with an expansion of the zones as sedimentation rate decreases, given a similar organic input. This is caused by the sediment having a longer residence time within any zone due to the low rate of burial, so that the fullest thicknesses of zones may develop.

1.10.2.3) Source of Oxidants.

Most waters contain dissolved oxygen, so that an Ox zone develops despite often being only a few millimetres thick. However, anoxic bottom waters can occur, and result in O.M. becoming less degraded once within the anaerobic part of the water column. SR does operate within anaerobic waters, but apparently at a much slower rate In such cases, the quantity and quality of O.M. entering the sediment is high, and more substantial quantities of O.M. remains unaltered during early diagenesis, ultimately providing an oil prospect.

The abundance of sulphate in sea water leads to a dominance of SR over other early diagenetic reactions in normal marine sediments, whilst the loss of sulphate by SR is balanced by diffusive recharge. Freshwater does not contain significant sulphate, and hence does not support an SR zone within the sediment. Therefore, once below the Ox zone,

O.M. is oxidised by the Me process, and if Fe is available, siderite precipitates extensively forming sideritic muds and concretions.

The source of Fe and Mn oxides is controlled by sediment type and rate of deposition. Curtis (1985) suggests three essentially different forms of Fe^{III} present in fine-grained detrital sediments:

a) Soil 'sesquioxides', Fe_2O_3, FeOOH, and amorphous Fe hydroxides.

b) Interlayer Al - Fe^{III} hydroxides in soil clay vermiculites.

c) Dioctahedrally co-ordinated in beidellite - illite, and nontronite - glauconite minerals.

Of these (a) is the most reactive and will be used first in FeR, so that a sediment rich in these particles, such as derived from a lateritic soil profile, is likely to lead to extensive iron reduction.

1.10.2.4) Bioturbation and Reworking.

The degree of bioturbation of a sediment is controlled by many factors including oxygen availability, sedimentation rate, nutrient supply, degree of reworking, position within the sedimentary basin etc., and has significant implications for O.M. preservation. Bioturbation increases the vertical permeability of the sediment by mixing layers, and producing burrows that can act as conduits for sea water (and oxygen) introduction into the sediment. The supply of oxygen is hence increased, and the depth of the Ox zone may be many times the thickness than that if the sediments were unbioturbated. High degrees of bioturbation also indicate that infaunal macro-organisms were present that lived off the detrital organics, thus further depleting the O.M. supply for SR and FeR/MnR during diagenesis.

The degree of physical reworking has a similar effect of increasing oxygen introduction to the sediment. Constant reworking of a sediment package does not allow a diagenetic zonation to develop, and mineral phases containing Fe^{2+} are rapidly oxidised during the reworking event.

1.10.2.5) Grain Size of the Sediment.

Sediment grain size is related to the environment and energy of deposition. Coarser grained sediments are usually associated with shallow water settings where bioturbation and reworking are high, resulting in intense organic degradation. Mudrocks are associated with lower depositional energies, organic preservation, and diagenetic zonation. However, the grain size also has an independent effect on diagenesis in that vertical permeability is considerably higher in coarser sediments. Consequently, increased diffusive recharge of oxygen and sulphate into the sediment may result in a much thicker Ox zone in coarser sediments. Therefore, although the post-oxic zones were recognised in deep water mudrocks, if O.M. is highly degraded, thick post-oxic zones may also develop in nearshore coarser sediments (up to a few metres thickness).

1.10.3) Diagenetic Processes Indicated by $\partial^{13}C$ Stable Isotopic Analysis.

Trends in the $\partial^{13}C$ isotopic signature of bicarbonate within sediment pore fluids may be shown to vary with depth, similar to that of cation concentrations (for example Presley and Kaplan 1968). Systematic analysis of these trends reveals that the $\partial^{13}C$ values may be used to approximate the diagenetic zone in which the bicarbonate was formed. The $\partial^{13}C$ signature is also reflected in carbonates precipitated from the pore fluids, and hence recognition of ancient diagenetic environments can be obtained from the $\partial^{13}C$ isotopic composition of the carbonates formed (see for example Curtis 1987, Irwin *et al.* 1977, and papers cited in the introduction to section **1**.10 above).

The differences in $\partial^{13}C$ values result largely from a mixing of marine and organic derived HCO_3^- within the precipitating pore fluids. HCO_3^- derived from the marine environment will have a $\partial^{13}C_{PDB} \approx 0$, as the PDB standard is a marine precipitate (see appendix A.2.2). The $\partial^{13}C_{PDB}$ value of plants varies with the photosynthetic pathway utilised, but all have a negative $\partial^{13}C_{PDB}$ of around -9‰ to -37‰ (see Hoefs 1980). However, analyses of organic matter in sediments (for example Nissenbaum and Kaplan 1972) suggest that a value of $\partial^{13}C_{PDB}$ around -20‰ to -25‰ is a good approximation. The CO_2 generated from the decay of this organic matter is found to be similar to that of the plant material from which it

is derived, and will be reflected in any carbonate precipitated from this source. The degree of mixing of marine and organically derived HCO_3^- in pore waters is therefore represented by a variation in $\partial^{13}C_{PDB}$ values between 0‰ to approximately -25‰ respectively. The $\partial^{13}C_{PDB}$ signatures of carbonates precipitated via the reactions given above in the introduction to this section (**1**.10) therefore allow the approximation of ancient diagenetic environments.

Cements precipitated in the Ox zone by a purely inorganic process will have a $\partial^{13}C_{PDB}$ isotopic signature of around zero, as although HCO_3^- is being supplied through O.M. oxidation, diffusive mixing with the marine reservoir is high. SR, MnR, and FeR, produce light (≈-25‰) HCO_3^- through the oxidation of organic matter, and the $\partial^{13}C_{PDB}$ value of any carbonates precipitated, reflects the relative abundance of marine and organic derived HCO_3^- in the pore water, of which the former predominates at shallower depths. Hence $\partial^{13}C_{PDB}$ values within precipitated carbonate should get lighter through the MnR, FeR and SR zones respectively, if the diagenetic zonation given above is followed (see figure 1.12).

$\partial^{13}C_{PDB}$ values of carbonate in the Me zone are different, because in addition to CO_2, CH_4 is produced that preferentially incorporates the lighter ^{12}C isotope ($\partial^{13}C_{PDB}$ of ≈-75‰). Measurements of coexisting CO_2 are generally $\partial^{13}C_{PDB}$ positive (up to +15‰), and ancient carbonates believed to have precipitated in the Me zone commonly exhibit $\partial^{13}C_{PDB}$ values up to +10‰. Cements of the Me zone should hence be isotopically heavy, clearly differentiating them from other zones. This is particularly useful in distinguishing siderites precipitated from the FeR and Me reactions.

The isotope values associated with particular reactions in diagenetic zones are summarised in table 1.3 and figure 1.18. This situation is however considerably complicated by zone overlap and diffusion of CO_2 and CH_4 into adjacent zones. In particular, upwardly migrating CH_4 from the Me zone may be utilised as a substrate for sulphate-reducing bacteria in the SR zone (see for example Devol and Ahmed 1981), or may be oxidised in the Ox zone, imparting anomalously light isotopic signatures on precipitated

Figure 1.18. Diagenetic Scheme with Carbon Isotopic Signatures of CO2 Produced in Each Zone. Taken From Irwin *et al*. (1977).

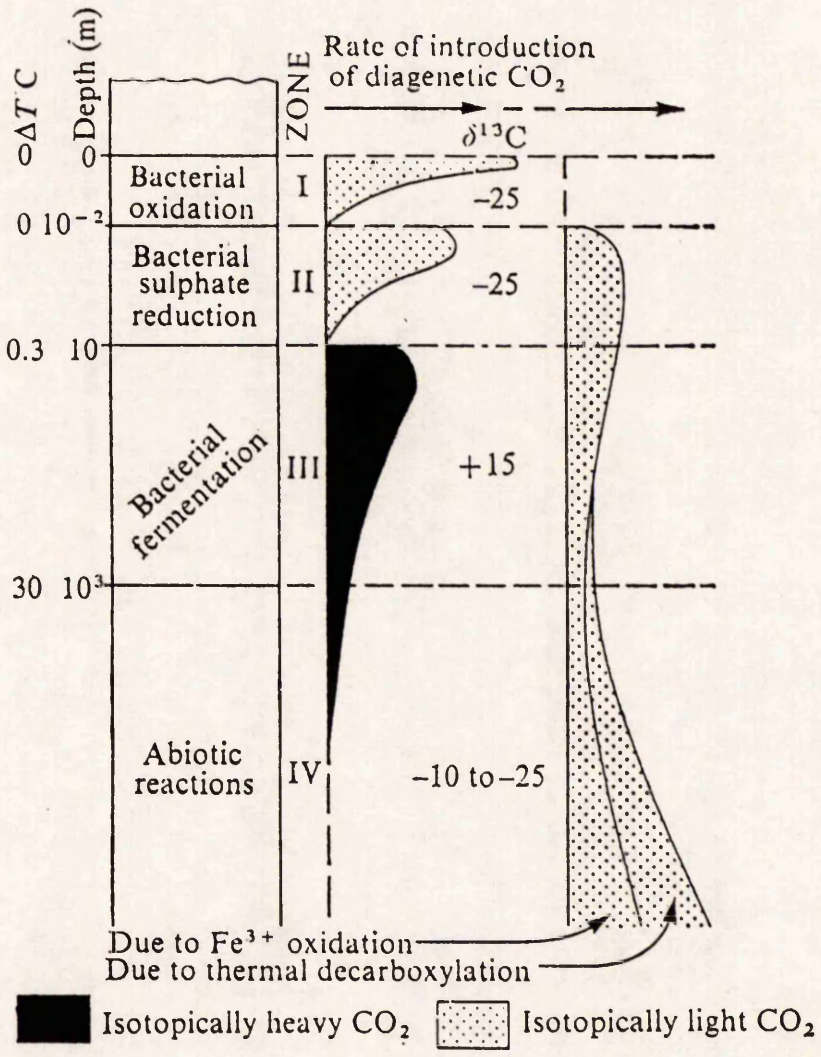

Introduction of diagenetic CO_2 within different diagenetic zones.

carbonates. The particular influences of the SR and Me processes on adjacent diagenetic zones are shown in figure 1.19. This diagram also shows the strong influence of FeR on the diagenetic processes.

Figure 1.19. The Influence of Iron, and the Diffusion of Gaseous Products from the SR and Me Zones, on Sediment Mineralogy and Carbon Isotopic Composition of Precipitated Carbonate. Taken From Curtis (1987b).

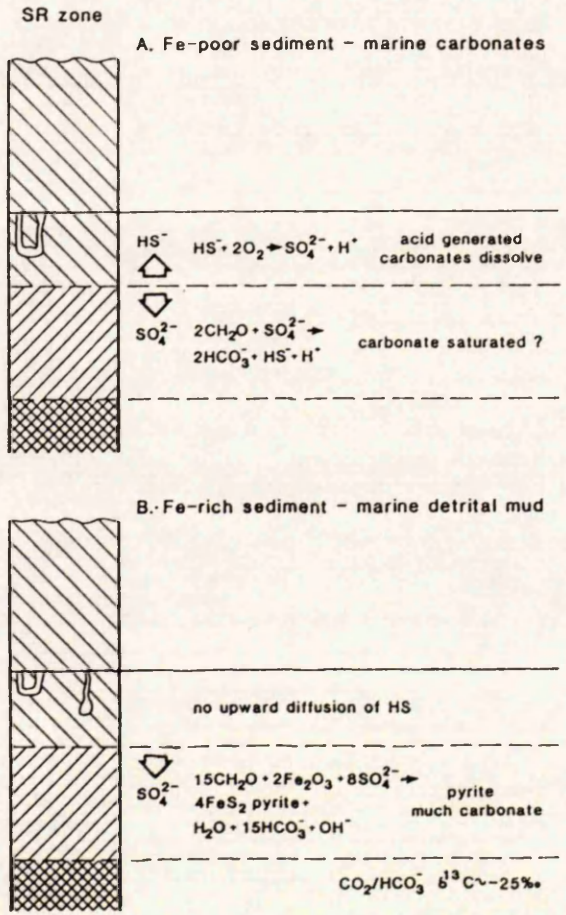

Sulphate reduction zone: influence of sediment iron content.

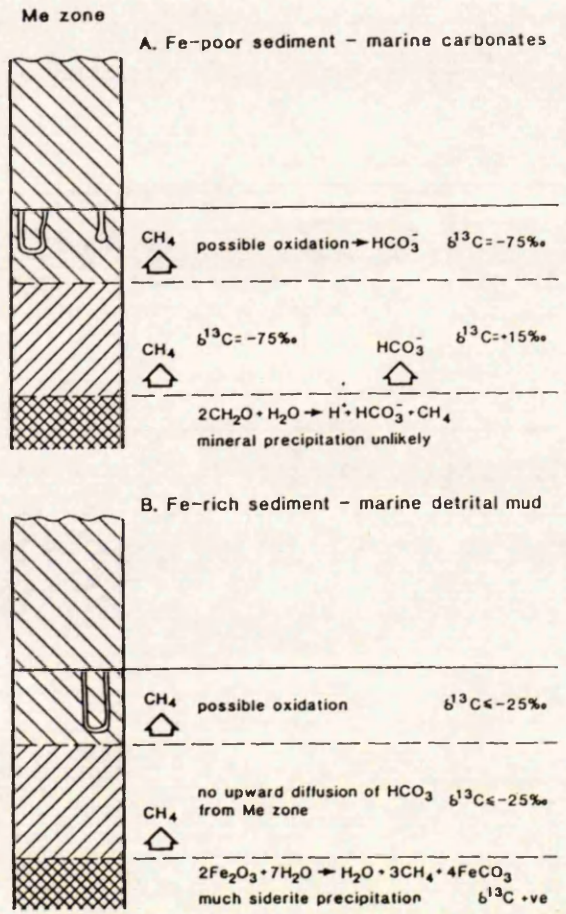

Microbial methanogenesis zone: iron-poor and iron-rich cases.

1.11) RESEARCH AIMS AND METHODOLOGY.

The literature review that precedes this section outlines the complex nature of ooidal ironstones and the problems associated with their study. Much research has concentrated on sedimentological description of ironstones including ooid genesis, with less being written to describe the detailed mineralogy and geochemistry. Advances in the understanding of diagenetic processes acting within the sediment during deposition, have however allowed a re-examination of ironstone mineralogy and origin in the light of this new work. In particular, the relative roles of sulphate reduction and iron/manganese reduction in the microbial oxidation of organic matter within ironstones could be examined. It was proposed as the hypothesis behind this research that post-oxic processes (iron and manganese reduction) dominated over sulphate reduction during the early stages of ironstone diagenesis, resulting in the widespread formation of iron-silicates and carbonates, but not iron sulphides that are so ubiquitous in most 'normal' marine sediments. The research has wider implications in that redox reactions involving iron and manganese with organic matter oxidation strongly affect the diagenesis of most sediments.

Preliminary fieldwork and thin-section examination suggested that the Frodingham Ironstone Formation of Scunthorpe, England, was the most suitable ironstone-formation for this study, due to its accessibility to fresh outcrop and core material, and the varied mineralogical assemblage it contains. Other ironstone-formations were examined with the view to comparing models of ironstone genesis based upon the Frodingham Ironstone Formation, to other British Jurassic ironstones. The sedimentology of the Formation was studied in outcrop and core, in order to provide a depositional framework on which to base this petrological and geochemical study. However, detailed palaeoecological studies were not carried out due to such research presently in progress by Mr. D. Parsons of Taunton Museum. A wider examination of the relationships of the ironstone-formation to the evolution of the East Midlands Shelf, lateral facies variation and palaeogeography, was also not undertaken in detail due to the imminent publication of a British Geological Survey Sheet Memoir for the Brigg Sheet, in which this is discussed (R. W. O'B Knox, T. P. Fletcher pers.comm.).

Detailed thin-section petrography was followed by analytical work utilising a number of techniques, of which Electron Probe Micro-Analysis (E.P.M.A.) was the most important. E.P.M.A. allows relatively rapid and detailed analysis of all mineral phases present in the ironstone. In addition to E.P.M.A., X-Ray Diffraction (X.R.D), Scanning Electron Microscopy (S.E.M.), stable isotopic analysis of C and O, and luminescence petrography were applied. Such a detailed analytical study of the complete ironstone mineralogy as opposed to only a single species (usually berthierine) had not before been seriously attempted. By examination of the iron minerals in these iron-rich deposits, it was also hoped that the mineral genesis for more 'normal', less iron rich sediments, may be better constrained.

Ooid petrography and mineralogy was studied in detail, as these particles characterise these deposits, and their origin is controversial. Ideas based on ooid growth mechanisms and mineralogical development have been used to imply sedimentological, diagenetic and palaeogeographical constraints on ironstone formation, and hence must be an integral part of all ironstone research.

Models for the genesis of the iron-silicate berthierine have usually been based on bulk-rock analyses, or from a small suite of microprobe analyses. Petrographic examination of the Frodingham berthierines however revealed very different occurrences of the same mineral, whose possibly differing compositions had never been considered. E.P.M.A. was used as the only rapid and direct method of testing this. Carbonates within the ironstone-formation were similarly examined, and these results can be applied to wider aspects of carbonate cementation of sediments. The unique mineral assemblage of the ironstone-formation allowed qualitative analysis of nucleation effects on carbonate precipitation, element incorporation into carbonates, replacement mechanisms etc., whose previous study had been restricted largely to fully carbonate sediments.

CHAPTER 2. THE FRODINGHAM IRONSTONE FORMATION: INTRODUCTION AND SEDIMENTOLOGICAL ASPECTS.

2.1) Introduction.

The Frodingham Ironstone Formation of South Humberside, England, provided a source of iron for the Romans, but it was not until 1859 that full scale quarrying of the ore started. Output rose steadily until the Second World War, but has since declined, and today extraction has ceased. The town of Scunthorpe developed around the the steel works which were built to process the ore, and expanded eastwards onto back-filled land. The steel works remain, but are now processing imported ore, using Frodingham ironstone only as an iron-rich flux during the last years of extraction.

The general local geology of the area has been described by Cross (1875), Ussher (1890), and Wilson (1948). A new British Geological Survey Memoir of the Brigg sheet is in preparation, and shortly to be published. Figure 2.1 is a geological map showing the outcrop of the Frodingham Ironstone Formation and associated strata. The structure of the area is not complex, with north-south striking strata, dipping uniformly 1-2 degrees to the east. The outcrop of the Formation shown, reflects quarrying activity rather than thickness variation, or surface topography. The tectonic structure of the field is described in detail by Whitehead *et al.* (1952, pages 73-74), and is shown in figure 2.2. In general the ironstone-formation follows the local dip of strata 1-2° to the east, but has been faulted in the area of Risby Warren, by two normal faults that form a minor graben of approximately 15-30m (50-100ft) throw.

2.2) Age of the Formation.

The Frodingham Ironstone Formation is Sinemurian in age and ranges from the *Arnioceras semicostatum* Zone (*Euagissiceras sauzeanum* Subzone) to the *Oxynoticeras oxynotum* Zone (*Oxynoticeras simpsoni* Subzone), although the *O. simpsoni* Subzone is restricted to the north of the outcrop (Cope *et al.* 1980). Hallam (1963) records a progressive sequence of ammonites in the lower part of the succession, although a possible

Figure 2.1. Geological Map of the Area Around Scunthorpe, South Humberside, Showing the Outcrop of the Frodingham Ironstone Formation.

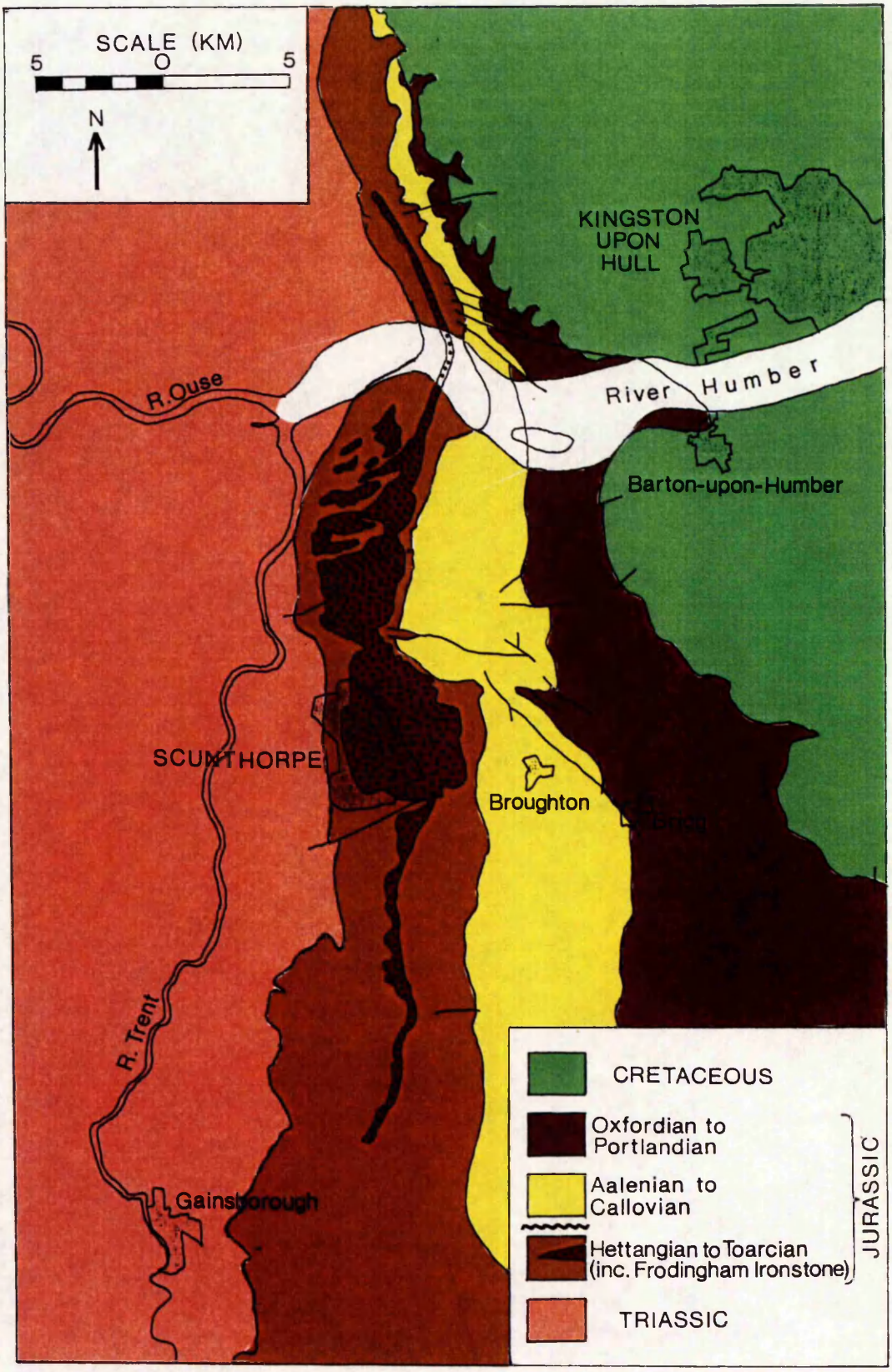

FIGURE 2.2

CONTOURS ON THE TOP OF THE FRODINGHAM IRONSTONE FORMATION

(From Whitehead et al., 1952)

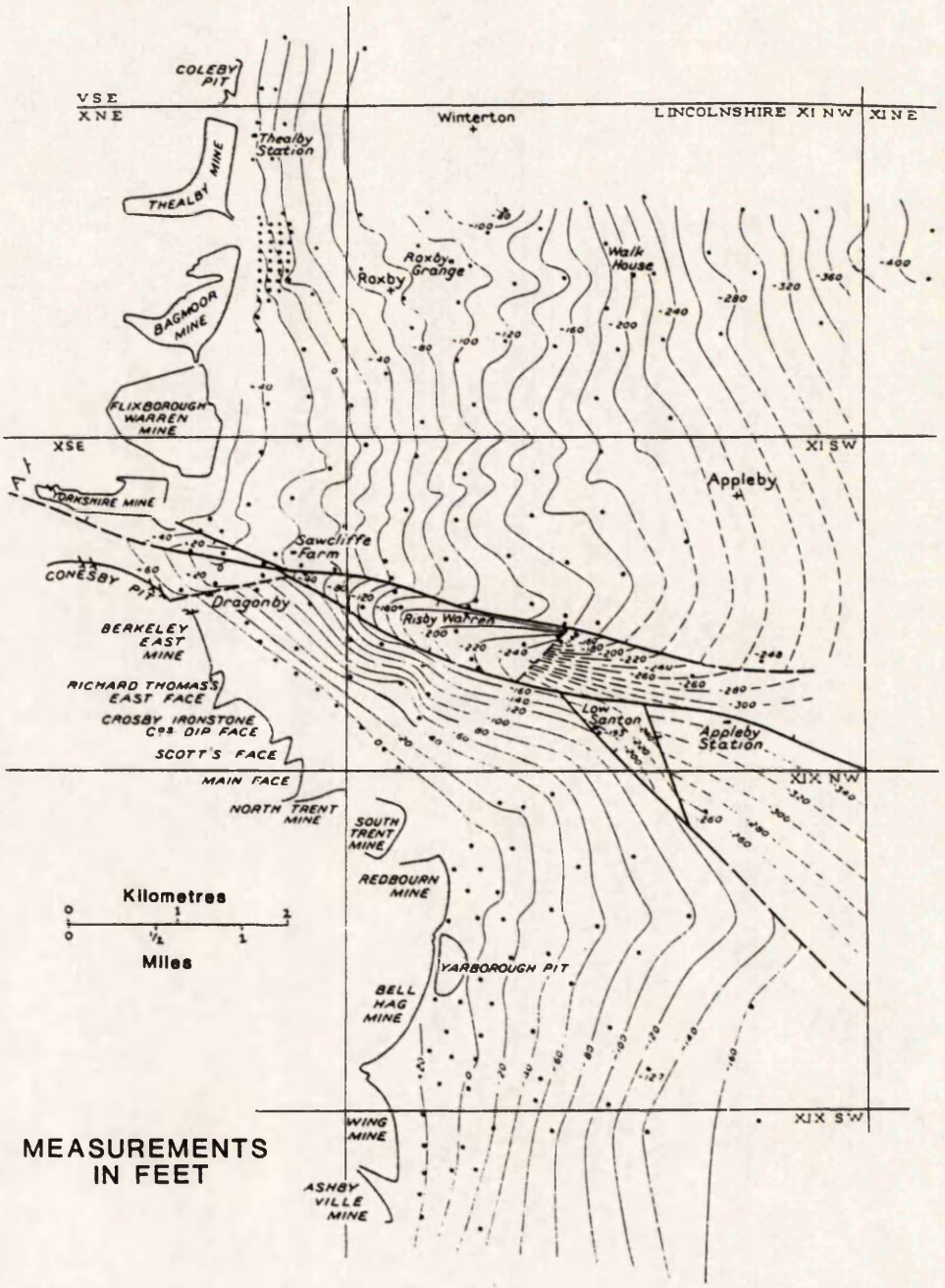

non-sequence is present in the lower *obtusum* Zone. The mixed ammonite assemblage recorded by Whitehead *et al.* (1952) led Cope *et al.* (1980) to suggest reworking of ammonite zones in the upper part of the ironstone-formation.

2.3) Stratigraphy.

2.3.1) Vertical Sequence.

The ironstone-formation occurs within the Lower Lias, which is dominantly mudrock, with subordinate silts and limestones. The deposit is condensed relative to equivalent strata in North Yorkshire which are three times as thick as the ironstone-formation, and to southern England where five times the thickness is present. The full Lower Lias sequence encompasses three thin ironstones: the Frodingham (<10m), Pecten (≈1m), and Marlstone Rock Bed (≈ 2.5m) (figure 2.3), separated by thicker sequences of clays with nodules. The Pecten Ironstone and Marlstone Rock Bed are often visible in outcrop in the quarries, but were never seriously exploited. The Marlstone Rock Bed is laterally equivalent to the Kettleness Member of the Cleveland Ironstone Formation.

The stratigraphic sequence beneath the Frodingham Ironstone Formation is poorly exposed and consists of shales with thin limestones which become more abundant towards the top of the sequence. Section descriptions are given by Ussher (1890). There appears to be no coarsening-upward sequence present beneath the Frodingham Ironstone Formation, and the boundary between shale and ironstone is both indistinct and stratigraphically undefined. The upper boundary of the ironstone-formation is ubiquitously sharp, defined specifically by contrasting cementation. This feature was exploited during quarrying, by allowing the removal of shale overburden by dragline (see plate 1a). The shales above the ironstone-formation are dark grey, occasionally silty, with shell coquinas and nodule formation. The mineralogy of these shales is discussed below in section 4.3.1.

2.3.2) Lateral Facies and Thickness Variation.

The Frodingham Ironstone Formation is an extremely localised deposit in comparison to the associated strata. The deposit was described to be economically workable for a

Figure 2.3. Vertical Succession of the Lias in South Humberside (Simplified). Taken From Knell and Knell (1988).

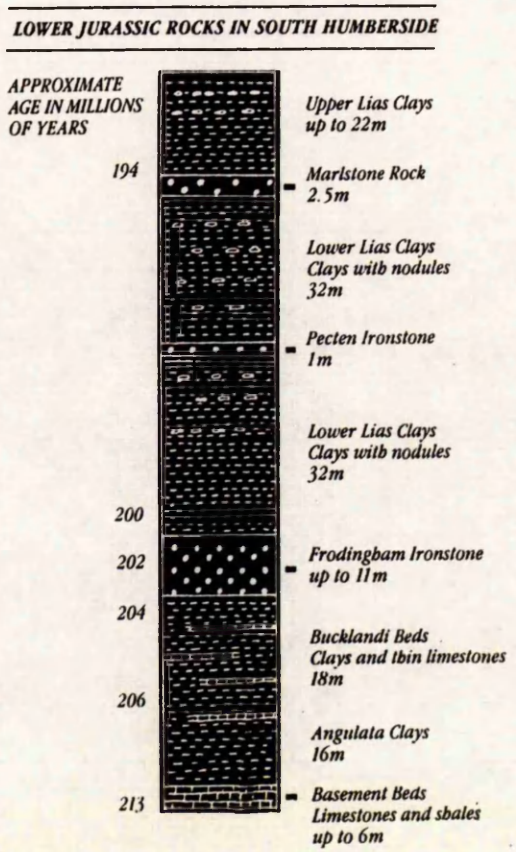

Figure 2.4. Isopach Map of Lower Jurassic Sediments on the East Midlands Shelf, Market Weighton Axis, and Cleveland Basin. Taken From Kent (1980).

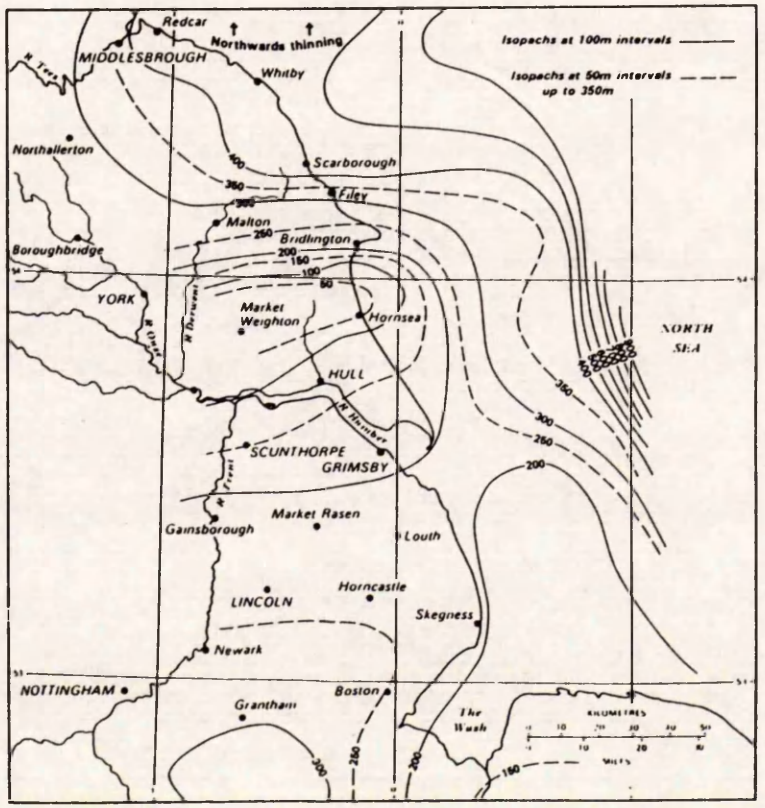

distance of approximately 10km along strike, and extended less than this distance, down dip towards the east.

The ironstone-formation ranges in thickness from 5.79m (19ft) to 9.75m (32ft) in the workable area (Whitehead *et al.* 1952), and thins to the north, south, and east. In the far north of the outcrop, north of the Humber River, the Whitton Ness (SE 9230 2434) and Cockle Pits (SE 9323 2865) Boreholes cored the formation (described by Gaunt *et al.* 1980). Here 3.46m of sideritic limestones with layers rich in "chamosite" ooids are described, but there is no full development of ironstone as seen at Scunthorpe. North of the Market Weighton axis, the Brown Moor (SE 8126 6203) and Howsham (SE 7430 6263) Boreholes cored ferruginous shales and silts in the Sinemurian strata (Gaunt *et al.* 1980). In the south-east, the Nettleton Borehole (TF 1245 9823) cored 2.93m of "limonitic", berthieroidal-rich siltstone, only 20% of which was ooidal, and further east, the Tetney Lock Borehole (TA 3315 0105) encountered 3.7m of "limonitic" and partly oolitic fine sandstones and siltstones (Bradshaw and Penney 1982). Similarly Kent (1953) describes a dominantly siliciclastic assemblage in the Spital Borehole (SK 9648 9162) to the south. The ironstone-formation therefore passes laterally to the north, south and south-east into siliciclastic facies, all of which are ferruginous.

Thinning of the sequence towards the north, mirrors that of the Lower Jurassic sediments in general, onto and over the Market Weighton axis (figure 2.4). The thinning of Lias sediments is associated with both regional attenuation and erosion, the latter of which is most important in the axis area, such that no strata equivalent to the Frodingham Ironstone Formation are recorded at outcrop near Market Weighton (Kent 1980). Thinning to the south-east and east must be depositionally controlled, as sedimentation decreased basinward across the East Midlands Shelf. This is however in contrast to the Lias shales and Marlstone Rock Bed, that are of similar or greater thickness in the Nettleton Borehole than to the north-west:

Sequence.	North Humberside[1]	South Humberside[1]	Nettleton Borehole[2]
Marlstone Rock Bed.	4m	2.5m	6.00m
Lower Lias Clays.	10m	27m	29.74m
Pecten Ironstone.	0.5m	1m	0.85m
Lower Lias Clays.	23m	30m	41.51m
Frodingham Ironstone.	3.5m	11m	2.93m
Lower Lias Clays.	35.1m	40m	>51.21m

1) Cope *et al.* (1980) 2) Bradshaw & Penney (1982)

2.4) Ironstone Description

The first geologically orientated description of the ironstone-formation with a few early analyses was given by Hallimond (1925). Lamplugh *et al.* (1920) based their work on mining and quarrying aspects with a few local details. The most comprehensive published petrographic description of the ironstones was given by Davies and Dixie (1951). Whitehead *et al.* (1952) remains the most complete published work on the Frodingham Ironstone Formation, summarising earlier work and adding a number of lithological pit-sections obtained during the 1939-1942 geological surveys of the area. Watkins (1972) described the bulk rock geochemistry of core from the Risby Warren area.

Davies and Dixie (1951) divided the ironstone-formation into four lithological types, and described sections and lateral variations on the basis of these. The types have been used in later descriptions of the ironstones and are described in their own terminology below;

TYPE A: Calcite shells and "limonite"-"chamosite" ooids, more or less replaced by siderite, coated with a thin "chamosite" rim, closely packed, with the interstices filled by siderite. The hand-specimen is a sponge-like mass of dark green "chamosite" with highly polished ooids.

TYPE B: Small rhombic siderite crystals are distributed among linearly arranged "chamosite" flakes. Ooids and coarse material are absent. This type usually occurs as thin bands among other ironstone types. The hand-specimen is a dense, tough, dark bluish grey rock, breaking with a granular fracture.

TYPE C: "Limonite"-"chamosite" ooids, more or less replaced by siderite, and calcite shells within a fine-grained "chamosite" and siderite matrix. Unlike type 'A', the

"chamosite" has partially replaced the shells and not simply coated them. The rock is soft when wet and contains polished "limonite" ooids scattered in a dark bluish grey matrix.

TYPE D: ("Limey Ore"). "Limonite"-"chamosite" ooids and calcite shells more or less replaced by siderite, set in a matrix of coarsely crystalline calcite. Pebbles of other types [intraclasts] can often be distinguished within. This rock-type is essentially a hard shelly limestone containing coarse iron-bearing particles.

To this classification, Watkins (1972) added a type 'E' to include the basal transitional beds within this scheme:

TYPE E: A silty "chamosite" mudstone, similar to types 'B' and 'C', but with an absence of siderite. Anhedral quartz grains, 20-30μm in diameter, occur in bedded lenses and pseudo-spherical accumulations. Discrete flakes of (?)plagioclase and tiny laths of mica occur along micro-laminations.

The ironstones are more variable than the above classification might suggest, but it provides a useful introductory description to the main types of ironstone present. It allowed Davies and Dixie (1951) to subdivide sequences of the ironstone-formation in a standard manner, and has been used by D. Parsons as part of his recent PhD. work on the palaeoecology of the ironstone-formation. However, though useful in field studies, it is not used extensively in this study for the following reasons. Petrography shows that complete variation between types occurs, and that more than one type may be found within a single thin-section. Geochemically, the rock-types are more complex than this classification would suggest, and in particular, the type of berthierine in type 'A' ironstones is undefined (pore-lining or fibrous). The pseudo-spherical accumulations of Watkins' (1972) type 'E' are believed to be misinterpreted burrow fills, and hence do not form a distinctive type.

2.5) Fauna and Palaeoecology.

The Frodingham Ironstone Formation contains an abundant and varied macrofauna dominated by invertebrates, especially bivalves and ammonites (plate 2), but Ichthyosaur

and Plesiosaur vertebrae have been found. The earlier research workers describe simply shell material, but a faunal and palaeoecological study was carried out by Hallam (1963) (table 2.1). Hallam showed that largely well oxygenated conditions had prevailed, but suggested that within the pyrite-rich "Snap Band", dwarfing occurred within some bivalves and brachiopods. He concluded that within the period of deposition of this bed, a deficiency of oxygen had occurred, but did not necessarily produce anaerobic conditions. Fauna found to be living within or on the sediment was found to be lacking in type 'B' ironstone. Types 'A' and 'C' showed an assemblage dominated by epibionts and nekton, with endobionts and sediment-eaters too. Type 'D' ironstone has much bioclastic debris, most of which is detrital, but Hallam concluded that some fauna may have existed there in quieter phases.

A more thorough palaeoecological investigation is in preparation by D. Parsons of Somerset County Museum, Taunton, to be submitted as a PhD. thesis. A summary of his work is included within Young *et al.* (1990), enclosed at the back of this thesis. In essence, he suggests that benthonic species formed a large percentage of the fauna, that lived in, or on, sediments akin to type 'C' ironstone. Bivalves dominate, of which most morphological and ecological types are present, and bioturbation of these sediments is common. Considerable reworking of the fauna has occurred in type 'D' ironstone, forming parauthochtonous deposits, and assemblages of low diversity. Firmgrounds probably developed, but hardgrounds did not, and scouring of up to 60cm is indicated.

2.6) Previously Interpreted Environments of Deposition.

It is generally agreed in the literature (for example Whithead *et al.* 1952, Hallam 1963) that water energy was a major factor in ironstone type formation. Type 'D' ironstones represent the highest energy, showing cross-lamination, shell hashes, and a lack of fine-grained material. Type 'B' ironstones represent a quieter water setting, with settling of finer debris into finely laminated beds with only thin shelled bioclastic debris. Type 'C' represents an intermediary between the two extremes, and the characteristics of type 'A' ironstones are largely diagenetic. Hallam's (1963) conclusion was that alternating phases of high and low energy conditions prevailed, including changes from oxidising to reducing

TABLE 2.1

FAUNAL LIST OF THE FRODINGHAM IRONSTONE FORMATION (From Hallam (1963, Table 1)

c = common o = occurs

AMMONITES
- *Aegasteroceras sagittarium* (Blake) c
- *Arnioceras* aff. *semicostatum* (Young and Bird) c
- *Asteroceras stellare* o
- *Caenisites* cf. *brooki* (J. Sowerby) o
- *Eparietites denotatus* c
- *E. tenellus* (Simpson) o
- *Epophioceras* aff. *carinatum* Spath o
- *Oxynoticeras simpsoni* (Simpson) o
- *Microderoceras birchi* (J. Sowerby) o
- *Pararnioceras* aff. *alcinoë* (Reynès) c
- *Sulciferites sp.* o

NAUTILOIDS
- *Nautilus striatus* J. Sowerby o

BELEMNITES
- *Nannobelus brevis* (Blainville) c

LAMELLIBRANCHS
Anisomyaria
- *Camptonectes lohbergensis* (Emerson) c
- *Chlamys* cf. *textoria* (Schlotheim) c
- *Entolium lunare* (Roemer) c
- *Gryphaea* aff. *arcuata* c
- *Lima gigantea* (J. Sowerby) c
- *L. succincta* Schlotheim o
- *? Liostrea sp.* o
- *Meleagrinella sp.* o
- *Modiolus sp.* o
- *Myoconcha sp.* o
- *Pinna hartmanni* Zieten o
- *Plicatula sp.* o
- *Terquemia arietis* (Quenstedt) o

Eulamellibranchia
- *Astarte obsoleta* Dunker c
- *Cardinia concinna* c
- *C. listeri* (J. Sowerby) o
- *Hippopodium ponderosum* J. Sowerby o
- *Pholadomya ambigua* (J. Sowerby) c
- *Pleuromya* cf. *striatula* (Oppel) c
- *Tutcheria cingulata* (Goldfuss) o

GASTROPODS
- *Amberleya sp.* o
- *Pleurotomaria anglica* (J. Sowerby) o
- Small forms seen in thin section c

BRACHIOPODS
- *Piarorhynchia juvenis* (Quenstedt) c
- *Spiriferina walcotti* (J. Sowerby) o
- *Zeilleria* cf. *perforata* (Piette) o

CRINOIDS
- Ossicles seen in thin section c

ECHINOIDS
- Spines seen in section o

FORAMINIFERA
- Seen in thin section c

TRACE FOSSILS AND BORINGS
- ? Sponges c
- *Rhizocorallium jenense* Zenker o
- *Diplocraterion parallelum* (Torell) c
- *Zapfella pattei* Saint-Seine c
- Algae c

conditions, resulting in the formation of banding in ooids. He envisaged the Frodingham Ironstone Formation as having formed on an offshore shoal with no evidence of a shoreline in the immediate proximity, due to the lateral transition in the north and south to marine shales, consequently invoking a possible 'clastic trap'.

Knox and Fletcher (1987a) invoke an offshore shallow marine environment of ironstone accumulation, separated from marginal berthierine forming lagoons by offshore sand bars of shell debris and oxidised ferruginous grains derived from the lagoons (figure 2.5). Exceptional storms partially breached the bars, resulting in redistribution of bar and lagoonal constituents offshore from the bar to form the deposit. Repeated storm activity led to the development of small-scale cyclicity in the ironstone, due to the reworking by storms and the subsequent deposition of finer material (figure 2.6). Knox and Fletcher (1987b) also give a palaeogeographic reconstruction based on this model (figure 2.7), that is discussed in detail below.

2.7) Sample Material and 'Field' Observation.

2.7.1) Yarborough Pit (SE 930 110) (Plate 1)

This was one of the last ironstone pits to be worked in the area, and was in operation at the start of this research. The pit is situated approximately 4 km east of the centre of Scunthorpe. Permission to enter and sample from the pit was obtained initially from the owners, Appleby Slag Reduction Co., but now all requests for access should be made through British Steel. The pit is presently being clay-lined in preparation for its use as a waste disposal site, and at the time of writing only half of the original exposure remains.

Only the top ≈8m of the ironstone-formation is usually exposed (plate 1c), as the lowest portion of the sequence has been left as a hard base for machinery to work on. The lithological successions at the pit are described by Whithead *et al.* (1952) and Hallam (1963) whose descriptive logs are redrawn in figures 2.8 and 2.9 respectively. This pit is particularly well suited for diagenetic studies since the Formation contains the "Snap Band", a pyritic berthierine rich type 'B' ironstone towards the top of the sequence that is not

Figure 2.5. Depositional Setting of the Frodingham Ironstone Formation. Taken From Knox and Fletcher (1987b).

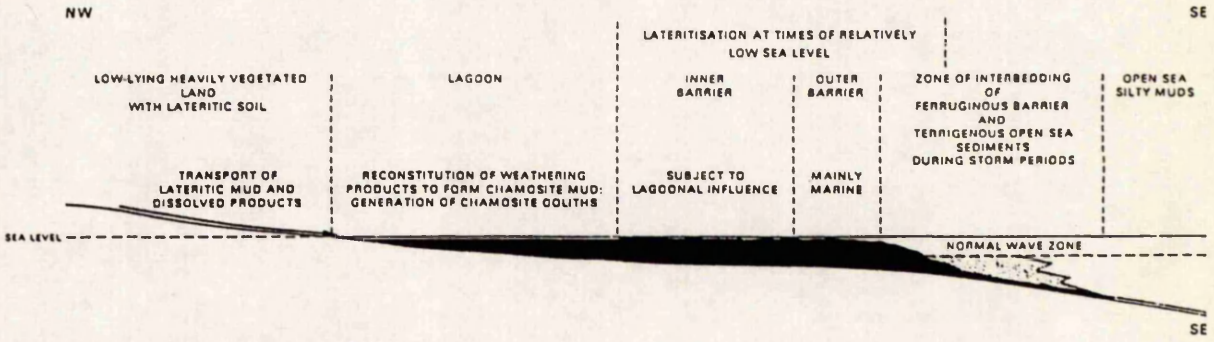

Figure 2.6. Generalised Depositional Cycle in the Frodingham Ironstone Formation. Taken From Knox and Fletcher (1987b).

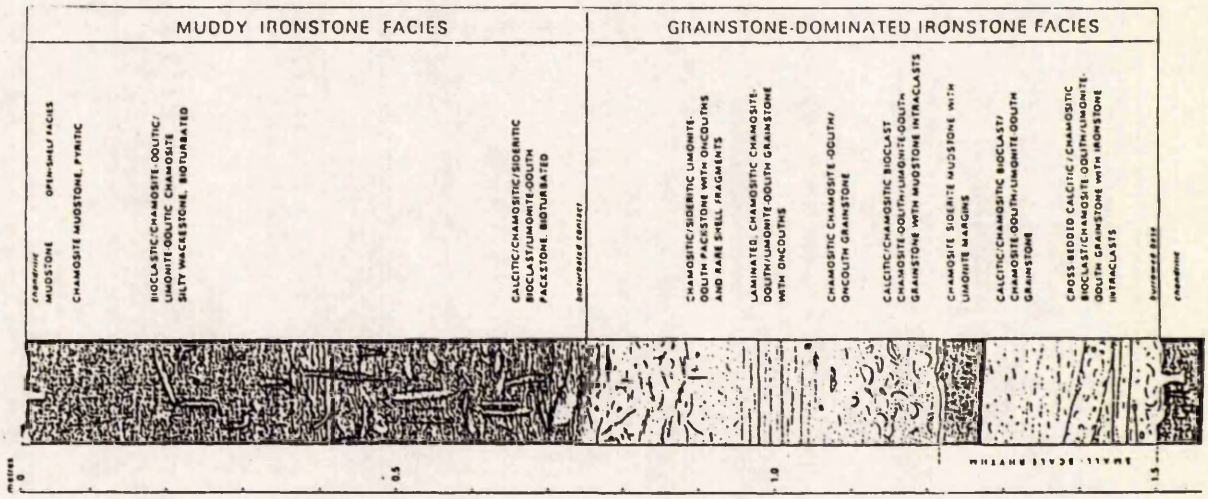

Figure 2.7. Palaeogeography of the East Midlands and Yorkshire at the time of Deposition of the Frodingham Ironstone Formation. Taken From Knox and Fletcher (1987b).

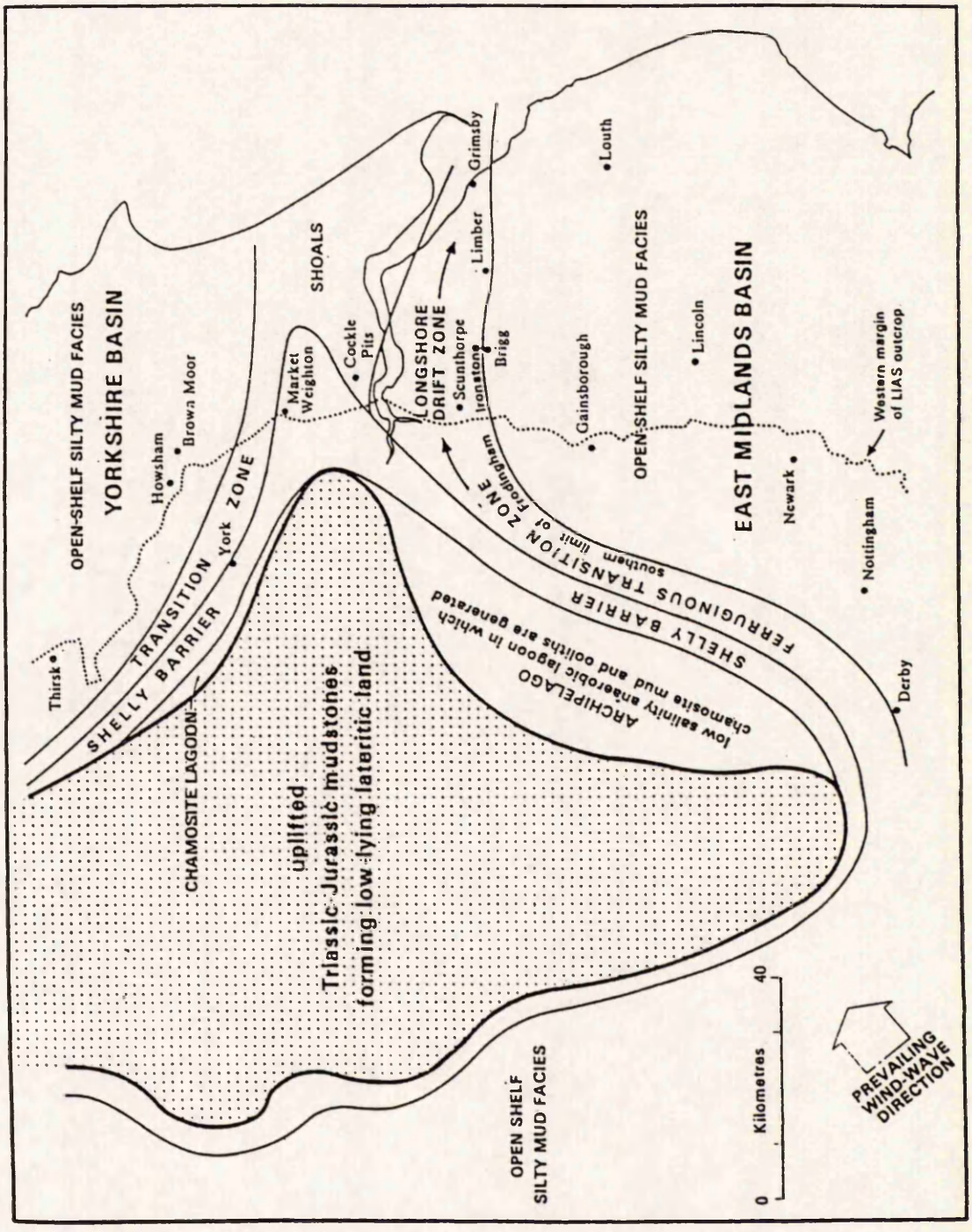

Figure 2.8. Section at the South End of Yarborough Pit, Scunthorpe. Redrawn From a Descriptive Section in Whitehead *et al.* (1952 page 91).

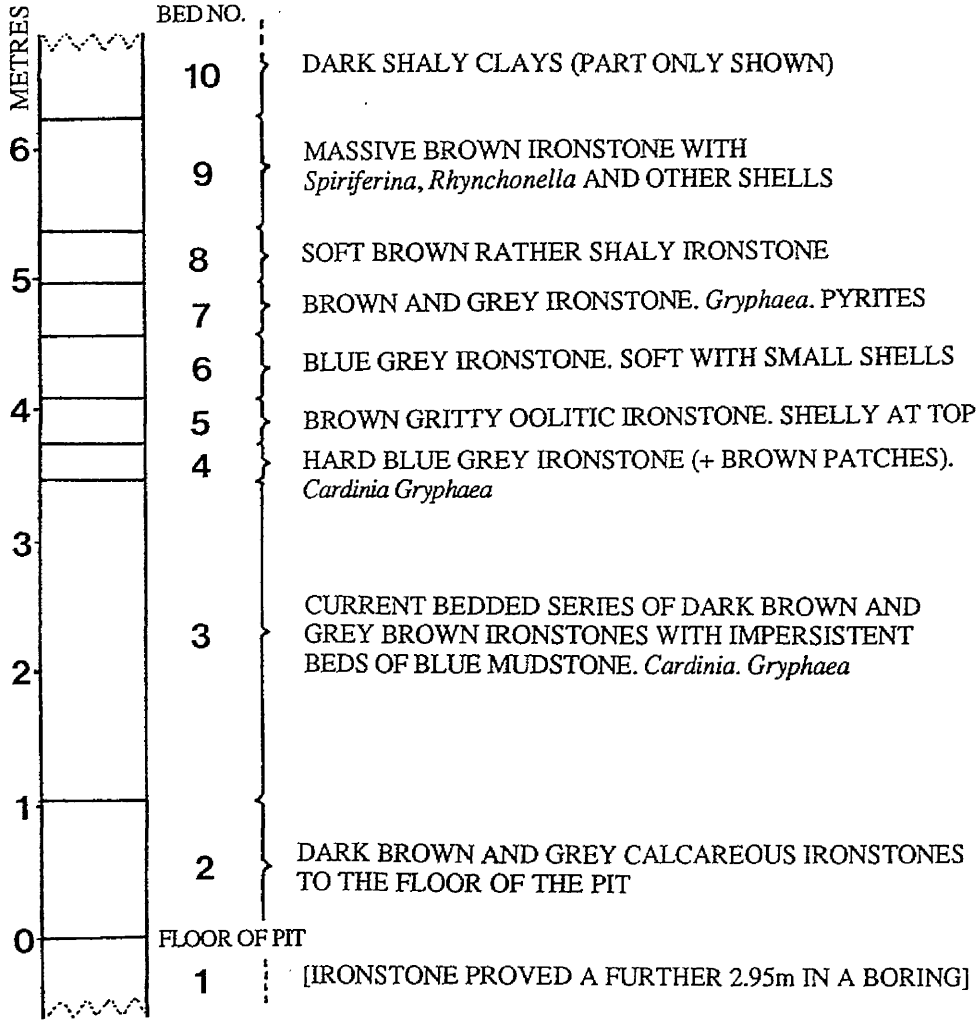

Figure 2.9. Section at the North End of Yarborough Pit, Scunthorpe. Redrawn From a Descriptive Section in Hallam (1963 page 155).

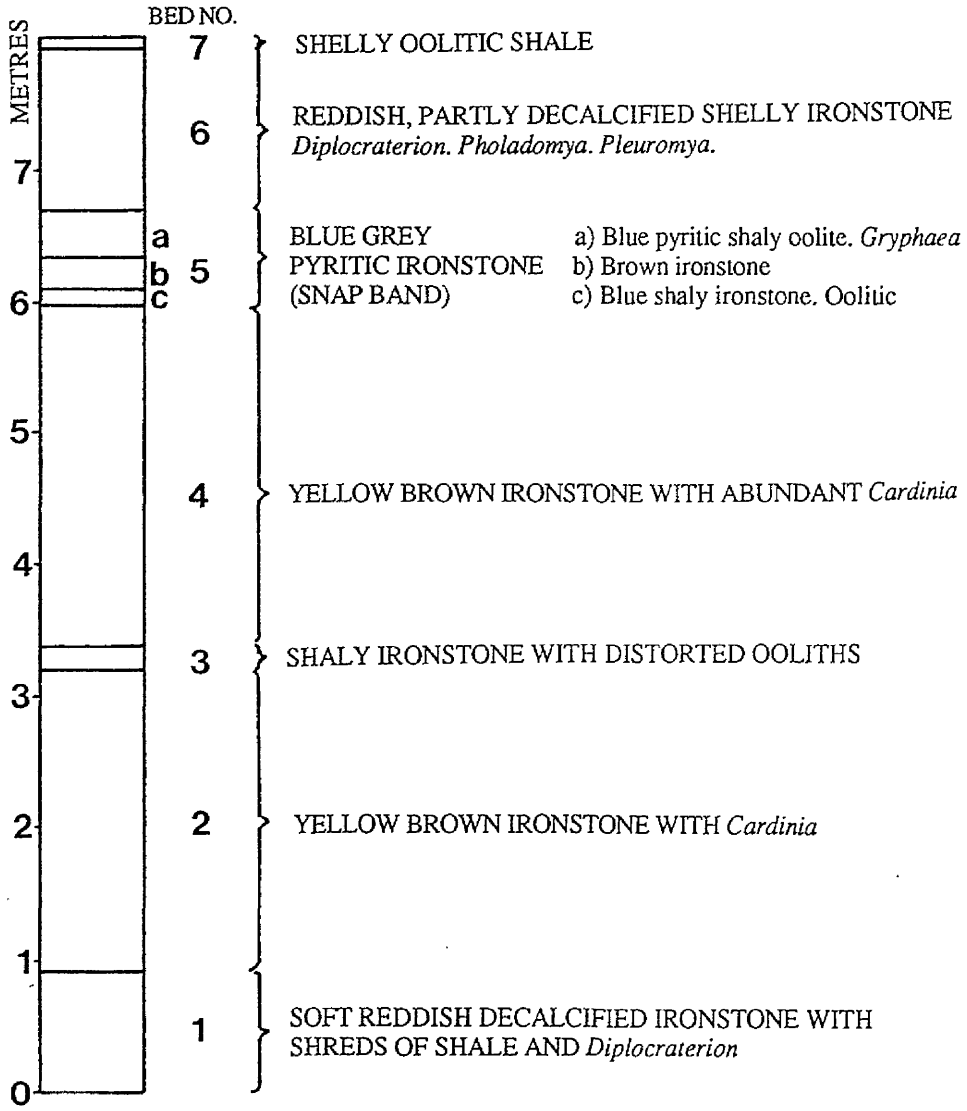

present in pits further to the north and south. A sedimentological log of the ironstone-formation from the centre of Yarborough Pit is given in figure 2.10, the top part of which is shown in plate 1d.

2.7.2) Core Material.

During the period that the ironstone was being worked, a number of exploratory boreholes were drilled, and core was taken. Many boreholes were drilled by British Steel, but the core material has become dispersed, and unfortunately much has been lost. The majority of remaining cores are now in the possession of the British Geological Survey at Keyworth. Of the cores in their possession, Dragonby 31 was chosen for detailed sampling since a virtually complete section through the ironstone-formation had been cored. Other cores examined either did not fully cover the complete depth of the Formation, or were incomplete in sections. A log of this core is given in figure 2.11.

Enquiries to ironstone workers who may have sampled or been given Frodingham material, revealed that Dr. P. Turner of Aston University was in possession of a few cores. Five accessible cores were examined, and the top 3.5m of core Y183 (from Yarborough) was logged and samples taken to include a full "Snap Band" sequence and the beds above it (not present in Dragonby 31). Field studies had shown that the most complex sedimentation and diagenetic modification within the sequence, was in the upper portion of the ironstone-formation. A detailed sedimentological log of this core is shown in figure 2.12, and was typical of the other cores examined.

2.8) Sedimentology of the Frodingham Ironstone Formation.

The logs in figures 2.10, 2.11, and 2.12, and plates 1-3 show the Formation to consist of a number of thin beds of variable average thickness from <1cm to rarely >1m. Individual beds may thin laterally, or may have slightly undulose bounding surfaces. The beds are often discontinuous, and in some cases may be traced over only a few metres. The precise occurrence of particular beds in the sequence is also largely unpredictable, such that logs of the same outcrop will vary in detail. In general however, the lower part of the sequence

Figure 2.10. Sedimentological Log of the Frodingham Ironstone Formation Exposed in the Centre of Yarborough Pit, Scunthorpe.

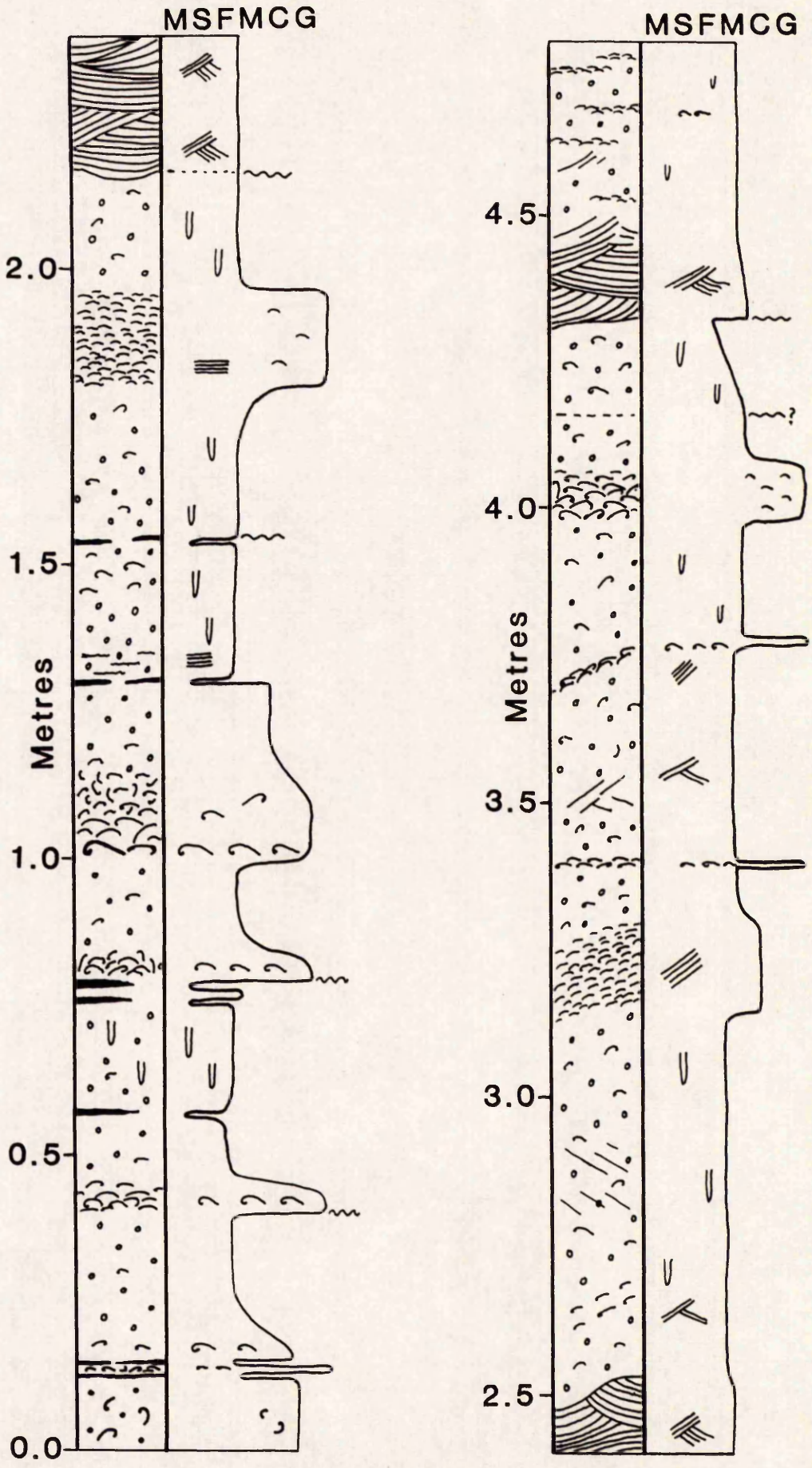

Figure 2.10. (Continued).

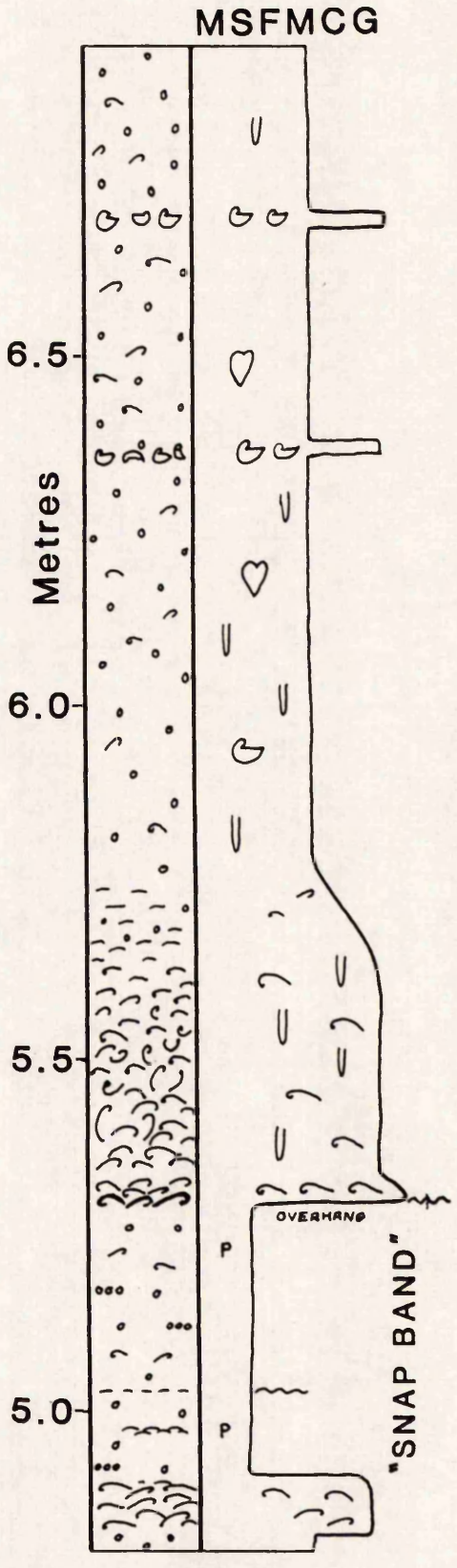

FOR A KEY TO THE SYMBOLS SEE THE END OF FIGURE 2.11.

Figure 2.11. Sedimentological Log of Borehole Core Dragonby 31, Frodingham Ironstone Formation.

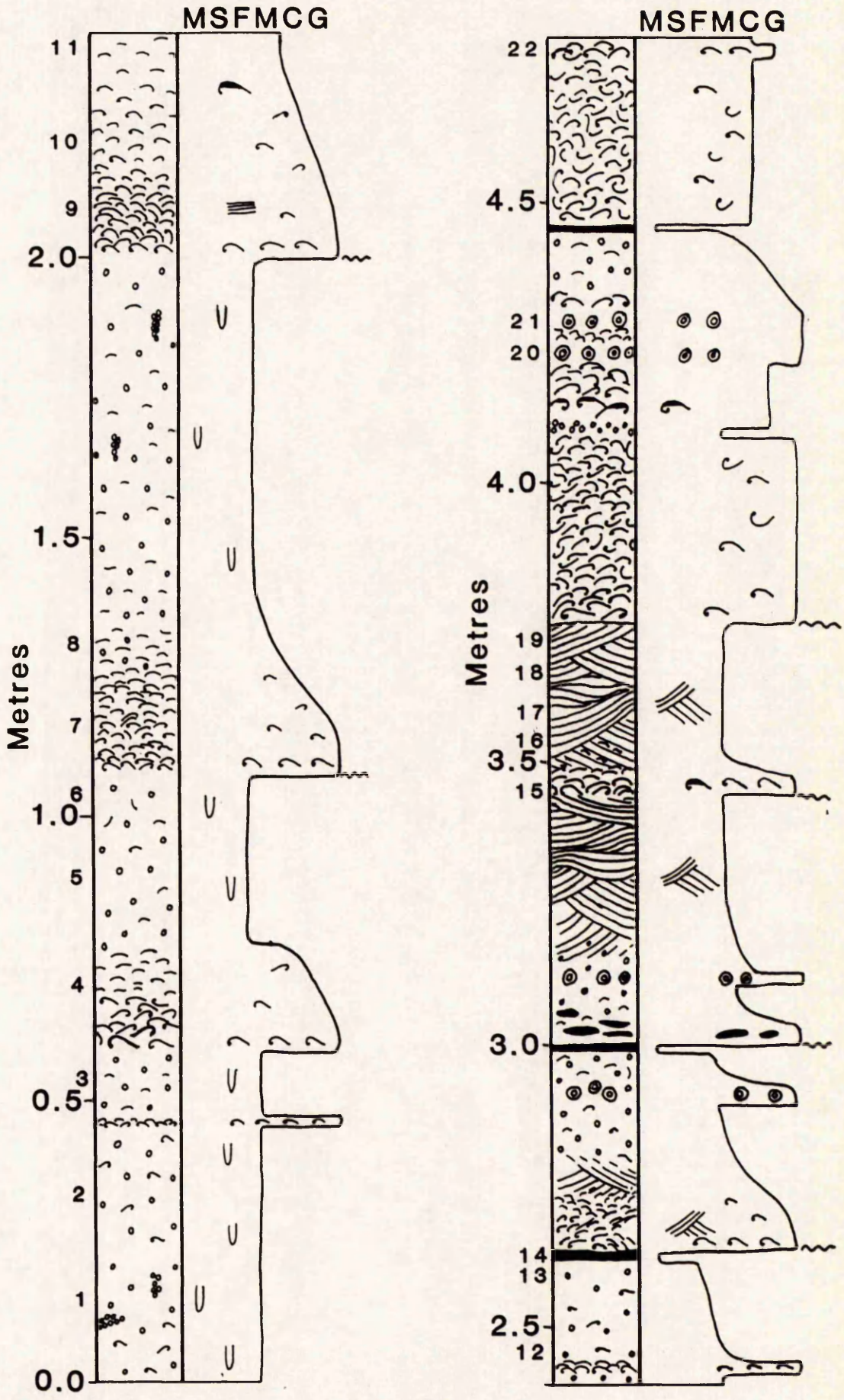

Figure 2.11. (Continued).

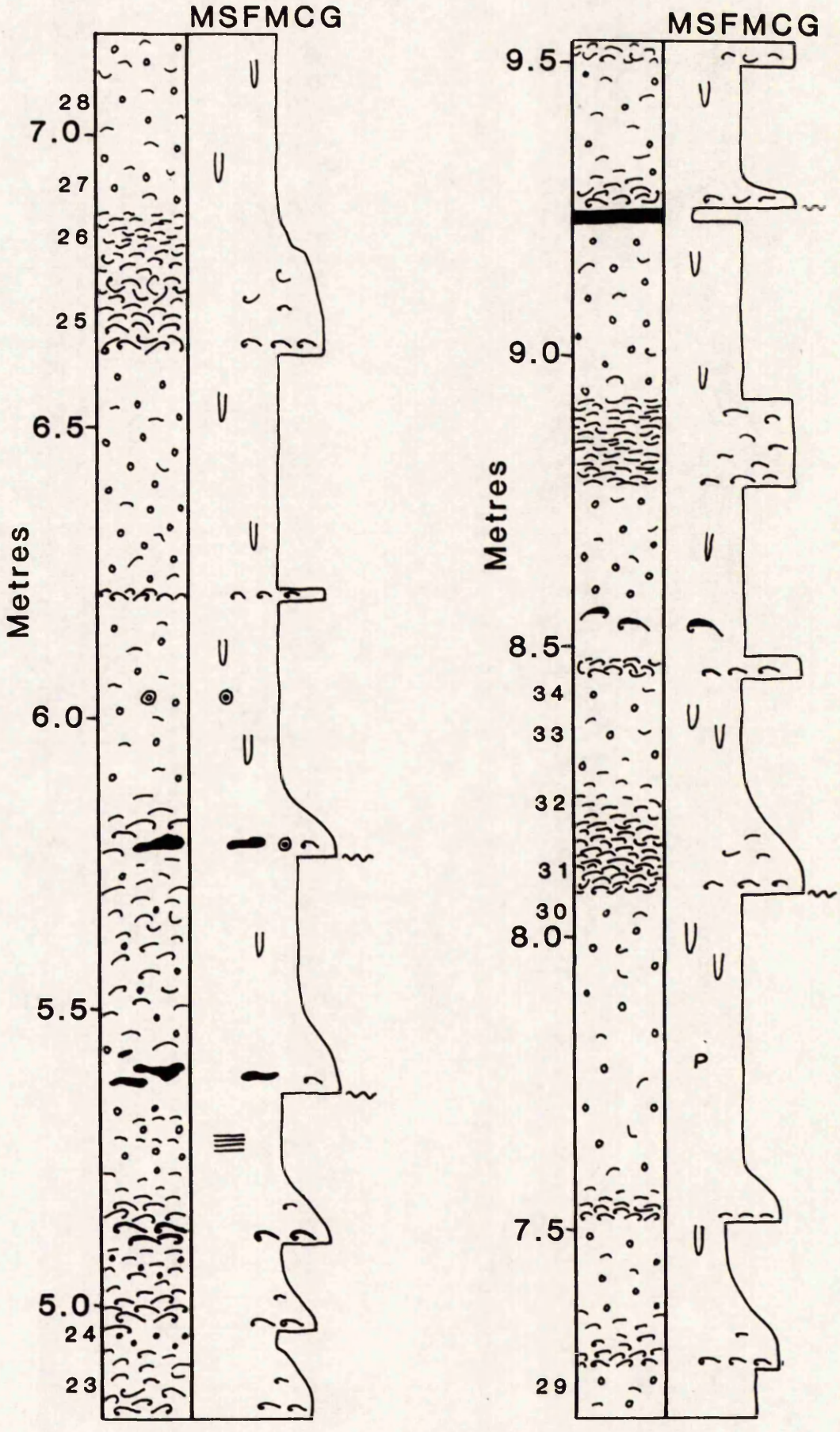

Figure 2.11. (Continued).

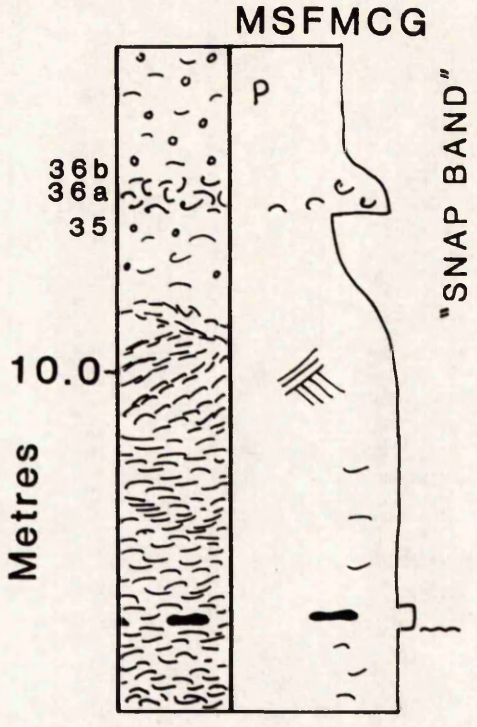

KEY

- SHELL FRAGMENTS, DISARTICULATED
- THIN FRAGMENTED SHELLS
- THICK-SHELLED BIOCLASTS
- In situ Pholadomya
- INTACT Gryphaea
- SHELL WITH MUD ON CONCAVE SURFACE
- BELEMNITE
- OOIDS
- PISOIDS
- BIOTURBATION
- MUD CLAST
- PARALLEL LAMINATION
- WELL-DEFINED CROSS-LAMINATION
- POORLY-DEFINED CROSS-LAMINATION
- OBLIQUE LAMINATION
- MINOR EROSION SURFACE
- P PYRITE

8 SPECIMEN NUMBER
(PREFIXED BY DRAG. OR Y183. IN THE TEXT).

88.0 DISTANCE FROM BASE OF LOG.

- M MUDSTONE
- S SILTSTONE
- F FINE
- M MEDIUM } SAND
- C COARSE
- G GRAVEL

Figure 2.12. Sedimentological Log of the Upper Portion of Borehole Core Y.183 (Yarborough), Frodingham Ironstone Formation.

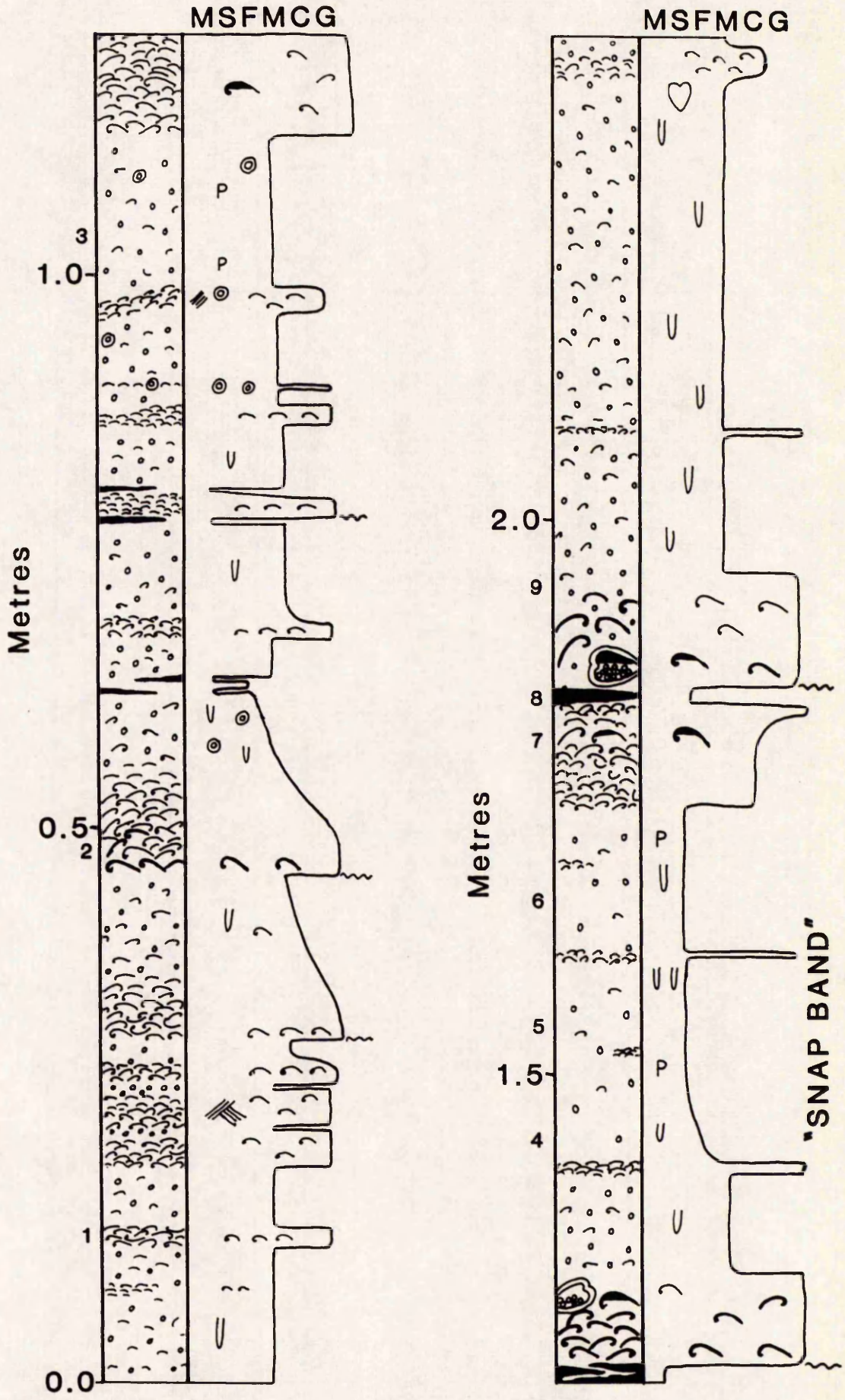

Figure 2.12. (Continued).

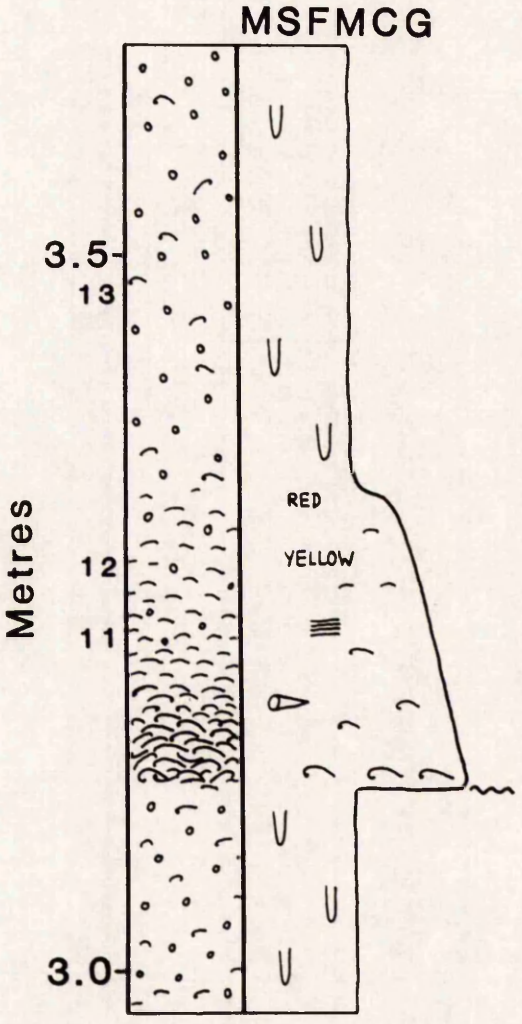

FOR A KEY TO THE SYMBOLS SEE THE END OF FIGURE 2.11.

61cm of core not logged due to its similarity with adjacent beds.

Specimen No.10 was taken at 2.70m.

PLATE 1

Yarborough Pit, Scunthorpe.

A) View looking south from the centre of the pit. The ironstone-formation is shown to the left, at the base of the pit (1). The Lias clays (2) have been removed by dragline and dumped at (3) following removal of the ironstone.

B) The sequence of Lower Lias clays above the ironstone-formation exposed in the pit. Base level on the photo is the top of the Frodingham Ironstone Formation. Approximately 20m of clay is exposed.

C) Sequence of the Frodingham Ironstone Formation exposed in the pit. The base of the Formation is not seen, as the pit is floored in ironstone. The blue-green "Snap Band" is arrowed towards the top of the sequence. The rucksack is 40cm high.

D) Detail of the upper part of the Frodingham Ironstone Formation logged in figure 2.10. The "Snap Band" (arrowed) is conspicuous by its green colour, and surface whitening due to gypsum precipitation. The height of the exposure is 4m 20cm.

A	B
C	D

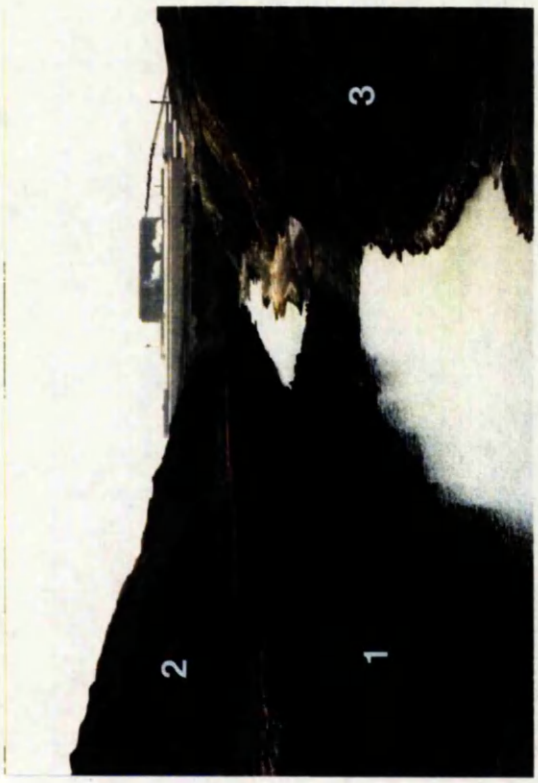
3
2
1

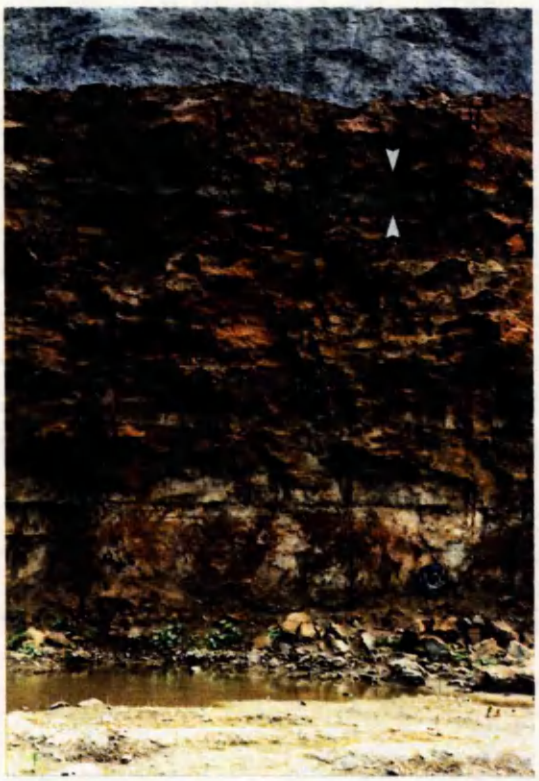

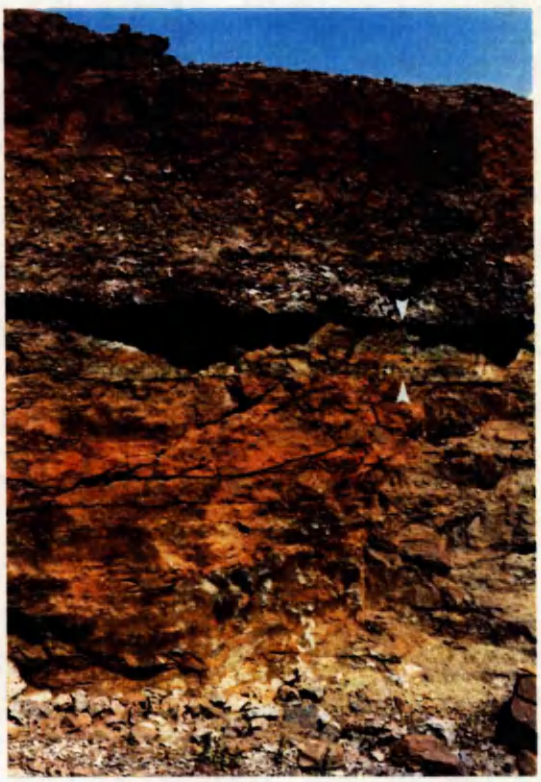

PLATE 2

Fauna of the Frodingham Ironstone Formation.

A) Fauna on a bedding plane, fallen block, Yarborough Pit. This assemblage is dominated by *Gryphaea* and *Cardinia*, slightly reworked and disarticulated. A small ammonite is arrowed. The lens cap is 5cm in diameter.

B) Bioturbated ooidal wackestone, hand specimen, Yarborough Pit. The rock has a mottled appearance of green mud-rich burrows and brown ooid-rich areas between them. A large *Rhizocorallium* burrow is seen, and was infilled with mud after penecontemporaneous oxidation of a thin layer of sediment in contact with the burrow (arrowed). The lens cap is 5cm in diameter.

C) Large ammonite sectioned perpendicular to the plane of coiling, fallen block, Yarborough Pit. The ammonite has remained uncrushed due to sediment infilling (1) and early calcite cementation (2). The calcite cement is both scalenohedral and coarsely crystalline. The lens cap is 5cm in diameter.

D) Reworked assemblage of bivalves and brachiopods, fallen block, Yarborough Pit. Much of the shelly material in the ironstone is disarticulated and reworked. The large *Cardinias* in this specimen (arrowed) have been replaced by scalenohedral and sparry calcite. The pen is 18cm long.

A	B
C	D

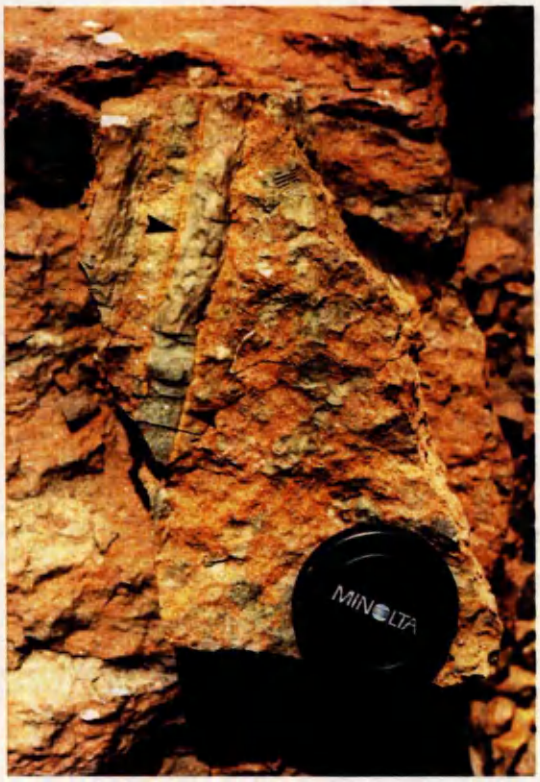
MINOLTA


1
2

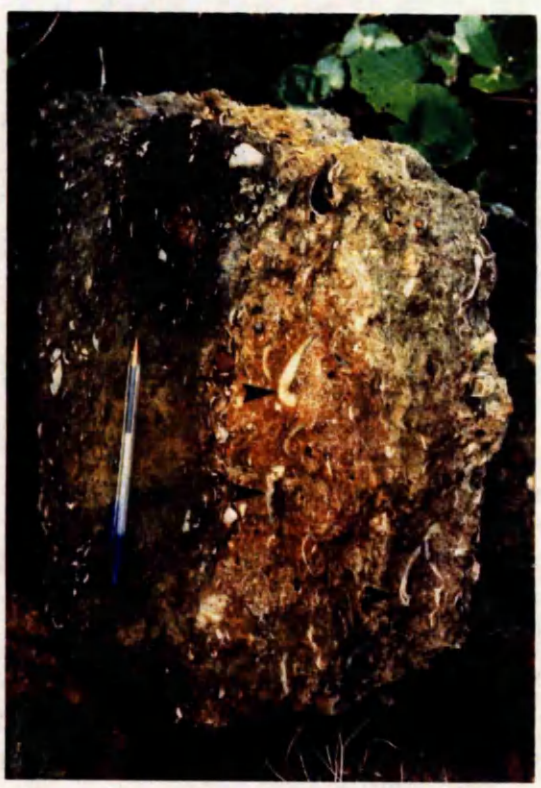

PLATE 3

Sedimentology of the Frodingham Ironstone Formation.

A) Parallel to cross-laminated bioclastic ooidal grain-ironstone. The darker layers are more ooid-rich. Loose specimen Yarborough Pit. The lens cap is 5cm in diameter.

B) Coquina largely composed of *Cardinia* shells, disarticulated and aligned roughly parallel to bedding. The coquina is shown in figure 2.10 at 4.00m. The discontinuity (erosion surface) at 4.16m in figure 2.10 is arrowed. The lens cap is 5cm in diameter.

C) Cross-laminated bioclastic ooidal grain-ironstone at 2.30m in figure 2.10. The lamination is produced by migration of small dunes, with subsequent erosion forming many truncation surfaces. The lens cap is 5cm in diameter.

D) Thin mud drapes (type 'B' ironstone) in bioclastic ooidal wacke-ironstones and grain-ironstones towards the base of the sequence. The hammer is 25cm long.

A	B
C	D

consists largely of goethite ooids and bioclastic debris in beds that may be cross-laminated (plate 3 a,c), and show signs of considerable reworking. Calcite cement is abundant in this part of the Formation. As the sequence is ascended, the proportion of mud increases and bioclast size increases due to reduced fracture and abrasion. Berthierine ooids are also found and bioturbation fabrics are more evident. Of particular note is the ≈40cm thick "Snap Band" (see plate 1 c,d) that is distinctive in the field due to the green berthierine ooids that are restricted in occurrence to this bed (plate 5d). The bed also contains a high pyrite content, and may be coated with a thin film of gypsum, due to pyrite oxidation generating sulphuric acid and subsequent reaction with carbonates. Above the "Snap Band", the beds are reddened and lacking in a primary sedimentary fabric due to the intense bioturbation. *In situ* *Pholadomya* are seen in life position within these beds, and *Gryphaea* are very common.

2.8.1) Grain-ironstones.

Grain-ironstones (see plate 4 a,b,c) are essentially of two types; bioclastic coquinas of shell debris, that are never more than a few centimetres thick; and bioclastic ooidal beds, often cross-laminated, with signs of reworking (scouring, lamination truncation, intraclastic material etc.). These two types were designated D_1 and D_2 respectively by D. Parsons (pers. comm. 1989). The former occur sporadically in the sequence, and indicate rapid deposition in some cases, but with subsequent minor reworking in others that aligned bioclastic material parallel to bedding in a convex-up orientation with high shelter porosity. To some extent these beds may represent lag deposits from winnowed, previously deposited shelly beds. The second type of grain-ironstone (D_2) contains substantial quantities of goethitic ooids with bioclastic debris that were reworked by current and wave action into small dunes (megaripples). Low angle cross-stratification is defined by differing proportions of ooids and bioclasts, forming laminae of a few millimetres to centimetres thick (plate 3a). Reactivation surfaces commonly truncate previously deposited sediment lamination. The laminae of individual sets are seen to thicken into the troughs and thin over the swells, so that the fabric cannot be assigned to hummocky or swaley cross-stratification. *In situ* fauna and bioturbation fabrics are generally lacking in the grain-ironstones.

PLATE 4

Thin-section Photomicrographs of Ironstone Textures 1.

A) Bioclastic, partly ooidal grain-ironstone, specimen YAR. 24 (stained). The bioclastic debris present consists of rounded and bored, unreplaced brachiopods and oysters (1); originally aragonitic bivalves replaced by ferroan calcite (2), siderite (3), and berthierine (+ferroan calcite) (4); and echinoderm fragments replaced by ferroan calcite (5). Photo length is equivalent to 6.7mm.

B) Ooidal bioclastic grain-ironstone, specimen DRAG. 31.10. The ooids are composed of dense goethite, and are randomly orientated. Most of the bioclastic debris is composed of echinoderm plates and spines. Photo length is equivalent to 6.7mm.

C) Intraclastic grain-ironstone, specimen YAR. 43. Intraclasts of reworked cemented grain-ironstones and wacke-ironstones are present in a bioclastic ooidal grain-ironstone. Photo length is equivalent to 6.7mm.

D) Ooidal wacke-ironstone, specimen Y183. 13. Ooids of dense goethite are present in a berthierine siltstone. A small mud-filled burrow crosses the photo. Photo length is equivalent to 3.3mm.

A	B
C	D


1
4
2

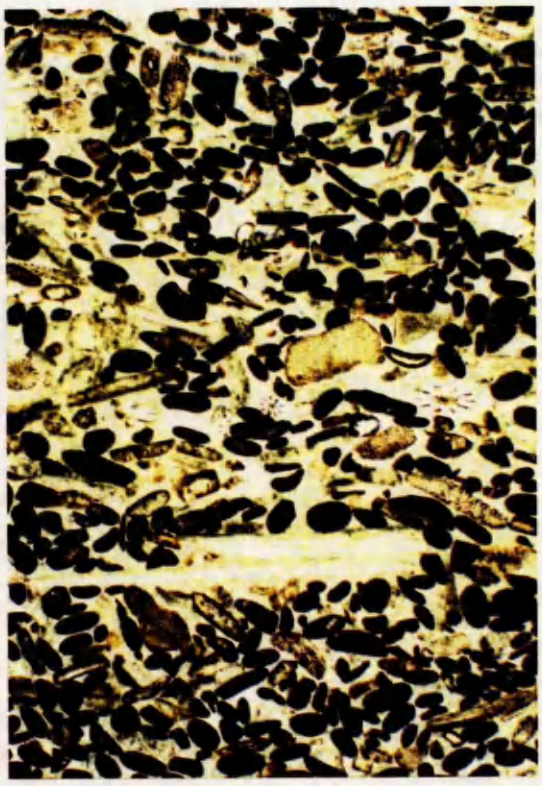

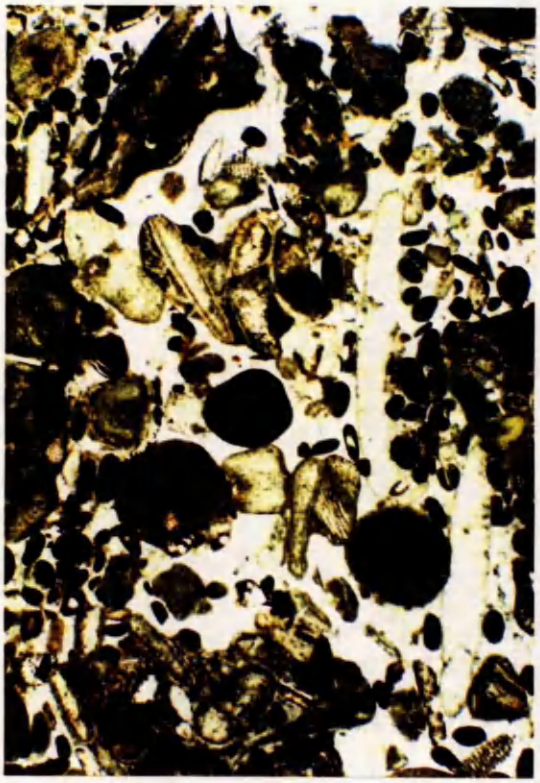

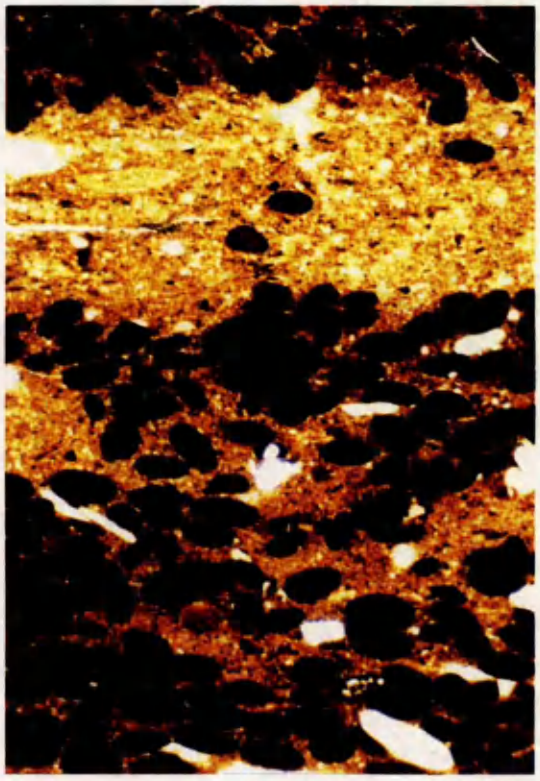

2.8.2) Pack-ironstones and Wacke-ironstones.

These beds (see plate 4d) are abundant in the sequence, and the muddier sediments are usually highly bioturbated (see plate 2b). Few examples appear to preserve much of the original texture of deposition, and it is often unclear whether the beds were formed by synchronous mud and ooid/bioclast deposition, or whether the sediment was originally an inter-layered sequence of muds and grain/pack-ironstones. The effects of bioturbation may be most clearly recognised where burrow-fills are of a different lithology to that of the surrounding and overlying sediment. Bioclastic debris is variable in content, and usually consists of fragmented thin-shelled bivalves which commonly align parallel to bedding. However, high angles of bioclast orientation are present in many cases, and form by rapid bulk deposition of high density suspended material, or by fabric distortion during bioturbation.

2.8.3) Mud-ironstones.

Mudstones (plate 5) are uncommon in the Formation, due to preservational, rather than depositional factors. Beds are always thin, with thicknesses >5cm being uncommon. They are not usually laterally continuous, and it is rare to be able to trace beds more than a few metres along outcrop. Many examples are fissile and exhibit a crude parallel lamination (plate 5b), but this depositional fabric may be lost during the transformation to berthierine (plate 5c). These beds were deposited during periods of quieter water conditions, as finer clay sized material was able to settle out of suspension. Subsequent higher energy reworking eroded these mud drapes by abrasion, utilising the erosive power of coarser material held in high density suspension and traction flows. Such erosion removed all of the drape in places (plate 3d), or reworked it to form intraclasts of cohesive mudstone, so that preservation potential of these mud drapes was low. Although removal of parts of the beds has occurred, it is not suspected that the original thicknesses of these units was much greater, because the amount of suspended material held in such shallow waters could not be large.

PLATE 5

Thin-section Photomicrographs of Ironstone Textures 2.

A) Bioturbated, sparsely ooidal, bioclastic wackestone from the transitional beds at the base of the ironstone, specimen DRAG. 31.5. The high proportion of quartz in the transitional beds is readily apparent. Photo length is equivalent to 3.3mm.

B) Detail of a mud drape, specimen DRAG. 31.13/14. The berthierine mudstone contains quartz (Q), muscovite (M) and organic matter (OM), and shows a primary lamination fabric. Photo length is equivalent to 0.7mm.

C) Recrystallised berthierine mudstone, specimen Y183. 8 (crossed polars). Any depositional fabric of the mud has been lost on recrystallisation and conversion to berthierine. The original detrital origin is however indicated by the presence of minor quartz, muscovite and other detrital particles. The low birefringence of berthierine is apparent in this photo. Photo length is equivalent to 1.3mm.

D) Typical "Snap Band", specimen Y183. 8. This bed is superficially apparent as a thick mudstone unit, but is actually formed largely of highly deformed berthierine ooids ('spastoliths'). Photo length is equivalent to 3.3mm.

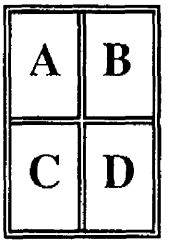

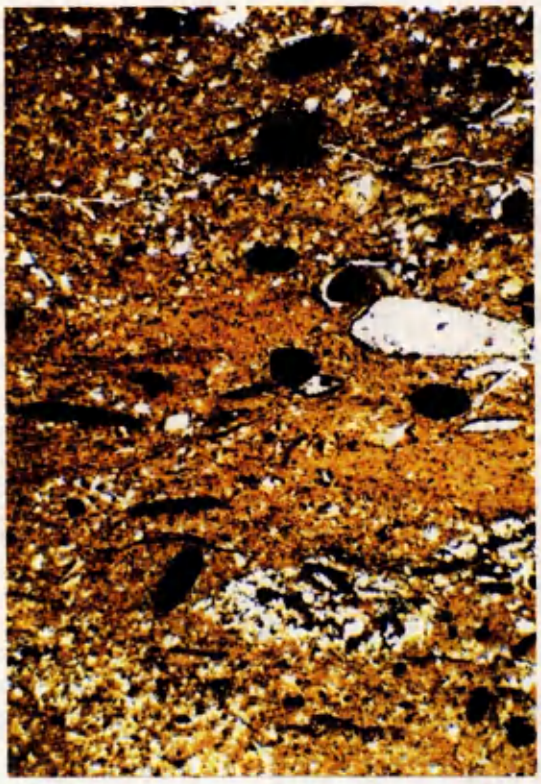

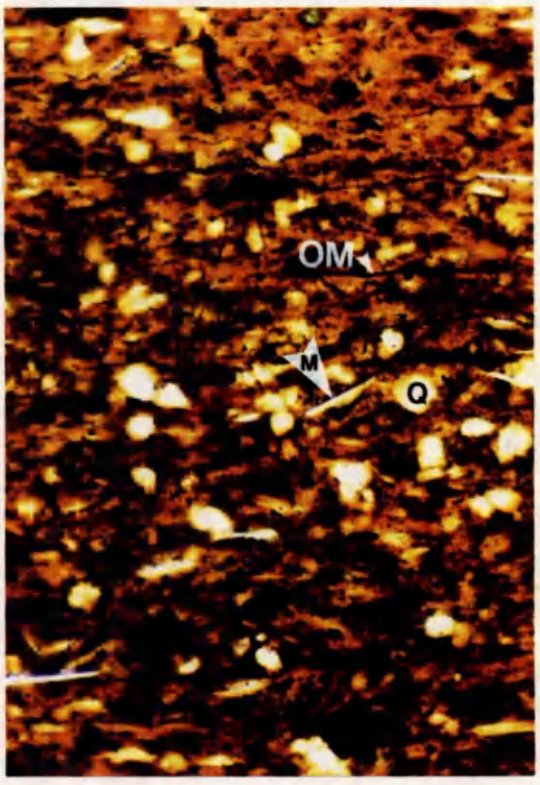
OM
M
Q

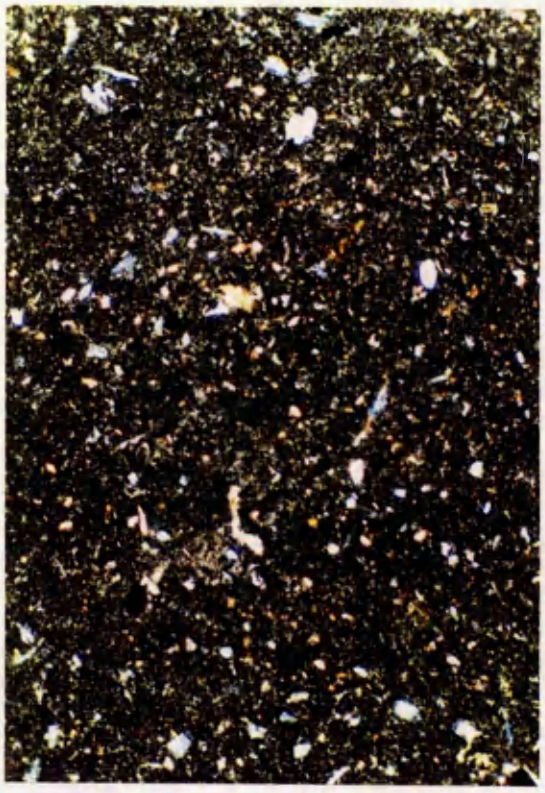

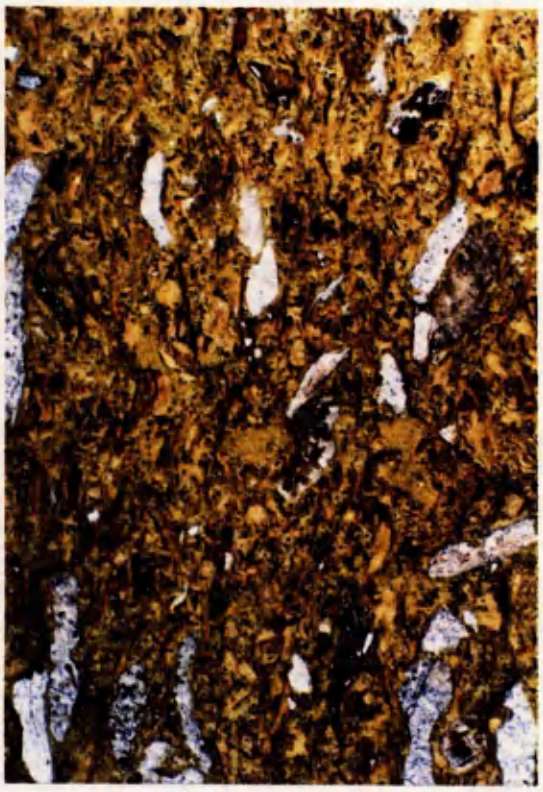

2.8.4) Terrigenous Clastics.

The common observation of ooidal ironstones being depleted in terrigenous clastic material has been discussed above (section 1.4.2), and the Frodingham Ironstone Formation is similar in this respect. Quartz and felspar are found in significant quantities only at the base of the sequence, in the transition from shale to ironstone deposition (plate 5a). They may also occur in muddier sediments including mud drapes, but are not common. 'Clastic trap' and hydrodynamic mechanisms have been implied to explain the absence of these particles, but are usually based upon hypothetical rather than sedimentological reasoning. In ironstones such as the Frodingham, in which the deposit represents a site of accumulation of various sediment types, ascertaining the source of the quartz relative to other particles is important if a separation mechanism (sorting), or changing sedimentation pattern is to be implied. In particular, it would be significant to ascertain whether iron-ooids and quartz were derived from the same source and later separated, or whether different sedimentary provenances need to be implied.

In the basal beds of the Dragonby 31 core, both quartz and iron-ooids are present along with bioclastic debris in a mud matrix (plate 5a). Point count data from thin-sections through these beds is shown graphically in figure 2.13. The brachiopod and bivalve shell count correlates well with echinoderm debris, indicating a single bioclastic source. Ooids show a partial correlation with them in the upper section, but most importantly quartz is seen to be inversely correlated with all three. This correlation is valid, given that the proportions of the individual particles under question are acting independently of the total particle abundance in the rock.

In effect figure 2.13 quantifies for the first time the observation of quartz depletion in ooidal ironstones. More significantly, it suggests that ironstone deposition represents a distinct change in sediment provenance from a quartz-rich facies to an ooid-rich facies, and not simply a depletion of only quartz. Brookfield's (1971) hydrodynamic separation hypothesis was hence probably not in operation here, and a clastic trap is also disputed since it cannot explain the depletion of ooids when quartz increases. Hence it is believed that the

Figure 2.13. Proportions of the Major Sediment Components within the Basal Beds of Borehole Core Dragonby 31, Obtained by Point-Count Analysis.

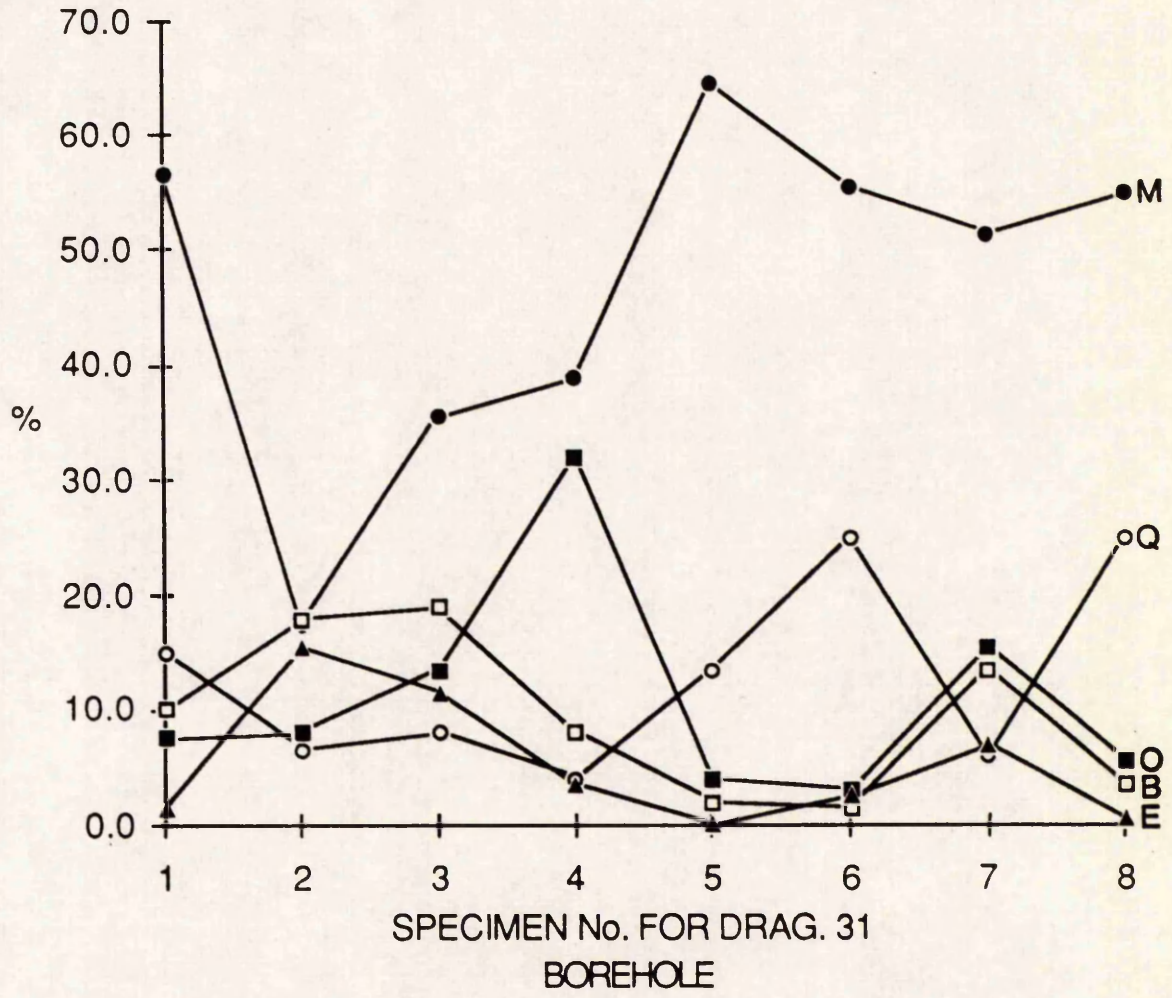

M-MATRIX
Q-QUARTZ
O-OOIDS
B-BRACHIOPODS/BIVALVES
E-ECHINODERMS

depletion of terrigenous clastics resulted from a change in sedimentation pattern, and not from a removal mechanism. This is supported by the thinning of sediments basinward during the time of ironstone deposition, suggesting that all sedimentation at this time was significantly reduced.

2.8.5) Cyclic Sedimentation and Depositional Models.

Within the sequence, small-scale cyclicity can be inferred, but subsequent reworking and extensive bioturbation has largely destroyed much of the primary fabric. This cyclicity is seen in the form of small fining sequences that are usually significantly less than 1m thick. The cycles were recognised by Knox and Fletcher (1987 a,b) and are also discussed by Young *et al.* (1990). Each cycle represents storm erosion and suspension of material, with subsequent deposition largely during the waning phase. The base of an ideal cycle is hence an erosional surface on which a shell lag, or allochtonous coarse shelly horizon is deposited, followed by grainstone deposition, then packstone through to mudstone. The 'fining' is defined by firstly an increasing proportion of mud up the cycle, and secondly a decreasing abundance of larger shelly material that is reworked (not to be confused with *in situ* fauna). Given that the ideal cycle therefore represents a single depositional event, the upper surface has the potential to be the site of intensive bioturbation, that would decrease in intensity with depth (i.e. a hierarchy of bioturbation develops). Fairweather sedimentation continues after the cycle is deposited, until the next storm event and subsequent cycle is formed.

Considerable variation on this cyclicity occurs according to; the amount of erosion; type of material eroded and re-suspended; storm strength and duration (i.e. amount of reworking during the episode); and later modification (fabric destruction) by bioturbation. Figure 2.14 gives a schematic representation of the 'ideal' cycle associated with this storm deposition, and the nature of the sediments deposited. Such variation is not restricted to the examples shown, but they serve to indicate the diversity possible. Coquinas may develop singularly by a pulse of strong current action, or be absent if erosion is slight and insufficient energy was available to suspend such material. Shellgrounds may develop which acted as sites for

Figure 2.14. Schematic Representation of an 'Ideal' Cycle of Storm Sedimentation in the Frodingham Ironstone Formation, and Examples of Variations Seen on This Model in Core and Outcrop.

i) Coarse Bioclastic Coquina.

ii) Ooidal Bioclastic Grain-ironstone.

iii) Cross-laminated, Bioclastic Ooidal Grain-ironstone.

iv) Bioclastic Ooidal Wacke/Pack-ironstone.

v) Mud-ironstone.

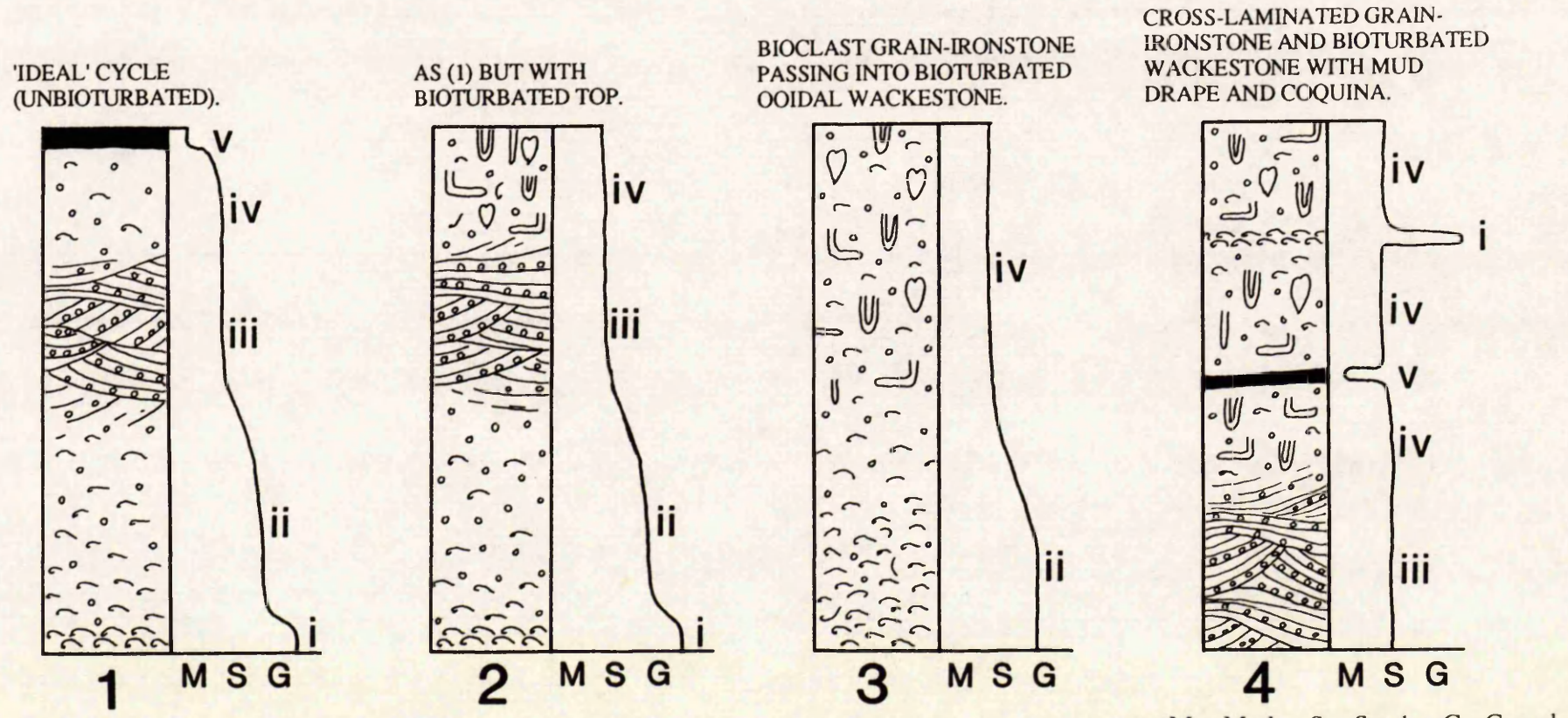

oyster and brachiopod attachment (as seen in specimens of large ammonites encrusted by oysters).

The grainstone facies may be rapidly deposited by mud free suspension fallout, or may be subsequently reworked into dunes or small bars. This is analogous to the formation of hummocky cross-stratification (Harms *et al.* 1975) that is believed to develop by the interplay of unidirectional and oscillatory flow on depositing sediment (for example Dott and Bourgeois, 1982). Though these bedforms (plate 3c) are not interpreted as hummocky cross-stratification, similar processes probably operated during storm activity when oscillatory wave motion is enhanced, and current strength in increased by storm surge ebb currents. Such currents may also supply material from the inshore zone, reworked and deposited in the zone of ironstone accumulation.

The muddier sediments are deposited during the waning of the storm, and also represent the background sedimentation, indicated from palaeoecological studies (D. Parsons pers. comm. 1989). Preservation of depositional fabric is unlikely if sufficient time lapses between storms for bioturbation to commence. Thin mudstone layers which represent the last stages of the storm cycle may be absent, and incorporated into the background sedimentation. A preservational, as opposed to primary factor for the presence of mudstone drapes is supported by the occurrence in mud drapes of only *Chondrites* burrows, that have a minimal effect on sediment disturbance. Further storm activity occurred prior to the onset of intense bioturbation of these muds, and mud preservation may therefore indicate faster rates of net sedimentation.

Sedimentation rate was therefore variable, and it is probable that although the net rate of sedimentation was low (≈10m in 2-4 Ma), individual packets of sediment, centimetres thick, were deposited within a single storm event. The deposit is condensed due to erosion, reworking and sporadic sedimentation, rather than due to continued low sediment input. A 30cm fining cycle may hence represent the preservation of one event in ≈60,000 years, and the disconformity at the base of cycles could represent the loss of many centimetres of

sediment. As indicated above, mud drapes representing storm fines deposition, are also not necessarily indicative of a slower sedimentation rate.

2.8.6) Site of Ironstone Accumulation.

The environment of deposition of the sections studied is thought to be constrained to the offshore-transition zone, i.e. between mean fairweather wave base and mean storm wave base (figure 2.15). The ironstones were hence largely undisturbed by wave action during normal fairweather periods, with background sedimentation having been derived from suspension and minor traction currents. During storms, the sediments were eroded and reworked into the structures described above. The cyclicity is similar to the model of idealised storm-generated hummocky-cross-stratification (Dott and Bourgeois 1981), but with a modified bedform. The faunal element suggests free access to open marine conditions (ammonites, belemnites), with an *in situ* fauna living both on and within the sediment, in well-oxygenated, clear, shallow water conditions. Bioturbation was intense during fairweather periods, and the trace fossils (for example *Chondrites*, *Diplocraterion*, *Rhizocorallium*) are consistent with the *Cruziana* facies of the sublittoral environment (see Frey 1975). It is worth specifically noting that the depositional environment is is not restricted to ironstones, but comparable to other mixed carbonate-clastic systems.

2.8.7) Palaeogeography.

It is impossible on the basis of cores and outcrop studied to ascertain the palaeogeography of the area, particularly with reference to the position of a shoreline. The palaeogeography as described by Knox and Fletcher (1987 a, b, figure 2.7) is considered to be highly interpretive, particularly as the majority of the reconstruction in the west of the region, is not represented at all in outcrop or subcrop, and based on their interpretation of ooid formation as requiring low salinity lagoons. Hallam's (1963) interpretation of ironstone formation on a shoal with no evidence of a near shoreline cannot be tested either, as the ironstone facies as described could form either on a shoal, or a simple non-barred coastal shelf. Again however, the palaeoenvironmental model was constrained by an assumption, which in this case was that a clastic trap was in operation at time of deposition.

Figure 2.15. Zone of Accumulation of the Frodingham Ironstone Formation in Relation to Shallow Water Environments, Processes and Facies. Modified From Reading (1986, figure 7.3 p.157).

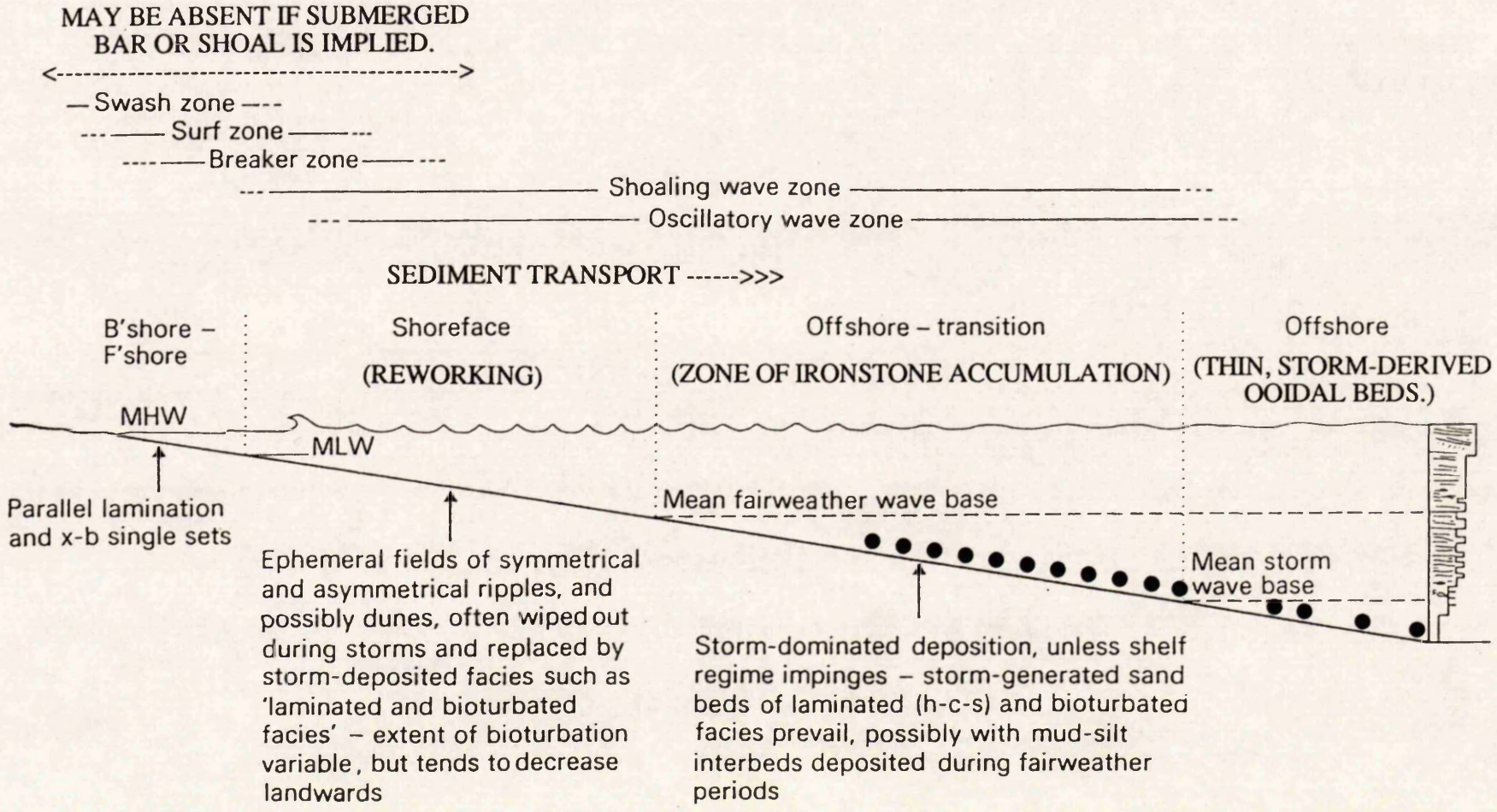

The discussion given in section 2.8.4 with regard to the lack of terrigenous material, suggests that a shoal need not be implied, but that its absence cannot be confirmed or dismissed. The only confirmed palaeogeographic feature of the models proposed, is that the Market Weighton Axis formed a topographic rise, but the depth or absence of water upon it cannot be ascertained due to the subsequent extensive erosion of the strata in that area

An attempt was made to ascertain the nature of the adjacent landmass in this study by analysis of the U, Th, and K content of various particles in the ironstone-formation by using E.P.M.A., in comparison to the work of Myers (1989). If the landmass was undergoing lateritic weathering, and hence presumed to be highly weathered and low-lying, then it was hoped lateritic particles could be distinguished on the basis of their U and Th content, lending support for this hypothesis. The results and methodology of this study are given in appendix B, but the data were considered to be inconclusive.

2.8.8) Transgressive/Regressive Nature of Deposition.

The change in deposition from shale to bioclastic ironstone at the base of the sequence, suggests that a shallowing of the water occurred between the two. Similarly, a deepening of the water is inferred to have followed ironstone deposition. Though the shales beneath the ironstone-formation do not show signs of regression in the form of a coarsening upward sequence, the section has been correlated with regressive sequences elsewhere (Hallam and Bradshaw 1979). The exact timing of ironstone deposition in general with regard to regression, transgression, or a stillstand is however debatable (see section 1.4.3.1), and requires a full facies analysis. However, it is possible that the gradual basal transition with quartz depletion and increasing ooid and bioclast input, through deposition of reworked storm deposited bioclastic grainstones and muddier ooidal facies towards the top, may represent sedimentation during minor regression and transgression, as opposed to the formation of distinct erosional and drowning surfaces. The regressive phase is represented by the transitional beds, with ironstone deposition associated with the initial stages of transgression. During this transgressive phase, terrigenous input would be significantly depleted if the source (i.e landmass) was low-lying, and became inundated with marine

waters (Hemingway 1951 and Hallam 1963). As the transgression proceeded, the sequence became slightly muddier, but the full effect of the transgression is assumed to have postdated the ironstone deposition, as the uppermost beds of ironstone are considerably reworked (Hallam 1963), and hence imply relatively shallow water. The ironstone-shale contact that could provide information on the cessation of ironstone deposition, is unfortunately largely destroyed or inaccessible at outcrop, and to my knowledge is not present within borehole core.

CHAPTER 3. PETROGRAPHY OF THE GRAINS AND MATRIX WITHIN THE FRODINGHAM IRONSTONE FORMATION.

3.1) Introduction.

This chapter describes, and discusses the origin of, the various particles that were deposited to form the ironstone-formation, in terms of their formation, nature and mineralogy. Emphasis is placed on fabrics and description of the components as sedimentary particles, but includes some discussion on mineralogical development that may be associated with the formation of authigenic cements. Most of the chapter is devoted to the iron-ooids that are characteristic of this type of ironstone, and contain important information on the geochemical evolution of ironstone deposits.

3.2) Iron-Ooids.

3.2.1) Introduction.

Iron-ooids are superficially similar to carbonate ooids in having a nucleus, around which consecutive laminae have been accreted to form a rounded, spherical to sub-spherical particle. The mineralogy is the obvious difference, with iron-ooids consisting of an iron oxide (here goethite) and/or iron silicate (here berthierine), but more subtle contrasts in shape and form can be shown to occur. These differences from carbonate ooids have meant that iron-ooids have attracted much attention in the literature (section 1.5), and their origin is widely debated due to the lack of modern analogues. This section describes in detail the petrography, mineralogy and composition of iron-ooids within the Frodingham Ironstone Formation, and then discusses the features described with respect to the varying hypotheses previously suggested for iron-ooid formation.

The Frodingham iron-ooids may be usefully subdivided mineralogically into two types; those of a dominant goethitic mineralogy; and those composed of berthierine. The internal fabric and occurrences of these two types are different, and may therefore be genetically, as well as mineralogically distinct. Goethitic ooids are by far the most abundant type, and most of the detailed petrographic and analytical work on iron-ooids in this research has been based

on this type. Berthierine ooids are however described first, so that the similarities and differences between goethitic and berthierine ooids can be borne in mind during the more wider discussion on goethitic ooid genesis.

3.2.2) Berthierine Ooids.

Berthierine ooids (plate 6) are difficult to study petrographically, as the majority of such ooids have been extensively deformed during compaction. Intact examples usually occur only where cementation was early, and formed a sufficiently rigid structure to avoid brittle fracture around the ooids (see section 3.2.7 for a full description of ooid deformation fabrics). Examination of intact berthierine ooids suggests that they are distinct from goethitic ooids in internal fabric and mineralogy, but not in size or shape. The following description concentrates on these fabric differences.

There are three common types of berthierine ooid nuclei; rounded particles that show a random orientation of crystals under crossed-polars; 'flakes' that possess a parallel foliation similar to that of the ooid cortices; and fragments of broken ooid cortex. Nucleus shape is usually equant, with highly elongate forms such as shell fragments not seen. The mineralogy of all nuclei is always berthierine. There is a high proportion of ooids that have no apparent nucleus, and this is higher than can be accounted for by assuming that the ooid has been obliquely sectioned through the cortex only. A sizable nucleus may therefore not be necessary for these ooids to form. Where no nucleus is present, the lamination of the cortex passes gradually inwards to a finely crystalline interior of berthierine with randomly orientated crystals.

The cortices of berthierine ooids do not possess distinctive continuous laminae that may be traced around the ooid, but consist of tiny (a few microns long) berthierine particles aligned in an apparently tangential fabric. A preferred crystal orientation is also indicated by the presence of a clear extinction cross within the ooids when viewed under crossed-polars (plate 6 b,c). This alignment is contrast to the findings of Hughes (1989), who using Transmission Electron Microscopy (T.E.M.). failed to find any preferential crystal alignment

PLATE 6

Berthierine Ooids and Peloids in Thin-section.

A), B) Berthierine ooids within the "Snap Band", Yarborough Pit, specimen YAR. 30. These berthierine ooids lack an obvious visible internal structure, but are seen to possess a laminated cortex under crossed polars (**B**). These ooids have been preserved intact due to the berthierine matrix having been extensively replaced by siderite, enabling resistance to compaction. Parts of the siderite have been oxidised to goethite (brown staining to the crystals). Photo length is equivalent to 1.3mm.

C) A single berthierine ooid seen under crossed polars, specimen DRAG. 31.36A. The ooid is orientated to show that the arms of the extinction cross are not perpendicular, nor parallel, to the analyser or polariser direction (which correspond to the edges of the photograph), when the ooid long axis is also oblique to these directions. Photo length is equivalent to 0.7mm.

D) Berthierine peloids within the "Snap Band", specimen Y183. 8. These peloids are formed of berthierine mud, and lack any laminated internal structure. Their size is similar to the ooids (here plucked in thin-section preparation), but are believed to be of a different origin (possibly faecal). Photo length is equivalent to 3.3mm.

A	B
C	D

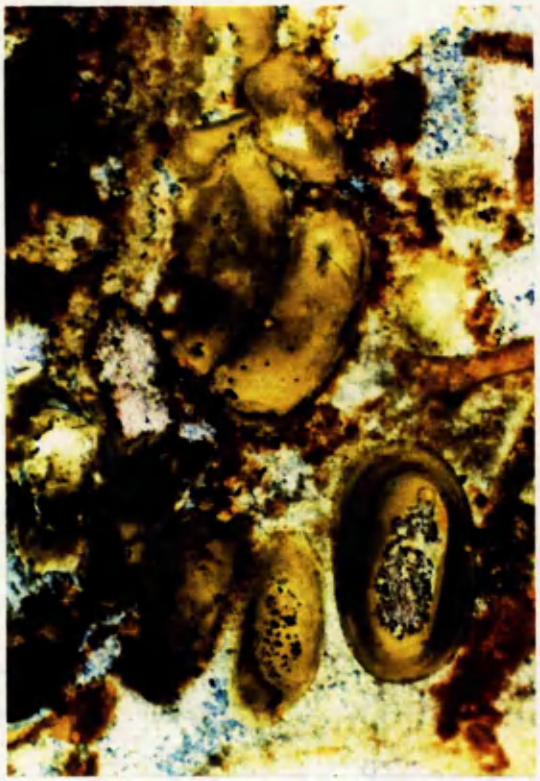

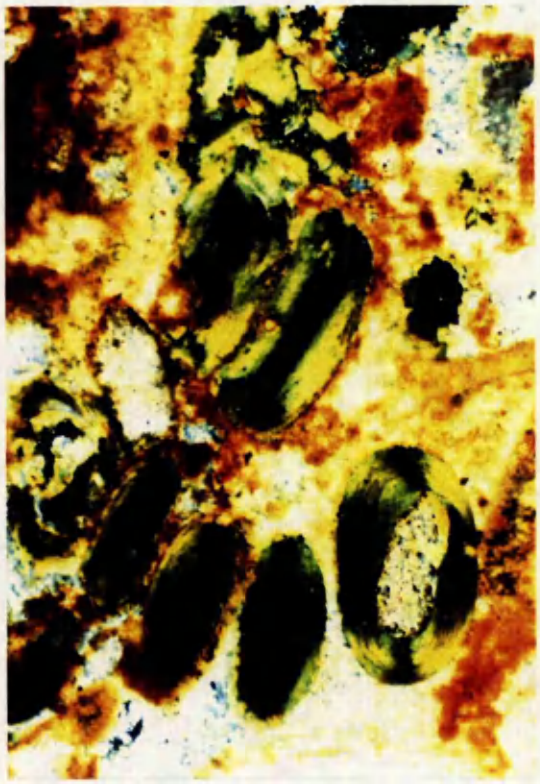

within ooid cortices of this ironstone-formation. Though the fabric is apparently tangential, the aligned particles as described may not be single crystals (found to be <0.1μm long by Hughes 1987, 1989), and may therefore represent aggregates within which the orientation could be radial. It is important to distinguish between tangential and radial fabrics in ooid cortices, as these fabrics have been proposed as resulting from mechanical particle accretion, and precipitation modes of growth respectively.

The apparent orientation of crystals in the ooid cortex, can be tested in thin-section using a quartz tint plate, assuming that the fast and slow vibration directions of a berthierine crystal are known. The optical properties of berthierine have not been fully described, but radial spherules of berthierine in the Raasay Ironstone; berthierine flakes in the Cleveland Ironstone Formation; and authigenic pore-lining berthierine in the Frodingham Ironstone Formation, all show berthierine to have the slow vibration direction parallel to the long crystal diameter in thin-section. By insertion of a tint plate, it was possible to suggest from the birefringence colour pattern, that the crystals are aligned with the slow vibration direction parallel to the lamination, and that the ill-defined orientation is tangential rather than radial. However, the complex diagenetic history of the ironstone-formation means that this cannot be assigned with confidence to a primary texture, as later recrystallisation and fabric modification cannot be ruled out.

The extinction cross present within berthierine ooids viewed under crossed-polars, has a further implication for ooid genesis. When the ooid is aligned with the longest diameter parallel to the analyser or polariser direction, the extinction cross has a 90° rotational symmetry. If the stage is then rotated by 45° to this, the cross becomes flattened, with both arms of the cross in the same quadrant as the longer axis (figure 3.1, plate 6c). This is consistent with a crystal orientation parallel, or normal, to the lamination at that point. If each successive layer had been precipitated syntaxially with that of the last, then this fabric could not form. This therefore means that the accretion process that operated in iron-ooids was such that accreted particles (by whatever mechanism), were orientated with respect to

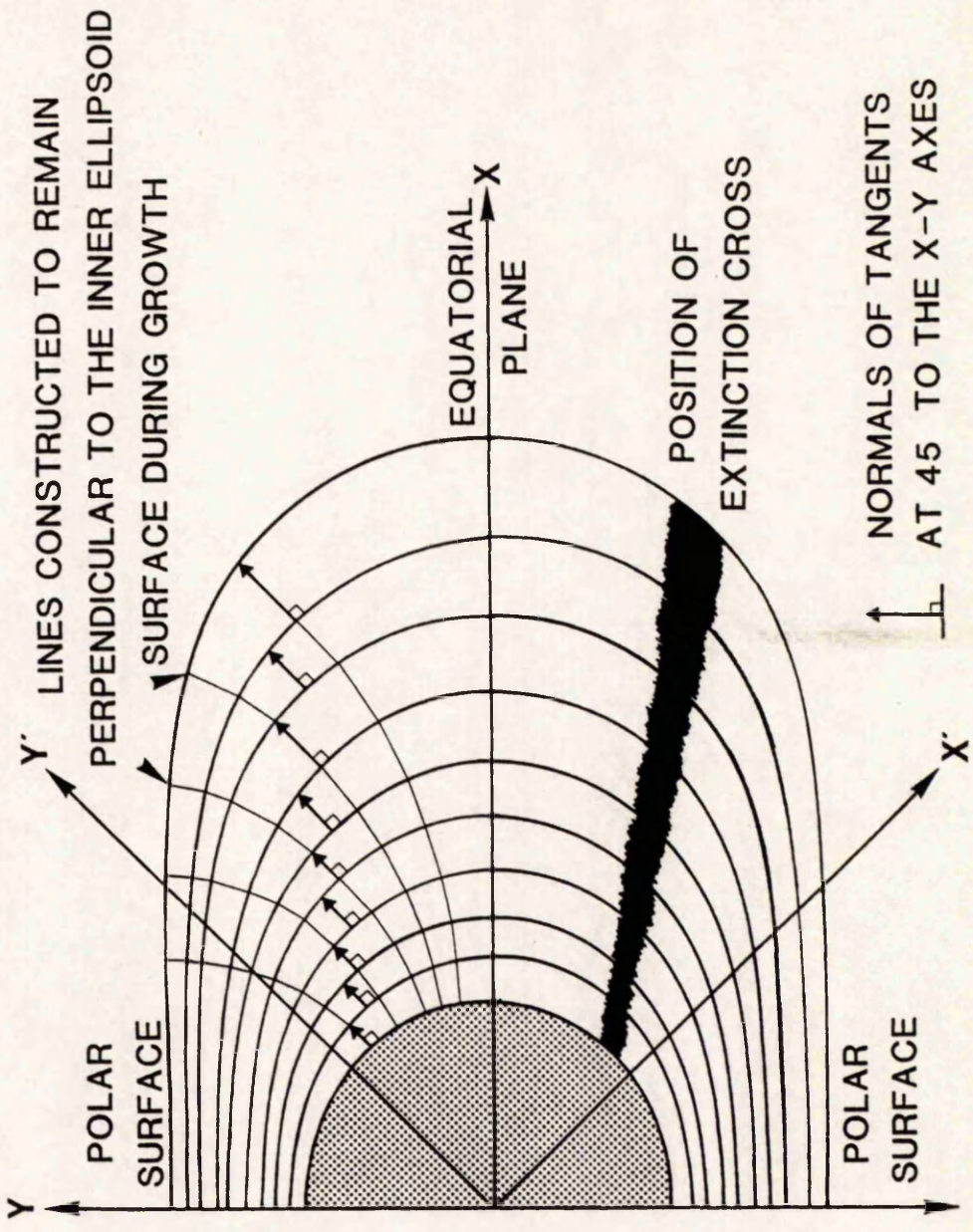

Figure 3.1. Diagrammatic Representation of Half a Berthierine Ooid to Show how the Orientation of the Extinction Cross Changes on Rotation in Thin-Section.

With the analyser and polariser crossed and parallel to X and Y, the ooid in the orientation shown yields an extinction cross in the X and Y directions.

With the analyser and polariser orientated at 45° to the above at X' and Y', the orientation of the extinction cross is as shown, and at an angle to X' and Y'. The reason for this can be seen in the top quadrant where lines have been constructed to remain perpendicular to the ellipsoid, that are parallel to Y'. Crystals parallel or perpendicular to the arrows within these lines, would be in extinction at this time.

the surface morphology at that time, and are apparently unaffected by the crystal orientation present in that surface. The implications of this are discussed later in this chapter.

Within Y183. 8, ooid sized elongate particles may be seen, whose internal structure is similar to that of the matrix in which they are present (plate 6d). Their similarity in shape to the ooids suggested a possible genetic link, but no further comparison exists and they are best termed peloids. Since they are restricted to one thin-section, it is unlikely that they represent ooid-precursors, and are more likely to be of a faecal origin or reworked mud clasts. Their composition was however obtained, and is described below in section 4.5.

3.2.3) Goethite Ooids.

Ooids composed of predominantly goethite are abundant in the ironstones, and are absent only in highly reworked coquinas, mud drapes, and much of the "Snap Band". The ooids may be opaque in thin-section (plate 4 b,c), so that examination of the structure is possible only in reflected light. More commonly the ooid cortex consists of alternating light and dark laminae of mixed goethite and berthierine, of which the latter provides the lighter colour (plate 7). The laminae that contain higher proportions of berthierine show a tangential fabric and may yield an extinction cross under crossed-polars, as for berthierine ooids. The laminae are generally continuous, appearing thicker than berthierine ooids, but these thick laminae are seen under high power to be defined by a number of mineralogically similar, thinner units. The colour of the laminae does not change significantly around the cortex, and dense opaque layers are not seen to pass into lighter areas. This shows that the proportion of goethite and berthierine within the laminae does not change significantly around the cortex. The internal fabric of these ooids is discussed in detail later, but some typical textures seen within goethite ooids are shown in figure 3.2.

Most goethitic ooids possess a distinct nucleus, with only a small proportion that apparently do not have when viewed in thin-section. Those ooids without a nucleus can usually be seen to have been obliquely sectioned, by the increasing lamination thickness towards the centre of the ooid, and diffuse interior. The nuclei are most commonly particles

PLATE 7

Photomicrographs of Goethitic Ooids

A) Ooids of goethite and berthierine with obvious nuclei of goethite particles, specimen DRAG. 31.28. Note the fracturing within the particles (arrowed), and the complex cortical development in these ooids. The cements are as described for plate 13. Photo length is equivalent to 1.3mm.

B) Goethitic ooids in a ferroan calcite cemented grain-ironstone, specimen YAR. 7. Nuclei of goethite particles, broken ooids and bioclasts are present within the ooids The specimen has been over-stained to reduce contrast between the cement and the ooids. Photo length is equivalent to 3.3mm.

C) A single ooid showing a clear stage two and stage three accretion pattern, specimen YAR. 7 (over-stained). The transition between the two stages (arrowed) is marked by the onset of more significant accretion on the polar surface. Photo length is equivalent to 0.7mm.

D) Area of specimen YAR. 7 (over-stained), showing two ooids (1) and (2) which possess a similar pattern of accretion to that shown in **C**. Photo length is equivalent to 1.3mm.

A	**B**
C	**D**

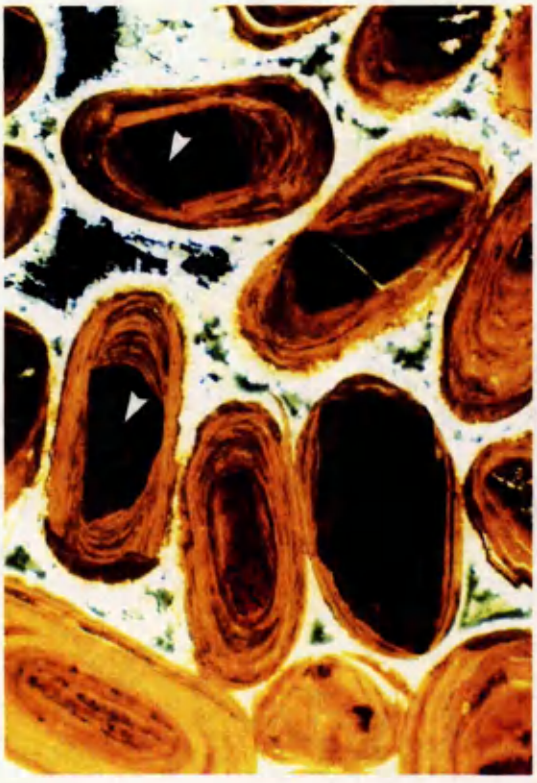

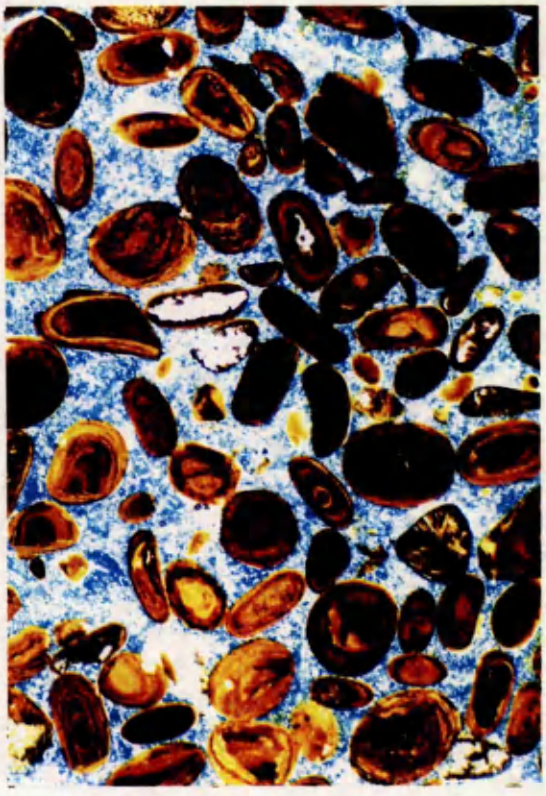

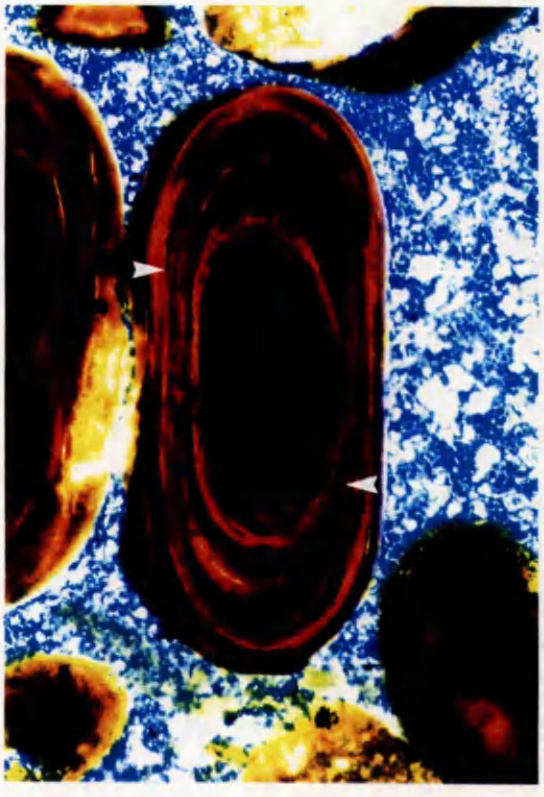

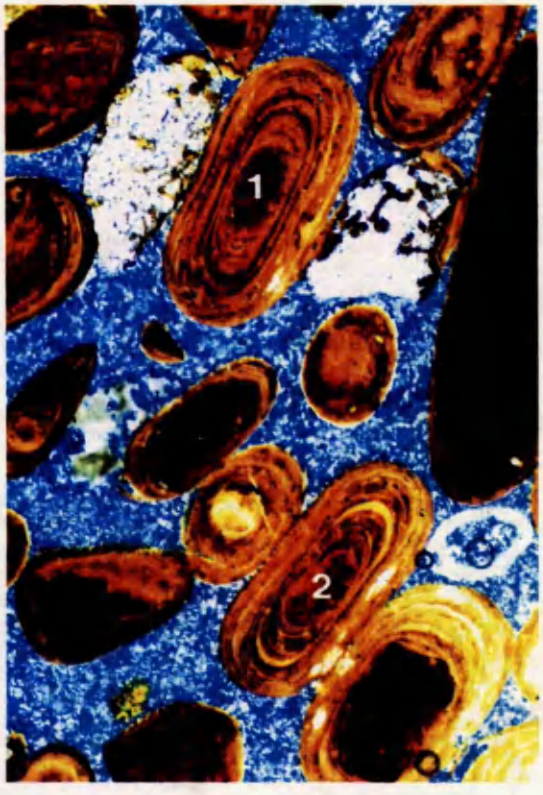
1
2

Figure 3.2. Examples of the Fabrics and Internal Textures of Goethitic Iron-Ooids of the Frodingham Ironstone Formation.

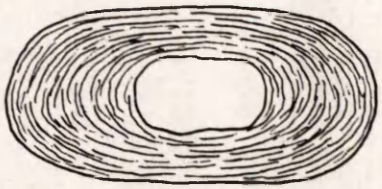

SINGLE STAGE ACCRETION LEADING TO THE FORMATION OF AN OBLATE SPHEROIDAL OOID.

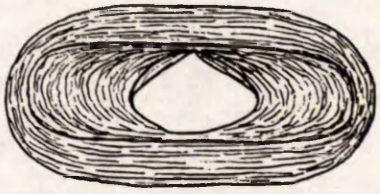

THREE STAGE ACCRETION, OF INITIAL NUCLEUS ROUNDING; PREFERRED ACCRETION FORMING AN EQUATORIAL PLANE; AND DOMINANT POLAR ACCRETION INCREASING SPHERICITY.

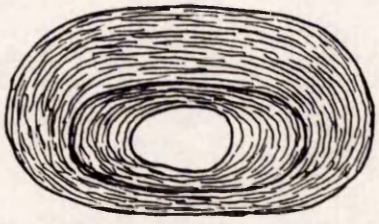

TWO STAGE GROWTH PATTERN, WITH THE LATTER STAGE SHOWING MARKED ASYMMETRY.

TWO STAGE GROWTH PATTERN IN WHICH THE OOID EQUATORIAL PLANE HAS BEEN ROTATED DURING ACCRETION.

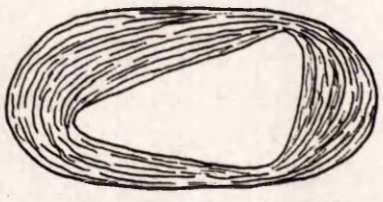

ACCRETION UPON AN ASYMMETRIC NUCLEUS. PREFERRED ACCRETION HAS OCCURRED ON THE AREAS OF LEAST CURVATURE OF THE NUCLEUS.

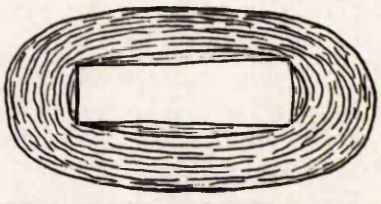

TWO STAGE ACCRETION ON A RECTANGULAR NUCLEUS. THE EARLIEST ACCRETION INCREASES THE ROUNDNESS, PRIOR TO THE MAJOR ELLIPSOIDAL ACCRETION.

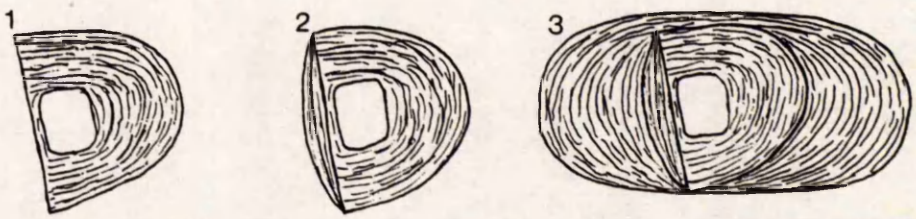

DEVELOPMENT OF AN OBLATE SPHEROIDAL OOID FROM A NUCLEUS OF A PREVIOUSLY FRACTURED OOID. ALL STAGES MAY BE SEEN INDIVIDUALLY. THE ORIGINAL NUCLEUS (1) HAS PREFERENTIAL ACCRETION ON THE BROKEN SURFACE TO INCREASE THE ROUNDNESS AND SPHERICITY (2). FURTHER ACCRETION LEADS TO THE DEVELOPMENT OF AN EQUATORIAL PLANE (3), AS SHOWN FOR THE ABOVE EXAMPLES.

of dense unstructured goethite (plate 7a), or fragments of broken ooids. Bioclastic nuclei are uncommon, and are usually a shell fragment or foraminiferida, or rarely echinoderm grains (see plate 7b). The broken ooid nuclei are similar in all respects to that of the ooids themselves, but neither the broken ooids nor the goethitic particles are found in any significant quantity as individual grains within the ironstones. Large partially broken goethitic ooids may also be seen with a small amount of accretion occurring on the broken surface only. The particles of goethite acting as nuclei (plate 7a) may be dense, massive, and opaque to translucent with a weak to well formed fracture pattern. Such fracturing is similar to that seen in lateritic goethites, which formed due to shrinkage during desiccation, and has led some authors to suggest a lateritic origin to these particles. A shrinkage mechanism has also been implied for the generation of broken ooids (Adeleye 1975). He proposed that shrinkage fracture planes would have formed in the ooids as a result of desiccation, weakening the ooid and aiding subsequent breakage, as opposed to simple collision fracturing in high energy environments. This may also be true for the Frodingham ooids, as although broken ooids occur which form ooid nuclei, there is no sign of significant ooid fracture even in the grain-ironstones that represent the highest energies of depositition.

The fabric of goethitic ooids within rock chips was examined using Scanning Electron Microscopy (S.E.M.) by secondary electron imaging (see appendix A.1.4). This showed (plate 8) that within the laminae of the cortex were highly rounded and polished surfaces similar to that of the ooid outer surface. Between these bounding surfaces a fabric of crystal aggregates was observed in which there was no distinctive alignment. Occasionally, authigenic berthierine was seen nucleating on the polished inner surface, possessing a distinct platy structure with crystals growing perpendicular to the substrate. These were apparently unrelated to the ooid fabric as a whole, and are considered to unrepresentative of the overall crystal orientations.

3.2.4) Iron-Ooid Shape and Form Study

The shape of transported sedimentary particles is dependent on many factors involving provenance and mode of transportation. Particle shape is modified by abrasion or accretion

PLATE 8

Scanning Electron Microscopy Photomicrographs

(Secondary Electron Imaging).

A) Detail of a goethitic ooid cortex, specimen YAR. 6. The photo shows polished surfaces between groups of laminae in the cortex, with an undefined orientation of the crystal fabric between these bounding surfaces. Taken at 3000X magnification.

B) Detail of a single lamina within a goethitic ooid cortex, specimen YAR. 7. Polished surfaces are well defined, and a degree of tangential lamination within the cortex is visible between the surfaces. The inner part of the ooid has separated from the outer during breakage of the specimen. Taken at 1000X magnification.

C) Goethitic ooid cortex, specimen YAR. 7. This ooid shows less well defined surfaces within the cortex than **A** or **B**, with little visible lamination present. Taken at 800X magnification.

D) Authigenic berthierine cement, specimen DRAG. 31.28. This photo illustrates the fabric of berthierine cements, which form a platy morphology typical of the chlorite group of clay minerals. The berthierine is post-dated by a single pore-filling crystal of siderite. Taken at 3000X magnification.

A	**B**
C	**D**

to a form more suited to the environment, but may be constrained by rock type and mineralogy. Iron-ooids are generally oblate ellipsoidal in shape, unlike carbonate ooids which are of a generally high sphericity, and ellipsoidal only when the nucleus is elongate or platy The shape of iron-ooids could therefore be related to the environment of formation, particularly as strong evidence will be presented to show that the shape is a primary feature and not related to compaction.

Detailed investigations of iron-ooid shape and form during growth have never been attempted. Previous work has simply referred to ovoid ooids as flattened or squashed, and ooid shape has never been quantified. Knox (1970) recognised a distinct two-stage process of iron-ooid formation in the Winter Gill Ironstone, but did not quantify the growth fabric. For these reasons it was decided to carry out a qualitative and quantitative study of iron-ooid shape, form and growth fabrics. An ooidal grain-ironstone (YAR. 7) containing goethite/berthierine ooids was chosen for the study, as the ooids could be chemically separated, and thin-section examination had showed clear growth fabrics within the ooids. The use of one sample alone, means that the ooids have been naturally sorted, simplifying interpretation that may be complicated by multi-modal distributions often found in less sorted deposits.

3.2.4.1) Iron-Ooid Shape

To extract ooids for measurement, the ooidal grain-ironstone was treated with weak HCl to dissolve the calcite cement. The ooid residue was diluted, poured onto a glass slide and dispersed so that individual ooids did not impinge on each other, and were orientated parallel to the slide. After the water had evaporated, a microscope glass slide with adhesive on one edge was gently lowered onto an ooid to attach it to the edge. By this method, the three mutually perpendicular axes (long (L), intermediate (I) and short (S)) that form the basis to all particle shape analyses, could be measured under the microscope using a graticule. By viewing the slide end on, the long and intermediate diameters could be obtained, with the short diameter measured by viewing the slide face on (see figure 3.3). A lens system with a large depth of field is preferable to reduce error. Fifty ooids from the

Figure 3.3. Methods used to Measure the Long, Intermediate, and Short Axes of Iron-Ooids Following Separation From the Rock Matrix.

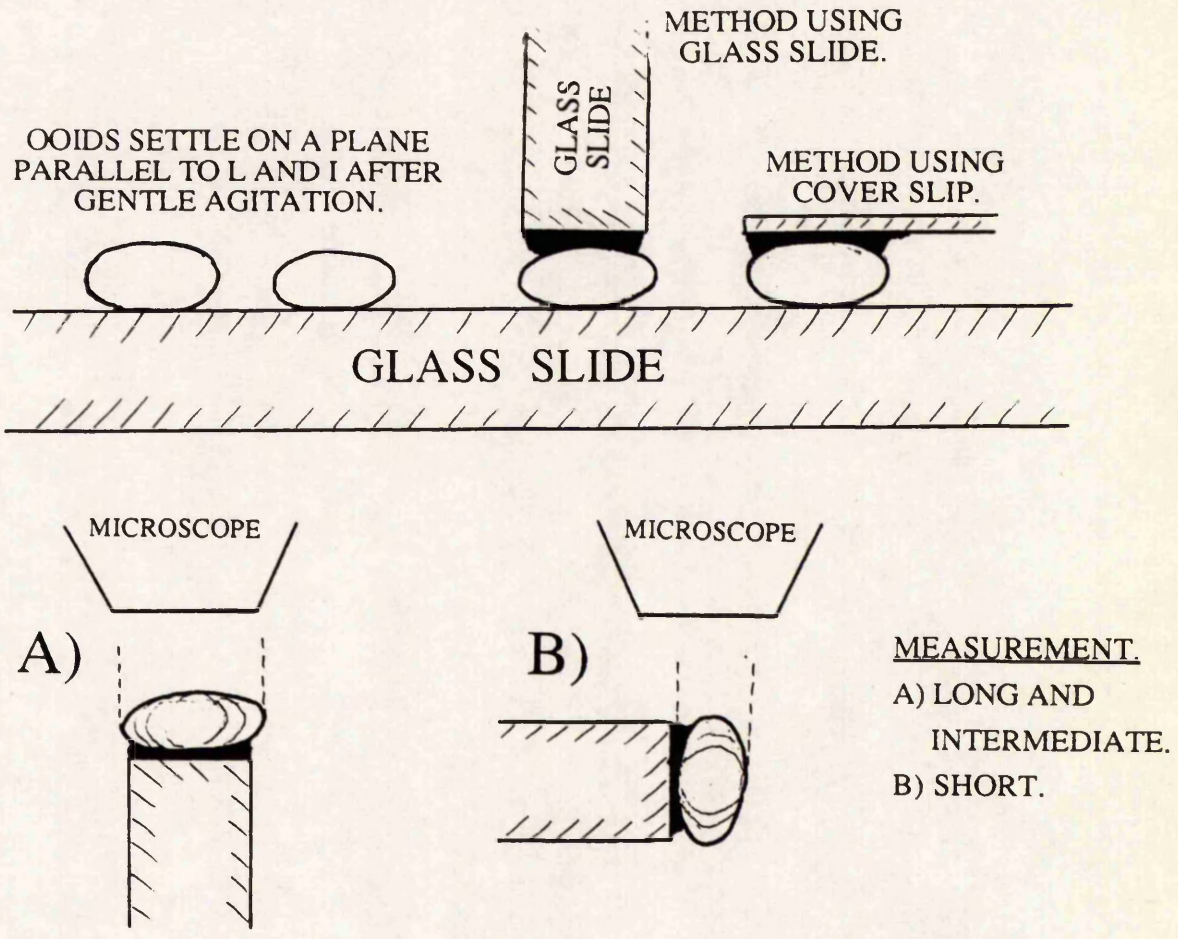

Figure 3.4. Zingg Plot Showing the Characteristics of each Class Within the Diagram. Taken From Tucker (1981).

CLASSES.

A) PLATY (DISC SHAPED).
B) EQUANT (SPHERICAL).
C) BLADED.
D) PROLATE (ROD SHAPED).

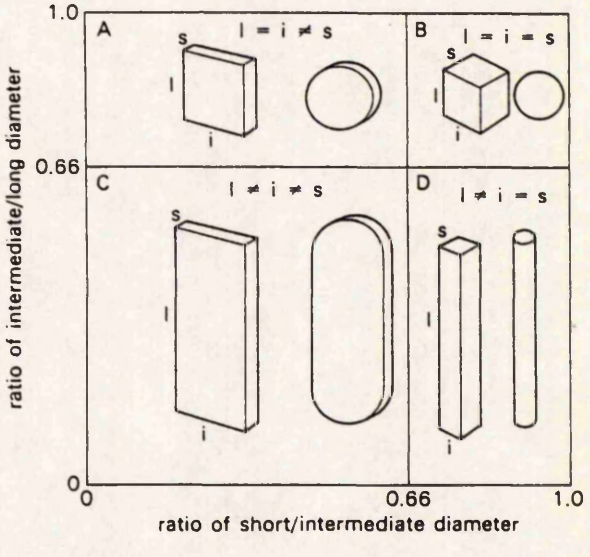

Frodingham grain-ironstone were separated and measured by this method, and a further fifty were measured from the Abbotsbury Ironstone (locality 1), where a 'sand' of residual ooids occurs on weathering. The measurements are given in tables 3.1 and 3.2

Many parameters have been defined to describe aspects of particle shape or form. In those defined on a theoretical basis (for example using the particle surface area), many methods have also been employed to estimate the true value from easy to measure parameters such as L, I, and S. These methods have been reviewed by Barrett (1980) who indicates that no one parameter can be devised to fully characterise the shape of a rock particle. Each parameter relates measurements to a reference standard, or defines a specific change in form. The data obtained in the iron-ooid study have been used to calculate various parameters designed to quantify aspects of form that have been used in the literature (see tables 3.1 and 3.2). For comparison, some standard shapes with simple axial ratios have been added. These shape parameters will be used to specifically define iron-ooid shape below. The formulas used to define each shape parameter with their significance are:

Wentworth (1922)

Flatness. $\frac{L+I}{2*S}$

This parameter measures flatness described by a high L and I relative to a low S.

Luttig (in Sames 1966)

Elongation. $\frac{I*100}{L}$

Flatness. $\frac{S*100}{L}$

Form is expressed using two parameters, elongation and flatness, taking the long axis as the reference.

Sneed and Folk (1958)

Flatness. $\frac{S}{L}$

Table 3.1. Average Size Data and Shape Parameters Calculated for 50 Measured Iron-Ooids, Sample YAR. 7., Frodingham Ironstone Formation, in Comparison with Standard Shapes. See Text for Calculation Formulae.

OOIDS (n=50)	LONG (mm)	INTERM.(mm)	SHORT (mm)	NOMINAL DIAMETER	WENTWORTH 1922 Flatness Index	ZINGG 1935 I/L	S/I	LUTTIG 1966 Elongation	Flatness	SNEED&FOLK 1958 Flatness	Flatness*I
AVERAGE	0.29	0.25	0.17	0.23	1.65	0.88	0.67	87.65	58.44	0.58	0.30
STDEV	0.05	0.04	0.03	0.03	0.29	0.08	0.10	7.56	8.66	0.09	0.18
MAXIMUM	0.47	0.40	0.24	0.34	3.08	1.00	0.90	100.00	80.00	0.80	0.83
MINIMUM	0.22	0.15	0.10	0.16	1.19	0.68	0.37	68.18	29.21	0.29	0.00
TEST DATA	1.00	1.00	1.00	1.00	1.00	1.00	1.00	100.00	100.00	1.00	(n.c.)
	2.00	1.00	1.00	1.26	1.50	0.50	1.00	50.00	50.00	0.50	1.00
	2.00	2.00	1.00	1.59	2.00	1.00	0.50	100.00	50.00	0.50	0.00
	3.00	1.00	1.00	1.44	2.00	0.33	1.00	33.33	33.33	0.33	1.00
	3.00	2.00	1.00	1.82	2.50	0.67	0.50	66.67	33.33	0.33	0.50
	3.00	2.00	2.00	2.29	1.25	0.67	1.00	66.67	66.67	0.67	1.00
	3.00	3.00	1.00	2.08	3.00	1.00	0.33	100.00	33.33	0.33	0.00
	3.00	3.00	2.00	2.62	1.50	1.00	0.67	100.00	66.67	0.67	0.00

OOIDS (n=50)	KRUMBEIN 1941 Intercept Sph.	SNEED&FOLK 1958 Max.Proj.Sph.	ASCHENBRENNER 1956 Working Sph.	DOBKINS&FOLK 1970 Obl.Prol.Index	ASCHENBRENNER 1956 Shape Factor F	WILLIAMS 1965 Shape Factor	Calculations for Sneed-Folk Diagram X	Y	Z
AVERAGE	0.80	0.73	0.91	-3.55	0.77	0.23	58.44	29.21	12.35
STDEV	0.05	0.07	0.03	3.05	0.16	0.15	8.66	9.27	7.56
MAXIMUM	0.90	0.89	0.95	5.30	1.32	0.54	80.00	50.56	31.82
MINIMUM	0.62	0.47	0.79	-8.55	0.46	-0.24	29.21	6.58	0.00
TEST DATA	1.00	1.00	0.96	(n.c.)	1.00	0.00	100.00	(n.c.)	(n.c.)
	0.63	0.79	0.86	10.00	2.00	-1.00	50.00	0.00	50.00
	0.79	0.63	0.88	-10.00	0.50	0.50	50.00	50.00	0.00
	0.48	0.69	0.74	15.00	3.00	-2.00	33.33	0.00	66.67
	0.61	0.55	0.82	0.00	0.75	0.25	33.33	33.33	33.33
	0.76	0.87	0.92	7.50	1.50	-0.50	66.67	0.00	33.33
	0.69	0.48	0.80	-15.00	0.33	0.67	33.33	66.67	0.00
	0.87	0.76	0.93	-7.50	0.67	0.33	66.67	33.33	0.00

Table 3.2. Average Size Data and Shape Parameters Calculated for 50 Measured Iron-Ooids, Locality 1, Abbotsbury Ironstone, in Comparison with Standard Shapes. See Text for Calculation Formulae.

OOIDS (n=50)	LONG (mm)	INTERM.(mm)	SHORT (mm)	NOMINAL DIAMETER	WENTWORTH 1922 Flatness Index	ZINGG 1935 I/L	S/I	LUTTIG 1966 Elongation	Flatness	SNEED&FOLK 1958 Flatness	Flatness*I
AVERAGE	0.49	0.42	0.21	0.35	2.23	0.85	0.52	85.45	43.60	0.44	0.28
STDEV	0.06	0.08	0.07	0.06	0.51	0.10	0.15	9.56	10.29	0.10	0.21
MAXIMUM	0.70	0.60	0.58	0.62	3.91	0.99	0.97	99.10	83.45	0.83	0.96
MINIMUM	0.38	0.27	0.12	0.27	1.12	0.55	0.28	54.95	23.23	0.23	0.02
TEST DATA	1.00	1.00	1.00	1.00	1.00	1.00	1.00	100.00	100.00	1.00	(n.c.)
	2.00	1.00	1.00	1.26	1.50	0.50	1.00	50.00	50.00	0.50	1.00
	2.00	2.00	1.00	1.59	2.00	1.00	0.50	100.00	50.00	0.50	0.00
	3.00	1.00	1.00	1.44	2.00	0.33	1.00	33.33	33.33	0.33	1.00
	3.00	2.00	1.00	1.82	2.50	0.67	0.50	66.67	33.33	0.33	0.50
	3.00	2.00	2.00	2.29	1.25	0.67	1.00	66.67	66.67	0.67	1.00
	3.00	3.00	1.00	2.08	3.00	1.00	0.33	100.00	33.33	0.33	0.00
	3.00	3.00	2.00	2.62	1.50	1.00	0.67	100.00	66.67	0.67	0.00

OOIDS (n=50)	KRUMBEIN 1941 Intercept Sph.	SNEED&FOLK 1958 Max.Proj.Sph.	ASCHENBRENNER 1956 Working Sph.	DOBKINS&FOLK 1970 Obl.Prol.Index	ASCHENBRENNER 1956 Shape Factor F	WILLIAMS 1965 Shape Factor	Calculations for Sneed-Folk Diagram X	Y	Z
AVERAGE	0.71	0.60	0.86	-5.82	0.63	0.38	43.60	41.86	14.55
STDEV	0.06	0.10	0.04	4.86	0.27	0.24	10.29	14.72	9.56
MAXIMUM	0.90	0.93	0.95	8.68	1.76	0.65	83.45	60.23	45.05
MINIMUM	0.57	0.40	0.74	-12.01	0.35	-0.43	23.23	1.80	0.90
TEST DATA	1.00	1.00	0.96	(n.c.)	1.00	0.00	100.00	(n.c.)	(n.c.)
	0.63	0.79	0.86	10.00	2.00	-1.00	100.00	0.00	0.00
	0.79	0.63	0.88	-10.00	0.50	0.50	50.00	50.00	0.00
	0.48	0.69	0.74	15.00	3.00	-2.00	100.00	0.00	0.00
	0.61	0.55	0.82	0.00	0.75	0.25	50.00	25.00	25.00
	0.76	0.87	0.92	7.50	1.50	-0.50	100.00	0.00	0.00
	0.69	0.48	0.80	-15.00	0.33	0.67	33.33	66.67	0.00
	0.87	0.76	0.93	-7.50	0.67	0.33	66.67	33.33	0.00

Flatness with I relative to L. $\frac{L-I}{L-S}$

Form is again expressed by two parameters to distinguish the degree of compactness (flatness), and the platy or elongate nature of the particle respectively. The second parameter measures whether the I axis is closer to L or S. The two parameters are usually plotted together in a form triangle.

Krumbein (1941)

Intercept Sphericity. $\sqrt[3]{\frac{I*S}{L^2}}$

This is an approximation of Wadell's (1932) true sphericity, by assuming a triaxial ellipsoidal shape and ratioing its volume to that of the circumscribing sphere. The long axis is used as the reference.

Sneed and Folk (1958)

Maximum Projection Sphericity. $\sqrt[3]{\frac{S^2}{I*L}}$

A parameter designed to express particle behavoir in a fluid, derived from the ratio of a sphere of volume equal to the particle, to that of a sphere with the same maximum projection area. A particle with a Maximum Projection Sphericity of 0.60 has a maximum projection area 1.00/0.60 that of a sphere of equal volume, and will settle at approximately 60% of the spheres velocity. The short axis is the reference axis.

Aschenbrenner (1956)

Working Sphericity. $\frac{12.8*\sqrt[3]{(I/L)^2*(S/I)}}{1+((I/L)*(1+(S/I)))+(6*\sqrt[2]{1+((I/L)^2*(1+(S/I)^2))}}$

True sphericity is defined here as the ratio of the surface area of the particle to that of a reference form. The reference is a tetrakaidekahedron, a plane sided figure thought to be more representative of natural sedimentary particles.

Dobkins and Folk (1970)

Oblate-Prolate Index (O.P.I.). $\frac{(10*((L-I)/(L-S)))-0.5}{(S/L)}$

A parameter designed to combine Sneed and Folks (1958) form triangle parameters. This is then used in conjunction with the Maximum Projection Sphericity to define the form. The O.P.I. defines disks as negative and rods as positive. A true blade will have an O.P.I.= 0.00.

Aschenbrenner (1956)

Shape Factor F. $\frac{L*S}{I^2}$

The shape factor is used in conjunction with the working sphericity to describe variations in form for particles of equal sphericity.

Williams (1965)

Williams Shape Factor. $1-((L*S) / I^2)$ If $I^2 > L*S$

or

$(I^2 / (L*S))-1$ If $I^2 < L*S$

A modification of Aschenbrenners (1956) Shape Factor F to scale it between -1 and +1. From 0 to +1 oblateness increases, 0 to -1 prolateness increases.

The nominal diameter ((L+I+S)/3) was used to indicate the grain-size distribution of the ooids within the specimen (figure 3.5). As expected for a continuously reworked grain-ironstone, the distribution is unimodal and well-sorted with minor skewness. It is therefore apparent that the ooids have been sorted in the same way as any 'normal' sedimentary particle would have been. If the bioclastic content of the rock were added to the histogram, then the distribution would be negatively skewed (coarse tailed), or bimodal, due to the winnowing of fines. This is consistent with deposition in a nearshore high energy environment.

The most common use of particle size measurement of this type of study, is to calculate the S/I and S/L ratios and plot a Zingg (1935) diagram, to represent the shape graphically. This allows a simple quantified description of shape on the basis of the three parameters measured (L, I, and S), by subdividing all possible particle shapes into four classes (oblate, equant, bladed or prolate. See figure 3.4). Diagrams constructed for the Frodingham and Abbotsbury ooids are shown in figure 3.6. These plots show that there is a difference in ooid shape between the Frodingham and Abbotsbury samples, with the Frodingham ooids clustering within the oblate field, but those of the Abbotsbury clustering over the oblate-equant boundary. The Abbotsbury ooids are therefore of a greater sphericity than the Frodingham ones. More specifically, these plots show that most ooids within a given sample are restricted to a given shape, though this cannot be related to ooid size. The

Figure 3.5. Frequency Histograms Showing the Size Distribution of the Measured Frodingham and Abbotsbury Ooids, Using the Nominal Diameter ((L+I+S)/3).

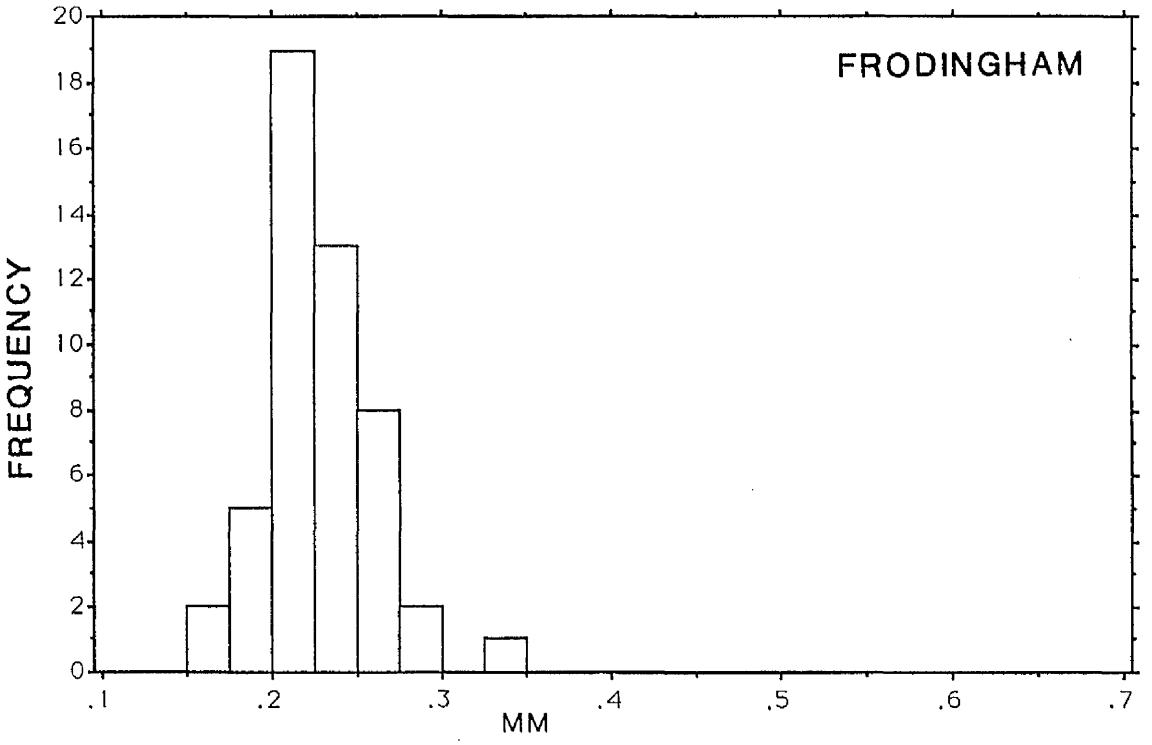

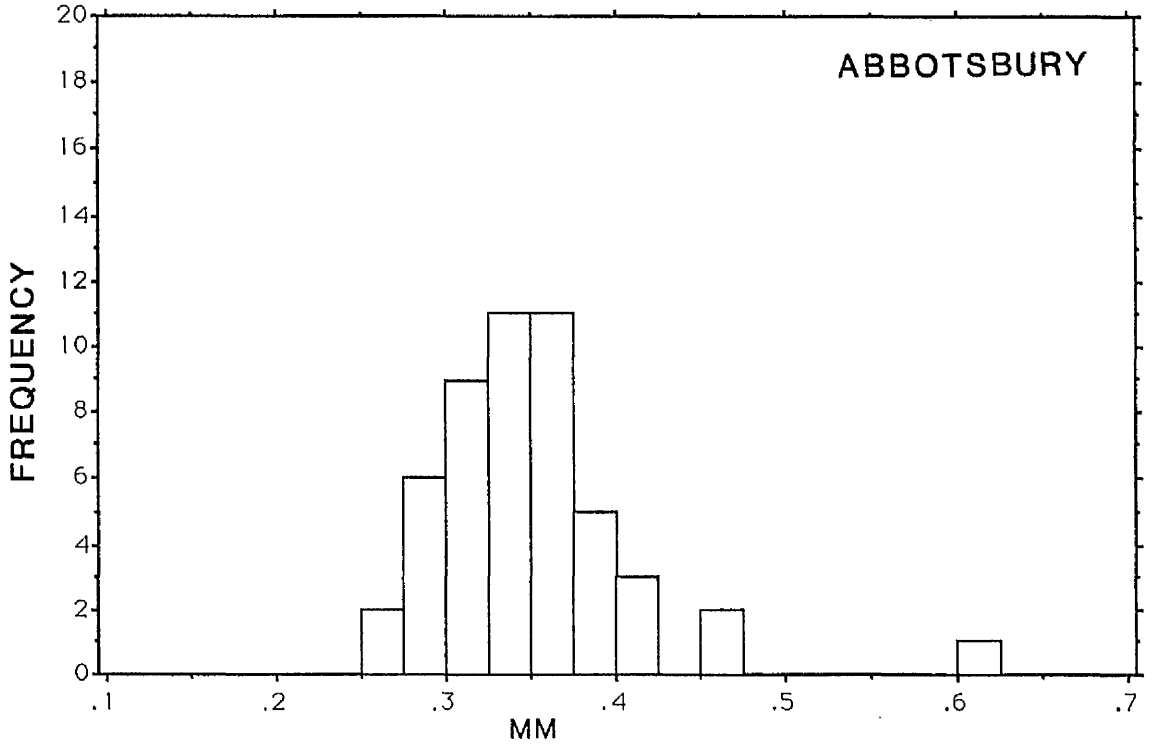

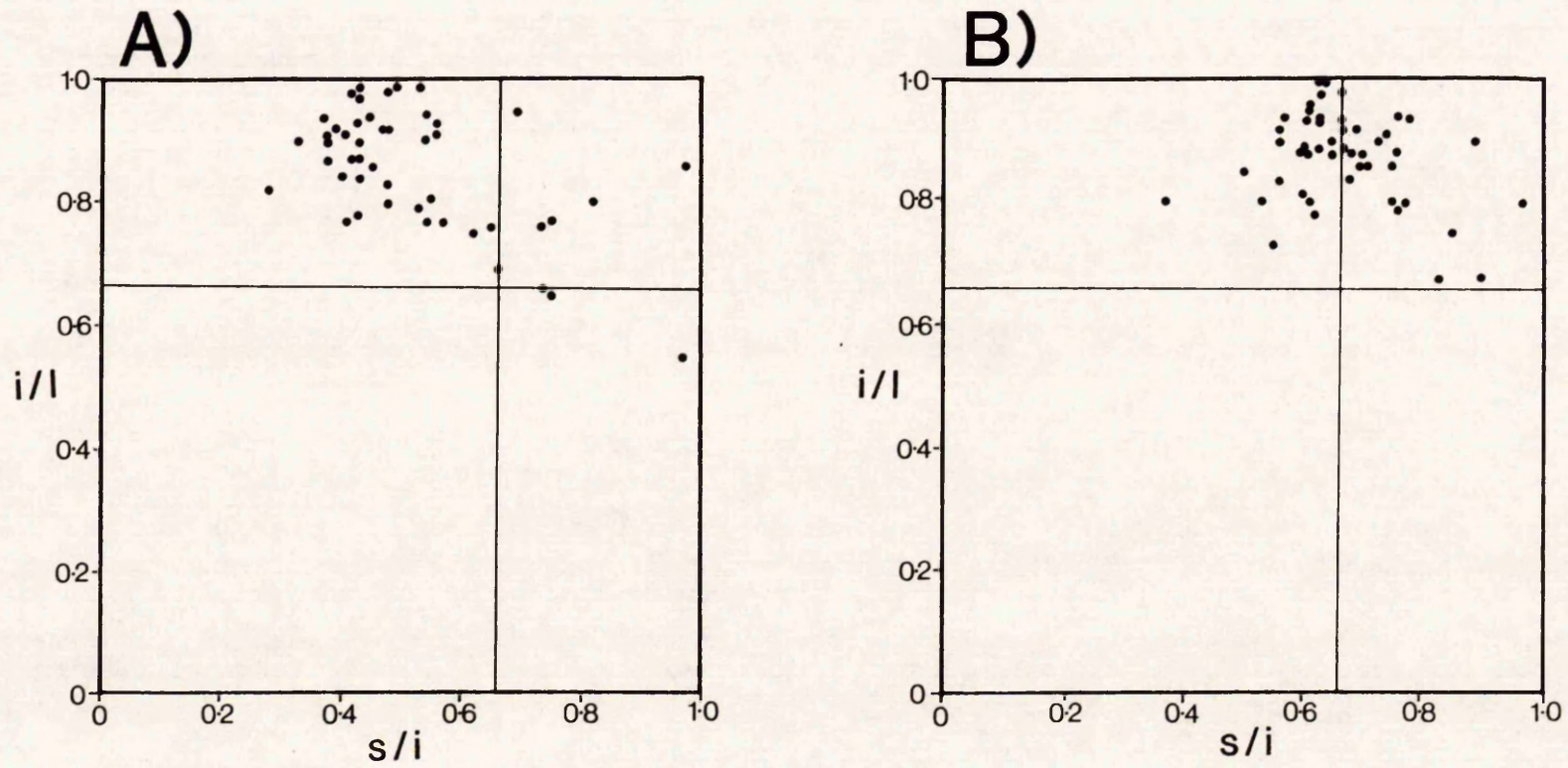

FIGURE 3.6

ZINGG PLOTS OF SEPARATED AND MEASURED OOIDS FROM:

A) FRODINGHAM

B) ABBOTSBURY

s-short, i-intermediate, l-long diameters

clustering suggests that iron-ooid formation is not a random accretion process, but results in a specific oblate to equant shape, with prolate and bladed forms being uncommon.

For a more precise description of shape, a Sneed/Folk Sphericity Form diagram was constructed. A standard triangular plotting program can be used to plot this diagram by the formulas:

$$\text{Top Corner} \quad (X) = ((S/L)*100)$$

$$\text{Lower Right} \quad (Z) = ((L-I)/(L-S))*(100-X)$$

$$\text{Lower Left} \quad (Y) = 100-X-Z.$$

This plot subdivides particle shapes into ten classes, again based upon the three mutually perpendicular axes L, I, and S, but is a much more sensitive indicator of particle form, as it may separate particles of similar sphericity but different form (see review in Barrett 1980).

Diagrams constructed for the Frodingham and Abbotsbury ooids are shown in figures 3.7 and 3.8 respectively. A distinct difference in form between the two sets of ooids is again picked out, with the Frodingham sample dominating the platy field, whereas the Abbotsbury ooids are more compact-platy in shape. As these diagrams are more sensitive to form, the clusters are more open than the Zingg plots, but the distributions do not show distinctive trends. In particular there is no apparent trend between compact and platy ooids within each sample, as would be expected if ooids had undergone progressive compaction from an initial spherical body.

If the data are plotted as a bivarient graph to represent the Sphericity-Form diagram on conventional axes (see Barrett 1980), by plotting Oblate-Prolate Index (Dobkins and Folk 1970) against Maximum Projection Sphericity (Sneed and Folk 1958), a more distinctive trend is seen, and this imparts a certain predictability to ooid shape (figure 3.9). Although there is again much scatter, the data show a trend from platy particles (lower left) to compact-bladed (upper right), with a true bladed particle (Oblate-Prolate Index = 0, (L-I) = (I-S)) occurring at a Maximum Projection Sphericitity of around 0.7. Similarly, the Zingg Plot may be represented by plotting Williams Shape Factor (Williams 1965) against Working

Figure 3.7. Sneed-Folk Sphericity Form Diagram For 50 Ooids of the Frodingham Ironstone Formation.

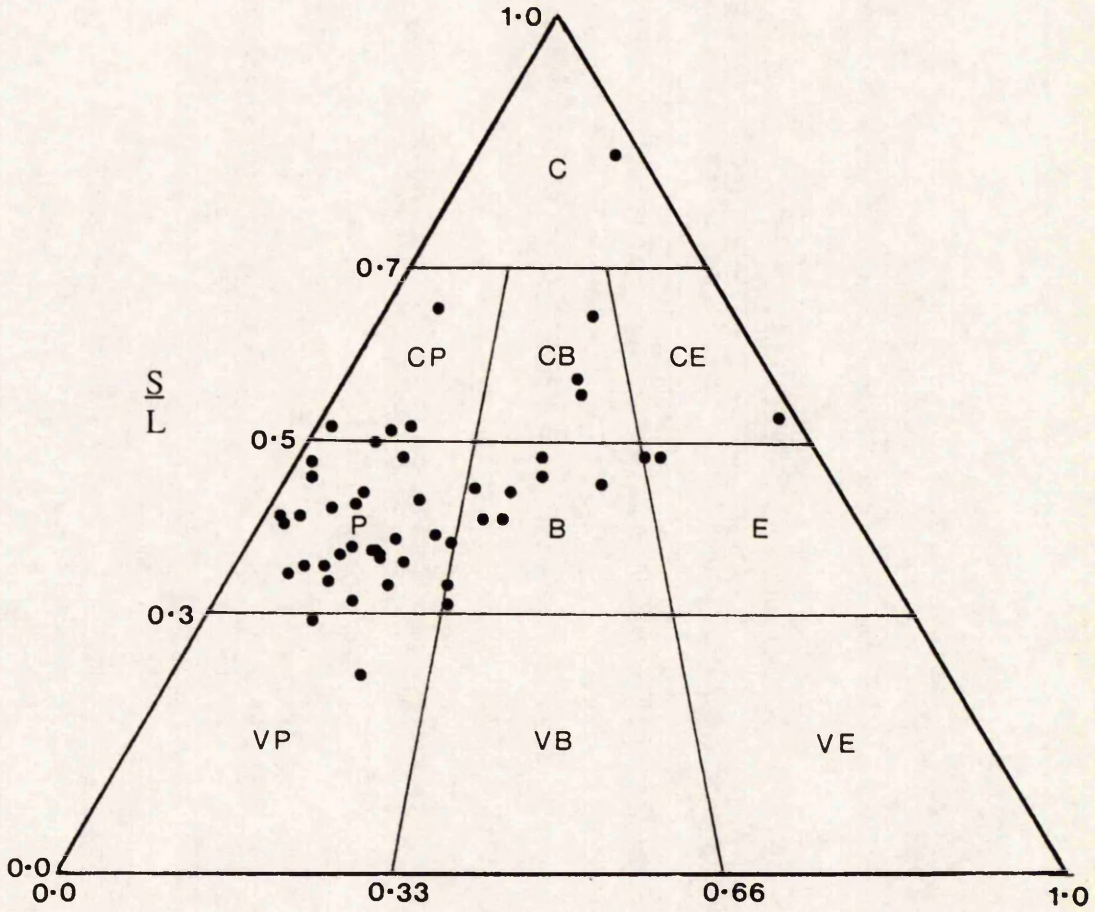

C = Compact. CP = Compact-Platy.

CB = Compact-Bladed. CE = Compact-Elongate.

P = Platy. B = Bladed.

E = Elongate. VP = Very Platy.

VB = Very Bladed. VE = Very Elongate.

L = LONG; I = INTERMEDIATE; S = SHORT DIAMETERS.

Figure 3.8. Sneed-Folk Sphericity Form Diagram For 50 Ooids of the Abbotsbury Ironstone.

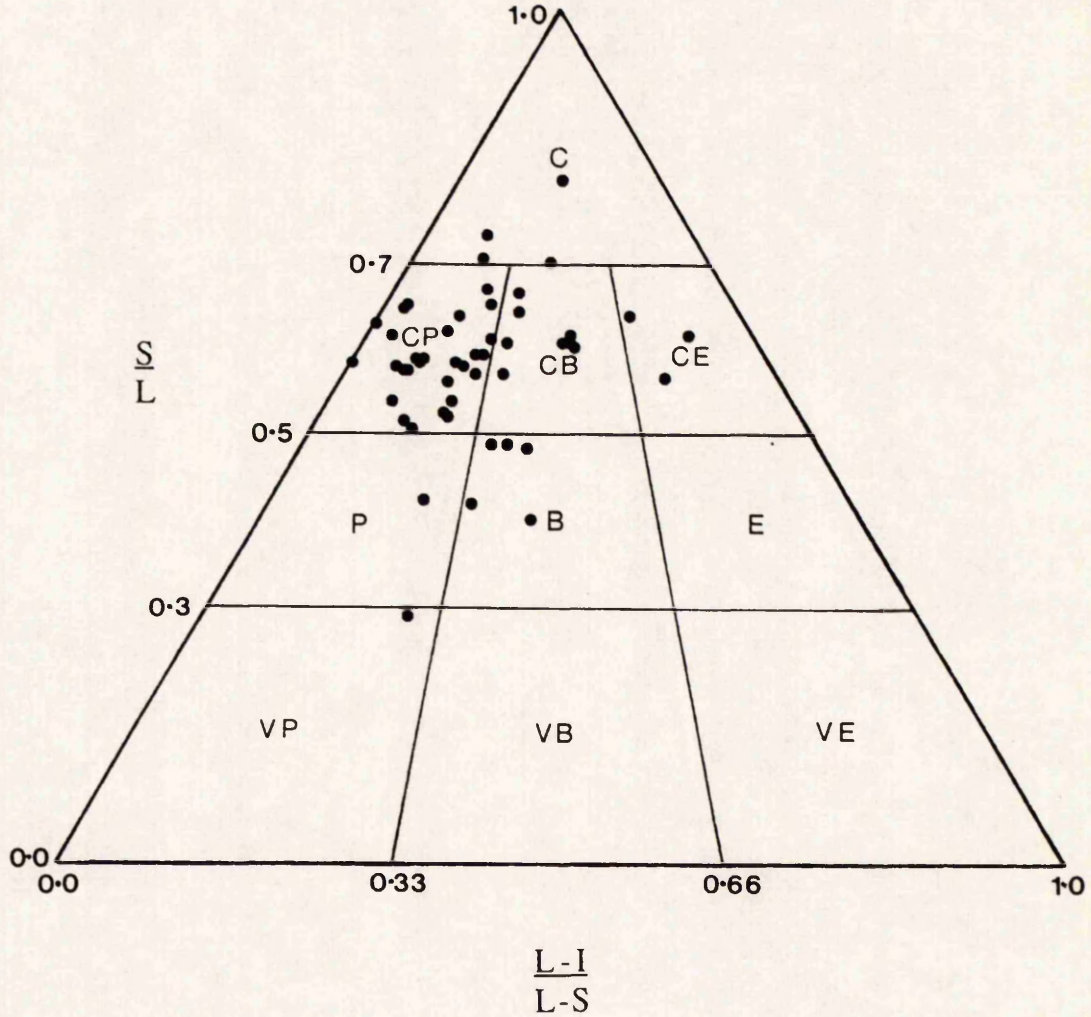

C = Compact. CP = Compact-Platy.

CB = Compact-Bladed. CE = Compact-Elongate.

P = Platy. B = Bladed.

E = Elongate. VP = Very Platy.

VB = Very Bladed. VE = Very Elongate.

L = LONG; I = INTERMEDIATE; S = SHORT DIAMETERS.

Figure 3.9. Oblate - Prolate Index Versus Maximum Projection Sphericity Graph, for Measured Frodingham Ooids, Illustrating the Form Distribution.

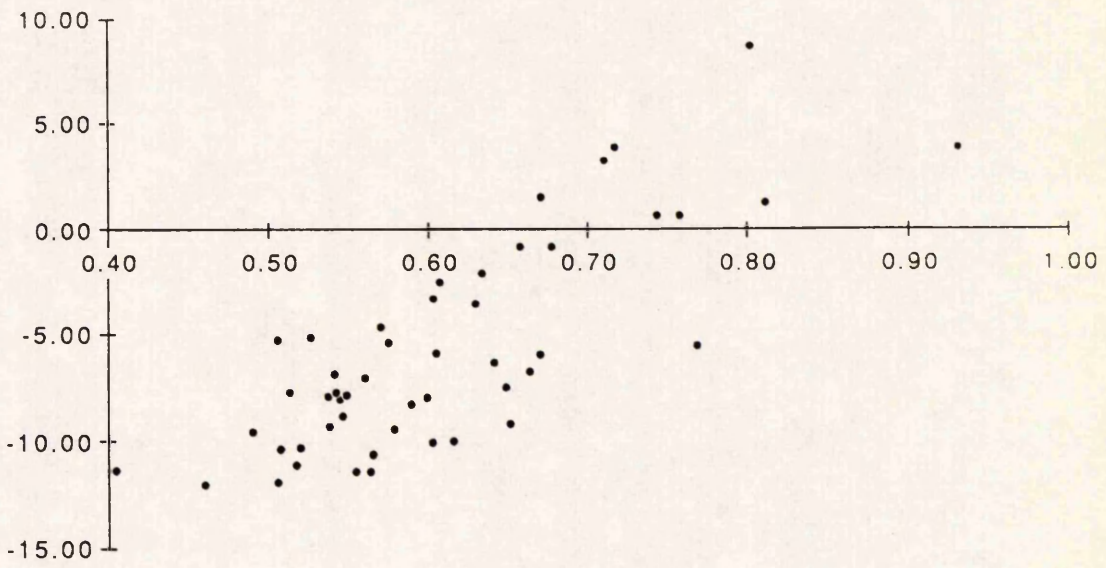

Figure 3.10. Williams Shape Factor versus Working Sphericity Graph, for Measured Frodingham Ooids, Illustrating A Similar Form Distribution to the Above.

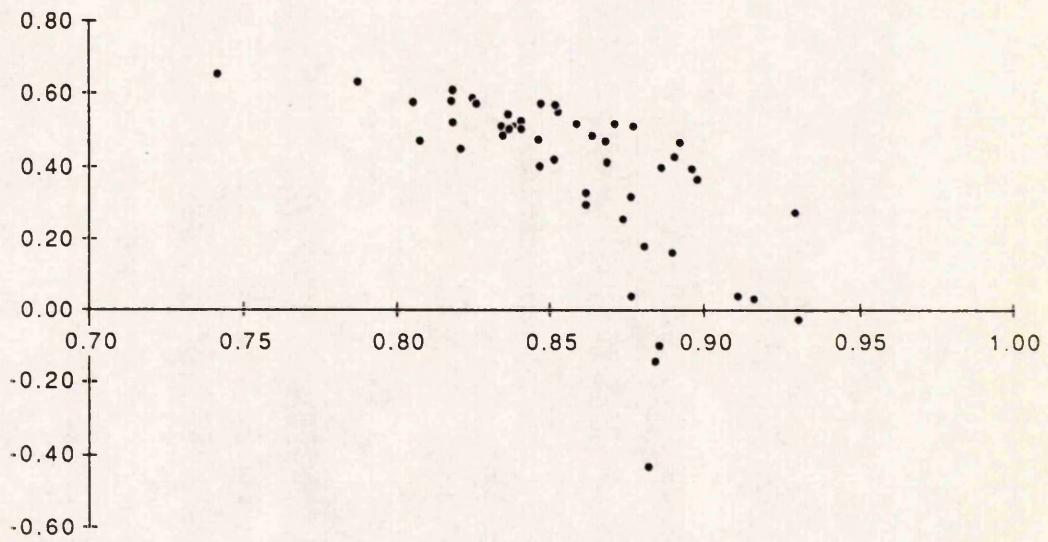

Sphericity (Aschenbrenner 1956) (figure 3.10), and again the trend is good, defining a more specific shape predictability than is expected from the Zingg and Sphericity-Form plots. The plots in figure 3.9 and 3.10 also allow direct comparison of the validity, and usefulness of such diagrams in form analysis. Barrett (1980) concluded the the Maximum Projection Sphericitity and Oblate-Prolate Index were the preferred method for particle shape analysis. This is supported here, for the graph in figure 3.9 shows a much better distribution over a wider range, than that of figure 3.10 for the Williams Shape Factor against Working Sphericity, and is arguably easier to understand.

The above plots have defined a specific shape to the samples of iron-ooids, but cannot show how the shape develops throughout growth. A simple, and easy to understand method of modelling this, is to plot the three axes against each other. This should show which, if any, of the axes is controlling the growth pattern. The 3 plots were constructed and are shown in figures 3.11 and 3.12. Plotting the data in this way should show trends expected during the growth of the ooids, assuming that the smaller ooids would evolve into the larger ones.

During the growth of Frodingham ooids (as L and I increase) there appears to be poor correlation between the short and long (correlation coefficient 0.56), or short and intermediate (correlation coefficient 0.38) axes. The short axis is the hardest to measure accurately, and some of the scatter may be attributed to experimental error. A clear correlation is seen between the intermediate and long axes (correlation coefficient 0.81) in the measured ooids, and that as L and I both increase, they trend towards I=L at around 0.60mm. This possibly suggests that as the particles grow, an initial difference in the nucleus I and L diameters is later removed by accretion. There is however no distinct trend in the S diameter that might allow a predicted shape when I=L.

Ooids from the Abbotsbury Ironstone generally show a better correlation between axes during growth (figure 3.12). The short axis increases with both L and I (correlation coefficients 0.48 and 0.52 respectively) but again the long and intermediate diameters show

FIGURE 3.11

PLOT OF OOID DIMENSIONS
FRODINGHAM IRONSTONE (YAR. 7).

L = LONG AXIS.
I = INTERMEDIATE AXIS.
S = SHORT AXIS.

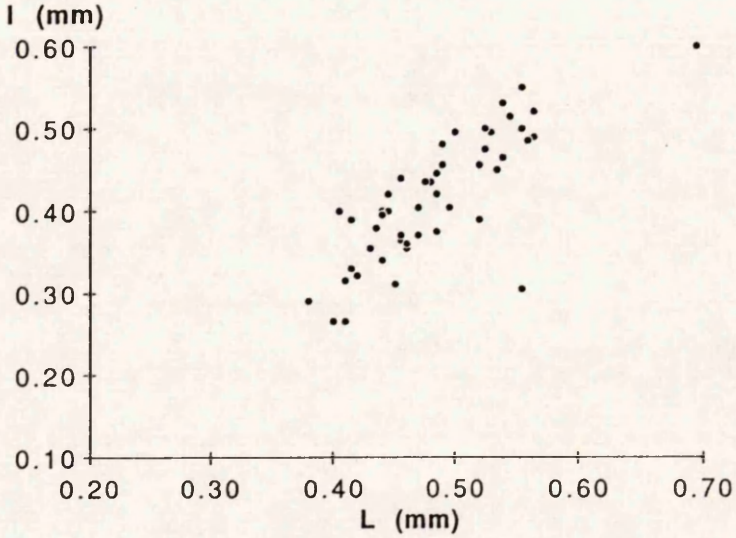

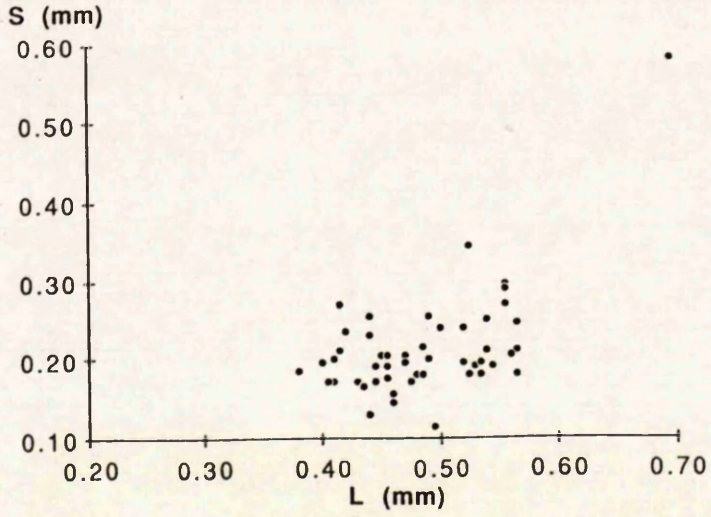

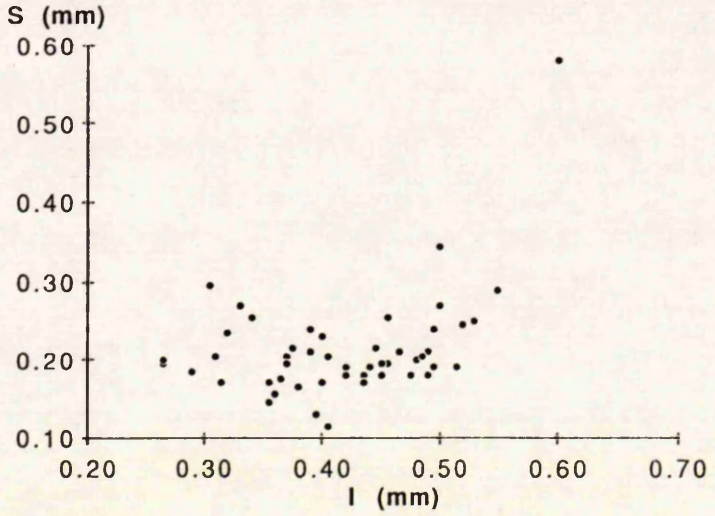

FIGURE 3.12

PLOT OF OOID DIMENSIONS
ABBOTSBURY IRONSTONE (ABB. 1).

L = LONG AXIS.
I = INTERMEDIATE AXIS.
S = SHORT AXIS.

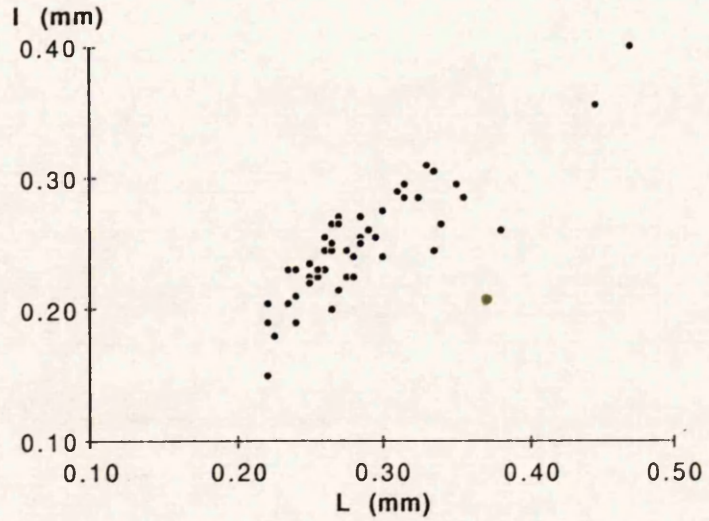

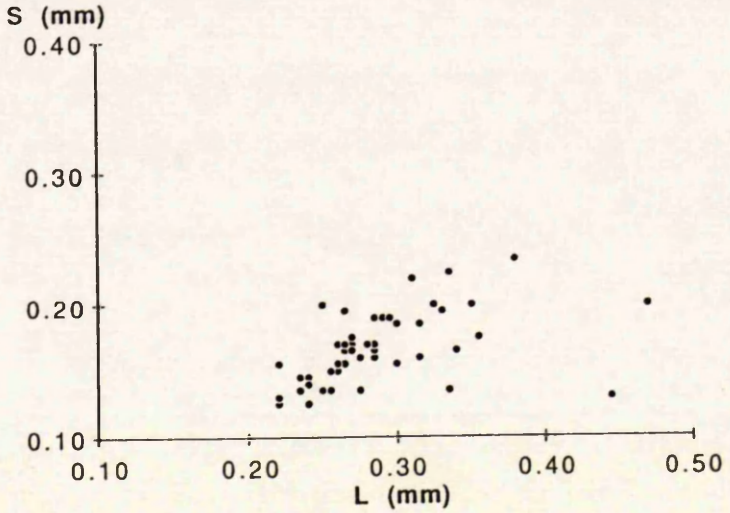

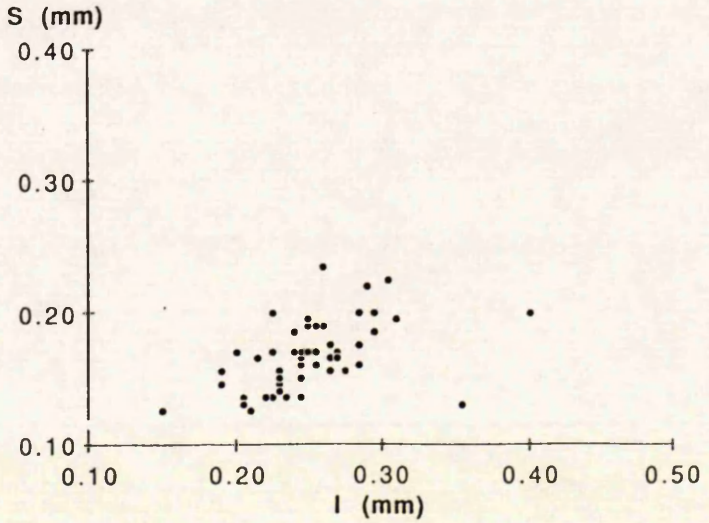

FIGURE 3.13

GROWTH STAGES OF A FRODINGHAM IRONSTONE GOETHITE/BERTHIERINE OOID.

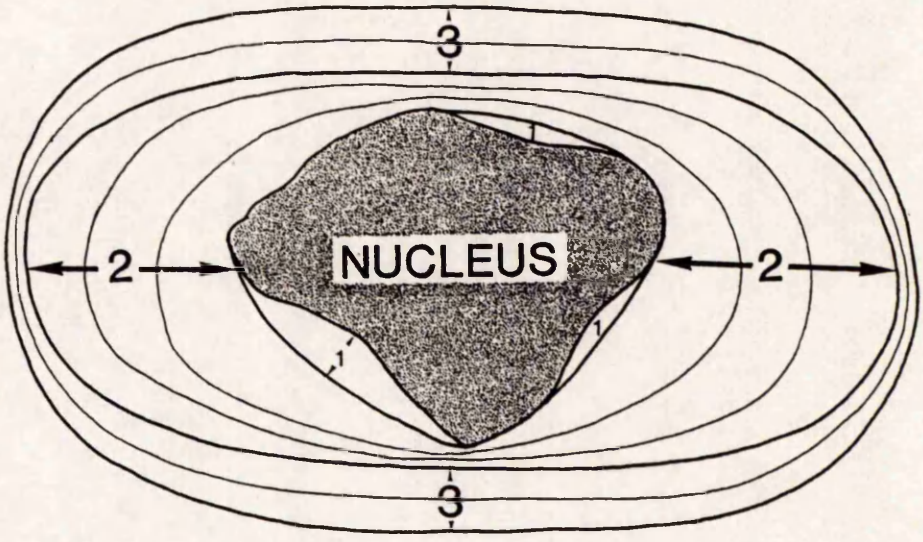

Figure 3.14. Terminology of Iron-Ooid Description Based Largely Upon Knox (1970).

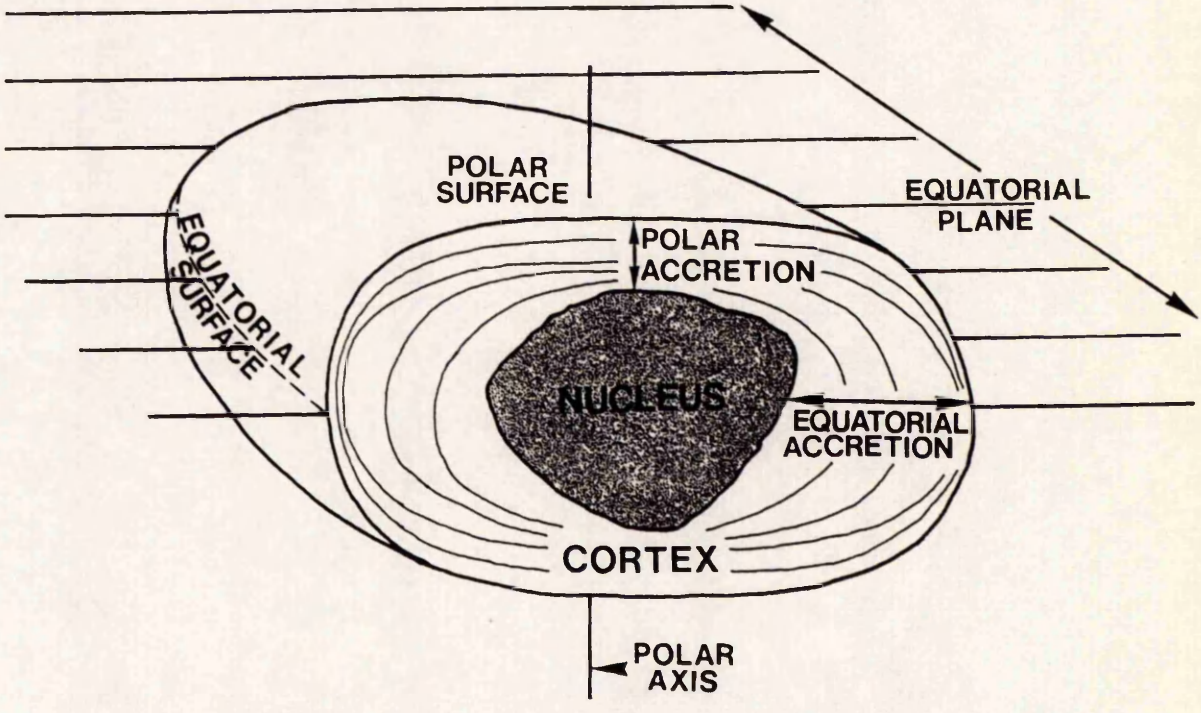

the strongest correlation coeficient of 0.87. It is interesting to note that the slope of the intermediate versus long graphs for both ironstone-formations are similar, at 0.65 for the Frodingham and 0.73 for the Abbotsbury, based on a linear regression.

3.2.4.2) Ooid Growth Fabric

Thin-section examination of iron-ooids reveals a three stage accretion process in many ooids, which is not apparent from ooid shape alone (see figure 3.13, plate 7 c,d). Knox (1971) described a similar fabric in the ooids of the Winter Gill Ironstone, using terms summarised in figure 3.14. These terms are also used here. The first stage of accretion increases the roundness of the nucleus without significantly changing the sphericity. Concave or flat surfaces are preferentially coated to achieve this, with no accretion on pronounced apices, so that continuous laminae around the cortex are not formed. After the cessation of stage one accretion, the degree of particle roundness is always high. Stage one accretion is most conspicuous where the nucleus is of a low initial roundness and sphericity such as a shell fragment.

The second stage is seen in the development of an equatorial plane due to preferred accretion in a single plane, with little or no accretion in the direction perpendicular to this. The plane is not necessarily parallel to the equatorial plane of the nucleus, but is normally close to it particularly where the nucleus is itself oblate or bladed. Accretion is symmetrical around the nucleus in most examples, and is most apparent where the nucleus is small and equant. As accretion continues, a pronounced, flattened polar surface is developed. The stage two process is present to varying degrees in all ooids, and is the most important in terms of volume of material accreted.

The third stage of ooid growth is shown by a sudden switch of preferred accretion from the equatorial plane to the polar surfaces. Accretion on the equatorial plane usually continues, but may be reduced or less commonly absent during this stage. The effect is to increase sphericity, with maximum accretion at the centre of the polar surface, although the shape still remains markedly oblate. Accretion is usually symmetrical on both polar

surfaces, and laminae may be traced continuously across both. This stage is not present in all ooids, and usually forms only a small part of the total accretion.

In order to model the ooid accretion process, measurements were taken from photographs of ooids in thin-section (for example plate 7c). The same sample (YAR. 7) was used as for the ooid shape study so that comparison could be made to the discussions on ooid shape development given above. Ooids were chosen that were cut perpendicular to the equatorial plane so that they would show both equatorial and polar accretion if present. All the ooids showed a visible measurable nucleus of moderate sphericity. The distances from the centre of the ooid to the nucleus edge and various accretion laminae, were measured for a quarter of an ooid. This reduces errors introduced when attempting to correlate laminae around the whole ooid cortex, especially over the polar surface where extensive thinning often occurs.

Using such data obtained from 28 ooids, plots were constructed to examine the following:

a) Differences in total equatorial and polar accretion relative to;

i) Nucleus size.

ii) Final size and size at time of accretion.

b) The stage 2-3 transition relative to;

i) Final size and size at time of transition.

ii) Total accretion at time of transition.

The relative rate of accretion at any instant in the equatorial and polar directions is immeasurable due to inaccuracies in measurement of the small amounts of polar accretion.

The plots produced have certain limitations that need to be mentioned. Firstly, the number of measurements for a single ooid is determined by the number of clearly visible laminae. Secondly, it is assumed that the ooid has been cut at 90° to the equatorial plane, although in reality deviations from this plane will have occurred. Finally, and most significantly, the distinction cannot be made as to whether the long or intermediate diameter is being seen and measured. This will clearly increase scatter in the plots relative to the equatorial accretion.

The variation can however be estimated from the intermediate versus long axis plots of the separated ooids (see section 3.2.4.1), which suggests that I ≈ 0.65 * L. Due to this uncertainty, the measurements are referred to as polar (PLR) and equatorial (EQL), rather than short and long/intermediate diameters.

Graph 1: PLR diameter, against EQL diameter.(Figure 3.15).

The simplest method of graphically representing the accretion process is to plot PLR diameter against EQL diameter. The change in total growth in the two directions can be compared by examination of the gradient, and can be related to the nucleus size (lower end of the curve), and final size (upper end). Each line on the graph represents the growth curve of a single ooid (twenty eight in total).

The growth curves are non-linear with gradients varying between ooids for a given value of EQL diameter or PLR diameter. Initial gradients are low due to EQL accretion with only a minor addition to the polar surface. In many cases, a sharp increase in gradient indicates the onset of stage three accretion, though in other ooids the change is more subtle. A number of important points arise from the graph:

1) In general, the gradient only increases during growth, indicating that there is no switch back to EQL dominant accretion.
2) None of the ooids has a final gradient much over 1, indicating that EQL accretion does not cease during stage three (otherwise the gradient is infinite).
3) Gradients are not necessarily greater at high EQL diameter values, suggesting that the onset of PLR accretion is not controlled by elongation (oblateness) of the ooid at that time, or the absolute values of PLR or EQL diameter.
4) Nucleus size does not effect the accretion process. In particular, smaller nuclei do not have rapid initial PLR accretion to increase their size, prior to the EQL dominant accretion.
5) The nucleus elongation, shown by the relative distance from the line EQL diameter = PLR diameter, does not appear to affect the accretion process, even when the nucleus

Figure 3.15. Ooid Growth Plot. Graph 1. PLR diameter against EQL diameter.

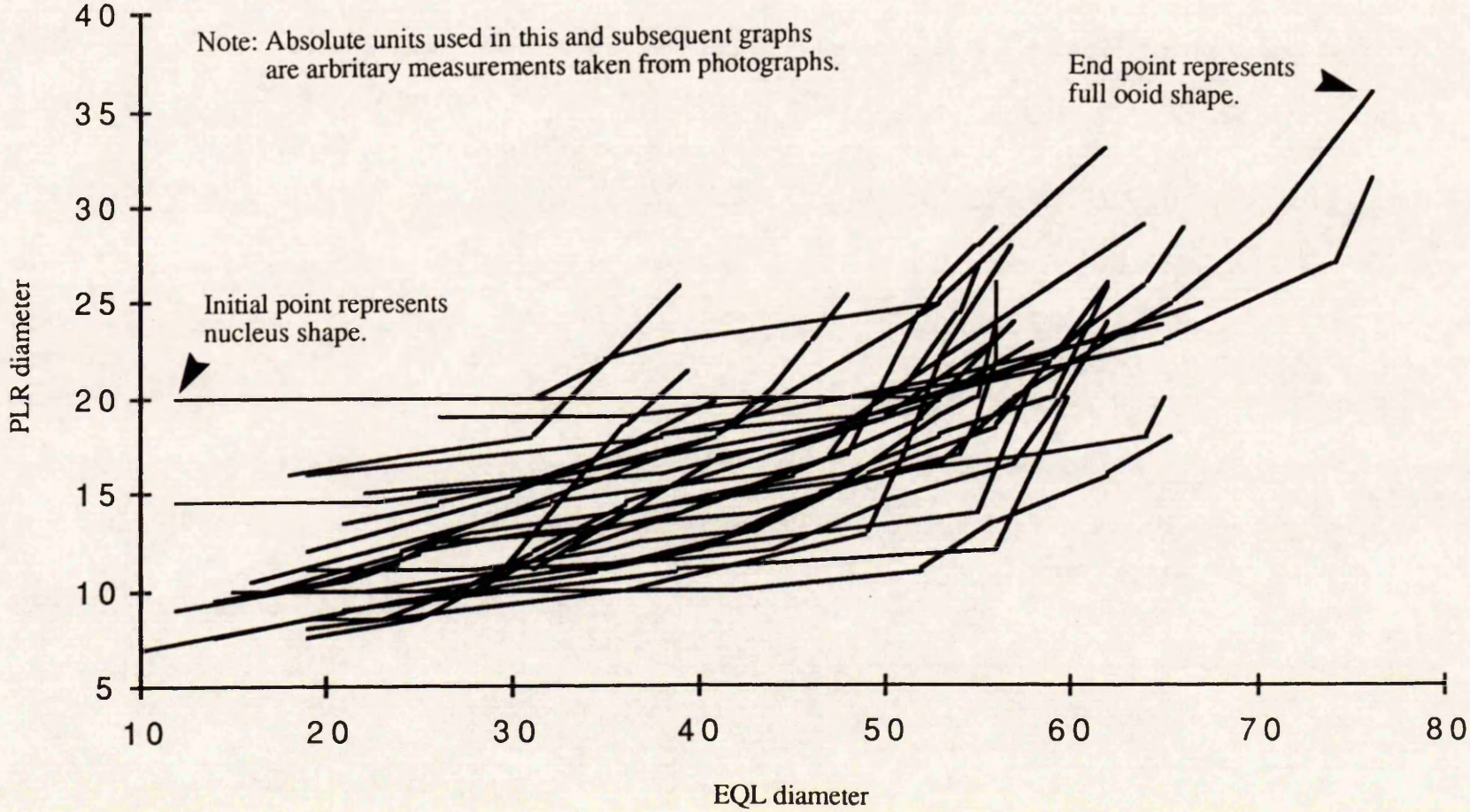

orientation is preferentially in the PLR direction (i.e. when the nucleus long diameter is perpendicular to the ooid long diameter).

Graph 2: (EQL diameter / PLR diameter), against EQL diameter.(Figure 3.16).

A more sensitive indicator of the timing of the stage two - stage three transition is constructed by plotting EQL diameter / PLR diameter against EQL diameter. The EQL measurements are used in preference to PLR on the X-axis as the reference to size, for the reasons of accuracy in measurement mentioned above. In this way, the point of transition from EQL to PLR dominant accretion is marked by the point of inflexion of the growth curve. Stage two has a positive gradient (sphericity decreasing), and stage three a negative gradient (sphericity increasing). Therefore the change can be specifically related to the EQL diameter (an indicator of ooid size) or the EQL/PLR diameter ratio (an indicator of ooid shape), at that point in time. Again a number of points arise from the graph:

1) It is clear by inspection alone that the transition points appear unrelated to the actual size of the ooid at that time.
2) It is more apparent here than in the previous graph, that ooid elongation (EQL diameter / PLR diameter) is not significant in constraining the timing of the transition.
3) Relatively low values of EQL/PLR diameter for the nuclei (lower end of growth curve) will form ooids of generally lower EQL/PLR diameter (higher end of growth curve). This is significant in that accretion must therefore be occurring on the equatorial surface of the nuclei regardless of its overall form.
4) Nucleus size and shape does not affect transition timing.
5) Shallower curves occur when the maximum EQL diameter / PLR diameter ratio remains low, than for higher values. In the latter, the value may drop sharply, suggesting that the greater elongation presented a greater shape disequilibrium at the onset of stage three accretion.

Figure 3.16. Ooid Growth Plot. Graph 2. (EQL diameter / PLR diameter) against EQL diameter.

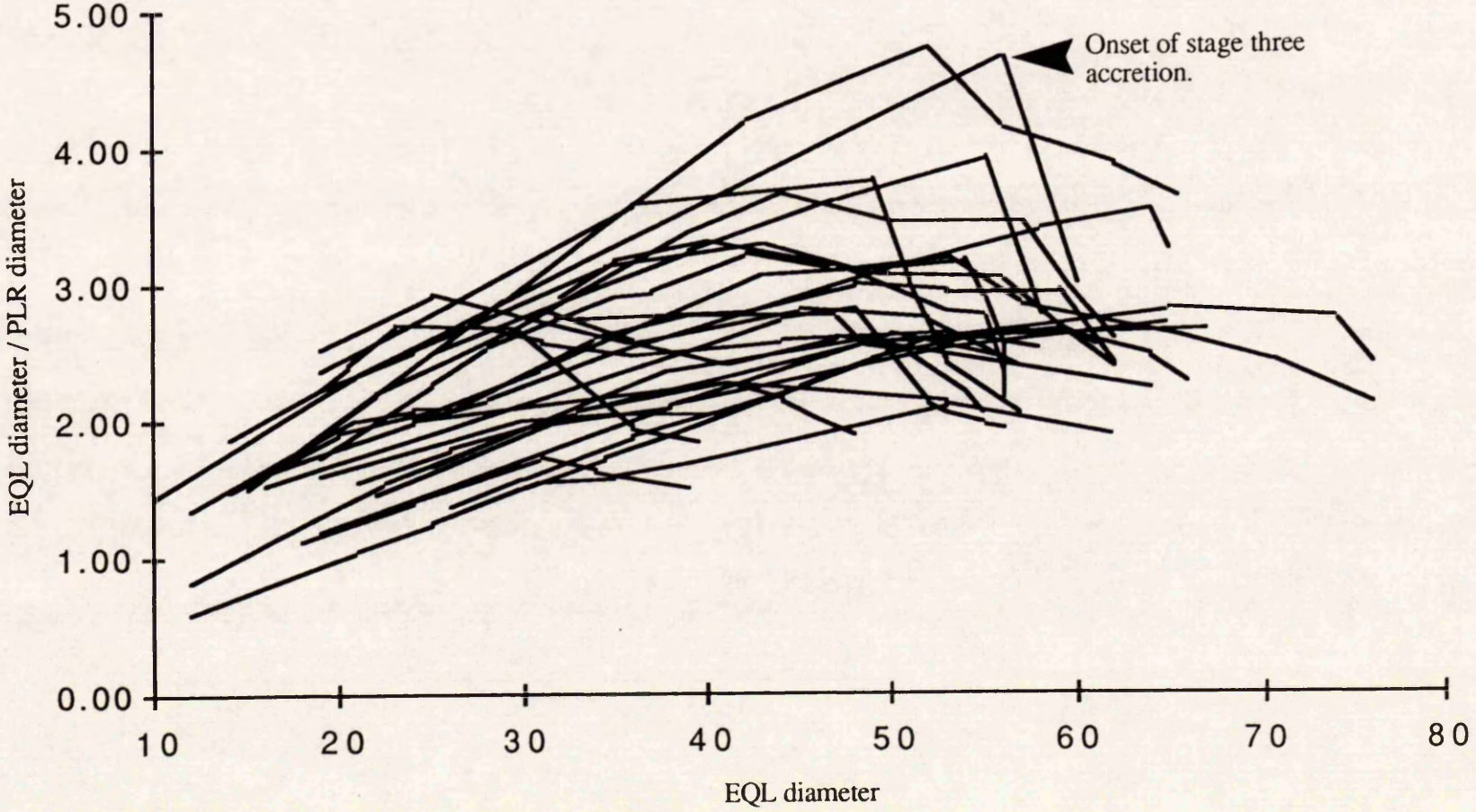

Graph 3: (PLR diameter - PLR nucleus diameter), against (EQL diameter - EQL nucleus diameter).(Figure 3.17).

The third graph shown measures the actual accretion in both the PLR and EQL directions, i.e. the size of the nucleus has been subtracted from the actual measurement. All graphs therefore pass through the origin, and the gradient is equal to the rate of PLR versus EQL accretion.

This graph serves to emphasize that the change in actual accretion from PLR to EQL (seen in this graph by a steepening gradient), will occur totally independently of the nucleus shape. The oblateness is hence process controlled, and not governed by initial factors such as nuclei shape and orientation. In general, the gradients of the graphs at the last accretion stage are higher for those ooids with higher EQL accretion. This perhaps emphasises point five above for graph two, that the more elongate ooids (with higher EQL accretion) have the more active PLR accretion in the latter stages.

Graph 4: (EQL diameter / PLR diameter), against (EQL diameter - EQL nucleus diameter).(Figure 3.18).

The fourth graph relates the position of the transition relative to the actual EQL accretion. The graph is essentially a normalised version of graph two, in which the nucleus diameter has been subtracted from the measurements, so that all the curves start at the origin. The transition points show no correlation at all with the actual amount of accretion, which shows that the amount of accretion is likely to play far less a role in ooid growth patterns and the stage two - stage three accretion, than the overall size development.

Graph 5: (EQL diameter / PLR diameter), against EQL diameter (normalised).(Figure 3.19).

The final graph is designed to test the synchrony of the stage two - stage three transition on the assumption that if rates of accretion in ooids were constant, and all the ooids were formed at the same time, the transition points would be similar. The shapes of all the ooids if growth was continued, can also be estimated and easy comparison made between ooids. EQL diameter / PLR diameter was plotted against EQL diameter, normalised so that the total

Figure 3.17. Ooid Growth Plot. Graph 3. (PLR diameter - PLR nucleus diameter) against (EQL diameter - EQL nucleus diameter).

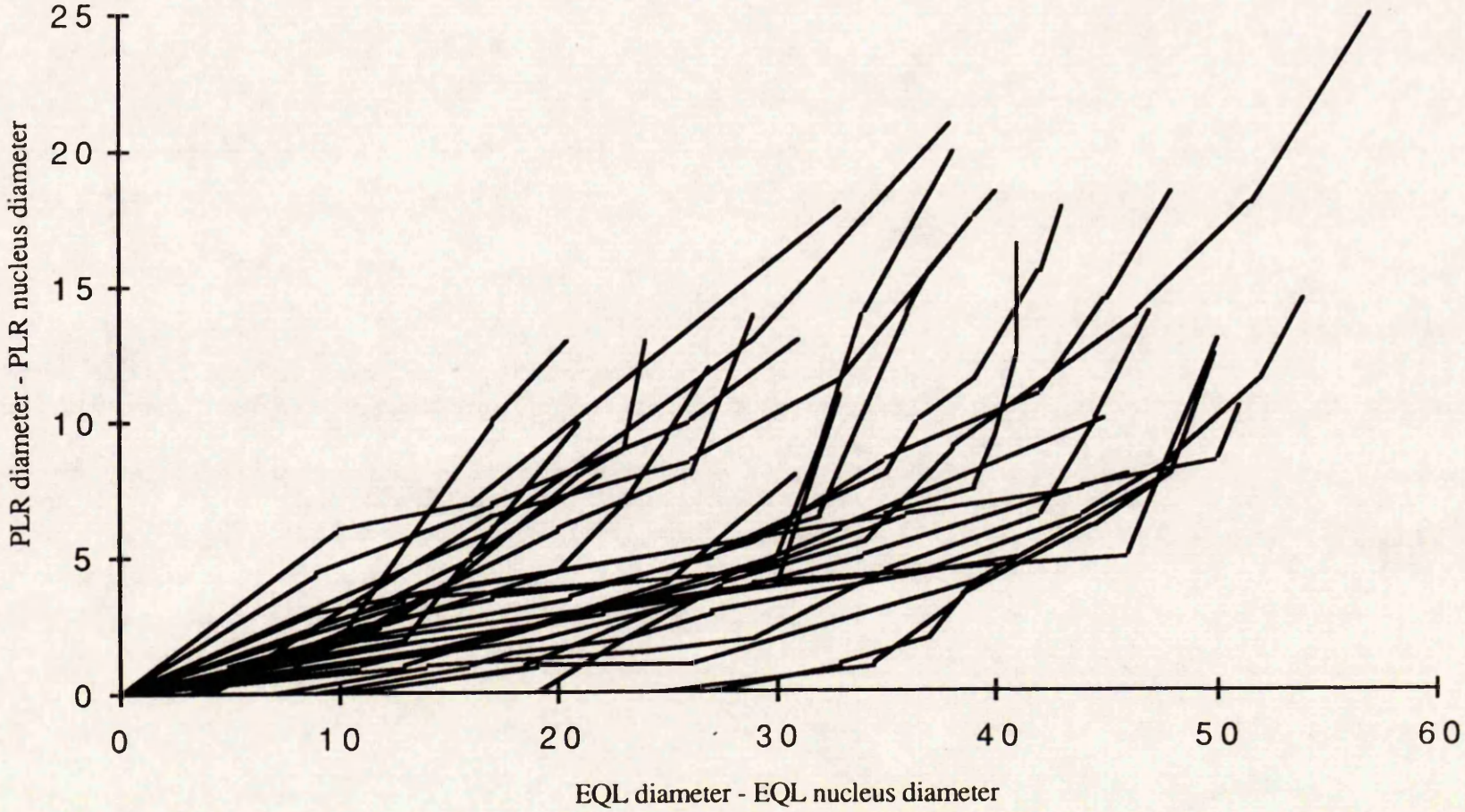

Figure 3.18. Ooid Growth Plot. Graph 4. (EQL diameter / PLR diameter) against (EQL diameter - EQL nucleus diameter).

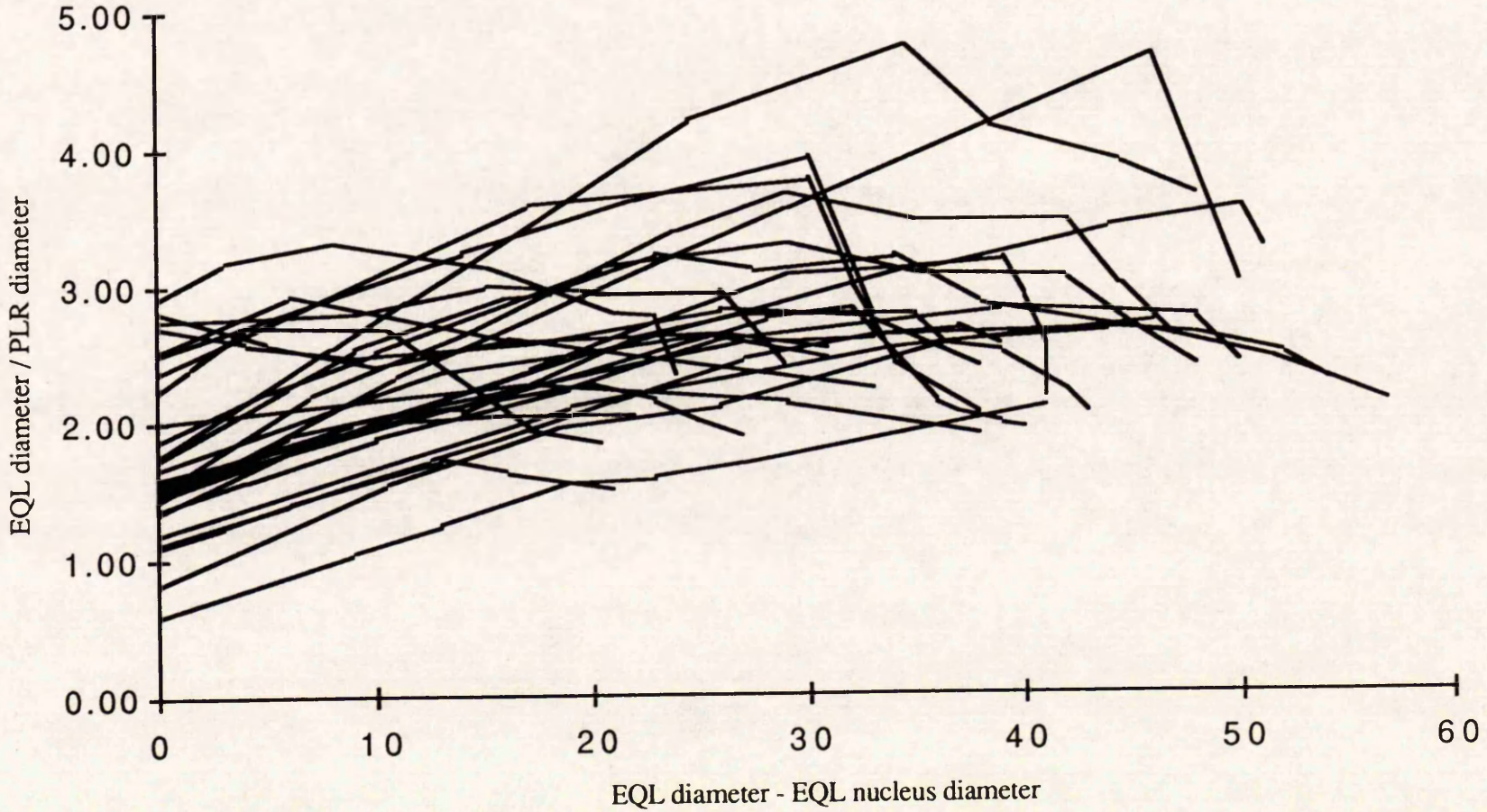

Figure 3.19. Ooid Growth Plot. Graph 5. (EQL diameter / PLR diameter) against EQL diameter (normalised).

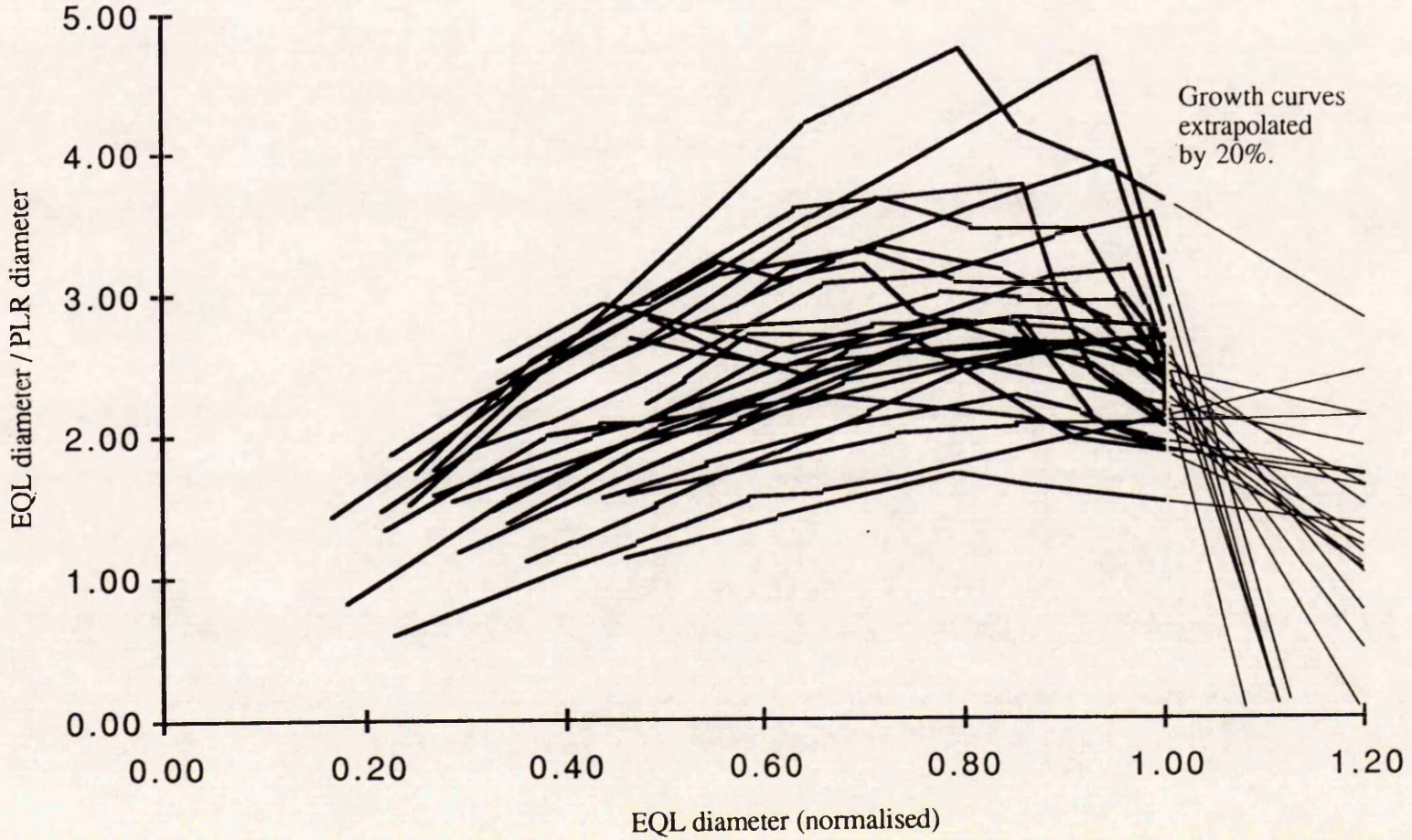

length of each ooid = 1. The growth curves were extrapolated assuming that the gradient at the last accretion stage remained constant. The plot shows:

1) A lack of correlation (overlap) of transition points between ooids. This suggests that, on the assumptions given, the stage two - stage three transition was not a synchronous event for all ooids. However, most ooids incurred the change after 70% of their present size, and scatter is less than for the other graphs.
2) Extrapolation of ooid growth to 120% of present size shows most ooids tend to an elongation ratio between 1.3 and 2.7. This is a surprisingly narrow range considering that the same ratios during growth of the ooid cover 0.6 to 4.7.

3.2.5) Goethitic Ooid Mineralogy.

The mineralogy and composition of the goethitic iron-ooids were studied using X.R.D. and E.P.M.A. respectively. Those of a berthierine composition are described separately below in section 4.5. Hughes (1989) studied goethitic ooids using T.E.M. and found that the laminae were composed of goethite and berthierine only, but his studies were restricted to a small amount of material. Goethitic ooids were studied in this research to ascertain:

i) The mineralogy of a wider suite of samples, including the possible recognition of other mineral phases.
ii) The relative abundance of elements / minerals within the ooids.
iii) Any systematic mineralogical or compositional change across the ooid that might reflect growth mechanisms or diagenetic modification.

X.R.D. analysis of a number of samples revealed only goethite, and a weak ≈7Å peak of a clay mineral, presumed to be berthierine. No aluminium oxides or hydroxides were detected. The presence of minor kaolinite would however not be distinguishable from berthierine using X.R.D.(see section 4.3.2).

E.P.M.A. of laminae in the ooid cortices represent the bulk composition of the crystal assemblage, due to the large size of the analysis area relative to the crystals, whose small (submicron) size was distinguished by T.E.M. (Hughes 1989). This use of probe data is

discussed in more detail below in section **4.2**, and if, treated statistically, much information can be obtained from such 'bulk-rock' data. From the analyses (table 3.3, figure 3.20) it is clear that a pure goethite composition (FeOOH) is rarely obtained, and examples that are close to berthierine are even rarer. Most analyses therefore have significant quantities of Si, Al, and Mg associated with the Fe (approximately 2 weight percent (wt%) Si and Al, and 0.6wt% Mg, see table 3.3). Most analyses also contain a small amount of phosphate, (P content usually between 0.1-0.4 wt%), and a very small amount of pyrite (seen as < 0.1 wt% S). Totals are variable due to differing porosity and surface polish of various parts of the ooids, so to facilitate comparison of the data between samples, the data were recalculated to a standard mineral formulae. Since the more complex mineral present is berthierine, the analyses have been recalculated to a berthierine structural formulae based on 14 (O,OH) (see appendix A.2.1), as opposed to that of a goethite. This also allows direct comparison with berthierine analyses described in chapter 4, rather than requiring further recalculation, and also facilitates the easy subtraction of an ideal pure berthierine analysis from the mixture, to give the composition of the remaining goethitic fraction (see below). It must be remembered however, that the valencies of the elements are hence assumed to be in the reduced state, but the method is valid given that a pure composition and structural calculation is not being implied, and that the resulting data are used only on a relative basis to other analyses.

The simple mixing trend between goethite and berthierine in the ooids is most clearly seen in figure 3.20, where E.P.M.A. compositions obtained from spot analyses of the ooid cortices have been plotted on an Si - (Fe+Mg) - Al(Total) triangular diagram as used for chlorite compositions (see section **4.2**). The majority of the analyses lie nearer to the Fe+Mg pole than the berthierine end-member, showing a clear dominance of goethite over berthierine in most samples studied. In this area of the plot, it was noted that the spread of analyses is at its greatest, and that the Al/Si ratio is on average higher than that of berthierine. This can also be seen from the averaged analyses of all samples, given in table 3.3, that shows an Al/Si ratio of ≈1.05, as opposed to an average berthierine composition (section **4.7**) of ≈0.52. This difference could be due to three major possibilities:

Table 3.3. Average Compositions of Goethitic Iron-Ooid Laminae Obtained By E.P.M.A. Spot Analyses. The Data have been Recalculated to a Berthierine Structural Formulae, and the Average Frodingham Berthierine Composition has been Subtracted From the Formula by Normalisation via Si and Mg. See text for full procedure.

	AVERAGE	ST.DEV.
Si	2.184	1.278
Ti	0.129	0.068
Al	2.192	0.605
Fe	32.643	7.797
Mn	0.165	0.176
Mg	0.610	0.269
Ca	0.651	3.071
Na	0.236	0.158
K	0.133	0.077
P	0.287	0.186
S	0.055	0.061
O	15.073	2.061
TOTAL	54.359	8.390
BerthCalc.		
Si	1.196	0.601
Al(TOT)	1.262	0.282
Ti	0.042	0.022
Fe	9.089	1.797
Mn	0.048	0.049
Mg	0.386	0.147
Ca	0.002	1.106
Na	0.161	0.107
K	0.053	0.029
OH	8.000	0.000
OoidCalc - Berth. (Si normalised)		
Si	0.000	0.000
Al(TOT)	0.644	0.221
Ti	0.041	0.022
Fe	7.687	2.411
Mn	0.046	0.049
Mg	0.069	0.131
Ca	-0.025	1.107
Na	0.126	0.112
K	0.050	0.028
OoidCalc - Berth. (Mg normalised)		
Si	-0.262	0.496
Al(TOT)	0.508	0.320
Ti	0.041	0.022
Fe	7.381	2.238
Mn	0.045	0.048
Mg	0.000	0.000
Ca	-0.031	1.106
Na	0.118	0.108
K	0.049	0.029

Figure 3.20. Si - (Fe+Mg) - Al(Total) Ternary Plot of Goethitic Iron-Ooid Spot Analyses Obtained by E.P.M.A. and Recalculated to Berthierine Structural Formulae. (n=208).

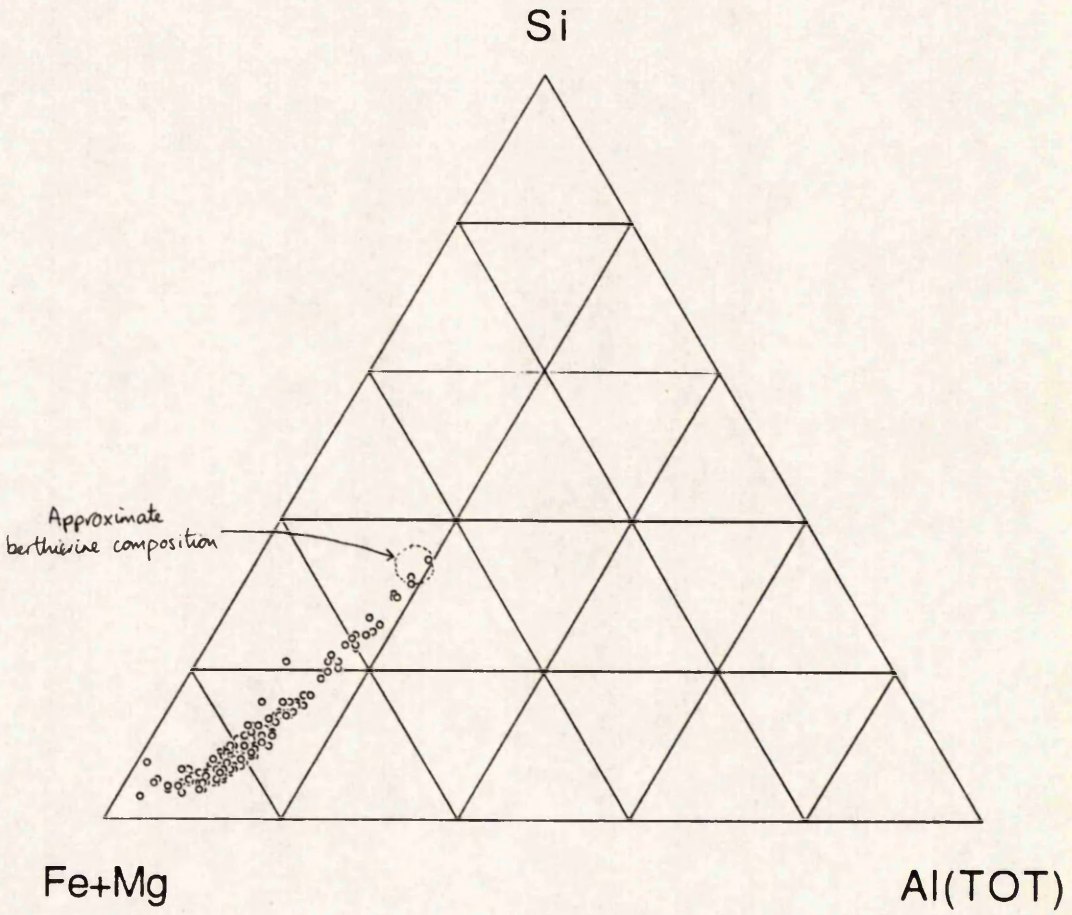

i) The composition of the berthierine within the ooids is different to that for all other Frodingham berthierines.

ii) A separate aluminous mineral phase is present that is indistinguishable by X.R.D.

iii) The goethite is aluminous and not pure FeO(OH).

These possibilities were investigated in three ways:

3.2.5.1) Subtraction of an Average Berthierine Composition From the Ooid Cortex Analyses.

Each individual analysis was recalculated to a berthierine structure as described above, so that the average authigenic berthierine cement composition of the Frodingham Ironstone Formation (section 4.7), could be easily subtracted from the ooid analyses. This method allows direct comparison of the berthierine within the ooid cortex to that of the cements, and includes a similar correction for the presence of minor pyrite and phosphate in the analyses. The recalculation was made by subtracting a quantity of each element in proportion to that of the authigenic berthierine, with the absolute values controlled by the Si content of the analysis, thus assuming that all the Si is present within berthierine. A similar recalculation was then made relative to Mg instead of Si. The former method has the advantage that larger absolute quantities of Si than Mg are present which provides greater confidence in the data, but suffers in that Si may be possibly present as quartz or kaolinite, or may substitute for Fe in the goethites (as can Al). Mg is a less significant constituent of berthierine, but is possibly a better element to use as its occurrence is probably restricted to this mineral alone. The averages of such calculations of all 208 analyses are given in table 3.3. There is good agreement between both sets of berthierine subtracted data, suggesting that Si is probably restricted to the berthierine and not present as a separate mineral, particularly as a negative value is recorded in the Mg normalised data set. The excess Fe from goethite is clearly demonstrated, and of all the other elements analysed, only Al shows a significant anomaly away from the expected value of zero, showing an excess associated with the goethitic fraction.

3.2.5.2) Graphical Representation of Al and Si.

Figure 3.21 shows a plot of Al against Si for the data recalculated to berthierines, and confirms the distinct trend shown in figure 3.20. If the data trend in figure 3.20 represented simple mixing of goethite and berthierine or kaolinite, then the data would be expected to lie along one of the lines shown. As can be seen, this is not the case, and the excess of Al relative to berthierine clearly increases as the proportion of Si decreases. The trend is also evident in the Si/Al against Mg plot (figure 3.22), that indicates the trend in Si/Al ratio as a function of berthierine presence (i.e. Mg). The excess Al is greater than that possible from kaolinite mixing, and must hence be due to Al substitution for Fe in the goethite, or a separate mineral phase such as an Al oxide/hydroxide that is undetectable by X.R.D.

3.2.5.3) X.R.D. Analysis of Goethite.

Goethite may have significant quantities of Al substituting for Fe in the structure (up to 33 mol% AlO(OH), see Brown (1980), and hence it is possible that the Al anomaly is associated with possible substitution. The amount of Al within goethites can be tested by using X.R.D., and also has potential as a geochemical indicator for the environment of goethite formation.

The method commonly used for approximating the mol% Al-substitution is to obtain the $d_{(111)}$ spacing of the goethite. This spacing is proportional to the amount of Al-substitution (see discussion in Brown 1980 p. 365) and can be calculated from the expression;

$$\text{mol\% AlO(OH)} = 714\ (2.448 - d_{(111)}).$$

Other peaks cannot be used, as the relationship is non-linear. The data obtained can only be used as an approximation, as other ions such as Cr^{3+}, Ti^{4+} and Mn^{3+} may replace the Fe^{3+}, also displacing the structure (Brown 1980). The $d_{(111)}$ peak was scanned in selected samples of Frodingham ironstone, from 36-38°2θ (Cukα radiation) shown in figure 3.23, and samples were shown to have low Al-substitution of the goethites. Values of less than 3.3 mol% AlO(OH) were calculated from the peak positions. Such amounts are not

Figure 3.21. Al versus Si Plot of Goethitic Iron-Ooid Spot Analyses Obtained by E.P.M.A. Recalculated on the Basis of a Berthierine Structural Formula. (n=208).

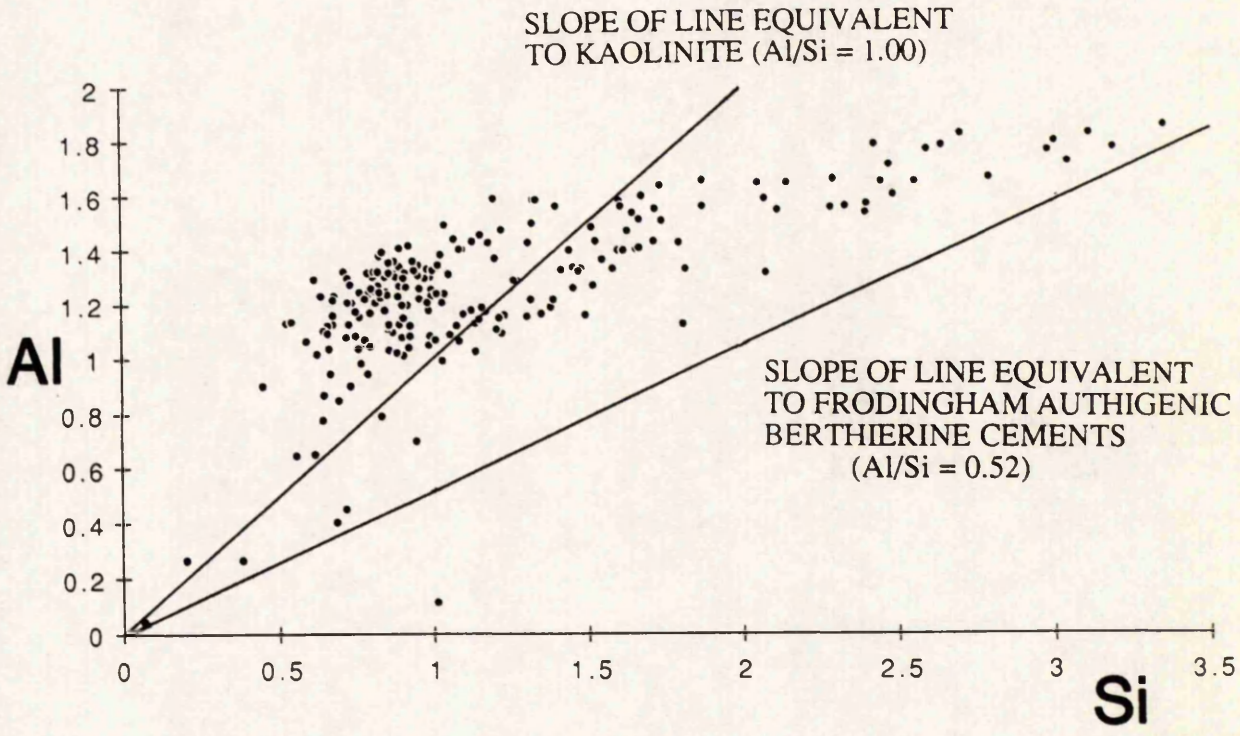

Figure 3.22. Si/Al versus Mg Plot of Goethitic Iron-Ooid Spot Analyses Obtained by E.P.M.A. Recalculated on the Basis of a Berthierine Structural Formula. (n=208).

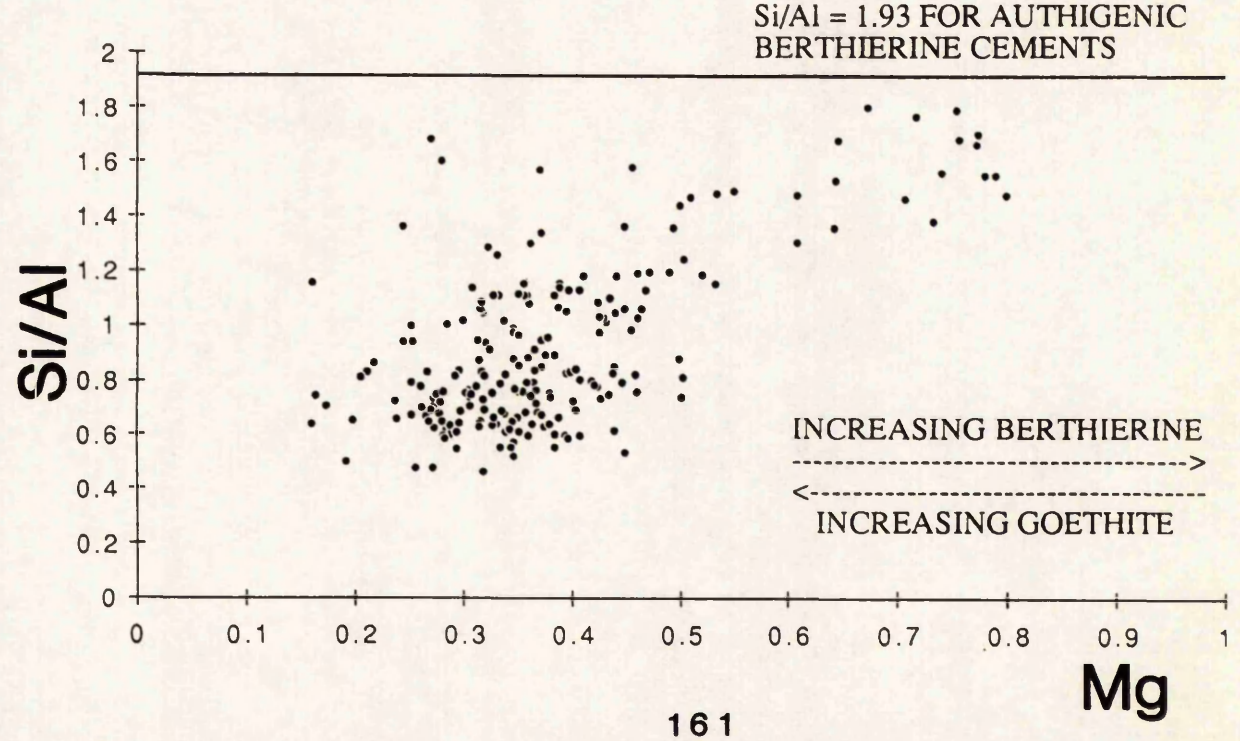

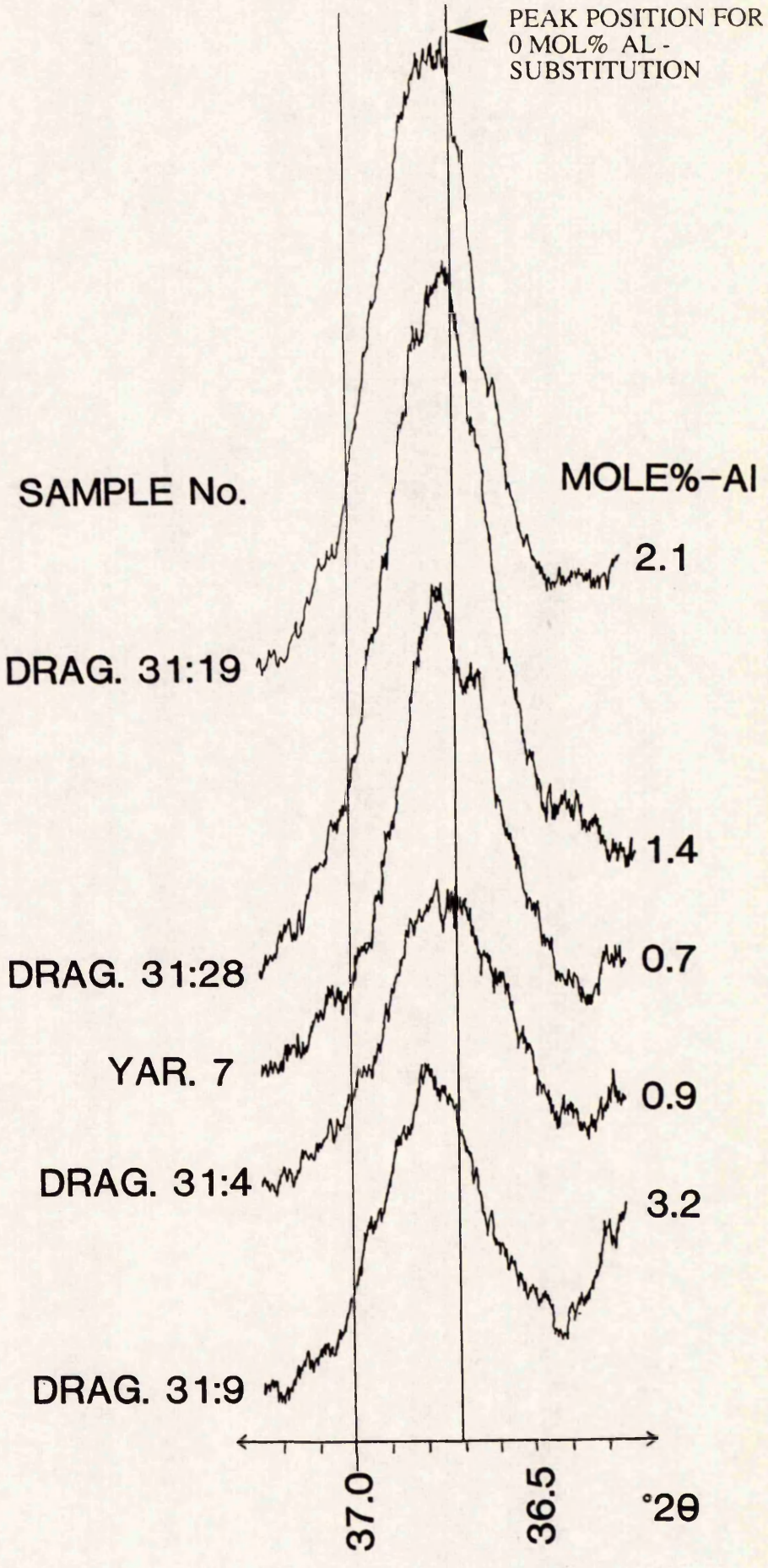

Figure 3.23. X-Ray Diffraction Traces of the $d_{(111)}$ Peaks for Goethite in Frodingham Ironstone Samples, Used to Estimate the Mol% Al - Subtitution in the Structure (see text).

significant enough to account for the anomaly shown by E.P.M.A., and a separate Al oxide/hydroxide phase is interpreted as being present in minor quantities within the ooids.

The amount of Al substituting for Fe in goethite can also be used as a geochemical indicator to the origin of detrital goethite particles and ooids. Siehl and Thien (1989) have summarised their own data and that of other workers, and derived an approximate relationship between environment of formation and mol% Al-substitution (see their figure 10). In particular, they used the high Al-substitution seen in many ooid goethites to imply ooid genesis in hydromorphic and lateritic environments (for example as soil pisoids), where Fe, Si, and Al, are concentrated. Gehring (1989) however describes ooids with <2 mol% Al-substitution in Middle to Upper Jurassic ironstones of the Jura Mountains, Switzerland, and therefore disputes a lateritic origin to all ooids.

3.2.5.4) Compositional Variation of Ooid Cortices.

Attempts were made in a number of samples to ascertain by E.P.M.A.variations in iron-ooid composition in a similar way to that of Rohrlich (1974). In particular, geochemical investigations were based upon studying any variation;

i) Between ooids of the same sample.

ii) Between ooids of different samples.

iii) Within the ooids themselves (i.e. across the cortex).

Compositions of ooid cortices obtained by spot analysis have been shown to comprise a suite of data which plot on a goethite-berthierine mixing trend. Analyses taken from a single ooid, or group of ooids from a single sample, tend to cluster within a small range of the major trend. This means that dense goethitic ooids do not occur alongside berthierine-rich ooids. Compositional variation within ooids was studied by obtaining lines of E.P.M.A. spot analyses across the cortices. Any systematic change could indicate primary mineralogical precipitation variation during growth, or subsequent diagenetic modification. Two examples of ooids analysed in this way are shown in figures 3.24 and 3.25. These

Figure 3.24. Plots Showing the Variation in Element Concentration (recalculated on the Basis of a Berthierine Structural Formula) From Ooid Exterior to Centre (1 to 10), for a Single Goethitic Ooid from DRAG. 31.28. Open and Filled Circles Represent Lines of Analyses From Opposite Ends of the Ooid.

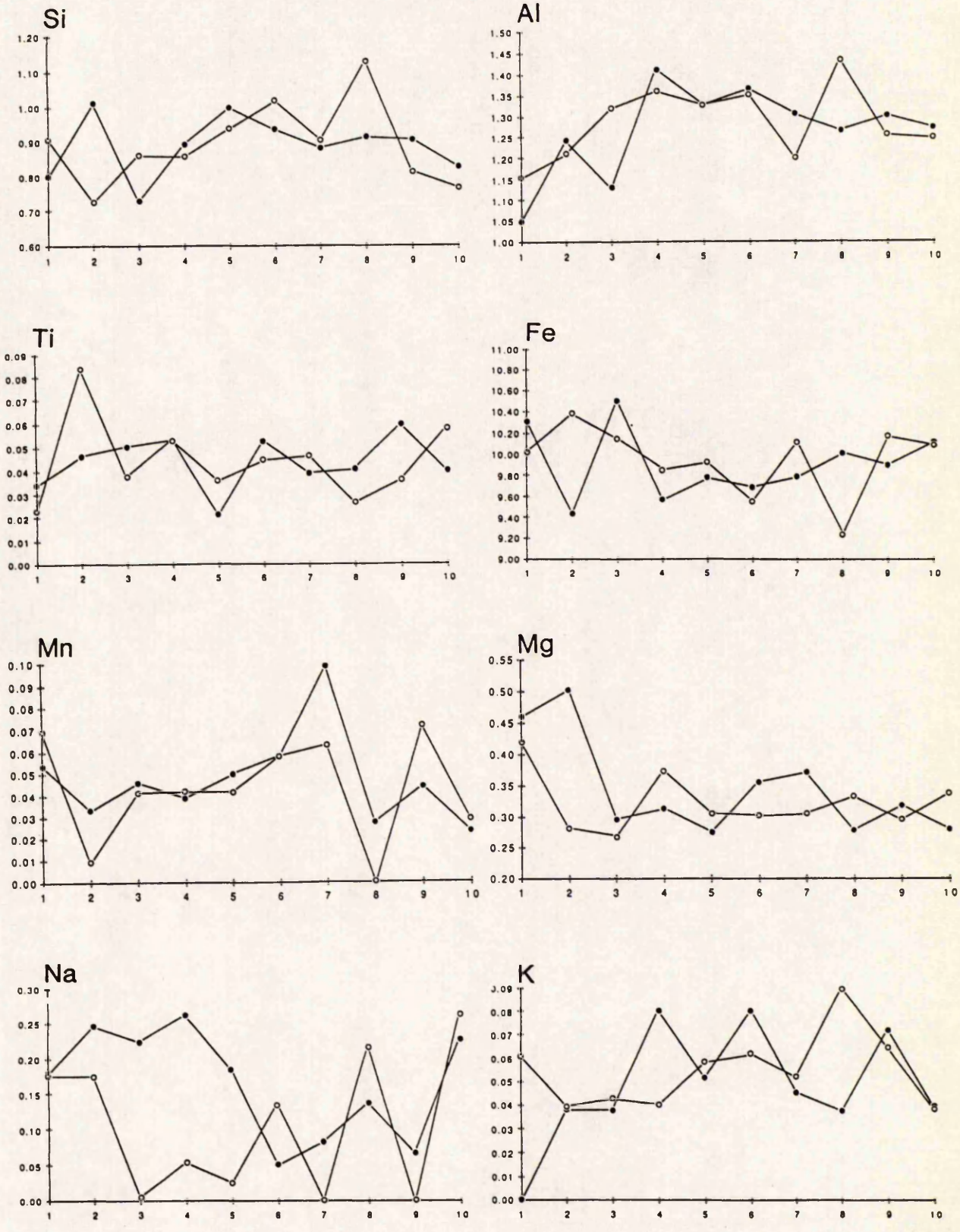

Figure 3.25. Plots Showing the Variation in Element Concentration (recalculated on the Basis of a Berthierine Structural Formula) From Ooid Exterior to Centre (1 to 11), for a Single Goethitic Ooid from YAR. 7. Open and Filled Circles Represent Lines of Analyses From Opposite Ends of the Ooid.

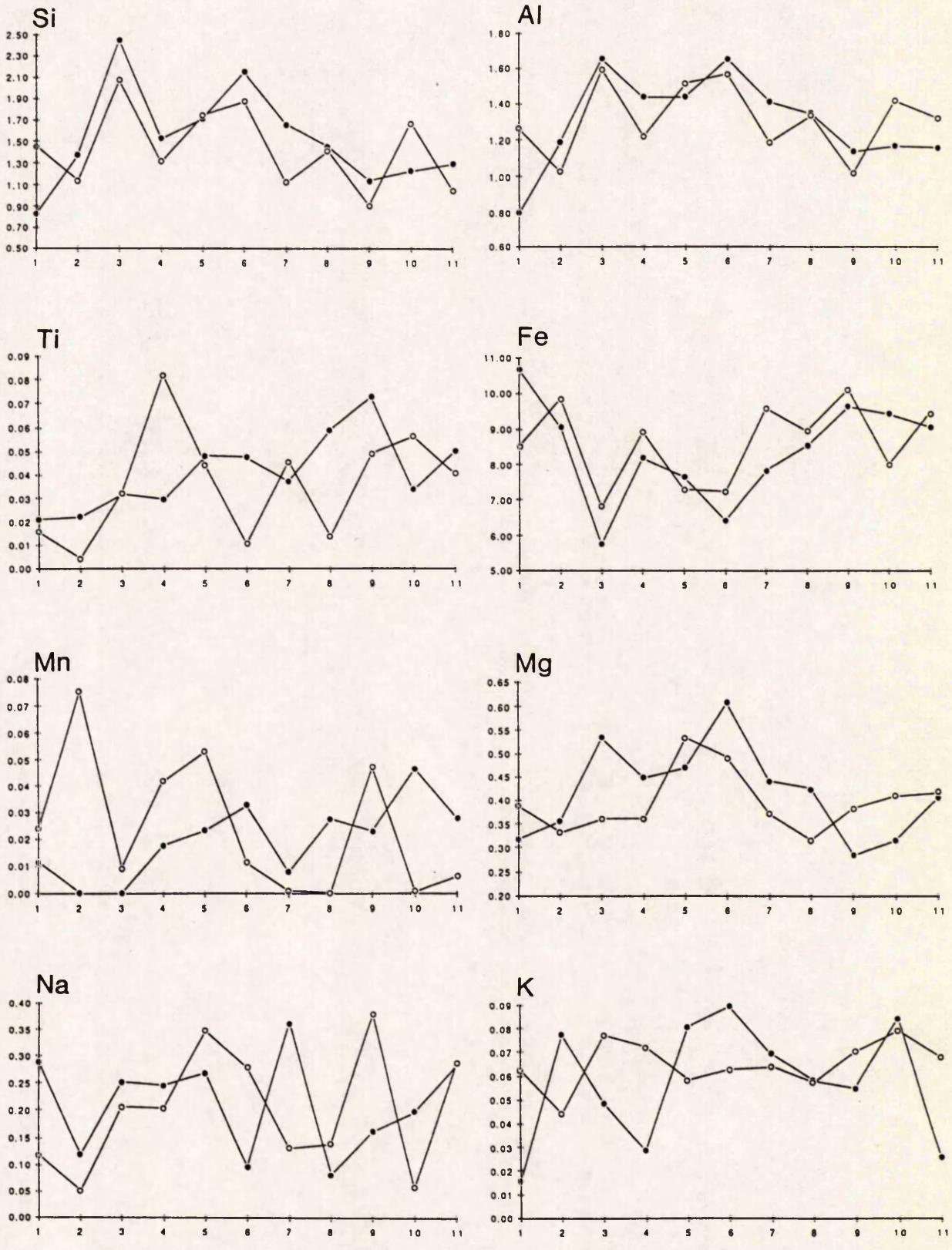

may be considered typical of the 22 ooids analysed by this method. In general, the following may be stated for the analyses obtained:

1) The variation in any element abundance across an ooid is not predictable.

2) Any variations detected were usually localised, with general compositional trends (such as a systematically increasing element concentration) being uncommon. Geochemical correlation around the cortex is hence often not possible but the graphs of Si, Al, and Fe abundance in figure 3.25, are examples of where correlation has been possible.

3) Comparison between single analyses, usually yields a good positive correlation between the elements Si, Al, and Mg. All these elements are negatively correlated to Fe. This is consistent with goethite-berthierine mixing. The minor elements Ti, Mn, Na, and K do not show any systematic correlation with any of the major elements.

3.2.5.5) Nucleus Composition.

The composition of the goethitic particles that act as nuclei for many ooids was studied specifically in DRAG. 31.28 (plate 7a), where examples of this type of nuclei are clearly seen and well differentiated from the cortex. E.P.M.A. compositions obtained from these are given in table 3.4. In general, such particles show a greater Fe content than the ooid cortices, but are not pure FeOOH, as concentrations of 1-2 wt% Si and Al, and 0.5-0.8 wt% Mg were measured. To ascertain whether the Si, Al, and Mg content was due to the presence of berthierine, the analyses were recalculated to a berthierine structural formulae, and the average Frodingham berthierine composition was subtracted from the analyses as described previously. Unlike the analyses obtained from ooid cortices (section 3.2.5), there is not a good similarity between the Si and Mg normalised sets of data, with an excess of Al and Mg in the Si normalised set, and a considerable Si depletion within the Mg normalised data. This can also be seen within analyses of other ooid nuclei in the data given in table D1 appendix D. It is hence believed that berthierine is not present within these particles, and that the analyses are simply consistent with compositions obtained from goethites in modern laterites, as given in table 3.5.

Table 3.4. Compositions of Goethitic Iron-Ooid Nuclei in DRAG. 31.28. The Data have been Recalculated as Described in the Text.

	DRAG. 31.28 OOID NUCLEI									
	1	2	3	4	5	6	7	8	AVERAGE	STDEV
Si	1.357	1.083	1.108	1.156	1.397	1.300	1.198	1.118	1.215	0.121
Ti	0.055	0.022	0.102	0.032	0.024	0.015	0.032	0.000	0.035	0.031
Al	2.634	1.661	1.703	1.374	1.267	1.251	1.350	1.744	1.623	0.455
Fe	48.013	49.272	45.401	50.295	50.346	50.795	50.244	47.841	49.026	1.836
Mn	0.172	0.170	0.153	0.250	0.212	0.160	0.253	0.163	0.192	0.041
Mg	0.759	0.614	0.663	0.588	0.818	0.496	0.660	0.686	0.661	0.100
Ca	0.125	0.103	0.161	0.148	0.172	0.160	0.148	0.095	0.139	0.028
Na	0.489	0.377	0.493	0.059	0.307	0.384	0.000	0.000	0.264	0.212
K	0.019	0.062	0.000	0.000	0.049	0.000	0.082	0.072	0.036	0.035
P	0.548	0.562	0.664	0.744	0.695	0.713	0.833	0.573	0.667	0.100
S	0.000	0.000	0.122	0.000	0.055	0.000	0.000	0.000	0.022	0.045
O	19.160	18.206	17.426	18.469	18.840	18.648	18.642	17.823	18.402	0.563
TOTAL	73.331	72.132	67.996	73.115	74.182	73.922	73.442	70.115	72.279	2.156
BerthCalc.										
Si	0.602	0.508	0.553	0.547	0.643	0.606	0.567	0.537	0.570	0.044
Al(TOT)	1.216	0.811	0.885	0.676	0.607	0.607	0.665	0.873	0.792	0.205
Ti	0.014	0.006	0.030	0.009	0.006	0.004	0.009	0.000	0.010	0.009
Fe	10.709	11.627	11.378	11.959	11.640	11.905	11.961	11.567	11.593	0.414
Mn	0.039	0.041	0.039	0.060	0.050	0.038	0.061	0.040	0.046	0.010
Mg	0.389	0.333	0.383	0.321	0.435	0.267	0.361	0.381	0.359	0.051
Ca	-0.328	-0.365	-0.445	-0.482	-0.428	-0.450	-0.547	-0.384	-0.429	0.069
Na	0.265	0.216	0.301	0.034	0.173	0.219	0.000	0.000	0.151	0.122
K	0.006	0.021	0.000	0.000	0.016	0.000	0.028	0.025	0.012	0.012
OH	8.000	8.000	8.000	8.000	8.000	8.000	8.000	8.000	8.000	0.000
OoidCalc - Berth. (Si normalised)										
Si	0.000	0.000	0.000	0.000	0.000	0.000	0.000	0.000	0.000	0.000
Al(TOT)	0.905	0.548	0.599	0.394	0.275	0.294	0.372	0.595	0.498	0.209
Ti	0.014	0.005	0.029	0.008	0.006	0.003	0.008	-0.001	0.009	0.009
Fe	10.004	11.032	10.730	11.318	10.886	11.195	11.296	10.937	10.925	0.425
Mn	0.038	0.040	0.038	0.060	0.049	0.037	0.060	0.039	0.045	0.010
Mg	0.230	0.198	0.236	0.177	0.265	0.107	0.211	0.239	0.208	0.049
Ca	-0.342	-0.376	-0.457	-0.495	-0.442	-0.463	-0.559	-0.396	-0.441	0.069
Na	0.247	0.201	0.285	0.018	0.154	0.201	-0.016	-0.016	0.134	0.122
K	0.004	0.020	-0.002	-0.001	0.014	-0.002	0.026	0.023	0.010	0.012
OoidCalc - Berth. (Mg normalised)										
Si	-0.868	-0.750	-0.892	-0.667	-1.000	-0.403	-0.797	-0.902	-0.785	0.185
Al(TOT)	0.456	0.161	0.138	0.049	-0.243	0.085	-0.040	0.128	0.092	0.197
Ti	0.013	0.005	0.028	0.007	0.004	0.003	0.007	-0.002	0.008	0.009
Fe	8.987	10.153	9.684	10.536	9.714	10.723	10.363	9.879	10.005	0.559
Mn	0.037	0.039	0.037	0.059	0.047	0.037	0.059	0.038	0.044	0.010
Mg	0.000	0.000	0.000	0.000	0.000	0.000	0.000	0.000	0.000	0.000
Ca	-0.361	-0.392	-0.477	-0.509	-0.464	-0.472	-0.577	-0.416	-0.459	0.068
Na	0.222	0.180	0.259	-0.001	0.125	0.189	-0.039	-0.042	0.112	0.122
K	0.002	0.017	-0.004	-0.003	0.012	-0.003	0.024	0.021	0.008	0.012

Table 3.5. Goethite Compositions Given by Taylor (1987 tables 2.2a and 2.2b)

	1	2	3	4	5	6	7	8	9
Fe2O3	73.90	88.50	81.30	73.70	72.7	74.8	69.9	71.7	59.2
Al2O3	8.68	-	0.30	2.96	4.17	2.6	3.71	3.61	11
TiO2	1.53	0.70	0.02	0.01	-	-	-	-	-
V2O5	-	3.00	-	-	-	-	-	-	-
MnO	-	-	0.34	0.65	0.65	0.33	0.85	1.53	1.15
ZnO	-	2.15	-	2.93	-	-	-	-	-
CuO	-	0.10	-	-	-	-	-	-	-
MoO3	-	1.42	-	-	-	-	-	-	-
P2O5	2.16	2.66	4.43	0.03	-	-	-	-	-
SO3	0.70	-	0.08	-	-	-	-	-	-
SiO2	1.20	-	0.30	5.02	3.27	2.4	1.99	2.69	4.88
MgO	-	-	-	-	0.63	0.4	0.81	0.43	1.42
Cr2O3	-	-	-	-	2.93	2.92	3.51	3.6	3.31
NiO	-	-	-	-	1.27	1.01	1.92	1.49	1.86
CoO	-	-	-	-	0.11	-	-	0.03	0.11

1-4) E.P.M.A. Analyses of Goethites.
1) Queensland. (single crystals).
2) Goethite-rich V shale.
3) Cobar district, New South Wales. (Gossan).
4) Broken Hill, New South Wales.
5-9) Chemical Analyses of Lateritic Goethites.
5-7) New Caledonia.
8-9) Philippines.
(- indicates no data obtained)

3.2.6) Discussion on Ooid Shape: Primary or Compaction Formed?

It is extremely important to ascertain the initial shape and fabric of the ooids, since many theories of iron-ooid formation rely on the assumption than an initially spherical ooid was compacted to produce the ellipsoidal form seen today. However, examination of the mechanisms of compaction, and the fabrics that would be expected to have been formed by compaction, has not previously been undertaken. It is important to point out at this stage, that iron-ooids always show a variety of orientations in thin-section, and that the oblate shape was formed prior to the ooids being incorporated into the ironstone-formation. If a compactional process for ooid shape formation is implied, the ooids must have been subsequently reworked.

In the compactional regime, the major stress σ_1 is vertical, with the minimum stress occurring in the horizontal plane, so that $\sigma_2 \approx \sigma_3$. A particle under such a regime is therefore likely to undergo deformation in the form of a pure shear as opposed to a simple shear (see figure 3.26). This means that the principle strain axes coincide with the directions of the principle stresses, and remain unchanged in this orientation during deformation (figure 3.26b). Shortening occurs in the σ_1 direction, with synchronous extension in the direction of minimum stress, if material is not lost from the distorting particle. A homogenous sphere undergoing such deformation (homogenous strain) will initially deform to a perfect uniaxial ellipsoid that is oblate (but not flattened) in shape (see figure 3.26b). Further compaction merely increases the oblateness. Superficially therefore compaction appears to be a valid argument for the development of the oblate iron-ooid shape, but other factors need to be considered.

3.2.6.1) Range of Ooid Shapes

The small range in ooid shape as described above in section 3.2.4.1, is a very strong argument that the ooids were not originally spherical and later deformed. Petrographic examination of the ooids, coupled with the quantification of ooid shape, shows clearly that ooid shape is not random, but restricted to a subset of oblate flattened ellipsoids. If these ooids represent deformed spherical particles, it would be expected that the ooids

Figure 3.26. A) Representation of Pure and Simple Shear on a Homogenous Body. In a) the strain axes X and Z do not change during deformation, but in b) the axes are rotated. From Park (1983, figure 6.7 p.40).

B) Axially Symmetric Shortening of a Homogenous Body (X=Y>Z). A sphere is deformed to an oblate uniaxial ellipsoid. From Park (1983, figure 6.8 p.41).

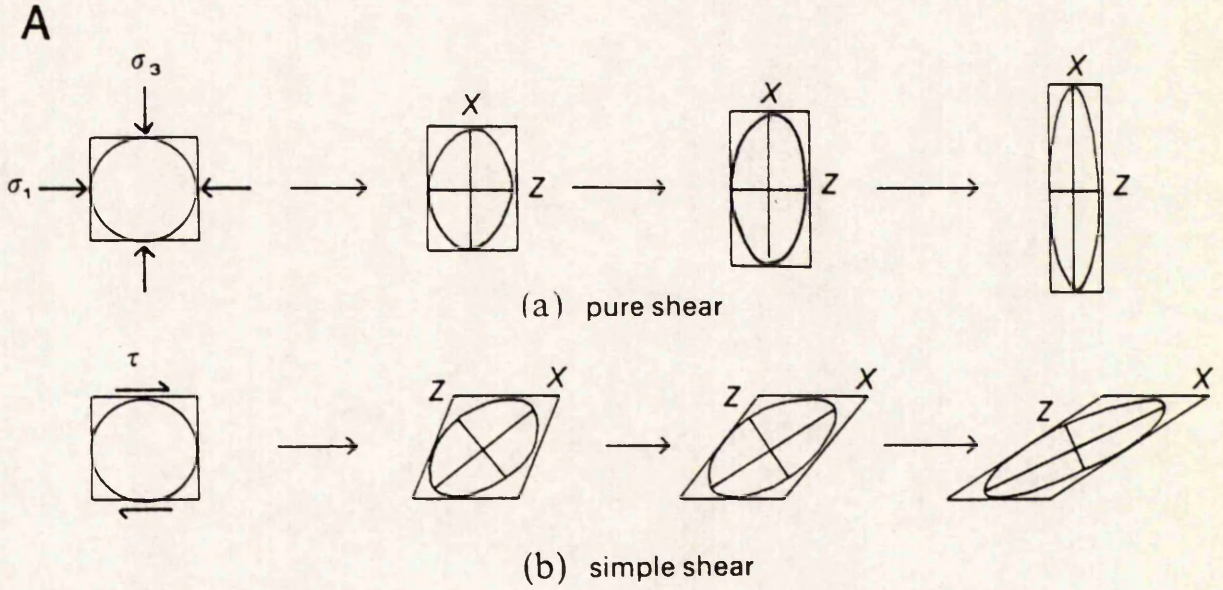

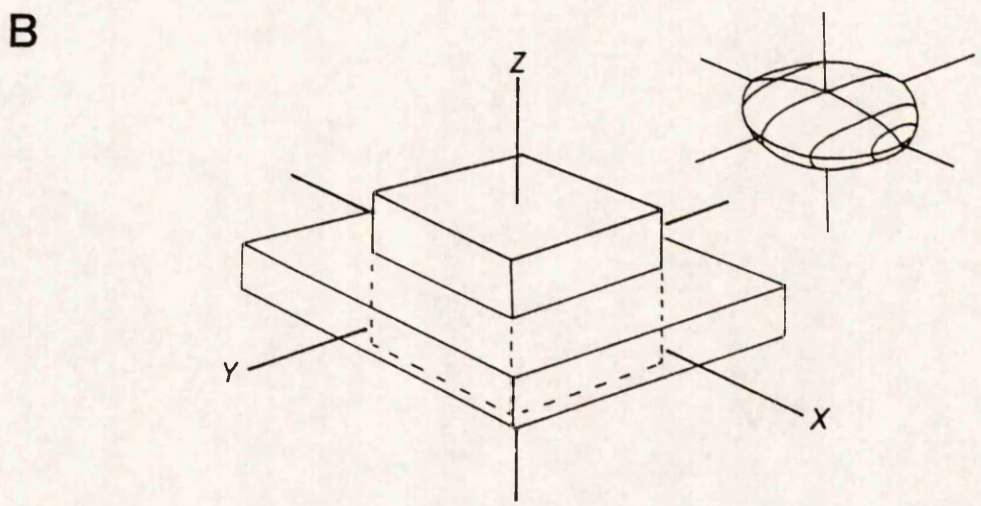

would show a complete range of shapes between spheres and highly flattened ellipsoids, due to varying degrees of ooid plasticity. This is not the case, and the latter are particularly rare. It is suggested that this fact alone is significant enough to suggest a primary ooid oblateness.

3.2.6.2) Ooid Shape Relative to an Ellipsoid.

Neither the external shape nor the internal laminae of iron-ooids are perfect ellipsoids, as would be expected for deformation of a homogenous sphere under the compactional regime described above. The shape alone is however not proof that compaction has not occurred, as the ooids are not homogenous, with differences occurring not only between the nuclei and the cortex, but also between successive laminae within the cortex. This heterogeneity may induce the difference in shape seen, between the theoretical compactionally formed perfect ellipsoid, and that of the more flattened iron-ooids. However, no experimental studies of iron-ooid deformation have been undertaken, and hence quantitative data are not available to validate or discredit the compaction argument. It should also be remembered, that if an ooid formed within a stress regime similar to that described above, that the shape may well reflect the differential stresses involved. This is clearly demonstrated by the formation of oblate concretions in mudrocks, and will be discussed as a mechanism later.

3.2.6.3) Ooid Internal Fabric.

Major arguments against ooid shape resulting from compaction are found on examination of the ooid internal fabric. If a sphere consisting of concentric laminae is compressed, then assuming homogeneity the resultant shape formed will consist of concentric ellipses. In iron-ooids the laminae do not form ellipses, and they are commonly non-concentric, with many ellipses meeting on the polar surface. This effect could be due to the presence of a nucleus that is sufficiently rigid so that the cortex deforms around it and mass transfer occurs in the direction of σ_2/σ_3, i.e. horizontal. However, goethitic ooids are unlikely to undergo plastic deformation, as is discussed in section 3.2.7. Such a mechanism of mass transfer would hence be assumed to have occurred via pressure solution

and re-precipitation, but none of the features associated with pressure dissolution fabrics such as stylolite formation are present. There is also no sign in any ooids of actual cortical deformation over the nucleus in the form of distorted laminae, that would be expected to either plastically distort around it, or undergo brittle fracture at the point of contact.

Compaction after ooid formation cannot reasonably account for the stage three accretion. If the outer ellipsoidal shape of the iron-ooid is restored to that of a sphere then the internal fabric would remain elliptical if a stage three accretion was present. Similarly, if the fabric of the stage two accretion was made spherical, then the stage three accretion would be ellipsoidal. Under these criteria, it would hence have to be assumed that the compactional phase predated the stage three accretion. However, this still cannot explain the fabrics described above.

3.2.7) Ooid Deformation Fabrics.

The deformation of iron-ooids is variable (plate 9), and the resulting fabrics reflect the ooid mineralogy. Ooid shape may become distorted by plastic or brittle deformation, which is directly related to the dominance of berthierine or goethite in the ooid or layer involved.

3.2.7.1) Goethitic Ooids.

Goethite ooids are rarely deformed, and where deformation fabrics are present, the result is only minor dislocation of the outer part of the cortex. This fracturing may be related to berthierine formation and growth within the ooid (plate 9a, 14a), and is discussed further in section 4.4.2. No broken ooids are found within the ironstone-formation, though evidence for the previous fracture of whole goethite ooids is abundant due to the presence of broken ooids acting as nuclei. Some cortex distortion may be associated with siderite replacement, but the effect is minor. An unusual form of distortion can be seen in Y183.3 in which deformation following carbonate cementation has resulted in the carbonate crystals being forced into the ooids, but in irregular patches, forming a castlelated fabric (plate 9b).

PLATE 9

Ooid Deformation Fabrics in Thin-Section

A) Fractured goethitic ooids and berthierine cement, specimen DRAG. 31.28. The goethitic ooids have undergone brittle fracture, and parts of the cortex have become detached and are supported within the berthierine cement. Photo length is equivalent to 1.3mm.

B) "Castlelated ooids", specimen Y183. 3. A peculiar form of ooid deformation fabric unique to this specimen, in which parts of the siderite cement have become indented into the cortices of the goethitic ooids. Photo length is equivalent to 1.3mm.

C) "Spastoliths", specimen Y183. 8 (crossed polars). The berthierine ooids within the "Snap Band" have become intensely deformed on compaction, resulting in an undulating foliation parallel to bedding. This is best seen under crossed polars. Photo length is equivalent to 3.3mm.

D) "Hooked" or "sheared" ooids, specimen Y183. 8. This fabric results from compaction of originally oblate spheroidal berthierine ooids cemented by calcite. The calcite cement framework has broken, but the pieces still retain the shape of the original pore that was cemented. The ooids have plastically deformed. Photo length is equivalent to 3.3mm.

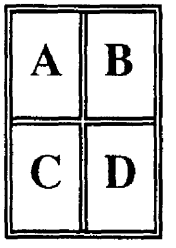

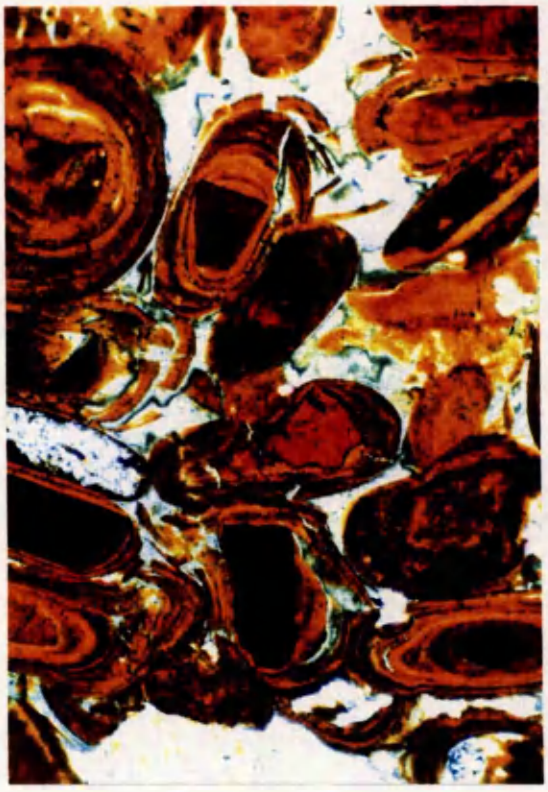

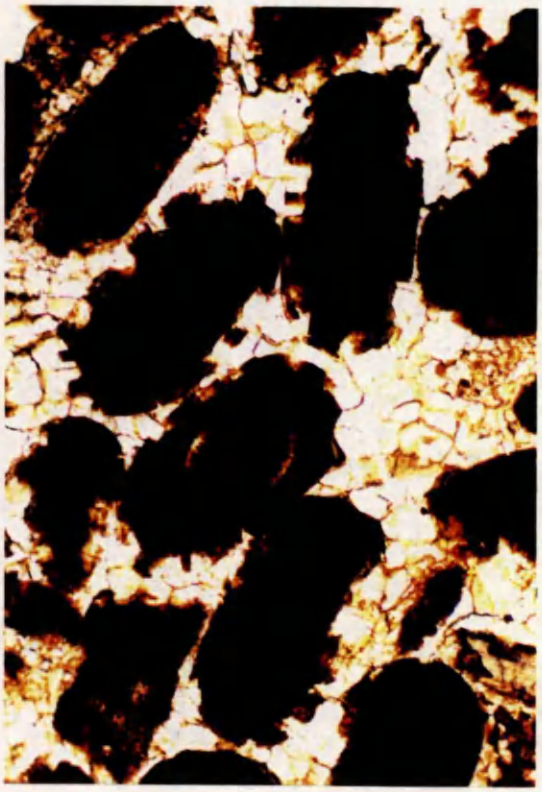

3.2.7.2) Berthierine Ooids.

Ooids of a predominantly berthierine mineralogy undergo plastic deformation (plate 9c). Such ooids have been reported to be able to undergo compaction to length/width ratios exceeding 10 (Kimberley 1983). It is clear from the large number of deformed berthierine ooids relative to those that have remained intact, that berthierine ooids are very soft and easily deformed. Scenarios for the preservation and deformation of berthierine ooids are given in figure 3.27. Note that solution is not implied for any fabrics seen, unlike the "eggshell diagenesis" (Wilkinson and Landing 1978) of carbonate ooids. Various terms have been used to describe ooids whose shape has been modified, and these are also given. "Spastoliths" *sensu* Rastall and Hemingway (1940), involve simple deformation via compactive stresses acting largely perpendicular to bedding. The shape formed is dependent on the stresses involved and the heterogenous nature of the matrix/cement.

The 'sheared' or 'hooked' ooids (figure 3.28 b,c, plate 9d) are evidence for post-cementation compactional stresses, that acted in a direction not necessarily perpendicular to bedding. After cementation, stresses are carried through the cement, and brittle fracture of the cement occurs at the points of greatest weakness, which are near to or at the points of ooid contact. Fracturing of the cement may be accompanied by some lateral movement, and result in the formation of 'hooked' ooids by plastic deformation of the ooid itself. This process is shown diagrammatically in figure 3.28b. These textures have been observed in ooidal limestones, and have been interpreted as being due to distortion during sedimentation in agitated conditions (Carozzi 1961); as compaction prior to cementation (Kettenbrink and Manger 1971); and by the above mechanism of shearing and compaction after external cementation, but associated with ooid dissolution and later pore-fill (Conley 1977). The discussion here therefore follows Conley (1977) with the modification that deformation could occur without dissolution of the ooids mineralogy.

Figure 3.27. Preservation and Deformation Fabrics of Berthierine Ooids as a Function of Diagenetic History.

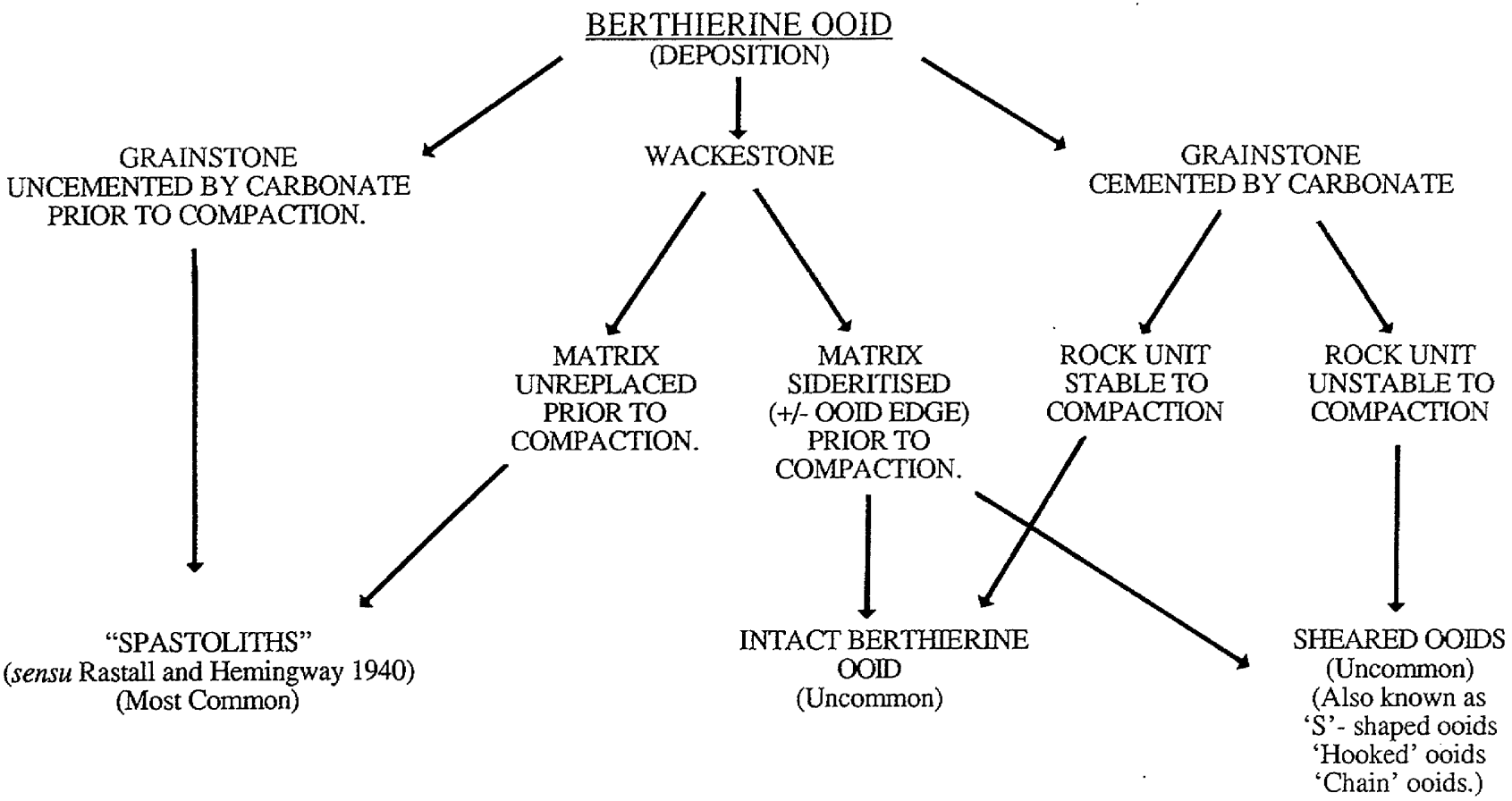

Figure 3.28. The Formation of 'Sheared' or 'Hooked' Ooids.

A) Undeformed, cemented ooidal grain-ironstone.

Points of fracture in B) and C) are indicated by arrows.

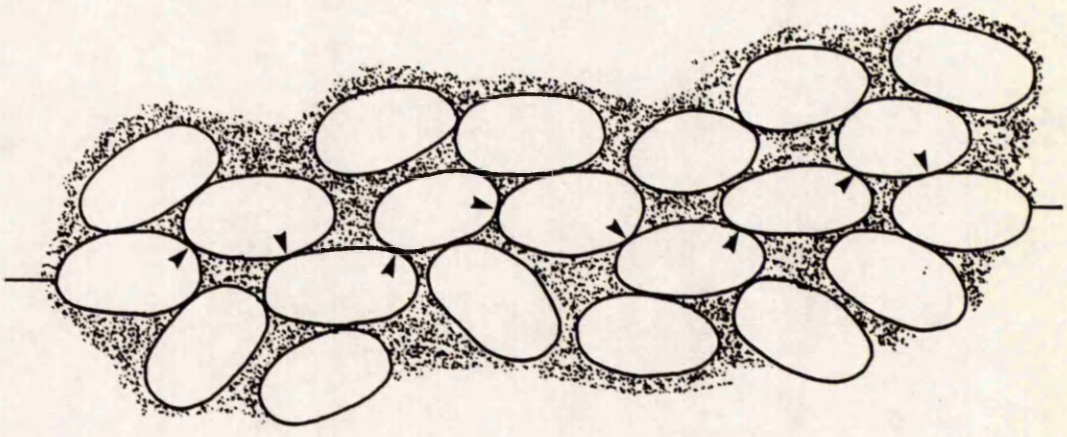

B) Formation by compaction.

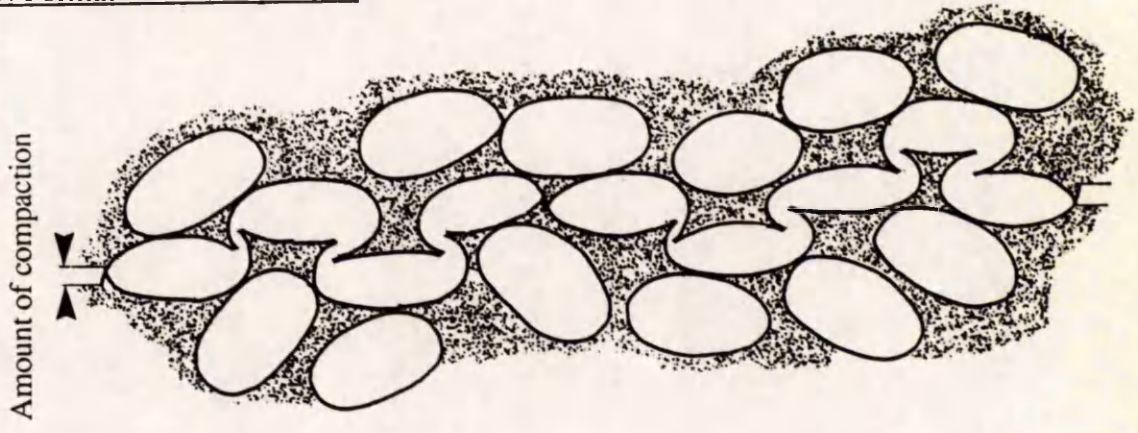

C) Formation by shear. (A small amount of dilation is included to emphasize the shape formed.)

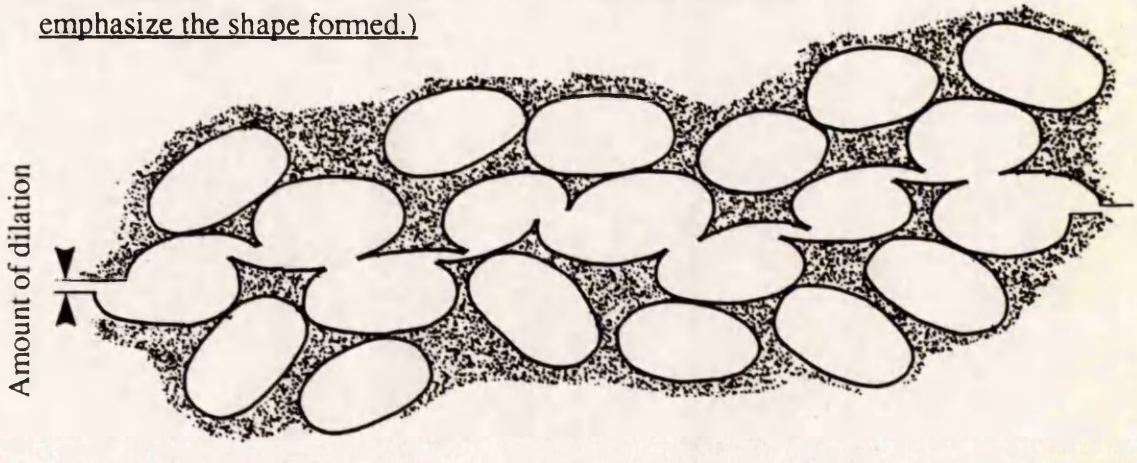

3.2.7.3) Implications for Ooid Genesis.

Three main implications for ooid genesis are suggested from the above:

1) The ellipsoidal shape of ooids is not compatible with formation by compaction. The fact that goethite ooids do not deform plastically, would necessitate the assumption that they were initially of berthierine. The argument would then fail when the narrow range of shape variation seen in goethite ooids is compared to the high degree of deformation in berthierine ooids within the ironstones, that have undergone similar compactive stresses.
2) The soft nature of the berthierine ooids makes it unlikely that they were transported far in their undeformed state. If a genetic link of berthierine oxidation to goethite is implied, then repeated episodes of berthierine production and oxidation would be necessary to give the ooid enough structural support for transport.
3) The lack of apparent plastically deformed goethite ooids, suggests that berthierine ooids were not reworked and oxidised following compaction, and confirms the primary goethitic mineralogy of these ooids at the time of cementation and compaction.

3.2.8) Ooid Mineralogy: Primary or Diagenetic?

The majority of iron-ooids in the Frodingham Ironstone Formation have been shown to consist of low Al goethite and berthierine in varying proportions within the cortex. A separate Al-bearing mineral phase, possibly an Al oxides/hydroxide, may also be present in small quantities within the ooids along with a small amount of phosphate and pyrite. The major question with regard to ooid mineralogy is whether the goethite and berthierine were primary constituents of the ooids, or whether they formed at a later stage.

Precipitation of goethite occurs during the formation of present day lateritic soil pisoids, and its formation on berthierine oxidation may be readily demonstrated by examination of ironstone weathering (section **6**.5.7). The formation of berthierine as a direct precipitate is seen as cements within the ironstone-formation, and an *in situ* modification of an aluminosilicate precursor is proposed below for berthierine mudstone formation. Therefore, a primary berthierine or goethite mineralogy to the ooids is geochemically possible. A mechanism exists for the transformation of berthierine ooids to goethitic ooids by single or

multiple event oxidation, and also from goethitic to berthierine ooids by solution of the goethite during microbial iron-reduction, with subsequent berthierine precipitation. In terms of actual formation and incorporation of goethite or berthierine into an ooid, there are hence a number of possibilities:

Goethite	i) Primary precipitation.	
	ii) Primary accretion.	
	iii) Oxidation of berthierine.	
Berthierine	i) Primary precipitation.	
	ii) Primary accretion.	
	iii) Diagenetic replacement of	a) An aluminosilicate precursor.
		b) Goethite, following iron-reduction.

It is possible that a single ooid may have undergone more than one of these processes during its formation, with the end mineralogy being dependent on the dominance of a particular process or processes. The complexity involved by the interaction of these processes can be demonstrated by the model in figure 3.29. The model is extremely simplified and not intended to show all possible pathways of ooid development, but illustrates how reworking, repeated introduction to oxidising/reducing conditions, transport, and *in situ* diagenetic mineralogical changes within the ironstones, may all contribute to ooid mineralogy. Other factors that are not considered in the model include the possibility of an initial mixed precipitation, degrees of berthierine and/or goethite formation, timescale, and the formation of other minerals. Despite this, a suite of variation is shown in the end mineralogy. With this in mind, it becomes clear to see how so many hypotheses of iron-ooid formation and mineralogy have been proposed and debated. It is also clear how ooid formation cannot be distinguished upon mineralogy alone, and that delineating the mineralogical development, must rely upon more than just thermodynamic considerations.

3.2.9) Iron-Ooid Formation: Models Discussed.

The detailed analysis of goethitic iron-ooids by petrographic and analytical methods given above, provides much new information on the nature of these particles. The

Figure 3.29. Possible Pathways of Ooid Mineralogical Development as a Function of Original Mineralogy, Reworking, Transport, and Diagenetic Modification.

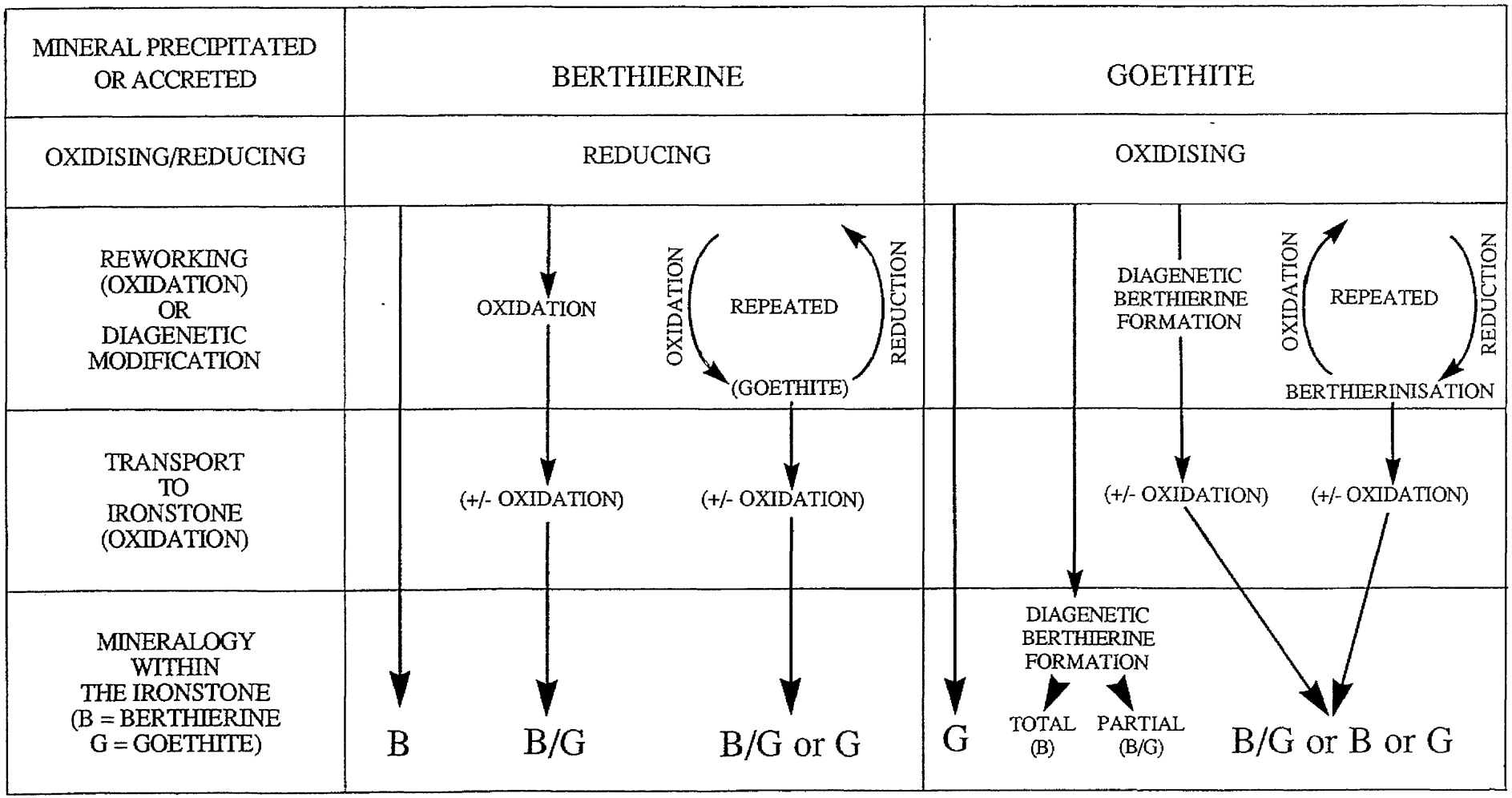

conclusions to these studies are briefly reviewed below, and then the various models of ooid formation proposed in the literature are tested in the light of this new data. The discussion is based upon the goethitic ooids, and extended later to fully berthierine ooids.

Iron-ooid shape has been shown to be of a primary oblate nature, and does not result from compaction. The oblateness developed by a three stage process of particle accretion, of which the second stage is always dominant, and led to the formation of an equatorial plane. Laminae within the goethitic ooids are composed of mixed goethite and berthierine crystals, which show a poorly defined tangential orientation. The laminae are continuous in goethitic ooids, but thin over the polar surface. Goethitic ooid nuclei are generally ooid fragments or goethitic particles. Berthierine ooids have less well defined lamination; nuclei of berthierine particles or ooid fragments; are usually compactionally deformed; and are restricted in occurrence to the "Snap Band".

Of the hypotheses given in the literature for iron-ooid formation (see section 1.5), a number cannot be proposed as possibilities for the generation of the Frodingham ooids. Replacement of carbonate ooids cannot be advocated as a mechanism for iron-ooid formation, due to the pronounced differences in ooid shape, internal fabric, nuclei type, and composition. Carbonate ooids do not form markedly oblate forms, whereas iron-ooids are ubiquitously this shape. Freeman (1962) showed that non-concentric cortices may develop within carbonate ooids, but the examples cited were rare and were not oblate. Though replacement of carbonates by iron minerals is seen in some limestones, such a replacement usually destroys the internal fabric. The nuclei of the Frodingham ooids are inconsistent with those of carbonate ooids, as the latter tend to nucleate on quartz or bioclastic debris, whereas the iron-ooids often nucleate on particles of goethite that show no signs of replacement. Petrography and E.P.M.A. has shown no examples of clear relict calcite within any iron-ooid, and berthierine or goethite replacement of carbonate particles has been shown to result in fabric destruction after dissolution and re-precipitation (see section 4.4.4 below).

Growth on the sea floor by either direct precipitation or mechanical accretion of free particles by a 'snowball effect', is not favoured here. The shape of the iron-ooids is in conflict with a formation by both precipitation and mechanical accretion onto a freely mobile ooid. Precipitation of a mineral onto an ooid surface would result in an isopachous fringe, and ultimately lead to the formation of a spherical particle. The oblate ooid shape is unsuited to rolling, and mechanical accretion would occur preferentially on parts of a non-spherical body to increase roundness and sphericity. Similarly, rounding would occur via abrasion during movement. A quiet water origin would hence need to be implied for development of a non-spherical ooid, but does not therefore answer how precipitation resulted in an oblate shape, or how particles were accreted if the ooid did not move. Knox (1970) attempted to explain this by suggesting non-movement of the ooid within a fluid flow containing a fixed concentration gradient of suspended material. It assumes a flat sediment surface, no grain interaction, and a constantly changing flow direction without changing sediment concentration levels. Such a scenario is however considered to be extremely unlikely in a natural environment.

Ooid mineralogy is also in conflict with ooid formation on the sea floor. To precipitate berthierine (or to have free detrital berthierine particles), significantly depleted oxygen levels would need to be implied (see sections **1.8**, **1.9**), but conditions at the site of ironstone accumulation were highly oxic, and there is no indication of widespread anoxia. It is also extremely unlikely that significant levels of dissolved Si, Al, and Fe could develop above the sediment-water interface. The berthierine must therefore be diagenetic. If a primary goethitic mineralogy is implied, then the ooids must have formed at or near the oxic-anoxic boundary within the sediment, or at the sediment-water interface. This is because the Fe is already in the oxidised state within oxic waters and chemically immobile. The formation of berthierine and goethite, are therefore both in conflict with a precipitation mechanism in agitated (and hence oxic) waters.

A pedogenic origin is unlikely for the Frodingham ooids, but the processes involved in the formation of soil pisoids may be strongly related to that of the formation of iron-ooids.

Ooid size, shape, and internal fabric are all different to soil pisoids (Bhattacharrya and Kakimoto 1982), but the goethitic mineralogy is compatible with a similar mechanism of formation. The composition of the Frodingham ooid goethites are non-aluminous, which is in contrast to most lateritic soil pisoids, but formation within a soil horizon could account for the presence of unstructured goethitic nuclei, and the fracturing of particles following desiccation during seasonal drying of the soil profile. There is therefore the potential mechanism for goethite precipitation, but not that for the development of oblate particles, of a regular and consistent shape. Polishing of ooid laminae is almost certainly related to bed transport of the ooid, and it appears unlikely that such transport could repeatedly erode from, and re-deposit into, a soil horizon.

3.2.10) A Model for the Formation of Frodingham Ironstone Ooids.

The favoured method of goethitic iron-ooid formation based on the findings of this work, is that the ooids formed within a sediment. This theory explains most, but not all, of the features seen in goethitic ooids. These features are now discussed with reference to their applicability and specific relevance to the development of a genetic model based upon a concretionary origin. Berthierine ooids are discussed separately at the end of this section.

The oblate ellipsoidal shape is strong evidence for postulating growth within the sediment ..The ooid would be effectively immobile, so that any process of non-uniform accretion would be reflected in the ooid shape. It is believed that non-uniform accretion (by precipitaion) was preferentially directed parallel to bedding, and controlled by either the compactional stress regime, or a differential horizontal and/or vertical permeability of the sediment. This is similar to the mechanism of formation of oblate concretions in ancient sediments (for example see Raiswell 1971, 1988). If reworking of the sediment occurred during ooid formation, then the ooid would re-settle parallel to the sea floor due to its oblate shape, and further accretion after deposition of a sediment cover would increase the oblateness.

The stage two accretion fabric that produces the oblate shape of the ooid, is compatible with this model, as maximum precipitation would occur in the direction of minimum stress, parallel to bedding. The actual stress regime necessary to produce this fabric is however not known. Stage one accretion could be due to transport and erosion of a coated nucleus prior to the main accretionary stages, which abraded away precipitates on convex surfaces of the nucleus, to give a rounded shape. Stage three accretion is however incompatible with this model, unless the ooids were reworked into an environment of less differential stress/permeability, such as that found within a shallower sediment cover. It would then be possible for accretion to occur on the polar surface, but this does not account for why accretion may actually decline on the equatorial surface. A mechanism similar to type one accretion, in which sphericity is increased to a more easily transported shape in a higher energy environment, is unlikely for this stage, as this fabric is unlikely to result from erosion.

The actual shape of the laminae and their development relative to other concretionary bodies, cannot easily be tested, for similar internal structures are not found in ancient concretions other than soil ooids and pisoids. The distinct break between successive laminae precipitation, and polished surfaces to groups of laminae, are assumed to indicate periods of reworking of the ooids from the sediment, with relatively short periods of polishing in agitated conditions. Little abrasion occurs at this stage, because although the laminae thin over the polar surface, the fabric remains intact and laminae are not truncated by erosion surfaces in any ooids. It is hence unlikely that the development of broken ooids is associated with this polishing (unless the ooids were weakened by desiccation), as current energies were sufficient to only polish, and not fracture the ooids.

The tangential fabric distinguished within the ooids does not support a precipitation mechanism, as precipitation would be normally be expected to form a radial fabric, and can be seen to do so within berthierine cements of this ironstone-formation. Studies of carbonate ooids have however shown that both radial and tangential fabrics are found (see review by Richter 1983), and both may be formed by an initial precipitation mechanism.

The formation of carbonate ooids is still widely debated and the literature is too vast to be discussed here, but experimental work by Davies *et al.* (1978) and Deelman (1978), suggests that a tangential fabric can be formed in carbonate ooids by precipitation, without mechanical 'snowball' accretion. Davies *et al.*(1978) argue that carbonate ooids with a tangential fabric grew in suspension, where the degree of turbulence induced grain impacts of sufficient energy to inhibit crystal growth other than in a tangential direction. Deelman (1978) suggests a similar precipitation, but that the tangential orientation is related to ooid movement along the bed, with polishing during intermittent agitation. Both these mechanisms invoke agitated water, but Richter (1983, p. 79) points out that coated grains in calcretes possess a tangential orientation of calcite in the cortex, proving an independence of such a fabric from water agitation. It is proposed here that the common link between these occurrences and proposed mechanisms, is that radial growth was inhibited by physical forces, either by impact between grains or the bed, or by formation in a constrained regime. There is no doubt that calcretes form by *in situ* calcite precipitation within the sediment, and hence the fabric of calcrete ooids would be expected to form in other types of precipitated ooid under the same regime.

The T.E.M. studies of Hughes (1989) showed that the apparent tangential fabric could not be strongly defined, as preferred alignment was not visible. This is consistent with calcrete and Bahama-type ooid fabrics whose fabrics show only statistical tangential orientation (Richter 1983), and would hence not be clearly visible under such a high-resolution technique. It should be remembered however, that such a fabric could equally be a primary or diagenetic fabric, but the discussion above demonstrates that formation of a tangential fabric in an ooid cortex need not be assigned to precipitation under agitated conditions.

During the course of this research much work was carried out on the composition and origin of the berthierine in the ironstone-formation, which is described in detail below within sections **4**.8 and **4**.9. The conclusion to these studies was that authigenic berthierine formed because a detrital assemblage of illitic/kaolinitic clay and iron-oxide/hydroxides, was

unstable under post-oxic diagenesis. The berthierine formed either as a replacement to the mud, occasionally undergoing recrystallisation as it did so, or as an authigenic cement. It is here postulated that the berthierine within goethitic ooids was similarly derived, and formed within goethitic ooids as both a replacement and as a cement, as it is seen to possess both orientated and random fabrics. The novel basis to this hypothesis, as opposed to previous interpretations, is that berthierine need not be assumed to have precipitated at the time of ooid formation, and neither did a separate precursor clay mineral. Instead, the scenario is simplified by assuming that the ooid formed in the same way as normal concretions, by precipitation of a mineral (here goethite) within the pore space of detrital clays. The mineralogy of these clays was that described in section 4.3, and the assemblage became unstable during post-oxic diagenesis leading to the formation of berthierine. The mechanism implies breakdown of the detrital clays and repreciptation of berthierine within the sediment, such that the resultant fabric would be similar to that of a primary precipitate, and may develop a tangential fabric as described above. Complex diagenetic alternations between berthierine and goethite precipitation may have occurred, but are hence not necessary for ooid formation.

The tangential fabric of the berthierine within ooids may hence possibly result from either primary precipitation of berthierine, or from later diagenetic modification of clay minerals trapped within the ooid during formation. The latter scenario implies initial goethite precipitation only, with the berthierine-rich laminae representing layers in which there was little iron precipitation, as is demonstrated in the formation of Liesegang rings. Oxidation of berthierine to form the goethite fails to explain the reason why thick isopachous rims of goethite do not occur around ooids. Given the porous nature of the ooids shown by T.E.M. (Hughes 1989), oxygen would be expected to diffuse to an equal depth in the ooid, producing an isopachous goethitic rim as opposed to thick goethite laminae at the equatorial surface, thinning to the polar surface.

The site of formation of the ooids is assumed to have been onshore of, or adjacent to, the site of ironstone accumulation, to allow for their derivation by storm activity. If goethite is

the only mineral precipitated, there is no need to imply surface reducing conditions or restricted lagoons, but the possibility of berthierine formation at the site of ooid formation is not necessarily discounted. As the ironstone-formation itself can be demonstrated to have undergone post-oxic diagenesis (this research), it is sensible to assume that the iron for ooid formation was derived from the post-oxic reduction of iron-oxides, and hence formation within the marine environment is possible. A marine origin also readily explains how the ooids could be reworked and polished during minor bed transport, prior to re-incorporation within the sediment.

3.2.10.1) Ooids of 'Pure' Berthierine.

Ooids composed of only berthierine are of a different nature to the goethitic ooids and are extremely difficult to study as indicated above in section 3.2.7.2. The interpretation of ooid formation given above was based on goethitic ooids, and its applicability to berthierine ooids is assessed here. The berthierine ooids were almost certainly also formed during post-oxic modification of an unstable detrital assemblage, but the major question given the absence of goethite, is whether the ooid itself was initially of berthierine. The similarities in shape and internal fabric between berthierine and goethitic ooids, suggests that the berthierine ooids formed within the sediment in a similar way to goethite ooids. However, differences in mineralogy and nuclei type, an inability to be transported without oxidation, and their restricted occurrence to the "Snap Band", suggests a separate.source from goethitic ooids.

Two possibilities exist for the formation of the pure berthierine ooids based upon the conclusions for berthierine formation given above and within section 4.9. The first is that berthierine precipitated as a cement, forming a primary berthierine ooid, and the second is that the ooid was originally of a separate mineralogy. In the latter possibility, it would appear that the mineralogy of the precursor ooid must have been goethitic, because there is no clear mechanism to suggest why any other mineral phase should be both precipitated, and form ooids within the sediment. The possibility of a mechanism whereby goethitic ooids could be reduced and liberate Fe to form berthierine has been discussed above (section

3.2.8). Although theoretically possible, the likelihood of full reduction of all the goethite within the ooid seems unlikely, due to the large volumes of goethite that would need to be reduced. Though the porosity of ooid cortices is high (Hughes 1989), with small and hence potentially reactive particles of goethite, the nuclei are dense and less likely to react. The ooids described here also do not show any relict goethite within the ooid.

It is believed that the berthierine ooids are primary precipitates, and not replacements of a former mineralogy. It is assumed that they formed within a muddy sediment that became unstable due to post-oxic diagenesis, but whether the mud itself was extensively berthierinised is unclear. The sediments in which the ooids are found within the sequence, are muddy, and also highly bioclastic. It is hence thought that the ooids were not formed at the present site, but were reworked and deposited with much of the mud that was possibly already transformed to berthierine. The reworking event must have been rapid, as oxidation of the ooids did not take place, but any slight oxidation that occurred may have been reversed during post-oxic diagenesis of the ironstone-formation itself. The actual site of formation of these ooids is unclear.

3.3) Non-Ooidal Ironstone Components.

3.3.1) Non-Ooidal Coated Grains.

Under the terminology of section 1.2.2, the particles described here (plate 10) are pisoidal, of uncertain origin. The internal fabric of all these particles is markedly different to the iron-ooids, implying they are not simply evolved ooids, but specific evidence to define these particles as soil pisoids, vadoids or oncoids is lacking and discussed below. The particles are not abundant in the sequence and are often restricted to particular thin beds where they may form a high proportion of the rock. Examples of both goethitic and berthierine varieties may be seen. The goethitic ones are much more common and vary in size from 1-11mm, do not necessarily possess a nucleus, are not well rounded, and have a variable shape. The lamination within the cortex is not as regular as ooids, with development of wavy lamination through to distinctly domed structures in some specimens. Ooids and bioclastic fragments may be incorporated within the lamination. Examination of

PLATE 10

Thin-section Photomicrographs of Larger Coated Grains ('Pisoids')

A) Goethitic pisoid in ooidal grainstone, specimen YAR. 21 (stained). This specimen is fractured and contains a large proportion of siderite in the layering and within fractures. Photo length is equivalent to 3.3mm.

B) Goethitic/berthierine pisoid from the "Snap Band", specimen YAR. C. This pisoid is finely laminated, with the layering picked out by alternating goethite and berthierine laminae. Siderite has partially replaced part of the pisoid. The large size of this specimen is indicated by comparison to the accompanying ooids. Photo length is equivalent to 6.7mm.

C), D) Fully berthierine pisoid, specimen YAR. C. The lamination within this specimen is poorly defined, and largely evident only under crossed polars (**D**). A large amount of recrystallisation has hence taken place on conversion to berthierine. Siderite cements the rock, and partially replaces the pisoid, particularly at the edge. Photo length is equivalent to 6.7mm.

A	**B**
C	**D**

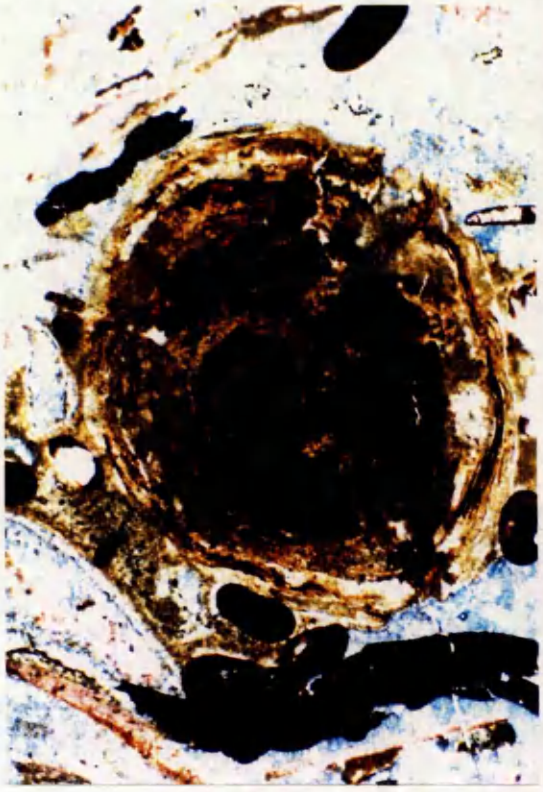

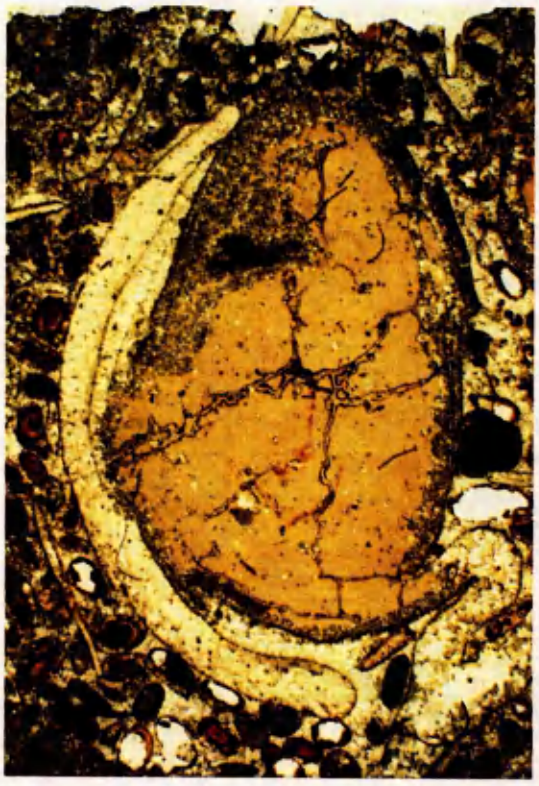

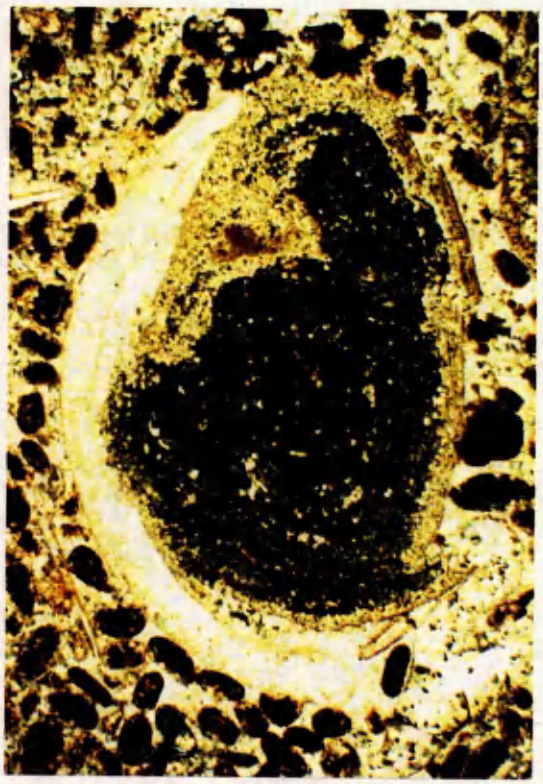

these particles under Ultra Violet light failed to reveal the presence of any organic matter within the laminae.

Berthierine pisoids, and berthierine laminae within goethitic pisoids, are distinctive as they lack a fine lamellar structure, and possess a fabric that is largely composed of randomly orientated crystallites of berthierine . In the case of fully berthierine pisoids, the structure is poorly represented suggesting that the fabric was destroyed during berthierinisation (plate 10 c,d).

The interpretation of large coated grains has attracted much discussion in the literature (see papers in Peryt 1983), and in particular the differentiation between inorganically precipitated vadoids (concentrically laminated particles which originated within the vadose zone) and biogenically formed oncoids, has been problematical. Vadoids may be fluvial, shallow-marine, evaporitic, and also form within soils and caves, so are not environmentally diagnostic. They are commonly calcitic, but soil vadoids are commonly ferruginous. Most oncoids are calcitic, but ferruginous oncoids have been reported, including the "Snuff Boxes" of the Inferior Oolite of southern England. These large (up to 30cm) oncoids were studied by Gatrall *et al.* (1972), who considered that their ferruginous nature was due to their formation in epicontinental seas, but were unspecific as to whether the iron was inorganically or biogenically formed. Palmer and Wilson (1990) recently concluded that the iron oxide/hydroxide layers in these oncoids were precipitated under the influence of non-photosynthetic, iron-oxidising bacteria, on the underside of the oncoids. There is therefore the possibility that ferruginous coated grains may be either vadoids or oncoids.

The pisoids of the Frodingham Ironstone Formation are tentatively assigned here to the inorganically precipitated vadoids, as opposed to true oncoids. The strongest argument for this is the total lack of algally produced biogenic sediments in the ironstones other than the particles under discussion. This is in contrast to the "Snuff-Boxes" that are clearly associated with stromatolites. It is assumed that the vadoids formed by a similar process to that of the iron-ooids, but in a way that resulted in a less well defined internal structure.

This internal fabric and mineralogy is similar to soil vadoids, but the inclusion of bioclastic debris in some laminae suggests a marine origin. The presence of iron-ooids within these vadoids supports a similar origin within the sediment to that of the ooids described above, as it is unlikely that large particles such as ooids would adhere to a freely moving pisoid. These vadoids would have formed in a similar region to that of the iron-ooids, in order that the ooids could be overgrown and incorporated during vadoid growth. They are however more restricted in occurrence than ooids , and are commonly concentrated within thin beds, as opposed to having a uniform distribution throughout the sequence. These particles hence underwent the same diagenetic modifications as the iron-ooids which resulted in similar fabrics to those discussed above for the ooids.

3.3.2) Bioclastic Material.

The Frodingham Ironstone Formation contains a large proportion of bioclastic material, that is dominated by bivalves, brachiopods, echinoids, crinoids, and ammonites, with belemnites, nautiloids, gastropods and foraminifera also present (plates 2, 3 and 4). This material is most commonly seen as reworked allochems, evidenced by shells that have been disarticulated, broken, and abraded to varying degrees. The size of bioclastic material is controlled largely by the type of particle and its resistance to breakage. Most shell debris is fragmented, but echinoderm particles remained as intact plates following disarticulation. Particle sizes therefore range from a millimetre scale to over 10 cm. Abundance of a particular bioclast type is largely unpredictable, but shelly material is usually in a greater proportion to that of echinoderm debris. Diagenetic modification and preservation of bioclastic debris, is described in detail within section 5.7.2, but shell material has also been extensively modified, and ultimately destroyed, by boring organisms.

3.3.2.1) Microborings.

Microborings are produced by the penetration of hard substrates by microorganisms, referred to as endolithic organisms. Cyanophytes (blue-green algae), chlorophytes (green algae), rhodophytes (red algae), sponges, fungi, and possibly bacteria, are all represented. The substrates (wood, bone, carbonate etc.), boring size (usually 1-

100μm), and morphology vary considerably, and modern studies are able to distinguish many forms (for example Budd and Perkins (1980) recognised 27 types off the coast of Puerto Rico). Most types of boring are marine, though some are known from freshwater environments (Golubic *et al.* 1975). Endolithic organisms require light, and their occurrence is restricted to the photic zone. In the tropics this limits depth to 80-100m (Budd and Perkins 1980), which decreases with latitude as the proportion of the suspended material increases and the angle of sunlight decreases. The most intensive boring is in the shallowest waters. Borings can therefore be used as limited depth indicators. Sedimentologically, their importance is in the destruction of carbonate grains either by direct boring, or by rendering the grain more susceptible to erosion (Bathurst 1966). In carbonate sediments borings are commonly infilled with carbonate mud (micritisation).

Investigation of the morphology of borings within the Frodingham Ironstone Formation revealed three groups: which will be designated Types I-III (plate 11). Subdivisions of these groups was not attempted.

Type I. This type consists of fine filaments 2-4μm thick, which extend into shell fragments roughly perpendicular to the shell surface. Bifurcation may occur, and be repeated, but usually only a single filament is present. A near spherical 8-25μm sac structure (sporangia?) at the termination of the filament, or off a short branch near the end of the boring is common. The type I boring is the most common, and may be of fungal origin due to the small width of the tubes (Bathurst 1975).

Type II. The second type has wider borings (6-8μm), with less consistency in width. They frequently branch at high angles, but are not associated with any sac-like structure. The inconsistency of width, and the larger size, suggest an algal origin. These borings are much less common.

Type III. The final group essentially forms a micrite envelope of roughly equal thickness, without any distinct individual bores extending into the shell. This cannot

PLATE 11

Borings Within Bioclasts

(Thin-Section Photomicrographs)

A) Type I boring, specimen YAR. 24 (stained). The original shell material has dissolved and is replaced by ferroan calcite, but the goethitic lined borings have remained intact. This bored specimen is unusual in possessing an outer portion in which the borings have been lost on replacement. The external outline of the shell is still visible (arrowed). Photo length is equivalent to 1.3mm.

B) Detail of Type I borings, specimen YAR. 7 (stained). The finely filamentous structure of this type of boring, and sac-like termination is clearly visible. A sac has been sectioned, and shows the thin goethitic lining within (arrowed). Photo length is equivalent to 0.35mm.

C) Type II boring in an unreplaced fragment of oyster shell, specimen YAR. 21 (stained). Photo length is equivalent to 0.7mm.

D) Type III boring in an unreplaced fragment of oyster shell, specimen YAR. 21 (stained). This type of boring does not deeply penetrate the shell, and results in a 'micritic' envelope on the bioclast. Photo length is equivalent to 0.7mm.

A	B
C	D

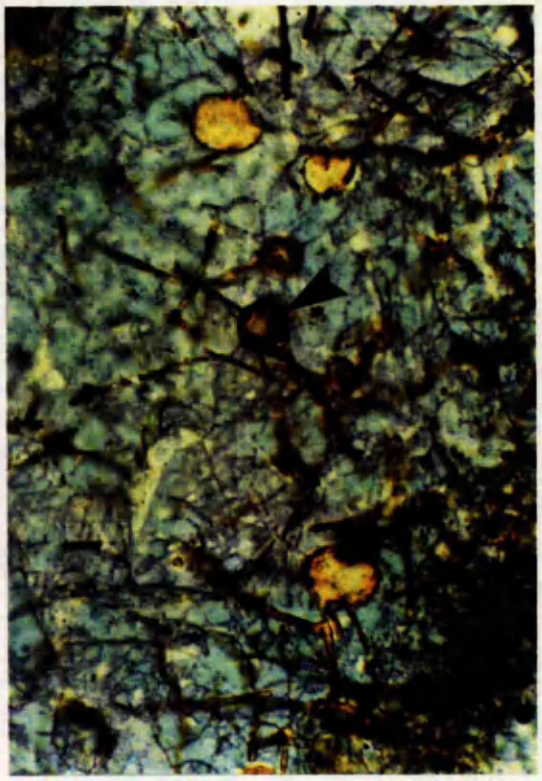

hence have been produced by either of the processes suggested by types I or II, and is therefore assigned to a third category. No internal structure to the envelope can however be seen.

Borings of type I and II may extend across the whole shell fragment, but the micrite envelope is restricted to an outer layer of variable thickness. All types occur both independently, and in any combination, suggesting a similar depth and environmental relationship. No correlation between rock-type and boring-type could be established, though in general, bioclasts are more highly bored in the grain-ironstones. This is due to a higher residence time in the water column as constant reworking of these beds occurred. Petrogaphic examination shows the borings to be usually lined with goethite a few microns thick, though berthierine has also been seen. Purely qualitative microprobe analysis of this goethite suggested a small amount of Si and Al to be also present.

Boring is confined to shell fragments, with no indications of boring having occurred in echinoderm fragments or iron-ooids. Borings are usually well developed only on bioclasts in which the structure has remained intact . Since the preservation of borings may be possible due to the goethitic inner coating (see discussion, section **5**.7.2.2), this occurrence suggests that the borings were concentrated in the originally low magnesium calcite shells of the brachiopods and oysters (especially *Gryphaea*).

3.3.3) Detrital Clays.

Most of the terrigenous detrital component within the ironstone-formation itself as opposed to the transitional beds, is present as a mud to silt-sized fraction of detrital clay, muscovite, and organic material (see plates 5 and 12). The clay is green, low birefringent berthierine, and is interpreted to be a diagenetic modification of a former detrital assemblage that became unstable during post-oxic diagenesis. This is discussed in detail within section **4**.3.2. Muscovite occurs sporadically as small <60μm long particles, and is apparently not affected by this modification. The organic matter is described separately below.

PLATE 12

Organic Matter, Examined Under U.V. Light

A), B), C) Examples illustrating the nature and type of organic matter preserved in the berthierine mudstones of this ironstone-formation, specimens DRAG. 31.27, Y183. 9, and Y183. 5, respectively. Much of the organic matter fluoresces yellow, and is composed largely of acritarchs/dinoflagellates and spores (exinite). Non-fluorescent woody material (vitrinite) is also present, and is arrowed in C. Photo length in each case is equivalent to 0.35mm.

D) Acitarchs/Dinoflagellates in a ferroan calcite cemented ooidal grain-ironstone, specimen DRAG. 31.27. The presence of these microfossils suggests that during the last stages of cementation of this specimen (believed to be by meteoric water), marine water passed through the pore. Photo length is equivalent to 0.35mm.

A	B
C	D

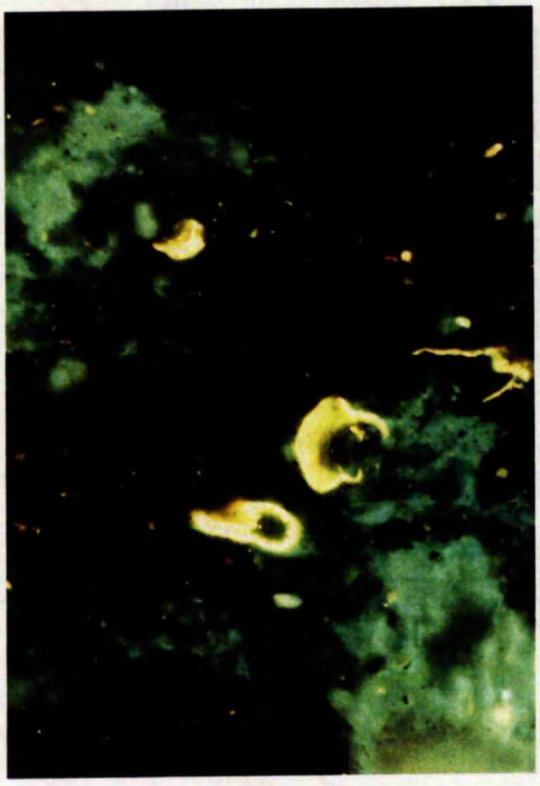

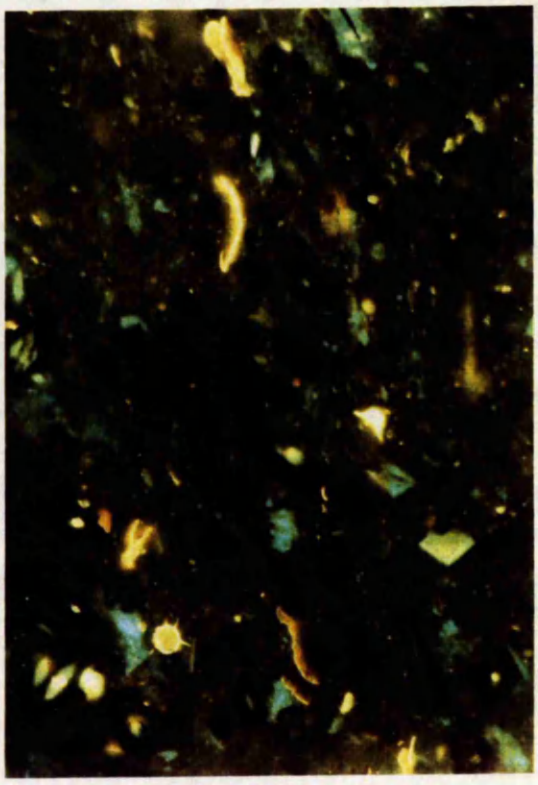

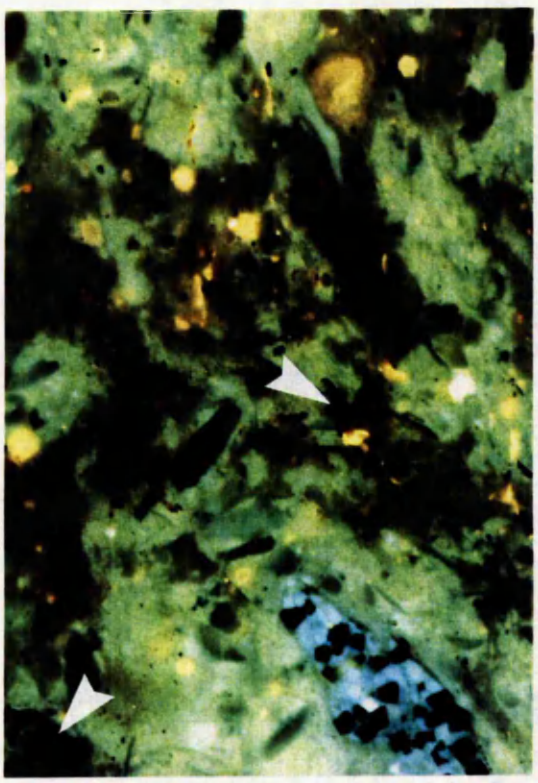

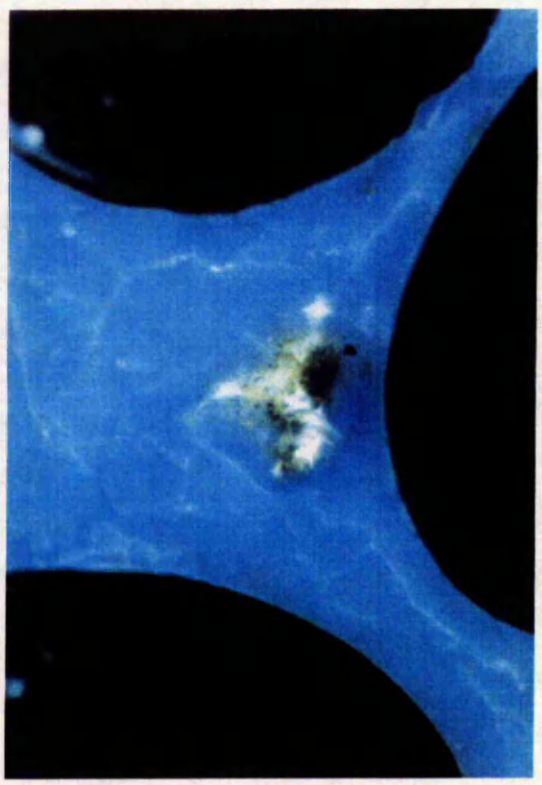

The muds occur throughout the sequence, but are easiest to study within the thin mud drapes (Type 'B' ironstone). The fabric is typical of mudstones in having parallel lamination that may give the mud a fissile nature. Where bioturbation has been intensive, all detrital fabric is lost, and this may be also the case where extensive sideritisation and/or berthierinisation has occurred. Sideritisation (or ferroan calcite replacement) merely replaces the mud, but berthierinisation may cause recrystallisation of the fabric to a random orientation of berthierine crystals.

3.3.4) Organic Matter (O.M.).

The type and nature of O.M. within a sediment, has a significant effect on microbial reactions that may occur during early diagenesis. In particular, the development of post-oxic zonation is thought to occur via the intensive biodegradation of O.M. to levels unable to support sulphate-reduction. The O.M. remaining within the sediment would hence be expected to be refractory, and highly degraded relative to 'normal' sediments. For this reason, organic petrography using Ultra-Violet (U.V.) light, was undertaken to briefly ascertain the possible source. type, and nature of the O.M. within the ironstones (see plate 12). Full O.M. analysis of the ironstone-formation was beyond the scope of this research, due to its time consuming nature, and complexity of interpretation.

Polished thin-sections of the ironstones, particularly mudstones, were examined under U.V. light to reveal O.M. type by its fluorescent properties. Distinction was made between the four basic types of O.M. in sedimentary rocks. These are listed below with the coal maceral type in parentheses:

Type I. (Alginite). Algally derived O.M. commonly of lacustrine origin (sapropel). This O.M. is highly reactive, and in sufficient quantity forms an excellent oil source rock. Highly fluorescent.

Type II. (Exinite, includng sporinite (spores), and cutinite (plant cuticle)). This has an intermediate derivation of mixed continental and marine types of O.M., including algal tissue, pollen, spores, and dinoflagellates. Fluorescent.

Type III. (Vitrinite, including telinite (preserved woody structures), and collinite (essentially structureless matrix)). This is humic O.M. of terrestrial woody origin. Non-fluorescent.

Type IV. (Inertinite, including fusinite (fossil charcoal), and sclerotinite (fungal spores)). Oxidised or altered O.M., that is essentially organically inert. Non-fluorescent.

The O.M. of the ironstone-formation was found to fit well with that of a Type II / Type III mixed assemblage, with the greatest abundance of O.M. occurring within the mudstones. Dinoflagellate cysts/acritarchs and spores are the most conspicuous O.M. due to their strong fluorescence, though the proportion of woody non-fluorescent vitrinitic material is also high. Within the latter, tellinite of a distinct structure may be visible, but much of the non-fluorescent O.M. has an irregular outline and no internal structure. Amorphous, algal-derived, Type I material was not seen. The assemblage is typical of a marginal marine setting with mixed marine (dinoflagellate/acritarch), and terrestrial (spores, vitrinite) organic matter.

CHAPTER 4. BERTHIERINE PETROGRAPHY AND COMPOSITIONAL VARIATION.

4.1) Introduction.

This chapter aims to describe the various textures and morphologies of berthierine seen within the ironstone-formation, to distinguish their primary or replacement origin, and attempt to explain berthierine formation within the Frodingham Ironstone Formation. Compositional data obtained by E.P.M.A., allow geochemical comparison between types of berthierine in this Formation and with those of other ironstones.

4.2) E.P.M.A. of Berthierines, and Graphical Data Representation.

Clay minerals are not ideally suited to analysis by E.P.M.A. due to the high porosity of the structures they form, coupled with their variable morphology and orientation in thin-section. Individual crystals of berthierine are too small to be analysed singly by E.P.M.A., and even using Analytical Transmission Electron Microscopy (A.T.E.M.) may require analysis of several crystals (each only 20 x 500-1000nm in size, Hughes 1989). It was not the intention of this work to obtain the purest composition of berthierine possible, as E.P.M.A. cannot compare with A.T.E.M. in this respect, and analyses of Frodingham berthierines, have already been obtained by this method (Hughes 1987, 1989). This work attempted to ascertain the variation in composition between the different morphologies of berthierine seen within thin-section (not seriously attempted previously), such as ooids, cements, muds, replacement fabrics etc., and between various occurrences of the same type of berthierine. Such an undertaking using A.T.E.M. would be beyond the scope of this research, as it would be extremely time-consuming, with possibly similar conclusions. E.P.M.A. of berthierines was successfully used by Maynard (1986). The preparation methods, precautions to avoid beam damage, and recalculation procedures used are all given in appendix A.2.1. It is important to note that the valency of iron is here assumed to be two, i.e. that of the reduced species (Fe^{2+}), as indicated by published wet chemical analyses that indicate a minimal, or near absent, Fe^{3+} content (see appendix E).

The E.P.M.A. analyses have been used in the construction of various plots to graphically represent the data. Chlorite compositions have usually been represented on a Si - Fe(+/-Mg) - Al(Total) ternary plots to indicate the proportions of the major cations in the structure. Though structurally different, berthierines have a similar composition to the chlorites, and hence may be similarly represented. Fe - Mg - Al(Total) plots have also been widely used (for example Humphreys *et al.* 1989, Jahren and Aagaard 1989, Curtis *et al.* 1984, Curtis *et al.* 1985), but a more significant variation on this plot is that of a Fe - Mg - Al(Octahedral) ternary plot, that represents the composition of the octahedral sites (for example Hughes (1989)). To allow for full comparison with other published berthierine compositions that have been variably represented in graphical form, all three plots have been utilised where necessary. The Velde (1977) MR^3 - $2R^3$ - $3R^2$ plot is not of use in chlorites due to the low or absent interlayer cations in the chlorite structure. Data are also given on a Hayes (1970) plot for chlorites, a simple graphical construction of tetrahedral Al versus (octahedral) Fe/(Fe+Mg), after recalculation of berthierines to a chlorite formulae.

4.3) 'Detrital' Muds.

The greatest proportion of berthierine in the ironstone is present as 'detrital' muds within mudstones, packstones and wackestones. The petrography of such muds, associated detrital particles, organics, and other authigenic minerals, has been given above (see sections 3.3.3 and 3.3.4), so this section will deal only with the mud fraction composition. The muds were analysed by E.P.M.A., and the results are given in tables 4.1 and 4.2. It is not intended that these represent pure compositions of a single mineral species, but that they represent a bulk mineral composition of the clay sized fraction of the mudrocks, free of carbonates, pyrite and organics. With careful beam positioning it is possible to avoid these latter phases even on a defocussed electron beam. The samples were also analysed by X.R.D., to examine the mineralogy of the clays, using the methods described in appendix A.2.3.

When plotted on a Si - (Fe+Mg) - Al(TOT) plot (figure 4.1), each sample gives a cluster of values, indicating that the composition of the analysed areas is approximately similar

Table 4.1. Average Matrix Compositions For DRAG. 31.1 and 7, Obtained By E.P.M.A. The Data have been Recalculated to Both Berthierine and Illite Structural Formulae.

	DRAG31.1		DRAG 31.7	
	AVERAGE	STDEV	AVERAGE	STDEV
Si	16.393	2.740	13.262	3.275
Ti	0.235	0.078	0.100	0.058
Al	9.153	1.290	7.621	1.940
Fe	7.713	1.101	11.477	2.309
Mn	0.038	0.050	0.075	0.054
Mg	1.506	0.163	1.953	0.348
Ca	0.260	0.099	9.300	5.993
Na	0.575	0.243	0.313	0.155
K	2.262	0.548	1.674	0.544
P	0.003	0.006	0.058	0.061
S	0.303	0.218	0.047	0.055
O	30.957	3.763	30.789	4.023
TOTAL	69.397	7.288	76.669	6.310
BerthCalc.				
Si	4.219	0.240	3.399	0.432
Al(T)	-0.219	0.240	0.601	0.432
Al(O)	2.684	0.137	1.432	0.669
Ti	0.036	0.014	0.015	0.008
Fe	0.982	0.203	1.483	0.152
Mn	0.005	0.007	0.011	0.008
Mg	0.454	0.059	0.584	0.053
Ca	0.047	0.021	1.842	1.380
Na	0.190	0.103	0.099	0.046
K	0.419	0.088	0.307	0.067
OCT.	4.161	0.127	3.524	0.817
INT.	0.656	0.123	2.249	1.331
CH	8.000	0.000	8.000	0.000
IlliteCalc.				
Si	6.630	0.378	5.341	0.679
Al(T)	1.370	0.378	2.659	0.679
Al(O)	2.503	0.215	0.535	1.051
Ti	0.057	0.022	0.023	0.013
Fe	1.543	0.319	2.331	0.239
Mn	0.008	0.010	0.017	0.013
Mg	0.713	0.093	0.918	0.084
Ca	0.074	0.032	2.895	2.168
Na	0.298	0.162	0.156	0.072
K	0.659	0.138	0.483	0.105
OCT.	4.898	0.199	6.719	0.901
INT.	0.957	0.170	0.639	0.115
CH	4.000	0.000	4.000	0.000
	n=9		n=10	

Table 4.2. Average Matrix Compositions for DRAG. 31.13/14, 21, and YAR. 7, 24. The Data have been Recalculated to Berthierine Structural Formulae Only.

	DRAG. 31.13/14		DRAG. 31.21		YAR. 7		YAR. 24	
	AVERAGE	STDEV	AVERAGE	STDEV	AVERAGE	STDEV	AVERAGE	STDEV
Si	12.918	0.400	10.665	0.841	6.098	1.678	1.524	0.626
Ti	0.204	0.050	0.155	0.053	0.015	0.018	0.028	0.026
Al	8.282	0.264	6.376	0.504	3.451	0.903	0.832	0.415
Fe	24.717	1.773	25.007	1.689	14.207	3.198	4.311	2.440
Mn	0.238	0.165	1.881	1.777	0.155	0.160	0.344	0.010
Mg	2.293	0.237	2.205	0.115	1.246	0.339	0.614	0.090
Ca	0.482	0.197	1.194	0.904	15.146	8.472	31.952	2.967
Na	0.234	0.119	0.176	0.099	0.194	0.132	0.130	0.140
K	0.642	0.356	0.158	0.063	0.259	0.289	0.129	0.139
P	0.017	0.029	0.006	0.011	0.228	0.271	0.128	0.135
S	0.027	0.023	0.032	0.027	0.118	0.108	0.028	0.033
O	31.306	0.537	not calculated	not calculated	21.422	1.885	17.226	0.590
TOTAL	81.359	1.631	47.854	0.924	62.536	5.992	57.244	1.153
BerthCalc.								
Si	3.294	0.068	3.073	0.142	2.310	0.653	0.706	0.263
Al(T)	0.706	0.068	0.927	0.142	1.690	0.653	3.294	0.263
Al(O)	1.492	0.104	0.985	0.228	-0.333	0.989	-2.894	0.447
Ti	0.031	0.008	0.026	0.009	0.004	0.005	0.008	0.007
Fe	3.167	0.221	3.623	0.194	2.709	0.675	0.999	0.536
Mn	0.031	0.022	0.284	0.280	0.031	0.035	0.083	0.005
Mg	0.676	0.068	0.736	0.042	0.550	0.164	0.332	0.041
Ca	0.084	0.036	0.244	0.197	3.968	2.381	10.501	1.324
Na	0.073	0.037	0.063	0.037	0.089	0.060	0.074	0.078
K	0.117	0.064	0.033	0.013	0.070	0.075	0.043	0.044
OCT.	5.397	0.112	5.654	0.071	2.961	1.605	-1.473	0.964
INT.	0.274	0.063	0.339	0.208	4.126	2.381	10.617	1.279
OH	8.000	0.000	8.000	0.000	8.000	0.000	8.000	0.000
	n=12		n=10		n=6		n=4	

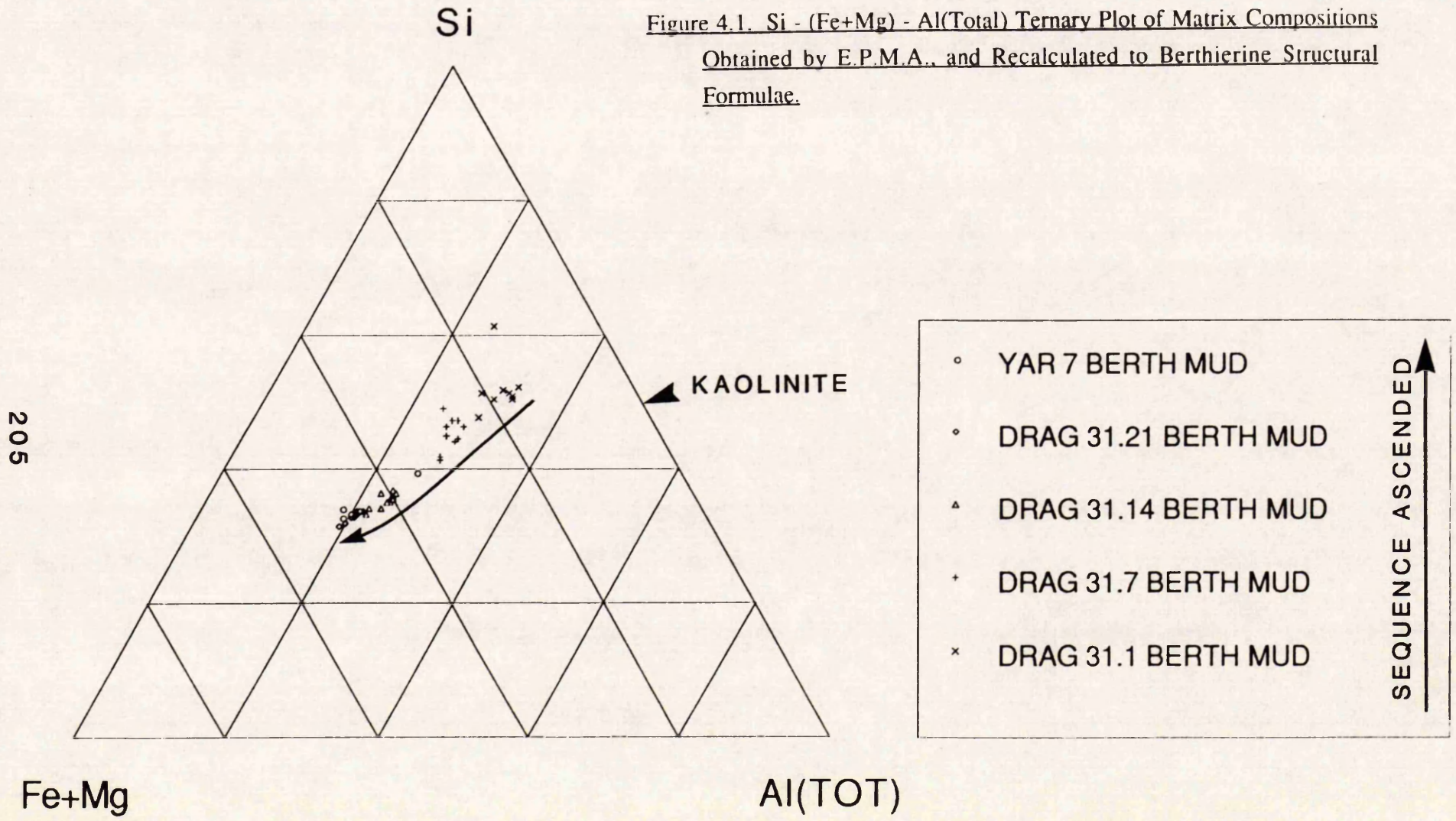

Figure 4.1. Si - (Fe+Mg) - Al(Total) Ternary Plot of Matrix Compositions Obtained by E.P.M.A., and Recalculated to Berthierine Structural Formulae.

within the sample, and that therefore the mixture of clay mineral types is approximately equal across the thin-section. When all the analyses are plotted together however, a clear trend is evident between a berthierine composition and that of a low Fe, Mg, aluminosilicate. The trend could be assigned to a distinct compositional change of a single clay mineral species, or to mixing between between berthierine and the end-member described. There are two likely possibilities for the 'end member', that of a single aluminous illitic phase such as reported by Warren and Curtis (1989), with an Si/Al ratio of around 1.4, or a mixture of a more siliceous illite with kaolinite. X.R.D. analysis was attempted to resolve these problems in two ways; by scanning the d_{001} peak of berthierine and d_{002} peak of illite between 7-14° 2θ (Cukα radiation) to qualitatively describe the relative abundance of these two minerals; and by scanning the d_{002} peak of berthierine at around 25° 2θ (figures 4.2 and 4.3), in an attempt to identify any minor kaolinite presence from a peak doublet. This analysis was undertaken on the samples analysed by E.P.M.A.

As the ironstone sequence is ascended (sample number increases) the d_{002} peak of illite is seen to gradually diminish in the muds relative to the berthierine d_{001} peak. This trend is consistent with the compositional trend shown by E.P.M.A. in figure 4.1. The variation in abundance of illite within the clay-sized fraction of the mudstones is hence thought to be controlling the variation in composition. The trend shown in figure 4.1 is controlled by the mixing of illite and berthierine, as opposed to a single mineral species undergoing transformation or compositional change.

The presence of kaolinite in a sample of berthierine may be difficult to detect using X.R.D. due to the similar structure of the two minerals. The d_{001} spacing is similar (7.12 Å for berthierine-1H, 7.17 Å for kaolinite-1T), so that peaks can feasibly be resolved only by examination of the d_{002} spacing (d_{002} berthierine-1H = 3.55Å (25.08° 2θ), d_{002} kaolinite-1T = 3.58Å (24.88° 2θ). Peak separation is accentuated if both structural types of berthierine are present (mixed), when the spacing may decrease to 3.52Å (25.30° 2θ). Examination of the muds in this way failed to distinguish a clear kaolinite peak, suggesting a minimal presence within any of the ironstone samples (given the constraints of this technique).

Figure 4.2. X-Ray Diffraction Traces in the Range 5-14°2θ for a Suite of Mud-ironstones/Wacke-ironstones, from the Frodingham Ironstone Formation, and that of the Overlying Shale. The Berthierine d(111) Peak has been Standardised to Show the Decrease in Relative Height of the Illite d(111) Peak up the Sequence.

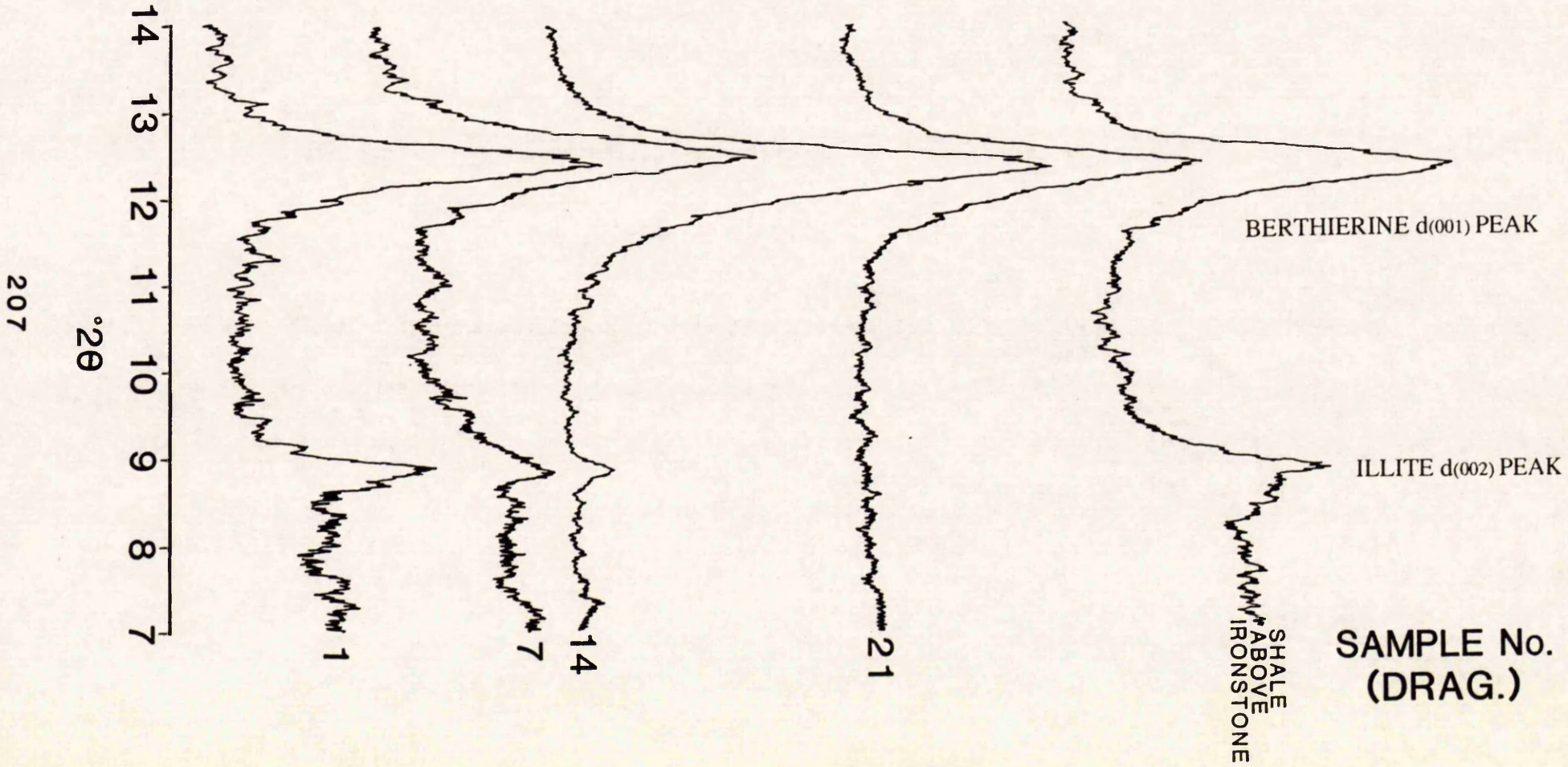

Figure 4.3. X-Ray Diffraction Traces in the Range 24-26°2θ for a Suite of Mud-ironstones/Wacke-ironstones, from the Frodingham Ironstone Formation, and that of the Overlying Shale, Showing the Berthierine (and Kaolinite) $d_{(002)}$ Peak. All Samples were run under Similar Operating Conditions (see text).

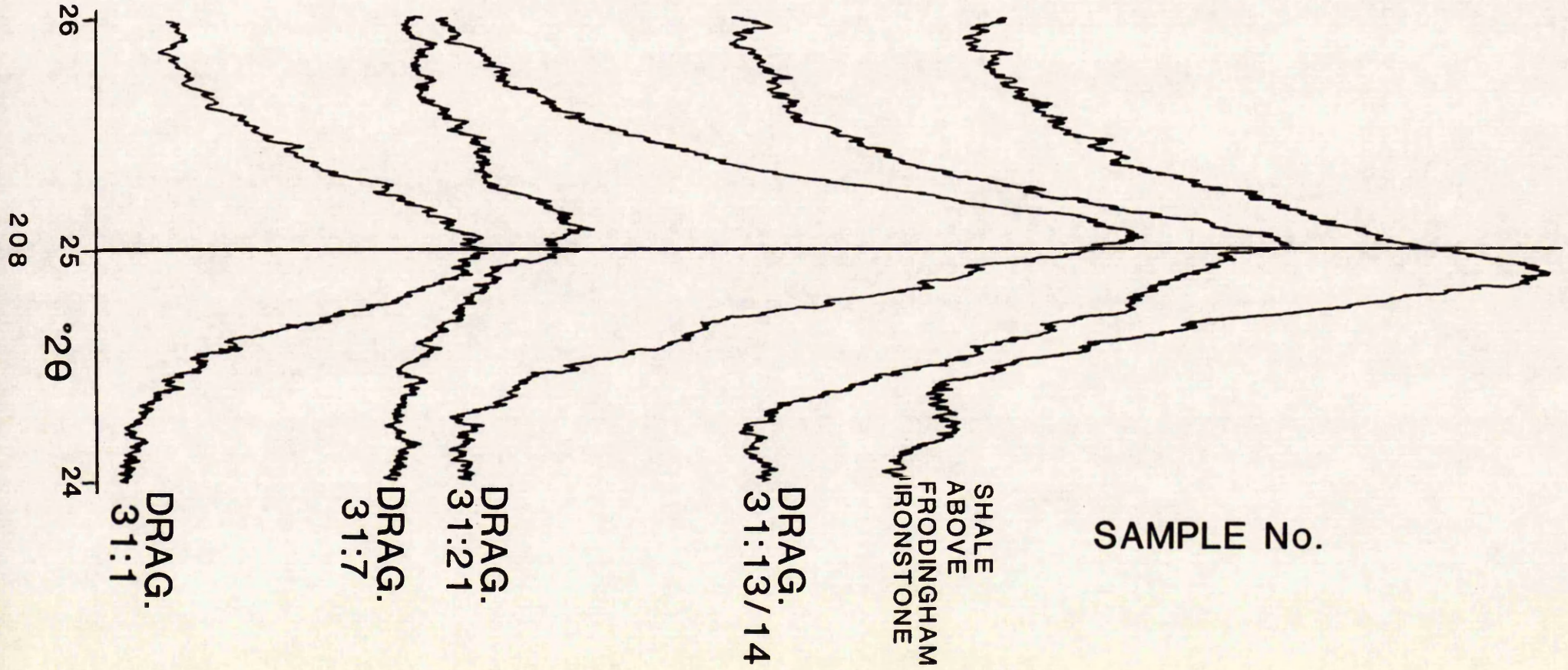

However, the DRAG 31.21 peak is asymmetric, which has also been seen in analysed samples of the "Snap Band" of Yarborough Pit. The asymmetry moves the peak towards higher d_{hkl} spacings, and though possibly suggestive of kaolinite mixing, the asymmetry extends further than expected for kaolinite, and may be complicated by a muscovite (24.59° 2θ) or siderite (24.78° 2θ) peak. The position of the peaks is also unusual in DRAG. 31.14 and DRAG. 31.1, where the peak lies between that expected for either berthierine or kaolinite, but without the marked asymmetry.

4.3.1) Shales Above the Ironstone-Formation.

Shale samples from above the ironstone-formation in Yarborough Pit (plate 1b) were examined using X.R.D., in a comparison to the ironstone muds (see figures 4.2 and 4.3). These figures show an obvious illite presence similar to that of DRAG. 31.1 at the base of the sequence. Unlike DRAG.31.1 however, a dominance of kaolinite is clearly seen by the peak occurrence at 28.8° 2θ with a slight asymmetry of the d_{002} peak towards lower d_{hkl} spacings. This suggests that within this sample, smaller quantities of berthierine are mixed with predominantly kaolinite. The shales above the ironstone-formation are hence illitic and kaolinite, with possible small quantities of admixed berthierine.

4.3.2) 'Detrital' Clay Mineralogy : Discussion.

Results of X.R.D. analysis suggests that there is a decrease in illite content of the muds as the ironstone sequence is ascended, and that there are probably only small quantities of kaolinite admixed with the berthierine in the ironstones. This is in contrast to the kaolinitic, illitic clays of the Lower Lias shales above the ironstone-formation. Unfortunately, the occurrence of kaolinite in the shales beneath the ironstone sequence cannot be directly proven from this borehole data, as the lowest beds of the sequence examined contained only berthierine and illite (figures 4.2 and 4.3). However, it seems extremely likely that the mineralogy of the mudstones above and below the ironstone are similar, from descriptions given in the literature from lateral equivalents of this Lower Lias sequence (Gaunt *et al.* 1980, Bradshaw and Penney 1982). The presence of kaolinite in

muds beneath the Formation will therefore be assumed, and three mechanisms to explain this pattern of kaolinite 'absence' and decreasing illite are hence thought possible:

1) Cessation of clay mineral input.

2) A loss by solution.

3) Reaction to form berthierine.

The importance of the first two can only be ascertained if that of the third is known, i.e. the origin of berthierine. It is assumed in the following discussion that the berthierine muds were formed from a detrital precursor clay mineral *in situ* and not deposited from suspension. This assumption is based on the calculated thermodynamic instability of berthierine in marine oxic waters (sections **1**.8 and **1**.9), and the presence of authigenic berthierine cements within the ironstone-formation (see below), that clearly indicates *in situ* berthierine formation could occur. However, even without the assumption, the arguments discussed below are still valid, as long as the degree of transport of the berthierine mud was minimal.

It is the view of many workers that kaolinite is strongly involved in berthierine formation (section **1**.9). If this view is followed, then the general absence of kaolinite in the ironstones is readily explained by its transformation (by whatever mechanism) to berthierine. The decreasing illite content must therefore be attributed to a reduction in the actual detrital input, rather than by its subsequent removal. This has sedimentological implications, since it therefore points to a change in detrital mineralogy from a kaolinite-illite detrital assemblage to kaolinite only in the upper part of the sequence. Return to 'normal' marine shale sedimentation resupplied the illite input. A second possibility is that illite may itself contribute to berthierine formation, and that its decrease represents a progressive berthierinisation of a constant input. However, unless kaolinite is inferred to have been used in this process, a separate precursor clay mineral must be implied to have been deposited in place of kaolinite to explain its absence.

The data in figure 4.1 have significant implications for berthierine formation, and could only have been obtained by E.P.M.A. This shows that despite the overall compositional

change within the muds, the Si/Al ratio remains fairly uniform, and is similar to that of authigenic berthierine cements. Hence the trend not only shows a mixing effect, but suggests that the bulk compositional change is also consistent with the addition of Fe+Mg to an Al-silicate. Figure 4.4, constructed from the same data, shows that this change can be further constrained to that of Fe addition only, with the Mg content remaining largely unchanged. It is therefore possible that the mud fraction is undergoing wholesale conversion to berthierine by Fe addition. The trend of the data suggests that it is not only kaolinite involved in berthierine formation, but a full discussion of this, with possible reaction pathways and geochemical considerations, is left to later (section 4.9) after the other occurrences of berthierine have been fully described.

A detailed clay mineralogical and T.E.M. study of the microfabrics, was beyond the scope of this research, but would considerably aid the interpretation of fabrics and compositions noted above, including the possible recognition of clay mineral solution textures and reprecipitation fabrics. Such a study would help in elucidating the roles of individual clay mineral species, and the bulk mudrock composition, on the formation of berthierine.

4.4) Cement Fabrics.

Berthierine cements are common in the ironstones, though the formation of these cements is not readily predictable. There are three readily distinguishable occurrences; a pore-lining to pore-filling type; replacements of bioclasts; and a thin coating that forms on bioclasts and produces the 'green fossils' of the Frodingham Ironstone Formation. These are described in turn with compositions obtained by E.P.M.A..

4.4.1) Intergranular Cements.

Berthierine cements are most commonly seen as a first formed, pore-lining, 10-30μm thick, light green cement, which is postdated either by a second pore-filling generation, siderite or ferroan calcite (see plate 13). The isopachous cement has a poor radial fabric that is distinguished under crossed-polars, and is seen in places to show crystals diverging

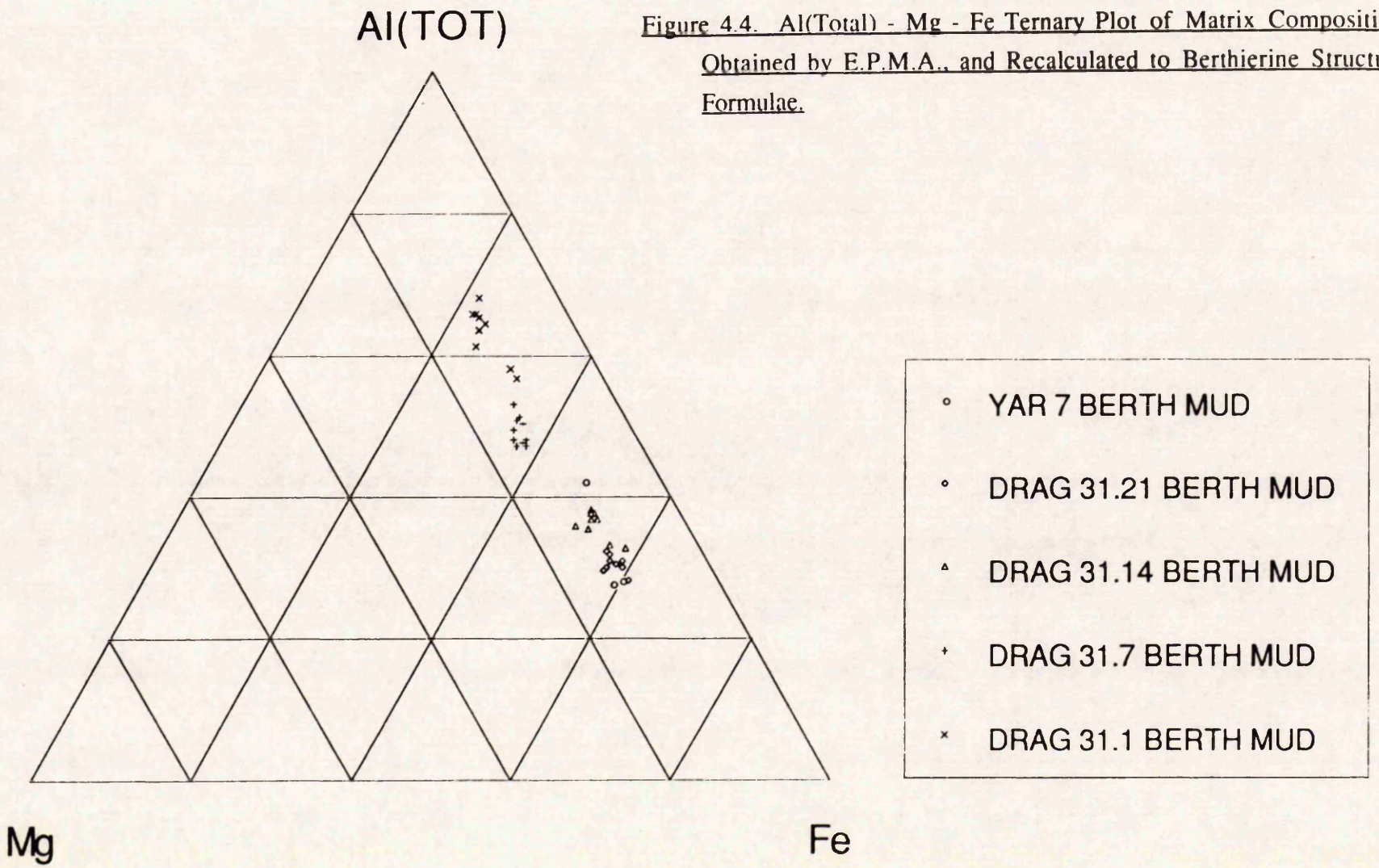

Figure 4.4. Al(Total) - Mg - Fe Ternary Plot of Matrix Compositions Obtained by E.P.M.A., and Recalculated to Berthierine Structural Formulae.

PLATE 13

Berthierine Intergranular Cements.

(Thin-section Photomicrographs).

A) Isopachous pore-lining berthierine cement nucleating on goethitic ooids in a grain-ironstone, specimen TY0106 (loaned from Dr. T. Young). The pores are filled with siderite.. Photo length is equivalent to 1.3mm.

B) Fully berthierine cemented grain-ironstone, specimen DRAG. 31.33. Two light green generations of berthierine are present, separated by a darker layer, also of berthierine. Photo length is equivalent to 1.3mm.

C) Remnants of a former berthierine cement within a grain-ironstone, specimen DRAG 31.22. The cement has been largely replaced by the later ferroan calcite, but relicts have been preserved in the interstices of the pores at the points of ooid contact (arrowed). Photo length is equivalent to 0.7mm.

D) Berthierine cemented grain-ironstone, specimen DRAG. 31.28. In this specimen, the berthierine has been replaced by siderite in the first generation (1), and in both generations (2). Platy pyrite has also formed and replaces the second generation (3). Photo length is equivalent to 3.3mm.

A	B
C	D

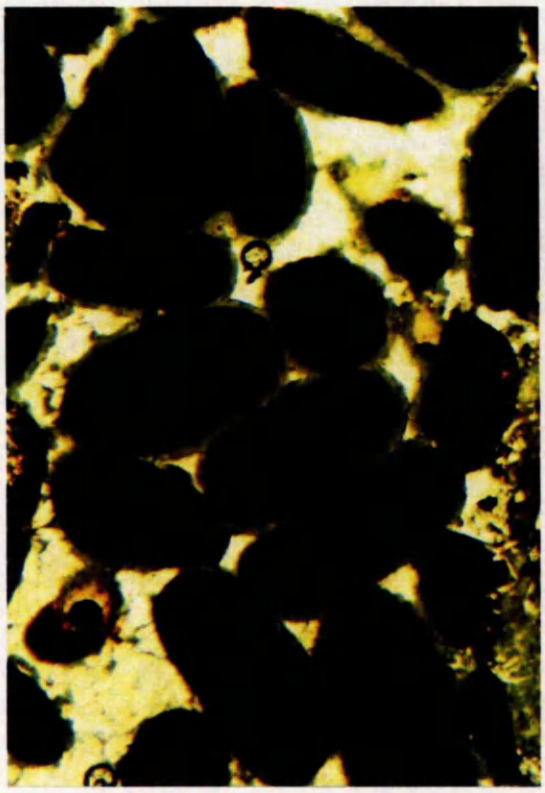

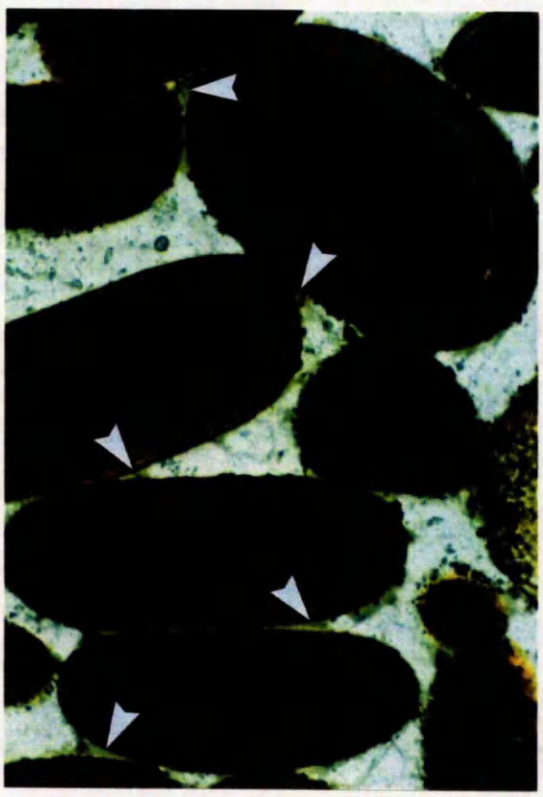

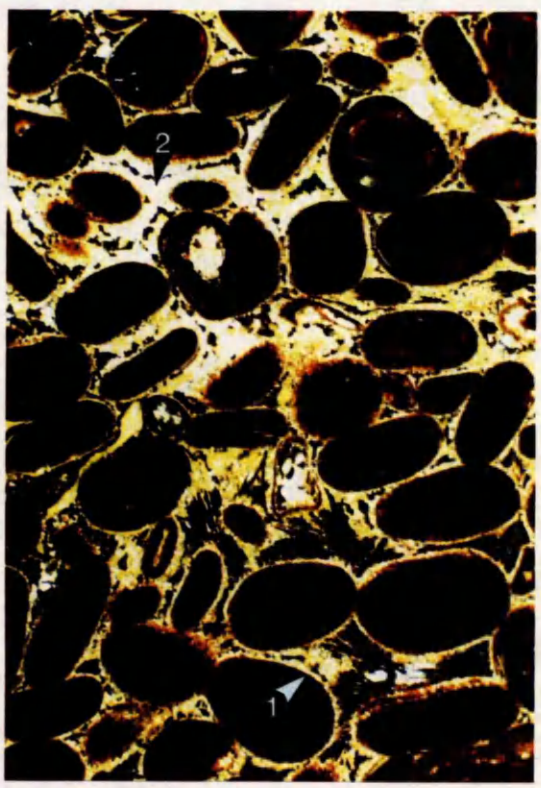
2
1

slightly at a few degrees, suggesting single site nucleation with partial radial growth. The effect is however minimal when compared to the Raasay spherulites (section **6**.6.3). The edge of the generation usually terminates abruptly, but in DRAG 31.19, the outer edge has a more 'wispy' appearance, with fine crystals extending a few microns into the pore (now calcite cemented). The second pore-filling generation has a random orientation of crystals, seen under crossed polars as elongate crystal aggregates a few microns long. The boundary between the two generations is usually indistinct, but may be marked in some cases (for example DRAG.31. 28 & 33) by a zone of darker berthierine (plate 13b), that is non isopachous, and occasionally fills the pore. Under very high magnifications, particularly in reflected light, the zone is seen to be mottled with sub-micron sized crystals increasing in abundance over a short area to form an apparently continuous sheet. The berthierine cements can be readily demonstrated to be primary as opposed to replacement of a former isopachous carbonate, by the lack of any fibrous or prismatic carbonate cements forming on ooids within the grainstones, indicating that iron-ooids were not good sites for carbonate nucleation (see section **5**.11.2.2).

Petrographic examination of some grain-ironstones, suggests that berthierine cements may have been previously slightly more extensive than seen at present. In DRAG. 31.22 for example, at the point of contact of some ooids there is a small amount of berthierine cement, that is elsewhere absent in the section (plate 13c). It is extremely unlikely that such textures are miniscus cements as described for carbonate cements precipitated in the meteoric vadose environment, due to the marine deposition of the ironstones, and the extremely unlikely event of berthierine saturated vadose waters. The surface of these cements exposed to the pore is also irregular, and does not possess a concave outline that would be expected if precipitation directly in the pore corner had taken place. These cements do not represent recrystallised geopetal sediments either, as they form on all sides of the pore. The texture is hence interpreted as a relict fabric from former berthierine cements that have been extensively replaced by ferroan calcite.

4.4.2) Ooid Fracture Cements.

Berthierine cements may also be found within goethite ooids, and are distinct from the berthierine which forms part of the cortex (plates 9a, 14a). These cements occur where part of the outer cortex has been displaced outwards, with the formation of berthierine in the area vacated (plate 14a). Such features are common where berthierine cements are associated with goethite/berthierine ooids, but not dense ooids of predominantly goethite. There are two possibilities for the formation of this texture; firstly that the ooid cortex was displaced by compactional stress fracture, with later berthierine precipitation; and secondly that berthierine formation displaced the outer ooid cortex, by a mechanism similar to the splaying of detrital muscovites on conversion to kaolinite in sandstones (for example see Burley *et al.* 1985). The former hypothesis is supported by the presence, of ooids with displaced cortices with and without berthierine cement. However, the discussion above (section 4.4.1) suggests that berthierine cement could be replaced by ferroan calcite, and replacement of berthierine mud by this mineral is also common. Compactional fracture is also supported by the formation of berthierine within fractures that cut across the ooid cortical fabric and into the nucleus. It is extremely unlikely that this particular fracturing could be produced by crystal growth stresses alone. The second hypothesis seems probable in explaining the occurrence of such cortex fracturing in areas unlikely to have undergone compactional stress fracture, for example where the outer ooid cortex is displaced into pore space. Both processes may have interacted to produce the fabric, that is most prevalent where berthierine cement formation is widespread.

It is believed here that berthierinisation of the ooids or recrystallisation of berthierine in the cortex may have weakened the ooids in particular layers/areas, allowing brittle fracture of the more competent layers during minor compaction. These areas may have then acted as sites for berthierine cement nucleation, which may have further displaced the cortex. It is thought that the force of crystallisation of clay mineral growth, would not in itself be sufficient to cause cortical fracture.

PLATE 14

Berthierine Fracture-Filling Cements, and Replacements of Bioclasts, (Thin-Section Photomicrographs)

A) Fractured berthierine/goethitic ooid with authigenic berthierine cement, specimen YAR. 7 (stained). The ooid cortex has fractured in a number of places (arrowed), and authigenic berthierine has precipitated in the void space formed. Photo length is equivalent to 0.35mm.

B) Berthierine replacing shell fragments, specimen DRAG. 31.25. The original aragonite of the bioclast dissolved, and berthierine precipitated as a cement in the void, postdating scalenohedral calcite formation (arrowed). Replacement did not occur *in situ*. Photo length is equivalent to 1.3mm.

C) Berthierine replacing a shell fragment within an ooidal grain-ironstone, specimen TY0106 (loaned from Dr. T. Young). Borings (type I) have been preserved during the replacement. Photo length is equivalent to 3.3mm.

D) Berthierine spherules in a replaced bivalve, specimen YAR. 7 (stained). The bioclast has been replaced by an early generation of scalenohedral calcite (1), berthierine spherules (2), authigenic phosphate (3), and a later pore-filling ferroan calcite (4). Photo length is equivalent to 1.3mm.

A	B
C	D

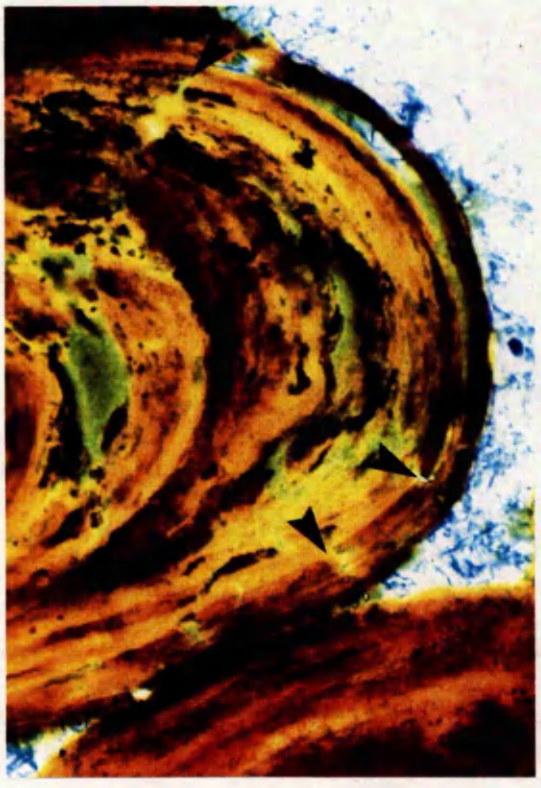

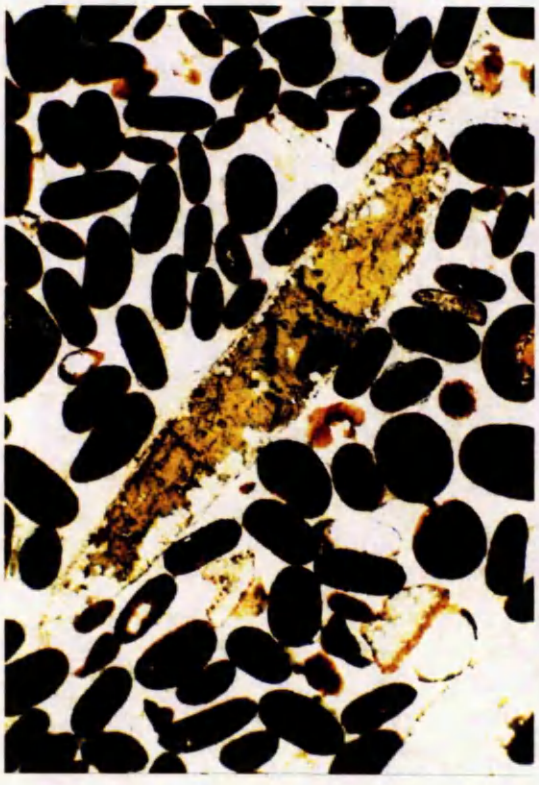

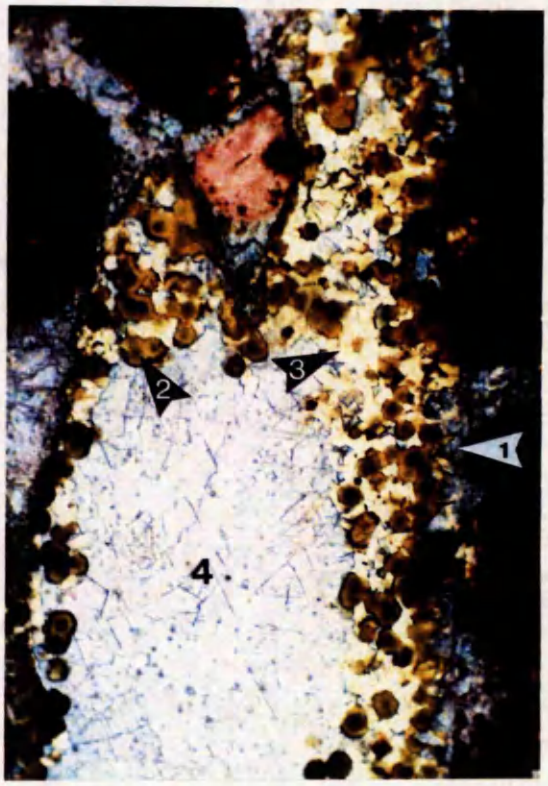
2
3
1
4

4.4.3) Intergranular and Fracture-Filled Cement Compositions.

The compositions of berthierine cements are remarkably consistent within a generation, and could be nearly identical within the error of E.P.M.A. Despite an extensive data collection of the cements in DRAG. 31.28 (table 4.3), no significant compositional difference could be found between the first and second light green generations; areas replaced by siderite and/or pyrite and those unreplaced; and authigenic berthierine occuring within broken ooids with displaced cortices. Analyses between thin-sections are also in excellent agreement of each other, producing a very small range of data. This consistency is best seen on a standard Si - (Fe+Mg) - Al(Total), ternary plot shown in figure 4.5.

The darker, mottled areas of berthierine were expected to produce analyses with increased Fe content due to oxidation, or FeO(OH) precipitation along with the berthierine. However, the analyses are essentially similar to the light green berthierine (table 4.3). As can be seen from figure 4.5 there is no shift of the data towards the Fe pole, as would have been expected by either of these possibilities, and it therefore suggests that the darker nature and mottled appearance relates to a morphological difference. Scanning Electron Microscopy (S.E.M.) however failed to resolve a clear difference.

4.4.4) Replacements of Bioclastic Debris.

Berthierine replacing bioclastic debris is common (plate 14 b,c), and is seen within both grainstones and wackestones. The fabric usually consists of randomly orientated crystals, light to dark green in colour, but in some samples a semi-isopachous fringe coating early scalenohedral calcites may be seen. This calcite nucleated on the bioclast inner surface following aragonite dissolution (see section **5**.7.1.3), and indicates that the berthierine precipitated within the void. Berthierine is not seen replacing bioclasts in which the structure remains intact.

The presence of berthierine replaced bioclasts in grainstones that are otherwise free of authigenic berthierine formation (plate 14 b,c), suggests that the berthierine replacement occurred prior to the bioclast incorporation within the sediment. They are therefore strictly

Table 4.3. Average Compositions of Berthierine Cements, Obtained By E.P.M.A. The Data have been Recalculated to Berthierine Structural Formulae.

	DRAG. 31.19				DRAG. 31.28							
	One end of slide		Other end of slide		GEN. 1		GEN. 2		GEN. 2 (SID./PYR.)		Ooid fracture-filling	
	AVERAGE	STDEV	AVERAGE	STDEV	AVERAGE	STDEV	AVERAGE	STDEV	AVERAGE	STDEV	AVERAGE	STDEV
Si	9.830	0.743	10.304	0.555	8.778	0.907	8.026	0.989	8.833	0.567	9.544	0.394
Ti	0.010	0.010	0.007	0.016	0.017	0.017	0.020	0.028	0.015	0.022	0.011	0.017
Al	5.949	0.649	6.451	0.332	4.086	0.509	3.826	0.328	4.070	0.356	4.660	0.167
Fe	25.961	2.652	27.571	2.231	19.455	3.129	16.764	2.959	19.270	1.895	22.838	1.194
Mn	0.049	0.068	0.036	0.055	0.015	0.020	0.030	0.029	0.036	0.039	0.051	0.061
Mg	1.621	0.152	1.654	0.180	2.215	0.127	2.184	0.206	2.314	0.110	2.306	0.106
Ca	0.310	0.234	0.187	0.113	0.177	0.048	0.179	0.041	0.184	0.051	0.143	0.045
Na	0.167	0.100	0.255	0.072	0.215	0.121	0.225	0.128	0.223	0.123	0.187	0.110
K	0.021	0.039	0.013	0.020	0.026	0.025	0.025	0.015	0.020	0.014	0.031	0.029
P	0.000	0.000	0.000	0.000	0.003	0.012	0.003	0.007	0.008	0.018	0.003	0.007
S	0.020	0.014	0.001	0.001	0.045	0.037	0.054	0.046	0.092	0.052	0.043	0.028
O	25.201	2.167	26.646	1.423	20.836	2.428	18.966	2.388	20.912	1.543	23.227	0.906
TOTAL	69.138	6.118	73.125	4.260	55.867	7.110	50.301	6.880	55.977	4.441	63.043	2.701
BerthCalc.												
Si	3.114	0.039	3.084	0.012	3.367	0.062	3.379	0.038	3.376	0.041	3.278	0.023
Al(T)	0.886	0.039	0.916	0.012	0.633	0.062	0.621	0.038	0.624	0.041	0.722	0.023
Al(O)	1.070	0.021	1.094	0.017	0.997	0.065	1.062	0.080	0.993	0.030	0.945	0.055
Ti	0.002	0.002	0.001	0.003	0.004	0.004	0.005	0.007	0.003	0.005	0.002	0.003
Fe	4.126	0.095	4.146	0.119	3.722	0.176	3.521	0.169	3.681	0.108	3.937	0.068
Mn	0.008	0.011	0.005	0.008	0.003	0.004	0.006	0.007	0.007	0.007	0.009	0.011
Mg	0.595	0.062	0.575	0.085	0.989	0.095	1.066	0.061	1.025	0.067	0.917	0.056
Ca	0.069	0.051	0.040	0.025	0.047	0.012	0.052	0.008	0.048	0.015	0.034	0.010
Na	0.066	0.043	0.094	0.031	0.098	0.049	0.118	0.073	0.104	0.054	0.077	0.044
K	0.005	0.009	0.003	0.004	0.007	0.006	0.007	0.004	0.005	0.004	0.008	0.007
OCT.	5.802	0.054	5.821	0.041	5.715	0.045	5.660	0.051	5.710	0.043	5.810	0.039
INT.	0.140	0.071	0.137	0.054	0.151	0.052	0.177	0.067	0.157	0.060	0.118	0.046
CH	8.000	0.000	8.000	0.000	8.000	0.000	8.000	0.000	8.000	0.000	8.000	0.000
	n=5		n=5		n=16		n=8		n=11		n=6	

Table 4.3 (Continued).

	DRAG. 31.28 (Cont.)		DRAG. 31.33				Y183. 3		YAR. 7	
	Darker Berth.		Cement		Darker Berth.		Cement		Cement	
	AVERAGE	STDEV	AVERAGE	STDEV	AVERAGE	STDEV	AVERAGE	STDEV	AVERAGE	STDEV
Si	9.741	1.378	9.096	0.789	8.995	0.442	9.435	0.862	8.749	0.430
Ti	0.025	0.032	0.036	0.023	0.016	0.022	0.022	0.025	0.028	0.043
Al	4.527	0.445	4.331	0.394	4.215	0.204	4.909	0.831	4.843	1.153
Fe	22.456	4.096	22.421	2.614	21.520	1.102	23.228	2.977	19.595	1.322
Mn	0.066	0.147	0.023	0.036	0.023	0.028	0.033	0.049	0.054	0.044
Mg	2.566	0.325	1.996	0.163	2.118	0.226	1.996	0.131	1.953	0.127
Ca	0.225	0.120	0.183	0.038	0.163	0.039	0.184	0.047	0.407	0.061
Na	0.178	0.154	0.154	0.110	0.325	0.070	0.217	0.083	0.151	0.116
K	0.029	0.040	0.014	0.027	0.015	0.024	0.019	0.031	0.031	0.041
P	0.001	0.005	0.005	0.012	0.004	0.011	0.013	0.018	0.011	0.027
S	0.019	0.023	0.028	0.022	0.021	0.027	0.027	0.037	0.019	0.023
O	23.442	3.129	22.117	2.057	21.758	1.034	23.278	2.606	20.999	1.108
TOTAL	63.276	9.015	60.401	5.917	59.171	2.766	63.362	7.330	56.840	3.069
BerthCalc.										
Si	3.261	0.238	3.284	0.031	3.299	0.032	3.245	0.077	3.262	0.153
Al(T)	0.739	0.238	0.716	0.031	0.701	0.032	0.755	0.077	0.738	0.153
Al(O)	0.856	0.323	0.911	0.030	0.908	0.053	0.989	0.055	1.130	0.213
Ti	0.006	0.006	0.007	0.004	0.003	0.005	0.005	0.006	0.006	0.009
Fe	3.901	0.427	4.058	0.096	3.967	0.129	3.998	0.087	3.671	0.225
Mn	0.028	0.065	0.004	0.007	0.004	0.005	0.006	0.010	0.010	0.008
Mg	1.019	0.076	0.834	0.044	0.896	0.069	0.796	0.049	0.841	0.034
Ca	0.072	0.071	0.044	0.010	0.040	0.011	0.037	0.016	0.104	0.017
Na	0.099	0.109	0.070	0.050	0.145	0.030	0.092	0.035	0.067	0.051
K	0.011	0.017	0.004	0.007	0.004	0.006	0.004	0.007	0.008	0.011
OCT.	5.809	0.185	5.814	0.046	5.779	0.029	5.793	0.040	5.657	0.045
INT.	0.182	0.179	0.118	0.053	0.189	0.035	0.133	0.035	0.179	0.056
CH	8.000	0.000	8.000	0.000	8.000	0.000	8.000	0.000	8.000	0.000
	n=12		n=8		n=8		n=8		n=6	

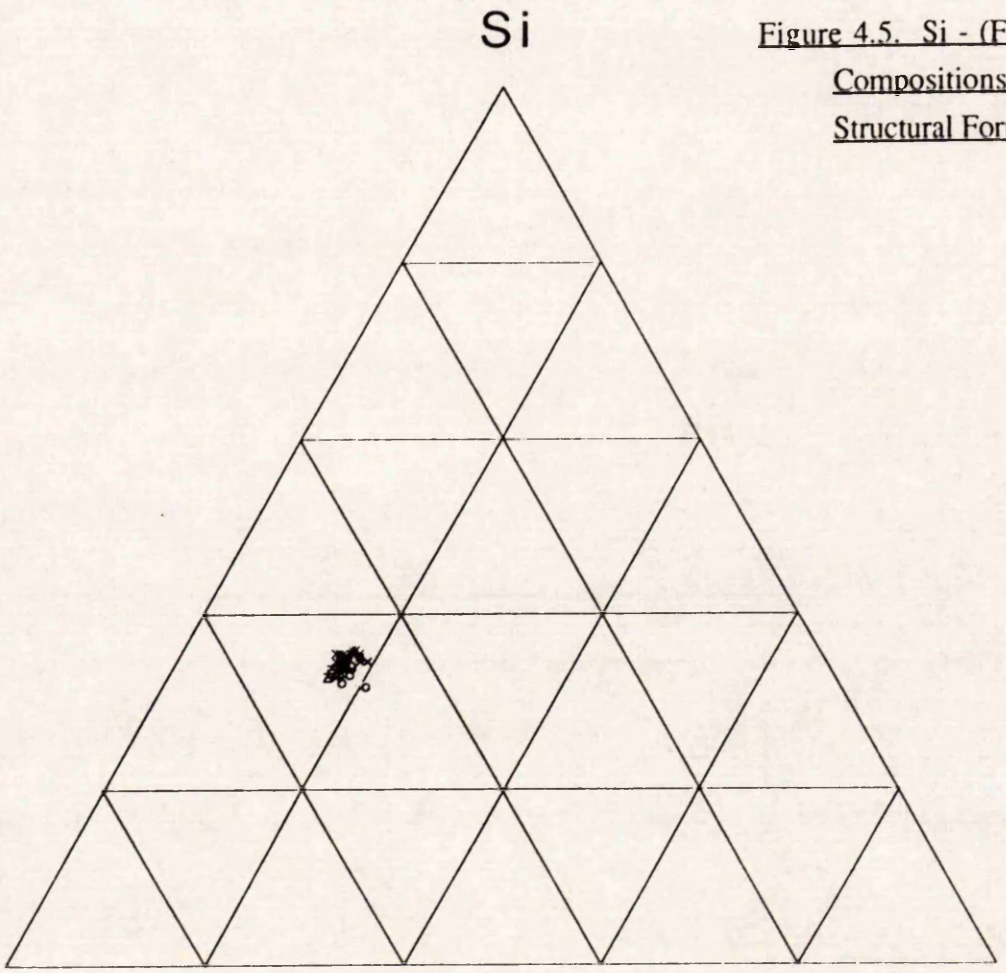

Figure 4.5. Si - (Fe+Mg) - Al(Total) Ternary Plot of Berthierine Cement Compositions Obtained by E.P.M.A., and Recalculated to Berthierine Structural Formulae.

- ○ Y183.3 AUTH. BERTH.
- ◇ YAR 7 AUTH. BERTH.
- △ DRAG 31.33 AUTH. BERTH.
- + DRAG 31.33 AUTH BERTH. DARK
- × DRAG 31.28 AUTH.BERTH
- DRAG 31.19 AUTH BERTH

intraclasts of reworked ironstone. Given that no similar external berthierine cements are seen on the bioclasts, and that berthierine replaced bioclasts also occur within berthierine muds, it is probable that precipitation occurred within the bioclast after aragonite dissolution whilst enclosed within the mudstone. Unconsolidated muds may then have been reworked, releasing the replaced bioclasts. Whether the authigenic berthierine was protected from oxidation by the scalenohedral (or thin) calcites, biofilm formation, or simply rapid reworking and deposition, remains unclear.

Berthierine also replaces bioclasts in the form of small 30-80μm sized spherules, apparently suspended within a calcite cement (plate 14d). The spherules often have a darker core, similar to the berthierine cements described above, and possess a poor radial fabric, that is evident under crossed-polars. Adjacent spherules may coalesce, to form a botryoidal texture. The spherules are not necessarily related to borings, and are not berthierine filled sacs of the type I boring (see section 3.3.2.1). Where the bioclast has been bored, the borings have been seen preserved in both berthierine and calcite replaced bioclasts, with the directions of the boring being unrelated to the spherules. It is not suspected that the spherules are replacing the calcite, since there is often a gradation from bioclast wall to centre of berthierine cement, through the botryoidal fabric to spherules, rather than random spherule formation. This berthierine cement stratigraphy may also postdate a scalenohedral to sparry ferroan calcite attesting to its cement origin, and since the ferroan calcite internal and external to the bioclast is similar, it would be expected that both would be replaced should a replacement origin be inferred. A mechanism for berthierine cation transport through calcite cement is also lacking and unrealistic. In order that the spherules could form therefore, it is suspected that an organic medium supported the spherules (algal filaments?) which was removed during bioclast cementation. This is partly supported by the occurrence of authigenic phosphate cements associated with spherule formation (plate 14d).

The compositions of the bioclast-replacing berthierines (table 4.4) are remarkable in being nearly identical to those of the intergranular cements described above, despite their apparently dissimilar origin (compare figures 4.5 and 4.6). The Ca content is however

Table 4.4. Average Compositions of Berthierine Cements Replacing Shell Fragments. The Data have been Recalculated to Berthierine Structural Fomulae.

	YAR 7		YAR 21		YAR 24	
	AVERAGE	STDEV	AVERAGE	STDEV	AVERAGE	STDEV
Si	10.180	1.268	11.486	0.438	9.965	2.380
Ti	0.021	0.032	0.039	0.055	0.009	0.015
Al	4.968	0.658	6.233	0.122	5.309	1.250
Fe	24.141	3.826	27.727	1.642	24.149	6.690
Mn	0.023	0.054	0.052	0.016	0.046	0.099
Mg	2.175	0.242	2.538	0.191	2.025	0.355
Ca	0.680	0.697	0.761	0.091	1.937	1.741
Na	0.232	0.155	0.404	0.107	0.135	0.123
K	0.084	0.066	0.212	0.073	0.122	0.101
P	0.107	0.317	0.000	0.000	0.347	0.589
S	0.042	0.039	0.112	0.025	0.048	0.040
O	24.892	3.553	28.772	1.295	25.639	6.040
TOTAL	67.544	10.027	78.335	3.828	69.732	16.298
BerthCalc.						
Si	3.291	0.061	3.187	0.023	3.152	0.172
Al(T)	0.709	0.061	0.813	0.023	0.848	0.172
Al(O)	0.961	0.090	0.988	0.069	0.905	0.191
Ti	0.004	0.006	0.006	0.009	0.001	0.003
Fe	3.903	0.117	3.854	0.058	3.797	0.357
Mn	0.004	0.010	0.007	0.003	0.012	0.029
Mg	0.814	0.032	0.813	0.024	0.755	0.073
Ca	0.130	0.083	0.148	0.011	0.459	0.630
Na	0.093	0.058	0.136	0.030	0.053	0.045
K	0.018	0.012	0.043	0.016	0.026	0.020
OCT.	5.685	0.064	5.669	0.019	5.471	0.465
INT.	0.242	0.126	0.326	0.025	0.538	0.645
CH	8.000	0.000	8.000	0.000	8.000	0.000
	n=4		n=2		n=7	

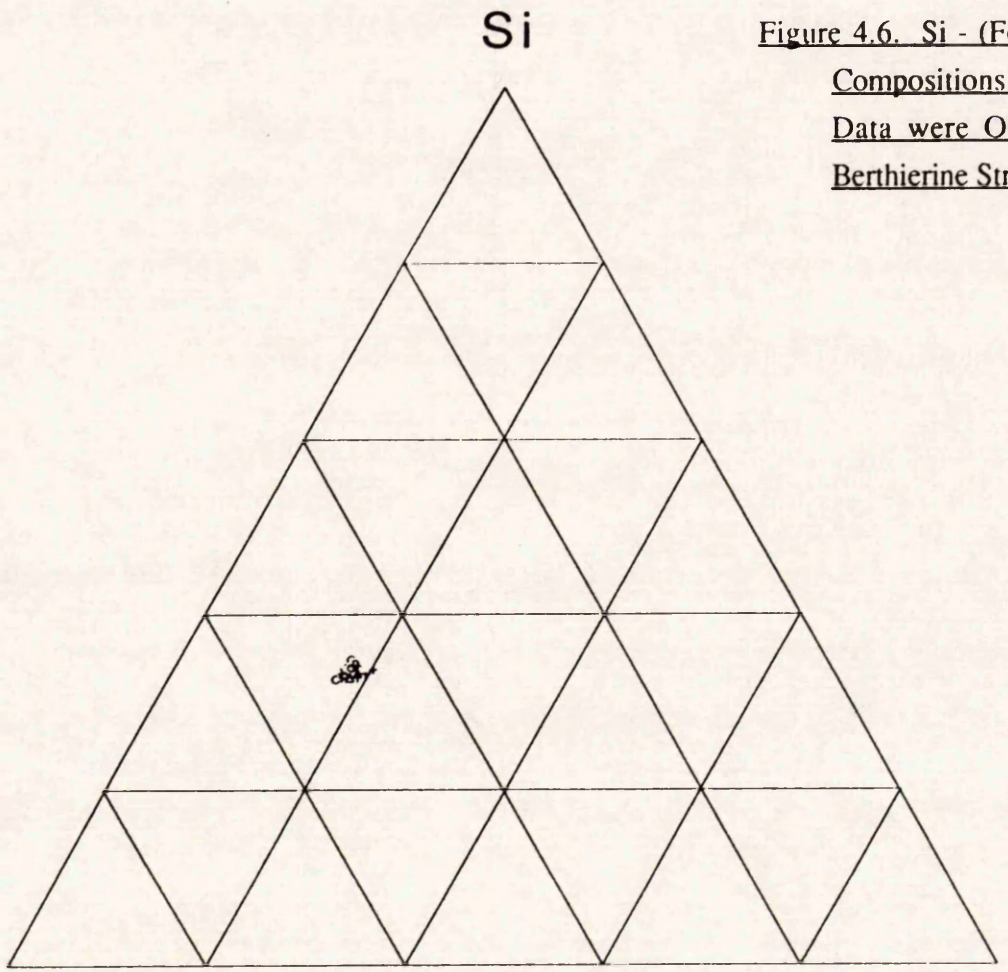

Figure 4.6. Si - (Fe+Mg) - Al(Total) Ternary Plot of Berthierine Cement Compositions Precipitated Within Void Space in Dissolved Bioclasts. Data were Obtained by E.P.M.A., and has been Recalculated to Berthierine Structural Formulae.

slightly elevated, due almost certainly to the inclusion of small amounts of residual calcite, rather than present within the berthierine structure as indicated within the calculation used in table 4.4.

4.4.5) Fibrous Cements Formed Predominantly on Bioclastic Debris: The "Green Fossils".

Thin, fibrous semi-isopachous cements of berthierine are found within some samples, particularly at Yarborough Pit. These cements are less than 15µm thick (usually considerably less), and are unusual in that they occur predominantly on reworked shell fragments (plate 15 a,b). Ooids within the same sample may have some minor berthierine development, but the full fibrous habit is present only on the bioclastic debris, forming the "green fossils" (plate 15a).

Examination of bioclast surfaces under incident light reveals the berthierine coating to be continuous, which indicates that it was formed prior to the bioclast being incorporated within the grain-ironstones at the present site. As with berthierine replaced bioclasts, it is thought that this berthierine formed on bioclastic debris deposited within mudstones, and was subsequently reworked. Evidence for this is seen by the presence of bioclastic debris sited within berthierine mud, possessing a (even more well-defined) fibrous berthierine fringe at the point of contact (plate 15c). It is suspected that this fringe forms during the berthierinisation of the muds, whereby some recrystallisation of the mud took place, and lead to nucleation of berthierine on the bioclast. As an iron silicate would not be expected to nucleate on a carbonate, it is thought that the presence of a biofilm on these bioclasts was a controlling factor in the formation of this fabric. These films are interpreted to have been biogenically formed as opposed to adsorption produced, in order to explain the absence of well-defined fringes on ooids. Reworking and subsequent deposition would have been rapid, in order that the berthierine was not oxidised in the process. In some samples, bioclasts are coated with a very thin layer of goethite, and this is believed to result from oxidation of berthierine films due to a greater residence time within oxic waters. Storm

PLATE 15

Berthierine Coatings on Bioclasts, and Berthierine Flakes.

A) Berthierine coated *Cardinias* in an ooidal grainstone, hand specimen YAR. 9, Yarborough Pit. The scale bar is divided in centimetres.

B) Thin berthierine coatings on bioclasts that form the green fossils of (A) within a thin-section of specimen YAR. 9. The coating (arrowed) is present on both replaced and unreplaced shell fragments. Some framboidal pyrite is present in the cements. Photo length is equivalent to 0.7mm.

C) Fibrous berthierine fringe (arrowed) on unreplaced shell fragments within a wacke-ironstone, thin-section, specimen YAR. 7. The fringe appears to form syntaxially to the structure of the bioclast. Photo length is equivalent to 0.7mm.

D) Berthierine flakes/stacks, thin-section, specimen YAR. 2. A poor parallel foliation in the flakes may be seen (arrowed). Photo length is equivalent to 3.3mm.

A	B
C	D

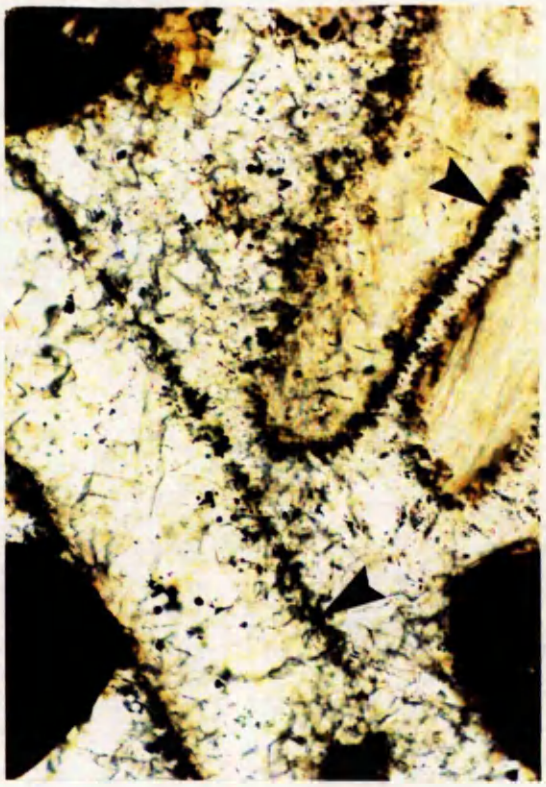

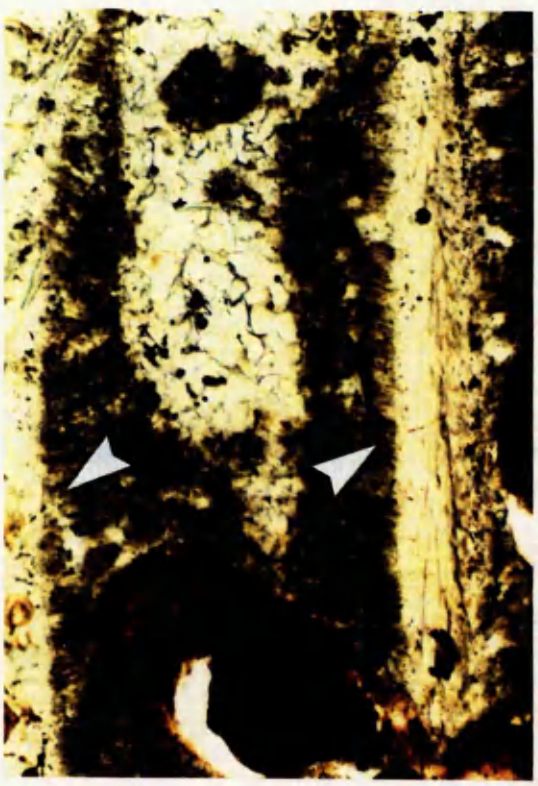

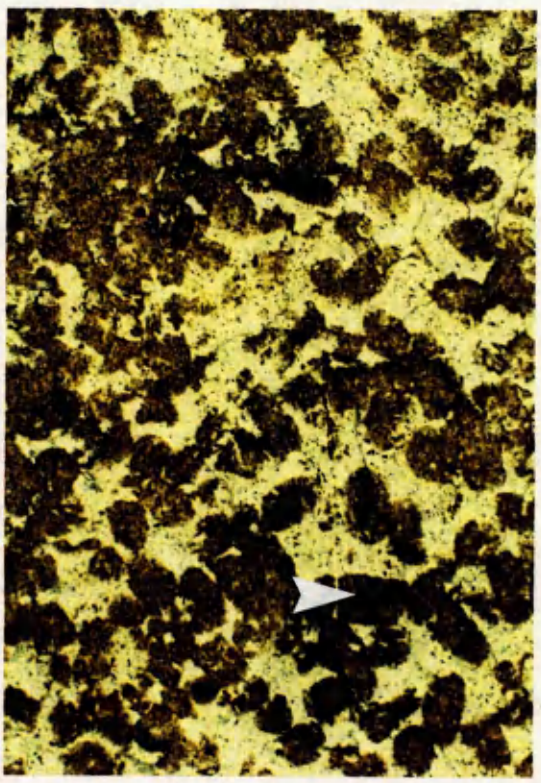

activity may have been instrumental in preserving these fabrics, by rapid erosion and deposition.

The crystal size of such fringes is too small to be accurately analysed by E.P.M.A., so the composition was not obtained. The mineralogy was confirmed to be berthierine, by X.R.D. analysis of samples scraped from bioclast surfaces.

4.5) Berthierine Ooids and Peloids.

The petrography and mineralogy of berthierine ooids and rare peloids, are described above in section 3.2.2. This section deals only with the compositions of the ooids and peloids obtained by E.P.M.A., compared to the other berthierine compositions described in this section. Analyses of berthierine ooids are given in table 4.5, and are plotted as before on an Si - (Fe+Mg) - Al(Total) plot in figure 4.7. These data show both variation between analyses of single ooids (3 examples), and between random analyses of ooid cortices within the same thin-section (Y183. 8). There are two main points to note about these data; firstly the lower Fe+Mg content of the ooids relative to authigenic cements; and secondly, the trend of the data in having a near constant Si/Al ratio despite variation in Fe+Mg content. As discussed for berthierine muds, compositional differences or mixing trends could be implied to explain these points, but evidence points to the latter. This is because the compositional variation in true authigenic berthierines has been shown to be highly consistent between different occurrences, and is hence unlikely to be markedly different within ooids. The compositional trends described for the ooids are also aligned with those described for berthierine muds, that clearly represent a mixing curve. It is hence believed that the ooids examined contain a small proportion of illite or illite/kaolinite, that is slightly variable in actual amount, but always present within a single analysis, so that a pure berthierine composition is never obtained. This is in contrast to the T.E.M. work of Hughes (1987, 1989) who found only berthierine and goethite in Frodingham ooids.

The berthierine peloid compositions are given in table 4.6, and are rich in apatite (francolite?) that is extremely fine grained, and not visible in thin-section. However, the

Table 4.5. Average Compositions of Berthierine Ooids, Obtained By E.P.M.A. The Data have been Recalculated to Berthierine Structural Formulae.

	YAR. 30						Y183.8	
	BERTH. OOID 1		BERTH. OOID 2		BERTH. OOID 3		10 OOIDS	
	AVERAGE	STDEV	AVERAGE	STDEV	AVERAGE	STDEV	AVERAGE	STDEV.
Si	9.762	1.075	8.186	0.871	8.451	1.299	11.701	1.202
Ti	0.134	0.094	0.112	0.053	0.078	0.046	0.358	0.308
Al	5.425	0.785	4.864	0.675	4.934	0.407	7.500	0.649
Fe	16.137	0.950	14.332	3.048	15.600	4.949	19.865	3.471
Mn	0.029	0.038	0.051	0.060	0.046	0.046	0.045	0.062
Mg	1.848	0.171	1.517	0.330	1.678	0.328	1.786	0.121
Ca	0.443	0.108	1.646	3.891	0.250	0.058	0.337	0.082
Na	0.187	0.113	0.259	0.108	0.143	0.112	0.343	0.143
K	0.575	0.246	0.315	0.107	0.327	0.193	0.713	0.426
P	0.106	0.097	0.010	0.016	0.046	0.076	0.022	0.026
S	0.048	0.036	0.072	0.029	0.043	0.035	0.034	0.038
O	22.380	2.138	19.671	2.084	19.931	3.337	27.548	2.031
TOTAL	57.075	4.804	51.034	5.813	51.528	9.989	70.252	4.959
BerthCalc.								
Si	3.514	0.110	3.328	0.137	3.408	0.105	3.390	0.154
Al(T)	0.486	0.110	0.672	0.137	0.592	0.105	0.610	0.154
Al(O)	1.542	0.136	1.389	0.361	1.499	0.240	1.654	0.216
Ti	0.028	0.018	0.026	0.012	0.019	0.012	0.062	0.056
Fe	2.929	0.206	2.906	0.461	3.090	0.410	2.901	0.502
Mn	0.005	0.007	0.011	0.013	0.010	0.010	0.007	0.010
Mg	0.771	0.057	0.713	0.136	0.779	0.067	0.600	0.032
Ca	0.054	0.032	0.458	1.095	0.042	0.032	0.059	0.013
Na	0.083	0.049	0.131	0.057	0.074	0.063	0.123	0.054
K	0.147	0.049	0.093	0.030	0.102	0.061	0.147	0.081
OCT.	5.275	0.130	5.045	0.898	5.397	0.191	5.223	0.271
INT.	0.284	0.079	0.682	1.143	0.218	0.098	0.328	0.117
CH	8.000	0.000	8.000	0.000	8.000	0.000	8.000	0.000
	n=11		n=8		n=10		n=10	

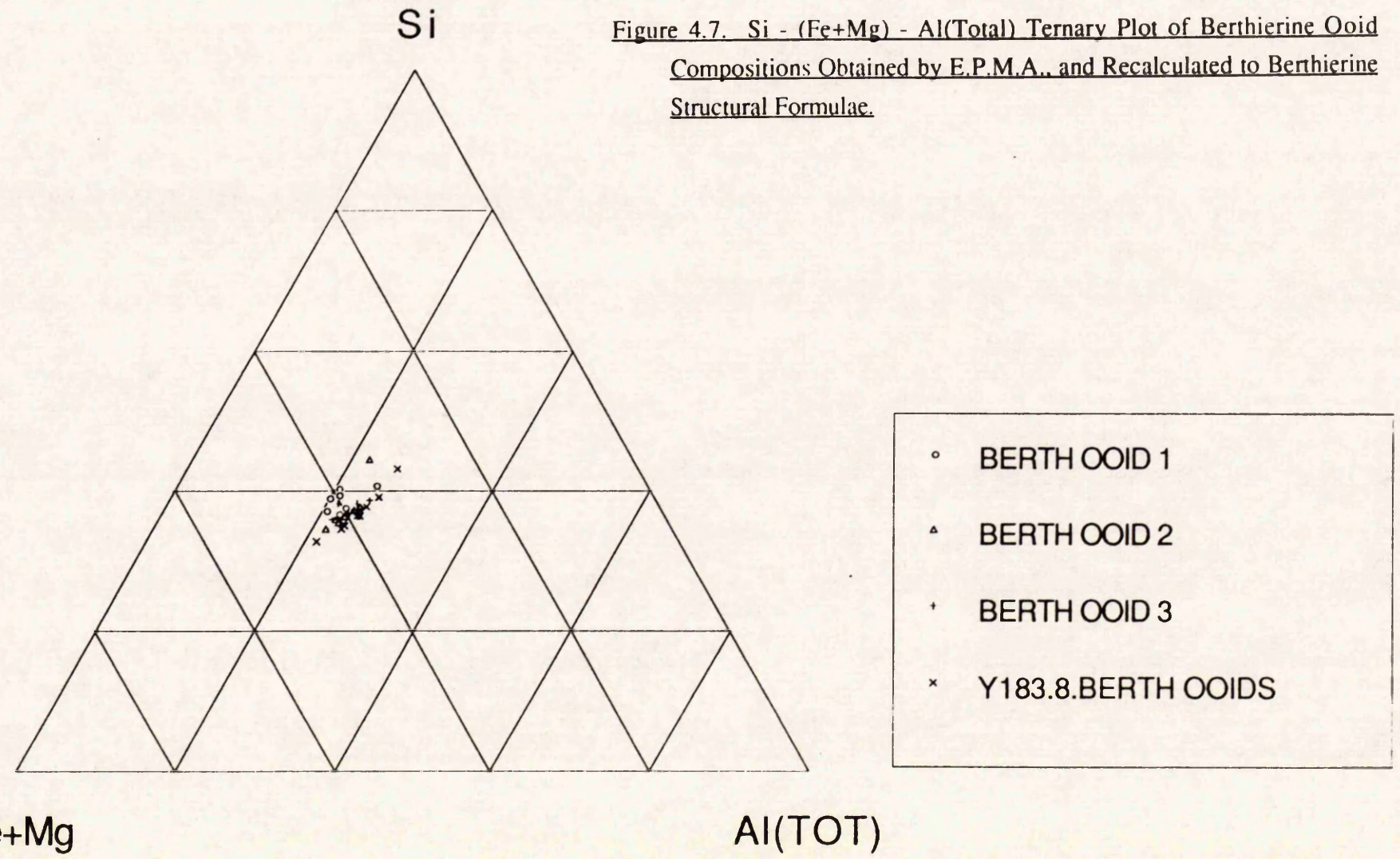

Figure 4.7. Si - (Fe+Mg) - Al(Total) Ternary Plot of Berthierine Ooid Compositions Obtained by E.P.M.A., and Recalculated to Berthierine Structural Formulae.

Table 4.6. Average Compositions of Berthierine Peloids in Y183.8., and Flakes in YAR.2. The Data have been Recalculated to Berthierine Structural Fomulae.

	Y183. 8		YAR. 2	
	BERTH. PELOIDS		BERTH. FLAKES	
	AVERAGE	STDEV.	AVERAGE	STDEV.
Si	3.308	0.618	3.364	0.301
Ti	0.006	0.010	0.072	0.126
Al	2.015	0.353	1.874	0.281
Fe	7.440	1.443	8.112	1.317
Mn	0.028	0.034	0.608	0.136
Mg	0.513	0.056	0.879	0.121
Ca	27.058	2.305	23.774	1.200
Na	0.835	0.123	0.153	0.085
K	0.180	0.040	0.118	0.128
P	10.479	0.623	0.494	0.509
S	0.201	0.039	0.010	0.008
O	32.706	0.472	18.833	0.682
TOTAL	84.768	1.239	58.293	1.567
BerthCalc.				
Si	2.594	0.242	1.510	0.111
Al(T)	1.406	0.242	2.490	0.111
Al(O)	0.241	0.372	-1.615	0.215
Ti	0.003	0.004	0.019	0.033
Fe	2.862	0.322	1.833	0.311
Mn	0.012	0.016	0.140	0.032
Mg	0.473	0.076	0.456	0.056
Ca	2.529	0.848	7.140	0.427
Na	0.817	0.179	0.083	0.045
K	0.101	0.014	0.037	0.041
OCT.	3.591	0.615	0.833	0.360
INT.	3.448	0.997	7.261	0.454
CH	8.000	0.000	8.000	0.000
	n=4		n=7	

phosphate content has been corrected for during recalculation, and shows that the peloids have a berthierine composition that is tightly constrained, and plots on the berthierine mud mixing-line close to the true authigenic berthierine composition (figure 4.8). The peloids resemble the associated muds in thin-section, so it is not surprising that the composition is identical to that expected for a berthierine mud. The phosphatisation may reflect a faecal origin, with phosphate being released on the degradation of contained organic matter.

4.6) Berthierine Stacks / Flakes.

Within the first generation of calcite cement that precipitated in the inner void of a *Cardinia* shell (YAR. 2), are small (80-200μm), rounded, slightly oblate berthierine particles with a poorly developed parallel lamination / cleavage (plates 15d and 17c). This foliation is nearly identical to the thin fibrous cements which formed on bioclasts (section 4.4.5) within this and other thin-sections, and may have formed in the same way. Larger particles of a similar width but more elongate nature, suggest that the flakes formed by disaggregation and reworking within the void of a similar mud fringe. Reworking within the bioclast, meant that particles could be rounded without undergoing oxidation.

The compositions of these flakes are given in table 4.6, and show a high Ca content due to replacement by calcite. This replacement is evident by the single extinction of the flake, and calcite crystal boundaries cutting through the particles. Plotting the composition on a Si - (Fe+Mg) - Al(Total) ternary plot as used before (figure 4.8), shows that the flakes are composed of berthierine. Calcite replacement of the berthierine has therefore involved wholesale dissolution of the latter without subsequent compositional or mineralogical modification of the berthierine.

4.7) The Chemical Composition and Classification of Frodingham Ironstone Berthierines.

From the above discussions, it has been shown that the compositions of berthierine muds, peloids, and almost certainly ooids, represent mixing curves between berthierine and an illite/ illite-kaolinite mixture. In this section the composition of the authigenic cements formed in intergranular and dissolution pore space is discussed. These cements are thought

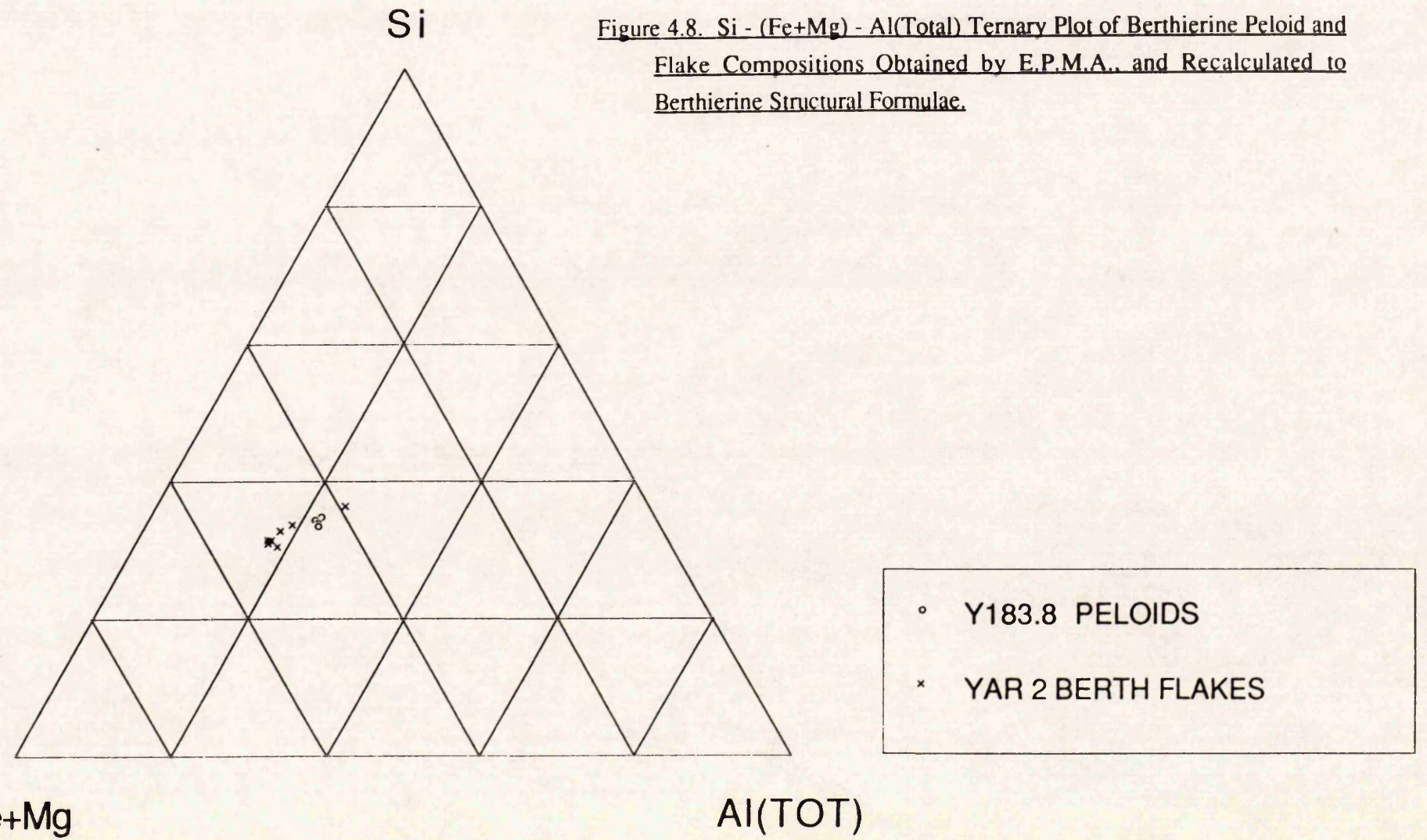

Figure 4.8. Si - (Fe+Mg) - Al(Total) Ternary Plot of Berthierine Peloid and Flake Compositions Obtained by E.P.M.A., and Recalculated to Berthierine Structural Formulae.

to have the end member compositions of the above mixing trends, and hence the true composition of the Frodingham berthierines. These cements have been shown to cover a narrow compositional range, that can be seen by plotting the analyses together with published berthierine compositions. 37 analyses from various sources and localities described in the literature (Appendix E) are shown in figure 4.9. The range of published analyses is seen to be far greater than those of the Frodingham samples. The significance of this narrow spread of data is discussed in detail below (section 4.8), and allows an average composition of Frodingham berthierines to be calculated from 92 analyses based on an $O_{10}(OH)_8$ structure (standard deviations given in parentheses):

$Al_{0.709(0.100)}$ $Si_{3.291(0.100)}$ (TETRAHEDRAL)

$Fe_{3.857(0.218)}$ $Mg_{0.871(0.154)}$ $Mn_{0.005(0.007)}$ $Ti_{0.004(0.005)}$ $Al_{0.992(0.077)}$ (OCTAHEDRAL)

$Ca_{0.073(0.070)}$ $Na_{0.095(0.053)}$ $K_{0.009(0.012)}$ (INTERLAYER)

The berthierine consists essentially of (assumed) tetrahedrally coordinated Si and Al, with the octahedral sites dominated by Fe. Al and Mg are also present within the octahedral sites but in significant though much lower quantities. The dominance of R^{2+} species (i.e. metal cations with a valency of two), assigns berthierine to the trioctahedral clay minerals. Mn is only a minor constituent of all berthierines, and is present here in very low quantities despite the abundance of Fe. Ca, Na, and K are almost certainly sited in the interlayer portion if present within the structure as opposd to separate phases. Maynard (1986) noted the occurrence of K in Frodingham berthierines which was supported by the T.E.M. work of Hughes (1989). This is in contrast to the higher values of Na reported here. Low octahedral totals coinciding with the presence of K led Hughes (1989) to suggest that K may be sited within the berthierine structure, but this is extremely difficult to test on the basis of mineral compositional data alone.

The suite of figures and discussion that follows, shows that the composition of the Frodingham silicate fits within the published data set for berthierines (figure 4.9), with the 1:1 structure confirmed by X.R.D. analysis. The relationship of berthierine composition to

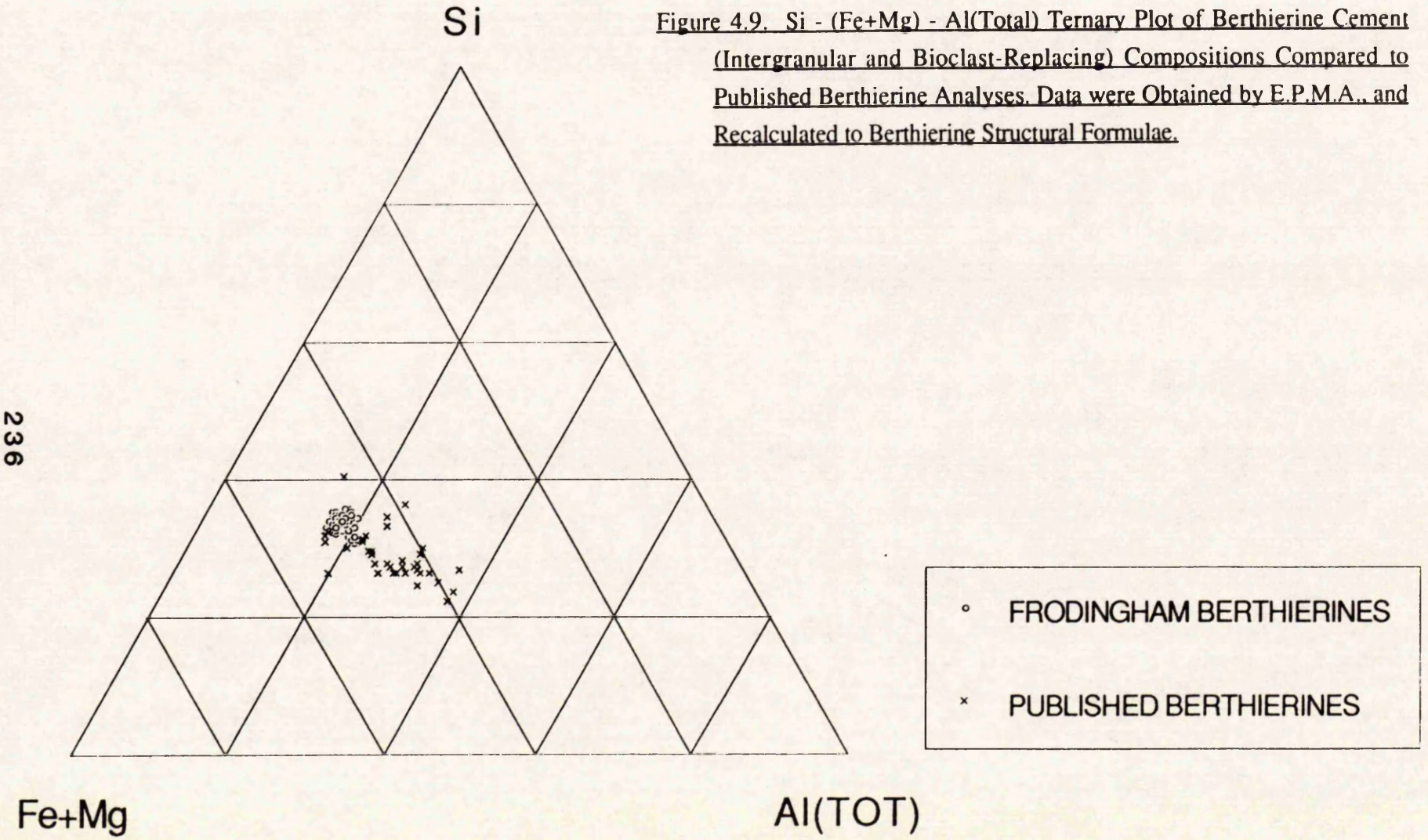

Figure 4.9. Si - (Fe+Mg) - Al(Total) Ternary Plot of Berthierine Cement (Intergranular and Bioclast-Replacing) Compositions Compared to Published Berthierine Analyses. Data were Obtained by E.P.M.A., and Recalculated to Berthierine Structural Formulae.

similarly structured chlorite-like minerals is shown in figure 4.10, taken from Nelson and Roy (1958) (berthierines are here termed "septechamosites"). This gives a clear, but simplistic view of the relationship between berthierine and two important similar mineral species, greenalite ($Fe_6Si_4O_{10}(OH)_8$) and amesite ($(Mg_4Al_2)(Si_2Al_2)O_{10}(OH)_8$). These two minerals may be compared to berthierine, by Fe and Si replacement for Al; and Mg replacement for Fe, respectively. A more complex, but complete, classification scheme for the 1:1 phyllosilicates has recently been produced by Wiewiora (1990), and is shown in figures 4.11, 4.12 and 4.13. The 1:1 phyllosilicates containing Mg, Fe^{2+}, Al, and vacant sites (❑) in the octahedra are classified in a polyhedron (figure 4.11). Pure end-member berthierine is here given the composition $(Fe^{2+}_{2.5}Al_{0.5})(Si_{1.5}Al_{0.5})O_5(OH)_4$ (note that the number of oxygens used here is half that used above), and can be compared to that of greenalite and amesite in figures 4.12 and 4.13, that represent the polyhedron base with side, and polyhedron top, respectively. Silicate compositions cannot be plotted directly on these figures, as all five variables Fe, Mg, Al, Si, and ❑ are represented only in the polyhedron. However, the authigenic cement compositions of the Frodingham Ironstone Formation can be best classified as berthierines relative to its closest neighbours in this scheme, on this basis of:

1) High Al relative to greenalite [$Al_{0.85}$ as opposed to $Al_{0.00}$(14,O(OH))].

2) Low Mg relative to amesite [$Mg_{0.44}$ as opposed to $Mg_{2.0}$ (14,O(OH))].

3) Higher Fe/Al ratio (≈2.3) relative to Fe^{2+}-amesite (1.0) and brindleyite (≈1.2).

The analyses would hence plot near the berthierine end-member, but with a vector component directed from the defined berthierine composition towards the greenalite, brindleyite and lizardite end-members.

Figures 4.14, 4.15 and 4.16, show that the Frodingham berthierines have a significantly lower, though not unreasonable, Al content in terms of both total and octahedral Al (figures 4.14 and 4.15 respectively). The analyses hence fall in the low Al area of berthierine compositions defined from published analyses (see also figure 4.16 a and b). This is consistent with the berthierines of the Frodingham samples forming part of the iso-cation substitution series R^{2+}, Si = Al^{iv}, Al^{vi} relative to those of higher Al content, i.e. the lower

Figure 4.10. Classification of Magnesian and Ferroan Chlorites Based Upon Four End-Member Compositions. Taken From Nelson and Roy (1958). Berthierine is Here Termed "Septechamosite".

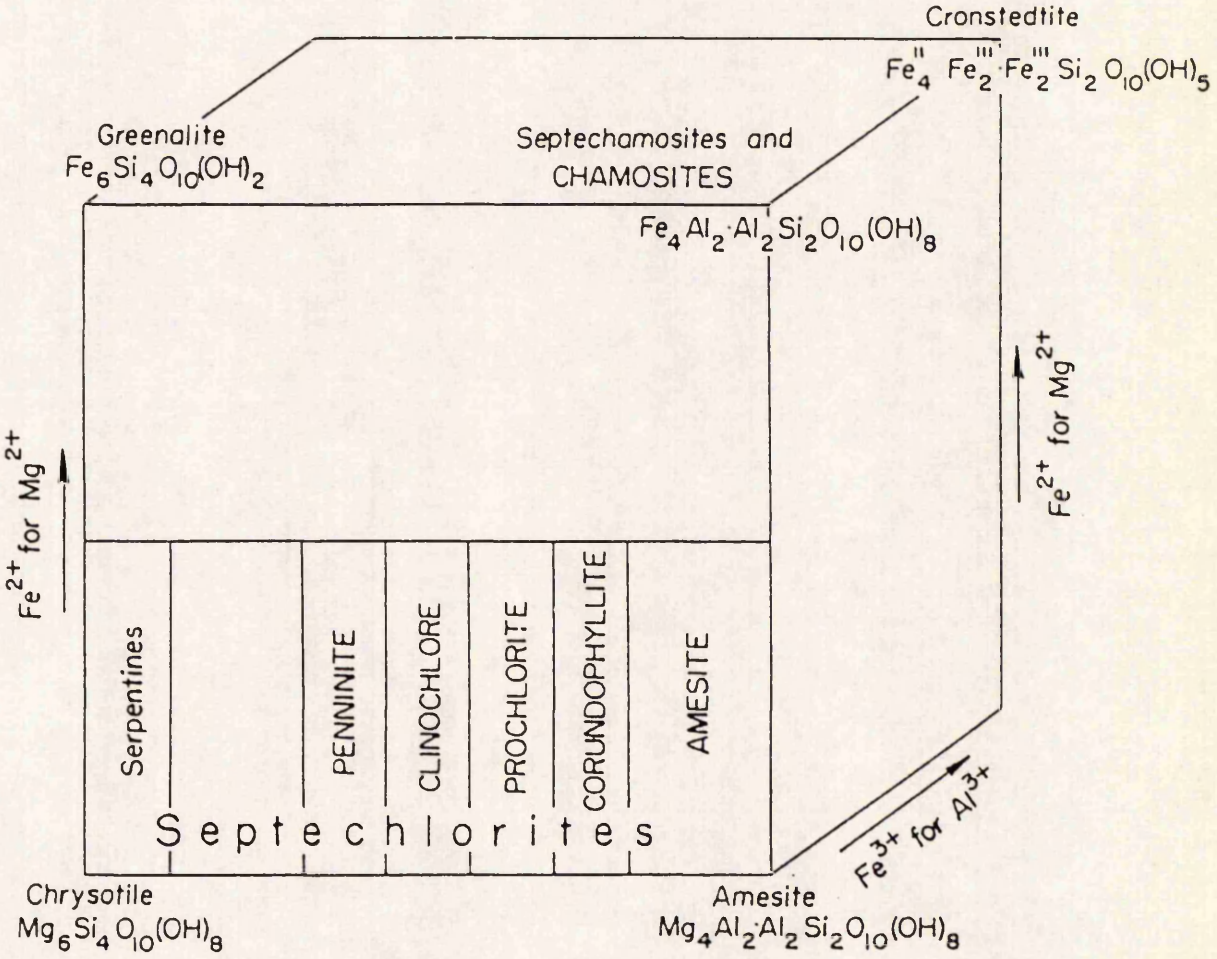

Figure 4.11. Composition Polyhedron for Classification of the 1:1 Phyllosilicates with Mg, Fe^{2+}, Al, and ❑ in Octahedra. Taken From Wiewiora (1990).

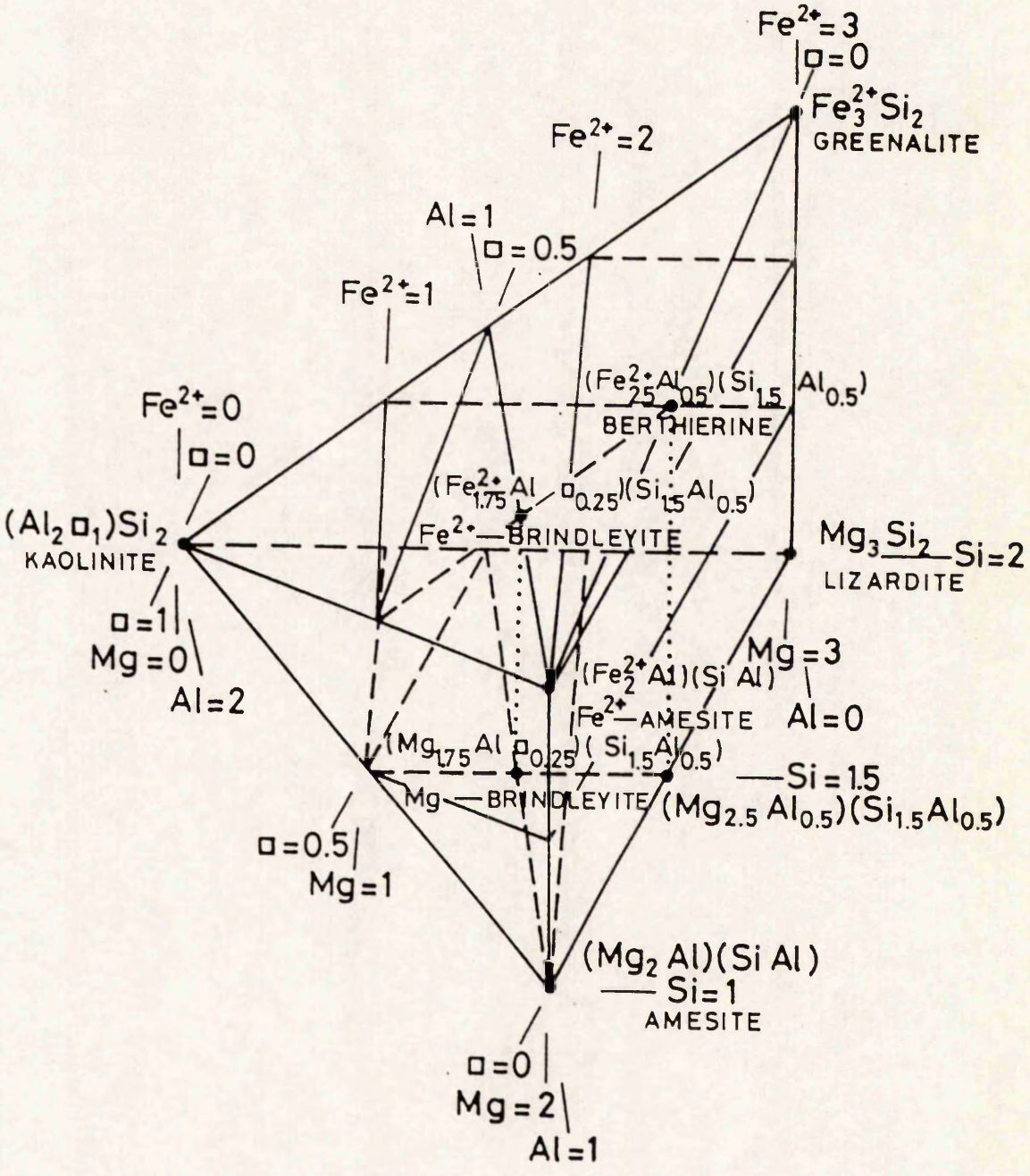

Figure 4.12. Projection Field for 1:1 Phyllosilicates with Mg, Al, and ❑ (Base of Polyhedron in Figure 4.11) and with Mg, Fe^{2+}, and Al (Side Wall of Figure 4.11). Taken From Wiewiora (1990).

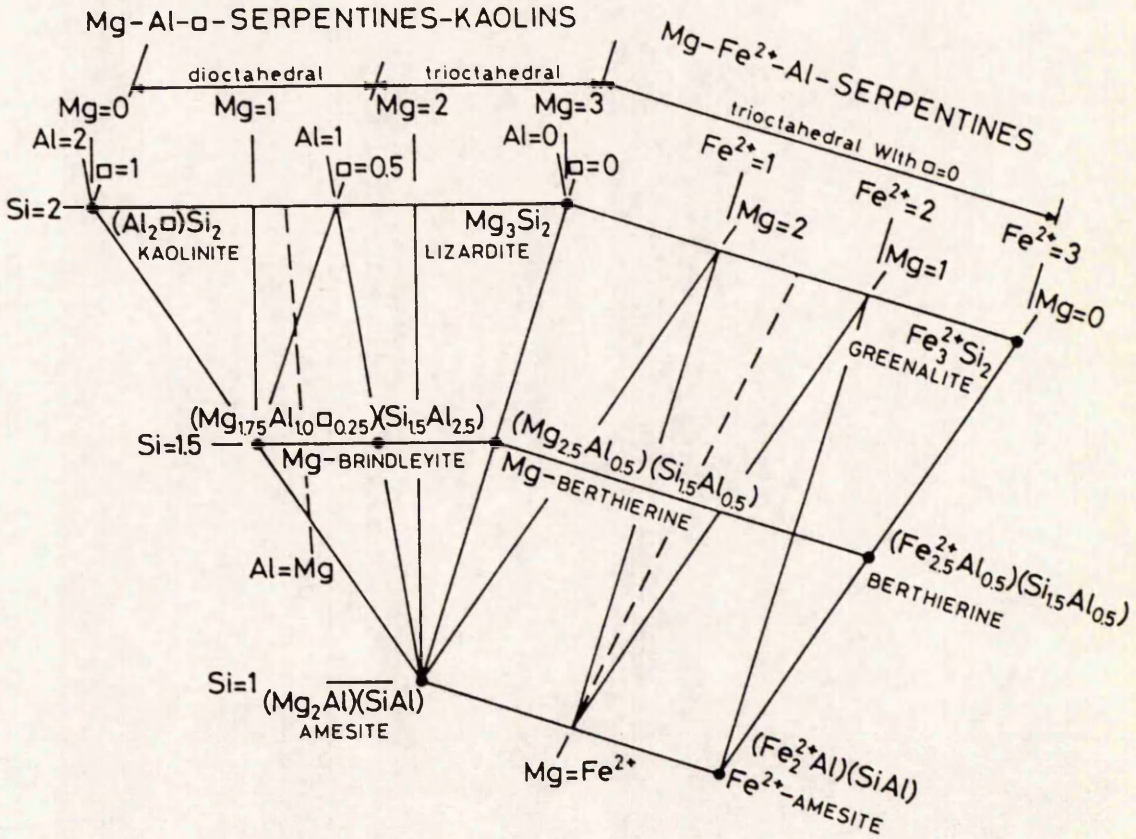

Figure 4.13. Projection Field for 1:1 Phyllosilicates with Fe^{2+}, Al, and ❑ in octahedra (Top of Polyhedron in Figure 4.11). Taken From Wiewiora (1990).

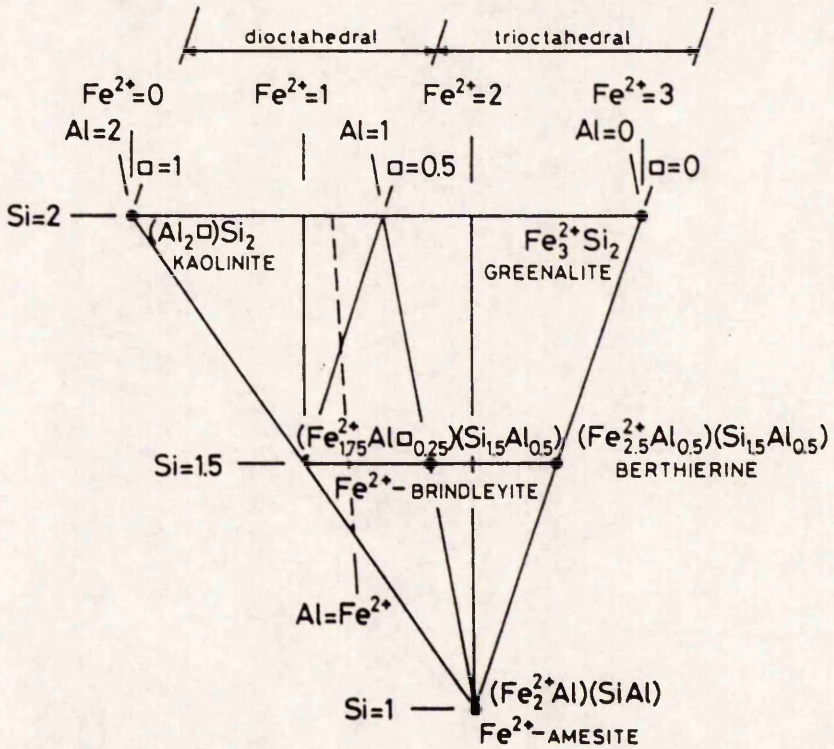

Figure 4.14. Al(Total) - Mg - Fe Ternary Plot of Berthierine Cement Compositions Compared to Published Berthierine Analyses. Data were Obtained by E.P.M.A., and Recalculated to Berthierine Structural Formulae.

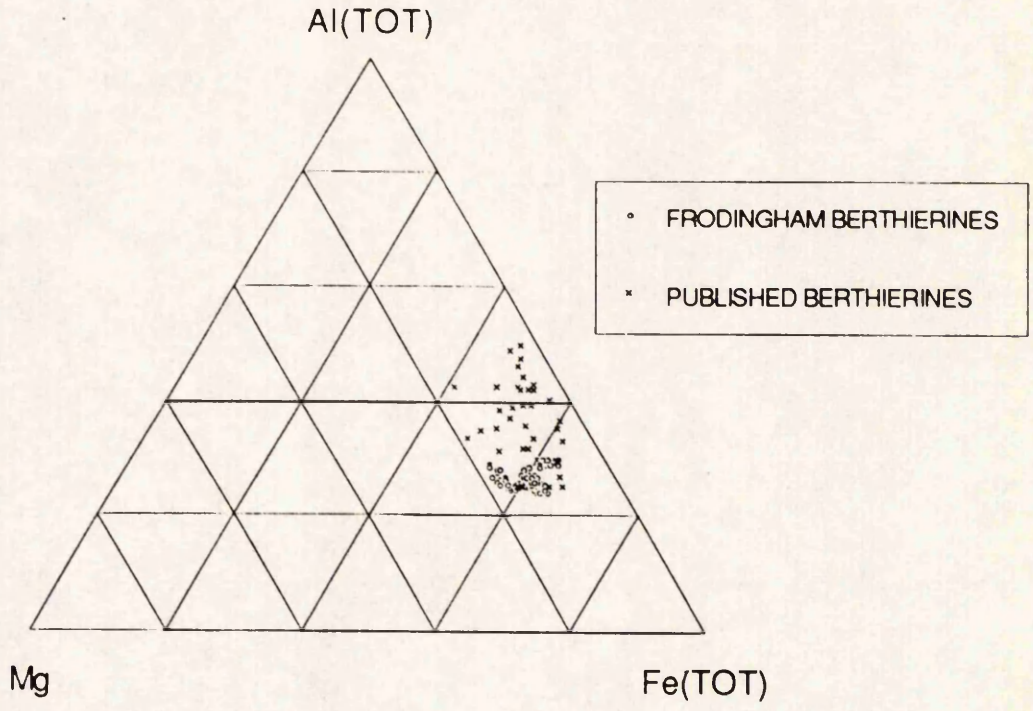

Figure 4.15. Al(Octahedral) - Mg - Fe Ternary Plot of Berthierine Cement Compositions Compared to Published Berthierine Analyses, Illustrating the Composition of the Octahedral Layer. Data were Obtained by E.P.M.A., and Recalculated to Berthierine Structural Formulae.

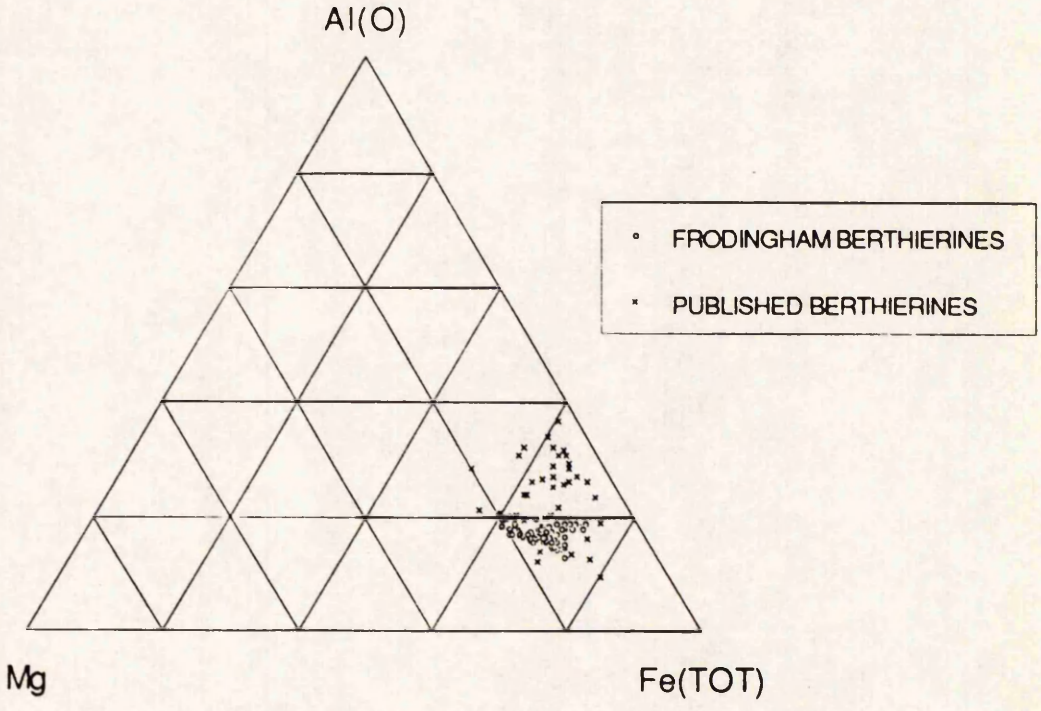

Figure 4.16. Authigenic Berthierine Cement Compositions Plotted on a Haves (1970) Plot. After Recalculation to a Chlorite Structural Formula.

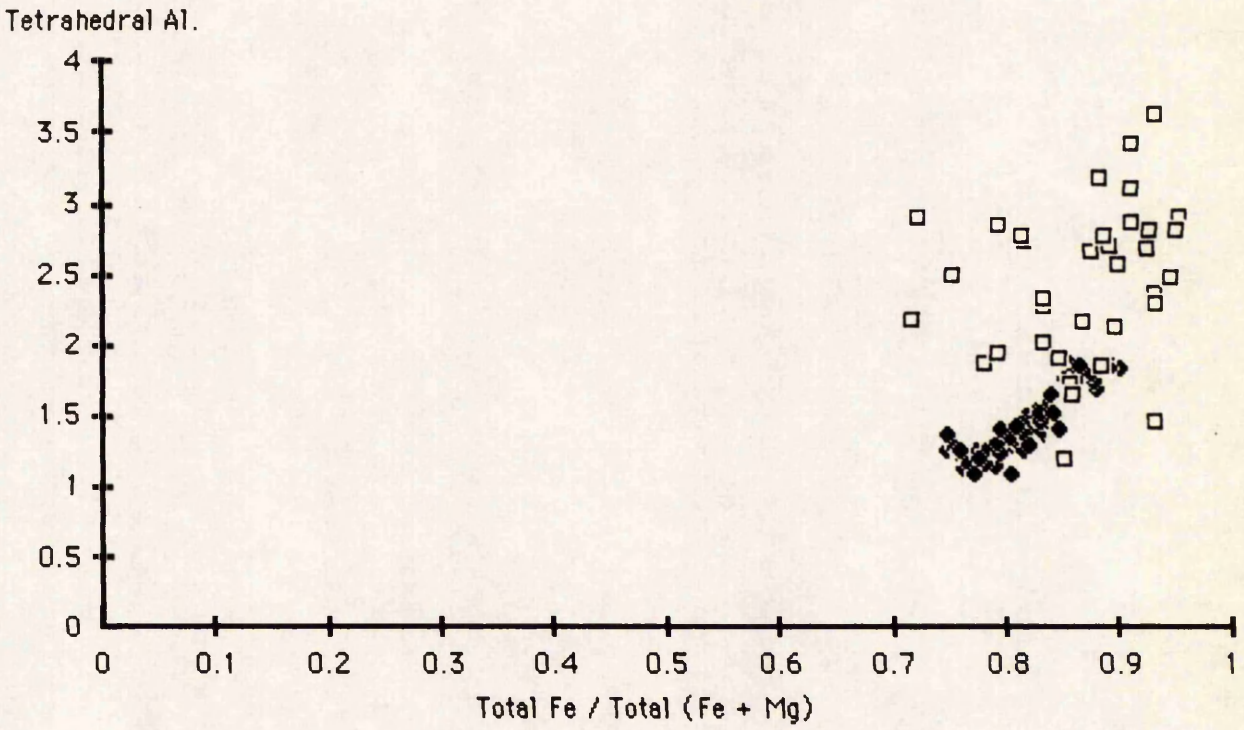

Detail of the Data Set Shown Above.

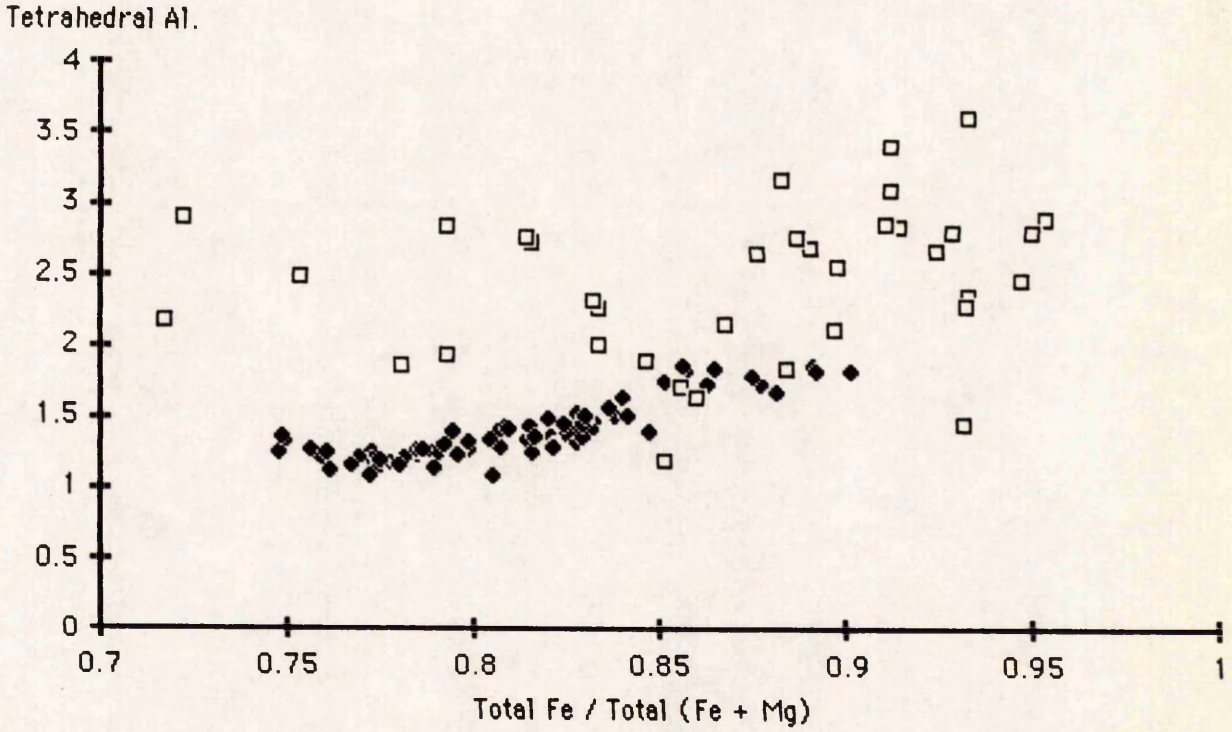

Al is balanced by an increased Si and R^{2+} content. From figures 4.14 and 4.15, there is little evidence of this series occurring within the Frodingham samples themselves, but the trend shown in figure 4.16 shows this to be the case. As tetrahedral Al increases (due to Si decrease), the Fe/(Fe+Mg) ratio also increases, i.e. the proportion of Fe in the octahedral sites is also increasing. It is therefore primarily Fe that is used to balance the charge when Si is the predominant tetrahedral cation.

4.8) The Timing of Berthierine Formation.

The narrow spread of data between analyses of a single precipitated generation of berthierine, and between different thin-sections described above, suggests three possible scenarios for berthierinisation, that are here discussed in detail:

1) Berthierine was precipitated/transformed from a precursor clay mineralogy, in near equilibrium with a pore fluid, by a single berthierinisation event.

2) As (1) but berthierinisation was a multi-occurrence process.

3) Berthierine has a single stable composition, for a variety of pore fluid types and microenvironments encountered in the Frodingham Ironstone Formation.

These three possibilities, and their implications for berthierine formation in the Frodingham Ironstone Formation, are discussed below.

1) Single Event Berthierinisation.

A single berthierinisation event would imply that muds and cements were synchronously transformed, and precipitated, respectively. This would imply deposition of the full ironstone sequence prior to berthierine formation. Progressive berthierinisation of the muds during deposition would hence be discounted, and the mud compositional trend (section 4.3) would instead be controlled by either a surface controlled effect (i.e. diagenetic zonation) or initial composition of the deposited muds. Given that berthierine is always an early cement, the ironstones would have had to have remained largely uncemented for the 2-4 Ma of deposition. This has support, in that no hardgrounds are seen to have formed during this period (see descriptions in section 2.8), but is unusual given the long timescale and the continuous deposition over the span indicated. Petrographic examination reveals the

ironstone-formation to be well suited to carbonate cementation, due to the high proportion of bioclastic debris, coupled with the fact that full cementation occurred prior to significant compaction. This hypothesis would also indicate that the berthierine ooids, and berthierine laminae in goethitic ooids, obtained their present mineralogy during this single event, in which case a precursor clay mineral or full diagenetic *in situ* precipitation mechanism is to be implied. The interpretations suggested in this thesis for the mud compositional trends; suitability for early cementation; and detrital origin of the ooids; are all in contrast to the conditions described above, and hence the model has significant problems, and is not supported here.

2) Multi-Stage Berthierinisation by a Single Pore Fluid Composition.

This hypothesis involves a number of finite berthierinisation events, or a continuous progression of berthierine formation during the deposition of the Formation. The mechanism of berthierine formation is implied to be related to an unchanging process, continually attained within the sequence, as opposed to a single diagenetic event. Berthierine is assumed to have been precipitated from a pore fluid whose composition did not change significantly during the 2-4 Ma of deposition. This hypothesis has advantages over (1) above, in that it explains signs of penecontemporaneous oxidation which occurred during reworking of previously formed berthierine. This suggestion implies that Fe^{2+} was present within the sediment during ironstone deposition.

3) Multi-Stage Berthierinisation With Variable Pore Fluid Composition.

It is not implied within this hypothesis that pore fluids underwent large scale changes in composition during berthierine formation, such as from marine to meteoric waters, but that more subtle changes in solute concentrations may have occurred that did not significantly effect the composition of the precipitate formed. This hypothesis suggests that precipitated berthierine was confined to a small range of compositions relative to that of the pore fluid. This is a more likely scenario than (2) above, for unless an abundant supply of constant composition (i.e. sea water) is implied as the precipitating fluid, pore water compositional changes through diagenesis are inevitable. It is hence possible that the actual

range of possible berthierine compositions is more restricted than published analyses might suggest, with the variation seen being due largely to analytical error. Fully testing such a hypothesis is however impossible, as the error on analyses quoted is poorly constrained, and considerable contamination may be present in many analyses.

4.9) Pore Fluid Composition and the Origin of Berthierine.

The pore water from which berthierine precipitated, was almost certainly of an original marine composition. The ironstone-formation has been shown to have been deposited in marine waters of normal salinity (section **2.5**), and entrapped pore waters would have been of a marine composition. High porosity and permeability would have allowed further diffusion of ions from sea water into the substrate. The major cations of berthierine, Si, Al, and Fe, are all in low concentrations within sea water, and would need to be enriched within pore fluids to allow berthierine formation, though the degree of enrichment necessary is undefined. The presence of authigenic berthierine cements within the ironstone-formation shows that free cations or complexes of Si, Al and Fe, were present in pore waters, but gives little indication of the source of these cations. This is discussed below.

The presence of detrital fabrics in berthierine mudstones, coupled with its instability in oxic marine waters, and implied *in situ* development, suggest that berthierine formed from a precursor clay mineral (or minerals) deposited at the time of ironstone accumulation. The clay mineralogy of the shales above the ironstone-formation suggests that this would have been kaolinite and/or illite. Kaolinite has been postulated by many workers to be the precursor mineral to berthierine formation due to its similar structure. However, simple kaolinite dissolution and berthierine precipitation would not account for the different Si/Al ratios found between kaolinite, and Frodingham berthierines (1.00 and 1.93 respectively). An extra source of Si would hence need to be sought if kaolinite only was involved. Detrital quartz is a possibility, but this is uncommon in the ironstones, and a mechanism for total quartz dissolution is lacking. An alternative view is suggested by the trend seen within analyses of the ironstone muds, from pure berthierine towards an illitic composition of equal Si/Al ratio to that of the berthierine cements. If the original detrital mineralogy were of this

illitic/kaolinitic composition, then mud dissolution would supply Si and Al to pore waters. Reprecipitation could occur with the addition of Fe to form berthierine of the same Si/Al ratio. Both illite and kaolinite may be involved in this process in order to explain the clay mineralogical trends seen.

It is here proposed that the berthierines of the Frodingham Ironstone Formation were formed in response to a detrital assemblage of kaolinite, illite, and iron oxide/hydroxides becoming unstable during early diagenesis of the ironstones, resulting in the formation of a more stable mineral phase, berthierine. Formation by this mechanism requires no external input of Si, Al, or Fe to the system after deposition, with the small amount of Mg within berthierine being derived from sea water. The destabilisation of the detrital mineralogy is assumed to have occurred during post-oxic diagenesis, as Fe was being liberated into solution by the bacterial reduction of detrital iron-oxides/hydroxides. As indicated in section 1.10, iron-reduction significantly increases the pH, which would tend to destabilise aluminosilicates, most of which have a minimum solubility at near-neutral pH values. Detrital muds underwent varying degrees of dissolution and re-precipitation, leading to the formation of cements and recrystallisation textures, or little modification and fabric preservation. Despite the differing fabric modifications, destabilisation apparently resulted in Si and Al release in a consistent Si/Al ratio, and the released Si and Al reacted with the excess Fe to form berthierine of a relatively fixed composition. Berthierine formation could hence have been a continuous process, and not a single event. The mechanism of berthierine generation by detrital clay destabilisation without external cation input, also explains the variation in published berthierine analyses, that probably result from different initial detrital clay assemblages undergoing the same post-oxic modification.

CHAPTER 5. NON-SILICATE MINERALOGY, PETROGRAPHY AND COMPOSITION.

This chapter is divided into two parts, the first part of which forms the majority of the chapter and deals with the description and discussion of the carbonates within the ironstone-formation. The second part describes the other minerals present within the sequence, that are in subordinate quantities relative to both the silicates and carbonates.

PART 1: CARBONATES.

5.1) Introduction.

The Frodingham Ironstone Formation has a high carbonate content, particularly in the lower beds, and much of this is authigenic. Deposition in high energy conditions that winnowed muds, coupled with the high sphericity of iron-ooids relative to other sedimentary particles, produced a high primary porosity. This was accentuated where storm-generated coquinas of intact shell debris were deposited preserving high shelter porosity. Cementation of the pores occurred early, prior to significant compaction, and so the total volume of authigenic minerals is high, the vast majority of which are carbonates. Petrographic studies show that carbonate cementation in the ironstones can be extremely variable, and often complex. Within a single thin-section, up to eight distinct carbonate fabrics could be seen, and these may be absent in another part of the slide, or texturally different.

The carbonate cements were examined using petrographic techniques (outlined below), in conjunction with E.P.M.A., and stable isotopic analysis of carbon and oxygen. The intention was to study three major areas of interest in detail;

1) Cementation of the ironstones relative to other sedimentary rock types, particularly those of an iron-rich mineralogy.
2) Changes in pore fluid chemistry during cementation of;
    a) Individual samples.
    a) The whole ironstone-formation.

3) Variations in cementation type between rock;

a) Fabric; the effect of mud, porosity etc.

b) Mineralogy; the effect of the presence or absence of other authigenic minerals.

5.2) Staining Technique and Acetate Peels.

Petrographic examination of the carbonate portion of these rocks is considerably enhanced by staining with Alizarin Red S and Potassium Ferricyanide (see for example plates 4a, 11, 14d, 16d, 19c). The method used was a modified version of Dickson (1965, 1966) and is outlined in appendix A.1.1. The best results were achieved by application of a light stain to thin-sections polished using 1/4 μm alumina powder. Heavy staining or lack of polish has only detrimental effects to petrography. More complex staining techniques such as those outlined in Friedman (1959) were not attempted as E.P.M.A. facilities were available.

The method of staining was found to be extremely useful, in that the three major carbonate types present in the ironstone-formation, non-ferroan calcite, ferroan calcite, and siderite are readily distinguished. Though semi-quantitative analysis of Fe proportion in calcite has been attempted by staining methods (Lindholm and Finkelman 1972), a purely qualititative approach was applied here to ascertain the carbonate phases present, with later compositional analysis by E.P.M.A. Staining thin-sections has also proved useful in photography, in reducing the contrast between iron oxide/silicate and carbonate (plate 7). 'Ghost' reflections and light diffraction under higher transmissions from clear carbonate are significantly reduced by staining without loss of textural detail. Photographic results are hence improved by the preservation of detail in both light and dark areas of the view.

Acetate peels were produced from stained rock slabs of the more carbonate-rich samples, in an attempt to examine larger rock areas, and extend the thin-section database. The peels were however found to be of generally poor quality despite varying times of etching or

grinding. This was largely due to the high proportion of iron-rich particles that did not peel well, often plucking and rendering the peel impossible to flatten.

5.3) Luminescence and Fluorescence Petrography.

The technique of cold-cathode cathodoluminescence (C.L.) has been used extensively in the study of carbonate sediments, and has been extended to the examination of ironstones (for example Hagni 1986). In the initial part of this research, C.L. was used as a standard petrographic method, and good luminescence was achieved from the calcite cements despite being ferroan, due to the high proportion of Mn present (see appendix A.1.3 for operating details). The siderites were predictably non-luminescent. Despite the good luminescence of the calcites, C.L. proved to be of little value in deciphering the diagenetic history of the ironstones, because zoning within crystals was rarely observed. Slight luminescence variation between crystals occurred, but was not generally systematic, and crystal orientation was probably of greater importance on the luminescence characteristics than compositional variation. There was hence no possibility for correlation of cement stratigraphies based upon luminescence properties, and normal optical petrography coupled with E.P.M.A. was found to provide more usable data.

Ultra-Violet (U.V.) fluorescence has been shown to be of considerable use in carbonate petrography as an aid to the delineation of diagenetic recrystallisation fabrics in some rocks (Dravis and Yurewicz 1985). It has also been used to show complex zoning within siderites, that would not be visible by conventional methods of optical and C.L. petrography (Mozley 1989). The causes of fluorescence in minerals have not yet been systematically evaluated, and the technique is limited to fabric, and not compositional analysis. Despite the aesthetically pleasing luminescence seen in Frodingham carbonates (for example plate 20a), the technique did not reveal significantly different textures to those readily seen by normal optical petrography, and extensive recrystallisation is assumed not to have taken place.

5.4) Electron Probe Micro-Analysis (E.P.M.A.)

E.P.M.A. (see appendix A.2.1) was used as the standard tool to obtain the chemical composition of the carbonate phases. It allows analysis of very fine crystals that are common in the ironstone-formation, though the accuracy and precision limits its use to the more abundant elements, Ca, Mg, Fe, Mn, Sr, and Na. The common occurrence of detrital material as micro-inclusions would also invalidate trace-element data. For this reason all analyses incorporated Si and Al determinations as an indicator of the presence of detrital inclusions. Phosphorus was analysed to check for authigenic phosphate formation and phosphatisation of bioclasts.

Probing of carbonates is particularly time consuming, as all analyses were made by Wavelength Dispersive Spectrometry, taking up to 15 minutes per analysis. The thin-sections chosen for E.P.M.A. were hence carefully chosen to test the variation in carbonate compositions within the ironstone-formation, and to highlight specific areas of interest, such as multi-generation cements and previously undescribed morphologies.

5.5) Terminology of Cement and Replacement Textures.

Many terms have been employed in the description of carbonate cement textures, and confusion often exists on precise definitions. Cement texture descriptions in this study are based upon the terminology of Bathurst (1975) but to avoid any possible confusion, the following terms are described in detail:

Replacement: Used as a general term to imply that the present mineralogy is in place of a former phase or fabric. No specific genesis is implied.

Cementation: The filling of pore space by precipitation from solution of a mineral phase. See Bathurst (1975 p. 417) for criteria of cement fabric recognition.

Neomorphism: This was defined by Folk (1965) as a term of ignorance encompassing all transformations between one mineral and itself or a polymorph, independent of fabric change. It does not include cementation.

Recrystallisation: A form of neomorphism where the fabric changes without a change in mineralogy. The high-magnesian to low-magnesian calcite reaction is not included.

Polymorphic Transformation: (Bathurst 1975, equivalent to 'inversion' Folk 1965). A neomorphic change from one polymorph to another (aragonite to calcite), as a wet *in situ* transformation.

Aggrading Neomorphism: A complex process combining recrystallisation and polymorphic transformation of micrite, to a sparite ('neomorphic spar' Bathurst 1975).

Calcitisation: The replacement of a mineral by calcite involving gradual (not wholesale) dissolution and precipitation, possibly preserving the internal fabric. The thin-film process of aragonite dissolution, and calcite precipitation, is such an example.

In addition to the above, the terms High Magnesian Calcite (>4 mol% $MgCO_3$, abbreviated to H.M.C.), and Low Magnesian Calcite (<4 mol% $MgCO_3$, abbreviated to L.M.C.) will be used. This division is arbitrary, but serves to differentiate between the naturally formed calcites with high Mg contents found in bioclastic fragments (often 10-20 mol% $MgCO_3$, Chave 1954) and calcites precipitated from sea water (thermodynamically predicted at 12 mol% $MgCO_3$, Walter and Morse 1984), with those of calcites deposited by meteoric waters and H.M.C. that has lost Mg during diagenesis.

The term ferroan calcite is used for calcites which can be stained blue by standard staining techniques (see above), and non-ferroan for those that are coloured pink-red (i.e. containing less than a few hundred parts per million (p.p.m.) Fe). Mn content cannot be determined by simple staining methods, but where E.P.M.A. data are available, the composition may be further clarified by the terms manganoan or manganoan/ferroan if Mn > Fe.

5.6) Crystallography.

Within the ironstone-formation, calcites and siderites are the only common carbonates present, which are isostructural, and crystallise in the **3** 2/m class. Many crystal forms exist in calcite, but the commonest clearly identifiable habit is the scalenohedron {2131}. This

may be tipped by a rhombohedron {1011}, but is usually poorly developed. Where crystals grow significantly far out from the substrate, the first-order prism {1010} may form. This cement is henceforth described as scalenohedral. Where a mucilage or thin micrite envelope has retained the bioclast outline during solution-replacement, twins on {0001} may develop by growth in both directions. Prismatic calcite (based primarily on {1010}) occurs as a fibrous cement fringe on bioclastic debris that retains the internal structure. Other calcite cements do not possess clear crystal form, due to crystal interference and compromise boundary development. Siderite typically crystallises as simple, single rhombohedrons, though curved crystal faces are ubiquitous.

5.7) Ferroan Calcite Cements and Replacement Textures.

5.7.1) Cement Fabrics.

The fabrics described in this section, are those produced by calcite precipitation alone. Siderite cements and carbonates associated with berthierine cement formation are described later. The rocks that are solely cemented by ferroan calcite form the bulk of the lower part of the sequence, and are the most carbonate-rich. They were originally highly porous, composed of iron-ooids, bioclastic debris, and occasional pisoids, mud-clasts, and intraclasts. Petrographic examination suggests that full cementation occurred in a single time-span, and not via multi-phase burial cementation.

The cements can be divided into four groups for description; syntaxial overgrowths on echinoderm fragments; fibrous and prismatic cements nucleating on unreplaced bioclastic debris; scalenohedral crystals; and pore-filling sparites, which include radiaxial calcites and larger void cementation. Compositions of these cement types are given within table 5.1 that lists the analyses by thin-section, so as to allow comparison of differing morphologies within the same sample.

5.7.1.1) Syntaxial Overgrowths on Echinoderms.

The formation of syntaxial overgrowths on echinoderm grains has been well documented (see discussion in Bathurst 1975). Within the ironstone-formation, most

Table 5.1. Average Compositions of Authigenic Calcites, Obtained By E.P.M.A. The Data are Recalculated to Calcite Formulae.

	DRAG. 31.1		DRAG. 31.2		DRAG. 31.7		DRAG. 31.10			
	Rep. Bio.		Rep. Bio.		Rep.Bio.		GEN. 1 (Scalenohedral)		GEN. 2 (Pore-fill)	
	AVERAGE	STDEV	AVERAGE	STDEV	AVERAGE	STDEV	AVERAGE	STDEV	AVERAGE	STDEV
Ca	36.875	1.201	36.646	0.268	37.738	0.595	37.602	0.231	37.134	0.249
P	0.006	0.013	0.011	0.016	0.000	0.001	0.004	0.006	0.000	0.000
Sr	0.065	0.041	0.049	0.008	0.041	0.021	0.036	0.005	0.041	0.012
Si	0.035	0.032	0.031	0.031	0.013	0.011	0.012	0.005	0.008	0.004
Al	0.014	0.024	0.013	0.021	0.005	0.005	0.002	0.004	0.008	0.011
Mg	0.296	0.089	0.340	0.040	0.299	0.170	0.146	0.014	0.112	0.007
Na	0.121	0.104	0.013	0.007	0.000	0.000	0.015	0.024	0.007	0.005
Fe	1.029	0.758	1.471	0.233	1.191	0.481	0.681	0.064	0.616	0.080
Mn	0.470	0.383	0.372	0.075	0.822	0.641	1.173	0.215	1.612	0.095
O	15.462	0.263	15.457	0.094	15.870	0.293	15.676	0.151	15.569	0.077
TOTAL	54.372	0.868	54.403	0.317	55.979	0.994	55.348	0.552	55.105	0.248
CarbCalc.										
Ca	0.956	0.022	0.950	0.005	0.951	0.009	0.959	0.005	0.953	0.004
Fe	0.019	0.014	0.027	0.004	0.022	0.009	0.012	0.001	0.011	0.001
Mn	0.009	0.007	0.007	0.001	0.015	0.012	0.022	0.004	0.030	0.002
Mg	0.013	0.004	0.015	0.002	0.012	0.007	0.006	0.001	0.005	0.000
Sr	0.001	0.000	0.001	0.000	0.000	0.000	0.000	0.000	0.000	0.000
Na	0.005	0.005	0.001	0.000	0.000	0.000	0.001	0.001	0.000	0.000
	n=10		n=5		n=5		n=3		n=4	

Table 5.1. (Continued)

	DRAG. 31.10 (cont.)								DRAG. 31.23	
	Ech.Ovgth.		GEN. 1 (Fibrous)		GEN. 2 (Pore-fill)		Line (Pore-fill)		GEN.1 (Rep. Bio.)	
	AVERAGE	STDEV	AVERAGE	STDEV	AVERAGE	STDEV	AVERAGE	STDEV	AVERAGE	STDEV.
Ca	37.351	0.070	37.547	0.255	37.330	0.372	36.982	0.484	38.984	2.304
P	0.000	0.000	0.011	0.019	0.007	0.019	0.023	0.020	0.000	0.000
Sr	0.036	0.006	0.040	0.004	0.043	0.010	0.042	0.016	0.120	0.016
Si	0.007	0.001	0.012	0.004	0.011	0.005	0.019	0.015	0.000	0.001
Al	0.001	0.001	0.000	0.000	0.001	0.002	0.000	0.000	0.002	0.003
Mg	0.139	0.015	0.156	0.018	0.217	0.100	0.162	0.052	0.403	0.066
Na	0.012	0.008	0.021	0.007	0.013	0.007	0.009	0.007	0.025	0.006
Fe	0.609	0.136	0.799	0.035	1.018	0.182	0.740	0.153	0.839	0.085
Mn	1.495	0.071	1.002	0.185	0.893	0.200	1.409	0.312	0.890	0.071
O	15.631	0.051	15.655	0.122	15.632	0.153	15.555	0.225	16.360	0.979
TOTAL	55.279	0.186	55.244	0.429	55.166	0.584	54.941	0.736	57.624	3.438
CarbCalc.										
Ca	0.954	0.001	0.959	0.002	0.955	0.007	0.952	0.003	0.951	0.002
Fe	0.011	0.002	0.015	0.001	0.019	0.003	0.014	0.003	0.015	0.001
Mn	0.028	0.001	0.019	0.003	0.017	0.004	0.027	0.006	0.016	0.001
Mg	0.006	0.001	0.007	0.001	0.009	0.004	0.007	0.002	0.016	0.002
Sr	0.000	0.000	0.000	0.000	0.001	0.000	0.000	0.000	0.001	0.000
Na	0.001	0.000	0.001	0.000	0.001	0.000	0.000	0.000	0.001	0.000
	n=2		n=3		n=7		n=5		n=3	

Table 5.1. (Continued)

	DRAG. 31.23 (cont.)				Y183.10					Y183.13	
	GEN.2 (Rep. Bio.)		Cementing Ooids		Cements		Rep. Bio.			Ferroan	
	AVERAGE	STDEV.	AVERAGE	STDEV.	AVERAGE	STDEV	AVERAGE	STDEV		AVERAGE	STDEV
Ca	38.209	0.539	37.375	0.828	35.635	2.362	35.861	0.387		37.560	1.382
P	0.000	0.001	0.006	0.011	0.006	0.008	0.008	0.010		0.035	0.041
Sr	0.070	0.003	0.059	0.012	0.036	0.008	0.025	0.017		0.048	0.015
Si	0.003	0.003	0.004	0.005	0.691	0.813	0.156	0.300		0.182	0.198
Al	0.002	0.002	0.004	0.002	0.435	0.544	0.101	0.188		0.100	0.104
Mg	0.130	0.013	0.215	0.222	0.306	0.222	0.250	0.037		0.165	0.036
Na	0.009	0.004	0.016	0.008	0.029	0.026	0.011	0.012		0.025	0.025
Fe	0.870	0.080	0.814	0.086	1.886	1.203	1.613	0.072		1.169	0.233
Mn	1.543	0.107	1.389	0.317	0.459	0.126	0.301	0.120		0.558	0.280
O	16.058	0.237	15.731	0.286	16.299	0.974	15.315	0.621		15.959	0.213
TOTAL	56.894	0.868	55.613	1.129	55.781	1.533	53.639	1.463		55.800	1.036
CarbCalc.											
Ca	0.950	0.003	0.949	0.005	0.940	0.034	0.952	0.002		0.960	0.009
Fe	0.016	0.001	0.015	0.002	0.036	0.025	0.031	0.001		0.022	0.005
Mn	0.028	0.002	0.026	0.006	0.009	0.002	0.006	0.002		0.010	0.005
Mg	0.005	0.001	0.009	0.009	0.014	0.010	0.011	0.002		0.007	0.002
Sr	0.001	0.000	0.001	0.000	0.000	0.000	0.000	0.000		0.001	0.000
Na	0.000	0.000	0.001	0.000	0.001	0.001	0.000	0.001		0.001	0.001
	n=3		n=3		n=5		n=4			n=4	

Table 5.1. (Continued)

	Y183.13 (cont.)		YAR. 2							
	Non-Ferroan		Radiaxial. Rep. Bio.		GEN. 1 (Fibrous)		GEN.2 (Pore-fill)		Cementing Ooids	
	AVERAGE	STDEV	AVERAGE	STDEV	AVERAGE	STDEV	AVERAGE	STDEV	AVERAGE	STDEV
Ca	37.557	0.683	39.371	1.229	39.279	0.233	39.864	0.610	38.372	0.565
P	0.007	0.012	0.006	0.013	0.000	0.000	0.000	0.000	0.005	0.009
Sr	0.065	0.021	0.041	0.013	0.049	0.005	0.042	0.024	0.067	0.006
Si	0.018	0.029	0.005	0.003	0.004	0.002	0.002	0.001	0.006	0.006
Al	0.007	0.008	0.004	0.009	0.000	0.000	0.000	0.000	0.000	0.000
Mg	0.271	0.095	0.269	0.148	0.158	0.021	0.172	0.086	0.283	0.060
Na	0.031	0.069	0.006	0.006	0.013	0.010	0.008	0.008	0.014	0.016
Fe	0.004	0.006	1.269	0.392	1.016	0.055	0.898	0.253	1.266	0.216
Mn	0.002	0.003	1.414	0.936	1.110	0.082	1.289	0.564	1.203	1.101
O	15.226	0.250	16.695	0.256	16.416	0.123	16.672	0.117	16.248	0.415
TOTAL	53.187	0.926	59.078	0.919	58.044	0.452	58.945	0.276	57.465	1.772
CarbCalc.										
Ca	0.987	0.004	0.942	0.018	0.955	0.003	0.955	0.008	0.944	0.017
Fe	0.000	0.000	0.022	0.007	0.018	0.001	0.015	0.004	0.022	0.003
Mn	0.000	0.000	0.025	0.016	0.020	0.001	0.023	0.010	0.021	0.019
Mg	0.012	0.004	0.011	0.006	0.006	0.001	0.007	0.003	0.012	0.003
Sr	0.001	0.000	0.000	0.000	0.001	0.000	0.000	0.000	0.001	0.000
Na	0.001	0.003	0.000	0.000	0.001	0.000	0.000	0.000	0.001	0.001
	n=10		n=6		n=3		n=4		n=3	

fragments of echinoderm possess an overgrowth (plate 16a), though the thickness varies, largely dependent on the amount of other suitable carbonate nucleation sites in the rock, and the surrounding porosity. The largest overgrowths are therefore present where the rock is a grainstone, consisting largely of echinoderm fragments and iron-ooids (for example parts of DRAG. 31.22), such that carbonate precipitation was hence directed towards overgrowth development.

5.7.1.2) Fibrous and Prismatic Cements on Bioclasts.

Fibrous cements form on bioclasts where the shell has remained intact (unreplaced), and the structure is finely foliated, such as the abundant *Gryphaea*, and brachiopod debris (plate 16 c,d). Individual fibres (i.e. acicular prismatic crystals) are 30-100μm long, but may not be apparent due to replacement. . . . Their shape is then defined by poorly defined inclusion trails and aligned extincton. The long-axis of the crystals may not be perpendicular to the shell face, but are orientated parallel, or perpendicular to, the foliation within the bioclast at the shell surface, and thus form an epitaxial cement fringe. These cements are usually not found on ooids, or on bioclasts in which the shell structure has been replaced or recrystallised. Coarser prismatic cements (with a lower length/width ratio) also occur, probably resulting from fewer nucleation sites on or in the bioclast structure. Some indication of competitive growth fabric can be seen, but the texture is usually poorly developed, and may also have undergone recrystallisation.

Analysis of these cements by E.P.M.A. in DRAG. 31.10, DRAG. 31.23, and YAR. 2, showed them to have usually between 1-2 mol% $FeCO_3$ and $MnCO_3$, with the Mn/Fe ratio showing inconsistency between samples. The Mg content reaches only 0.1 mol% $MgCO_3$, and though slightly elevated relative to later cements in DRAG. 31.22, is not consistently so. Similarly, Sr was not found to be enriched, and so an original H.M.C. or aragonite cement cannot be proven on geochemical means. The origin of this and other early cements are discussed in detail in section 5.12.1 below.

PLATE 16

Scalenohedral and Fibrous/Prismatic Calcite Cements.

(Thin-Section Photomicrographs)

A) Early ferroan/manganoan calcites in an ooidal grain-ironstone, specimen DRAG. 31.10. A replaced bioclast is cemented by scalenohedral calcites (1), and a later sparry calcite (2). The grain-ironstone is here largely cemented by echinoderm overgrowths (3), and the later sparry ferroan calcite. A biofilm on the bioclast remained intact during the dissolution of the shell material, and acted as a site for calcite precipitation. Photo length is equivalent to 1.3mm.

B) Scalenohedral calcite in a replaced shell fragment, specimen DRAG. 31.23. A sparry ferroan calcite cements the grain-ironstone, and postdates the scalenohedral form. Photo length is equivalent to 1.3mm.

C) Early fibrous/prismatic calcite cement on an unreplaced shell fragment, specimen DRAG. 31.10. A sparry ferroan calcite postdates this inclusion-rich generation. A broken biofilm (arrowed) has also acted here as a site for poorly scalenohedral calcite precipitation. Photo length is equivalent to 1.3mm.

D) Early fibrous/prismatic calcite cement precipitated syntaxially on two unreplaced oyster shells in a grain-ironstone, specimen YAR. 21. Note that the ooids do not possess a cement rim of this type. Photo length is equivalent to 1.3mm.

A	B
C	D

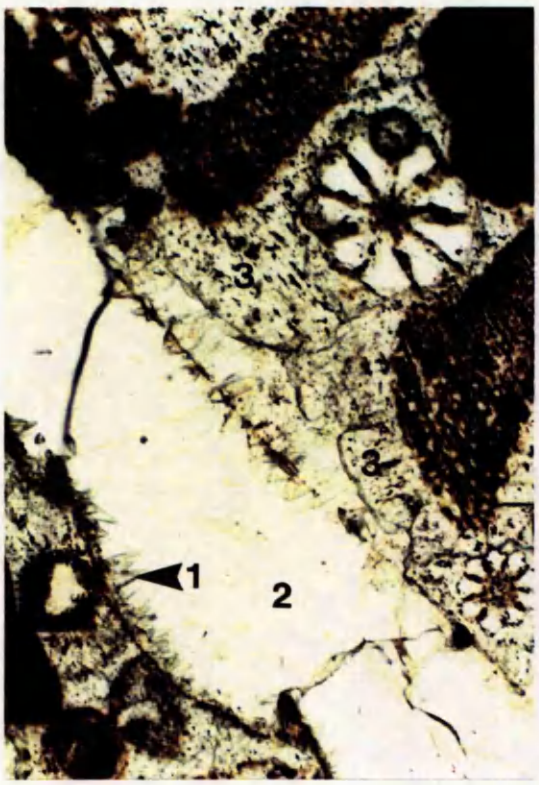
3
3
1
2

5.7.1.3) Scalenohedral Calcite.

The commonest occurrence of scalenohedral calcite is as the first cement generation within replaced shell fragments, attesting to the full solution of the primary aragonite or calcite, with void formation (plate 16 a,b). The size of the crystals formed is dependent on the number grown, which in turn is related to nucleation site availability. The morphology of these cements has been discussed above in section 5.6. Development of the habit outside the bioclast is always less pronounced, due to the presence of impinging particles, and sometimes other cement fabrics. Generally, the cement outside such a bioclast, though similarly nucleated, is finely crystalline and indistinct in form. Where a mucilage or thin micritic layer is present, and space allows, both surfaces may develop a clear crystal fabric, and twinning may occur with one crystal acting as nucleation site to the other.

The composition of these scalenohedral calcites is similar to the fibrous varieties, and to the ferroan calcites as a whole. 1-2 mol% $FeCO_3$ and $MnCO_3$ were found, with an Mn/Fe ratio of 1-2. In DRAG. 31.23, a magnesium anomaly was found relative to the later ferroan calcite (0.04 wt% relative to 0.13 wt%), and may suggest a possible H.M.C. precursor.

5.7.1.4) Pore-filling Sparites.

Ferroan and manganoan calcites form the largest proportion of the cements in the Frodingham Ironstone Formation, and the pore-filling variety is the most abundant of these (for example see plates 4, 7, 11, 16, 20, 21). The texture of pore-filling cements is seen to be largely dependent on the nature of the particles being cemented. Clearly identifiable cement fabrics of coarsely crystalline sparite with roughly equidimensional crystals and planar surfaces, are found usually only between ooids. It is suggested that this is due to the lack of suitable carbonate nuclei present in ooids, such that continued growth to large crystals occurred. A high bioclastic content appears to complicate cementation, so the crystal shape may be irregular with non-planar faces, few enfacial angles, and an appearance similar to neomorphic spar. The origin of this is however not neomorphic, for the following reasons:

1) Evidence of deposition in a high-energy environment, with well-sorted particles in depositional contact. Micrite is therefore unlikely to have been present.

2) This fabric is also seen as a second generation (unlikely in neomorphism).

3) Fabrics in which crystal size increases into pore centres also contain this texture, which are typical of a cement.

Care is hence needed in the interpretation of these cements relative to a primary or replacive origin, and other criteria are considered to be of greater importance in interpreting these cements, such as inclusion fabrics and relic textures.

Many analyses by E.P.M.A., were made of these pore-filling calcites, in order to fully categorise the composition of this most abundant cement of the ironstones. The calcites are ferroan/manganoan with usually 1.0-4.0 mol% $FeCO_3$ and 0.5-3.0 mol% $MnCO_3$, with higher values of one associated with a lower value of the other, giving a negative correlation and a total $(Fe+Mn)CO_3$ of around 3.0-5.0 mol%. The Mn/Fe ratio therefore ranges from approximately 0.2-3.0. The negative correlation between Mn and Fe can be seen in figure 5.1, which plots Mn against Fe as mol% carbonate for random analyses of a single thin-section of a grain-ironstone, DRAG. 31.10. This feature is not true of all samples, which often gave a random distribution, but when data from many sources (DRAG. 31.10, 23; Y183.10; YAR. 2, 21, 22; AMM. 2) are compared, the approximate correlation is again seen, with the greatest scatter at lower $FeCO_3$ values.

Initial attempts to pick up compositional variation across single crystals in an intergranular setting between ooids, showed little evidence for compositional change during growth. Lines of analyses were made in YAR. 21, and are averaged in table 5.2. Analyses of calcites taken from pore edge to pore centre of larger voids, occasionally showed systematic variation in Fe and Mn content, but this variation was inconsistent between samples, such that both Fe and Mn enrichment may occur. It is therefore not possible to suggest an overall change in pore fluid composition during precipitation of these pore-filling calcites.

Figure 5.1. Plots of $MnCO_3$ versus $FeCO_3$ for Pore-Filling Sparites in:

1) A Single Thin-Section (DRAG. 31.10).

2) Many Samples (DRAG. 31.10, 23, YAR. 2, 21, 22, Y183. 10, AMM. 2)

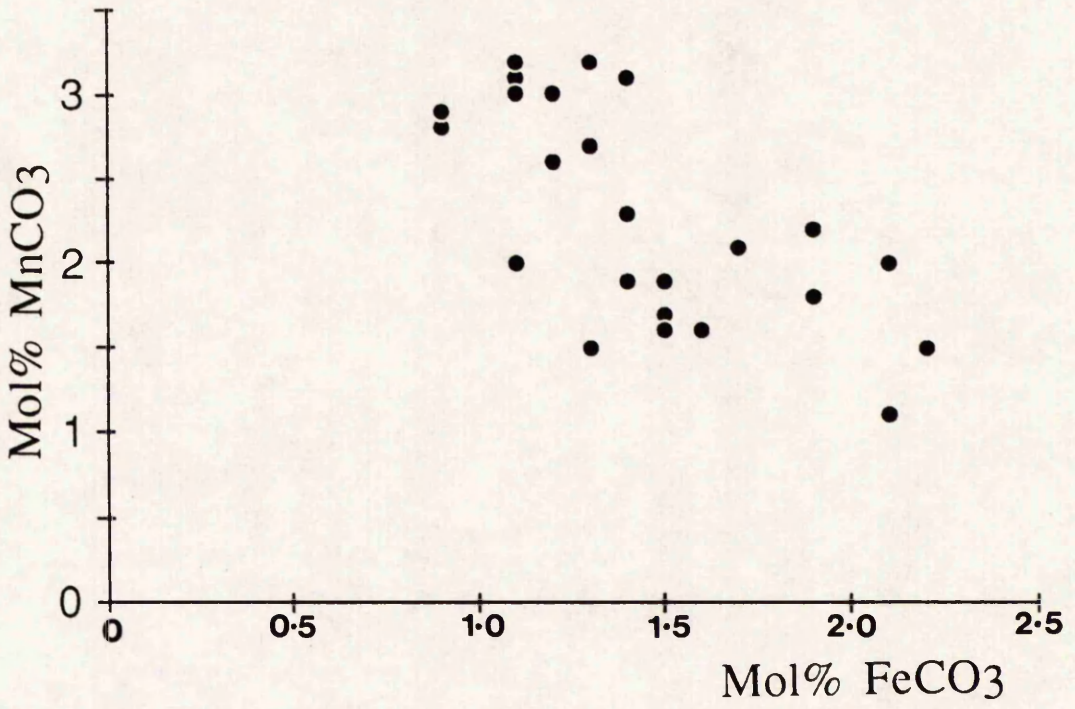

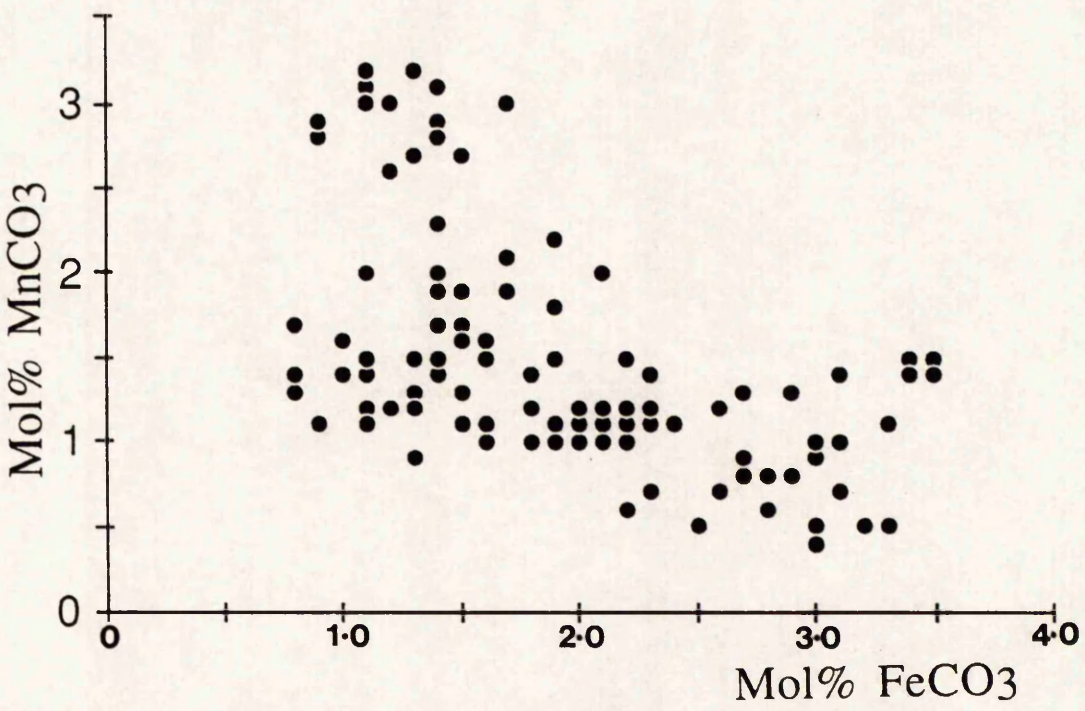

Table 5.2. Average Compositions of Pore-Filling Calcites in YAR. 21, Analysed by Lines of Single Spot Analyses Across the Cement. Data was Obtained By E.P.M.A. The Data have been Recalculated to Calcite Formulae.

		YAR. 21									
		Line >>>			Line >>>			Line >>>			Line >>>	
		AVERAGE	STDEV		AVERAGE	STDEV		AVERAGE	STDEV		AVERAGE	STDEV
Ca		37.432	0.765		38.201	0.343		37.856	0.340		36.883	0.641
P		0.006	0.011		0.032	0.038		0.033	0.022		0.025	0.038
Sr		0.069	0.030		0.061	0.015		0.044	0.009		0.032	0.010
Si		0.049	0.114		0.004	0.008		0.000	0.000		0.003	0.005
Al		0.027	0.067		0.003	0.006		0.000	0.000		0.000	0.000
Mg		0.419	0.085		0.370	0.078		0.445	0.024		0.439	0.049
Na		0.006	0.006		0.004	0.005		0.012	0.005		0.040	0.044
Fe		1.560	0.192		1.346	0.131		1.643	0.071		1.603	0.079
Mn		0.493	0.129		0.518	0.197		0.508	0.040		0.359	0.112
O		15.911	0.155		16.091	0.135		16.079	0.116		15.631	0.239
TOTAL		55.971	0.697		56.629	0.482		56.620	0.389		55.014	0.760
CarbCalc.												
Ca		0.944	0.006		0.951	0.003		0.942	0.003		0.944	0.003
Fe		0.028	0.004		0.024	0.002		0.029	0.001		0.030	0.002
Mn		0.009	0.002		0.009	0.004		0.009	0.001		0.007	0.002
Mg		0.017	0.003		0.015	0.003		0.018	0.001		0.019	0.002
Sr		0.001	0.000		0.001	0.000		0.000	0.000		0.000	0.000
Na		0.000	0.000		0.000	0.000		0.001	0.000		0.002	0.002
		n=6			n=6			n=5			n=5	

The magnesium content of the calcites is usually less than iron or manganese, but may occasionally attain a greater proportion than the latter (less so the former). Values of 0.5-1.5 mol% $MgCO_3$ are typical, though up to 2.0 mol% has been recorded. Such values are however not suggestive of a H.M.C. replacement. Magnesium content shows a general positive correlation with Fe (and hence negative with Mn), shown in figures 5.2. The significance of these trends are discussed in detail later in section **5**.12.2.1.

Non-ferroan calcites were found in only one specimen Y183.13, at the top of the ironstone-formation, where it forms sparry cement in a dense ooidal wacke-ironstone. Zero mol% $FeCO_3$ and $MnCO_3$ were detected with 1.2 mol% $MgCO_3$. Also present within the section was ferroan calcite with 2.2 mol% $FeCO_3$, 2.1 mol% $MnCO_3$, and 0.7 mol% $MgCO_3$, forming around 40% of the cement.

5.7.1.5) Radiaxial Calcites.

Cement fabrics in voids and within formerly aragonitic bivalves, were often found to be of a fabric similar to radiaxial fibrous calcite (*sensu* 'radiaxial fibrous mosaic', Bathurst 1959), which for reasons given below is shown to be a primary cement fabric. The occurrence of this fabric (plate 17 a,b) is of importance to the understanding of radiaxial calcite formation, since to my knowledge, ferroan calcite examples have not been previously described. Radiaxial fibrous mosaic is defined (Bathurst 1959, 1975) by three textures within calcite crystals, usually of a radial-fibrous/prismatic habit. These textures are:

1) Convergent optic axes.

2) Diverging subcrystals.

3) Curved twin planes.

Full textural descriptions of these calcites are given in Bathurst (1959, 1975), Kendall and Tucker (1973), and Kendall (1985). The relationship of radiaxial calcites relative to fascicular-optic (Kendall 1977), bladed-prismatic (Braithwaite 1979), and other replacement fabrics are well reviewed by Mazzullo (1980). In this study, these calcites are referred to as simply radiaxial, since both these examples and those in the literature, are considered to be better described as prismatic rather than fibrous.

Figure 5.2. Plots of $MgCO_3$ versus $FeCO_3$ for Pore-Filling Sparites in:

1) AMM. 2.

2) Many Samples (DRAG. 31.10, 23, YAR. 21, 22, Y183. 10, AMM. 2)

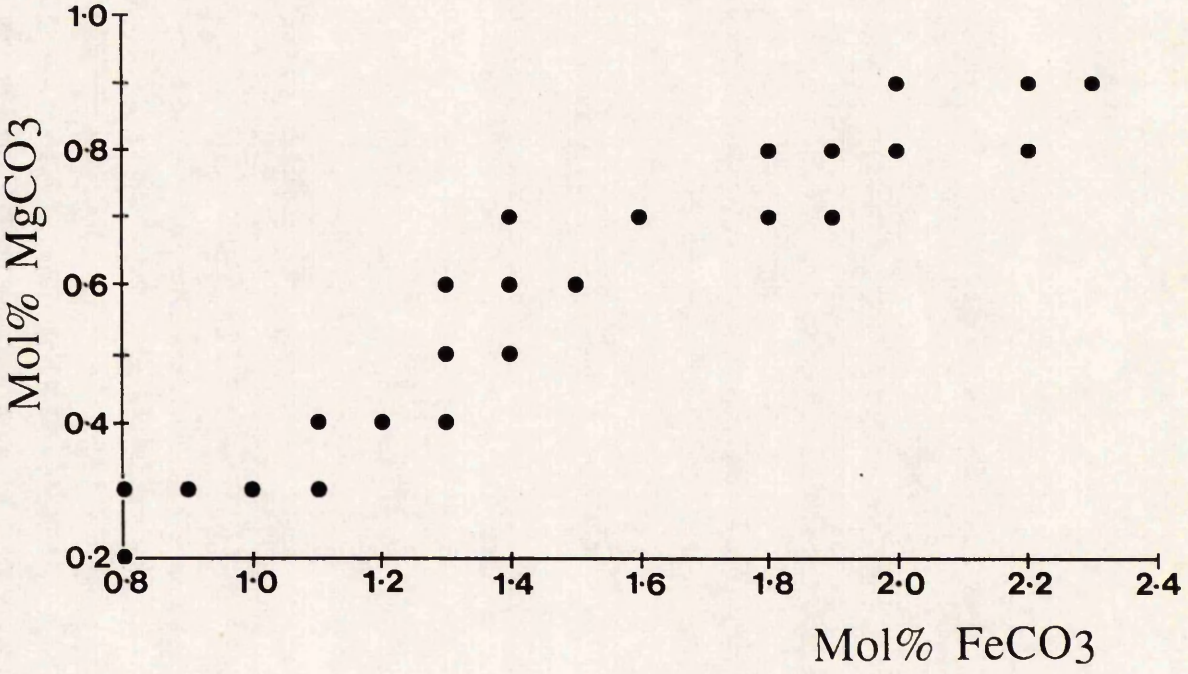

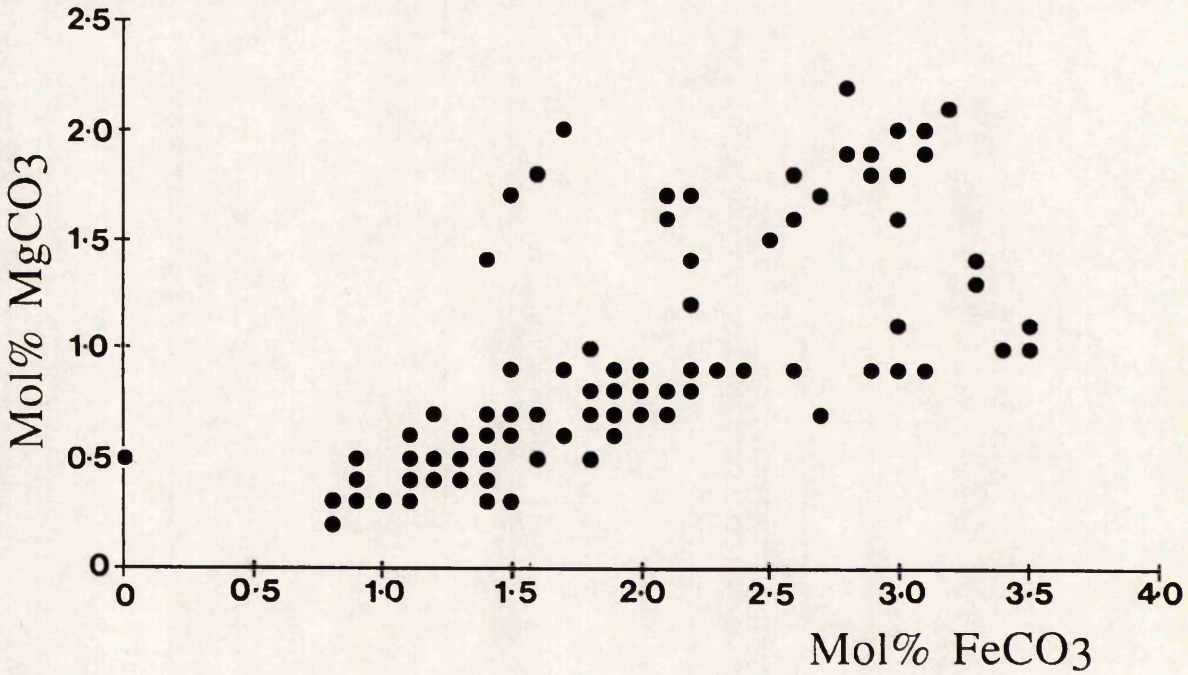

The calcite crystals are elongate, with a preferred orientation perpendicular to the shell edge. Crystal size increases away from the substrate in a competitive growth fabric, and may be seen in some cases to be terminated in a rhombohedron. The size of these crystals is limited by the pore size: the largest crystals seen occur where nucleation was on one side of a void only, so that crystal length may reach 6mm. Intercrystalline boundaries are irregular. The crystals usually show slight undulose extinction under crossed-polars, sweeping across the crystal within 5-15° of stage rotation, but not all crystals within the same specimen do so. The extinction pattern shows that optic axes in the crystal are convergent, distinguishing the texture as radiaxial rather than fascicular-optic (Kendall 1977) calcite. Subcrystals can be seen, and are usually irregular in shape with non-specific orientation, other than approximately aligned with the long axis of the parent crystal. Twin planes are not always present, and show only minor curvature in certain examples. Most radiaxial calcites in the literature are inclusion-rich, with inclusions aligning along twin lamellae, subcrystal boundaries, or related to crystal growth patterns (Kendall and Tucker 1973). These examples are virtually inclusion-free, and hence show no signs of replacement structures or previous stages of growth.

Although the calcite described here is different in many respects from previously described examples of radiaxial calcite, the extinction fabric is considered a strong enough criteria for applying the term radiaxial in this instance, and discussing its origin relative to "true" radiaxial calcites. Bathurst (1959, 1975) originally assumed a primary cement origin to radiaxial calcites, but later (Bathurst 1982) followed other workers in accepting an altered marine cement formation for radiaxial calcites of stromatactis cavities, as opposed to a recrystallisation of host carbonate. Kendall and Tucker (1973) put forward a series of arguments for replacement after acicular carbonate, that was supported by Lohmann and Meyers (1977) and Prezbindowski (1985). Later Kendall (1985) reinterpreted the fabrics to represent a primary rather than a neomorphic origin, suggesting that asymmetric growth within calcite crystals (assumed to be originally HMC) undergoing split growth resulted in a composite radiaxial crystal. Saller (1986) has reported radiaxial calcites in Miocene limestones, with stable isotopic values consistent with marine precipitation, and suggests

aragonite undersaturation, burial sea water circulation, and fluctuating conditions of calcite supersaturation and crystal growth rate, as factors controlling precipitation. Most recently, Mazzulo *et al.* (1990) have recognised 4 generations of radiaxial calcite within a subconformity in the Northern Calcareous Alps of Austria, and interpreted them as forming by direct precipitation as H.M.C. from marine fluids in the shallow burial environment (< 180m).

The composition of a radiaxial calcite cement in a replaced *Cardinia* shell (YAR. 2) was studied by E.P.M.A., specifically to ascertain whether replacement may be detected on geochemical grounds. This showed that the composition was within the range shown by pore-filling calcites (≈ 2 mol% $FeCO_3$ and $MnCO_3$), with only 1.1 mol% $MgCO_3$ on average, and no significantly elevated Sr content. There is hence no suggestion of former H.M.C. or aragonite cements. The Mn/Fe ratio is also seen to vary from 0.1 to 1.9 through the crystals, which would be unexpected for wholesale replacement of former cements, and hence a primary cement origin is favoured. Similar conclusions were made for other occurrences of radiaxial calcite such as those in DRAG. 31.36a (section **5**.9.2).

A primary cement origin is favoured for the Frodingham Ironstone Formation examples, for the following reasons:

1) The fabric is consistent with a competitive growth formation, with crystal size increasing away from the substrate, and the preferred survival of crystals aligned perpendicular to the substrate.
2) The texture is typical of many bladed-prismatic primary cements, but with slight undulose extinction.
3) Cavity growth is indicated by collapse of shells following dissolution, rhombohedral terminations to crystals, and interference growth with crystals growing on the opposite side of the void.
4) No relic structures such as inclusion outlines of former cements are visible in the crystals, or microdolomite inclusions suggested to indicate former H.M.C.

The application of this model to all radiaxial calcites would be unrealistic, due to the significant differences between the fabrics mentioned above. However, it may be possible that this fabric is intermediary between bladed-prismatic, and radiaxial calcite. There is no reason to assume the primary mineralogy was anything other than ferroan calcite, and so such fabrics are shown to be not restricted simply to the 'normal' marine phreatic environment. Though these particular radiaxial-like cements are described in detail here, undulose extinction is present in many of the calcites (and siderites) of the Frodingham Ironstone Formation. This further emphasises the argument that undulose extinction fabrics are not in themselves indicators of carbonate replacement.

5.7.1.6) Void Cementation in Bivalves and Ammonites.

The initial porosity of the ironstone-formation was in some cases around 50% due to the packing of highly spheroidal particles with bioclastic debris and extensive mud winnowing. This porosity is however intergranular and does not allow formation of multigeneration cements, due to the restricted pore size. To examine whether several phases of cements may occur by repeated precipitation or reworking events, several bivalves and ammonites were examined in which calcite had precipitated within the larger voids of the central cavity, and chambers, respectively (see plates 2c, 17). In some cases, two phases were seen; an early inclusion-rich fibrous to scalenohedral cement, followed by a larger prismatic to scalenohedral generation. These calcite cements were analysed in YAR.2 which gave a manganoan/ferroan composition (Mn/Fe $\approx$ 1.0-1.5) with little detectable variation across the generation. It is however interesting to note that the Mn/Fe ratio is slightly elevated in the second cement. The retention of most of the initial porosity by incomplete cementation in some bivalves, indicates that the system was closed during, or as a result of, this cementation; that the source of the HCO_3^- was not exhaustive; or most probably a combination of the two.

Many ammonites were crushed prior to cementation, and retained their shape only by sediment infilling. Pore-filling cements often consist of only one or two generations of sparry ferroan calcite, with crystal size reaching a few millimetres in size. One particular

PLATE 17

Cementation of Large Voids.

A) Radiaxial calcite cementing a *Cardinia* shell, thin-section of specimen YAR. 4 (crossed polars). The bioclast edge is arrowed, and the cement possesses a competitive fabric of growth away from this edge. The undulose extinction of the crystals is apparent, and corresponds to a radiaxial fabric. Photo length is equivalent to 3.3mm.

B) Cement stratigraphy of specimen AMM. 2 (thin-section, crossed polars). The generations are numbered as described in the text. Photo length is equivalent to 6.7mm.

C) Sectioned *Cardinia* shell, hand-specimen YAR. 2. Note the geopetal infill of iron ooids and berthierine stacks (1). Solution collapse of the shell at (2) predated cementation by radiaxial calcite. A thin fibrous cement internal to the bivalve is postdated by a scalenohedral form, but significant porosity remains. The scale bar is divided into centimetres.

D) Detailed calcite microsampling for isotopic analysis, specimen ISO. YAR. 22B (thin-section, crossed polars). The width of a single groove is indicated by arrows. Photo length is equivalent to 6.7mm.

A	B
C	D


1
2
3
4

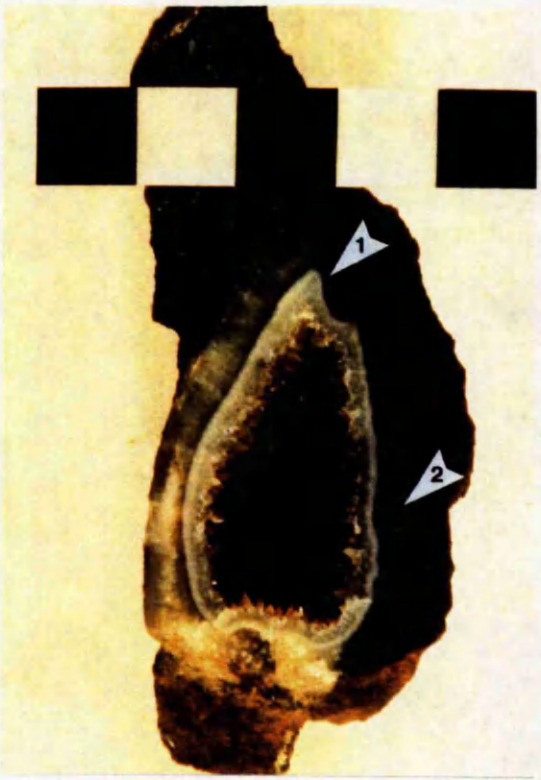
1
2

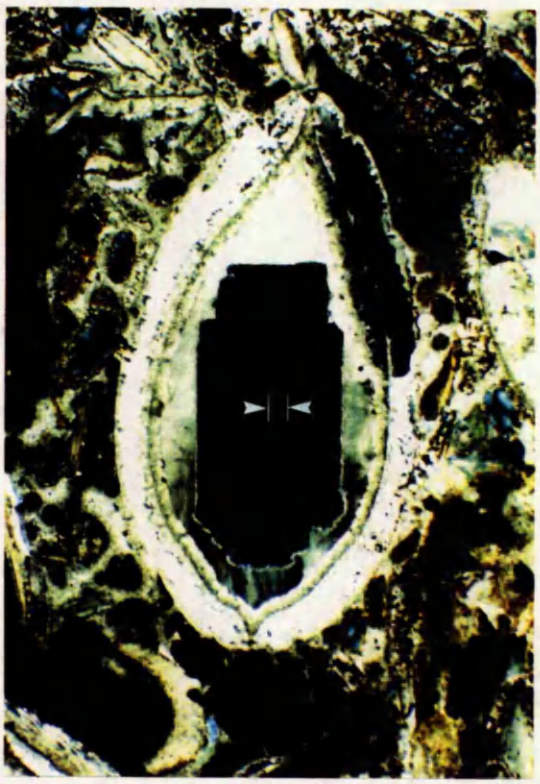

specimen AMM.2 was examined in detail since four generations of ferroan calcite were identified in thin-section (plate 17b). Generations (1) and (3) are prismatic calcites with euhedral rhombic terminations, separated by a micritic layer. Generation (4) is a pore-filling sparry calcite. Compositions of these generations obtained by E.P.M.A.are given in table 5.3. All compositions were found to be manganoan/ferroan calcite with a $FeCO_3 + MnCO_3$ value averaging 2.4-3.3. It is evident from the analytical data, that morphology is not controlled by composition. The Fe/Mn ratio is relatively consistent at approximately 1.0 within generation (1), but increases slightly to 2.0 in generation (3), decreasing within this generation and into generation (4). This is in contrast to an expected transition for diagenetic carbonate evolution where the Fe/Mn ratio is expected to increase (section **1**.10). The trend described reflects a decrease in Fe (rather than an Mn increase) and is suggestive of a gradual and non-predictable change in the relative roles of iron and manganese reduction. The decrease in Mg accompanying this change might be expected if Mg is incorporated into the calcite, without recharge from sea water. The compositional change seen within all Frodingham samples of void-filling calcite cements is extremely subtle relative to cement stratigraphies described for other formations. For example, Marshall (1981) describes up to 9 zones of ferroan/non-ferroan alternation in Middle Jurassic ammonites of Skye.

The importance of studying these void fills is that they show that the later stages of cementation in which large voids were filled (not necessarily late burial), produced only ferroan manganoan calcite and not complex cement stratigraphies. The fact that cement compositions are not seen to change significantly, suggests that there was not a long history of cementation involving various burial formation waters.

5.7.2) Bioclast Diagenesis.

The faunal list of the Frodingham Ironstone Formation (table 2.1) suggests that bioclastic debris was initially present as aragonite (mainly bivalves, gastropods, and cephalopods), L.M.C. (mainly brachiopods and oysters), and H.M.C. (essentially echinoderms). The stable L.M.C. brachiopods and oysters (especially *Gryphaea*) remained intact during diagenesis, but the H.M.C transformed to L.M.C. (by direct Mg loss), and the

Table 5.3. Average Compositions of Calcite Cements Within Specimen AMM. 2, Obtained By E.P.M.A. The Data have been Recalculated to Calcite Formulae.

	GEN. 1						GEN. 2		GEN. 3						GEN. 4	
	INNER		MIDDLE		OUTER				INNER		MIDDLE		OUTER			
	AVERAGE	STDEV	AVERAGE	STDEV	AVERAGE	STDEV	AVERAGE	STDEV	AVERAGE	STDEV	AVERAGE	STDEV	AVERAGE	STDEV	AVERAGE	STDEV
Ca	38.150	0.807	38.224	0.411	37.234	1.114	38.566	1.232	37.241	1.056	37.477	2.182	37.333	1.186	39.324	0.927
P	0.012	0.021	0.000	0.000	0.023	0.021	0.008	0.017	0.006	0.011	0.000	0.000	0.009	0.016	0.004	0.007
Sr	0.048	0.002	0.060	0.009	0.039	0.002	0.045	0.020	0.066	0.014	0.071	0.020	0.074	0.024	0.052	0.018
Si	0.000	0.000	0.000	0.000	0.003	0.006	0.000	0.000	0.000	0.000	0.000	0.000	0.000	0.000	0.000	0.000
Al	0.000	0.000	0.000	0.000	0.000	0.000	0.000	0.001	0.000	0.000	0.000	0.000	0.000	0.000	0.000	0.000
Mg	0.143	0.020	0.130	0.025	0.092	0.011	0.085	0.015	0.214	0.011	0.187	0.024	0.163	0.004	0.143	0.061
Na	0.013	0.008	0.014	0.006	0.009	0.003	0.006	0.005	0.002	0.001	0.006	0.009	0.006	0.004	0.008	0.006
Fe	0.751	0.009	0.752	0.085	0.588	0.026	0.599	0.088	1.178	0.112	1.100	0.177	0.941	0.071	0.865	0.289
Mn	0.730	0.027	0.714	0.074	0.720	0.070	0.680	0.101	0.584	0.008	0.600	0.050	0.543	0.023	0.744	0.202
O	15.780	0.281	15.784	0.110	15.347	0.447	15.842	0.485	15.536	0.467	15.589	0.842	15.466	0.471	16.274	0.328
TOTAL	55.627	1.034	55.678	0.363	54.056	1.529	55.832	1.688	54.825	1.638	55.029	2.948	54.535	1.698	57.414	1.147
CarbCalc.																
Ca	0.966	0.002	0.967	0.004	0.971	0.001	0.972	0.002	0.957	0.002	0.960	0.006	0.964	0.001	0.965	0.006
Fe	0.014	0.000	0.014	0.002	0.011	0.000	0.011	0.002	0.022	0.002	0.020	0.004	0.017	0.001	0.015	0.005
Mn	0.014	0.001	0.013	0.001	0.014	0.002	0.013	0.002	0.011	0.000	0.011	0.001	0.010	0.001	0.013	0.004
Mg	0.006	0.001	0.005	0.001	0.004	0.000	0.004	0.001	0.009	0.000	0.008	0.001	0.007	0.000	0.006	0.003
Sr	0.001	0.000	0.001	0.000	0.000	0.000	0.001	0.000	0.001	0.000	0.001	0.000	0.001	0.000	0.001	0.000
Na	0.001	0.000	0.001	0.000	0.000	0.000	0.000	0.000	0.000	0.000	0.000	0.000	0.000	0.000	0.000	0.000
	n=3		n=3		n=3		n=9		n=3		n=3		n=3		n=9	

aragonitic bioclasts were subject to solution or neomorphic replacement by calcite (calcitisation). The resulting fabrics formed by these processes, as seen within the Frodingham Ironstone Formation, are discussed in this section.

5.7.2.1) Echinoid Diagenesis and the H.M.C.- L.M.C. Transition.

Echinoids are originally composed of H.M.C., with up to 43% $MgCO_3$ being reported in echinoid teeth (Schroeder *et al.* 1969). Usually however the value is much lower than this, with the exact value varying with water temperature (Chave 1954), and within different parts of the skeleton (Weber 1969). Harris and Pilkey (1966) have also shown a temperature dependence on the trace elements Sr, Na, Mn, and Fe content of recent echinoids. During the early stages of diagenesis, the Mg is lost as H.M.C. transforms to L.M.C. The mechanism of this transformation is thought to be by congruent dissolution (Land 1967, Bathurst 1975), with pairs of Mg^{2+} and CO_3^{2-} ions being lost synchronously to preserve charge balance, though Mg^{2+} diffusion to the surface with subsequent replacement by Ca^{2+} by incongruent dissolution may however also be possible. Congruent dissolution better explains re-equilibrium of the stable isotopic composition during freshwater diagenesis of H.M.C. by CO_3^{2-} loss, reported for some rocks (see discussion in Bathurst 1975, pp. 337-338). Richter and Fuchtbauer (1978) support the loss of $MgCO_3$ as the mechanism of the transition, and favour an 'epitactical' replacement, pseudomorphing the crystal lattice in the same orientation as the replaced phase (calcitisation). Experimental work on the H.M.C.- L.M.C. transition undertaken by Friedman (1964) and Land (1967) proved to be inconclusive.

In the Frodingham Ironstone Formation, all echinoderm fragments are seen to be replaced by low magnesian ferroan/manganoan calcite, or less commonly berthierine, goethite or phosphate. This 'replacement' requires some discussion because its nature is an important indicator of diagenetic conditions. The most important factor is to ascertain that the structural calcite itself has been replaced. The porosity of echinoderms may exceed 50% (Bathurst 1975) due to the fenestral structure with large pores (25μm in recent examples (Matthews 1966). These pores may fill with detrital fine-grained material, or possibly act as

a microenvironment for authigenic mineral precipitation. The pore morphology and size is often similar in appearance to the structural component of the grain, so that a fragment may appear replaced when it is in fact simply infilled.

Where the present mineralogy is ferroan calcite, staining reveals that the structure has clearly been replaced and that no non-ferroan calcite remains. The mechanism of Fe and (often considerable) Mn introduction into the structure is however unclear. It can be implied however, that the incorporation of Fe and Mn occurred during the loss of Mg from the H.M.C.-L.M.C. transition. Replacement could not post-date the change, as the resulting calcite would be stable and similar to the non-ferroan L.M.C. calcite shell material that remains unreplaced. Incorporation of Fe and Mn prior to the transition appears unlikely due to the lack of a suitable mechanism, and the improbability of there being free Fe^{2+} and Mn^{2+} in pore waters at such an early stage before the H.M.C.-L.M.C. transition is seen to occur. This being the case, it appears that the H.M.C.-L.M.C. transition occurred via a replacement process whereby Mg^{2+} ions are exchanged synchronously with Ca^{2+} and Fe^{2+}, with possible (probable?) exchange of CO_3^{2-} ions as described by Richter and Fuchtbauer (1978). Stable isotopic analysis of the fragments was however impossible due to the small size of the fragments, which would have otherwise resolved whether CO_3^{2-} ions were exchanged. Analyses obtained by E.P.M.A., show that a direct replacement of Fe^{2+} and Mn^{2+} for Mg^{2+} is not viable, as relatively little Fe^{2+} or Mn^{2+} is included relative to the presumed original Mg^{2+} content. Ca^{2+} must therefore be exchanged to complete the charge balance, whether by incongruent or congruent dissolution.

A second indicator of an early replacement of echinoderm debris is given by E.P.M.A. which often gives an Mn/Fe ratio >1 (table 5.4). Higher Mn^{2+} contents relative to Fe^{2+} are expected in earlier cement and replacement fabrics in the post-oxic diagenetic realm (section 1.10). In some cases, for example DRAG. 31.2, considerable change of pore fluid composition must have occurred between echinoid replacement and calcite cementation, as indicated by the differing Mn/Fe ratios of 1.3 and 0.25 respectively. E.P.M.A. also revealed the existence of a 'magnesium memory' (Tucker and Wright 1990), with up to 3 mol% $MgCO_3$ retained in the echinoid fragments relative to < 1 mol% $MgCO_3$ in the

Table 5.4. Average Compositions of Unreplaced Bioclasts and Echinoid Fragments, Obtained By E.P.M.A. The Data have been Recalculated to Calcite Formulae.

	DRAG. 31.2 Ech. Frags.		DRAG. 31.7 Ech. Frags.		DRAG. 31.22 Ech. Frags.		DRAG. 31.1 Unalt. Bio.		DRAG. 31.7 Unalt. Bio.	DRAG. 31.10 Unalt. Bio.	DRAG. 31.23 Unalt. Bio.
	AVERAGE	STDEV	AVERAGE	STDEV	AVERAGE	STDEV	AVERAGE	STDEV			
Ca	36.524	0.785	34.824	2.622	37.046	0.478	38.239	0.756	39.157	39.393	39.018
P	0.019	0.032	0.019	0.019	0.005	0.009	0.034	0.027	0.017	0.000	0.000
Sr	0.062	0.021	0.043	0.016	0.063	0.032	0.070	0.014	0.044	0.128	0.149
Si	0.226	0.128	0.544	0.665	0.021	0.006	0.023	0.008	0.000	0.013	0.002
Al	0.118	0.074	0.323	0.425	0.003	0.004	0.004	0.003	0.000	0.003	0.000
Mg	0.344	0.153	0.543	0.395	0.382	0.316	0.109	0.025	0.078	0.133	0.045
Na	0.027	0.021	0.017	0.029	0.040	0.046	0.224	0.023	0.108	0.277	0.213
Fe	0.975	0.238	1.968	1.124	0.608	0.193	0.009	0.012	0.036	0.014	0.021
Mn	1.282	0.206	1.139	0.551	1.131	0.327	0.003	0.004	0.012	0.118	0.109
O	15.867	0.362	16.100	0.683	15.602	0.118	15.504	0.230	15.765	15.989	15.748
TOTAL	55.444	1.073	55.520	0.971	54.902	0.726	54.216	0.875	55.217	56.068	55.305
CarbCalc.											
Ca	0.942	0.004	0.916	0.046	0.950	0.005	0.989	0.002	0.993	0.985	0.989
Fe	0.018	0.005	0.038	0.022	0.011	0.003	0.000	0.000	0.001	0.000	0.000
Mn	0.024	0.004	0.022	0.011	0.021	0.006	0.000	0.000	0.000	0.002	0.002
Mg	0.015	0.006	0.024	0.017	0.016	0.014	0.005	0.001	0.003	0.005	0.002
Sr	0.001	0.000	0.001	0.000	0.001	0.000	0.001	0.000	0.001	0.001	0.002
Na	0.001	0.001	0.001	0.001	0.002	0.002	0.010	0.001	0.005	0.012	0.009
	n=5		n=5		n=3		n=2		n=1	n=1	n=1

enclosing cements (DRAG. 31.22, and to a lesser extent DRAG.31.7). However, it is clear in the data obtained from DRAG. 31.2, that in some cases all magnesium is lost in the process.

Actual replacement by berthierine and/or goethite is uncommon, but pores are often filled by either mineral, the latter often seen as an oxidation product of the former. Berthierine replacement is well defined in DRAG. 31.20, where it results in a loss of texture in the fragment. Replacement appears to occur via infilling of pore space followed by calcite dissolution and precipitation of berthierine on the infilling material. The actual skeletal material diminishes, and a complete transition from berthierine filled, to berthierine replaced fragment can be seen. Though the replacement mechanism must be by congruent dissolution, the overall shape is preserved. This, and the fact that other bioclastic debris is replaced only by ferroan calcite, suggests that berthierine replacement is occurring due to the inherent instability of H.M.C., as only this debris is affected. Replacement by phosphate occurs in DRAG. 31.22 associated with a complex suite of cements (see section **5**.9.1.2). As with berthierine replacement, phophate is restricted to echinoid fragments only, and again results in a destruction of the structure.

5.7.2.2) Shell Calcitisation and Solution-Replacement (Plate 18).

Original aragonitic shell material is unstable in the diagenetic environment, and may either dissolve or undergo calcitisation. The former is by far the most common mechanism of replacement in the Frodingham Ironstone Formation, but detailed petrography is required to clearly ascertain that this is the case. The criteria used for identification of cement versus neomorphic textures have been discussed in detail by Bathurst (1975). These criteria must be treated with caution in this work however, since the existence of neomorphic-like fabrics in primary cements has been demonstrated. Where two clear generations of calcite are present, such as a scalenohedral cement followed by a coarse calcite, this is clearly a primary cement fabric (plate 18a). Mollusc calcitisation may result in smaller crystals concentrated at the margins of the shell wall, and care is needed to distinguish this from a first generation

PLATE 18

Bioclast Diagenesis and Cement Dissolution.

(Thin-Section Photomicrographs)

A) Replaced shell fragment, specimen DRAG. 31.31. This specimen has been cemented by an early generation of fibrous prismatic calcite, and a later sparry calcite. Despite this, the borings inside the shell have remained intact. Photo length is equivalent to 1.3mm.

B) Partially replaced shell fragment, specimen YAR. 7 (stained). Only half of the bioclast (of original aragonite or H.M.C.) has dissolved, and been replaced by ferroan calcite and berthierine. The original outline of the shell is arrowed. Photo length is equivalent to 0.7mm.

C) Partially neomorphosed, partially solution-replaced shell fragment, specimen DRAG. 31.31. Some of the original structure of the shell has been preserved (arrowed) by a thin-film replacement process in half of the shell. Photo length is equivalent to 1.3mm.

D) Solution fabrics of early scalenohedral carbonate cements, specimen DRAG. 31.10. The anhedral nature of these crystals and the presence of concave surfaces on some examples suggests partial solution of the cement has occurred. Photo length is equivalent to 0.7mm.

A	B
C	D

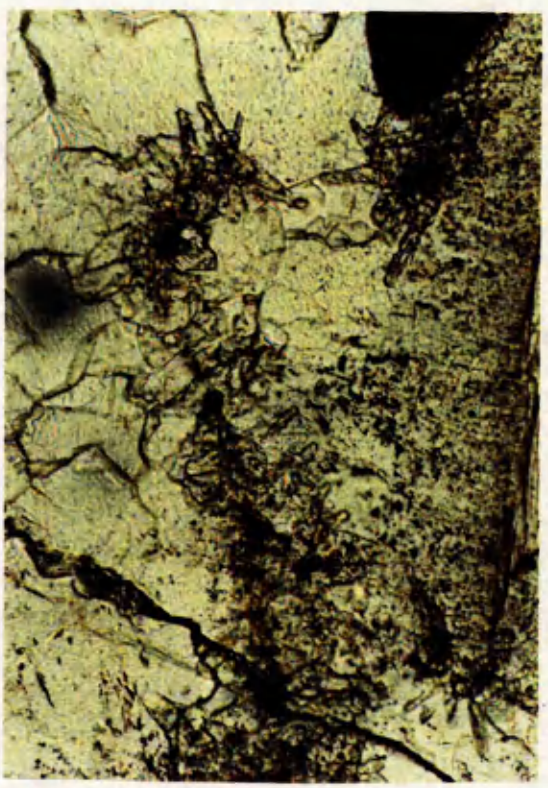

cement, or initial cement crystals terminated by competitive growth of their neighbours. This is further complicated where boring, and micrite envelope development has been active.

The only clear method of ascertaining bioclast calcitisation is where a relict structure has been preserved (plate 18c). This is uncommon in the ironstones, and is usually associated with a degree of ferruginisation of the bioclast prior to replacement, so that the relic structure is preserved in goethite. Even in these cases, the crystal fabric may show cement-like textures, in the formation of prismatic crystals along the wall edge (DRAG. 31.31).

Boring by fungi/algae is common in bioclasts (section **3**.3.2.1), and is found in both unreplaced non-ferroan calcite shells of brachiopods and oysters, and in replaced bioclasts of ferroan calcite. Usually, in the latter such structures would suggest that calcitisation had occurred as opposed to wholesale solution-precipitation. However, the borings are lined with goethite (section **3**.3.2.1) and such borings can be studied by dissolving the calcite (for example see Bathurst 1975 p. 383 figure 283, Dahanayake and Krumbein 1986). Micrite-filled borings are seen to survive dissolution of the bioclast (Bathurst 1975 p. 328 figure 252d) and there is therefore the possibility that such structures may remain largely intact, even if complete bioclast solution were to take place (plate 18a).

Goethite lined borings may not represent suitable nuclei to later calcite precipitation, as evidenced by the large size of crystals developed around goethitic ooids, due to the absence of nucleation sites. Development of a ferruginous envelope on a bioclast may produce an outer layer free of suitable carbonate nuclei, such that the cement would also precipitate as equant sparite. It is however worth remembering that borings can be preferential sites for precipitation of authigenic minerals. Alexandersson (1972) documents aragonite needles and rhombohedral H.M.C. growing in modern borings. Borings may hence influence bioclast diagenetic fabrics but are not themselves suitable indicators of bioclast neomorphism.

A curious feature of a few bioclasts, is the presence of an outer layer of clear ferroan calcite, despite the inside of the bioclast being highly bored (plate 11a). The inner edge of

this rim is marked simply by the termination of borings; there is no apparent crystal boundary surface, micrite or mucilage layer. In some of these examples a dense micritic patch is present in the layer, suggesting that the outer portion of the bioclast with the densest boring and micrite envelope development, was replaced. The continuation of the rim around the bioclast discounts the possibility of a mineralogical difference such as an aragonitic layer. The mechanism for this replacement remains uncertain.

5.7.2.3) Bioclast Coatings and Their Role in Timing Dissolution and Precipitation.

The presence of a thin outer coating on bioclasts, that may preserve the outline of a replaced bioclast, has already been briefly mentioned, and is distinguished from a micrite envelope by the lack of penetration into the shell. Such envelopes are best preserved where replacement of the bioclast has occurred, but are found to be no different to those of unreplaced bioclasts. This coating is important in that it not only preserves structure, but acts as the nucleation surface for subsequent cementation. Petrographic examination of these layers reveals little of their origin, and ultra-violet fluorescence microscopy fails to ascertain a clear organic signature. Such layers are however presumed to be films of organic matter produced from colonies of microorganisms (including algae and bacteria), living on the surfaces of these particles, as are present in carbonate sediments of the present. Suess (1973) suggests enough organic matter is dissolved in marine surface waters to produce a layer on every available carbonate surface by direct sorption processes.

The role of this layer in carbonate diagenesis as an inhibitor or promotor of carbonate cementation has not been conclusively determined (Suess 1973, Bathurst 1975, Mitterer and Cunningham 1985). Talbot (1971) however shows that in the Corallian of southern England, such layers were clearly sites for crystal nucleation of calcite, though he suggests that the layers are composed of finely divided material adhering to the sticky surface. Presuming this material was carbonate mud, this would act as nucleation sites when incorporated onto the layer.

Within the Frodingham ironstones, similar mucilage layers to those described by Talbot (1971) are also present (see plates 11a, 16 a,c, 18). Micritic calcite is not present within the ironstone-formation, so it is assumed that the layer itself forms the nucleation medium. Layers of mucilage (+ detrital material?) remained intact during the solution-replacement of the aragonitic shell, and acted as a site for precipitation of ferroan calcite on both the inner and outer surfaces of the film (plate 16 a,c). In some cases, both cement morphologies are scalenohedral calcite, suggesting in such cases that solution must have occurred early, prior to the onset of significant external cementation, in order to form similar cement fabrics both externally and internally. From this, it is apparent that the layer possessed a certain rigidity or cohesiveness at this stage, enough at least to support some compaction stresses. Early formation of calcite on the film would add extra support to the structure, before the bioclast was fully cemented, and presumably also prior to the development of the scalenohedral habit. It is clear from modern carbonate samples studied, that very little cement is in fact required to lithify a sediment, and such cements may therefore need only to be a matter of a few microns thick. Broken films with the thin scalenohedral calcites, cemented by pore-filling ferroan calcite, attest to a small amount of compaction prior to the last stage cementation. Uncemented relic films are rare.

In many cases, only the inner layer of scalenohedral calcite is well developed, with a poorly developed, non-uniform sparitic calcite cement present on the outer surface. In this case, it appears that external cementation occurred prior to bioclast dissolution, though cementation may not have been complete, allowing the influx of pore waters into the void and the precipitation of the scalenohedral calcite. This is clearly demonstrated where the first generations of calcite are inclusion-rich; the pore-filling calcites of replaced bioclasts are clear sparites; and clear sparitic cements are also present cementing the rock (usually around ooids). Recognition of cement generations exterior to the bioclast is however often difficult, as it is not easy to differentiate between a distinct cement generation, and a texture produced in response to nucleation site availability, i.e. the initial stages of a competitive growth fabric. This is due to the impingement of other grains, that reduce pore space and add

further complications due to growth interference between differing cement textures. In these cases, the rigidity of the mucilage envelope itself is not proven.

Complete external cementation of a bioclast prior to dissolution may be possible, with ion transfer along crystal boundaries, permitting cementation of the void. The precise mechanisms and magnitude of such transfer are as yet poorly understood, but suggest that such fabrics could develop without necessitating pore fluid access via a sizable pore throat. Compositionally however, external and internal cements do not vary sufficiently to ascribe to two very different phases of cementation (such as early and late burial), and this is supported by isotopic analysis (5.12.2.2). In all probability, for most of the Frodingham bioclastic material, solution and cementation were nearly synchronous.

It is evident from sectioned hand specimens of originally aragonitic bivalves from Yarborough Pit, that cementation did not always directly accompany aragonite dissolution. The presence of irregular shell thickening and thinning, suggests that collapse or compression of the shell biofilm occurred after dissolution, prior to cementation (plate 17c). In some cases cementation did not occur at all, as in specimens of *Pholadomya* that are found only as moulds with the external ornamentation impressed onto the inner cast, due to compaction/compression following aragonite solution. Ammonites are also found similarly preserved, especially towards the top of the sequence above the "Snap Band". Such features suggest that in these cases a stronger pH control may have been operating, so that reprecipitation did not take place, as opposed to the mechanism of unstable aragonite reverting to calcite via dissolution-precipitation in the above cases.

5.7.3) Cement Dissolution Textures.

The irregular crystal outline of the coarse sparry calcites has already been noted above, but this texture can form either by precipitation or recrystallisation. Early formed scalenohedral calcites are usually euhedral with planar crystal faces, but in cases the overall habit is similar, but the surface form is irregular (plate 18d). Small concave surfaces with rounded outlines on these crystals are unlikely to be produced by crystal growth, and are

suggested to result from partial solution of the calcite. Some early fibrous cements also have an irregular outer surface that may be ascribed to possible partial solution. The effect is obviously most visible where a distinct crystal shape has been modified, so the extent of the solution on other calcite cement types is unclear. These solution textures are not necessarily apparent across a whole thin-section, and apparently similar cement fabrics may be variably dissolved or left unaffected. This therefore suggests that solution was a very localised mechanism, and did not result from a marked pore water change.

Solution of carbonates will occur when a pH change of the pore fluid destabilises the previously precipitated cement. This change is almost certainly minor or short-lived in the Frodingham ironstones, since extensive solution is uncommon. The most likely cause of solution in this diagenetic environment is by organic matter oxidation or sulphate-reduction, becoming slightly more pronounced relative to iron-reduction (section 1.10). Both processes acidify pore waters, which may lead to carbonate dissolution. Oxidation of previously formed pyrite would also lead to dissolution via the generation of sulphuric acid:

$$2\ FeS_{2(s)} + 4\ H_2O_{(l)} + 7.5\ O_{2(g)} = Fe_2O_{3(s)} + 8\ H^+_{(aq)} + 4\ SO_4^{2-}{}_{(aq)} \qquad \text{(Curtis 1977)}$$

Some pyrite may form in post-oxic diagenetic regimes and would be expected to be localised. Tiny early framboids of pyrite could be easily oxidised, and would not be preserved, so this mechanism cannot be ruled out.

It is possible that these solution textures could be used as an indicator of primary cement mineralogy, since unaltered bioclastic material (L.M.C.) is apparently unaffected, but Walter (1985) has shown that the commonly accepted sequence of diagenetic alteration (H.M.C. > aragonite > L.M.C.), is only strictly the case at solution saturations above that of aragonite. Below this level microstructural control, based on the effective surface area, becomes important, and aragonite may preferentially dissolve.

5.7.4) Comparison With Ferroan Calcite Fabrics in Jurassic Limestones.

The fabrics described for the ferroan calcite cements above, were compared with those found in the Inferior Oolite of Gloucestershire and the Purbeck Marble of Dorset, to ascertain any differences between ironstone and limestone cementation by ferroan calcite. The limestones contain carbonate ooids, echinoderm debris, intraclasts, some micrite, and both unreplaced and ferroan calcite replaced bioclasts. The rocks are cemented by both ferroan and non-ferroan calcite.

The majority of the cement in the limestones is sparry ferroan calcite showing a competitive growth fabric with increasing crystal size into the pore. Crystal shape is often irregular, and crystal boundaries non-planar, similar to that described for the Frodingham Ironstone Formation. Acicular cements and scalenohedral calcites were absent in the sections studied, but a prismatic first generation is present in some thin-sections as crystals 8-15μm wide and up to 70μm long. This forms on carbonate ooids and bioclasts whose structure remains intact. Unlike the Frodingham Ironstone Formation, some cements contain phases of non-ferroan, or depleted-ferroan calcite precipitation, that is revealed by staining. This occurs both as distinct cement generations, and during crystal growth. Syntaxial overgrowths of ferroan-calcite on echinoderm fragments are present, occurring on both ferroan-calcite replaced, and unreplaced debris.

Bioclast replacement in the Purbeck Marble has resulted in the preservation of some structure within and between sparry ferroan calcite crystals, attesting to a neomorphic calcitisation replacement process. Much of the replacement in the Inferior Oolite is by solution-precipitation, producing a single generation of ferroan calcite possessing a competitive growth cement fabric within the bioclast. Most importantly however, the radiaxial calcite described replacing bioclasts in the Frodingham Ironstone Formation is also seen here, showing that the fabric is not restricted to this ironstone.

Overall, the sparry calcite cement fabrics described for the Frodingham Ironstone are similar to those of the ferroan limestones, and a similar origin for the cement might be

implied. More specific variations in crystal morphology in earlier generations of calcite between them, may be due to nucleation effects, in particular a higher abundance of carbonate particles (including ooids) and calcite mud in some samples. The significance of the scalenohedral calcite in the ironstones may be similarly related. Bioclast diagenesis results in similar textures, and the radiaxial calcite is shown to be present in both ironstone and limestone.

It is therefore apparent that though some specific textures of ferroan calcite cements in the ironstone are not directly comparable with the limestones, the overall difference between them is not significantly large to imply that the ironstone calcites have a uniquely different origin. It is also suggested that a detrital iron-rich mineralogy is not essential for the widespread formation of ferroan calcite cements, and the ideas proposed here may be applied to ferroan calcite cements in other rock types.

5.8) Siderite Cements and Replacement Textures.

5.8.1) Cement Fabrics.

Siderite forms only a few percent of the carbonate content of the ironstone-formation as a whole, but may be locally abundant, and is particularly associated with berthierine-rich beds. Unlike ferroan calcite, siderite is rarely a pore-filling phase, and is therefore usually present as a thin pore-lining cement fringe of variable morphology. It is commonly the first formed carbonate cement, but often post-dates authigenic berthierine formation where present. Siderite cement morphologies are more variable than that of ferroan calcite, and are commonly associated with complex generations of calcite and siderite. Two common forms, rhombohedral and crystalline sparite are described here, with an unusual, previously undescribed texture termed 'arboraceous' siderite. Other morphologies specific to individual samples are described in the complex cements section below. Fewer compositions of the siderites were obtained by E.P.M.A. than for the calcites, due to the lesser abundance of the former. They have hence been discussed together below in section 5.12.4.

5.8.1.1) Rhombohedral Siderite.

Rhombohedral siderite is a common cement fabric in the ironstone-formation, and forms the basic crystal shape to more complex cement morphologies (plate 19 a,c). It is particularly abundant in the "Snap Band" of Yarborough Pit (YAR. 30, YAR. 22). Crystals 10-150μm long with curved faces, nucleate on the pore edge and grow with good crystal shape as individual rhombohedrons. The orientation of a crystal relative to the substrate is however variable, and ranges from long axis parallel, to long axis perpendicular. These different orientations lead to cement textures variable between dog-tooth crystals and a rounded almost botryoidal fabric. It is difficult to ascertain the precise crystal shape in the latter, but the fabric difference may possibly relate to the orientation of the c-axis relative to the crystal formed, i.e. parallel, or perpendicular to, the crystal long axis.

5.8.1.2) Coarse Sparitic Siderite.

This cement type forms where the siderite crystal morphology is less well defined and crystal interference occurs, usually as a small pore is filled (plate 19b). Cementation probably initiated as the rhombic siderite described above. Siderite formation is never extensive enough for fully competitive growth fabrics to develop, so crystals remain small in size (< 100μm) and largely equant. Crystal boundaries are non-planar, as expected from growth interference between crystals withcurved faces. This fabric does however show a gradual increase in crystal size away from the pore edge, indicative of a cement fabric. This cement has been seen enclosing undeformed berthierine ooids attesting to its early formation.

5.8.1.3) 'Arboraceous' Siderite (Plate 19 c,d).

This fabric is seen in samples from the "Snap Band" at Yarborough Pit (for example YAR. 22, and to a lesser degree YAR. 30). The fabric appears to be a variation on the botryoidal type of texture described above. Crystals of rhombic siderite are apparently stacked upon each other with the long axis parallel to the substrate (and hence c-axis perpendicular to it), with crystal size apparently increasing into the pore. The crystals appear to overlap, and form a structure with the appearance of a child's drawing of a Christmas tree, hence the fabric is termed 'arboraceous'. The outer part of the structure is a continuous

PLATE 19

Siderite Textures in Thin-Section

A) Rhombic crystals of siderite grown syntaxially on a shell fragment, specimen DRAG. 31.36A (crossed polars). A small amount of oxidation is present, producing a brown tarnish (goethite) on the crystals. Photo length is equivalent to 1.3mm.

B) Siderite replacing berthierine mud, specimen YAR. 14. The siderite forms single rhombic crystals with curved crystal faces. Photo length is equivalent to 0.7mm.

C) Bioclastic grain-ironstone cemented by calcite and "arboraceous" siderite, specimen YAR. 22 (stained). Rhombic siderite is also present in the photo (arrowed). Photo length is equivalent to 3.3mm.

D) Detail of the "arboraceous" siderite, specimen YAR. 22 (stained). The cement stratigraphy has developed upon an unreplaced shell fragment (1), a large intraclast (2), and a replaced bioclast (3). Note the rhombohedral terminations of former cement crystals, presently outlined by inclusions within the siderite (arrowed). Photo length is equivalent to 0.7mm.

A	B
C	D

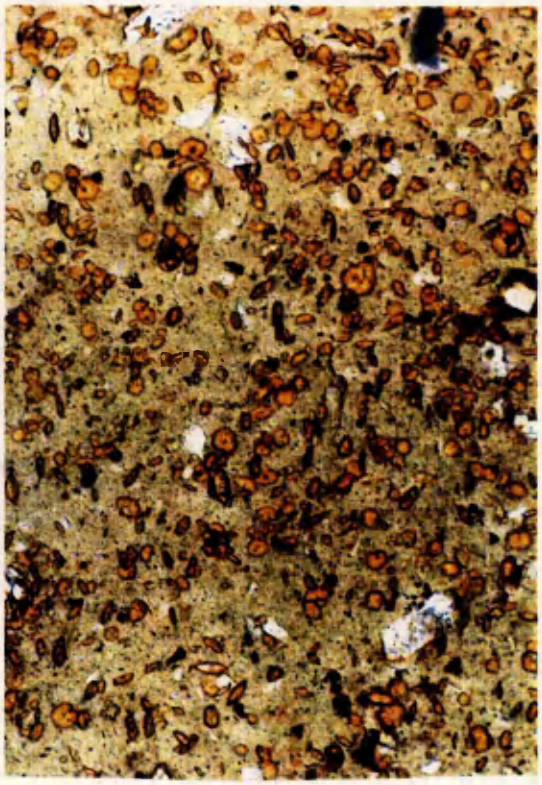

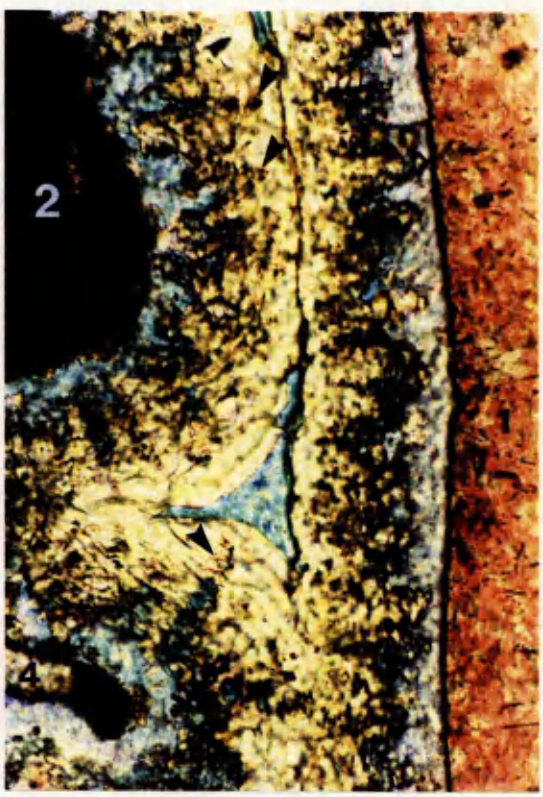
2
1
4

sheet of siderite, with the external edge identical to the fabric of the botryoidal type. The whole fabric is only 200μm thick, and is separated from the substrate by a coarsely crystalline ferroan calcite. External to the siderite fabric is a similar coarse pore-filling ferroan calcite with crystal size up to 1.2mm. Compositions of these carbonates are given in table 5.5.

The origin of this fabric remained problematical for most of the research period, but a re-examination together with other observed textures, tentatively suggests the following possible origin through six stages (see figure 5.3).

1) Initially a prismatic to scalenohedral cement fringe is precipitated on the wall of the pore (here shown as a bioclast).
2) A layer of microcrystalline cement may then form, or a very thin layer of material may be deposited from suspension, that may outline the crystal shape. Usually however this is absent, and crystal form remains largely unpreserved.
3) Siderite is precipitated in a layer on the prismatic cement, smoothing the surface topography to a slightly undulating upper face.
4) Dissolution of the prismatic cement occurred, but one or two points of contact supported the majority of the siderite layer away from the substrate.
5) Further siderite was precipitated on the inner surface, as small rhombic crystals that are complete where nucleated at, or near to, the original prismatic calcite growth interference boundaries.
6) The pore and inner void space are filled by coarse sparry ferroan calcite.

The original mineralogy of the prismatic cement is problematical. The morphology is suggestive of H.M.C. as opposed to aragonite, but echinoid debris remains intact and has not undergone dissolution. The L.M.C. bioclast is also unaffected. Since rhombohedral siderite crystals are seen cementing dissolved aragonitic bioclasts, the inference is that siderite precipitation post-dated aragonitic dissolution, or that these rhombic siderites formed

Table 5.5. Average Compositions of the Carbonates Within Specimen YAR.22, Obtained By E.P.M.A. The Data have been Recalculated to Carbonates of the Calcite Group.

	UNALT. BIO.		GEN. 1 Calcite		GEN. 2 Siderite		GEN. 3 Calcite (inner)		Calcite (outer)		Cementing Ooids Siderite	
	AVERAGE	STDEV	AVERAGE	STDEV	AVERAGE	STDEV	AVERAGE	STDEV	AVERAGE	STDEV	AVERAGE	STDEV
Ca	39.453	0.263	37.879	0.536	3.903	0.260	38.259	0.356	36.446	0.416	3.741	0.417
P	0.011	0.011	0.011	0.017	0.006	0.014	0.007	0.014	0.006	0.013	0.010	0.016
Sr	0.062	0.009	0.038	0.017	0.007	0.009	0.027	0.011	0.047	0.011	0.019	0.008
Si	0.000	0.000	0.000	0.000	0.158	0.446	0.003	0.002	0.002	0.004	0.006	0.008
Al	0.002	0.002	0.003	0.002	0.002	0.002	0.000	0.000	0.001	0.002	0.003	0.004
Mg	0.078	0.006	0.198	0.023	4.166	0.363	0.147	0.057	0.240	0.010	4.228	0.256
Na	0.174	0.033	0.013	0.026	0.079	0.073	0.005	0.005	0.002	0.003	0.010	0.012
Fe	0.019	0.015	1.097	0.082	32.637	0.671	1.201	0.365	1.812	0.080	32.815	0.435
Mn	0.005	0.007	0.618	0.036	2.038	0.588	0.722	0.077	0.755	0.018	2.240	0.430
O	15.895	0.099	15.774	0.234	14.462	0.520	15.944	0.303	15.467	0.160	14.360	0.171
TOTAL	55.698	0.321	55.630	0.826	53.554	1.185	56.315	1.120	54.779	0.520	53.692	0.699
CarbCalc.												
Ca	0.992	0.001	0.960	0.002	0.109	0.008	0.959	0.009	0.941	0.002	0.104	0.011
Fe	0.000	0.000	0.020	0.001	0.655	0.018	0.022	0.006	0.034	0.002	0.656	0.015
Mn	0.000	0.000	0.011	0.001	0.042	0.012	0.013	0.001	0.014	0.000	0.045	0.008
Mg	0.003	0.000	0.008	0.001	0.192	0.015	0.006	0.002	0.010	0.000	0.194	0.010
Sr	0.001	0.000	0.000	0.000	0.000	0.000	0.000	0.000	0.001	0.000	0.000	0.000
Na	0.008	0.001	0.001	0.001	0.004	0.004	0.000	0.000	0.000	0.000	0.000	0.001
	n=3		n=10		n=10		n=5		n=5		n=7	

FIGURE 5.3.
POSSIBLE STAGES IN THE DEVELOPMENT OF ARBORACEOUS SIDERITE.

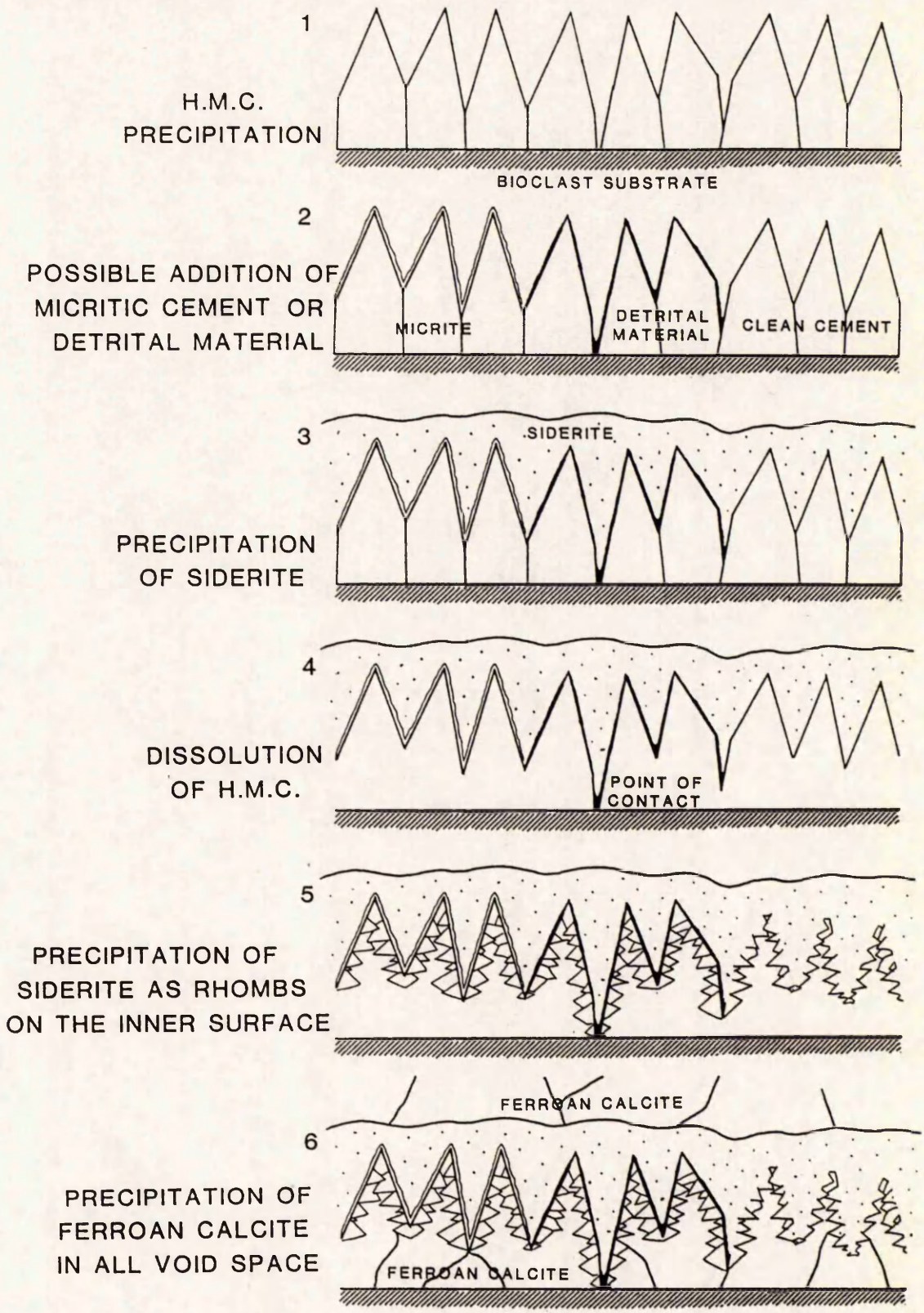

at the same time as the second generation of siderite precipitation in the model. The volumes of cement produced are however dissimilar.

5.8.2) Replacement Fabrics.

Siderite is not seen extensively replacing calcitic and aragonitic particles and cements, to the extent that ferroan calcite is seen to do. Bioclasts are replaced only by complete aragonite dissolution, and precipitation of siderite (rhombic) in the void, but siderite is seen replacing (pseudomorphing) original calcite cements (see DRAG. 31.36a below, plate 21c). This is however uncommon. Siderite widely replaces all morphologies of berthierine, and some goethitic ooids. It is these fabrics that are discussed in detail within this section.

5.8.2.1) Replacement of Berthierine.

Small euhedral rhombic crystals of siderite (usually < 30μm) with slightly curved faces, form as a replacement of berthierine mud (plate 19b). Crystal sizes in this morphology > 50μm are uncommon, with replacement occurring via new crystal nucleation as opposed to continued growth of existing crystals. Crystal orientation is random, but in some cases (DRAG. 31.21 and 37, YAR. 27), crystals are connected in groups aligned parallel to bedding. Some crystals show a darker core, but the occurrence of this texture is too sporadic to imply a preferred nucleation on certain debris. Nucleation does however occur preferentially on detrital carbonate. In YAR.9, small rhombs of siderite nucleate epitaxially to the shell structure and grow into the mud, replacing it, along with crystals within the mud itself.

Petrographically, the occurrence of such siderite cannot be readily predicted, as some berthierine mudstones are free of replacement. Abundance is variable, even within a single thin-section, and the rhombs are associated with and without ooids, bioclasts, quartz and muscovite. However, siderite is largely absent from the muds at the base of the ironstone-formation (DRAG. 31.1-7), and this type of siderite does not tend to replace thin laminae of deformed berthierine ooids (YAR. 30, Y183. 8 &9). Small *Chondrites* burrows in YAR.31

from a thick (4cm) mud drape are unreplaced, whereas the whole mudstone is almost totally sideritised.

A coarser fabric of anhedral, to occasionally euhedral shaped crystals around 100μm in length, or small accumulations of such crystals, is more typical of siderite replacement of berthierine ooids and mixed lamellae of ooids and mud. Replacement by this coarser siderite morphology may also be extensive but is much less common, and individual crystal size enlargement is more pronounced than the euhedral fabric described above.

Authigenic berthierine cements may also be replaced by siderite, though commonly siderite precipitates as a separate cement phase without berthierine replacement. In DRAG 31.28 however, the first pore-lining generation of authigenic berthierine is partially replaced by siderite, whose morphology reflects that of the radial nature of the original cement, by forming as small elongate crystals (plate 13d).

5.8.2.2) Ooid Replacement.

Berthierine and goethite/berthierine ooids are replaced in two forms; by preferential edge replacement that occurred prior to significant compaction and was associated with siderite cementation; and by anhedral crystals in a random position within the ooid. Edge replacement of berthierine ooids occurs within the "Snap Band" (for example YAR 30) where a thin rim of siderite crystals around 30μm thick is present at the ooid edge. Crystal form is poor to rhombic, with the long axis perpendicular to the ooid laminae. Replacement does not always distort the internal fabric of the ooid, and often ooids that possess a distorted fabric are themselves deformed, as seen by an irregular outer shape. In such cases, it is assumed that the siderite edge replacement occurred prior to compaction, and that later the ooid was plastically deformed, with the incompetent siderite crystals being forced in to the more plastic ooid, distorting the ooid laminae.

5.9) Complex Carbonate Cement Stratigraphies.

This section deals with cements that possess a complex morphology or suite of cement generations, that cannot easily be discussed in isolation relative to simply ferroan calcite or siderite cementation. Though unusual and not extensively formed, these cements hold many clues to the diagenetic history of the ironstone-formation, replacement processes, and morphological development of early diagenetic carbonates.

5.9.1) DRAG. 31.22: A Multi-Cemented Coquina (Plate 20).

DRAG. 31.22 is a coquina of horizontally aligned shell debris usually < 1cm long, echinoderm fragments and occasional ooids, within a goethite/berthierine ooidal grainstone. The coquina is only 2cm thick but possesses a complicated and completely different cement fabric to that of the enclosing grain-ironstone, and allows examination of porosity controls on cementation, and processes acting within such lag deposits. This sample was also shown to contain the only ankerite found during this study. At least seven cement generations are clearly visible in one part of the slide (plate 20c), but the variability of such cements is such that in the other part of the thin-section, the first five generations are present as only two fabrics. The seven generations are described below, with approximate thicknesses in parentheses.

Generation 1). (30μm). A fibrous (acicular) inclusion-rich calcite, largely recrystallised, similar to the fabrics described in section 5.7.1.2. It forms on bioclasts as an epitaxial cement, but is represented by an inclusion-rich overgrowth on echinoderm debris. Elsewhere, it may only be present as an irregular mosaic of small crystals.

Generation 2). (50μm). A clear sparry calcite with occasional rhombohedral terminations to the crystals, though usually with an irregular outer boundary. Crystals of this generation replace those of generation (1).

Generation 3). (70μm). Three mineral phases precipitated within this generation.

3a) Microcrystalline ankerite, dark grey in thin-section.

PLATE 20

Photomicrographs of Specimen DRAG. 31.22

A), B) Complex cement stratigraphy developed upon an unreplaced shell fragment (SF). The cement generations are numbered as described in the text. (**A**) is taken under incident U.V. light, and shows the highly fluorescent nature of generation 3. The fibrous calcite of generation 6 shows signs of dissolution in **B** (arrowed). Photo length of (**A**) is equivalent to 0.65mm, photo length of (**B**) is equivalent to 1.3mm

C) Cement stratigraphy developed within a pore bounded by two echinoderm plates (EP), and a replaced shell fragment (SF). The cement generations are numbered as described in the text. Photo length is equivalent to 1.3mm.

D) Upper boundary of the coquina with the enclosing grain-ironstone. Note the high proportion of phosphatised echinoderm fragments in the coquina. Photo length is equivalent to 6.7mm.

A	**B**
C	**D**


SF

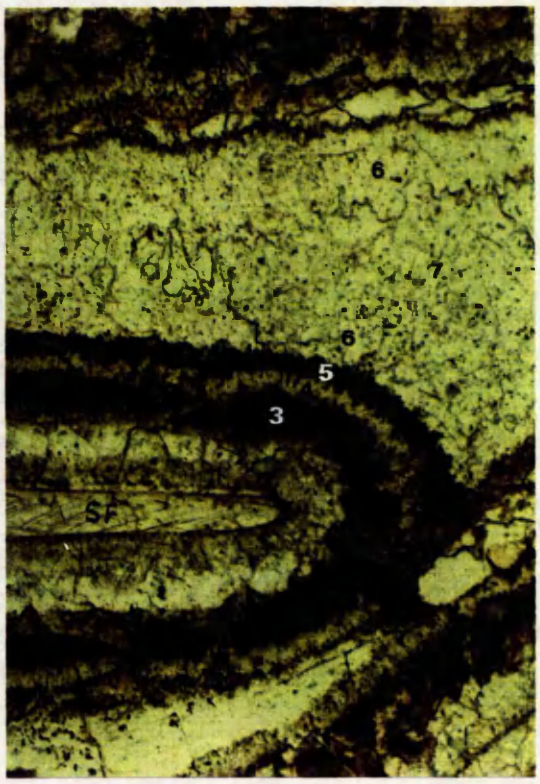
6
7
6
5
3
SF


EP
3b
3a
2
2
SF
6
EP

3b) Euhedral crystals of siderite up to 100μm aligned <45° from the bounding surface. Crystal edges have oxidised to goethite. The siderite apparently replaces the ankerite of generation 3a

3c) Small crystals of authigenic phosphate of elongated rhombohedral outline <60μm long, possesing low birefringence. Orientation is random.

Generation 4). (40μm). A thin layer of ankerite, structurally indistinct, but shown in places to be formed of stacked crystals of equal size, intergrown with long axes parallel, similar in morphology to the 'arboraceous' siderite (section **5**.8.1.3). A similar origin cannot however be invoked here due to the interlocking of the stacks.

Generation 5). (20-60μm). Two mineralogies were evident in this generation.

5a) A layer of crystalline siderite of variable thickness, similar to generation (3b), but more extensively developed with interlocking crystals and much less pronounced oxidation.

5b) Coarsely crystalline sparry calcite cement, less common than the siderite.

Generation 6). (70μm). A prismatic to scalenohedral calcite cement now largely replaced by the calcite of generation (7). The cement fabric is indicated by inclusion trails outlining the crystals.

Generation 7). (Pore-filling). A coarse sparitic pore-filling calcite with crystal size reaching nearly 1mm at the pore centre.

5.9.1.1) Chemical Compositions (E.P.M.A.).(Table 5.6).

Generations 1 and 2: The compositions of these calcites are similar, and are hence described together. All the calcites are manganoan and ferroan with an Mn/Fe ratio of ≈2 suggesting an early diagenetic origin. The magnesium content is not high (≈ 1 mol% $MgCO_3$), and neither Mg nor Sr is elevated to delineate the former mineralogy of generation (1). The replaced shell fragment that acted as the substrate to precipitation is also of this mineralogy.

Generation 3: The presence of ankerite was distinguished by E.P.M.A. only, but totals were low. Examination under U. V. light showed strong fluorescence in this generation (plate 20a), therefore suggesting a possible high organic content. The

Table 5.6. Average Compositions of Carbonate and Phosphatic Cements Within Specimen DRAG. 31.22, Obtained By E.P.M.A. The Carbonate Data have been Recalculated to Carbonates of the Calcite Group.

	REP. BIO.		GEN. 1		GEN. 2		GEN. 3a		GEN. 3b		GEN. 3c		GEN. 4	
	Calcite		Calcite		Calcite		Ankerite		Siderite		Phosphate		Ankerite	
	AVERAGE	STDEV	AVERAGE	STDEV	AVERAGE	STDEV	AVERAGE	STDEV	AVERAGE	STDEV	AVERAGE	STDEV	AVERAGE	STDEV
Ca	36.527	0.260	36.312	0.610	36.664	0.553	10.656	1.916	5.375	0.991	34.228	1.719	21.492	0.871
P	0.017	0.019	0.010	0.013	0.171	0.413	0.018	0.032	0.005	0.008	12.421	1.154	0.403	0.974
Sr	0.064	0.014	0.059	0.016	0.062	0.023	0.012	0.020	0.014	0.011	0.231	0.022	0.052	0.018
Si	0.002	0.002	0.009	0.006	0.006	0.008	0.058	0.028	0.007	0.004	0.004	0.001	0.007	0.004
Al	0.003	0.006	0.001	0.002	0.004	0.004	0.008	0.008	0.000	0.001	0.005	0.004	0.002	0.004
Mg	0.232	0.059	0.216	0.056	0.163	0.061	2.186	0.354	3.196	0.104	0.912	0.291	4.380	0.319
Na	0.001	0.001	0.012	0.007	0.009	0.018	0.070	0.017	0.008	0.007	0.531	0.068	0.051	0.072
Fe	0.829	0.228	0.771	0.047	0.918	0.122	5.151	0.922	30.676	0.872	2.955	0.801	10.331	0.526
Mn	1.670	0.187	1.435	0.258	1.481	0.209	1.265	0.214	3.415	0.380	0.761	0.151	2.772	0.200
O	15.496	0.198	15.315	0.281	15.682	0.488	7.659	1.310	14.052	0.164	31.611	1.680	15.787	1.270
TOTAL	54.840	0.734	54.140	1.000	55.157	0.807	27.083	4.708	56.749	0.291	83.659	3.328	55.276	2.468
CarbCalc.														
Ca	0.943	0.009	0.948	0.006	0.947	0.007	0.561	0.003	0.152	0.026			0.552	0.005
Fe	0.015	0.004	0.014	0.001	0.017	0.002	0.195	0.001	0.626	0.025			0.199	0.003
Mn	0.031	0.003	0.027	0.005	0.028	0.004	0.049	0.001	0.071	0.008			0.054	0.002
Mg	0.010	0.002	0.009	0.002	0.007	0.003	0.191	0.003	0.150	0.003			0.193	0.003
Sr	0.001	0.000	0.001	0.000	0.001	0.000	0.000	0.000	0.000	0.000			0.001	0.000
Na	0.000	0.000	0.001	0.000	0.000	0.001	0.007	0.002	0.000	0.000			0.003	0.004
	n=3		n=6		n=6		n=3		n=3		n=3		n=6	

Table 5.6. (Continued).

	GEN. 5a		GEN. 5b		GEN. 6		GEN. 7		Grainstone Below Coquina				Grainstone Above Coquina			
	Siderite		Calcite		Calcite		Calcite		Ech. Ovgrth.		Pore-fill Cement		Ech. Ovgrth.		Pore-fill Cement	
	AVERAGE	STDEV	AVERAGE	STDEV	AVERAGE	STDEV	AVERAGE	STDEV	AVERAGE	STDEV	AVERAGE	STDEV	AVERAGE	STDEV	AVERAGE	STDEV
Ca	5.608	1.745	35.904	3.024	36.172	1.243	36.663	0.707	35.890	1.047	36.090	0.921	36.507	0.833	37.074	0.802
P	0.005	0.009	0.005	0.007	0.047	0.029	0.007	0.010	0.002	0.003	0.027	0.025	0.004	0.008	0.007	0.010
Sr	0.024	0.006	0.045	0.021	0.050	0.025	0.039	0.014	0.045	0.015	0.033	0.008	0.034	0.006	0.046	0.009
Si	0.003	0.004	0.008	0.001	0.000	0.000	0.008	0.003	0.019	0.011	0.007	0.008	0.015	0.005	0.014	0.008
Al	0.001	0.002	0.001	0.001	0.007	0.003	0.004	0.003	0.003	0.004	0.001	0.002	0.001	0.003	0.003	0.002
Mg	3.241	0.166	0.124	0.008	0.246	0.105	0.173	0.039	0.208	0.137	0.145	0.044	0.127	0.047	0.181	0.107
Na	0.015	0.005	0.018	0.005	0.000	0.000	0.001	0.002	0.017	0.013	0.001	0.003	0.009	0.006	0.019	0.011
Fe	30.554	2.640	0.886	0.108	0.889	0.030	0.877	0.092	0.978	0.131	0.909	0.085	0.879	0.170	0.789	0.053
Mn	3.365	0.230	1.122	0.455	1.262	0.136	1.470	0.135	1.300	0.311	1.226	0.283	1.379	0.309	1.646	0.408
O	14.127	0.093	15.025	1.104	15.301	0.448	15.458	0.315	15.165	0.425	15.170	0.271	15.345	0.254	15.667	0.318
TOTAL	56.944	0.467	53.134	3.798	53.974	1.680	54.700	1.139	53.627	1.566	53.608	0.937	54.301	0.874	55.447	1.168
CarbCalc.																
Ca	0.158	0.049	0.955	0.010	0.948	0.004	0.948	0.004	0.946	0.005	0.952	0.008	0.951	0.007	0.946	0.012
Fe	0.621	0.058	0.017	0.001	0.017	0.001	0.016	0.001	0.019	0.003	0.017	0.002	0.016	0.003	0.014	0.001
Mn	0.069	0.004	0.022	0.010	0.024	0.002	0.028	0.002	0.025	0.005	0.024	0.006	0.026	0.006	0.031	0.007
Mg	0.151	0.007	0.005	0.000	0.011	0.005	0.007	0.002	0.009	0.006	0.006	0.002	0.005	0.002	0.008	0.004
Sr	0.000	0.000	0.001	0.000	0.001	0.000	0.000	0.000	0.001	0.000	0.000	0.000	0.000	0.000	0.001	0.000
Na	0.001	0.000	0.001	0.000	0.000	0.000	0.000	0.000	0.001	0.001	0.000	0.000	0.000	0.000	0.001	0.000
	n=3		n=3		n=3		n=5		n=5		n=5		n=5		n=5	

generation is however non-phosphatic as only insignificant amounts were detected. Recalculation to a molecular formula gives a similar composition to the analyses of generation (4).

The siderites are high in Mg and Ca, both of which comprise 15 mol%, with a Mn content of 7 mol% $MnCO_3$. This therefore has a Fe:Ca:Mg:Mn ratio very nearly 8:2:2:1. Generation (3c) gave an apatite composition, almost certainly francolite, due to the low P/Ca ratio expected for CO_3^{2-} inclusion into the phosphate sites, relative to other apatites. F and Cl were however not measured. This is discussed further in section **5**.14.

Generation 4: The composition of this ankerite is almost identical to that of generation (3a). Totals obtained during analysis are however more realistic, and the occurence of ankerite within the Frodingham Ironstone Formation is hence confirmed. The ankerite has an Fe/Mg ratio almost equal to one, comprising ≈20 mol% each, with 5 mol% $MnCO_3$.

Generation 5: Siderite composition is also identical to the earlier generation (3b).

Generations 6 and 7: These final calcite cements have compositions similar to each other, though generation (6) may show a possible Mg high. They have essentially the same composition as generations (1) and (2).

5.9.1.2) Phosphatised Echinoderm Fragments.

Within the coquina, echinoderm debris has been extensively replaced by phosphate, often associated with a small amount of berthierine replacement. All structure is lost, to be replaced by crystals similar to those described above. E.P.M.A. of the grains showed a composition nearly identical to the phosphates of generation (3c), showing that all calcite has been removed, though with probable Ca inclusion directly into the phosphate. The phosphates are apatites, almost certainly francolite and are discussed in section **5**.14.

5.9.1.3) Comparison with the Enclosing Grain-ironstone cements.

The cements of the grain-ironstones above and below the coquina (see plate 20d) are typical of similar samples elsewhere in the ironstone-formation. A high proportion of

ooids, with large amounts of echinoderm debris, has led to cementation via early syntaxial overgrowths on the echinoderm debris, and later pore-filling sparite. Compositionally, the cements of both above and below the coquina are comparable to those of generations (1), (2), (6) and (7), of the coquina. There are no atypical carbonate cement morphologies in either grain-ironstone.

5.9.1.4) Discussion.

The complex cementation of this coquina reveals a diagenetic history that is not easy to resolve. On the basis of mineralogy alone, a number of questions arise, specifically:

1) Calcite: How does the ooidal-grainstone cementation fit in with the generations (1), (2), (6) and (7), and what was the original mineralogy of generations (1) and (6)?
2) Ankerite: Why does ankerite form here and nowhere else in the ironstone-formation, and what factors control the morphology?
3) Phosphate: Was a single phosphatisation event responsible for phosphate cements and echinoderm replacement?
4) Siderite: Why does siderite apparently replace the ankerite in generation (3), and is the similar morphology in generation (5) replacive?

Strict answers to these questions are most likely impossible to obtain, but it serves to show the extreme complexity that may occur within the early post-oxic diagenesis of the ironstones, and the problems of interpretation that follow. What is apparent from the complex cementation of this coquina in comparison to other sections, is that complex cements form only in sections of high porosity, often associated with considerable phosphatisation. In effect, the coquina represents a minor phosphorite deposit, and is perhaps not a surprising find given the condensed nature associated with phosphorites and ironstones.

Low sedimentation rates and high organic productivity are usually assigned as factors in phosphorite formation, with subsequent reworking to concentrate the deposit. This model would appear to fit for this coquina which represents a lag deposit of shell fragments and

echinoderm debris. Organic matter breakdown liberated phosphate and almost certainly was responsible for the complex suite of cements seen. Pore waters were modified by iron and manganese reduction, supplying Fe^{2+} and Mn^{2+} to marine (Ca^{2+} and Mg^{2+} rich) waters, as the organic matter was degraded by post-oxic bacteria. The relative roles of post-oxic processes, and flushing with marine waters that diluted Fe^{2+} and Mn^{2+} concentrations, probably dictated the mineralogy precipitated. The formation of ankerite, that is otherwise absent in the ironstone-formation, is probably related to the high organic content, as seen in its association with a U.V. fluorescence zone and authigenic phosphate crystals. The reason for this is however unclear.

5.9.2) DRAG 31.36A: Complex Carbonate Morphological Development (Plate 21).

This sample is from the "Snap Band" of borehole DRAG 31, and is hence associated with extensive berthierine formation. As with DRAG 31.22, cementation is complex but involves only calcite and siderite. In particular, this section demonstrates the replacement of calcite by siderite, the formation of highly manganoan calcite, and evidence for the primary occurrence of aragonitic or H.M.C. cements, all pre-dating the pore-filling ferroan calcite cementation. Various morphologies are present, resulting from the following cement sequence, described for that seen in plate 21a, with compositions obtained by E.P.M.A. given in table 5.7.

Generation 1. (Highly manganoan calcite)

A probable initial H.M.C. cement forms prismatic to acicular crystals up to 150μm long, on ooids and bioclastic debris. The cement is light brown in colour (plate 21a) due to abundant <1μm inclusions throughout the cement, and produces birefringence colours of the first and second orders, within the crystals. The inclusions are seen to diverge slightly across the crystal, and a distinct cone shape is produced in a few examples. This suggests a probable fibrous cement origin. E.P.M.A. shows these cements to have the highest Mn content (averaging 27 mol% $MnCO_3$) of all samples studied in the ironstone-formation. Such a high Mn content is unusual, but not improbable, since Deer *et al.* (1962) suggest that manganese calcite in the range 0-50 mol% $MnCO_3$ can exist and be formed at relatively low

PLATE 21

Photomicrographs of Specimen DRAG. 31.36A

A) Cement stratigraphy developed within shelter porosity. The cement generations are numbered as described in the text. Note the extra cement generation within one of the pores (arrowed). Photo length is equivalent to 3.3mm.

B) Detail of the replaced radial fibrous cement of generation 2, and subsequent generations (crossed polars). Photo length is equivalent to 1.3mm.

C) Early scalenohedral calcite replaced by siderite, with small rhombic siderite crystals nucleated on the sides of the larger scalenohedral form, and also on the berthierine matrix. Photo length is equivalent to 0.7mm.

D) Fully botryoidal texture developed in generation 2, with subsequent siderite precipitation as small, parallel aligned, rhombic crystals on the exterior of the botryoidal fabric. Photo length is equivalent to 0.7mm.

A	B
C	D


1
5
1
2
2
3
4
5


4 3
2
5

Table 5.7. Average Compositions of Carbonate Cements Within Specimen DRAG. 31.36a, Obtained By E.P.M.A. The Data have been Recalculated to Carbonates of the Calcite Group.

	GEN. 1		GEN. 2		GEN. 3		GEN. 4		GEN. 5					
	CEMENTING OOIDS		(RADIAL)		SIDERITE 1		SIDERITE 2		PORE-FILL CALCITE		SIDERITE REP. BIO.		CALCITE REP. BIO.	
	AVERAGE	STDEV	AVERAGE	STDEV	AVERAGE	STDEV	AVERAGE	STDEV	AVERAGE	STDEV	AVERAGE	STDEV	AVERAGE	STDEV
Ca	22.702	3.707	34.825	1.702	4.473	0.460	4.619	0.396	36.213	0.874	3.822	0.309	37.615	0.435
P	0.014	0.016	0.019	0.027	0.007	0.013	0.017	0.022	0.013	0.018	0.026	0.035	0.000	0.000
Sr	0.026	0.015	0.091	0.035	0.021	0.021	0.014	0.008	0.049	0.011	0.016	0.014	0.076	0.019
Si	0.000	0.001	0.013	0.020	0.019	0.011	0.021	0.031	0.010	0.015	0.014	0.011	0.003	0.003
Al	0.007	0.005	0.007	0.014	0.000	0.000	0.000	0.001	0.003	0.002	0.004	0.007	0.002	0.003
Mg	1.499	0.223	0.459	0.283	4.323	0.121	3.746	0.305	0.339	0.019	3.175	0.347	0.297	0.054
Na	0.061	0.020	0.031	0.014	0.184	0.134	0.136	0.223	0.031	0.019	0.088	0.039	0.027	0.016
Fe	0.039	0.030	1.174	0.442	30.903	0.387	31.474	0.781	1.863	0.089	33.158	0.567	1.288	0.202
Mn	12.749	1.980	2.324	1.081	1.967	0.162	2.256	0.362	0.670	0.033	1.977	0.033	0.498	0.036
O	13.883	2.190	15.292	0.409	14.156	0.059	14.079	0.141	15.458	0.323	13.776	0.362	15.754	0.241
TOTAL	50.980	7.977	54.236	1.386	56.053	0.242	56.362	0.628	54.649	1.131	56.056	1.230	55.559	0.867
CarbCalc.														
Ca	0.656	0.010	0.912	0.034	0.126	0.014	0.130	0.010	0.937	0.003	0.107	0.010	0.954	0.006
Fe	0.001	0.001	0.022	0.008	0.627	0.006	0.643	0.017	0.035	0.002	0.696	0.004	0.023	0.003
Mn	0.270	0.011	0.045	0.021	0.041	0.003	0.047	0.008	0.013	0.001	0.042	0.001	0.009	0.001
Mg	0.072	0.003	0.020	0.012	0.202	0.005	0.176	0.014	0.014	0.001	0.152	0.013	0.012	0.002
Sr	0.000	0.000	0.001	0.000	0.000	0.000	0.000	0.000	0.001	0.000	0.000	0.000	0.001	0.000
Na	0.003	0.002	0.001	0.001	0.009	0.007	0.007	0.011	0.001	0.001	0.005	0.002	0.001	0.001
	n=5		n=13		n=3		n=6		n=5		n=3		n=3	

temperatures. The upper limit is based on the discovery of kutnohorite ($CaMn(CO_3)_2$) by Frondel and Bauer (1955). The occurrence of such cements at diagenetic temperatures, and morphologies produced are however poorly documented. It is suspected that Mn was introduced to a radial fibrous H.M.C. calcite, as 7 mol% $MgCO_3$ is recorded in this calcite. It is unlikely that both Mg^{2+} (from sea water) and large quantities of Mn^{2+} (from manganese reduction) would be present together, since the presence of Mg^{2+} via diffusion would also introduce oxygen. The site of Mn^{2+} occupation is problematical, since it would be expected to replace the Mg^{2+} on cation size alone, but rhodochrosites show only limited Mg incorporation (Deer *et al.* 1962). Replacement by congruent dissolution of $CaCO_3$ is hence implied, with the possible $MgCO_3$ loss remaining unknown, though an original dolomitic composition is highly unlikely on the basis of cement morphology. The cement is iron-poor with only 0.1 mol% $FeCO_3$ present.

Generation 2. (Manganoan/ferroan calcite)

The second generation of calcite (plate 21b) may have formed syntaxially with the first generation, and as the first generation underwent recrystallisation or partial solution, because the boundary separating these generations is indistinct and generation (1) may be absent. The cement is composed of sparite crystals whose edges may diverge and terminate in an arc, producing a botryoidal fabric. Uniform to indistinct extinction is seen, but the texture is highly indicative of replacement after a radial fibrous, acicular cement fabric, with growth interference between bundles of fibres. Angle of fibre divergence varies, so that in some cases a complete hemisphere may form. No compositional variation was found by E.P.M.A. along the crystals, which posses an Mn/Fe ratio of approximately two (4.5 mol% $MnCO_3$). Both Mg and Sr were very slightly elevated relative to the pore-filling calcite, so distinguishing between an aragonitic or H.M.C. precursor is unjustifiable.

Generation 3. (Siderite)

This siderite forms a thin (<15μm) generation as an isopachous cement of small crystals in the area being studied. Elsewhere, it is more fully developed, and forms larger rhombic crystals. Compositionally, the siderite has high Mg and Ca, with low Mn (20 mol% $MgCO_3$, 13 mol% $CaCO_3$, and 4 mol% $MnCO_3$), similar to the arboraceous siderite.

Generation 4. (Siderite)

This generation is remarkable in that it forms in only one pore, yet it is compositionally like that of generation (3). It is 60-80μm thick and also possesses a poor radial fabric due to its isopachous precipitation on an undulating surface. Prismatic crystals appear to be present, but have interlocking crystal edges and length-parallel crystals at the crystal terminations,suggesting that this fabric also results from parallel stacked siderites, here <15μm in length.

Generation 5. (Ferroan calcite)

Pore-filling ferroan calcite occurs as large sparry crystals, elongate prismatic in form, and possessing a radiaxial texture with undulose extinction and poorly developed subcrystals. The calcite is highly ferroan (3.5 mol% $FeCO_3$), with equal proportions of Mn and Mg (1.3 and 1.5 mol% respectively).

In addition to the morphologies described above, generation (1) apparently also formed as isolated scalenohedral crystals, upon which siderite nucleated and replaced the former (plate 21c) This is the only example seen of calcite replacement by siderite, and suggests an original (diagenetically unstable) H.M.C. precursor. The composition of this siderite, and other rhombohedral siderites associated with it were found to be similar, and no 'magnesium memory' was found. Other siderites form syntaxially on bioclasts. Plate 21d shows how generation two may develop a fully botryoidal texture, and how siderite may form stacked crystals, maintaining the approximate orientation, despite the changing orientation of the substrate.

5.9.2.1) Discussion.

The earliest cements of probable H.M.C. origin may have formed in the marine phreatic environment under 'normal' conditions of marine calcite precipitation. Replacement by large amounts of $MnCO_3$ occurred as manganese reduction began, and was possibly maintained for a period to allow sufficient replacement. Iron reduction would have accompanied manganese reduction to some extent, but Mn was preferentially incorporated

into the calcite. The reason for the replacement as opposed to precipitation of a new cement phase remains unclear, particularly in that the H.M.C. still contains considerable Mg.

A recharge of pore fluid may have re-introduced Ca and Mg to the system, fuelled by the dissolution of aragonitic shell debris, to allow a second generation of radial fibrous cement to form. A negative Eh was maintained and Mn and Fe were also included, but in much smaller amounts. An alternative possibility is that the introduction of Mn and Fe occurred during the phase of recrystallisation. Considerable iron-reduction followed, raising the Fe^{2+} concentration until the pore water became siderite saturated, and siderite precipitated as cement phases within primary porosity and bioclast voids. Siderite also replaced former H.M.C crystals as the calcites were destabilised by the high Fe/Ca ratio of the pore fluid. The generation (4) siderite cement shows how variable pore fluid composition must have been at this time, since siderite was precipitated for a longer period, possibly during a later stage of more localised iron reduction. The final phase of calcite cementation is similar to that described for other grain-ironstones.

The formation of berthierine must have occurred prior to all the above cementation, since the earliest calcites cement the muds and ooids. It is interesting to note that the first generation calcite is seen to nucleate on some (but not all) of the ooids, contradictory to that described for calcites in the ooidal grain-ironstones. Some authigenic phosphate may also be seen but is not extensive. Its formation is however strongly indicative of biogenic activity in the sample.

Though the cementation is complex, with considerable discussion possible on the above interpretation, an overall pattern of cement precipitation dominated by marine influences, manganese-reduction, and iron-reduction, in sequence, can be detected. This is consistent with the sample undergoing early diagenesis, with a mineralogy reflecting the modification of pore fluid composition as post-oxic diagenetic reactions followed 'normal' marine cementation.

5.10) Carbonates Associated With Berthierine Cement Formation.

The carbonate cements post-dating the formation of authigenic berthierine (for example plate 13 a,b) were studied to ascertain whether berthierine authigenesis significantly affected subsequent carbonate precipitation. If the system were relatively closed, then a depletion of the elements found within berthierine, would be expected in the later carbonate. DRAG. 31.19 & 28, and Y183.3 & 8, have carbonate precipitated after berthierine cements. DRAG 31.19 contains both siderite and calcite; DRAG. 31.28 contains only siderite, one morphology of which replaces the first generation of berthierine as a prismatic, radial cement, and the second of which is as a pore-filling cement.

The calcite and siderite of DRAG. 31.19 usually form only a few crystals within a pore, and of a similar mineralogy. This suggests that individual pores acted as separate microenvironments in which either siderite or calcite was precipitated, but in an overall open system to allow for solute recharge. The compositions of the calcite and siderite are similar to those from other lithologies (table 5.8). An Mn/Fe ratio of nearly two in the calcite may reflect either the predominance of manganese reduction at this stage, or the preferential incorporation of Fe over Mn into berthierine, as there is very little Mn in the silicate (section 4.7). Neither calcite nor siderite show any significant depletion in the elements Ca, Fe, or Mg, that might be removed by berthierine precipitation, and so if any pore fluid change did occur during formation, it did not effect the later carbonate precipitation.

The siderites of DRAG. 31.28 have a similar composition within the cements as the replacement textures, but are slightly depleted in Ca relative to other siderites possibly reflecting the small amount of original aragonitic shell material in this sample. Since the compositions are similar, it is suspected that replacement and precipitation occurred synchronously, but the reason for this is unclear, as no significant difference was found within the berthierines across the sample or between generations (section 4.4.3).

In conclusion to this section, it is evident that berthierine cement formation does not significantly effect the composition or morphology of carbonates that post-date its

Table 5.8. Average Compositions of Carbonate Cements Associated with Authigenic Berthierine Precipitation, Obtained By E.P.M.A. The Data have been Recalculated to Calcite Group Formulae.

	DRAG. 31.19				DRAG. 31.28 (Siderites)			
	Calcites		Siderites		Cements/ Rep. berth.		Surrounding ooids	
	AVERAGE	STDEV	AVERAGE	STDEV	AVERAGE	STDEV	AVERAGE	STDEV
Ca	38.215	1.349	3.991	0.235	3.302	0.240	3.242	0.957
P	0.004	0.007	0.016	0.036	0.052	0.054	0.041	0.059
Sr	0.058	0.014	0.032	0.011	0.035	0.013	0.052	0.025
Si	0.003	0.005	0.005	0.006	0.060	0.069	1.060	2.140
Al	0.000	0.000	0.000	0.000	0.035	0.035	0.669	1.451
Mg	0.125	0.021	2.702	0.146	3.268	0.396	3.138	0.324
Na	0.001	0.002	0.006	0.008	0.040	0.025	0.062	0.049
Fe	0.958	0.331	33.807	0.454	33.336	0.674	32.208	1.667
Mn	1.656	0.358	2.386	0.226	3.395	0.289	3.878	1.273
O	16.114	0.543	13.785	0.262	14.194	0.229	15.603	2.768
TOTAL	57.135	1.885	56.730	0.944	54.415	0.829	56.710	4.584
CarbCalc.								
Ca	0.947	0.004	0.115	0.007	0.091	0.008	0.091	0.024
Fe	0.017	0.005	0.705	0.006	0.683	0.015	0.675	0.047
Mn	0.030	0.007	0.051	0.004	0.071	0.006	0.082	0.024
Mg	0.005	0.001	0.129	0.005	0.154	0.017	0.150	0.008
Sr	0.001	0.000	0.000	0.000	0.000	0.000	0.001	0.000
Na	0.000	0.000	0.000	0.000	0.002	0.001	0.003	0.003
	n=4		n=6		n=6		n=8	

authigenesis, relative to siderites and calcites formed elsewhere. It must be remembered however that siderite formation is commonly associated with berthierine formation, but that the type of berthierine formed does not effect its composition. As the compositions of the later carbonates are similar between these samples and grain-ironstones, a similar origin can be inferred.

5.11) Discussion: Controls on Carbonate Precipitation, Morphology, and Composition.

Carbonate cementation of ironstones has not been studied in detail previously, despite the vast literature on ironstone formation. Ironstone cementation however allows an extension of theories of carbonate cementation mechanisms based on 'normal' carbonate cements, to wider diagenetic environments. The role of Fe^{2+} and Mn^{2+} on carbonate precipitation and replacement, can be coupled with kinetic effects such as porosity and nucleation site availability. The effect of lesser understood processes, such as PO_4^{3-} and SO_4^{2-} inhibition of carbonate precipitation, and organic-inorganic interaction, are also of probable greater importance in such a diagenetic scenario. These are discussed individually below, following a discussion on the basic thermodynamic considerations for precipitation, and pore water compositions, that control all carbonate formation.

5.11.1) Thermodynamic considerations.

The precipitation of carbonate minerals can be symbolised by the reaction:

$$MCO_{3(solid)} + H_2CO_3 \Leftrightarrow M^{2+} + 2HCO_3^- \qquad \text{(Krauskopf 1979)}$$

where M^{2+} represents Ca^{2+}, Mg^{2+}, Fe^{2+}, Mn^{2+}, Sr^{2+} etc. Though simplified, the reaction serves to indicate the controls on the precipitation or dissolution of carbonate, by a shift in reaction rate to the left or right respectively. The equilibrium of this reaction is shifted towards the left (and hence to carbonate precipitation), by the removal of CO_2 by heating or decreasing pressure, or more significantly here, by the addition of alkali, CO_2 removal by photosynthetic activity of plants, or M^{2+} and HCO_3^- addition by bacterial oxidation of organic matter by reduction of metal compounds (including oxides). The exact reactions involved are however more complex, and quantifying the above requires detailed knowledge

of activity coefficients, ion associations, and reactant concentrations, that are discussed in detail by Krauskopf (1979).

Calculations of solubility products have shown that the only simple carbonate besides $CaCO_3$ that approaches saturation in sea water is $SrCO_3$. The Ba^{2+} concentration is kept low because $BaSO_4$ is less soluble than $BaCO_3$ due to the high concentration of SO_4^{2-}, and pure $MgCO_3$ requires extreme Mg/Ca values, found only in salt lakes. Mg is however incorporated into dolomite. Fe and Mn carbonates are not formed in the marine oxic environment, because these metals are precipitated as oxides. Hence the only simple carbonate that forms on a large scale in the oxic environment is calcium carbonate.

In the diagenetic environment, Fe^{2+} and Mn^{2+} are added by bacterial reduction of their oxides, to the Ca^{2+} and Mg^{+} from trapped sea water. These four ions are incorporated into precipitating carbonate, that may give a diverse range of compositions by solid-solution. In the system $FeCO_3$-$MgCO_3$-$MnCO_3$, there is complete miscibility, but there is incomplete miscibility between $CaCO_3$, and $FeCO_3$, $MgCO_3$ and $MnCO_3$. In the latter system, the compounds $CaMn(CO_3)_2$ (kutnohorite) and $CaMg(CO_3)_2$ (dolomite) are stable, with up to 70 mol% $CaFe(CO_3)_2$ (ankerite) substitution for dolomite possible (Goldsmith 1983). Pure ankerite is not found.

5.11.1.1) Pore water Composition.

Pore water composition is the controlling factor on the carbonate species precipitated, but the precise elemental ratios of the solution are unclear (see Curtis and Coleman 1986). Calcite precipitation will occur from depositional sea water, until levels of Fe, Mn or Mg are sufficiently elevated to allow precipitation of other phases. As calcite precipitates it will however incorporate these elements into the lattice, and its composition will be related to the rates of cation production (or recharge), and incorporation into the crystal. The uptake of elements from pore water into a carbonate (here taken as calcite) is controlled by the partition coefficient (k) of that element, given in the simplest form by the equation:

$$({}^{m}Tr / {}^{m}Ca)_{(solid)} = k\,({}^{m}Tr / {}^{m}Ca)_{(liquid)}$$

where m indicates molar concentration, and Tr the trace constituent. This assumes a high water/rock ratio, i.e. the volume precipitated is insignificant relative to the volume of solution (a fully open system). Where $k > 1$, the trace element is preferentially incorporated into the solid phase; where $k < 1$ the ratio of Tr/Ca is less in the solid than the liquid; and where $k = 1$, the ratio is the same. Published values for k show considerable variation in some cases, with reported values of Sr; 0.027-0.4, Na; $2x10^{-5}$-$3x10^{-5}$, Mg; 0.013-0.06, Fe; 1-20, Mn; 5.4-30 (ranges reported in Veizer 1983). Though values are variable, this means that where available, Fe and (more so) Mn are preferentially incorporated into precipitating carbonate, whereas Mg and Sr would concentrate in the liquid. Given that the molecular weights of Fe and Mn are nearly identical, and assuming a $k_{Fe} = 5$, $k_{Mn} = 10$ (Tucker and Wright 1990), it follows from the above equation, that for a calcite containing equal amounts of Fe and Mn, the precipitating solution would have contained twice the amount of Fe than Mn (assuming the conditions outlined above).

The situation becomes considerably more complicated if the system is closed, as the pore fluid becomes progressively depleted/enriched in trace elements, and zoning occurs in crystals formed. Since the calcites of the Frodingham Ironstone Formation are however poorly zoned, and the preferential incorporation of Fe and Mn into calcites has been adequately described on the assumption of an open, homogenous precipitation, the discussion will not here be extended to closed systems (see Tucker and Wright 1990) and Moore (1989) for a full summary).

5.11.1.2) Replacement Mechanisms.

Carbonates may replace each other, and the reaction may be thermodynamically expressed by the reaction:

$$MCO_3 + m^{2+} \Leftrightarrow M^{2+} + mCO_3$$

where M and m are different cations of Ca, Fe, Mn, Mg etc. The equilibrium constant (K) for this reaction is calculated as the ratio of the solubility products of MCO_3 and mCO_3. For the replacement of calcite by siderite, K= 225 (Krauskopf 1979 p. 68) indicating that at

normal temperatures calcite should be replaced by siderite if the solution contains Fe^{2+} in a concentration more than 1/225 that of Ca^{2+}. For calcite replaced by pure $MnCO_3$, K= 9, suggesting that Fe^{2+} would replace a calcite before that of Mn^{2+}, if both concentrations increased to the same degree. However, kinetic factors may be important in such a replacement process.

Thermodynamically, the replacement of calcite by siderite as seen in DRAG. 31.36a is hence possible, and would be expected if the Fe concentration increased during diagenesis. The replacement process is however uncommon, and calcite replacement of siderite is not seen, favouring instead new mineral precipitation. Clearly, thermodynamics alone cannot explain carbonate fabrics, but provide an initial prediction of whether a reaction is possible.

5.11.2) Controls on the Morphology of the Unreplaced Carbonate Cements

5.11.2.1) Composition.

The Mg/Ca ratio of precipitating pore fluid and carbonate formed has long been held to be a major control on the species and morphology of carbonate cements (for example Muller *et al.* 1972, Folk 1974, Berner 1975, Longmann 1980), which is well reviewed by Chafetz *et al.* (1985), who support this premise. Walter (1986) also applies the Mg/Ca ratio to dissolution rates of carbonates. More unusual textures are assigned to irregular crystal growth (such as in radiaxial calcites, Kendall 1985), or incorporation of unusual ions such as the SO_4^{2-} ion, (for example Folk *et al.* 1985, see also section **5**.11.4). Given and Wilkinson (1985) describe carbonates of both meteoric and marine settings, and suggest that the kinetics of surface nucleation and concentration of reactants (principly carbonate ions) are of greatest importance.

Surprisingly perhaps, little has been written on ferroan/manganoan calcite morphologies, since if Mg^{2+} (0.80Å diameter) can control precipitation or cause lattice distortion by substitution for Ca^{2+} (1.08Å), then Fe^{2+} (0.86Å) or Mn^{2+} (0.91Å) might also be expected to do so. Although careful studies were carried out to test whether certain morphologies of cement within the Frodingham Ironstone Formation could be related to their composition, it

became evident that no correlation could be seen. It is however interesting to note the observation of widespread undulose extinction in many calcites, apparently unrelated to the composition of major elements. These calcites are often associated with accessory minerals (pyrite, phosphate) suggesting a possible incorporation of lattice distorting SO_4^{2-} or PO_4^{3-} ions (see also section 5.11.4 below).

5.11.2.2) Nucleation Effects.

The morphology and production of calcites and siderites in the ironstone-formation, has been shown to be strongly dependent upon nucleation site availability. Fibrous cements form syntaxially on unreplaced bioclasts, scalenohedral calcites in voids often associated with bioclast dissolution, and large sparry calcites in areas of apparently few nuclei (for example iron-ooids). Samples containing large amounts of bioclastic debris therefore have been preferentially cemented, whereas iron-ooid rich beds may have remained unlithified in part. There appears however to be no distinct compositional differences between the two. Siderite can be seen to precipitate upon calcitic bioclastic debris (syntaxially), and would therefore be similarly affected by nucleation factors as calcite.

The lack of suitable sites for nucleation of carbonate relative to pure limestones could have affected carbonate formation by changing rates of precipitation (rapid growth on available nuclei?), and pore fluid composition (over saturation with elements unable to precipitate?). These effects are however difficult to measure, but it appears that cementation was fairly rapid due to the lack of compactional features in the ironstones, and the absence of crystal zoning that might be expected with pore waters evolving over time.

Of the non-carbonate components within the ironstones, berthierine is apparently favoured over iron oxides as a nucleation for carbonate precipitation, particularly for the formation of siderite. Calcite uncommonly forms euhedral crystals when nucleated on berthierine mud, whereas this is common in siderite. Care is therefore needed when interpreting the formation of first-formed cements, because it is possible that calcite may not have precipitated prior to siderite on the muds, due to nucleation, rather than

thermodynamic, effects. Iron-ooids of predominantly goethite are not good sites for carbonate nucleation, indicating that they were not calcite at the time of deposition, nor did they apparently contain any significant calcite in the structure.

5.11.3) Porosity and Permeability.

The depositional porosity of the ironstone-formation was high, with Minus-Cement-Porosity (M.C.P.) values of grain-ironstones indicating up to 46% original porosity in a bioclastic ooidal ironstone (YAR. 21), but more commonly 20-30% where greater numbers of ooids are present (for example DRAG. 31.10). Where intact shell material is present, shelter porosity is high, reaching 57.5% in the coquina of DRAG. 31.22. If solution porosity of dissolved aragonitic bioclasts is added to these values, a further 5-20% may be added to the volume of authigenic carbonate precipitated. Such high values of M.C.P. indicate that little porosity was lost due to compaction, prior to the cementation.

The porosity of the grain-ironstones is fully inter-connected, so that the permeability of the grain-ironstones would also have been high, and high rates of fluid flow would have been possible. Large quantities of water would have had to flow through the ironstones, on the basis that inorganic cementation would require 10,000-100,000 pore volumes of water to supply the necessary $CaCO_3$ to cement the Formation, from any natural water type (see Scholle and Halley 1985). Flow rates would have been considerably restricted by the presence of muds, but complete permeability barriers are uncommon, as the thin mudstone bands that would provide the greatest restriction, are continuous for only a few metres. Storm-generated coquinas would act as conduits for fluid flow in these muddier lithologies. Permeability would be highest at the base of individual cycles of sedimentation, within the grain-ironstones, and these areas would themselves be interconnected due to the reworking and mud winnowing of the ironstone sediments. Similarly, the lower portion of the ironstone as a whole, contained the greatest initial porosity, as witnessed by the high proportion of grain-ironstones in this part.

Vertical permeability is also considered to have been high during the deposition of the ironstone-formation, with the possible exception of the "Snap Band" whose laterally extensive nature may have restricted such movement. It therefore seems extremely likely that continued recharge of ions into the sediment by direct water flow and diffusion was possible, particularly during deposition and reworking of the grain-ironstones.

Porosity (and hence permeability) does not show a correlation with mineralogy of carbonates precipitated, but may indirectly effect the morphology. Given and Wilkinson (1985) have suggested that magnesian calcite follows aragonite precipitation within the pores of the Capitan Formation, W. Texas, due to the kinetics of decreasing fluid shear as pore throats are occluded by cementation. Such factors may be involved in the formation of morphologies such as seen in DRAG 31.36a, but involving both calcites and siderites. In general however, no relationship between crystal shape, form or orientation with pore size could be found.

5.11.4) Possible Effects of SO_4^{2-} and PO_4^{3-} on Calcite Precipitation.

It is important here to specifically discuss the effect of SO_4^{2-} and PO_4^{3-} on calcite precipitation, because in the diagenetic environment, sulphate-reducing bacteria deplete SO_4^{2-} concentrations, and organic matter decay in general supplies PO_4^{3-}. Bischoff and Fyfe (1968) showed that SO_4^{2-} inhibits calcite formation relative to aragonite, and Busenberg and Plummer (1985) recently showed that SO_4^{2-} significantly reduces the rate of crystal growth in calcite. Walter (1986) carried out further experiments involving both SO_4^{2-} and PO_4^{3-}, and confirmed that calcite growth was selectively inhibited by SO_4^{2-}, and that aragonite was selectively inhibited by PO_4^{3-}. She concluded therefore that environments where PO_4^{3-} is released by organic matter degradation, and SO_4^{2-} is depleted by sulphate reduction, may be favourable sites for calcite or Mg-calcite precipitation.

It was therefore possible that examination of the calcites in the Frodingham Ironstone Formation might yield further information on this issue from an actual example. The post-oxic concept suggests that PO_4^{3-} would be formed by organic matter oxidation, but that

SO_4^{2-} levels would not be significantly depleted, unlike a more 'normal' diagenetic scenario. The ironstone-formation therefore provides an environment of high PO_4^{3-} and SO_4^{2-} in which $CaCO_3$ precipitation would be expected to occur. Petrographic examination of the cements reveals no evidence for calcite growth inhibition, particularly in the fact that early cementation was rapid and complete, since no signs of compaction features are evident in the samples. It is not however implied that SO_4^{2-} was depleted, and its presence may explain why dolomite did not form in the ironstones.

The effect of PO_4^{3-} on aragonite precipitation suggests that it would not form in preference to calcite in the diagenetic environment with relatively high PO_4^{3-} concentrations. The formation of aragonite relative to calcite in the early diagenesis of sediments other than limestones, has however not been investigated. The occurrence of early fibrous cements cannot unfortunately contribute to the debate due to their uncertain origin (see below section 5.12.1), but such experimental considerations must however add weight to the argument of a H.M.C. precursor cement (if any) rather than aragonite.

It is possible that incorporation of SO_4^{2-} or PO_4^{3-} into the calcite structure in place of CO_3^{2-} may be responsible for the undulose extinction textures seen in some carbonates. This is particularly likely for PO_4^{3-}, as phosphates are often associated with complex cements, and pore-filling calcites post-dating authigenic phosphate cements are often slightly undulose. E.P.M.A. is however not accurate enough to confirm this suspicion.

5.11.5) Organic Matter - Carbonate Interactions.

Interactions between organic matter (O.M.), grain surfaces and $CaCO_3$ precipitation have been excellently reviewed by Mitterer and Cunningham (1985). They suggest that O.M. interacts with $CaCO_3$ systems by being adsorped onto grain surfaces, with the formation of biofilms, and by complexation or chelation of free ions. The effect of biofilms on $CaCO_3$ precipitation and equilibrium between bioclast and sea water remains unclear (though suspected to be largely inhibitory), but complexation and chelation is thought to

inhibit $CaCO_3$ precipitation by reducing the concentration of Ca^{2+}. The overall effects of this are summarised in figure 5.4.

The model is restricted in diagenetic work in that it deals mainly with primary incorporation of O.M. into the sediment, but gives clear indications of the possible effects of O.M. - $CaCO_3$ interaction. The suggestion of such a model is that at lower values of Total Organic Carbon (T.O.C.), due to either low O.M. input or as biodegradation proceeds, the less effect O.M. has in inhibiting $CaCO_3$ precipitation. Hydrophobic O.M. becomes more hydrophilic under the effects of degradation or oxidation. Complexation of cations increases, and adsorption may occur, but the O.M. concentration will have decreased, and $CaCO_3$ precipitation may occur as less Ca^{2+} ions are held within the O.M.

As with the effect of SO_4^{2-} and PO_4^{3-}, it is here considered likely that organic matter had little effect on inhibiting $CaCO_3$ precipitation, for the same reason of evidence for rapid cementation. The uninhibited formation of calcite is consistent with depositional values of T.O.C. being relatively low and/or considerable biodegradation of the O.M. It is not suspected that original T.O.C. values were high, and it is clear that considerable O.M. oxidation will have occurred during diagenesis by aerobic and anaerobic processes. Complexation of cations will have occurred, including the formation of biofilms, but cation availability was probably not significantly reduced. Though unable to be quantified, possible complexation of Ca and Mg in the early stages of diagenesis may have aided early siderite formation, as Fe was liberated later during diagenesis. Although the actual effects of O.M. - carbonate interaction cannot be clearly ascertained, it can be suggested that the observations for the Frodingham Ironstone Formation are at least consistent with high O.M. degradation during microbially dominated diagenetic processes, such as within the post-oxic diagenetic concept.

5.12) Origin of the Carbonates of the Frodingham Ironstone Formation.

The carbonate content of the ironstone-formation has been shown to consist of; bioclastic debris (L.M.C.), often replaced; ferroan manganoan calcite; siderite; and rare ankerite and

Figure 5.4. A Model for the Interaction of Organic Matter With Calcium Carbonate. Taken From Mitterer and Cunningham (1985).

TOC	O_2 LEVEL	OM TYPE	EFFECT OF OM	TYPICAL ENVIRONMENT
HIGH	ANOXIC	HYDROPHOBIC (LIPID-RICH)	COMPLEXING OF Ca BY OM; NO PRECIPITATION	PORE WATERS IN FINE-GRAINED SEDIMENTS
MODERATE	↓ INCREASING LEVEL OF O_2	↓ INCREASING DEGREE OF OXIDATION	LIPID COATING; ISOLATION OF GRAIN; NO PRECIPITATION	OPEN MARINE BASIN
LOW		HYDROPHILIC (OXYGEN-RICH)	ADSORPTION OF OM AND COMPLEXING OF Ca; POSSIBLE PRECIPITATION OF $CaCO_3$ (EPITAXY?)	SHALLOW MARINE GRAINSTONE AND BOUNDSTONE
"ABSENT"	OXIC		NONE; PRECIPITATION FOLLOWS INORGANIC KINETICS	VADOSE

non-ferroan calcite cements. Plotted together on a standard $CaCO_3$, $MgCO_3$, $(Fe+Mn)CO_3$, triangular plot (figure 5.5), the overall suite of carbonate cements is apparent. The following discussion attempts to relate the carbonate phases seen in the ironstones, to former replaced cements (for the earliest generations), or other occurrences of iron and manganese bearing carbonates, and hence suggest the mechanism of origin of the Frodingham carbonates.

5.12.1) Early Ferroan Carbonate Cements, Primary or Replaced?.

Evidence was given in the discussion on radial fibrous cements in DRAG 31.36a (section 5.9.2) to suggest that the particular cement fabric was of a primary marine origin. Also, the formation of arboraceous siderite required that a precursor cement dissolved completely. Such fabrics suggest that either H.M.C., or aragonite, was precipitated during a phase of normal marine cementation, prior to the onset of bacterially controlled diagenesis. These cements are however restricted to the "Snap Band", whose diagenetic history was decidedly more complicated. For the ironstone-formation as a whole, early ferroan calcite fabrics need to be examined to establish the consistency of this suggestion. The early cements, of fibrous/prismatic and scalenohedral habit, are discussed as to whether their primary mineralogy was aragonite; H.M.C.; original ferroan calcite; or a more unstable precursor (for example ferromagnesium calcite). Clearly, this is of extreme importance in delineating the history of the ironstone, particularly in ascertaining the composition of the depositional waters.

To prove these cements to be originally of H.M.C. or aragonite, would suggest that the depositional pore water was of 'normal' marine composition, and that the usual processes affecting limestones during diagenesis were in operation. Modern carbonates are cemented by both these mineralogies, but the controls on their formation, and hence environmental interpretation, remain specifically undefined (see reviews in Bathurst 1975, Goldsmith 1983, Tucker and Wright 1990, and papers in Scneidermann and Harris 1985). To prove otherwise might infer a more restricted regime of perhaps differing salinity, oxia or temperature, or that early burial cements form similar textures to those of non-ferroan carbonates.

Figure 5.5. Ternary Plot of Carbonate Compositions Expressed as Mol% Carbonate for the Frodingham Ironstone Formation. The Lower Plot is an Enlargement of the >90% $CaCO_3$ Region of the Upper Diagram.

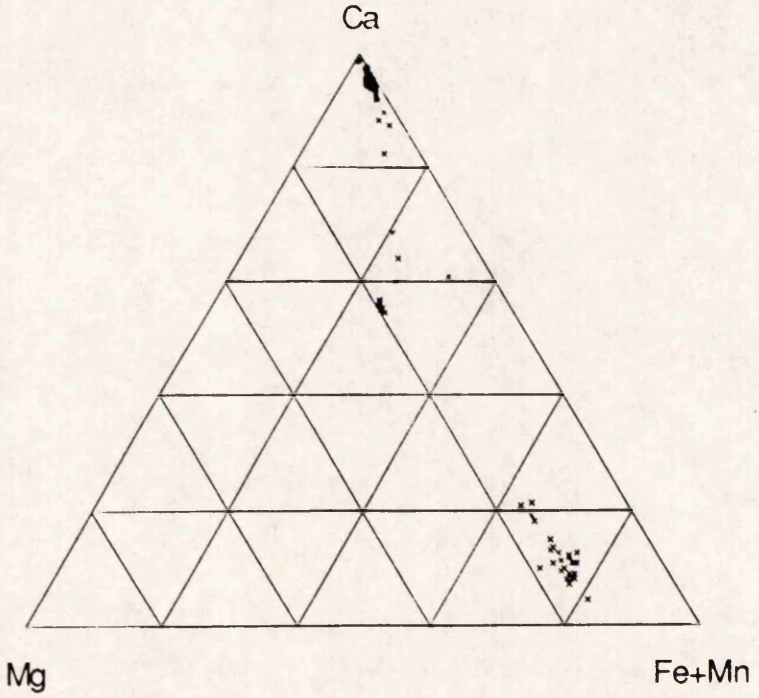

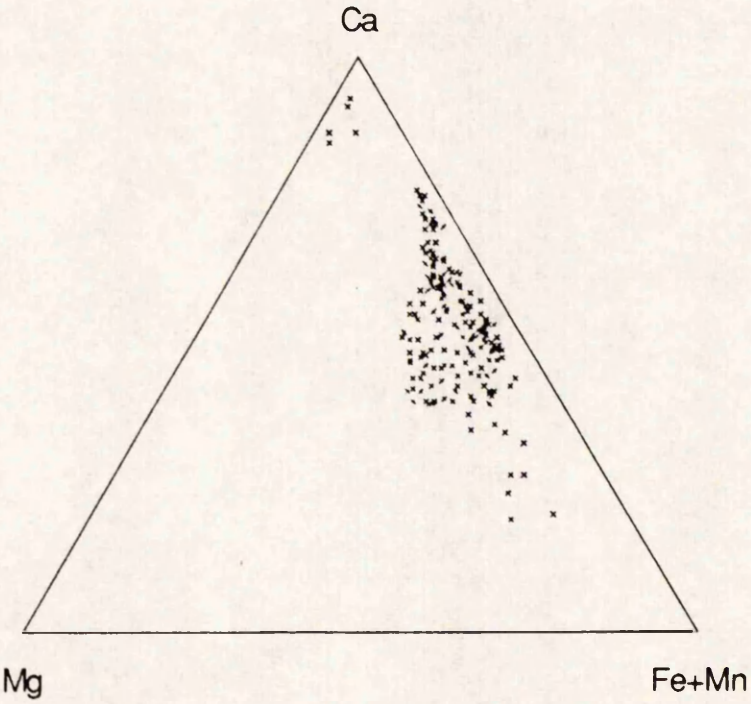

5.12.1.1) Morphological Considerations.

The morphology of early carbonate cements in ancient sediments has often been used to indicate an original aragonitic or H.M.C. cement, by a more acicular/fibrous or bladed habit respectively. However, both cement types may produce various morphologies, that overlap to a degree (see discussions in Given and Wilkinson 1985, Chafetz *et al.* 1985), and must therefore be treated with caution. This is particularly so where fibrous to prismatic cements are under discussion. The scalenohedral calcites are assumed to originally have been calcite as opposed to aragonite, due to the distinct form that orthorhombic aragonite would not produce. The initial iron or magnesium content is however unclear. The fibrous and prismatic cements are more problematical, with the complication that morphologies of early diagenetic ferroan calcites have not been fully categorised. Such cement fabrics have been assumed in the literature to be replacements of the more familiar H.M.C. and aragonite cements, without fully addressing the question as to whether ferroan calcites would produce similar morphologies in the marine phreatic environment to those of 'normal' limestones. If nucleation is a primary factor in the morphological control, then there is no apparent reason why this should not be so. If however the morphology is compositionally controlled, the situation is considerably complicated.

Solution textures are of little use in cement differentiation, as both H.M.C. and aragonite are diagenetically unstable, and all calcites would be attacked by acidified pore waters, particularly these earlier generations that have a large surface area. Inclusion fabrics indicate the initial morphology prior to recrystallisation, but are not microdolomitic, a suggested indicator of former H.M.C. cement (Lohmann and Meyers 1977).

5.12.1.2) Compositional Considerations.

The presence of high Mg or Sr in a L.M.C. or ferroan calcite cement relative to other cements of the same sample, has been used as a criteria for the identification of precursor H.M.C., or aragonitic cements respectively (for example see Lohmann and Meyers 1977, Prezbindowski 1985, Mazzullo 1980). However, Mg and Sr may be lost during diagenesis, with no recognisable anomaly. This loss is probably more likely where

other cations are involved during diagenesis such as Fe^{2+} and Mn^{2+}, that may displace these elements during replacement and recrystallisation. Mg^{2+} would be particularly vulnerable to replacement, in having a similar cation diameter to Fe^{2+} and Mn^{2+}, so such anomalies may be harder to detect within the ironstones, and ferroan calcites in general. Using an elevated Mg content to delineate a former H.M.C. mineralogy for ferroan calcites is also possibly flawed, in that ferroan calcites are themselves known to be able to contain significant Mg. Nash and Pittman (1975) record ferromagnesium calcites with 1-10 wt% $FeCO_3$, and 11-39 wt% $MgCO_3$ in sandstones, that were clearly not a former H.M.C. (*sensu strictu* of limestone diagenesis). Recrystallisation of an original ferroan calcite cement could therefore produce similar textures or marked Mg anomalies. E.P.M.A. was used to investigate these theories.

Within the samples of early fibrous/prismatic and scalenohedral calcites analysed, there was no general anomaly of Mg or Sr detected to any degree of certainty (see sections **5**.7.1.2 and **5**.7.1.3). However, slight Mg ano malies were found in two generations of fibrous calcite in DRAG 31.22, and more so in scalenohedral calcites of DRAG 31.23. Such values as detected in the latter were also obtained from pore-filling sparites elsewhere in the ironstone-formation (YAR 21), and must hence be considered inconclusive to a H.M.C. precursor, relative to a primary ferroan calcite origin.

5.12.1.3) Interpretation.

From the above, it is apparent that no conclusive origin of these early cements can be given. However, the scalenohedral calcites have almost certainly retained their mineralogy, if not their composition, and the fibrous and prismatic cements, if replaced, were probably originally H.M.C. Given that the morphology of carbonates is critically influenced by the substrate (shown by syntaxial overgrowths on detrital carbonate), there is a clear possibility that such morphologies are formed by initial ferroan calcite precipitation, without necessitating an unstable precursor.

5.12.2) Sparitic Ferroan/Manganoan Calcites.

5.12.2.1) Compositional Considerations.

Ferroan calcites have attracted only minimal attention in the literature relative to non-ferroan carbonates, often being assigned simply to a late stage influx of iron-bearing meteoric waters, with little attempt made to further categorise them. Typical occurrences of ferroan calcite with brief descriptions, are given by Oldershaw and Scoffin (1967), Colley and Davies (1969), Talbot (1971), Meyers (1974), Nash and Pittman (1975), Dickson and Barber (1976), Emery *et al.* (1988), a series of papers in Schneidermann and Harris (1985) and those papers listed in table 5.9. It cannot be overstressed however that the ferroan calcite cements described for the Frodingham Ironstone Formation are not true 'burial' cements. Compositions of ferroan calcites are also poorly published, the exceptions being Richter and Fuchtbauer (1978) who examined 37 specimens of ferroan calcite of various ages, analysing 10 in detail (table 5.9), and the work of Matsumoto and Iijima (1981) on the coalfields of Japan.

With reference to the published analyses of ferroan calcites (table 5.9), the cements of the Frodingham Ironstone Formation are:

1) Highly enriched in manganese.

2) Considerably depleted in magnesium.

3) Of average iron content.

These calcites are hence compositionally unlike the analyses given in table 5.9, including those of early diagenetic concretions. This is perhaps surprising because the early diagenetic nature of the Frodingham calcites might suggest a similar formation to concretions, and hence a comparable composition.

The manganese enrichment in the calcites can be readily explained in the concept of post-oxic diagenesis, in that Mn^{2+} is expected to be liberated into pore fluids as manganese oxides/hydroxides are reduced by bacterial oxidation of organic matter. This Mn^{2+} would be preferentially incorporated into precipitating calcites (see sections **1**.8 and **5**.11.1.1), accentuating the Mn/Fe ratio. Such high Mn/Fe ratios in calcite are unusual, and indicate a

Table 5.9. Mol% Carbonate Compositions of Ferroan Calcites From Various Localities, Cited in the Literature.

	1	2	3	4	5	6	7	8	9	10	11	12	13
Ca	89.3	87.9	81.4 - 85.8	95.2 - 94.7	89.4 - 99.1	n.d.	96.8	95.4	91.43 - 95.6	88.8 - 92.9	88.1 - 96.3	94.8 - 95.2	96.8 - 99.1
Mg	9.2	2.7	9.1 - 10.8	3.3 - 3.8	0.3 - 6.6	0.05 - 3.30	0.1	1.3	1.43 - 2.97	4.9 - 7.8	0.2 - 1.5	0.5 - 0.6	0.7 - 1.7
Fe	1.0	8.7	4.0 - 7.2	1.3 - 1.4	0.4 - 3.7	0.04 - 1.30	2.2	2.9	0.66 - 4.13	0.1 - 2.2	1.0 - 4.1	1.8 - 2.0	0.3 - 2.2
Mn	0.3	0.7	0.7 - 0.9	0.2 - 0.2	0.1 - 0.3	n.d.	0.1	0.3	0.26 - 2.97	0.4 - 1.1	0.4 - 6.4	n.d.	0.0 - 0.3

1	Curtis et al. (1985)	Concretion, L. Westphalian Coal Measures, Bull House Quarry, England.	
2	Pearson (1974a)	Within siderite concretion, Westphalian A, Hazlehead, England.	
3	Carpenter et al. (1988)	3 concretions, U. Cretaceous, Fox Hills Formation, N. Dakota.	a) Proximal Radial Fibrous Calcite.
4	" "		b) Distal Radial Fibrous Calcite.
5	" "		c) Equant Calcite.
6	Woronick & Land (1985)	Late calcite cement, Lower Cretaceous carbonates and shales, S. Texas.	
7	Hudson (1978)	Concretions, Oxford Clay, England. (Recalculated)	a) Main concretions.
8	" "		b) Early septarian concretions.
9	Boles and Ramseyer (1987)	Cements, Miocene Sandstone, San Joachim Basin, California.	
10	Boles et al. (1985)	Concretions, Palaeocene Moeraki Formation, New Zealand	a) Concretion Body.
11	" "		b) Septarian Vein.
12	Marshall & Ashton (1980)	Late void-filling cement, Hardground, Lincolnshire Limestone, (M. Jurassic), Cowthick Pit.	
13	Garzanti et al. (1989)	Cements, Ferruginous Oolite Formation, Jurassic, Zanskar, N. India.	

Analyses of ferroan calcites given in Richter and Fuchtbauer (1978)

	1	2	3	4	5	6	7	8	9	10
Ca	94.8	88.4	96.5	95.5	95.9	97.3	94.5	93.8	94.1	96.0
Mg	4.5	5.3	n.m	3.4	2.1	1.9	4.7	2.6	4.5	1.7
Fe	0.68	6.3	3.5	1.0	1.9	0.8	0.74	3.1	1.3	2.1
Mn	0.05	n.m.	n.m.	0.13	0.07	0.04	0.03	0.48	0.1	0.18

1	Santonian, Behobie/Biarritz, France, Intraclastic biocalcarenite.
2	Turonian, Ariyalur/Cauvery, S.India, Glauconitic sandstone.
3	Hauterivian, Rd. Weesoen-Arnden/Suisse, Glauconitic, phosphatic marl.
4	Mid. Kimmeridgean, Eldagsen/S. of Hannover, Oolite
5	Pliensbachian, Castrovido/N. Spain, Calcilutite.
6	Triassic/Jurassic, N.W. of Reinosa/Spain, Intraclastic biocalcarenite.
7	Triassic/Jurassic, Camino, N.W. Reinosa/Spain, Sedimentary breccia.
8	U. Triassic, Wilder Kaiser/E. Alps, Raibler Formation.
9	Middle Triassic, Neudenau/N. Heilbronn, Fossiliferous siltstone.
10	Devonian, Perlora/N. Spain, Coral limestone.

n.d. = no data
n.m. = not measured

strong influence of manganese reduction during calcite precipitation, more so than indicated by published examples.

The low Mg values could be implied to be in conflict with a hypothesis built solely on marine depositional waters undergoing post-oxic enrichment of Mn and Fe. In such a case, it would be expected that the calcites would also contain significant Mg, due to the high proportion of Mg in sea water and pore fluids derived from it. There are three major possibilities to explain this Mg depletion:

1) Mg was preferentially incorporated into a separate mineral phase.

2) The calcites precipitated from water low in Mg.

3) Fe and Mn were preferentially incorporated into the calcite lattice before Mg.

The first possibilty may be discounted as there is no apparent mechanism to account for Mg removal from pore fluids, other than by a small amount of complexation by organic matter. A meteoric water type could explain the Mg depletion because of the lower Mg/Ca ratio (≈ 0.3, Livingstone 1963) than sea water (≈ 5.3 Riley and Skirrow 1965). This would agree with the data of Matsumoto and Iijima (1980) who found that calcites precipitated in freshwater and brackish sediments have lower Mg, and higher Fe+Mn contents than those of marine sediments.

Preferential incorporation of Fe and Mn into a precipitating calcite is suggested by the element partitioning principle described in section **5**.11.1.1. Mg would also be expected to be incorporated, but the effect of high concentrations of Fe and Mn on the element partitioning is poorly understood. Figure 5.6 is a ternary plot for the major associated cations (Fe, Mn, and Mg) in the calcites described, showing that the major variable on composition is Mn. The trend from Fe to Mn reflects the relative rates of iron and manganese reduction during calcite precipitation. It should be stressed that the actual equilibrium quantities for Fe, Mn, and Mg incorporation calcite are unknown where all these elements are present, and that the higher Mg associated with higher Fe may reflect a Mn

Figure 5.6. Ternary Plot of Sparitic Calcites Expressed as Mol% Mg, Fe, and Mn Carbonate, Frodingham Ironstone Formation.

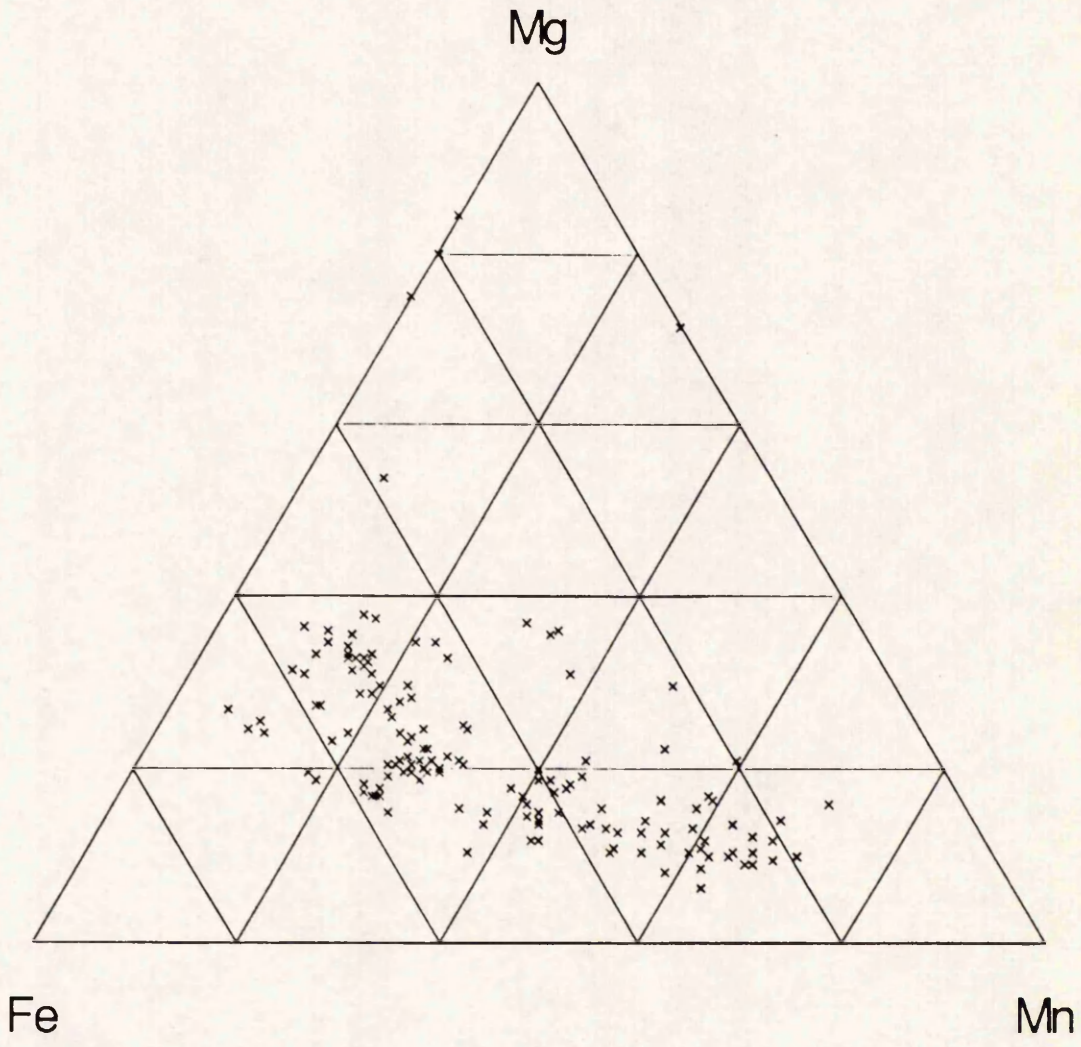

controlled process, in which extensive manganese incorporation in preference to Fe dominates both Fe and Mg concentrations.

If the average values of Fe, Mn and Mg, as mol% are plotted in relation to their position in the sequence (figure 5.7), then the Fe-Mg-Mn correlations described in section 5.7.1.4 and shown in figure 5.6 are quite striking. The highest Mn enrichment is seen to occur at the centre of the ironstone sequence associated with grain-ironstone development, with the higher Fe values occurring at the base and top of the ironstone-formation where the sequence is matrix rich. Whether this reflects processes acting within the sediment, or permeability constraints on meteoric water flux is not clear. However, the muds at the base of the sequence are not as berthieroidal as at the top of the ironstone-formation, invoking separate diagenetic conditions and processes, and supporting the latter.

5.12.2.2) Stable Isotopes.

In an attempt to resolve a possible meteoric water influx to the Formation that led to ferroan/manganoan calcite precipitation, stable isotopic analysis of C and O was carried out on these late stage sparry calcites. The methods, procedures and data are given in appendix A.2.2, and are shown plotted in figure 5.8. The analyses of various sparry ferroan/manganoan calcites, separated by drilling, have $\partial^{13}C_{PDB}$ of -3.6‰ to -22.1‰, and $\partial^{18}O_{PDB}$ of -6.0‰ to -9.4‰. Analyses taken from apparently unreplaced shells of Gryphaea and Pinna have values of $\partial^{13}C_{PDB}$ of +1.7‰ to +2.9‰, and $\partial^{18}O_{PDB}$ of -1.4‰ to -3.0‰.

The use of stable isotopes in carbonate sedimentology has been well reviewed in a number of publications (including Hudson 1977, Hoefs 1980, Anderson and Arthur 1983, Moore 1989, Tucker and Wright 1990, with references therein), and these should be referred to for detailed discussions of interpretation. The following discussion relates only to the data obtained in this study. The unreplaced shell debris is assumed to have remained isotopically unaltered since its formation, and hence retains an isotopic signature in equilibrium with the sea water from which it precipitated. A palaeotemperature for the ocean

Figure 5.7. Plot of Fe, Mn, and Mg Content of Pore-filling Sparites, Expressed as Mol% Carbonate, in Relation to Sample Position Within the Frodingham Ironstone Formation.

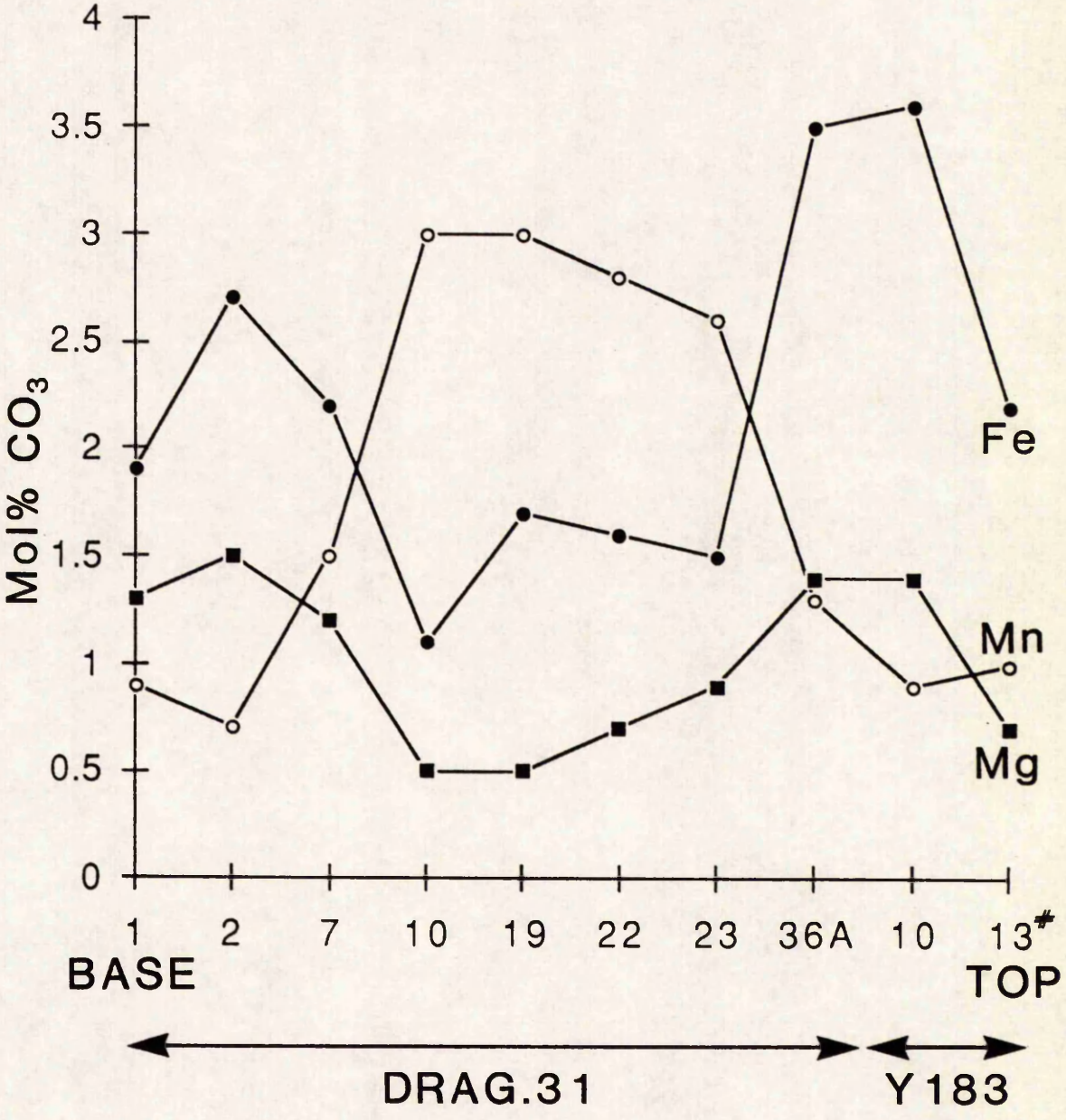

Non-Ferroan Calcites Included

Figure 5.8. Carbon and Oxygen Stable Isotopic Composition of Calcites Within the Frodingham Ironstone Formation.

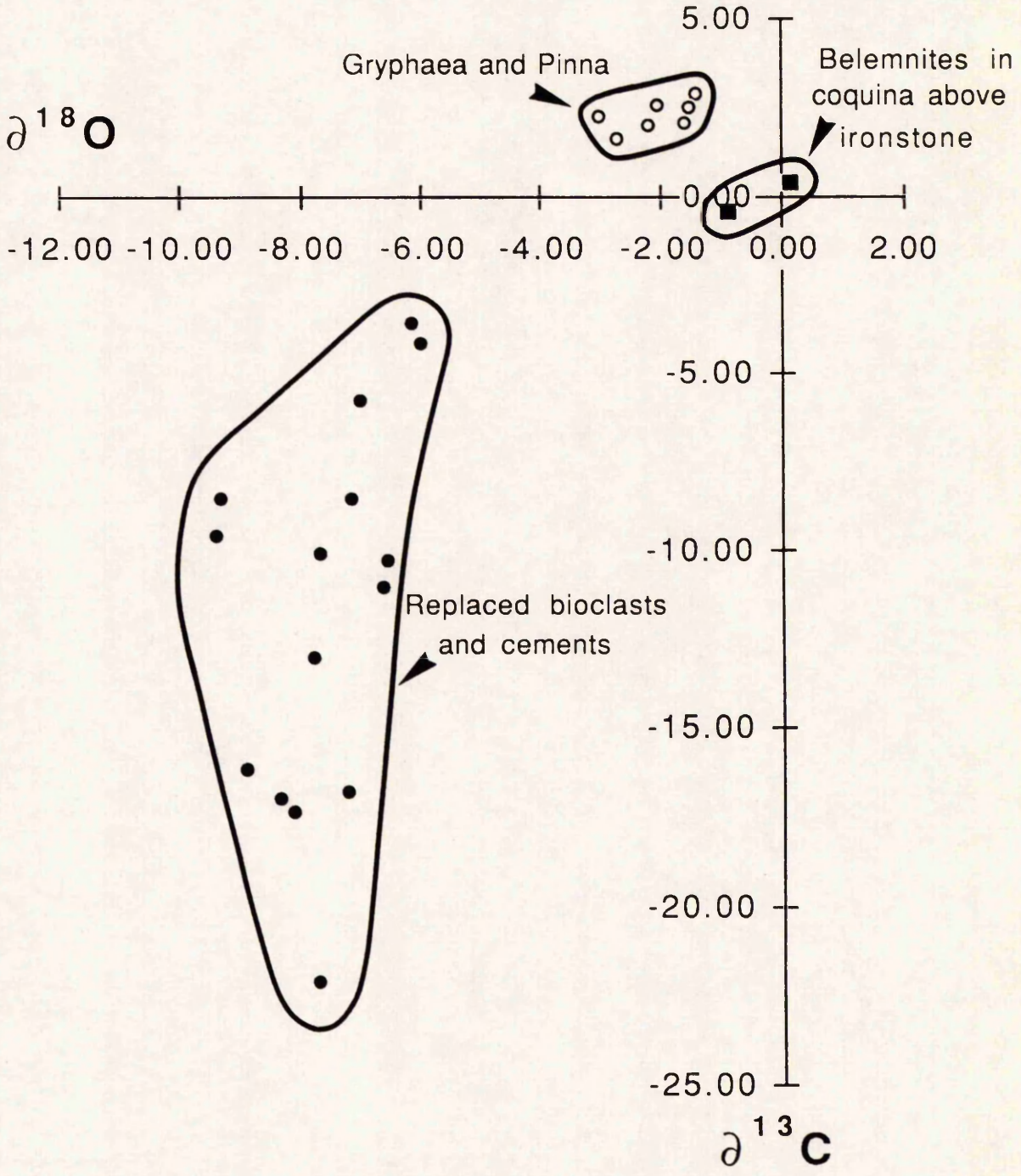

during precipitation may be estimated from the expression derived by Epstein *et al.* (1953), modified by Craig (1965), represented as:

$$t\ (°C) = 16.9 - 4.2(\partial_c^+ - \partial_w^+) + 0.13(\partial_c^+ - \partial_w^+)^2.$$

where ∂_c^+ is the $\partial^{18}O_{PDB}$ of CO_2 produced by the reaction of $CaCO_3$ in phosphoric acid at 25°C, and ∂_w^+ is the $\partial^{18}O_{PDB}$ of CO_2 in equilibrium with the water from which the carbonate precipitated. This can be modified to express the oxygen isotopic signature relative to the SMOW standard:

$$t\ (°C) = 16.0 - 4.14(\partial_c - \partial_w) + 0.13(\partial_c - \partial_w)^2.$$

where ∂_c and ∂_w^+ are equivalent, but ∂_w is the assumed $\partial^{18}O_{SMOW}$ of the precipitating water. The value of ∂_w is unknown, but can be estimated by assuming a pre-glacial ocean water with a $\partial^{18}O_{SMOW}$ isotopic composition of -1.2‰ (Shackleton and Kennett 1975). On this basis, a palaeotemperature of between 16.8 - 23.9°C can be obtained. This temperature assumes that no ^{18}O depleted meteoric waters mixed with the shallow marine ocean water. The values are consistent with modern precipitation, and similar to those published for the Oxford Clay (Upper Jurassic) fossils (Hudson 1978), the Lincolnshire Limestone Formation, Middle Jurassic (Marshall and Ashton 1980), and the marine portion of the Jurassic Great Estuarine Series of Scotland (Tan and Hudson 1974). It is hence suggested that these bivalves have retained their original isotopic signature, and record the palaeotemperature of a normal marine sea water.

The sparry ferroan/manganoan calcites give a very distinct trend on the isotope plot (figure 5.8), parallel to the $\partial^{13}C_{PDB}$ axis at low values of $\partial^{18}O_{PDB}$. Given that the samples represent a similar form and generation of calcite within the ironstones, and that no systematic variation was found between shell fragments, cements or radiaxial calcites, the trend is almost certainly an isotopic mixing trend, and not an evolutionary pathway. The trend is interpreted as representing the mixing of marine, and organically derived HCO_3^-.

$\partial^{13}C_{PDB}$ of carbonate precipitated from marine water should be near zero, and defines the upper limit of the scatter. However, the isotopic signature cannot differentiate between that

of HCO_3^- supplied directly from sea water, dissolution of aragonitic shell material within the sediment, or from previously deposited and dissolved carbonates. The $\partial^{13}C_{PDB}$ of organic matter is variable, and depends in plants on the photosynthetic pathway utilised, but if -20‰ to -25‰ is taken as a good approximation of the organic matter carbon isotope signature (section 1.10.3), then the values of $\partial^{13}C_{PDB}$ for the calcites analysed are within values expected for mixing of marine and organically derived HCO_3^-. They do not however give an indication of the timing of the organic matter oxidation, as to whether this occurred within the ironstone-formation or previously in the history of the meteoric fluid.

Similar trends in $\partial^{13}C_{PDB}$ values could be obtained within both the terrestrial and marine environment. In the former, organic matter oxidation would produce ^{13}C depleted CO_2 (≈ -25‰) that may dissolve forming carbonic acid that could dissolve previously deposited limestone of a marine isotopic signature (≈ 0‰). The resulting meteoric water may hence contain a range of $\partial^{13}C_{PDB}$ values depending on the number of moles of C derived from soil gas and limestone (see discussion in Moore 1989). Similar $\partial^{13}C_{PDB}$ values in the marine environment could result from both aerobic and anaerobic oxidation, with mixing from marine HCO_3^- and dissolving H.M.C. or aragonitic shell material. Further evidence as to the origin however, can be deduced from $\partial^{18}O_{PDB}$ signatures.

The values of $\partial^{18}O_{PDB}$ for the calcites are more consistent than for the $\partial^{13}C_{PDB}$, and hence represent a more constrained O origin. Two major factors control oxygen isotopic signatures of carbonates; temperature of precipitation, and the isotopic composition of the fluid. Using the temperature calculation given above, the data yield temperatures in the range 38.9 - 58.7°C for precipitation from a marine pore fluid of an $\partial^{18}O_{SMOW}$ isotopic composition of -1.2‰. Such temperatures cannot represent sea temperature, as this has been shown to be ≈ 20°C, and either a high heat flux in the sediment or precipitation at a burial depth of around 1km (assuming a thermal gradient of around 30°Ckm^{-1}) would need to be implied. Both are unlikely, as there is no evidence for a high heat flow on the East Midlands Shelf, and large burial depths were never attained for the Formation. The burial curve for the Bajocian Lincolnshire Limestone Formation given by Emery *et al.* (1988) may

be extrapolated, giving a maximum burial depth of around 600m during the late Cretaceous. A maximum burial temperature may be estimated by following the procedure of Emery *et al.* (1988) using their estimated parameters in the equation from Andrews-Speed *et al.* (1984);

$$T = T(s) + q(L/K).$$

where T = Temperature of the rock unit (°C); T(s) = surface temperature (°C); q = basal heat flow (Wm^{-2}); L = thickness of the overlying rock (m); K = conductivity of the rock unit of thickness L ($Wm^{-1}K^{-1}$). The estimates used by Emery *et al.* (1988) were T(s) = 15°C; q = $0.06Wm^{-2}$; and K = $1.66Wm^{-1}K^{-1}$. An additional thickness of 120m is added to the 522m overburden figure for the Lincolnshire Limestone, giving an approximate maximum burial temperature of 38°C. The isotopes are hence inconsistent with precipitation at high temperature alone, and it should be remembered that petrographic evidence strongly suggests cementation occurred early prior to any significant compaction, and are hence not "burial" cements.

Given that the normal marine isotopic signature is well defined, and temperature alone cannot explain the trend seen, the precipitating water is assumed to have been depleted in ^{18}O. Meteoric waters are a clear candidate for this precipitating fluid due to their large degree of possible variation in $\partial^{18}O_{PDB}$, but consistency within a given aquifer. Variation in $\partial^{18}O_{PDB}$ of meteoric waters reflects the amount of evaporation, condensation, and fluid-rock interaction that an initial marine water has undergone in the hydrological cycle. Evaporation at low latitude produces a ^{18}O depleted vapour due to the kinetic fractionation and preferential incorporation of the lighter ^{16}O isotope in the vapour phase. Rising of the vapour and poleward movement causes cooling and condensation, with subsequent rainfall heavier than the vapour phase, and continued ^{18}O depletion of the vapour. There is therefore a latitudinal control (see Yurtsever 1975) and continental effect (see discussion in Anderson and Arthur 1976). Given that the palaeoclimatology of the Jurassic world is largely unknown, it is impossible to predict the precise isotopic composition of meteoric water expected for Britain at this time, except that based on present day examples, it should be at least a few permil lower in $\partial^{18}O_{PDB}$. Marshall and Ashton (1980) and Emery *et al.* (1988) suggest that British Jurassic rainfall may have had a $\partial^{18}O$ of about -7 relative to the

sea water of that time based on a palaeolatitude of 35°N. The degree of interaction of the fluid with carbonate strata is undefined, particularly if a Pennine landmass is invoked in which Carboniferous Limestone would have been prominent. However, such light values of $\partial^{18}O_{PDB}$ are consistent with derivation of this carbonate cement from a meteoric source, and the whole isotopic trend is typical of a 'meteoric calcite line' as defined by Lohmann (1988).

A further possibility exists to explain the depletion of ^{18}O in the calcites, that of reduction of isotopically light soil-derived iron-oxides. It is possible in the development of lateritic type soil profiles, that Fe^{2+} liberated from basement rock could be oxidised by isotopically light meteoric waters, and thus retain a light $\partial^{18}O_{PDB}$ signature in precipitated goethites and hematites. This is supported by the extremely light $\partial^{18}O_{PDB}$ values recorded for Quaternary soils of the U.S.A. by Lawrence and Taylor (1971). They show that most weathering products in these soils have a $\partial^{18}O_{SMOW}$ of between +15 to +25‰ ($\partial^{18}O_{PDB}$ of -15.4 to -5.7‰). If these particles were transported and reduced in the marine environment, it is possible that this light oxygen could be incorporated into CO_2, and subsequently into calcite. Direct evidence for this is however lacking, and detailed isotopic data for soil iron-oxides are not apparent in the literature.

5.12.2.3) Interpretation.

On balance, the petrographic, compositional and isotopic data given above are suggestive of a significant input of meteoric water in the precipitating fluid for the sparry ferroan/manganoan calcites. This has important implications for the genesis of the Frodingham Ironstone Formation, with regard to the source of this water, and the input of significant quantities of Fe and Mn to this fluid. More specifically, an important question arises as to whether the waters themselves were enriched in Mn, or whether the Mn was added during post-oxic diagenesis within the sediment as described above. The former implies Mn enrichment towards the source of the water and not at the site of precipitation, whereas the latter possibility implies a meteoric water flux through the sediment during or shortly after deposition.

In situ Mn (and Fe) enrichment of low Mg/Ca meteoric waters within the sediment is favoured here due to:

1) The low solubility of Mn and Fe, prohibiting considerable transport in solution.

2) The lack of a suitable Mn-enriching mechanism other than the one proposed.

3) Clear evidence for post-oxic processes, operating prior to cementation by the ferroan calcite.

The implications of this to the diagenetic model for the formation of the ironstones, is discussed further in section **6**.3.

5.12.3) Non-Ferroan Calcites.

The non-ferroan calcites at the top of the ironstone-formation are highly restricted in occurrence, and their significance is uncertain. Their association with ferroan/manganoan calcites identical to those described above, suggests that their formation represents a local effect only, and possibly an event unrelated to the early diagenesis. However if primary, they indicate calcite precipitation from oxic waters in which no free Fe or Mn was present. The absence of pyrite discounts removal of Fe by the formation of the sulphide. Given that the beds above the "Snap Band" are reddened, it is possible that these calcites do record a period of higher oxygen input to the sediment associated with the more intense reworking of this upper sequence of the ironstone-formation.

5.12.4) Siderites.

As with ferroan calcites, the literature on siderite morphology, composition, and formation remains largely fragmentary, with particular concentration on its occurrence in fresh to brackish water sediments, relative to pyrite formation in marine sediments. Occurrences in the former regime are more common, with typical examples described by Ho and Coleman (1969), and Postma (1977 and 1982). Pye (1981, 1984), and Pye et al. (1990) describe siderite forming in modern saltmarsh sediments, and typical accounts of marine concretion formation are given by Hallam (1967), Raiswell (1971), and Gautier (1982) for example. Published analyses of these siderites are sparse, but some are given in table 5.10. The work of Matsumoto and Iijima (1981) is again of importance.

Table 5.10. Mol% Carbonate Compositions of Siderites From Various Localities, Cited in the Literature.

	1	2	3	4	5	6	7	8	9	10	11	12	13
Ca	0.1-7.6	4.2-11.3	11.1-18.8	9.0-11.1	26.9	3.0	2.0	2.0	9.0	10.0	11.0	10.0	11.0
Mg	1.1-19.8	6.5-19.1	12.9-16.2	14.1-15.6	6.2	10.0	12.0	9.0	11.0	11.0	11.0	13.0	16.0
Fe	73.5-89.8	72.7-86.0	64.1-71.9	68.4-81.5	66.8	75.0	81.0	85.0	79.0	78.0	78.0	76.0	72.0
Mn	1.0-14.3	0.8-4.1	0.9-1.7	1.8-2.3	n.d.	12.0	5.0	4.0	1.0	1.0	0.4	1.0	1.0

1	Curtis et al. (1986) — Concretions, L. Westphalian Coal Measures, Bull House Quarry, England.
2	Pearson (1974) — Concretions, Westphalian A, Hazlehead, England.
3	Carpenter et al. (1988) — 3 concretions, U. Cretaceous, Fox Hills Formation, N. Dakota.
4	Bjorlykke & Brendsdal (1986) — Cements, Rannock Formation, Brent Group, N.Sea.
5	Gehring (1990) — Cements, Northampton Sand Ironstone, Cowthick Pit, England. (Averaged)
6	Maynard (1986). E.P.M.A. Averages — Sokoman Iron Formation,Labrador Trough. Proterozoic.
7	" " — Weld Range, Australia. Archaean.
8	" " — Wabana Ironstone, Newfoundland. Ordovician.
9	" " — Mines a Poix, Hayange, France. Jurassic.
10	" " — Frodingham Ironstone, Scunthorpe, England. Jurassic.
11	" " — Northampts Ironstone, Corby, England. Jurassic.
12	" " — Marlstone Rock Bed, Wroxton, England. Jurassic.
13	" " — Cleveland Ironstone, Staithes, England. Jurassic.

The siderites of the Frodingham Ironstone Formation contain substantial Ca, Mg, and Mn, averaging 9.1-15.8 mol% $CaCO_3$, 12.9-20.2 mol% $MgCO_3$, and 4.1-8.2 mol% $MnCO_3$. They therefore span the range of compositions given in table 5.10, pure siderites being uncommon in sedimentary sequences. The high values of $MnCO_3$ are however unusual, being similar only to those values reported by Curtis *et al.* (1986) for the earliest cements within the concretions studied. The narrow range in values of the samples in this ironstone-formation, and the lack of low Mg, Ca, or Mn varieties is also noteworthy.

5.12.4.1) Discussion and Interpretation.

Siderite composition cannot be directly related to environment of formation, though it may be expected that high Ca-Mg varieties would be expected in siderites precipitated from marine waters due to the much higher concentrations of Ca^{2+} and Mg^{2+} in sea water. Matsumoto and Iijima (1981) found both high Ca-Mg, and low Ca-Mg siderites in freshwater sequences; Postma (1977) records high Ca-Mn siderite in a Recent Danish river bog, and later (1982), comparitively pure $FeCO_3$ at another locality; Curtis *et al.* (1986) showed freshwater siderites to have considerable compositional variation. Intertidal sediments of Norfolk, England, showed low Ca-Mg incorporation (Pye 1984, Pye *et al.* 1990) depite the marine influence. Matsumoto and Iijima (1981) and Carpenter *et al.* (1988) do however support a marine origin for high Ca-Mg siderites where sedimentological (and/or isotopic analysis) supports the interpretation.

Carpenter et al. (1988) commented that their siderite analyses of the Fox Hils Formation were almost identical to those of the brackish-marine Nanaura and Wakanabe Formations reported by Matsumoto and Iijima (1981). It is interesting, and possibly significant, to note that those of the Frodingham Ironstone are also similar, but further data from other sources (particularly of marine siderites) would be required before any inference is drawn from this.

Siderite formation is expected in sediments where maintained sulphide levels are very low, HCO_3^- is abundant, and Fe^{2+} is liberated into the pore waters (section 1.8 above), as found during post-oxic diagenesis, or methanogenesis. Ca and Mg are incorporated into the

siderite, from three main sources in the marine environment:

1) Pore fluids, either trapped or from sea water flow within the sediment.

2) Diffusion from overlying sea water.

3) Dissolution of carbonate debris and cements (with Mg from H.M.C.).

All three sources probably supplied Ca^{2+} and Mg^{2+} to the Frodingham siderites. The high permeability of the ironstone-formation would allow free fluid flow and diffusion, particularly important for Mg introduction, with the high proportion of bioclastic debris undergoing dissolution/replacement (with siderite as the carbonate replacement in some samples) supplying additional Ca and minor Mg.

The high Mn content of the siderites is particularly indicative of an early formation, as Mn^{2+} was liberated during early diagenesis. The Mn^{2+} levels were not significantly elevated by berthierine formation (section **5**.10), so that substantial manganese reduction must have taken place at the time of formation.

5.12.5) Ankerite / Ferroan Dolomite.

It is perhaps surprising given the presence of ferroan calcites and siderites, that ankerite or ferroan dolomite is not more common, being highly restricted in occurrence. This appears to be true of ironstones in general, with ankerite cementation subordinate to ferroan calcites and siderites (for example Garzanti *et al.* 1989). Most descripitions of ankerites in sedimentary rocks refer to reservior sandstones (for example Kantorowicz 1985, Boles 1978), but ankerite and ferroan dolomites has been found in coal measures sequences (Dunham 1960, Matsumoto and Iijima 1981, Curtis and Coleman 1986), and occasionally early diagenetic concretionary horizons (Irwin *et al.* 1977). Ankerite formation requires the presence of Mg and Fe that is usually assumed derived from marine pore waters, but at deeper diagenetic levels the illite-smectite transition (Boles 1978) and cation release from hydrocarbon source rocks (Kantorowicz 1985) has been inferred.

It would appear that despite the free availability of necessary cations present to form ankerite in the ironstone-formation, that the problem of its formation is directly akin to that

of dolomite, "...the most stubborn question in carbonate geochemistry..." (Krauskopf 1979 p 70), and cannot be resolved here. However, if as some authors have argued (for example Curtis and Coleman 1986), based on experimental work in the literature, that SO_4^{2-} inhibits dolomite precipitation, (see section **5**.11.4), then there is mineralogical evidence to suggest that SO_4^{2-} was not depleted during ironstone deposition. It is also interesting to note that most of the occurrences described above are organic-rich, or organic associated, and that the ankerite of the Frodingham Ironstone Formation is associated with a phosphatic horizon, and a highly U.V. fluorescent layer.

PART 2: OTHER MINERALS.

5.13) Sulphides (Pyrite).

Pyrite was the only sulphide mineral clearly identified in the ironstone-formation and forms only a small overall proportion of the iron minerals in the ironstones. It is usually most abundant in the muddier sediments. The most significant occurrence of pyrite is within the "Snap Band" where it is found replacing the whole fabric of the ironstone. Pyrite may be described as four forms within this ironstone-formation; framboidal, massive, cubic, and platy.

5.13.1) Framboidal.

Framboidal pyrite occurs as small dispersed aggregates in a spheroidal habit, usually <30μm across, but some framboids may exceed 60μm. This type of pyrite is largely absent within the ironstone sequence itself, even within the muddier sediments, but is common within the transitional beds at the base of the ironstone-formation, where it is commonly associated with organic matter.

5.13.2) Massive and Cubic.

Pyrite in the ironstone-formation does not readily form a distinct cubic habit, only doing so where the crystal size is small (plate 12c), so is usually of a massive form. Occasional cubic faces on outer surfaces may be present. Massive pyrite is uncommon in the bulk of the ironstones, but is present in significant quantities within the "Snap Band", where it preferentially replaces berthierine ooids (plate 22a) and matrix, and occasionally carbonate debris. The fabric of the matrix is usually totally destroyed, but the ooid shape and crude internal fabric may remain, suggesting preferred replacement of certain layers in the ooid. Significantly, these ooids are usually undeformed, and thus replacement must have occurred pre-compaction.

5.13.3) Platy.

Commonly, pyrite forms thin plates up to 2.5mm in length, that may radiate from a centre, interlock slightly, or be aligned roughly parallel to each other (plate 22b). The plates

PLATE 22

Pyrite, Phosphate and Barite in Thin-Section

A) Pyrite replacing ooids in the "Snap Band", specimen YAR. 22. Photo length is equivalent to 3.3mm.

B) Platy pyrite and authigenic phosphate, specimen YAR. 7 (crossed polars). A shell fragment in an ooidal wackestone has dissolved and been replaced by a thin isopachous rim of phosphate (PH), and large pore-bridging crystals of pyrite (PY). A ferroan calcite cements the pore. Photo length is equivalent to 3.3mm.

C) Pyritised coquina from the shales above the Frodingham Ironstone Formation, Yarborough Pit, specimen YAR. A. The degree of pyritisation in this coquina can be contrasted with the coquinas and grainstones of the ironstones under discussion. Photo length is equivalent to 3.3mm.

D) Barite precipitated within a *Gryphaea* shell, specimen YAR. 14. Photo length is equivalent to 0.7mm.

A	B
C	D

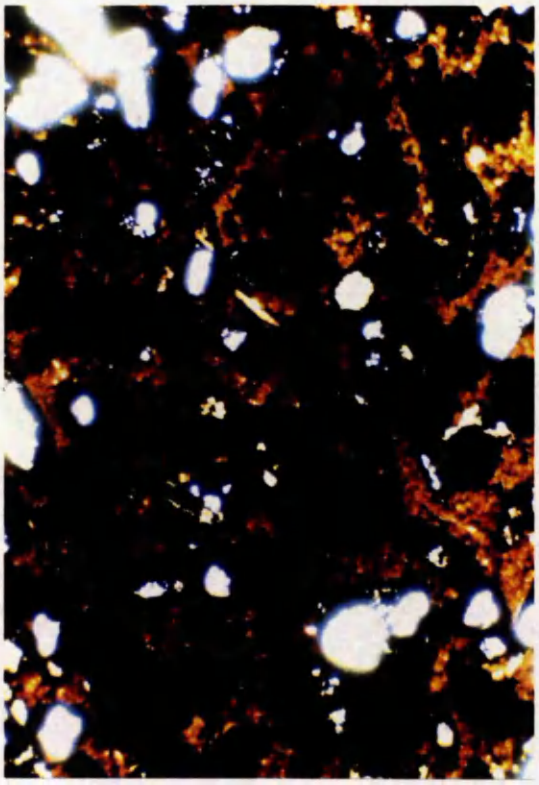


PY
K-PH

are straight to slightly curved, with rough faces and indistinct terminations. The plates occur as aggregates in grainstones through to mudstones, but occur only in voids within the latter. This pyrite often occurs in direct association with authigenic phosphate which predates it. Most indications of this form of pyrite suggest that it was formed later in the cementation history. In DRAG. 31.28, the pyrite postdates siderite and berthierine formation, and possibly replaces the second generation of the latter. It is however usually seen postdated by the ferroan/manganoan sparry calcite.

Under reflected light with near crossed polars, parts of the pyrite shows marked anisotropy suggesting the possible presence of marcasite, but X.R.D. traces of drilled sub-samples showed no iron sulphides other than pyrite. The anisotropy and crystal habit does however suggest that the pyrite is replacive after marcasite.

5.13.4) Discussion.

Framboidal and massive/cubic pyrite are typical habits of pyrite found within sediments in the geological record, and are abundant in the sediments above the ironstone-formation. The absence of pyrite within the ironstone-formation itself is an integral part of delineating the diagenetic history of the Formation, and suggests that the rate of supply of decomposable organic matter, dissolved sulphate, or reactive detrital iron minerals (Berner 1970, 1984) was possibly lowered during ironstone deposition. Given the iron-rich nature of the sediment deposited in fully marine conditions, it is apparent that the organic matter quantity and type was a primary controlling factor on pyrite absence. The post-oxic diagenetic concept suggests that organic matter was rapidly biodegraded by bacteria to levels unable to support sulphate reduction, so that sulphur was not released for pyrite formation. The general absence of pyrite within the Formation (compare plate 22c with all grain-ironstones) is hence in good agreement with this hypothesis. The abundance of pyrite within the "Snap Band" may therefore represent a period of greater sedimentation rate such that organic matter was rapidly buried to below the level of oxygen diffusion and intensive bioturbation, so that a larger amount of organic matter remained unoxidised and able to support sulphate reducing bacteria.

The presence of pyrite of a platy form, presumed to be replacive after marcasite, has significant implications for the genesis of the latter. Marcasite is an orthorhombic dimorph of pyrite (cubic) that is much less common, being described mainly from the Coal Measures and the Chalk. Little is known about the conditions necessary for marcasite formation relative to pyrite, but it is suggested that more acidic conditions favour marcasite precipitation (pH<5 Murowchick and Barnes 1986). Petrographic examination does not show the platy pyrite to be associated with extensive carbonate solution, and it seems unlikely therefore that the pH could have been lowered significantly. Krauskopf (1979) suggested that pyrite and marcasite give no quantitative information on pH, and this might be supported here.

It is here believed that the relative roles of iron and sulphate reduction may have affected the mineral species formed rather than pH, and in particular the dominance of iron reduction over sulphate reduction. No quantitative information can however be given. An organic control is likely, due to the common association of platy pyrite with authigenic phosphate formation.

5.14) Phosphates.

Authigenic phosphate cements have been identified in a number of sections from the upper part of the ironstone-formation, particularly from the "Snap Band" (plates 14d, 22b). The phosphate occurs as a thin, pore-lining cement, of small (<30μm) crystals of low birefringence, resembling chert or fine quartz. Discernable crystals are usually nearly square in section, with the expected hexagonal shape being much less common. These cements are not abundant, and rarely attain a thickness more than a few crystals thick. To some extent, the presence of phosphate may be predicted, as it is always associated with one or more of the following; authigenic berthierine formation, complex carbonate cements (including those with undulose extinction), and platy pyrite.

Phosphate crystals of a different morphology were found in DRAG. 31.22 where elongate rhombic crystals up to 60μm are associated with an ankerite cement. Similar

crystals as described above are also present replacing shell debris and echinoderm fragments (see section 5.9.1.2). Larger crystalline phosphate, with crystal size up to 250μm were observed in YAR.22 associated with the complex 'arboraceous' siderite. These crystals are nearly isotropic, and are zoned in one section.

Compositions of the phosphates were obtained by E.P.M.A. (table 5.11), and recalculated to a structural formula on the basis of 26 (O, OH, Cl, F) (Deer et al. 1962). More complex calculations, such as used by Manheim and Gulbrandsen (1979) were not attempted, as CO_2, Cl, and F were not measured. The intention here was to simply identify the mineral phases present. Though Cl was measured in one set of data, all analyses were similarly calculated without including Cl, to allow direct comparison. The data fit well with apatite compositions based upon a $Ca_{10}(PO_4)_6(OH,F,Cl)_2$ composition and structure. The total P is however less than the value of 6.00 indicated here (reaching as low as 5.27), suggesting the presence of $(CO_3^{2-}.F)$ substitution for the PO_4^{3-} (Binder and Troll 1989), and hence indicating a carbonate-apatite composition. Some SO_4^{2-} may however also be included within the replaced echinoids of Drag 31.22. Since F, Cl, and CO_2 were not measured, precise identification within the carbonate-apatites, perhaps to francolite (>1% F) or Dahllite (<1% F) is not possible, though the former is almost certainly the case due to the totals obtained. The Ca content is slightly higher than the expected value of 10, and may indicate the presence of admixed calcite within the phosphate, since the apatites of YAR. 7 were pre- and postdated by calcite cements, and the DRAG. 31.22 analyses were from replaced echinoid debris, and an ankerite cement generation. These apatites also contain small amounts of Fe, Mg, Na, and Sr, substituting for the Ca, consistent with the variable composition of the carbonate fluorapatites (see McClellan 1980).

5.14.1) Discussion.

Carbonate fluorapatite is the main constituent within present day marine phosphorites (Manheim and Gulbrandsen 1979), and may form either by authigenic precipitation, or by carbonate replacement. In the ironstone-formation, the former is represented by the finely crystalline, pore-lining apatites, that clearly form a cement generation, and the larger zoned

Table 5.11. Average Phosphate Compositions in the Frodingham Ironstone Formation, Obtained By E.P.M.A. The Data have been Recalculated to Phosphate Formulae (26 (O, OH, Cl, F)).

	YAR. 7.			DRAG. 31.22 ECHINOIDS			CEMENT.	
	AVERAGE	STDEV		AVERAGE	STDEV		AVERAGE	STDEV
Si	0.039	0.132		0.466	0.149		0.004	0.001
Ti	0.017	0.021		0.076	0.122		n.d.	n.d.
Al	0.039	0.065		0.350	0.085		0.005	0.004
Fe	1.063	0.463		1.294	1.053		2.955	0.801
Mn	0.071	0.081		0.143	0.205		0.761	0.151
Mg	0.046	0.059		0.197	0.130		0.912	0.291
Ca	36.720	0.630		36.810	1.252		34.228	1.719
Na	1.043	0.130		0.564	0.101		0.531	0.068
K	0.020	0.024		0.096	0.040		n.d.	n.d.
P	15.533	0.894		14.171	0.564		12.421	1.154
Sr	n.d.	n.d.		n.d.	n.d.		0.231	0.022
S	0.000	0.000		0.219	0.075		n.d.	n.d.
Cl	n.d.	n.d.		0.006	0.012		n.d.	n.d.
TOTAL	90.123	1.979		89.039	1.589		83.659	3.328
PhosphCalc.								
Si	0.018	0.061		0.199	0.061		0.002	0.001
Ti	0.004	0.005		0.019	0.031		n.d.	n.d.
Al	0.017	0.031		0.155	0.036		0.002	0.002
Fe	0.226	0.112		0.282	0.240		0.706	0.233
Mn	0.015	0.017		0.032	0.047		0.184	0.047
Mg	0.023	0.029		0.098	0.066		0.501	0.190
Ca	10.731	0.167		11.028	0.249		11.257	0.182
Na	0.531	0.061		0.295	0.052		0.304	0.026
K	0.006	0.007		0.029	0.013		0.000	0.000
P	5.867	0.176		5.492	0.106		5.277	0.225
	n=12			n=8			n=3	

crystals of YAR.22. The latter is seen in the replacement of echinoderm debris. Detrital phosphates such as bone or scales were not seen in any section, but may be collected in the field.

Phosphate is liberated from organic molecules during oxidation, that combines with Ca and other free cations to form authigenic precipitates. For example, in the oxidation of the 'Redfield (1958) molecule':

$$(CH_20)_{106}(NH_3)_{16}(H_3PO_4) + 106O_2 \text{ ----> } 106\ CO_2 + 16\ NH_3 + H_3PO_4 + 106H_2O$$

(Taken from Froelich *et al.* 1979).

Dissociation of the H_3PO_4 liberates $H_2PO_4^-$ (acid conditions) or HPO_4^{2-} (alkaline solutions), the latter of which is commonly used in apatite formation. Oxidation via oxidants other than O_2, has the same effect. The presence of authigenic phosphate in thin-sections is hence clear evidence for the microbial decay of organic matter.

5.15) Sulphates (Barite).

Barite ($BaSO_4$) was seen as large rectangular crystals up to 1.5cm long within a single specimen of a *Gryphaea* (plate 22d). The mineralogy was confirmed by X.R.D. The crystals are present within berthierine mud that fills the internal cavity of the *Gryphaea*, and probably grew replacing the matrix. The origin of this barite is uncertain, but of minor importance.

CHAPTER 6: CONCLUSIONS ON THE FRODINGHAM IRONSTONE FORMATION AND IMPLICATIONS FOR THE GENESIS OF OTHER OOIDAL IRONSTONES.

6.1) Introduction.

This chapter is divided into two parts. The first concludes the discussion on the genesis of the Frodingham Ironstone Formation, by summarising the present research and the proposed sedimentological and diagenetic models for its evolution. Other ooidal ironstones of the British Jurassic examined during this research are then briefly described in the second part, and compared to the Frodingham Ironstone Formation in order to refine and extend these models.

PART I. The Frodingham Ironstone Formation:

6.2) Summary and Discussion.

The Frodingham Ironstone Formation was deposited on the north-western margin of the East Midlands Shelf over approximately 2-4 Ma during the Sinemurian Stage, Lower Jurassic. It is a condensed sequence (11m maximum thickness) within the Lower Lias shales of South Humberside, and thins laterally to marine shales. Sedimentological evidence suggests that the ironstone-formation was deposited in 'normal' shallow-marine waters under the influence of storm activity, at or near storm wave base. Periodic storms were responsible for supplying sediment, and for producing minor fining sequences that were constantly reworked. A full shallow marine fauna existed during fairweather periods and resulted in extensive bioturbation of the sediment.

The non-authigenic component of the ironstones comprises ooids, bioclasts (principally bivalves, brachiopods, cephalopods and echinoderms) and detrital clays, with occasional pisoids and intraclasts. These components are present in variable quantities, and formed mud-ironstones through to grain-ironstones depending on the energy of deposition within the storm cycle, fair weather phase, or reworking event.

The iron-ooids are interpreted to have formed within the sediment, which resulted in the formation of a primary distinctive oblate spheroidal shape. A three stage cortical growth pattern developed in goethitic ooids by accretion upon a goethitic nucleus, but the constraints on the formation of this structure are poorly defined. It is believed that the goethite is primary, and that the berthierine within these ooids formed by direct precipitation within the sediment, or by later diagenetic modification of detrital clays trapped within the ooid cortex. Berthierine ooids are texturally different to goethitic ooids, but possess a similar shape, and are believed to have formed by direct precipitation of berthierine only.

Berthierine was usually the first formed authigenic mineral, but may postdate aragonite dissolution and the formation of early scalenohedral and 'fibrous' calcite cements. Berthierine replacement of echinoderm debris suggests that it was forming during the H.M.C.-L.M.C. transition. Berthierine composition is consistent despite the variety of morphologies and modes of occurrence of the mineral. An average composition of 92 authigenic berthierine cements is:

$(Ca_{0.073}Na_{0.095}K_{0.009})(Fe_{3.857}Mg_{0.871}Mn_{0.005}Ti_{0.004}Al_{0.992})(Si_{3.291}Al_{0.709})O_{10}(OH)_8$

It is believed that berthierine formed by the destabilisation of detrital clay minerals (illite/kaolinite) and iron-oxides during the early diagenesis of the ironstone-formation. This resulted in the *in situ* transformation of detrital muds to berthierine, and the formation of authigenic cements where full breakdown of the detrital clay into solution occurred. No post depositional enrichment of Si or Al was hence required for berthierine formation, with the small amount of Mg being obtained from sea water. The Fe was liberated during the microbial oxidation of organic matter for which iron-oxides were utilised as the oxidant. Berthierine formation is believed to have been continuous during the deposition of the ironstone, and was not restricted to a single post-depositional event.

Siderite precipitation postdates the berthierine formation and resulted in the partial replacement of all modes of occurrence of berthierine, and the precipitation of thin cements within pore space. The siderite contains significant Ca, Mg, and Mn (averaging 9.1-15.8 mol% $CaCO_3$, 12.9-20.2 mol% $MgCO_3$, and 4.1-8.2 mol% $MnCO_3$), and is interpreted to

have precipitated from marine pore waters enriched in Fe and Mn. Siderite was usually only formed in association with the berthierine rich beds, and exhibits a complex suite of morphologies. Ferroan/manganoan calcite forms the largest authigenic component of the ironstone-formation, comprising in places up to 57.5% of the rock. The Fe and Mn content varies inversely, with typical values of 1-4 mol% carbonate of each. The coarse sparitic calcite postdates both berthierine and siderite, and its low $\partial^{18}O$ isotopic signature (-6.0 to -9.43‰) and Mg content suggest that it was precipitated from meteoric waters. Ankerite was found in only one sample.

Minor authigenic phosphate was precipitated due to the breakdown of organic matter, and is usually associated with berthierine formation. Pyrite is present in significant quantity only within the "Snap Band" where it extensively replaces berthierine. 'Platy' pyrite is interpreted to have replaced marcasite, and usually postdates berthierine and siderite formation.

6.3) Diagenetic Evolution: Conclusions and Discussion.

The bulk mineral assemblage of the Frodingham Ironstone Formation fits well with the original hypothesis behind this research, i.e. that iron and manganese reduction dominated over sulphate reduction as the mechanism for microbial oxidation of organic matter, during the early 'sub-oxic' diagenesis of the ironstones. This resulted in the formation of berthierine, siderite and ferroan/manganoan calcites, but not pyrite. It is believed that the conditions of constant reworking by physical and biological processes degraded the available organic matter to levels unable to support sulphate reducing bacteria. Iron and manganese oxides/hydroxides were however reduced, which liberated these elements into pore fluids, and maintained the sediment in a post-oxic condition, similar to that reported for the muds of the Amazon River Delta by Aller *et al.* (1986). Production of these conditions was only possible due to the low net rate of sedimentation of the ironstones.

The formation of the major authigenic minerals may be tentatively given as:

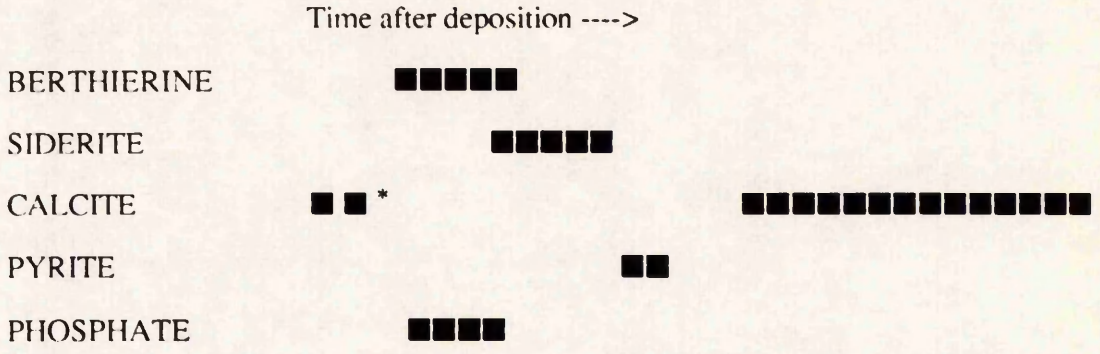

* indicates early scalenohedral and fibrous cements

The earliest calcite cements are believed to result from dissolution of aragonitc bioclastic material, with subsequent precipitation as thin scalenohedral and 'fibrous'/prismatic cements. Biofilms remained largely intact and acted as sites for subsequent carbonate nucleation. These cements are ferroan/manganoan, and it is suggested that this may be the primary mineralogy, and not necessarily a replacement of a former H.M.C. or aragonite cement.

The diagenetic sequence post-dating the earliest ferroan/manganoan calcites follows that which might be predicted for a sediment undergoing continued iron-reduction during minor burial with marine pore waters, followed later by a meteoric water influx. As described in section 1.10.1 the diagenetic reaction most likely to lead to the generation of iron-silicates is iron-reduction:

$$2Fe_2O_3 + CH_2O + 3H_2O \text{ -----> } 4Fe^{2+} + HCO_3^- + 7OH^-$$

It is believed that the onset of this reaction and increasing levels of Fe^{2+} within the sediment led to the destabilisation of the detrital clay mineralogy, and subsequent berthierine formation. Continued iron-reduction would however have lead to increasing concentrations of HCO_3^- which would not have been removed from pore waters by the precipitation of berthierine. The increasing HCO_3^- concentration led to iron-rich carbonate precipitation in favour of the silicate, and the available Fe was incorporated into siderite. Pyrite was formed later, when sulphate reducing bacteria utilised the free sulphate in any trapped sea water, as supplies of reactive detrital iron oxides/hydroxides became exhausted. The extensive pyrite

formation in the "Snap Band" is believed to have formed due to increased sedimentation rates for this berthierine ooidal bed, which led to the preservation of organic matter in greater quantity and of better quality than that of the rest of the ironstones, which allowed sulphate reduction to occur.

A meteoric water source for the generation of sparry ferroan/manganoan calcites is typical for many sediments, but requires some discussion here because the calcites of this Formation were not precipitated at any significant depth, and suggest that meteoric waters flushed through the ironstone-formation after only shallow burial. Possible sources of meteoric water for shallow marine sediments are outlined in figure 6.1. The scenario shown in 6.1(a) is unlikely to be of importance, because the meteoric water 'floats' on the denser marine water, and hence meteoric diagenesis would be expected to precede marine diagenesis. A gravity-driven flow of water is possible (figure 6.1(b)), but the lack of significant terrigenous clastics, and a kaolinitic/iron oxide detrital mineralogy to the Formation, suggests that any adjacent landmass was low lying, and that any hydraulic head can only have been small. The only available aquifer for fluid flow is the ironstone-formation itself, and use of this model is constrained by the lack of outcrop data for the more proximal ironstone sediments.

A localised floating meteoric lens as shown in figure 6.1(c) could have formed if the sediments had become exposed at some stage. This is more likely to have occurred if Hallam's (1963) suggestion of ironstone formation on a shoal is followed, but there are no signs of emergence within the sequence seen today. It is however possible that such evidence may have been subsequently removed during reworking and erosion.

Comparison of the Frodingham calcites can be made with those of the Lincolnshire Limestone Formation that also formed on the East Midlands Shelf, but later during the Bajocian Stage (Middle Jurassic). The Formation is described by Emery *et al.* (1988) who suggest that the late ferroan calcites of this formation were precipitated by mixed marine and meteoric waters moving updip from the basin. The $\partial^{18}O_{PDB}$ signature of the calcites

Figure 6.1. Possible Hydrologic Settings for the Introduction of Meteoric Water into the Shallow Marine Environment. Taken From Moore (1989, figure 6.9 p.173).

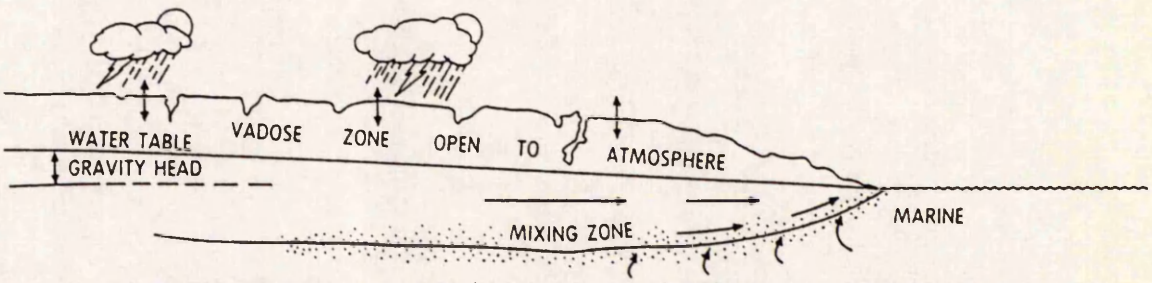

A. Unconfined Gravity-Driven Regional, Meteoric Aquifer Floating on Marine Water

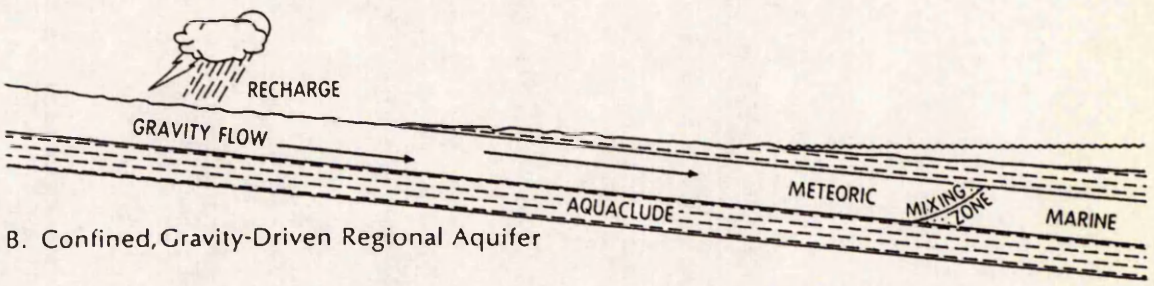

B. Confined, Gravity-Driven Regional Aquifer

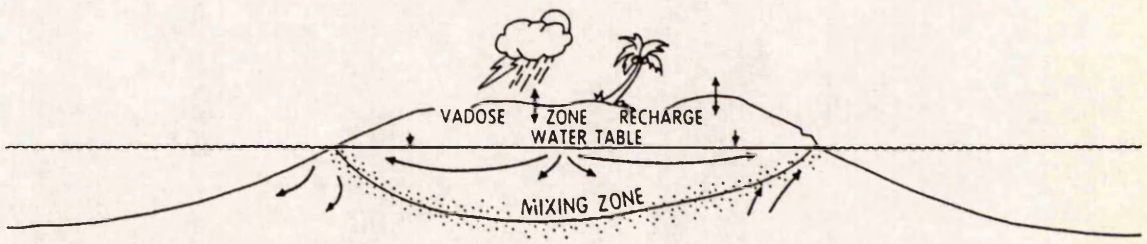

C. Local, Floating, Meteoric Lens

(≈ -6‰ to -11‰) is nearly identical to those reported here, but the $\partial^{13}C_{PDB}$ ranges from ≈ -2‰ to +3‰, and hence lacks the organic isotopic signature of the ironstone-formation. The presence of a similarly derived basinal fluid cannot be supported for the Frodingham Ironstone Formation due to the difference in $\partial^{13}C_{PDB}$ isotopic signatures, and more importantly the lack of a suitable aquifer for fluid movement, given that the Formation thins rapidly eastwards and passes into shales (section **2**.3.2).

The source of the meteoric water is hence problematical, as is the origin of the Fe and Mn within this water. Enrichment of Fe and Mn by similar post-oxic processes within the basin of ironstone deposition is favoured, as it is possible that iron and manganese reduction initiated during marine diagenesis could have continued after an influx of meteoric water. This would have further suppressed any sulphate reduction by dilution of dissolved sulphate, but whether this may have effected initial berthierine and siderite formation is unknown.

PART II. Other Jurassic Ooidal Ironstones.

Four other ooidal ironstone-formations of the British Jurassic, the Cleveland, Banbury, Raasay and Abbotsbury, were examined and compared to the Frodingham Ironstone Formation. The applicability of conclusions derived from the examination of the Frodingham ironstones to a wider suite of examples could hence be postulated. Unless otherwise stated, similar methods of analysis were used as for the Frodingham investigations.

6.4) The Cleveland Ironstone Formation.

6.4.1) Introduction.

The Cleveland Ironstone Formation was extensively mined in the earlier part of this century, but today mines are infilled and examination is restricted to natural exposures. The ironstone-formation outcrops around the edge of the North Yorkshire Moors (figure 6.2), though the inland exposures are few in number and of poorer quality than the coast. The type-section of the Formation is on the coast at Staithes (NZ 794183 to NZ 783191), where it is readily accessible at low tide (figure 6.3, plate 23a). The ironstone-formation has been recently studied on a lithostratigraphical and sedimentological basis by Howard (1985) following on from the work of Howarth (1955), Chowns (1968), Greensmith *et al.* (1980) and Rawson *et al.* (1982), who correlated outcrops and categorised the depositional cyclicity within the sequence. The geochemistry of the ironstones have however not been defined in detail, with bulk rock analyses of ironstones and overlying sediments having been described by Catt *et al.* (1971) and Gad *et al.* (1969) respectively.

Chowns 1986

The examination of this ironstone-formation was undertaken in collaboration with Dr. T. Young of Cardiff University. Thin-sections of the Staithes outcrop supplied by Dr. Young were examined petrographically and analysed by E.P.M.A., with the aim of combining these data with sedimentological investigations and bulk-rock analysis of the ironstone-formation being undertaken by Dr. Young. The combined data set will be published as a full joint publication, though preliminary results of this research are given in Young *et al.* (1990), enclosed at the back of this thesis. Also presented in this paper is a summary of the

Figure 6.2. Outcrop Map of the Staithes Sandstone and Cleveland Ironstone Formations in North-east Yorkshire. Taken From Howard (1985, figure 1).

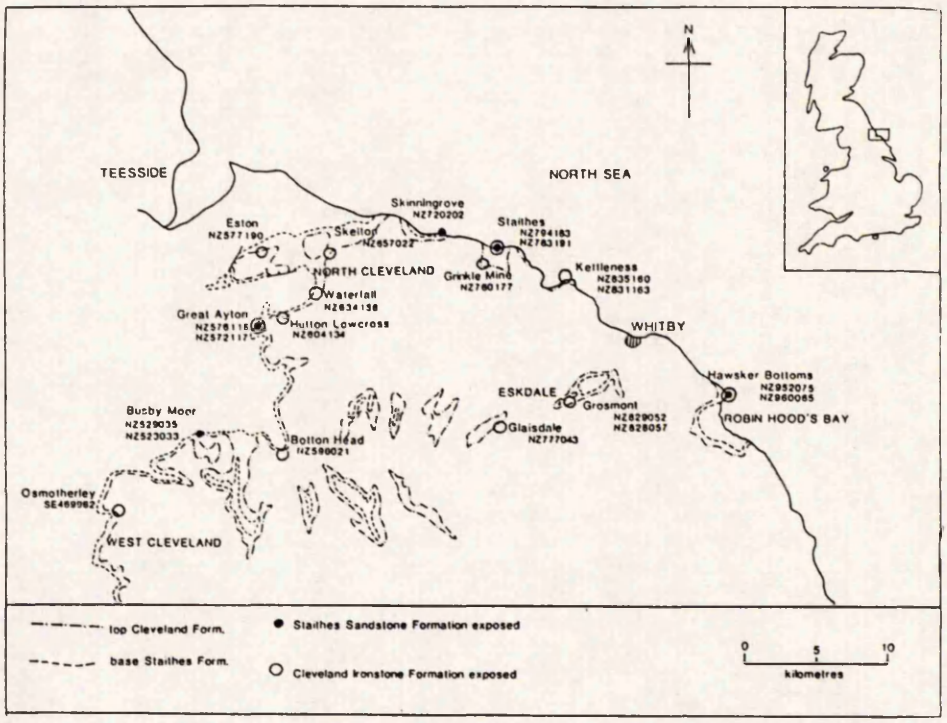

Figure 6.3. Geological Map of the Foreshore at Staithes, North-east Yorkshire, Showing the Outcrop of the Cleveland Ironstone Formation. Taken From Howarth (1955, figure 12).

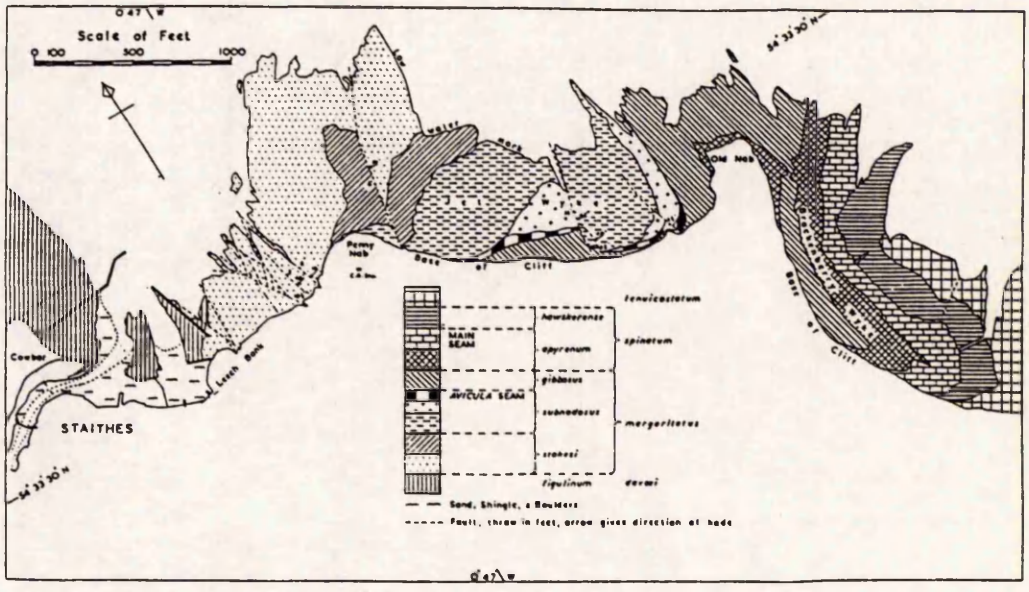

PLATE 23

The Cleveland Ironstone Formation 1.

A) Outcrop of the upper part of the Penny Nab Member, and full sequence of the Kettleness Member of the Cleveland Ironstone Formation at Old Nab, Staithes. The ironstone seams labelled are the Two Foot (TF), Pecten (P), Main Seam Lower (Ml) and Main Seam Upper (Mu).

B) Typical siltstone between ironstone seams, thin-section, specimen STH. 40. The rock is bioturbated and contains fine quartz, muscovite, detrital clay, organics and pyrite. Photo length is equivalent to 1.3mm.

C) Typical appearance of a siderirised ironstone seam, thin-section, specimen STH. 34. The initial rock texture (see **B**) has been totally lost on replacement by finely crystalline siderite. Photo length is equivalent to 1.3mm.

D) Intact berthierine ooids, thin-section, specimen STH. 45. The ooids have an oblate spheroidal shape with berthierine nuclei of unstructured particles and foliated flakes. The rock is cemented by coarse crystalline siderite. Photo length is equivalent to 3.3mm.

A	B
C	D


Mu
MI
P
TF

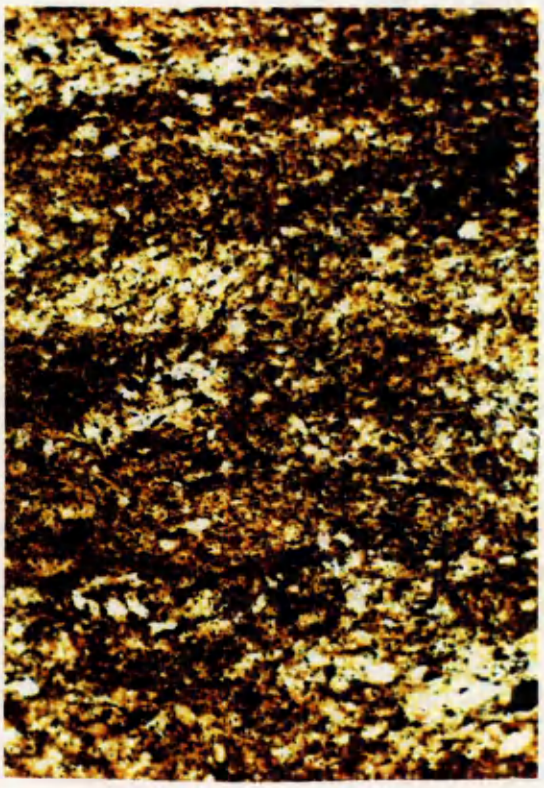

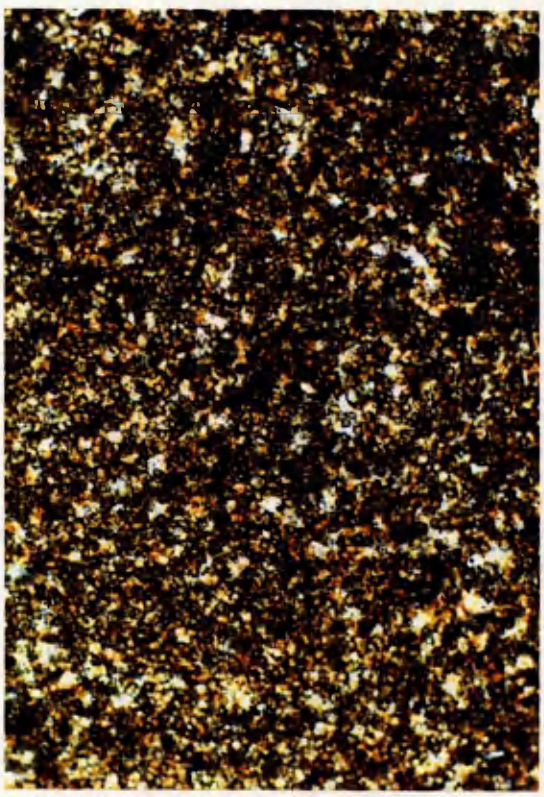

sedimentology of the sequence and so will not be duplicated here. The following is a petrographic examination of the ironstone-formation, with the E.P.M.A. results obtained, to compare the Frodingham and Cleveland ironstone-formations.

6.4.2) Petrography.

Figure 6.4 shows a sedimentological log of the ironstone-formation with the sample numbers as referred to in the text marked upon it. Point-count analyses of these samples are given in table 6.1, and indicate the relative abundance of the components described individually below. The present investigation, was particularly directed to identifying differences between ironstone seams which are prominant at outcrop, and the interbedded muds and silts, some of which are also ironstones. Typical fabrics are illustrated in plates 23 and 24.

6.4.2.1) Quartz.

Quartz is present as monocrystalline, angular to subrounded, silt to fine sand sized grains 30-100μm across, dispersed within the matrix, or occasionally concentrated by bioturbation. The greatest abundances (up to 15.5%) are found outside the ironstone seams, particularly between the Two-Foot and Pecten Ironstones. A few percent may be found within the seams, but the interbedded muds usually have a significantly greater proportion.

6.4.2.2) Muscovite.

Flakes of muscovite are small, typically 50-100μm long. Muscovite is associated with quartz, and a clear positive correlation in their abundances can be demonstrated. Muscovite is therefore most common in the interbedded muds, but rarely forms a significant proportion of the rock. Muscovite can be confused in some sections with berthierine flakes, especially where a green colouration has been imparted to the muscovite. Birefringence colour is then the only method of distinguishing between the two.

6.4.2.3) Berthierine Flakes.

Within the berthierine matrix of some specimens, a foliated structure can be seen that is commonly, but not always, a distinct particle (plate 24d). These particles have been

PLATE 24

The Cleveland Ironstone Formation 2.

(Thin-section Photomicrographs).

A) "Spastoliths", specimen STH. 36. These berthierine ooids have not been cemented or replaced by siderite, and have hence undergone extensive plastic deformation parallel to bedding during compaction. Photo length is equivalent to 1.3mm.

B) Goethite ooids, specimen STH. 46. This is the only occurrence of goethite ooids in the Staithes samples studied, and are present in the only grainstone. The ooids are considered to be oxidised berthierine ooids, as little structure is visible within them. Ferroan calcite cements the specimen. Photo length is equivalent to 3.3mm.

C) Kaolinite replacing berthierine ooids, specimen STH. 32 (crossed polars). Some relict berthierine is present within the ooids (arrowed), particularly at the edges. The matrix has been intensely replaced by siderite. Photo length is equivalent to 1.3mm.

D) Berthierine flakes, specimen STH. 30 (crossed polars). The difficulty in differentiating between berthierine flakes and muscovite is illustrated in this specimen, by comparison between the low to medium birefringent platy particles arrowed. Photo length is equivalent to 0.7mm.

A	B
C	D

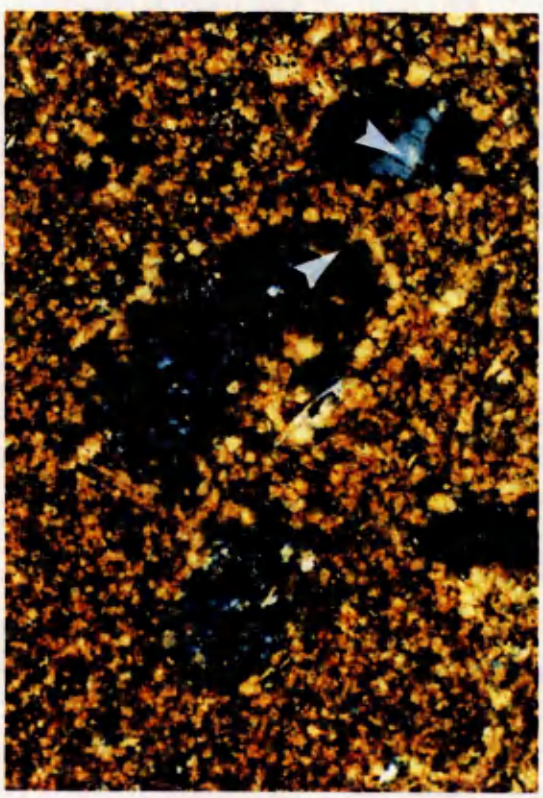

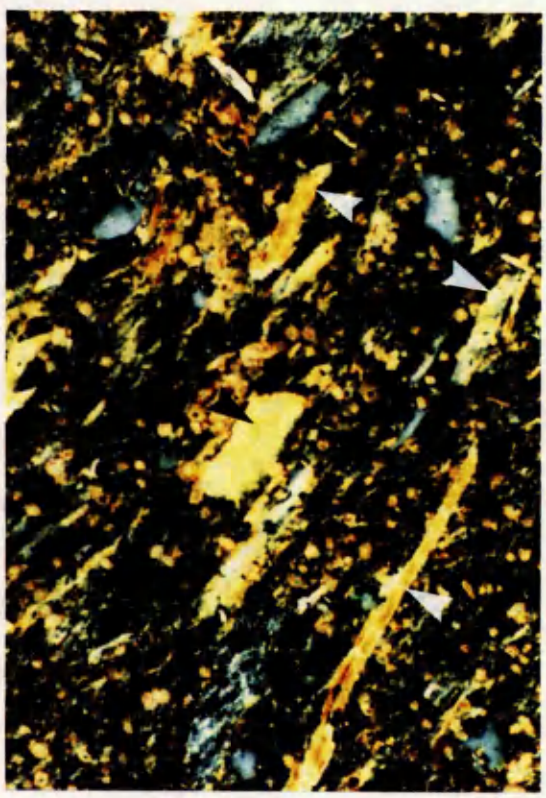

Figure 6.4. Sedimentological Log of the Staithes Section of the Cleveland Ironstone Formation, With Sample Numbers as Referred to in the Text.

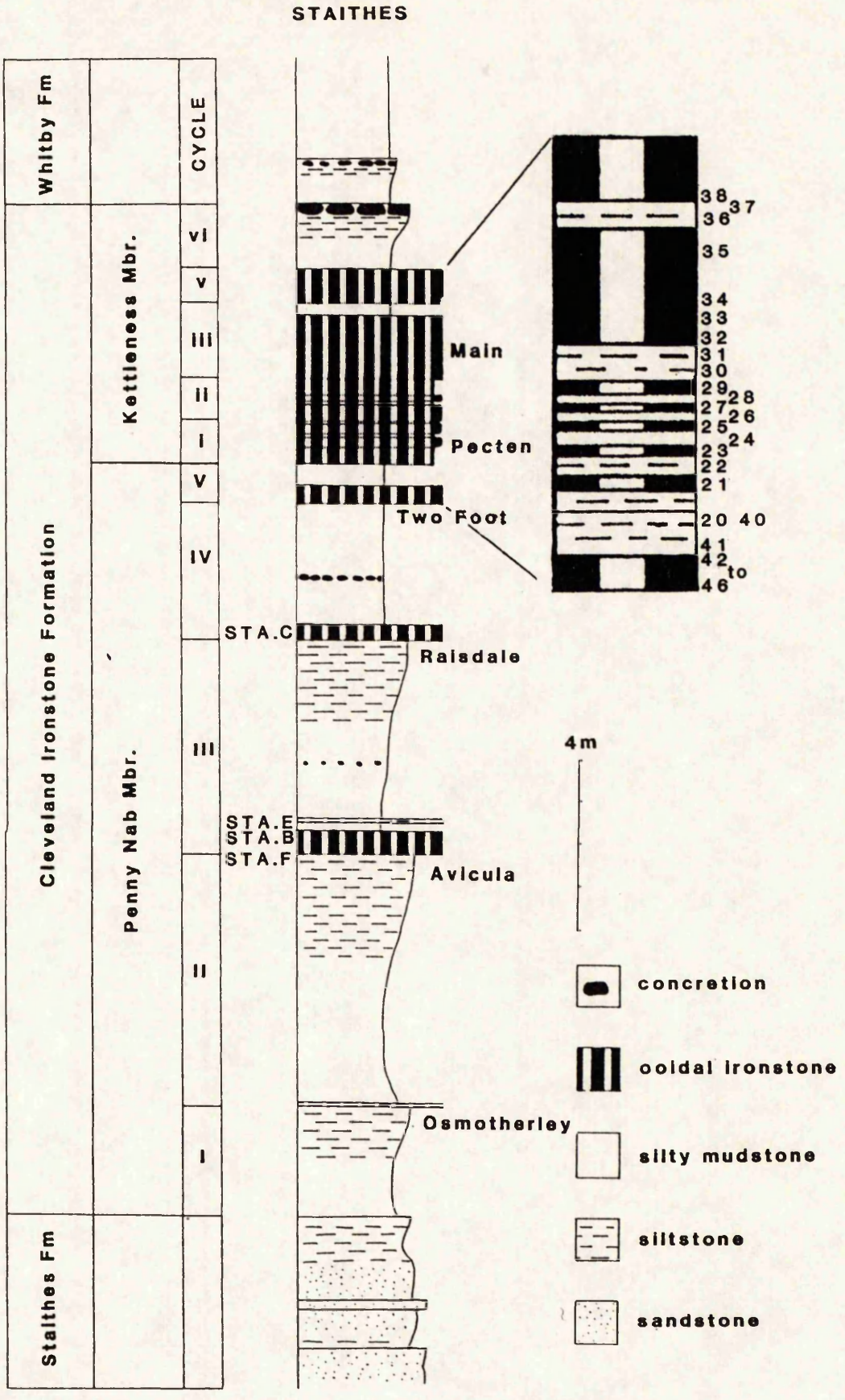

Table 6.1. Point-Count Data for the Samples of the Cleveland Ironstone Formation. See Text for Descriptions of the Various Components.

NUMBER	STA.F	STA.B	NODULE	STA.E	STA.C	46	45	44	43	42	41	40	20	21	22	24
OOIDS																
BERTHIERINE	0.0	0.5	0.0	0.5	0.0	0.0	42.5	27.0	0.0	5.0	0.0	0.0	0.5	1.0	1.0	2.0
BERTH./KAOL.	0.0	0.0	0.0	0.0	0.0	0.0	0.0	0.0	0.0	0.0	0.0	0.0	0.0	0.0	0.0	0.0
BERTH./CALC.	0.0	2.0	0.0	1.5	0.0	0.0	1.5	2.0	0.0	0.5	0.0	0.0	0.0	0.0	0.0	0.0
KAOLINITE	0.0	0.0	0.0	0.0	0.0	0.0	0.0	0.0	0.0	0.0	0.0	0.0	0.0	0.0	0.0	0.0
CALCITE	0.0	3.0	0.0	0.0	0.0	0.0	0.0	0.5	0.0	3.5	0.0	0.0	0.0	0.0	0.0	0.0
PHOSPATE	0.0	1.0	0.0	0.0	0.0	0.0	0.0	0.0	0.0	0.0	0.0	0.0	0.0	0.0	0.0	0.0
GOETHITE	0.0	0.0	0.0	0.0	0.0	15.0	0.0	0.0	0.0	0.0	0.0	0.0	0.0	0.0	0.0	0.0
GOETH./CALC.	0.0	0.0	0.0	0.0	63.5	0.0	0.0	0.0	62.5	0.0	0.0	0.0	0.0	0.0	0.0	0.0
SUB-TOTAL	0.0	6.5	0.0	2.0	63.5	15.0	44.0	29.5	62.5	9.0	0.0	0.0	0.5	1.0	1.0	2.0
MATRIX	7.0	0.0	69.0	1.0	2.0	7.0	2.5	1.0	7.0	0.0	62.0	70.0	7.0	13.0	16.0	63.0
SIDERITE	82.0	7.5	0.0	86.0	1.0	0.0	30.0	64.0	0.0	85.5	1.0	1.0	76.5	78.0	60.0	20.0
SIDERITE CEMENT	0.0	47.5	0.0	0.0	26.0	50.5	17.0	0.0	25.0	0.0	0.0	0.0	0.0	0.0	0.0	0.0
OPAQUE	1.5	0.5	3.0	1.0	0.0	0.5	0.5	1.0	0.0	1.5	5.0	3.5	4.5	1.5	3.0	1.5
PYRITE	1.5	3.0	7.0	1.0	4.5	2.0	0.0	0.5	2.5	1.0	7.5	6.5	2.5	2.0	2.0	1.0
QUARTZ	6.0	2.0	8.0	6.0	0.0	0.0	0.0	0.0	0.0	1.5	15.5	11.5	2.0	1.5	1.0	3.5
MUSCOVITE	1.0	0.0	1.0	1.0	0.0	0.0	0.0	0.0	0.0	0.0	2.0	1.5	1.5	0.5	0.5	1.5
SHELL FRAGMENT	0.0	10.5	0.0	0.0	1.5	8.5	0.0	0.5	1.5	0.0	0.0	0.0	0.5	0.0	9.5	0.0
CALCITE	0.0	0.0	1.0	0.0	0.0	0.0	1.5	1.0	0.0	0.0	0.0	0.0	2.0	0.5	0.0	0.0
TRANSLUCENT GOETH.	1.0	1.0	2.0	1.5	0.0	0.5	1.0	1.5	0.0	1.0	5.0	4.5	2.5	1.5	1.5	3.0
BERTH. FLAKE	0.0	0.5	9.0	0.5	0.0	0.0	0.0	0.0	0.0	0.0	2.0	1.5	0.5	0.5	5.5	4.5
REPLACED BIOCLAST	0.0	20.0	0.0	0.0	1.5	13.0	3.5	1.0	1.5	0.5	0.0	0.0	0.0	0.0	0.0	0.0
INTRACLAST	0.0	0.0	0.0	0.0	0.0	3.0	0.0	0.0	0.0	0.0	0.0	0.0	0.0	0.0	0.0	0.0
PHOSPHATIC CLAST	0.0	1.0	0.0	0.0	0.0	0.0	0.0	0.0	0.0	0.0	0.0	0.0	0.0	0.0	0.0	0.0
TOTAL	100	100	100	100	100	100	100	100	100	100	100	100	100	100	100	100

Table 6.1 (Continued).

NUMBER	25	26	27	28	29	30	31	32	33	34	35	36	37	38
OOIDS														
BERTHIERINE	3.5	0.0	5.5	2.5	0.5	0.5	7.0	2.0	2.5	1.5	0.0	60.0	0.0	1.0
BERTH./KAOL.	0.0	0.0	0.0	0.0	0.5	0.0	0.0	2.5	0.0	1.0	1.5	1.0	0.0	0.5
BERTH./CALC.	1.5	0.0	0.0	0.0	0.0	0.0	0.0	0.0	0.0	0.0	0.0	0.0	0.0	0.0
KAOLINITE	0.0	0.0	0.0	0.0	0.5	0.0	0.5	2.0	1.0	3.0	2.0	0.0	0.0	0.5
CALCITE	2.0	0.0	0.0	0.0	0.5	0.0	0.0	0.0	0.0	0.0	0.0	0.0	0.0	0.0
PHOSPATE	0.0	0.0	0.0	0.0	0.0	0.0	0.0	0.0	0.0	0.0	0.0	0.0	0.0	0.0
GOETHITE	0.0	0.0	0.0	0.0	0.0	0.0	0.0	0.0	0.0	0.0	0.0	0.0	0.0	0.0
GOETH./CALC.	0.0	0.0	0.0	0.0	0.0	0.0	0.0	0.0	0.0	0.0	0.0	0.0	0.0	0.0
SUB-TOTAL	7.0	0.0	5.5	2.5	2.0	0.5	7.5	6.5	3.5	5.5	3.5	61.0	0.0	2.0
MATRIX	36.0	56.0	10.0	43.0	10.0	58.5	35.5	25.0	5.0	8.0	4.0	32.0	38.5	32.0
SIDERITE	54.0	29.0	79.5	35.5	79.5	27.5	50.5	65.0	86.5	82.5	89.0	1.0	40.0	60.0
SIDERITE CEMENT	0.0	0.0	0.0	0.0	0.0	0.0	0.0	0.0	0.0	0.0	0.0	0.0	0.0	0.0
OPAQUE	0.0	1.0	0.5	4.0	1.0	0.5	2.0	0.5	2.5	0.5	1.0	0.0	1.0	0.0
PYRITE	1.0	1.0	2.5	3.5	3.5	3.5	1.0	1.0	1.0	0.5	1.0	0.5	5.0	1.0
QUARTZ	0.5	2.0	0.5	2.0	1.0	3.0	0.0	0.0	0.0	0.5	0.0	2.0	12.0	4.0
MUSCOVITE	0.5	1.5	0.5	1.5	0.0	0.5	0.5	0.5	0.5	0.0	0.0	0.5	1.5	0.5
SHELL FRAGMENT	0.0	0.0	0.0	0.0	0.0	0.0	0.0	0.0	0.0	0.0	0.0	0.0	0.0	0.0
CALCITE	0.0	0.0	0.0	0.5	0.0	0.0	0.0	0.0	0.0	0.0	0.0	0.0	0.0	0.0
TRANSLUCENT GOETH.	0.5	1.5	0.5	1.5	1.0	1.5	2.0	1.0	0.5	1.5	1.0	0.5	1.0	0.5
BERTH. FLAKE	0.5	8.0	0.5	6.0	2.0	4.5	1.0	0.5	0.5	1.0	0.5	2.5	1.0	0.0
REPLACED BIOCLAST	0.0	0.0	0.0	0.0	0.0	0.0	0.0	0.0	0.0	0.0	0.0	0.0	0.0	0.0
INTRACLAST	0.0	0.0	0.0	0.0	0.0	0.0	0.0	0.0	0.0	0.0	0.0	0.0	0.0	0.0
PHOSPHATIC CLAST	0.0	0.0	0.0	0.0	0.0	0.0	0.0	0.0	0.0	0.0	0.0	0.0	0.0	0.0
TOTAL	100	100	100	100	100	100	100	100	100	100	100	100	100	100

termed berthierine flakes. The green to brown colouration and low birefringence distinguishes them from muscovite, but confusion occurs where particles are small, or the section is ultra-thin. Care is therefore required to distinguish them from muscovite, and the simple foliation within the matrix itself. The flakes show a clear distinction in abundance between the ironstone seams and the interbedded mudstone, being up to sixteen times more abundant in the latter.

6.4.2.4) Matrix.

The term 'matrix' is here used to describe the clay mineral fabric and the very fine particulate/authigenic material largely unresolvable under 200X magnification. The matrix may possess some lamination, but a preferred orientation is usually difficult to ascertain under high power. No distortion of the fabric of the matrix, around detrital particles or authigenic cystals is evident.

6.4.2.5) Replacive Siderite.

This siderite in the point-count data refers only to that siderite replacing the matrix (see plate 23c). The siderite forms as small crystals (usually <10μm across, rarely greater than 30μm), that may form euhedral rhombs, but are more commonly subrounded. Some crystals may themselves be aggregates of smaller siderite subcrystals. Many crystals show a dark core 2-4μm across, that may resemble a particle of goethite in transmitted light. The shape of this core is of moderate to high sphericity, but of low roundness. However, polished surfaces under reflected light reveal only holes and not distinct particles. It appears unlikely that the cores have been plucked during section making, due to the excellent polish on the thin-section, and hence the loss of the core due to solution or degradation is implied. Not all crystals contain cores, and it is therefore not a controlling factor for siderite precipitation, but the crystals with cores are usually slightly larger, and may therefore have nucleated earlier. Crystal size appears to be restricted, probably due to the interaction between crytals as more nucleate and grow, so that the resultant fabric of sideritisation is one of a mosaic of small crystals, similar to that described for the Frodingham replacive siderites.

Siderite is most abundant within the ironstone seams, giving the prominant surface weathering profile and hematitic reddening on oxidation at outcrop (plate 23a), but siderite is also widespread within the interbedded muds. For the reasons given in appendix A.1.2 on point-counting, the actual proportion of siderite determined by this method must be considered as an estimate only.

6.4.2.6) Bioclasts.

The Cleveland Ironstone Formation contains little bioclastic material relative to other ironstones. Only 9 of the 30 thin-sections studied contained any bioclastic material, and only three sections contained significant quantities (STA. B, STH. 46 and STH. 22). STA. B and STH. 46 (plate 24b) are basal shell accumulations of the Avicula, and Two-Foot Seams, respectively. STH. 22 is a bioclastic mud-ironstone and contains shell debris (9.5%) with all structure intact. This is in contrast to the afore mentioned shell hashes, in which the majority of the shell material has been replaced. In STA. B, the phosphatic clasts may also be replaced bivalve shells.

6.4.2.7) Intraclasts.

Identifying intraclasts in thin-section was complicated by bioturbation that produced burrow-fills of allochthonous material, but it is suspected that intraclastic material is generally of very low abundance within the ironstone-formation. Distinct mud clasts are however present in STH. 46, in the higher energy deposition of the basal layer in the Two-Foot Seam.

6.4.2.8) Pyrite.

Almost all of the pyrite is present as dispersed framboids <20μm across, occasionally coalescing into a more massive form. Pyrite is most common in the interbedded muds between the Two-Foot and Pecten Seams, and in the mudstone separating the two halves of the Main Seam, but is ubiquitous throughout the sequence. This widespread occurrence is reflected in the Pecten Seam, where the distinction between

ironstone and mudstone based on pyrite abundance is unclear. Pyrite also shows a notably high abundance in the Avicula and Raisdale concretions.

6.4.2.9) Ooids.

As in the Frodingham Ironstone Formation, there are two main ooid types; berthierine and goethitic, but the latter are restricted in occurrence (see below). Other mineralogies are diagenetic modifications of the berthierine ooids. The possibility of a generic link between berthierine and goethite ooids, is discussed below.

Berthierine Ooids.

The most well preserved examples of berthierine ooids are seen in the Two-Foot Seam, particularly STH. 45 (plate 23d). Here the ooids can be seen to possess an oblate ellipsoidal shape, 0.3-0.5mm long, with an elongation ratio of 2:1 to 3:1. The nuclei are all particles of berthierine, many of which possess a layered structure similar to the berthierine flakes. Many are however distinctive in that the cleavage is perpendicular to the long axis, and are hence distinct from muscovite. Other nuclei are formed of very fine crystals in a random orientation. The cortex of the ooids is finely laminated with light and darker layers, but may be often only apparent under crossed-polars. The growth of the cortex is similar to that described for Frodingham ooids, i.e. a three stage growth process, but in this case stage 3 is marked more by an increased polar accretion than a pronounced dominance over equatorial accretion. Elsewhere in the sequence, the ooids have usually undergone a degree of deformation to "spastoliths", and the structure is difficult to ascertain. Replacement by other minerals also destroys the fabric.

The ooids are most abundant within the Two-Foot Seam (up to 44.0%), and in STH. 36 (61.0%) where intense deformation has occurred (plate 24a). In general, ironstone seams are more likely to contain ooids than the mudstones, but ooids also occur in the latter. The muds separating the Two-Foot and Pecten Seams are however devoid of ooids. The presence or absence of ooids does not therefore control the development of ironstone seams and siderite sheets.

Ferroan Calcite Replacement.

The ferroan calcite replacing berthierine ooids, has the appearance of being microcrystalline, but is usually composed of less than four crystals, and often only one. The nucleus is often preferentially replaced, which is in contrast to replacement by siderite where replacement occurs at the rim. The crystal formed does not undergo uniform extinction under crossed polars, but possesses a sweeping extinction with a few degrees rotation of the stage, that is unrelated to ooid structure. Ferroan calcite replacement occurs within the Two-Foot and Pecten Seams, but not within the Main Seam. Replaced ooids do not exceed 50% of those present in the rock, and the actual quantity of the replaced ooids does not appear to be related to ooid abundance.

Kaolinite Replacement.

The presence of intact berthierine cortices on the outer edge of many ooids partially replaced by kaolinite, suggests that kaolinite preferentially replaces the inner parts of the ooids (plate 24c). The kaolinite occurs as a finely crystalline mass, with individual crystal diameters up to 15μm, occasionally developing a 'book' structure. No preservation of ooid structure occurs on replacement. Kaolinite replacement of ooids is largely restricted to the lower ironstone block of the Main Seam. Ooid replacement by kaolinite is more extensive than shown by ferroan calcite, so that most ooids of a sample in which kaolinite is present usually show a degree of kaolinite formation.

Siderite Replacement.

Complete replacement of ooids by siderite is not seen, despite extensive sideritisation of the matrix in many samples. Siderite replacement occurs only as a rim on the edge of the ooids and is often difficult to distinguish from the sideritised matrix. It appears that this fabric results from a continuation of the matrix replacement process, but the reason for edge-only replacement is unclear, particularly when kaolinite and calcite preferentially replace the centre of the ooid.

Goethite Ooids.

Goethite ooids are restricted to a single occurrence in the basal shell bed of the Two-Foot Seam (STH. 46, plate 24b). They are opaque with no internal structure of the cortex seen in reflected light, but nuclei are seen that possess a layered and foliated structure, directly analogous to that of the berthierine flakes. The size (0.25-0.35mm in length), and oblate ellipsoidal shape (elongation ratio of 2:1 to 3:1), is similar to undeformed berthierine ooids of this ironstone-formation, and it is believed here that these ooids result from full oxidation of berthierine ooids, and that the cortical fabric was destroyed in the process. Many of these ooids are sheared, but are not deformed to spastoliths.

6.4.3) Electron Probe Micro-Analysis (E.P.M.A.).

6.4.3.1) Berthierines.

Analyses of the berthierine matrix and ooids are given in table 6.2, and plotted on an Si - (Fe+Mg) - Al(Total) ternary plot in figure 6.5. Kaolinites replacing ooids, and some muscovites were also analysed for comparison (table 6.3). Cleveland berthierines have an approximately similar Si content to the Frodingham berthierines, but considerably more Al occurs within the octahedral sites, at the expense of Fe. Mg contents are similar. In figure 6.5, the data are hence nearer the Al pole than the Frodingham analyses, but possess a similar mixing trend of data away from the Fe+Mg pole. The purest composition is obtained from the berthierine flakes. Applying the interpretations from the Frodingham investigation, suggests that berthierine in the Cleveland Ironstone Formation formed from a detrital clay of significantly higher kaolinite content.

Data obtained from muscovites, were highly variable, particularly in Mg and K content. If this reflects a true compositional variation, then it may be possible that muscovite is also destabilised during berthierine formation. The data set is however too small to test this hypothesis.

Table 6.2. Average Compositions of Berthierine in the Cleveland Ironstone Formation, Obtained By E.P.M.A. The Data have been Recalculated to Berthierine Structural Formulae.

	STH. 26				STH. 32			STH. 36			
	MATRIX		FLAKES		MATRIX		OOID	MATRIX		BERTH. OOIDS	
	AVERAGE	STDEV	AVERAGE	STDEV	AVERAGE	STDEV.	1 Analysis	AVERAGE	STDEV.	AVERAGE	STDEV.
Si	14.026	0.622	11.900	0.554	5.669	0.427	12.336	12.040	1.295	12.348	1.639
Ti	0.233	0.148	0.292	0.124	0.076	0.055	0.031	0.085	0.073	0.091	0.075
Al	11.173	0.428	10.062	0.487	4.409	0.341	9.792	10.463	0.725	10.711	0.864
Fe	20.755	1.399	26.648	0.652	7.757	1.160	6.629	20.499	2.061	24.567	2.397
Mn	0.027	0.037	0.041	0.022	0.017	0.032	0.000	0.013	0.018	0.025	0.032
Mg	1.902	0.115	3.131	0.219	0.698	0.117	1.177	1.671	0.126	1.972	0.310
Ca	0.136	0.040	0.038	0.033	17.880	1.978	0.350	0.078	0.018	0.081	0.035
Na	0.290	0.097	0.342	0.044	0.236	0.143	0.296	0.264	0.162	0.287	0.128
K	1.452	0.260	0.363	0.169	0.701	0.221	2.010	0.915	0.561	0.624	0.432
P	0.000	0.000	0.006	0.010	7.989	0.849	0.921	0.000	0.000	0.005	0.015
S	0.076	0.055	0.061	0.014	0.008	0.011	0.029	0.087	0.042	0.091	0.031
O	33.731	0.786	32.625	1.026	30.800	1.161	27.303	30.366	1.957	32.267	2.639
TOTAL	83.800	0.994	85.509	1.856	76.240	2.406	60.874	76.480	4.347	83.069	5.311
BerthCalc.											
Si	3.317	0.080	2.911	0.048	3.324	0.123	3.887	3.159	0.198	3.046	0.173
Al(T)	0.683	0.080	1.089	0.048	0.676	0.123	0.113	0.841	0.198	0.954	0.173
Al(O)	2.068	0.099	1.472	0.091	2.014	0.104	3.098	2.022	0.157	1.805	0.188
Ti	0.032	0.020	0.042	0.019	0.027	0.020	0.006	0.013	0.011	0.013	0.010
Fe	2.465	0.209	3.276	0.172	2.284	0.274	1.046	2.710	0.343	3.072	0.429
Mn	0.003	0.004	0.005	0.003	0.005	0.009	0.000	0.002	0.002	0.003	0.004
Mg	0.520	0.027	0.884	0.035	0.472	0.058	0.428	0.510	0.057	0.561	0.056
Ca	0.022	0.006	0.004	0.005	0.273	0.141	-0.361	0.014	0.003	0.012	0.010
Na	0.084	0.028	0.102	0.014	0.167	0.100	0.114	0.085	0.053	0.085	0.037
K	0.247	0.043	0.063	0.028	0.293	0.085	0.455	0.169	0.099	0.107	0.068
OCT.	5.088	0.115	5.679	0.067	4.801	0.184	4.579	5.255	0.231	5.454	0.226
INT.	0.353	0.061	0.170	0.019	0.733	0.158	0.208	0.268	0.098	0.204	0.095
CH	8.000	0.000	8.000	0.000	8.000	0.000	8.000	8.000	0.000	8.000	0.000
	n=6		n=6		n=5		n=1	n=5		n=8	

Table 6.3. Compositions of Kaolinite and Muscovites in the Cleveland Ironstone Formation. The Kaolinite Data have been Recalculated to Kaolinite Structural Fomulae (A Similar Structure to Berthierines).

	STH. 32					
	KAOLINITE REPLACING OOIDS					
	1	2	3	4	AVERAGE	STDEV.
Si	15.229	18.464	20.298	19.300	18.323	2.195
Ti	0.059	0.065	0.000	0.000	0.031	0.036
Al	14.359	17.117	19.218	17.655	17.087	2.025
Fe	0.798	1.133	0.335	0.158	0.606	0.443
Mn	0.000	0.000	0.047	0.035	0.021	0.024
Mg	0.028	0.188	0.153	0.120	0.122	0.069
Ca	0.262	0.048	0.000	0.051	0.090	0.117
Na	0.208	0.086	0.205	0.049	0.137	0.082
K	0.130	0.062	0.050	0.049	0.073	0.039
P	0.000	0.000	0.000	0.000	0.000	0.000
S	0.224	0.051	0.065	0.053	0.098	0.084
O	30.612	36.814	40.511	37.874	36.453	4.193
TOTAL	61.909	74.028	80.882	75.344	73.041	7.993
(BerthCalc.)						
Si	3.975	4.002	3.998	4.066	4.010	0.039
Al(TOT)	3.901	3.861	3.939	3.871	3.893	0.078
Ti	0.009	0.008	0.000	0.000	0.004	0.005
Fe	0.079	0.119	0.028	0.012	0.059	0.049
Mn	0.000	0.000	0.005	0.004	0.002	0.002
Mg	0.008	0.047	0.035	0.029	0.030	0.016
Ca	0.048	0.007	0.000	0.008	0.016	0.022
Na	0.066	0.023	0.049	0.013	0.038	0.025
K	0.024	0.010	0.007	0.007	0.012	0.008
OCT.	3.972	4.036	4.004	3.981	3.999	0.029
INT.	0.139	0.040	0.056	0.028	0.066	0.050
CH	8.000	8.000	8.000	8.000	8.000	0.000
	STH. 26					
	MUSCOVITES					
	1	2	3	4	5	
Si	21.157	20.274	16.247	14.787	15.910	
Ti	0.456	0.070	1.085	0.746	0.146	
Al	12.827	12.548	9.488	9.823	13.905	
Fe	6.304	7.599	13.353	17.521	17.277	
Mn	0.075	0.012	0.165	0.000	0.003	
Mg	1.617	1.722	7.308	5.542	1.880	
Ca	0.035	0.082	0.121	0.043	0.087	
Na	0.264	0.345	0.559	0.391	0.255	
K	8.203	4.085	3.354	2.848	0.865	
P	0.000	0.000	0.000	0.000	0.000	
S	0.020	0.231	0.056	0.001	0.088	
O	40.493	38.608	37.287	35.486	37.079	
TOTAL	91.451	85.576	89.023	87.188	87.495	

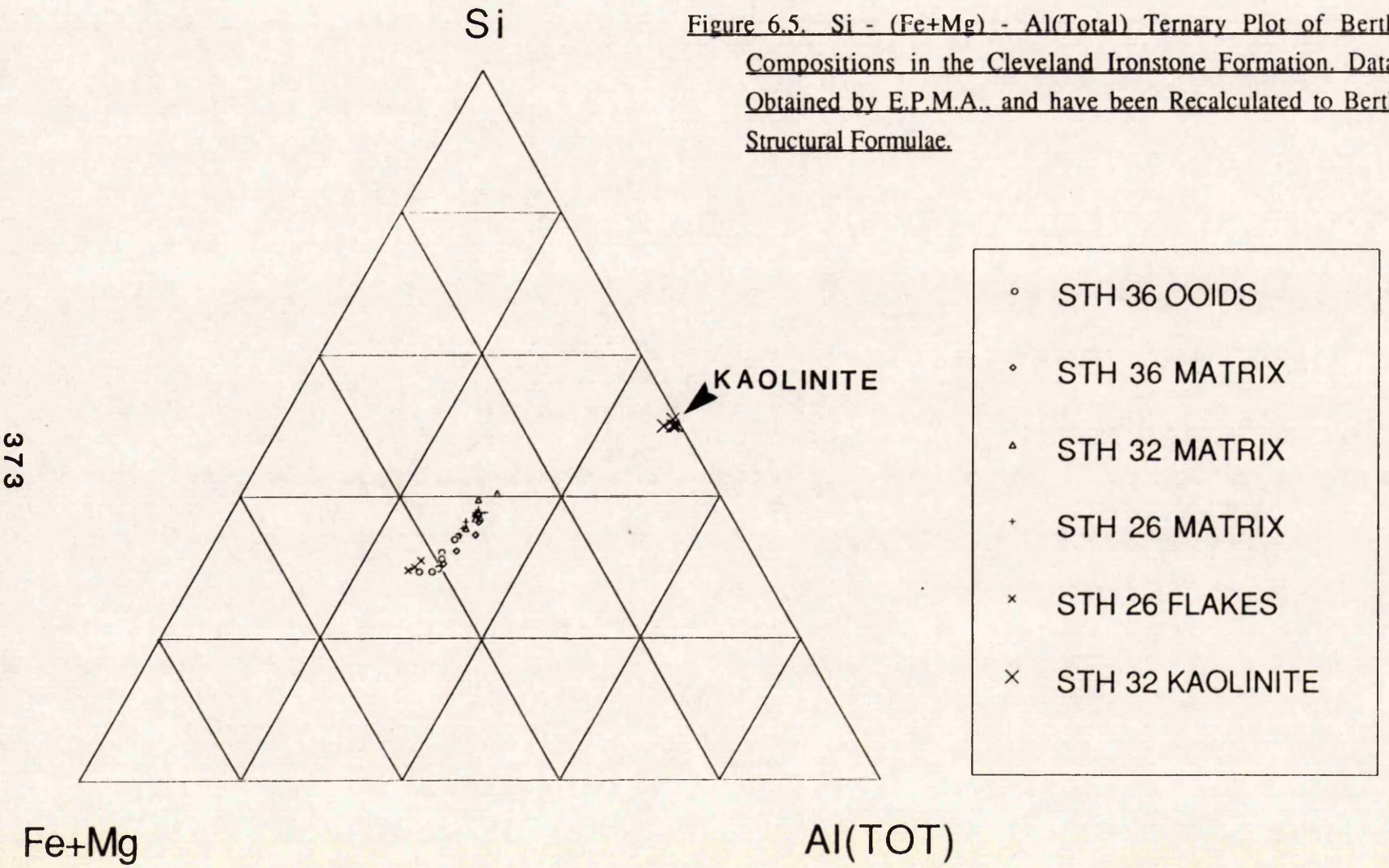

Figure 6.5. Si - (Fe+Mg) - Al(Total) Ternary Plot of Berthierine Compositions in the Cleveland Ironstone Formation. Data were Obtained by E.P.M.A., and have been Recalculated to Berthierine Structural Formulae.

6.4.3.2) Carbonates.

Siderites.

Analyses of siderites (table 6.4) show a narrow range of siderite composition between those of the same, and different, samples (averaging 77.8-79.7 mol% $FeCO_3$, 10.8-13.9 mol% $MgCO_3$, 7.0-8.9 mol% $CaCO_3$, and 0.8-1.3 mol% $MnCO_3$). The siderites are slightly higher in Fe, and lower in Mg and Ca than the Frodingham siderites, with the most significant difference being in Mn content, which is highly depleted in this ironstone-formation. High Ca and Mg tentatively points to marine precipitation of this siderite, but manganese reduction appears to have been less significant during siderite formation.

Calcites.

Calcite cements are uncommon in the Cleveland Ironstone Formation, probably reflecting the low bioclastic content (particularly aragonitic ones), and the low porosity and permeability due to a high mud content, that may have restricted later meteoric water fluxes. Analyses of the calcites replacing ooids in STH. 25 showed them to have an Fe/Mn ratio >10, with a high $FeCO_3$ content averaging 7.4 mol%. Some Si and Al were detected confirming the replacive origin, but this cannot account for the high Fe content that supports the apparent dominance of iron reduction over manganese reduction during early diagenesis.

6.4.4) Discussion.

The Cleveland Ironstone Formation has a complicated sedimentological history, but coarsening upward cycles beneath ironstone seams, the fauna contained within them, and the condensed, bioturbated and reworked nature of the seams is typical of 'Minette'-type ironstones. These features reflect conditions similar to those described for deposition of the Frodingham Ironstone Formation, that led to the development of a post-oxic diagenetic environment.

The Cleveland ironstones have a stronger diagenetic overprint than the Frodingham ironstones, especially due to the intense sideritisation of the berthierine matrix that makes primary fabric recognition difficult. However, other than quartz and berthierine flakes being

Table 6.4. Average Compositions of Carbonates Within the Cleveland Ironstone Formation, Obtained By E.P.M.A. The Data have been Recalculated to Carbonates of the Calcite Group.

	STH. 25		STH. 25		STH. 26		STH. 32			
	CALCITES REP. OOIDS		RHOMBIC SIDERITES		RHOMBIC SIDERITES		RHOMBIC SIDERITES		SIDERITES REP. OOIDS	
	AVERAGE	STDEV.	AVERAGE	STDEV.	AVERAGE	STDEV	AVERAGE	STDEV.	AVERAGE	STDEV.
Ca	30.448	5.759	3.004	0.332	2.560	0.695	5.060	1.740	0.401	0.076
P	0.000	0.000	0.137	0.085	0.133	0.166	1.027	1.106	3.528	0.396
Sr	0.067	0.019	0.049	0.009	0.030	0.022	0.052	0.033	0.043	0.073
Si	2.730	2.111	0.107	0.106	0.615	1.403	0.105	0.090	0.170	0.144
Al	1.719	1.314	0.080	0.074	0.512	1.184	0.079	0.060	0.175	0.132
Mg	0.527	0.169	2.606	0.664	2.721	0.566	2.184	0.613	2.099	0.151
Na	0.052	0.017	0.064	0.037	0.079	0.028	0.097	0.031	0.097	0.031
Fe	3.306	1.305	36.391	1.015	35.239	2.303	34.102	1.409	35.501	0.484
Mn	0.213	0.036	0.528	0.261	0.495	0.215	0.533	0.227	0.337	0.006
O	18.179	1.815	13.894	0.172	14.413	1.928	14.942	1.461	13.967	0.154
TOTAL	57.240	1.730	53.855	0.663	56.796	1.965	58.181	2.862	52.789	0.620
CarbCalc.										
Ca	0.893	0.051	0.081	0.011	0.070	0.011	0.089	0.025	0.083	0.011
Fe	0.074	0.038	0.778	0.031	0.778	0.022	0.781	0.045	0.797	0.012
Mn	0.005	0.001	0.011	0.006	0.011	0.005	0.013	0.006	0.008	0.000
Mg	0.027	0.012	0.128	0.031	0.139	0.033	0.113	0.024	0.108	0.008
Sr	0.001	0.000	0.001	0.000	0.000	0.000	0.001	0.001	0.001	0.001
Na	0.003	0.001	0.003	0.002	0.004	0.002	0.006	0.002	0.005	0.002
	n=4		n=5		n=7		n=5		n=4	

abundant in the interbedded silts, there is little petrographic difference between the prominant seams and less sideritised silts in terms of primary mineralogy of the sediment. In particular, ooids are present in many beds and are not responsible for initiating siderite formation. A similar though modified process of ooid formation can be inferred. Therefore, unlike the Frodingham ironstones where primary mineralogy and fabric has a strong influence on subsequent diagenesis, the Cleveland ironstones are possibly influenced more by depositional processes and the sedimentary environment.

E.P.M.A. data of berthierines tentatively suggest that berthierine formed from a more kaolinitic detrital clay assemblage than the Frodingham examples, and this would fit with the conclusions of Myers (1989). Berthierine is present as only matrix and ooids, and does not form visible cements, due to the low primary porosity and the lack of aragonitic bioclastic material that could be subsequently replaced. Siderite exhibits a similar composition and morphology on replacement of the matrix as the Frodingham examples. As with berthierine, cements did not form due to the low porosity. The widespread formation of berthierine and siderite without significant pyrite formation is similar to that described for the Frodingham ironstones, but unlike the latter (and the Banbury Ironstone, described below) there is no evidence for later flushing with meteoric waters.

6.5) The Banbury Ironstone.

6.5.1) Introduction.

The Banbury Ironstone is an informal name given to the ferruginous Marlstone Rock Bed quarried around Banbury, Oxfordshire. It occurs largely at the top of the Middle Lias in the *Pleuroceras spinatum* Zone (Edmonds *et al.* 1965), and may extend into the Toarcian *Dactylioceras tenuicostatum* Zone as the "Transitional Bed" (Howarth 1980). The Ironstone reaches up to 7.62m (25ft) in thickness (Woodward 1893). The structure and extent of the ironstone field, along with measured sections, are discussed in detail within Whitehead *et al.* (1952) and Edmonds *et al.* (1965), and these should be referred to for full details. A map showing the outcrop of the field and thickness variation across it is shown in figure 6.6.

Figure 6.6. Outcrop of the Banbury Ironstone Field (Marlstone Rock Bed), Showing Thickness Variations. Taken From Whitehead *et al.* (1952, figure 20, p.157.)

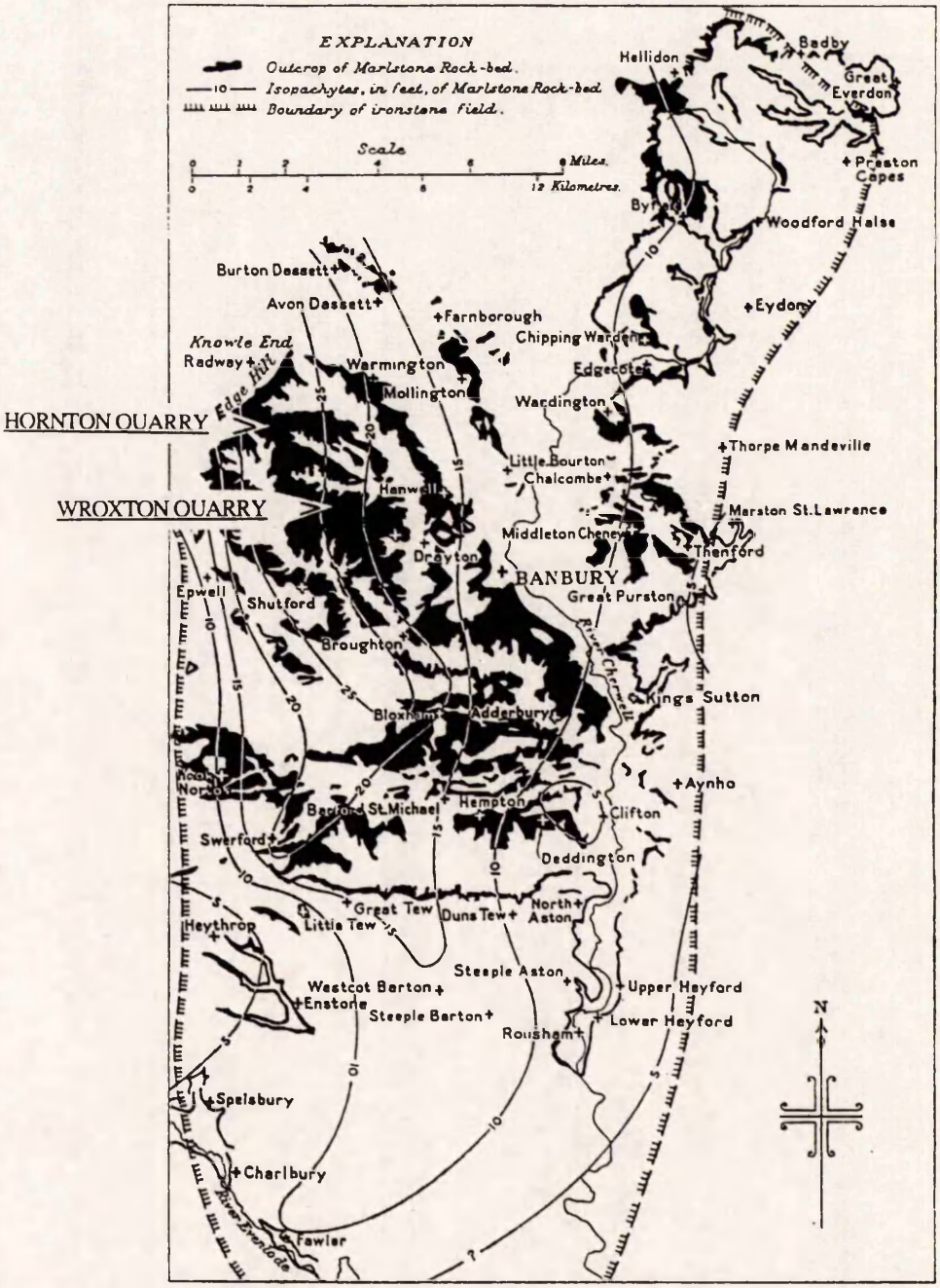

The Ironstone is essentially a bioclastic ooidal grain-ironstone, with ooids of berthierine (+/- goethite), cemented by siderite and ferroan calcite. A high proportion of echinoderm debris is common. The ironstone is poorly bedded, though flaggy in places, and vertical subdivisions usually hold for only a few metres along the outcrop. The only beds apparently common to the whole ironstone field are the phosphatic basal conglomerate, and the "Transition Bed" at the top, the latter of which shows oxidation prior to further sedimentation (Howarth 1980). Edmonds *et al.* (1965) recognised a two fold division of the ironstone sequence into a lower bluish-green, massive ironstone of a high carbonate content (the "bluestone"), and an upper, brown, flaggy ironstone (the "brownstone"). Cross-lamination and signs of current reworking are more conspicuous in the upper part of the sequence.

Whitehead *et al.* (1952) suggest that the Ironstone formed in shallow marine conditions undergoing current and wave reworking. They suggest that material was carried in and deposited on a shallow ridge, to allow for the absence of terrigenous clastics, trapped in deeper water between the ridge and the land (i.e. a clastic trap). Ager (1956) suggests that the "iron-rich waters" at this time restricted brachiopod migration, and that species abundances were also reduced for this reason.

6.5.2) Exposure and Sampling.

The Ironstone is no longer quarried as an iron ore, but is still extracted in places for building purposes. One such working quarry is Hornton Quarry (see figure 6.6) where samples of various lithologies were collected and the sequence studied. In particular, specimens of brachiopod 'nests' were collected in order to examine their preservation and cementation during early diagenesis. The exposure is variable, being highly weathered in places, but a small section was examined at the south end of the quarry, and is shown in plate 25. Wroxton Quarry (see figure 6.6) was also visited, but is now mostly filled and reclaimed, though the remaining small scarp still yielded fresh material on hammering.

6.5.3) Petrography.

The following petrographic descriptions are based upon material collected at Hornton Quarry, and in particular from the section shown in plate 25. Point-count analyses for the sequence are given in table 6.5, and the ironstone constituents are described below.

6.5.3.1) Ooids.

The ooids of the Banbury Ironstone are 0.15-0.3mm in length, and are composed of berthierine, or berthierine and goethite, and are similar to the Frodingham and Cleveland berthierine ooids. Most of the ooids are deformed to some degree, but the oblate ellipsoidal shape is seen within many examples, and shows the three growth stages described for the Frodingham ooids, suggesting that a similar genesis may be implied. Cortical fabric is also comparable, but the thickness is reduced, due to the relatively large nucleus in most examples, which is usually composed of a berthierine flake (plate 26a). Rounded particles of unstructured berthierine, and broken ooid fragments are also present as nuclei.

Whenever the berthierine/goethite ooids are present, siderite always shows signs of oxidation when present in the sample. This suggests that the goethite in these ooids results solely from the oxidation of the whole rock, in contrast to the Frodingham Ironstone Formation where no 'weathering' need have occurred. There is no pronounced goethite-berthierine banding in the cortices, instead an overall oxidation resulted in poorly defined layering, due to the preferential oxidation of certain layers within berthierine ooids. It not clear whether the oxidation was ancient or more recent, as both oxidised and unoxidised ironstone (i.e. "brownstone" and "bluestone") is present in fresh outcrop. This is further discussed in section 6.5.7 below.

6.5.3.2) Matrix and Berthierine Cement.

These two components are described together, since occasionally some of the "matrix" possesses a cement-like fabric, that is indistinguishable from the matrix in other sections. The matrix is a green to brown mud with randomly orientated particles of berthierine. The cement fabric occurs as an isopachous rim 4-8μm thick on ooids and

PLATE 25

Section of the Banbury Ironstone Exposed in Hornton Quarry.

The section shown is at the south end of the quarry. C. D. Curtis is pointing to a nest of terebratulid brachiopods, ≈10cm across, present within the sequence. Note that the goethitic nature (brown colouration) of this section cannot be ascribed to weathering on exposure, as the top of the sequence contains berthierine-rich beds that are green (unoxidised) at the surface. Sample numbers taken for thin-sectioning are given on the left, and a scale is given to the right of the photo.

TOP OF SECTION

MASSIVE BLUE-GREEN IRONSTONE

"BLUESTONE" ABUNDANT SHELL DEBRIS — HRT 25

"BROWNSTONE" — HRT 24

MASSIVE NON-LAMINATED IRONSTONE

RHYNCHONELLID NEST IN MASSIVE IRONSTONE — HRT 23

FRIABLE IRONSTONE GOETHITE VEINING — HRT 22

MASSIVE IRONSTONE. ABUNDANT FRAGMENTED SHELL DEBRIS. GOETHITE VEINING

INTACT AND BROKEN TEREBRATULID BRACHIOPODS — HRT 21

BASE OF SECTION

PIT FLOORED IN IRONSTONE

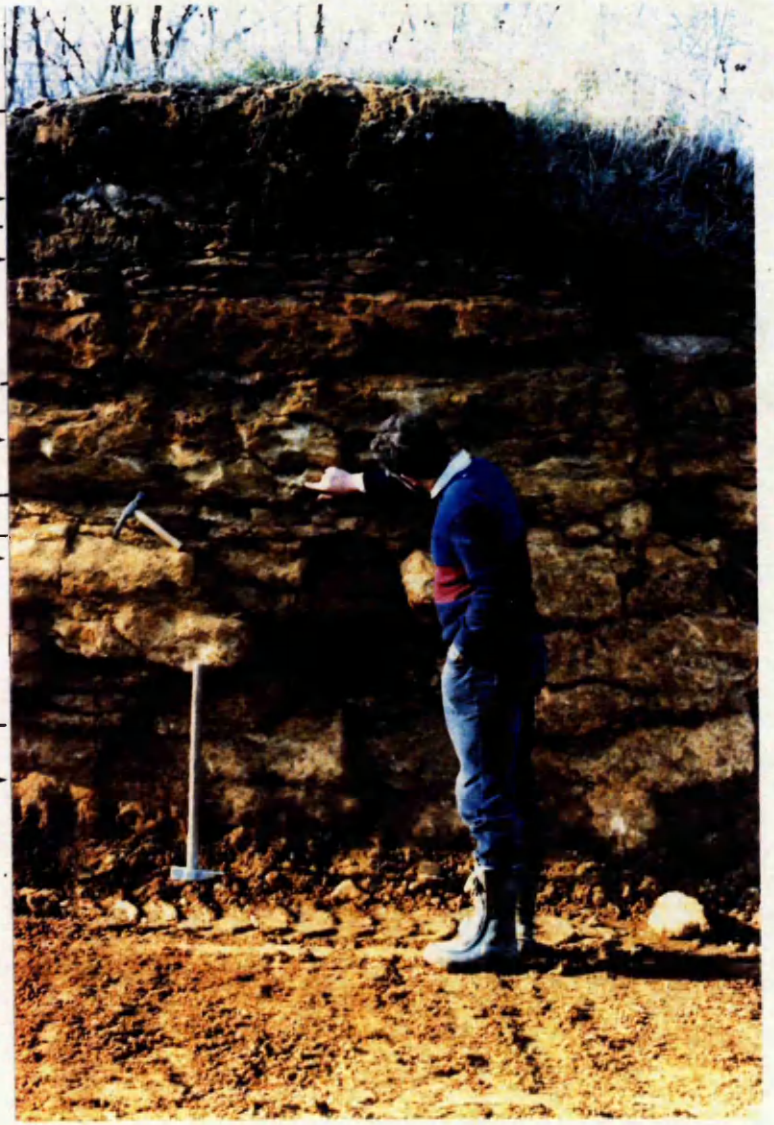

PLATE 26

The Banbury Ironstone 2

A) Typical thin-section of the Ironstone, specimen HRT. 25 (stained). Ooids of berthierine with large nuclei of unstructured particles (1) or flakes (2) of berthierine, are present with detrital mud and bioclastic debris (3). The rock is cemented by siderite (colourless) and ferroan calcite (blue). Photo length is equivalent to 1.3mm.

B) Specimen HRT. OX. This specimen is of a bioclastic ooidal berthierine pack-ironstone, with has an oxidised exterior of goethite. All the fabric of the pack-ironstone has been lost on oxidation of the berthierine to goethite. Photo length is equivalent to 6.7mm.

C) Broken terebratulid brachiopods showing the internal structure, preserved due to early calcite cementation. The specimen is 24cm at the base.

D) Thin-section through a brachiopod shell and internal cement, specimen HRT. C. This shows an early fibrous inclusion-rich cement (arrowed), and a later prismatic to sparry form. Photo length is equivalent to 3.3mm.

A	B
C	D

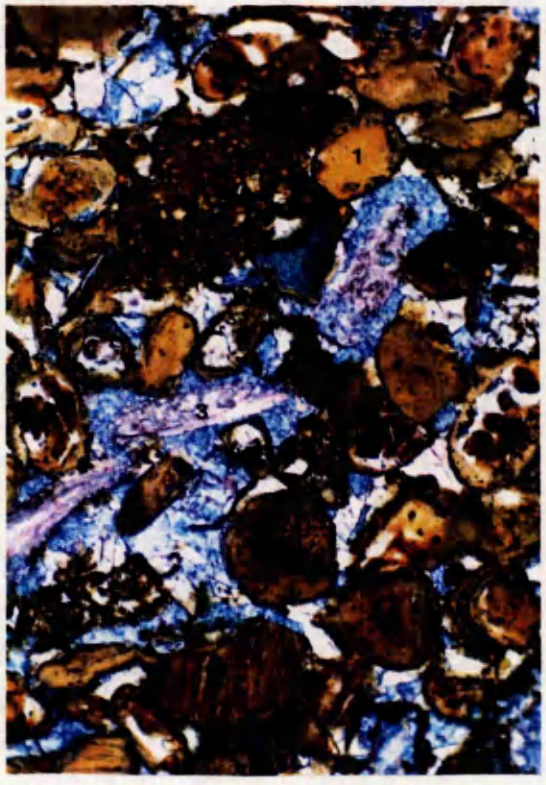
1

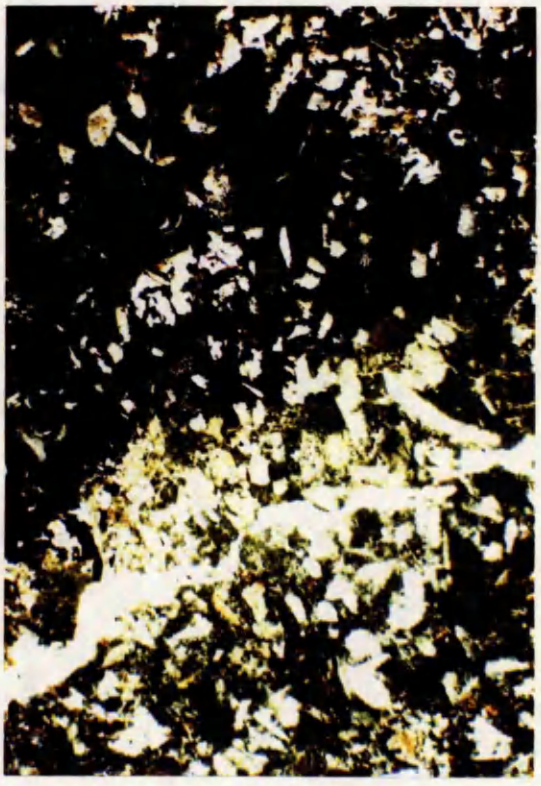

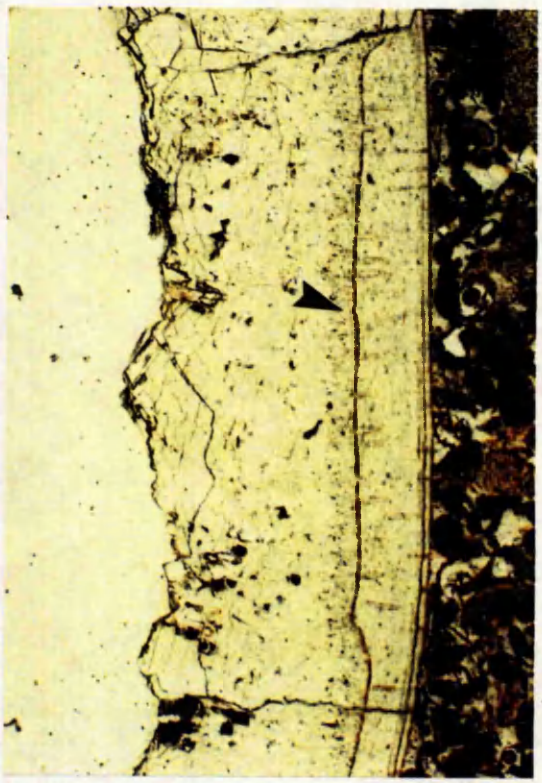

Table 6.5. Point-Count Data for the Samples of the Banbury Ironstone. See Text for Descriptions of the Various Components.

NUMBER	HRT 21	HRT 22	HRT 23	HRT 24	HRT 25	HRT.OX.IN.	HRT.OX.OUT.
OOIDS	10.5	10.5	11.0	12.5	24.5	13.5	-
MATRIX	26.0	6.5	28.0	36.0	14.0	22.5	3.5
SIDERITE REPLACING MATRIX	21.0	18.5	16.5	34.0	3.5	6.0	-
PHOSPHATIC CLAST	1.5	0.0	0.5	2.0	0.0	0.0	-
OPAQUE (Not-Pyrite)	0.0	1.0	0.0	0.0	0.0	0.0	-
PYRITE	0.5	0.0	0.0	0.0	0.0	0.0	-
SHELL FRAGMENT	8.5	14.0	8.0	0.0	9.5	9.0	7.0
TRANSLUCENT GOETHITE	2.0	2.0	1.0	5.0	0.0	9.5	-
BERTHIERINE FLAKE	6.0	0.0	14.5	10.0	3.0	12.0	-
REPLACED BIOCLAST	2.0	2.5	2.0	0.0	8.5	4.0	-
ECHINODERM FRAGMENT	9.0	12.5	4.5	0.5	3.5	5.0	2.0
SIDERITE CEMENT	1.5	0.0	0.0	0.0	15.0	15.5	-
FERROAN CALCITE CEMENT	5.5	15.0	11.0	0.0	16.5	3.0	6.5
FIRST GENERATION CALCITE	2.0	6.5	0.5	0.0	0.0	0.0	-
ECHINOID OVERGROWTH	3.5	7.0	1.0	0.0	1.5	0.0	-
NON-FERROAN CALCITE	0.5	4.0	1.5	0.0	0.5	0.0	-
TOTAL	100	100	100	100	100	100	19.0
							(81%GOETH.)

berthierine flakes, and also possesses a random fabric. The radial fabric of the authigenic cements in the Frodingham Ironstone Formation is largely absent.

The matrix is variably replaced by siderite, which occurs either as single rhombic crystals approximately 10-20μm across, or in aggregates. In HRT. 25, the "Bluestone" is replaced by siderite with dark brown cores in some crystals, similar to that described for the Cleveland siderites. Oxidation of siderite to goethite is common.

6.5.3.3) Berthierine and Goethite Particles.

Large flakes of berthierine up to 60μm across are a common feature of the Banbury Ironstone. Cleavage is parallel to the length of the flake, and splitting of the particle is common. Rounding by both abrasion and by accretion is seen, with the latter extending to the formation of 'superficial ooids'. More equant, rounded particles of berthierine are also present but much less abundant, and are believed to be reworked muds due to their similar structure. Particles described as goethite are considered to be oxidised berthierine particles, which now lacking visible structure.

6.5.3.4) Bioclasts.

Broken shell fragments that have retained their structure, and fragments replaced by ferroan calcite and/or siderite, are common. Many of the intact fragments are bored, and similar morphological types to the Frodingham Ironstone Formation can be seen. Usually the borings are lined or filled with goethite, but in HRT. 25, and other sections of the "bluestone", berthierine occurs as a micrite envelope and remains intact during the replacement process. Echinoderm debris is common, particularly in the lower part of the section studied (HRT. 21 and HRT. 22). The debris is extensively replaced by ferroan calcite, and less commonly berthierine, but some non-ferroan calcite (L.M.C.) remains in some examples.

6.5.3.5) Other Components.

Phosphatic clasts are reddish brown, rounded and unstructured, up to 0.2mm. None of the sections examined (including those of loose material) contained quartz or muscovite. Some organic matter (?vitrinite) was seen but is uncommon. Pyrite is considerably depleted relative to the other ironstones.

6.5.4) Berthierine Composition.

A few analyses of berthierine ooids and matrix were obtained using E.P.M.A. as part of an investigation into ironstone weathering (see below section 6.5.7). The analyses (table 6.7) are similar to the Cleveland Ironstone Formation (compare figures 6.8 with 6.5), but show signs of oxidation in the ooids, as the values have a slightly elevated Fe content and fall just outside the berthierine compositional field.

6.5.5) Carbonate Cement Fabrics.

The cementation of the Banbury Ironstone follows a similar pattern and textural development to the Frodingham ironstones. Only siderite and calcite were identified, and where present, the cement fabrics always post-date the berthierine cement (described above).

Siderite was the first carbonate phase to precipitate, and forms extensively in the "bluestone" where it nucleated on the berthierine, forming rounded rhombic crystals approximately 50μm long, or pore-filling sparites. Ferroan calcite postdates the siderite, and nucleated on the detrital carbonate debris, commonly filling available pore space. It forms thin 30-50μm thick prismatic cements on unreplaced shell debris; overgrowths on echinoderm fragments; and large (up to 0.3mm long) pore-filling cements. The cement fabric differs from that found in the Frodingham ironstones in that it has larger crystal sizes in earlier cement generations, and a more euhedral habit with often planar faces and enfacial junctions. In the larger pores, two sparry generations may be seen (for example HRT. 22), the first of which forms equant rhombohedral calcites rather that the scalenohedral fabrics seen in the Frodingham Ironstone Formation.

HRT. 22 had an initially high porosity, and contains a large amount of bioclastic debris which acted as a site for carbonate cement nucleation. This resulted in the formation of multi-cement generations which are usefully described in detail. In addition to the cements described above, non-ferroan calcite was precipitated during the formation of echinoderm overgrowths, and in the latter stages of the prismatic calcites on shell fragments. The crystal morphology remained unchanged during this pore fluid change. A second, less extensive, generation was precipitated following the sparitic ferroan calcites. The faces of the second ferroan calcite are coated with a micron-sized brownish film, suggesting that a small amount of oxidation was probably associated with precipitation of this last non-ferroan calcite.

The cement stratigraphy thus defined for HRT. 22 is:

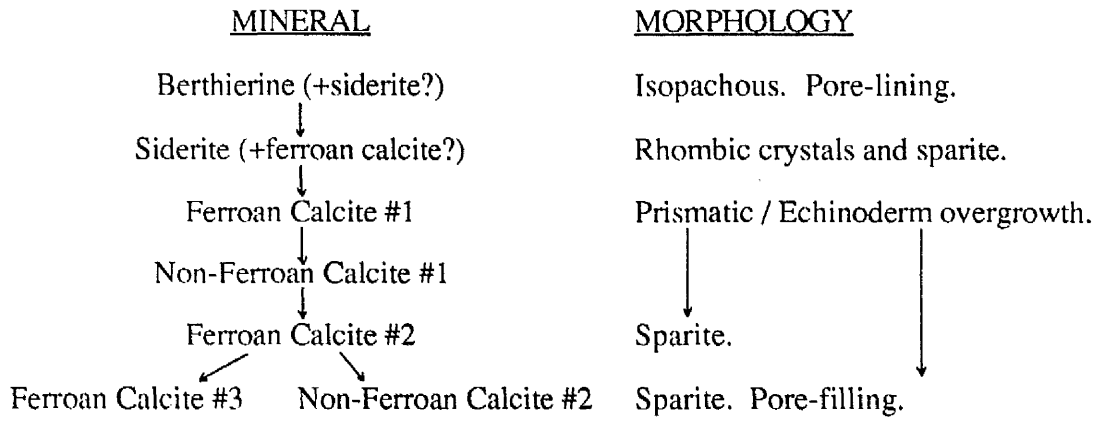

HRT. 21 and HRT. 23 differ from this diagenetic sequence, in that the initial ferroan calcite cement is absent, although the echinoid debris has been replaced. The second and third generations are not present. HRT. 25 has no non-ferroan calcite cements, and HRT. 24 contains no carbonate due to extensive weathering.

6.5.6) Brachiopod Preservation and Cementation.

Within the Banbury Ironstone, and throughout the Marlstone Bed outcrop, 'nests' of 1-3cm long complete brachiopods occur in small accumulations <30cm across (plate 26c). The valves are intact and geopetal fabrics indicate this to be a primary depositional fabric. The brachiopods of the Middle Lias were studied by Ager (1956) who defined a Banbury brachiopod Subprovince within a Midlands Province, characterised mainly by a

superabundance of *Tetrarhynchia tetrahedra* and *Lobothyris punctata* [syn. *Terebratula punctata*] ; an abundance of *Gibbirhynchia northamptonensis*; and a predominance of *Zeilleria indentata* among the long-looped terebratulids. The latter is however uncommon.

The brachiopods are significant to this study, due to the remarkable preservation of their internal structure by early calcite precipitation (plate 26c). The terebratulids have a brachidium in the form of a simple short loop, that within some specimens of *Lobothyris punctata* is preserved intact by the nucleation of a thin rim of calcite on the brachidium and cardinalia. The loop extends from the crura to about half way towards the anterior and has a single switch back to a posterior direction on the pedicle valve side. The two parts of the loop are close and nearly parallel, so that cementation fuses them together forming a two-pronged fork. Close examination however reveals the loop structure.

Rhynchonellids (including *Tetrarhynchia tetrahedra*) do not possess a full brachidium, only a pair of short crura projecting from the cardinalia towards the anterior. Cementation therefore usually results in a fused area of calcite in the umbonal region of the brachial valve, with little structural detail evident.

6.5.6.1) Carbonate Cement Textures.

Thin-sections taken across the brachiopods showed two distinct cement generations of ferroan calcite which were present in all examples (plate 26d). The first generation is thin (60-150μm thick), with a prismatic to scalenohedral habit of good crystal shape, and grows relative to the fabric of the brachiopod shell, so that it may not grow perpendicular to the surface. It is rich in inclusions, most of which are detrital iron oxides/hydroxides. This generation has been replaced by the second, that continues the growth outwards and preserves the former crystal outline in the inclusion pattern. In one part of HRT. C, zoning is revealed by the inclusion fabric within the first generation.

The second generation forms long prismatic crystals up to 5mm in length in a competitive growth fabric, with crystal size increasing into the pore. Inclusion fabrics are variable and

heterogenous, which suggests that recrystallisation may have taken place. The crystals do not possess a radiaxial or fascicular optic texture, undergo uniform extinction, and are terminated in rhombohedra unless interference occurs with opposing crystals in the void. Most brachiopods retain a large central void, preserving substantial porosity.

6.5.6.2) Electron Probe Micro-Analysis.

E.P.M.A. of the cements within the brachiopods are given in table 6.6. The calcites contain 1-3 mol% $FeCO_3$, with negligible Mn (<0.5 mol% $MnCO_3$). Mg content is also low (≈0.5 mol% $MgCO_3$), and is marginally higher in the first cement generation. The minimal Mg difference between the two generations, and the substantial decrease in Fe from generation one to two, suggests that the precurser was not an H.M.C., as high concentrations of Fe are not expected in such cements. Analyses and textures of cements within, and exterior to, the brachiopods were found to be similar, and are hence assumed to have precipitated synchronously.

6.5.6.3) Stable Isotopic Analysis of C and O in the Calcites.

Isotopic analysis of belemnites from the Ironstone (see figure 6.7) gave $\partial^{18}O_{PDB}$ values of -0.26 to -0.95‰ and $\partial^{13}C_{PDB}$ values of 0.29 to 2.33‰ which records the marine isotopic signature of the depositional waters. The ferroan calcites of generation two show a range of $\partial^{18}O_{PDB}$ values of -4.58 to -9.20‰ and $\partial^{13}C_{PDB}$ values of -4.89 to -10.31‰, and are hence significantly depleted in ^{18}O and ^{13}C relative to the belemnites. Following the arguments given in section **1**.10.3, and the specific discussion for the Frodingham isotope data in section **5**.12.2.2, a similar scenario of late meteoric water flushing and calcite precipitation may be implied, assuming that the Ironstone was not buried to significant depths at this time. This assumption is supported by petrographic evidence for an early calcite precipitation pre-compaction.

Unlike the Frodingham calcites, the $\partial^{13}C_{PDB}$ values are more restricted (compare with figure 5.8), suggesting that a more specific ratio of marine and organically derived HCO_3^- was incorporated in the calcites, with a dominance of the former. The spread of $\partial^{18}O_{PDB}$

Table 6.6. Average Compositions of Calcites Cementing Brachiopods in the Banbury Ironstone, Obtained By E.P.M.A. The Data have been Recalculated to Calcite Formulae.

	HRT. C											
	BRACHIOPOD 1				BRACHIOPOD 2				BRACHIOPOD 3			
	GEN. 1		GEN. 2		GEN. 1		GEN. 2		GEN. 1		GEN. 2	
	AVERAGE	STDEV	AVERAGE	STDEV	AVERAGE	STDEV	AVERAGE	STDEV	AVERAGE	STDEV	AVERAGE	STDEV
Ca	35.442	1.661	36.395	0.461	34.376	1.009	36.414	0.186	35.841	0.866	36.276	0.752
P	0.011	0.014	0.000	0.001	0.000	0.000	0.000	0.000	0.016	0.028	0.030	0.021
Sr	0.040	0.009	0.023	0.010	0.063	0.026	0.038	0.008	0.063	0.051	0.033	0.019
Si	0.036	0.017	0.010	0.005	0.314	0.214	0.009	0.007	0.028	0.006	0.009	0.003
Al	0.005	0.009	0.000	0.000	0.235	0.164	0.000	0.000	0.004	0.006	0.000	0.000
Mg	0.105	0.009	0.060	0.029	0.132	0.030	0.075	0.019	0.132	0.020	0.074	0.035
Na	0.036	0.003	0.031	0.006	0.040	0.019	0.031	0.004	0.034	0.004	0.035	0.005
Fe	0.848	0.135	0.529	0.114	1.319	0.456	0.541	0.078	0.802	0.096	0.388	0.385
Mn	0.166	0.013	0.157	0.050	0.104	0.002	0.123	0.002	0.103	0.025	0.162	0.186
O	14.588	0.693	14.793	0.156	14.810	0.305	14.804	0.056	14.734	0.354	14.755	0.250
TOTAL	51.276	2.444	51.997	0.543	51.393	0.843	52.034	0.194	51.758	1.117	51.761	0.909
CarbCalc.												
Ca	0.974	0.002	0.983	0.003	0.963	0.012	0.983	0.002	0.975	0.003	0.985	0.011
Fe	0.017	0.002	0.010	0.002	0.027	0.010	0.010	0.002	0.016	0.002	0.008	0.008
Mn	0.003	0.000	0.003	0.001	0.002	0.000	0.002	0.000	0.002	0.001	0.003	0.004
Mg	0.005	0.000	0.003	0.001	0.006	0.002	0.003	0.001	0.006	0.001	0.003	0.002
Sr	0.001	0.000	0.000	0.000	0.001	0.000	0.000	0.000	0.001	0.001	0.000	0.000
Na	0.002	0.000	0.001	0.000	0.002	0.001	0.001	0.000	0.002	0.000	0.002	0.000
	n=3		n=4		n=3		n=3		n=3		n=5	

Table 6.6. (Continued).

	HRT. A											
	BRACHIOPOD 4				BRACHIOPOD 5							
	GEN. 1		GEN. 2		GEN. 1		GEN. 2		GEN. 3		OOID	CEMENT
	AVERAGE	STDEV	AVERAGE	STDEV	AVERAGE	STDEV	AVERAGE	STDEV	AVERAGE	STDEV	AVERAGE	STDEV
Ca	37.931	1.740	39.112	0.247	38.265	1.686	37.825	0.840	38.406	0.691	38.680	0.617
P	0.015	0.015	0.000	0.000	0.015	0.026	0.000	0.000	0.000	0.000	0.036	0.032
Sr	0.028	0.003	0.045	0.014	0.041	0.011	0.037	0.014	0.031	0.008	0.138	0.195
Si	0.000	0.000	0.000	0.000	0.000	0.000	0.000	0.000	0.000	0.000	0.010	0.007
Al	0.001	0.000	0.001	0.001	0.004	0.002	0.003	0.003	0.004	0.004	0.018	0.023
Mg	0.085	0.003	0.113	0.027	0.156	0.028	0.122	0.032	0.093	0.022	0.130	0.018
Na	0.000	0.000	0.007	0.004	0.003	0.005	0.000	0.000	0.000	0.000	0.001	0.001
Fe	0.640	0.269	0.694	0.131	0.445	0.441	0.798	0.156	0.674	0.218	1.088	0.372
Mn	0.227	0.150	0.126	0.013	0.066	0.047	0.145	0.031	0.153	0.025	0.137	0.033
O	15.472	0.574	15.934	0.043	15.556	0.559	15.460	0.368	15.639	0.290	15.980	0.188
TOTAL	54.399	1.958	56.031	0.125	54.550	1.795	54.389	1.298	55.000	1.037	56.218	0.647
CarbCalc.												
Ca	0.980	0.008	0.980	0.004	0.983	0.011	0.977	0.004	0.981	0.005	0.971	0.009
Fe	0.012	0.005	0.012	0.002	0.008	0.009	0.015	0.003	0.012	0.004	0.020	0.007
Mn	0.004	0.003	0.002	0.000	0.001	0.001	0.003	0.001	0.003	0.000	0.003	0.001
Mg	0.004	0.000	0.005	0.001	0.007	0.001	0.005	0.001	0.004	0.001	0.005	0.001
Sr	0.000	0.000	0.001	0.000	0.000	0.000	0.000	0.000	0.000	0.000	0.002	0.002
Na	0.000	0.000	0.000	0.000	0.000	0.000	0.000	0.000	0.000	0.000	0.000	0.000
	n=3		n=3		n=3		n=3		n=3		n=5	

Figure 6.7. Carbon and Oxygen Stable Isotopic Composition of Belemnites, and Sparitic Calcite Cements Within Brachiopods, Banbury Ironstone.

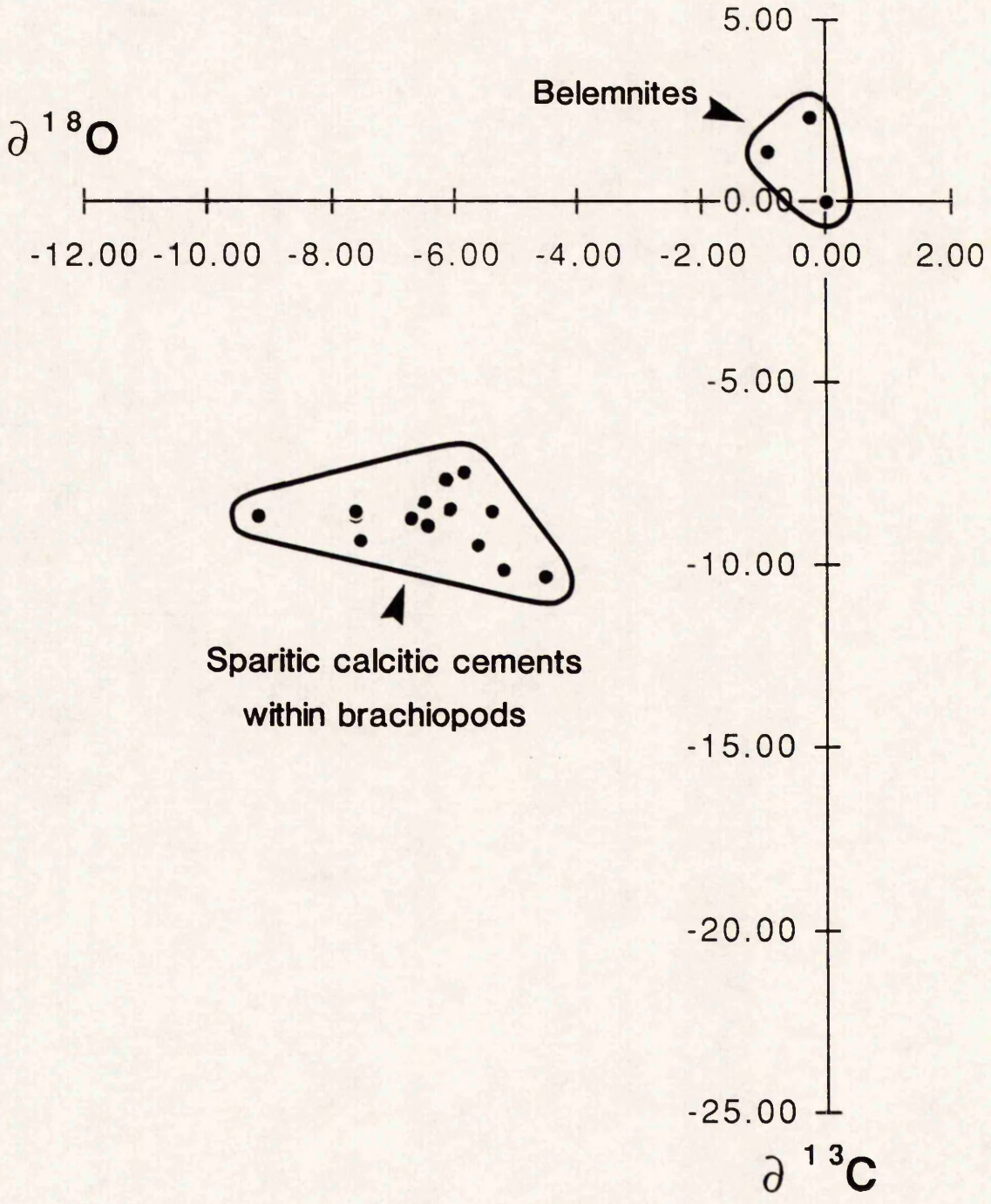

values is large, but if the two extreme values are removed then the range of $\partial^{18}O_{PDB}$ values from -5.42 to -7.64‰ is achieved, giving a more realistic range in isotopic values for meteoric waters, and a similar range to the Frodingham calcites. It is possible that some re-equilibrium of the calcites with later meteoric water may have occurred in this Ironstone to produce a large range in $\partial^{18}O_{PDB}$ values, given that the oxidation of the Ironstone in places is intense. However, the samples were drilled from both berthierine-rich, and goethitic beds, and no systematic difference in isotopic signature between the two was detected.

The isotopic signature of these later calcites may hence be compared directly to those of the Frodingham Ironstone Formation, and a similar genesis may be implied on the basis of the data obtained here.

6.5.7) Oxidation and Weathering of the Banbury Ironstone.

Many of the early accounts of ooidal ironstones from various localities, contain a section on the weathering of ironstones due to the enrichment of Fe that occurred on oxidation. Calcites are dissolved, and the Fe^{2+} in berthierine and siderite is oxidised during the formation of goethite. It is apparent from examination of weathered samples of the Banbury Ironstone that berthierine is more stable than siderite, as goethite pseudomorphs of siderite cements are found enclosing essentially fresh berthierine. It is therefore possible to gain an appreciation of the degree of weathering a sample has undergone by examination of the siderite present. The occurrence of goethite ooids within a clear siderite cement within ironstones is a clear indication that the goethite was present on deposition, and was not formed during recent weathering.

The weathered crust on the Banbury Ironstone is well defined, and provides direct information about the process of weathering and oxidation of ironstone minerals. In particular, the oxidation of berthierine to goethite has been proposed by many workers for the formation of goethite ooids. This could be tested by examination of the oxidation crust.

Petrography of a thin-section taken across the weathered surface (HRT. OX, plate 26b) showed that oxidation of a berthierine ooidal grainstone resulted in the obliteration of the texture of the ironstone, so that distinguishing original components within the goethite can be impossible, even in reflected light. Preservation of delicate fabrics on berthierine oxidation is therefore unlikely, and lends weight in favour of a primary goethite origin for ooids showing finely laminated cortices.

E.P.M.A. data of specimen HRT. OX are given in table 6.7, and plotted on a Si - (Fe+Mg) - Al(Total) ternary plot in figure 6.8. The berthierine ooid compositions show signs of slight oxidation relative to the matrix due to an elevated Fe content, or possible minor incorporated goethite. Analyses of the weathered crust show a complete trend towards the Fe+Mg pole from these berthierine compositions due to the loss of Si, Al and Mg and enrichment of Fe on oxidation. There is no systematic compositional difference between the inner and outer part of this crust, with all analyses containing residual Si and Al. This suggests that pure goethite (FeOOH) is unlikely to result from berthierine oxidation. Interestingly, X.R.D. analysis shows the goethite to contain ≈4 mol% AlOOH, indicating that the Al released is not necessarily incorporated into the goethite, and that high Al-goethites should not be expected from oxidation of ferrous aluminosilicates.

6.5.8) Discussion.

The Banbury Ironstone differs significantly from the Frodingham Ironstone Formation in that it contains an abunbance of berthierine ooids, but the high bioclastic content and dominance of grain-ironstones in the sequences are comparable. The diagenetic sequence is very similar, resulting in the formation of berthierine muds and cements, with siderite then ferroan calcite forming a high authigenic carbonate content later during diagenesis. The lack of a clear distinction between berthierine matrix and cement in this ironstone-formation suggests that the fabrics show a more *in situ* transformation with berthierine formation, rather than extensive liberation of elements into pore fluids. Siderite is widespread as a pore-filling cement, and may reflect the abundance of berthierine within

Table 6.7. Average Compositions of Berthierines and the Surface Oxidation Layer Within Specimen HRT. OX of the Banbury Ironstone, Obtained By E.P.M.A. The Data have all been Recalculated to Berthierine Structural Formulae to Facilitate Comparison Between the Data.

	BERTHIERINE MATRIX		BERTH./GOETH. OOIDS		GOETHITE OOIDS (INNER)		GOETHITE ZONE (OUTER)	
	AVERAGE	STDEV	AVERAGE	STDEV	AVERAGE	STDEV	AVERAGE	STDEV
Si	9.966	1.137	6.903	1.297	4.740	2.674	5.256	3.449
Ti	0.028	0.034	0.356	0.270	0.031	0.031	0.059	0.080
Al	7.177	0.847	5.132	0.857	2.764	2.320	3.610	2.536
Fe	26.822	2.589	23.610	5.190	40.536	9.947	38.918	4.616
Mn	0.020	0.023	0.053	0.036	0.147	0.088	0.250	0.151
Mg	1.335	0.206	1.139	0.368	0.564	0.469	0.697	0.176
Ca	0.294	0.062	0.418	0.199	0.285	0.077	0.671	0.178
Na	0.219	0.103	0.223	0.193	0.357	0.075	0.253	0.166
K	0.056	0.052	0.087	0.109	0.033	0.027	0.029	0.048
P	0.059	0.062	0.099	0.080	0.028	0.048	0.043	0.056
S	0.054	0.047	0.064	0.036	0.062	0.064	0.032	0.033
O	26.607	2.704	20.585	3.457	20.187	5.402	21.336	5.119
TOTAL	72.636	6.987	58.668	10.392	69.732	14.445	71.154	7.428
BerthCalc.								
Si	2.997	0.050	2.702	0.223	1.768	0.662	1.807	0.791
Al(T)	1.003	0.050	1.298	0.223	2.232	0.662	2.193	0.791
Al(O)	1.243	0.101	0.793	0.275	-1.221	1.390	-0.914	1.411
Ti	0.005	0.006	0.086	0.068	0.006	0.006	0.012	0.015
Fe	4.061	0.190	4.608	0.472	8.488	2.488	7.849	2.446
Mn	0.003	0.004	0.010	0.006	0.034	0.026	0.055	0.041
Mg	0.463	0.041	0.511	0.135	0.233	0.175	0.303	0.047
Ca	0.052	0.010	0.093	0.053	0.081	0.051	0.166	0.020
Na	0.084	0.047	0.103	0.088	0.187	0.072	0.132	0.098
K	0.012	0.012	0.026	0.031	0.008	0.006	0.007	0.010
OCT.	5.775	0.063	6.009	0.239	7.541	0.975	7.306	1.073
INT.	0.148	0.056	0.222	0.110	0.277	0.115	0.305	0.091
CH	8.000	0.000	8.000	0.000	8.000	0.000	8.000	0.000
	n=6		n=6		n=7		n=8	

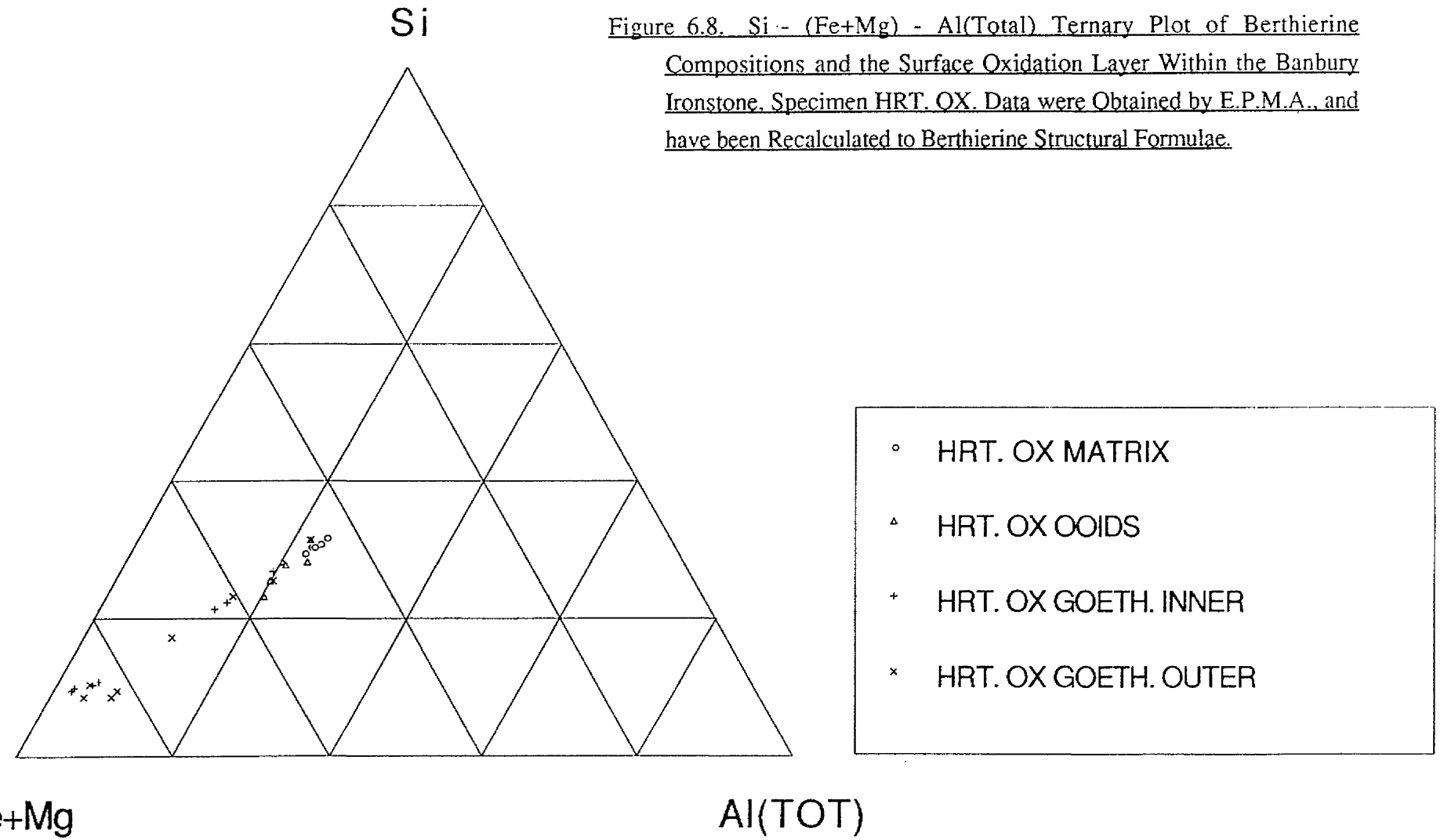

Figure 6.8. Si - (Fe+Mg) - Al(Total) Ternary Plot of Berthierine Compositions and the Surface Oxidation Layer Within the Banbury Ironstone, Specimen HRT. OX. Data were Obtained by E.P.M.A., and have been Recalculated to Berthierine Structural Formulae.

this ironstone. A marine origin for the siderites and berthierine can be postulated on the basis of the similarity between this and the Frodingham Ironstone Formation.

As in the Frodingham ironstones, the later ferroan calcite may be associated with a precipitation from meteoric water, based upon the isotopic evidence. Compared to the Frodingham Ironstone Formation, the small range of $\partial^{13}C_{PDB}$ values suggests that less O.M. degradation was occurring at the time of calcite precipitation, so that the $\partial^{13}C_{PDB}$ signature reflects that of the meteoric water alone.

6.6) The Raasay Ironstone.

6.6.1) Introduction.

The Raasay Ironstone is a berthierine-rich ooidal ironstone with a high proportion of echinoderm debris, that outcrops on the island of Raasay, N.W. Scotland (figure 6.9, plate 27a). It is 2.5m thick and Toarcian (U. Lias) in age, of the *Dactylioceras commune* and *Grammoceras thouarsense* subzones, with the three intervening ammonite zones being absent (Cope *et al.* 1980). The deposit is condensed, comparable to over 50m of strata in North Yorkshire, and local to Raasay as a ferruginous deposit. It occurs within Liassic shales, the sequence of which is described in detail by Lee (1920), with its lateral extension onto Skye, described by Anderson and Dunham (1966). The best description of the ironstone field, yields, and extent, is given by MacGreggor *et al.* (1920), but such a small ironstone field has generally received little attention in the literature. The most recent work involving this ironstone is by Kearsley (1989), who uses the Raasay ooids as part of his classification scheme.

The Ironstone can be divided into three convenient lithotypes; ferruginous crinoidal limestone (plate 27b); berthierine ooidal mudstone (plate 27c); and sparsely ooidal sideritic mudstone, with full transitions between the three. Beds are usually a few centimetres thick, but are obscured by weathering. As with other ironstones, bed variation over a few metres can be seen, and correlation becomes difficult. Some cross-lamination may be visible.

Figure 6.9. Geological Map of the Island of Raasay, North-west Scotland, Showing the Outcrop of the Raasay Ironstone. Taken From Macgregor *et al*. (1920, figure 16, p.199).

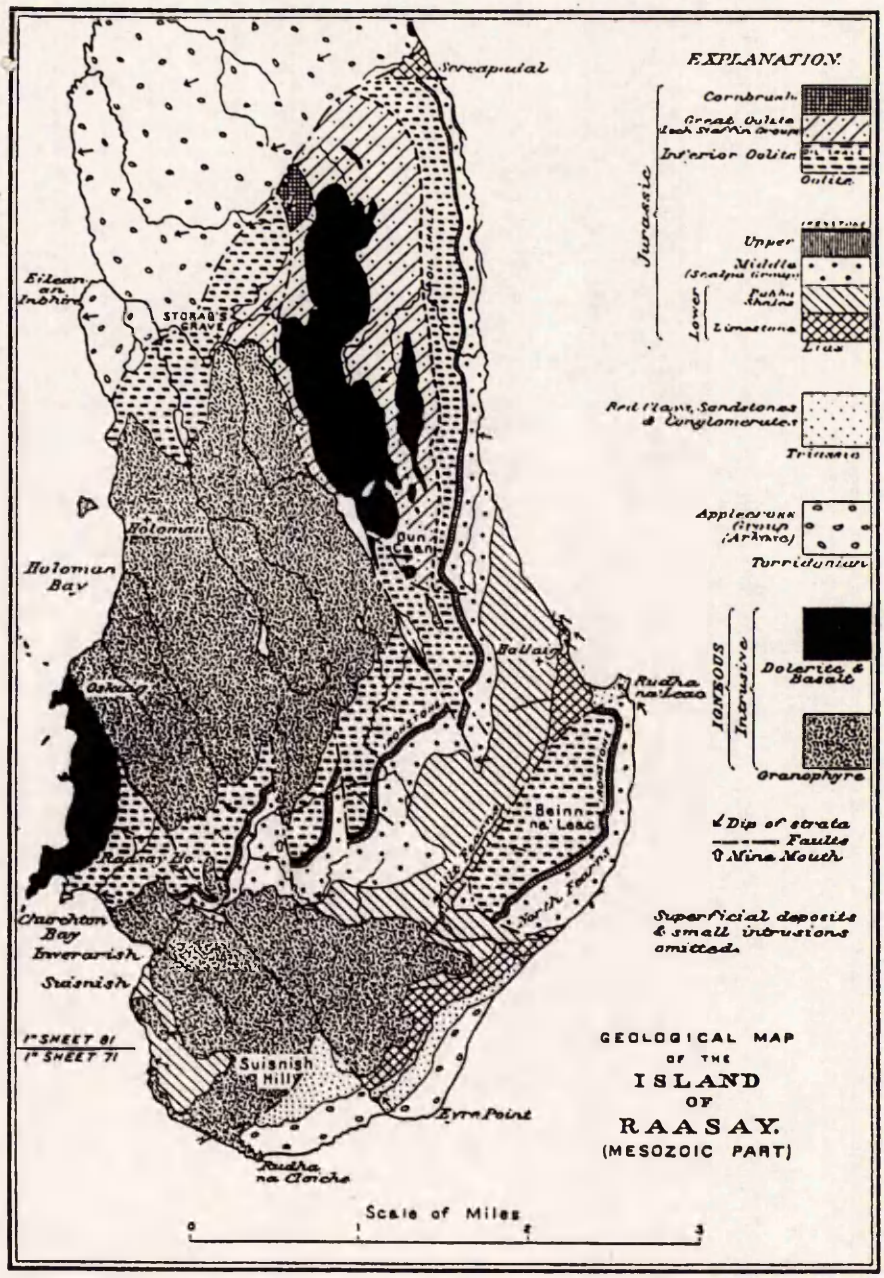

PLATE 27

The Raasay Ironstone

A) Outcrop of the Raasay Ironstone at the ironstone mines (see map, figure 6.9). The exposure shown is approximately 2m high.

B) Carbonate cement stratigraphy of an echinoderm grainstone, thin-section of specimen RSY. 6. The earliest siderite generation is arrowed for reference. Photo length is equivalent to 3.3mm.

C) Berthierine ooidal packstone, thin-section of specimen RSY. 4. The ooids are generally plastically deformed, but preserved in places where edge replacement by siderite has occurred (arrowed). The rock is cemented by siderite and berthierine. Photo length is equivalent to 3.3mm.

D) Spheroidal berthierine, thin-section (crossed polars) of specimen RSY. 4. The berthierine has nucleated on the ooids and cements the pore. Siderite replaces both the ooids and the cement. Photo length is equivalent to 0.7mm.

A	B
C	D

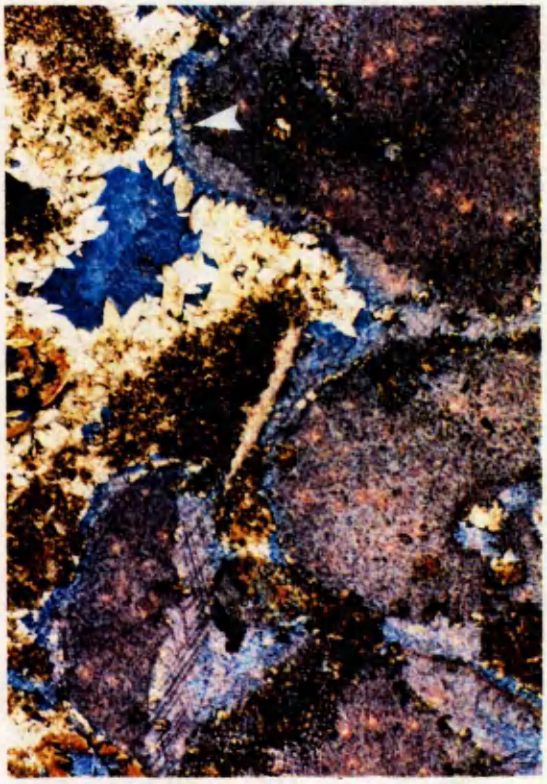

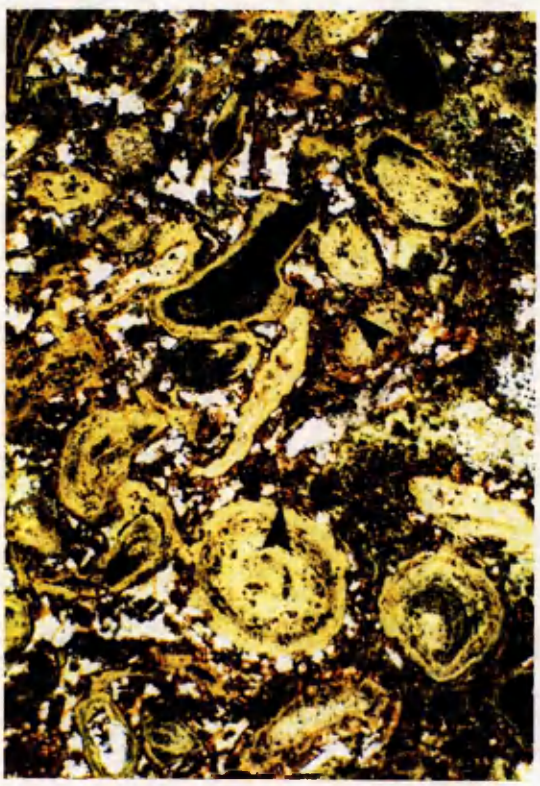

Belemnites are abundant and often show signs of reworking, leading to the interpretation of MacGreggor *et al.* (1920) that this is a *remanie* assemblage.

Samples were collected from outcrop, and thin-sections were made of berthierine ooidal ironstone and a crinoidal facies, with the intention of ascertaining a brief diagenetic comparison to the other ironstones. In particular, ooid morphology, berthierine composition, and relative timing of diagenetic events were studied.

6.6.2) Ooid Morphology.

Berthierine ooids form a large proportion of the rock and are spheroidal to ellipsoidal in shape but often highly deformed (plate 27c). Nuclei are often absent, and the cortex is concentrically laminated with no sign of complex cortical development as in the Frodingham ooids. They are also larger than the Frodingham examples, being 0.4-1.3mm across, mostly around 0.8mm. A similar mode of genesis to the Frodingham ooids is implied, that is growth as microconcretions but without development upon large nuclei, but formation within an area of less differential stress/permeability is suggested, that allowed a more perfect ellipsoidal shape to develop.

6.6.3) Berthierine Occurrence and Composition.

Berthierine occurs forming ooids (see above), mud (largely replaced by siderite), replacing bioclastic debris (especially echinoderm fragments), and as an authigenic cement. Only the latter is discussed here in detail, as the morphologies and interpretation of the other occurrences are similar to the Frodingham examples, and are interpreted to have similarly formed. The authigenic cement is unusual in that it occurs as spherules, or part spherules, of radiating berthierine crystals, up to 70μm long (i.e. full spherules are < 140μm), in an apparently previously undescribed morphology (plate 27d). The texture does not appear to be replacive, though the comparison to sphaerosiderites of other rock types is noted.

The composition of berthierine ooids and spherules was obtained by E.P.M.A., and are given in table 6.8, and plotted in figure 6.10. Compared to the Frodingham berthierines,

Table 6.8. Average Compositions of Berthierines in the Raasay Ironstone, Obtained By E.P.M.A. The Data have been Recalculated to Berthierine Structural Formulae.

RSY. 4	BERTHIERINES			
	OOIDS		SPHERULES	
	AVERAGE	STDEV	AVERAGE	STDEV
Si	8.497	0.767	9.038	0.285
Ti	0.088	0.048	0.050	0.052
Al	8.470	0.818	10.662	0.414
Fe	27.951	2.750	34.245	0.439
Mn	0.054	0.061	0.046	0.088
Mg	1.084	0.175	1.025	0.077
Ca	1.249	0.974	0.044	0.040
Na	0.160	0.178	0.169	0.131
K	0.049	0.056	0.000	0.001
P	0.564	0.513	0.387	0.133
S	0.037	0.044	0.019	0.024
O	27.303	1.570	30.852	0.755
TOTAL	75.507	4.837	86.505	1.673
BerthCalc.				
Si	2.550	0.085	2.367	0.052
Al(T)	1.450	0.085	1.633	0.052
Al(O)	1.193	0.109	1.282	0.059
Ti	0.016	0.008	0.008	0.008
Fe	4.210	0.138	4.525	0.066
Mn	0.009	0.010	0.006	0.012
Mg	0.376	0.050	0.311	0.024
Ca	0.276	0.227	0.008	0.008
Na	0.058	0.063	0.054	0.042
K	0.010	0.012	0.000	0.000
OCT.	5.803	0.159	6.132	0.030
INT.	0.344	0.219	0.063	0.045
CH	8.000	0.000	8.000	0.000
	n=7		n=9	

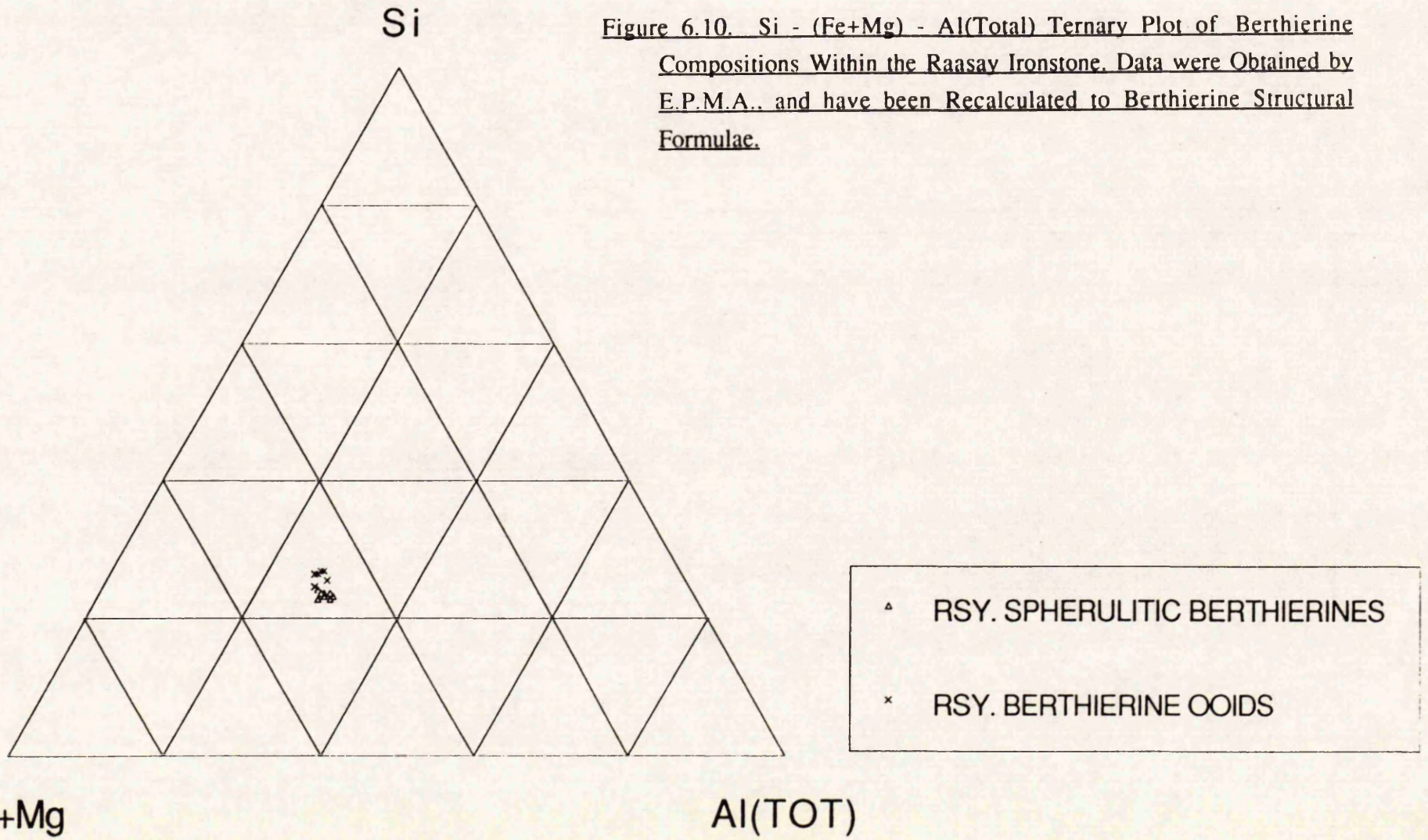

Figure 6.10. Si - (Fe+Mg) - Al(Total) Ternary Plot of Berthierine Compositions Within the Raasay Ironstone. Data were Obtained by E.P.M.A., and have been Recalculated to Berthierine Structural Formulae.

those of the Raasay Ironstone have a similar Fe+Mg content, though the Fe/Mg ratio is slightly higher. Both the ooids and spherulitic cement data cluster in the same area of the Si - Fe+Mg - Al(Total) ternary plot (figure 6.10). The Fe+Mg content is similar in the ooids and spherulites, but the Fe/Mg ratio is slightly higher (≈14.5 as opposed to ≈11.2), and Si/Al ratio slightly lower (0.81 as opposed 0.96), in the latter. Both sets of analyses have a significantly higher Al content than those of the Frodingham and other berthierines but remain within the range of published berthierine compositions. If the origin of berthierines within this ironstone is similar to that of the Frodingham berthierines, then it can be assumed that the lower Si/Al content results from a more Al-rich precurser detrital clay, almost certainly due to a higher proportion of kaolinite, similar to the Cleveland and Banbury ironstone-formations.

6.6.4) Carbonates.

The Raasay Ironstone has a high detrital carbonate content, which is largely composed of echinoderm fragments. Authigenic carbonates are also abundant where primary porosity was high. Ferroan calcite and siderite cements were identified by staining, the former of which has replaced most echinoderm fragments. Examination of a number of sections gives the following carbonate cement stratigraphy, the full development of which is associated with the crinoidal sediments (plate 27b):

CARBONATE	MORPHOLOGY
Siderite #1	Very thin fibrous cement with a poor radial fabric.
↓	
Ferroan Calcite #1	Sparite. Syntaxial overgrowths on echinoderm debris.
↓	
Siderite #2	Euhedral rhombic crystals with curved faces.
↓	
Ferroan Calcite #2	Sparite. Pore-filling.

In RSY. 4 where spheroidal berthierine has formed, a scalenohedral ferroan calcite has developed predating the berthierine, and was precipitated syntaxially on small crinoid stems that retain their non-ferroan calcite mineralogy. This clearly suggests that ferroan calcite can

form primary scalenohedral cements that are not replaced former H.M.C. cements, otherwise the crinoid stems (of H.M.C.) would also have been replaced.

6.6.5) Discussion.

Though there is more significant overlap in the development of the authigenic mineralogy in this ironstone to those described above, a similar diagenetic sequence of berthierine, siderite, and calcite precipitation is again displayed. Pyrite is uncommon, and the characteristic mineral assemblage as described for the other ironstones is again seen. The Raasay mineralogy differs most significantly from the other ironstones in the unusual morphology of the berthierine cement, but the constraints on the formation of this texture are undefined. The ferroan scalenohedral calcites precipitated on non-ferroan calcite of original H.M.C. provides strong evidence for the primary precipitation of scalenohedral and fibrous ferroan calcites, as postulated for the Frodingham Ironstone Formation.

6.7) The Abbotsbury Ironstone.

6.7.1) Introduction.

The Abbotsbury Ironstone is a localised deposit outcropping in and around the village of Abbotsbury, Dorset, 12km west of Weymouth (figure 6.11). The Ironstone consists of goethite-ooidal sandstones overlying ferruginous sandstones (Sandsfoot Grits of Arkell, 1936), and is about 8m thick (Brookfield 1973). The Ironstone was not extensively quarried due to the high silica content, despite an average iron content of over 30% (Lamplugh *et al.* 1920). The deposit is of Kimmeridgian age (Arkell 1933, 1936) in the *Rasenia cymodoce* zone (Brookfield 1973, Cope 1971) and is therefore a lateral extension of the Lower Kimmeridge Clay of Dorset. Within the Kimmeridge Clay, the zone is represented in the lower part by clays with two siltstone bands, and by pyritic shales in the upper part. The Oxfordian-Kimmeridgian boundary sequence consists of dark grey, bioturbated clays and silts with scattered goethitic ooids and phosphatic nodules overlying the Ringstead Coral Bed, and ferruginous ooidal clay (Cox and Gallois 1981).

Figure 6.11. Geological Map of the Abbotsbury Area. Taken From Brookfield (1973).

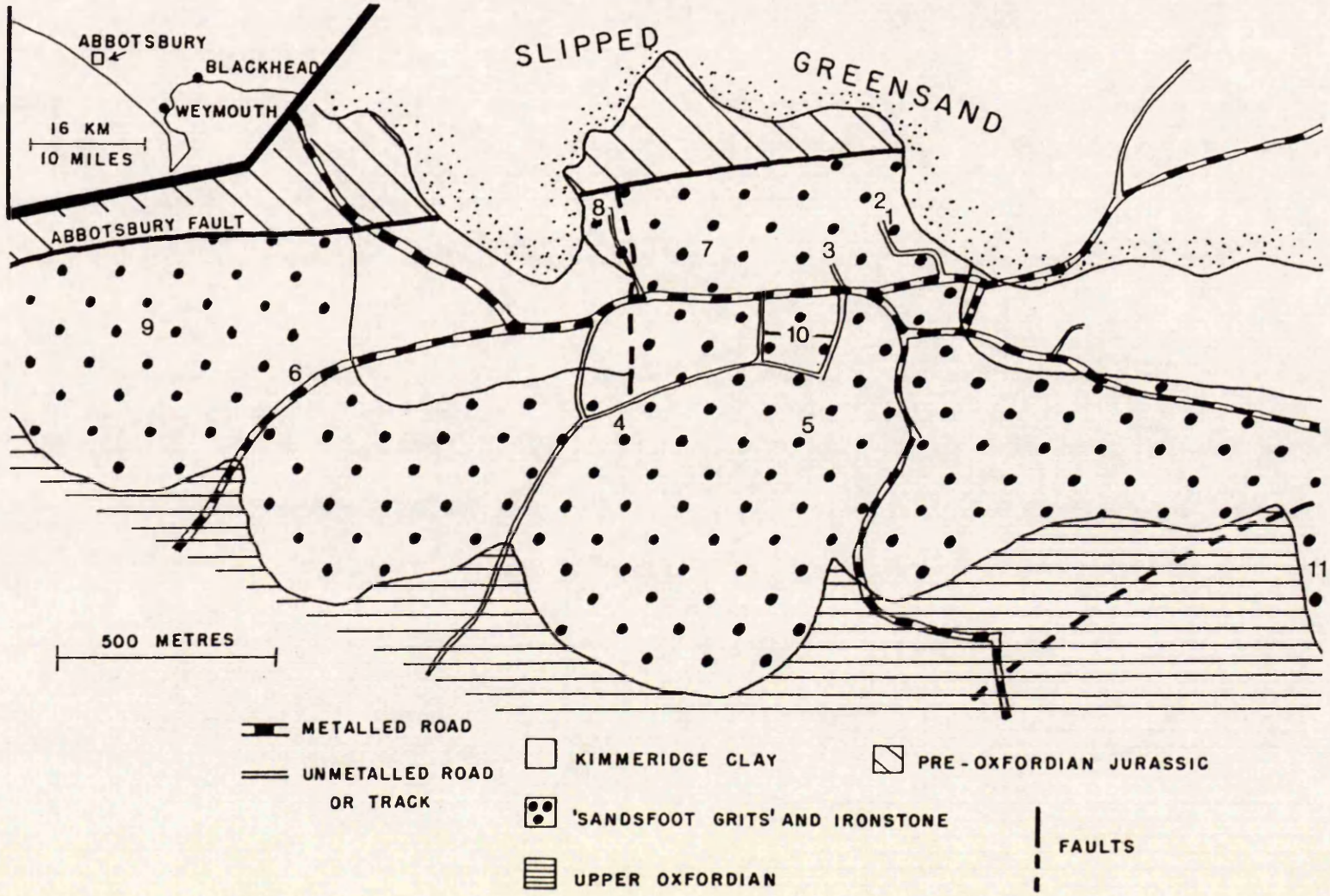

Early descriptions of the Ironstone were given by Arkell (1933, 1936) and Lamplugh *et al.* (1920). The most useful and modern work, is that of Brookfield (1973), who subdivided the Abbotsbury Ironstone and 'Sandsfoot Grits' into three lithofacies (see also figures 6.12 and 6.13):

1) Medium-bedded, moderately well-sorted, bioturbated, fine-grained, quartz sandstone.

2) Thin-bedded, poorly-sorted to moderately well-sorted, fine-grained, quartz sandstone.

3) Massive, poorly-sorted, "limonite"-ooidal fine-grained, quartz sandstone. (Two faunal sub-facies.)

A nearshore environment, or marginal to an offshore (barrier) bar, was proposed for the environment of ironstone formation, with the different facies largely reflecting the degree of water agitation.

6.7.2) Exposure and Ironstone Description.

Localities of the Ironstone indicated in Brookfield (1973) were visited (figure 6.11). Many are now apparently no longer present, or in a poor condition, but the following localities may still be found, whose numbers refer to locations in figure 6.11.

Locality 1). A small cutting at the edge of a wood along a footpath leading northwards from the village. The outcrop is highly weathered ooidal ironstone with a 'sand' of ooids weathered out at the base. The exposed surface is friable and lacks signs of bedding or lamination. Fossils are uncommon, though bioturbation is seen as dispersed burrows. The ooids are brown-black and closely packed forming the framework of the rock (pack-ironstone). Symmetrically zoned goethite veins up to 1cm thick cut the outcrop. Ooids were collected at this locality for shape analysis (section 3.2.4.1).

Locality 2). A small cutting ≈40m north of locality 1, of ferruginous sandstone with scattered ooids. Thin-section examination shows fine to medium sand grade, mono- to polycrystalline, rounded to angular quartz (38%); similar sized feldspars (2%) and uncommon ooids (1%), in a matrix of dark brown oxidised mud (59%). Quartz sphericity is variable, measured (as elongation) up to 3:1.

Figure 6.12. Sections of the Abbotsbury Ironstone. Taken From Brookfield (1973).

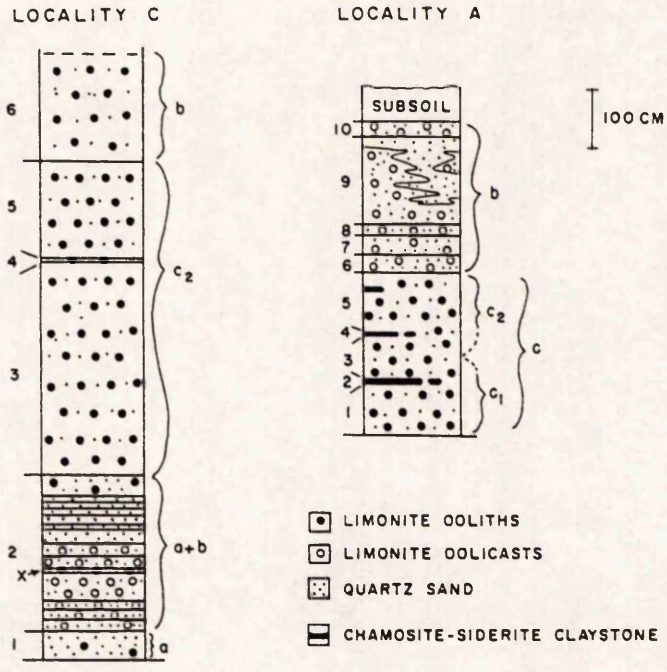

Figure 6.13. Facies Distribution of the Abbotsbury Ironstone with Characteristic Fauna. Taken From Brookfield (1973).

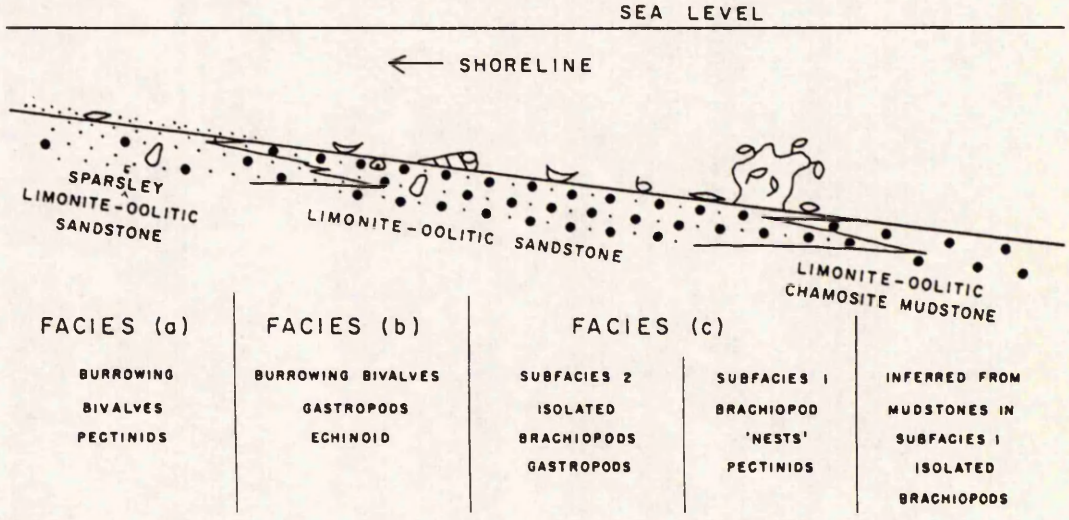

Locality 3). Small disused (now being infilled as rubbish tip), and overgrown quarry. The locality is innaccessible without permission and is of poor quality. Brookfield's (1973) log of this exposure is given in figure 6.12.

Locality 5). Very small exposure next to the footpath. The rock is a weathered, non-ooidal ferruginous sandstone, containing fine to medium grade, mono- and polycrystalline, subrounded to subangular quartz (59.5%); feldspar (2%) and glauconite (<0.5%), in a tangential grain-coating, and interstitial, matrix (38.5%).

Locality 6). Road Cutting (plate 28a). The exposure consists of massively-bedded ooidal ironstone with goethitic veining. Two thin-sections revealed quartz (31% and 21%); ooids (23% and 33%); matrix (36% and 25%); and goethite pseudomorphs after siderite (10% and 21%). The quartz is similar to that described above, but is here partly corroded by the siderite. The analysed specimen ABB. 13 is from this locality.

6.7.3) Ooids.

The shape of the ooids in the Abbotsbury Ironstone were examined in detail as a comparison to those of the Frodingham Ironstone Formation in section 3.2.4.1. The Abbotsbury ooids have a greater sphericity than the Frodingham ooids, and this is reflected in their internal structure which shows better defined cortical lamination in a continuous growth pattern (plate 28b). Growth stages one and two defined for the Frodingham ooids are present here, though stage two does not develop a strong equatorial plane. There is no stage three cortical accretion.

The nuclei of these ooids are similar to the Frodingham ooids, comprising unstructured goethitic particles which may show a random fracture pattern. No quartz nuclei are present despite the abundance of the mineral in the Ironstone, suggesting differing sources for the ooids and quartz sand.

6.7.4) Mineral Compositions.

The compositions of the iron-ooids (goethitic) and matrix were determined using E.P.M.A. Calcites have often been leached during weathering, and siderite has been

PLATE 28

The Abbotsbury Ironstone

A) Outcrop of the Abbotsbury Ironstone at locality 6. The outcrop shown provides the most readily accessible exposure of the ironstone at present.

B) Ooidal sandstone, thin-section of specimen ABB. 14. The ooids show a finely laminated cortex and oblate shape. The "chamositic" matrix has been partially replaced by siderite (arrowed) that is now pseudomorphed by goethite due to recent weathering of the outcrop. Photo length is equivalent to 3.3mm.

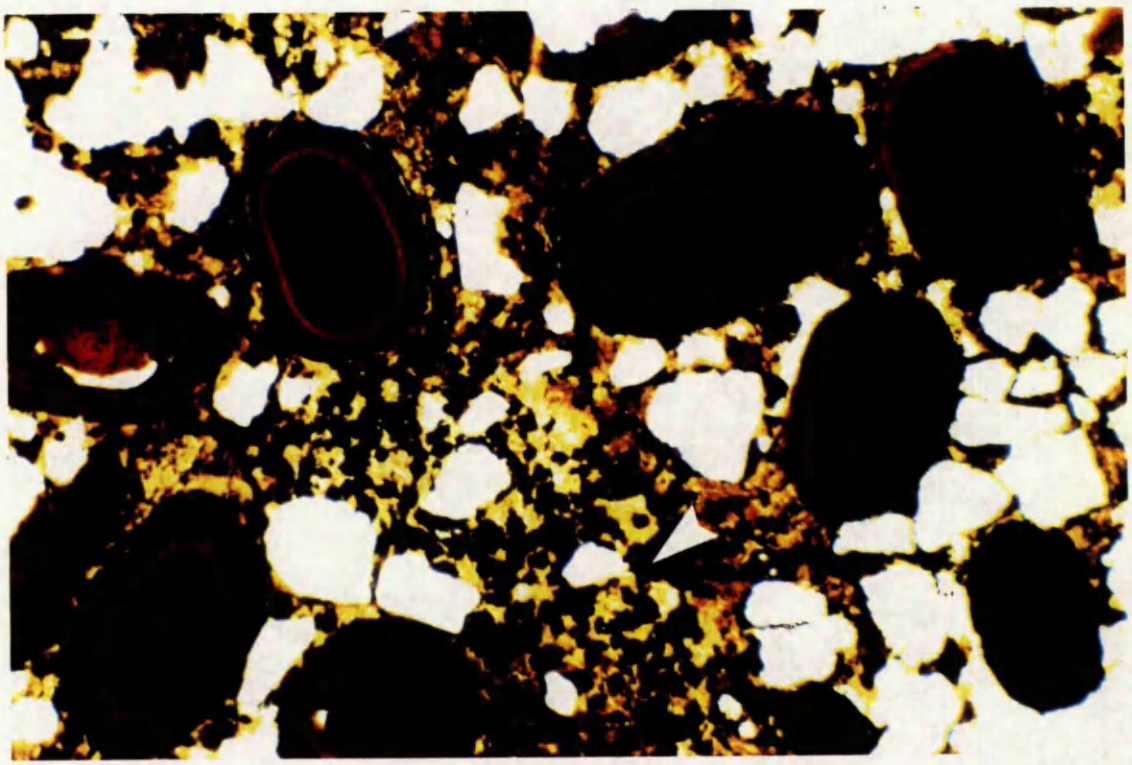

pseudomorphed by goethite, so these minerals were not analysed. Analyses of the ooids and matrix are given in tables 6.9 and 6.10, and are plotted together in figure 6.14. The ooid compositions are similar to those obtained from the Frodingham ironstones, in that they contain a small quantity of Si and Al within the cortex that is attributed to admixed clay. This is confirmed by the trend of data seen in figure 6.14 from the Fe+Mg pole towards the matrix composition. X.R.D. analysis of the goethites suggests that they are non-aluminous.

X.R.D. analysis of sample ABB. 13 failed to identify the mineral of the matrix, but this has been previously described as "chamosite" (for example Brookfield 1973). Analyses of the matrix gave widely varying results shown by a large scatter in figure 6.14. The Abbotsbury Ironstone contains significant quantities of quartz, and the high Si content is probably due to contamination by fine grained SiO_2, so that these analyses do not represent the bulk clay mineral composition.

6.7.5) Discussion.

The Abbotsbury Ironstone is unusual amongst the British Jurassic ooidal ironstones as it contains a high proportion of silt and sand sized quartz. The lack of quartz nuclei in the ooids indicates that the detrital assemblage in this deposit represents reworking of (at least) two very distinct sources of sediment; one ooid rich and the other quartz rich.

The presence of "chamosite" mud in the Ironstone is in conflict with the commonly held view that a low detrital input is required for ironstone formation. This therefore suggests that either the mud was transported as original "chamosite" or that the presence or absence of quartz does not control the formation of iron silicates. The occurrence of siderite replacing the matrix is strong evidence to suggest that iron-reduction was occurring within this sediment, and that "chamosite" formed *in situ*. It is therefore proposed that ironstone formation associated with a lack of terrigenous clastic material is due to sediment starvation allowing post-oxic conditions to form during constant reworking, and not due to the lack of abundant silica in the system.

Table 6.9. Compositions of Goethitic Ooid Cortices in the Abbotsbury Ironstone, Obtained By E.P.M.A. The Data have been Recalculated to Berthierine Structural Formulae to Allow Direct Comparison With the Frodingham Ooid Data.

	ABB. 13	GOETHITIC OOIDS										
	1	2	3	4	5	6	7	8	9	10	AVERAGE	STDEV
Si	2.028	3.339	2.796	1.543	1.981	2.040	2.461	2.307	2.158	3.415	2.407	0.607
Ti	0.200	0.228	0.231	0.428	0.263	0.175	0.141	0.100	0.142	0.273	0.218	0.093
Al	1.717	2.431	2.279	1.406	1.651	1.802	1.841	1.957	1.781	2.393	1.926	0.339
Fe	38.036	37.870	41.164	40.673	41.646	42.106	37.700	36.453	44.173	35.830	39.565	2.751
Mn	0.023	0.035	0.049	0.080	0.115	0.000	0.087	0.000	0.000	0.175	0.056	0.058
Mg	0.375	0.394	0.525	0.317	0.314	0.349	0.242	0.513	0.530	0.525	0.408	0.107
Ca	0.070	0.129	0.211	0.138	0.149	0.337	0.169	0.129	0.132	0.202	0.167	0.072
Na	0.122	0.261	0.191	0.150	0.015	0.180	0.054	0.364	0.229	0.330	0.190	0.111
K	0.289	0.342	0.231	0.081	0.149	0.201	0.199	0.228	0.181	0.456	0.236	0.105
P	0.271	0.200	0.491	0.422	0.505	0.423	0.338	0.301	0.303	0.421	0.368	0.100
S	0.000	0.004	0.053	0.005	0.000	0.028	0.000	0.047	0.000	0.000	0.014	0.021
O	15.601	17.708	18.352	15.846	16.820	17.121	16.084	15.830	17.702	17.696	16.876	0.983
TOTAL	58.732	62.941	66.573	61.089	63.608	64.762	59.316	58.229	67.331	61.716	62.430	3.190
(BerthCalc.)												
Si	1.077	1.541	1.290	0.824	1.004	1.004	1.278	1.213	1.009	1.622	1.186	0.253
Al(Total)	0.949	1.168	1.095	0.781	0.871	0.923	0.995	1.071	0.867	1.183	0.990	0.136
Ti	0.062	0.062	0.062	0.134	0.078	0.050	0.043	0.031	0.039	0.076	0.064	0.029
Fe	10.158	8.791	9.543	10.920	10.617	10.417	9.847	9.627	10.391	8.560	9.887	0.772
Mn	0.006	0.008	0.012	0.022	0.030	0.000	0.023	0.000	0.000	0.043	0.014	0.015
Mg	0.230	0.210	0.280	0.196	0.184	0.198	0.145	0.312	0.286	0.288	0.233	0.055
Ca	-0.191	-0.098	-0.274	-0.289	-0.334	-0.198	-0.204	-0.192	-0.171	-0.235	-0.219	0.067
Na	0.079	0.147	0.108	0.098	0.009	0.108	0.034	0.234	0.131	0.191	0.114	0.067
K	0.110	0.113	0.077	0.031	0.054	0.071	0.074	0.086	0.061	0.156	0.083	0.035
CH	8.000	8.000	8.000	8.000	8.000	8.000	8.000	8.000	8.000	8.000	8.000	0.000

Table 6.10. Compositions of "Chamositic" Matrix of the Abbotsbury Ironstone, Obtained By E.P.M.A. The Data have been Recalculated to Berthierine Structural Formulae.

	ABB. 13								
	1	2	3	4	5	6	7	AVERAGE	STDEV.
Si	15.183	13.357	14.768	8.239	15.332	13.995	17.953	14.118	2.969
Ti	0.000	0.000	0.076	0.032	0.000	0.216	0.508	0.119	0.188
Al	5.808	5.252	5.565	3.866	3.400	6.709	8.219	5.546	1.637
Fe	20.776	26.459	23.028	33.153	18.770	16.789	17.469	22.349	5.832
Mn	0.026	0.000	0.069	0.000	0.000	0.000	0.038	0.019	0.027
Mg	1.572	1.485	1.676	1.389	0.695	1.055	1.377	1.321	0.338
Ca	0.318	0.432	0.319	1.017	0.374	0.172	0.429	0.437	0.270
Na	0.924	0.927	0.790	1.095	0.463	0.587	0.634	0.774	0.224
K	0.910	0.774	0.719	0.369	0.458	1.723	2.394	1.050	0.739
P	0.108	0.243	0.127	0.612	0.264	0.049	0.128	0.219	0.189
S	0.138	0.164	0.441	0.156	0.085	0.095	0.092	0.167	0.125
O	30.231	29.412	30.258	24.912	27.071	28.248	35.071	29.315	3.174
TOTAL	75.994	78.505	77.836	74.840	66.912	69.638	84.312	75.434	5.787
BerthCalc.									
Si	4.041	3.692	3.942	2.790	4.617	3.969	4.118	3.881	0.557
Al(T)	-0.041	0.308	0.058	1.210	-0.617	0.031	-0.118	0.119	0.557
Al(O)	1.650	1.204	1.488	0.152	1.683	1.950	2.079	1.458	0.644
Ti	0.000	0.000	0.012	0.006	0.000	0.036	0.068	0.017	0.026
Fe	2.765	3.659	3.040	5.622	2.832	2.383	2.006	3.187	1.192
Mn	0.004	0.000	0.009	0.000	0.000	0.000	0.004	0.002	0.004
Mg	0.483	0.474	0.517	0.543	0.242	0.346	0.365	0.424	0.109
Ca	0.016	-0.018	0.008	-0.072	-0.041	0.013	0.025	-0.010	0.036
Na	0.300	0.313	0.258	0.453	0.170	0.203	0.178	0.268	0.099
K	0.174	0.154	0.138	0.090	0.099	0.351	0.395	0.200	0.122
OCT.	4.902	5.336	5.067	6.324	4.756	4.714	4.523	5.089	0.605
INT.	0.490	0.449	0.404	0.471	0.228	0.568	0.597	0.458	0.121
CH	8.000	8.000	8.000	8.000	8.000	8.000	8.000	8.000	0.000

Figure 6.14. Si - (Fe+Mg) - Al(Total) Ternary Plot of Goethitic Ooid and Berthierine Compositions Within the Abbotsbury Ironstone. Data were Obtained by E.P.M.A., and have been Recalculated to Berthierine Structural Formulae.

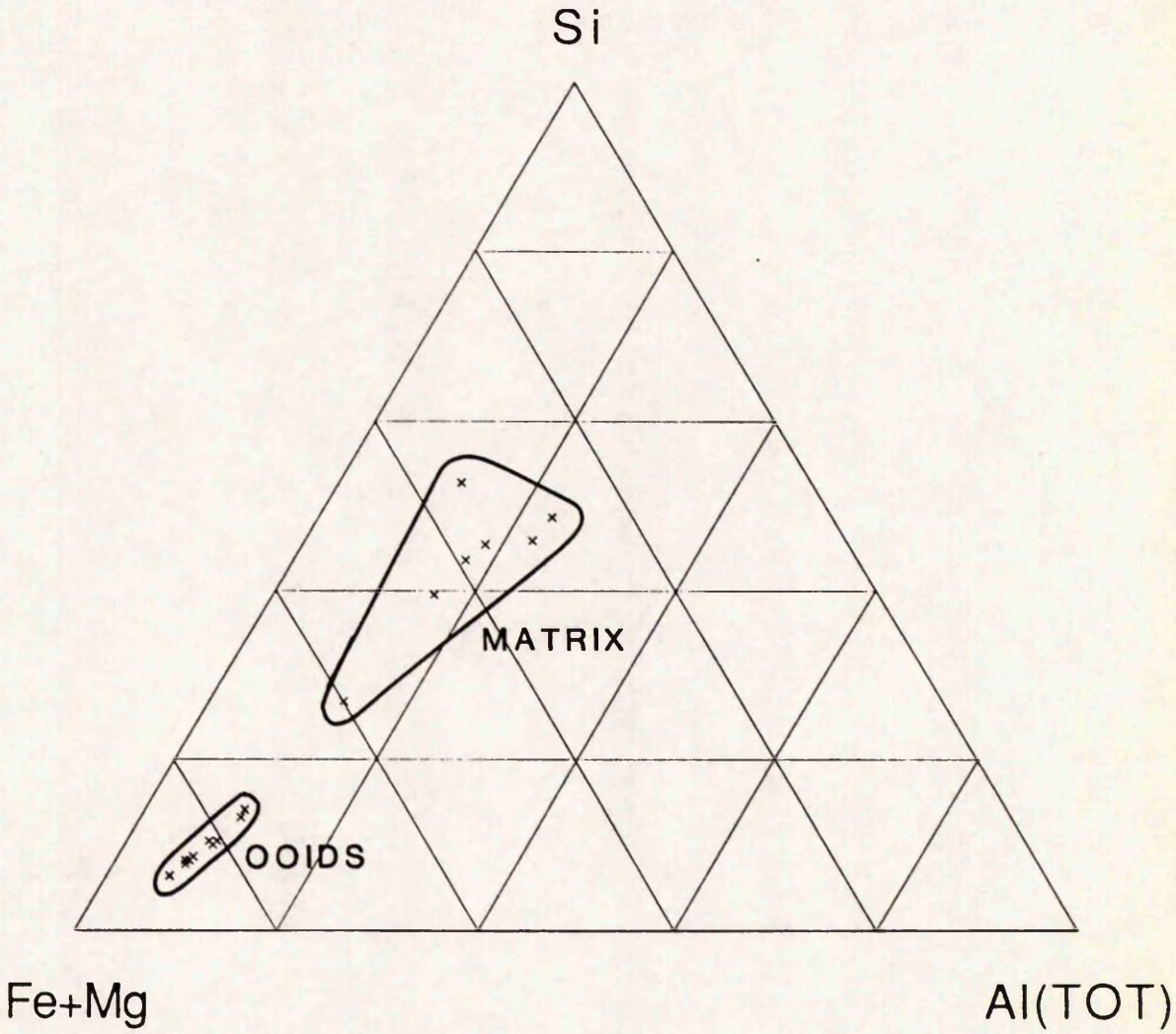

6.8) Summary of Ironstone Genesis in the Frodingham Ironstone Formation Compared to Other British Jurassic Ooidal Ironstones.

The descriptions and interpretations given for the Cleveland, Banbury, Raasay, and Abbotsbury ironstones, suggest that the conclusions of ironstone genesis proposed for the Frodingham Ironstone Formation can be applied to other ironstones with slight modification. Sedimentologically, all of these ironstone-formations consist of a condensed sequence of marine, reworked and bioturbated ooidal bioclastic sediments, deposited in shallow water, although the precise facies may vary.

The Frodingham ironstones differ most significantly from the others described in having a high proportion of goethitic ooids relative to fully berthierine ooids, the latter of which are extremely difficult to study. Therefore, applying the models of ooid genesis from the goethitic Frodingham examples to other ironstones containing predominantly berthierine ooids, should be avoided unless comparison is made on a purely textural, rather than a mineralogical basis. The oblate spheroidal ooid shape is consistent within all the ironstones studied, and an origin for ooid genesis within the sediment may be extended to these ironstones. A full three stage cortical development is however not always present, even in the goethitic Abbotsbury ooids, and hence cannot be applied to ooids in general. Nuclei type in the goethitic and the berthierine ooids is similar between ironstones, but the Cleveland and Banbury ironstone-formations are distinct in that particles comprising ooid nuclei are also present within the matrix. There is hence the possibility for ooid genesis within the sediment at the site of accumulation in these examples, whereas the goethitic ooids of the Frodingham and Abbotsbury Ironstones, are believed to have been fully derived from a zone onshore.

The suggested origin of the Frodingham berthierine, as having formed from the destabilisation of a detrital kaolinitic / illitic / iron-oxide mineralogy, is believed to extend to the other examples described. The compositional variation and differing morphological development of the berthierine probably reflects local variations in sediment type, and kinetic factors (nucleation, porosity etc.) respectively. Siderite may be similarly compared between ironstones. Late meteoric-derived calcite cements in the Frodingham and Banbury

Ironstones are texturally and isotopically similar, and the early formation of these calcites may have significant implications for both 'late' ironstone genesis, and the interpretation of ferroan/manganoan calcites in other sediments.

The diagenetic sequence described for the Frodingham Ironstone Formation of:

(calcite) - berthierine (+/- siderite) - siderite - (pyrite) - ferroan/manganoan calcite

indicates a full post-oxic diagenetic sequence with a late meteoric influence. The diagenetic assemblage of the other ironstones fits with part or all of this sequence. The Cleveland and Abbotsbury Ironstones show berthierine and siderite formation only, whereas the Banbury and Raasay Ironstones show a nearly complete succession. This development has also been seen in the Northampton Sand Ironstone (Gehring 1990). Therefore, although local variations occur, this sequence may be proposed as a "typical" diagenetic sequence for the British ooidal ironstones. The common development in ironstones of this authigenic mineralogical assemblage, described in detail within this thesis for the Frodingham Ironstone Formation, gives confidence to suggest that a post-oxic dominated diagenetic history can be invoked for all ironstones where berthierine and siderite have formed *in situ*.

CHAPTER 7: CONCLUSIONS.

The major conclusions to this research are outlined below with some recommendations for future work.

1) Sedimentological studies of the Frodingham Ironstone Formation at outcrop (Yarborough Pit) and in borehole core (Dragonby 31 and Y183), suggests that it comprises a number of storm-generated fining cycles usually < 1m thick deposited at or near storm wave base. An 'ideal' cycle comprises a scoured base and coarse bioclastic coquina, overlain by ooidal bioclastic grain-ironstones grading into highly bioturbated ooidal wacke-ironstones and pack-ironstones, with a thin mud-ironstone drape. The cycles have been mechanically and biologically reworked with similar subordinate background sediments. Beds are variably composed of ooids, bioclasts (principally bivalves, brachiopods, cephalopods, and echinoderms) and detrital clays with occasional pisoids and intraclasts. Conditions were well-oxygenated, and a rich, diverse *in situ* macrofauna is present.

2) Ooids are composed of goethite +/- berthierine, or berthierine alone. Goethitic ooids are oblate ellipsoidal in shape and commonly show a three stage growth development. Ooid form and fabric have been qualitatively and quantitatively assessed in this thesis, and are believed to be of primary origin, representing growth of ooids as micro-concretions within a sediment under conditions of differential horizontal and vertical stresses or permeabilities. Compaction from spherical bodies is inconsistent with; the narrow range in ooid form; the three stage accretion fabric; the lack of cortical deformation around the goethitic nucleus; and the brittle fracturing of goethitic ooids. The ooids were formed by direct precipitation of goethite, similar to that seen today in laterites, as Fe^{2+} liberated from detrital particles during iron-reduction was oxidised in the upper (oxidised) layers of the sediment. Reworking of the ooids resulted in surface polishing, prior to re-incorporation of the ooid within the sediment and subsequent precipitation of the next goethitic layer. Illitic/kaolinitic clays trapped within the ooids were diagenetically altered to berthierine under conditions of post-oxic diagenesis, at the time of goethite precipitation or after incorporation within the ironstone.

Berthierine ooids also formed as micro-concretions, but it is believed that they might result from direct precipitation of berthierine within illitic/kaolinitic muds undergoing diagenetic alteration (see below). Berthierine ooids would not remain intact during significant reworking, as is demonstrated by their irregular plastic deformation on compaction, so were not transported far. It is hence considered unlikely that berthierine ooids were oxidised during reworking to form the goethitic ooids.

3) Berthierine cements are common and are of similar composition. They may form intergranular pore-lining to pore-filling cements; fill fractures in ooids; replace bioclastic debris; or form thin, non-isopachous fibrous cements on shell fragments. The berthierines have a low Al content and higher Fe/(Fe+Mg) ratio relative to most published berthierine compositions. Berthierine mudrocks with minor illite and kaolinite become purer as the sequence is ascended, with a compositional change consistent with the addition of Fe to the bulk clay mineralogy. Berthierine formed in response to a detrital assemblage of illitic/kaolinitic clays and iron oxide/hydroxides becoming unstable during early post-oxic diagenesis, with no necessity for significant external ionic input

4) Carbonate cements dominate the authigenic mineralogy and consist of ferroan/manganoan calcite, siderite, with rare ankerite and non-ferroan calcite. All carbonates exhibit a variety of morphologies that reflect variations in substrate rather than compositional changes. Frodingham calcites are highly enriched in manganese, depleted in magnesium, and of average iron content relative to published analyses. They formed early before compaction, as evidenced specifically by the preservation of intact berthierine ooids where calcite cementation occurred, and stable isotopic analysis suggests precipitation from a meteoric water source. Siderite is subordinate to calcite which it predates, and is usually found in association with berthierine. The siderites are calcian and magnesian, with elevated levels of Mn suggesting an early formation from marine porewaters.

5) Pyrite, phosphate and rare barite are the only other identified mineral phases within the ironstone-formation. The mineralogical assemblage results from post-oxic

processes (iron and manganese reduction) acting within the top few metres of the iron-rich sediment under shallow marine conditions. Continued biodegradation of organic matter in the oxic zone via mechanical and biological reworking resulted in the incorporation of highly degraded organic matter into the sediment unable to support sulphate-reduction, and thus suppressing pyrite formation. Instead, a post-oxic diagenetic assemblage of iron silicates and carbonates formed respectively, possibly aided by a meteoric water input for the later ferroan calcite precipitation.

6) The mineralogical assemblage of the Frodingham Ironstone Formation has been examined in detail both qualitatively and quantitatively in relation to depositional and diagenetic processes. Comparison with other British Jurassic ironstone-formations (Cleveland, Banbury, Raasay and Abbotsbury) suggests that the conclusions drawn in this research may be applied to the genesis of many ooidal ironstones, by application of minor modifications to account for local variations as detailed within this thesis.

Similar detailed geochemical studies of other ooidal ironstones would undoubtedly increase our understanding of the diagenetic processes involved in ironstone formation. In particular, clay mineralogical studies of ironstones and associated sediments would be extremely useful in delineating the extent to which post-oxic processes extend beyond the zone of ironstone deposition. Further geochemical analyses of carbonates in ironstones would give more precise information on early diagenetic carbonate precipitation. It is also hoped that future workers will expand the database on ooid shape and growth patterns for a variety of ironstones so that the concretion hypothesis may be fully tested As this thesis has shown, detailed examination of ironstones has implications far beyond the genesis of these enigmatic deposits.

APPENDIX A: METHODS USED IN THIS STUDY.

A.1) PETROGRAPHIC.

A.1.1) Thin-section Preparation and Staining.

Thin-sections of 30μm thickness were prepared, and finished with 1μm carborundum powder for standard petrographic use. Cover slips were added with immersion oil to facilitate easy removal if required for other techniques. For cathodoluminescence petrography only, a hand polish using 0.3μm alumina powder was considered satisfactory, but for E.P.M.A. and S.E.M., fully polished thin-sections were produced. Most were prepared using water as the lubricant, but some of the silicate samples were prepared in paraffin. Due to the soft nature of these rocks, most were impregnated with unstained araldite resin prior to grinding. Carbonates polished easily, but the oxides and silicates less so, with the greatest problems in polishing occurring where a mixed mineral assemblage was present. Plucking of iron-ooids, incorporation of grinding powder into softer material within the section, and overthinning, were particular problems encountered in the thin-section preparation. Many thin-sections were stained after hand polishing using 0.3μm alumina powder, to facilitate identification of the carbonate phases. The method used is given in table A.1.

A.1.2) Point-Counting.

Quantitative analysis of the various ironstone constituents, allows direct and precise comparison of the amount and type of sediment input, and authigenic mineral formation. This was obtained by point-counting thin-sections under the microscope in both transmitted and reflected light. It is important to outline here the limitations on the use of these data, particularly on the analysis of fine-grained rocks.

Accurate modal analysis of fine-grained rocks in thin-section is possible only by using reflected light, or a similar method relying on the surface alone. In transmitted light, over-estimation of fine-grained components may occur, due to their distribution within the section. For example, the high relief and birefringence of siderite makes it visually more

TABLE A1. METHOD OF CARBONATE IDENTIFICATION IN THIN-SECTION BY STAINING (MODIFIED FROM DICKSON 1965).

A) METHOD USED:

1) Stain Preparation:
   a) To 300ml of 0.5% HCl, add 0.6g Alizarin Red S (A.R.S.).
   b) To 200ml of 0.5% HCl add 4g Potassium Ferricyanide (P.F.).
   c) Mix the two solutions.
2) Etch thin-section in 1% HCl for 5 seconds.
3) Stain thin-sections for 15-60 seconds in the combined solution until clear differentiation of cement mineralogies can be seen.
4) Gently rinse with distilled water.
5) Dry the sections vertically so that excess water drains off.

B) RESULTS:

The following colours are obtained by this method for differing carbonates:

CARBONATE.	STAINING COMPONENTS.		
	A.R.S.	P.F.	A.R.S. + P.F.
CALCITE	pink	---	pink
FERROAN CALCITE	pink	blue	mauve-purple royal blue
DOLOMITE	---	---	---
FERROAN DOLOMITE	(mauve if Fe-rich)	blue/turquoise	turquoise/green
SIDERITE	---	---	---
MAGNESITE	---	---	---
RHODOCHROSITE	---	pale brown	pale brown
ARAGONITE	pink	---	pink

(--- indicates no stain produced)

apparent than berthierine matrix, and may be counted accordingly, no matter how deep in the section. Comparison of siderite abundance measured by point-counting and by CO_2 determinations for the Cleveland ironstones, suggest that the error in standard point-counting may be as high as 100% in certain cases (T. Young pers. comm. 1990). When comparing data, the thickness of the sections becomes important because thick sections will accentuate this problem.

Polished thin-sections are however more expensive and timely to produce, and point-counting was restricted to transmitted light, even where a section was polished, so that consistency was maintained. The effect was significantly reduced by counting only that which was in focus on the upper surface of the section, and attempting where possible to maintain thin-section thickness. However, abundance data of the finer grained phases were used only qualitatively.

A.1.3) Cathodoluminescence (C.L.) and Ultra Violet (U.V.) Fluorescence Petrography.

Cathodoluminescence petrography was carried out using a Technosyn Cold Cathode Luminescence 8200 Mk II unit, connected to an Olympus BH2 microscope. A voltage of ≈ 15 KV, and a current of 0.4-0.6mA was found to produce optimum luminescence. Its use in this study was limited, as little significant variation in C.L. properties were found.

U.V. fluorescence petrography was undertaken using both a direct U.V. light source and a white light source with U.V. filters, on an Zeiss Axioskop microscope.

A.1.4) Scanning Electron Microscopy. (S.E.M.).

A small amount of S.E.M. examination of small rock chips was undertaken on an International Scientific Instrument's (I.S.I.) Super-II Scanning Electron Microscope, after gold coating the specimen in an I.S.I. PS-2 Coating Unit.

A.2) ANALYTICAL.

A.2.1) Electron Probe Micro-Analysis (E.P.M.A.).

All E.P.M.A. was carried out at the Manchester Geology Department on a C.A.M.E.C.A. Camebax Microprobe, and forms the bulk of the data used in this thesis. The probe has two Wavelength Dispersive (W.D.) spectrometers, and a Link Systems 860-500 Energy Dispersive (E.D.) spectrometer system. ZAF-4/FLS software was used initially for manual E.D. analysis whilst undergoing training, but the majority of work used the 'SPECTA' software on automated E.D. and E.D./W.D. analyses. The probe is operated at a 15KV accelerating voltage, with a 3nA beam current for E.D. analysis, and 14.5nA current for E.D./W.D. work. All analyses were taken from polished thin-sections coated with a 20nm carbon film.

For E.D. analysis, all elements were standardised against a pure sample of Co. For W.D. calibration a variety of standards were used:

Si	Wollastonite.	Al	Corundum.	Ti	Rutile.
Fe	Fayalite.	Mg	Periclase.	Mn	Tephroite.
Ca	Wollastonite.	K	Orthoclase.	Na	Jadeite.
P	Apatite.	S	Pyrite.	Sr	Celestite.
Th	Thoria	U	Uraninite.		

Samples were analysed for 100s using E.D., but required considerably longer for W.D. (up to 15 mins.). W.D. analysis has a greater accuracy and detection limit (0.02 weight percent (wt%) of an element) than E.D. analysis (detection limit ≈ 0.2 wt%), but causes significantly greater specimen damage and possible element loss (for example Na). E.D. analysis also has the advantage that it permits the detection of elements not necessarily undergoing analysis. All analyses quoted are given in full numerical form to allow for computer data handling, but no emphasis is given in the interpretations to any analyses at around the detection limits given above. The accuracy of the Manchester probe is within 5% of the wt % quoted on E.D. analysis during normal operation (G. Wayte pers. comm. 1990).

E.D. Analysis of Non-Carbonate Phases.

Iron oxides (goethite) and silicates (berthierine), with a few samples of phosphate and sulphides, were analysed using E.D. only. The nature of the crystals and growth habits which result in a high porosity and hence high surface area, means that beam damage is common even at a 100s analysis time. Visible burn marks on berthierine attest to this fact. W.D. analysis is hence not suitable due to the highly extended analysis times and higher beam currents employed. The beam is defocussed to minimise specimen damage. Totals obtained (wt %) from these analyses are invariably low, for the above reasons and the large number of OH groups. However consistency (precision) was good, and the analyses usable.

W.D. Analysis of Carbonates.

Carbonates are better suited to E.P.M.A., since they are denser and obtain a better polish than the oxides/silicates. Mixed E.D./W.D. analysis was used since accuracy in the minor elements was of particular importance. The common elements Ca, Mg, Fe, Mn, Sr, and Na were analysed along with Si and Al to check for replacement of aluminosilicates. Similarly, phosphorus was added in case of mistaken identification with a clear phosphate (the optics are of a poor quality). Carbonates are also susceptible to beam damage, particularly during this W.D. analysis, so a defocussed beam of $\approx 8\mu m$ was used as standard. Analyses of Na are considered less reliable, as the element is rapidly lost from the specimen during analysis.

W.D. Analysis of Uranium and Thorium.

For analyses of U and Th, special standards were prepared of Uraninite (UO_2) and Thoria (ThO_2) for use in W.D. analysis. Files for peak analysis had to be carefully prepared to avoid Th, U, K, and Fe overlap (figure A.1). This was particularly important for Fe, that may have significantly effected other peaks when analysing goethites. Standards were specially mounted for these analyses, and had to be removed afterwards, so only a small, but representative suite of samples were studied.

Figure A.1. Scan of U, Th, K, and Fe, X-Ray Peaks in the Range 0.4-0.5 sin 2θ Analysed by Electron Microprobe (PET crystal), Illustrating Peak overlap. Analysed Peaks are Underlined.

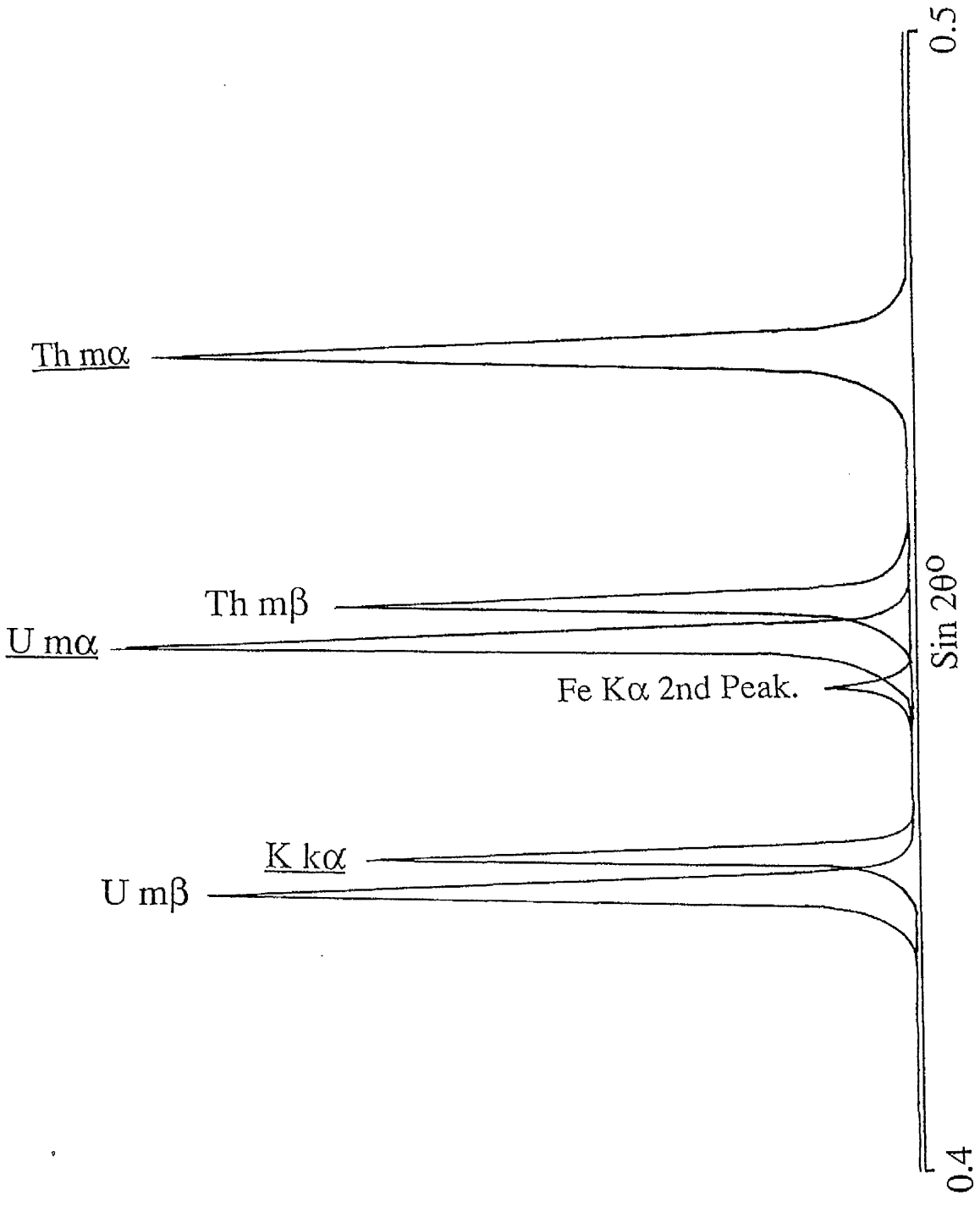

Mineral Recalculations.

Berthierine formulas were calculated by the standard method of Deer, Howie, and Zussman (1962) on the basis of 14 (O,OH). A tetrahedral total of 4.00 was assumed, consisting of all the calculated Si, plus enough Al to complete the total. The excess Al, and all Ti, Fe, Mn, and Mg were assigned to octahedral sites. Ca, Na, and K are given as interlayer cations, though the presence of such elements within the structure of berthierine is debated. Analyses containing significant amounts of S or P were discarded, but for small amounts and greater accuracy, a small correction was made on Fe assuming all S was present as pyrite (FeS_2), and another correction made on Ca, assuming all P was present as apatite (essentially $Ca_5(PO_4)_3(OH,F,Cl)$).

Data obtained from goethitic iron-ooids were recalculated on the basis of a berthierine formula as described above. The reasons for this are described in the text, along with methods used for a recalculation based on the subtraction of a berthierine formulae from the analysis, in order to ascertain the composition of the goethitic phase.

Carbonate analyses were recalculated (omitting Si, Al, and P) on the basis of a standard carbonate formula MCO_3 (M = Ca, Mg, Fe, Mn, Sr, Na). 3 rather than 6 oxygens were chosen, as ankerites were found late in the study. Actual analyses are quoted as wt% element rather than as oxides, as the oxide has little relevance in carbonates, and values in parts per million by weight (p.p.m.) can be directly read off the tables.

A.2.2) Stable Isotopic Analysis of C and O in Carbonates.

Stable isotopic analyses of calcites and siderites were carried out at the British Petroleum (B.P.). International Research Centre at Sunbury-on-Thames. The help of the staff and students in the isotope laboratories is gratefully acknowledged.

Sample Preparation of the Calcites.

For coarse sparry calcites, such as those replacing or filling large bioclastic fragments, samples could be obtained via the use of a small drill with steel or tungsten

carbide drills. To sample inter-particle cements without bioclastic debris becoming incorporated, more careful sampling was required. This was possible with the B.P. microsampler, that consisits of an ultrasonically vibrated tungsten carbide needle fitted to a microscope stage. Thin-sections of 50-100μm in thickness were prepared, and samples drilled whilst viewing through the microscope. The needle forms a groove 0.15-0.2mm in width when the stage is moved, and the sample is vacuum sucked onto a glass filter. Very precise sampling is hence possible by this method (see plate 17d). Various pore-filling ferroan calcites were sampled, but the early fibrous to prismatic cements are too thin to be sampled even by this method.

Isotopic Analysis.

Prior to analysis of the carbonates, any organic carbon was removed from the sample by an oxygen plasma in a Tegal Plasmod. The glass filters were also treated in this way. The analysis was carried out using a Finnegan Mat 251 Mass Spectrometer fitted with a Carbonate Sampling Device. The advantage of this system is that all processes are automated (i.e. acid addition, separation of evolved CO_2 and H_2O, and isotopic analysis of the CO_2), and in the ability to analyse very small sample volumes of ≈ 0.1mg. A standard was run after every 4 samples, to be used in calibration, and as a check on consistency. The accuracy is variable, with a standard deviation of approximately 0.1-0.3‰ on both $\partial^{13}C_{PDB}$ and $\partial^{18}O_{PDB}$. The calculation scheme and corrections used for the B.P. isotope laboratories are given in Rouse and Shirley (1988).

All values are reported using the standard ∂-notation defined as:

$$\partial = 10^3.\left(\frac{R_{SAMPLE} - R_{STANDARD}}{R_{STANDARD}}\right)$$

where R is the isotopic ratio ($^{13}C/^{12}C$ or $^{18}O/^{16}O$). The standard used is given in abbreviated subscript after the element, so that PDB indicates the standard to be *Belemnitella americana*, a belemnite from the Pee Dee Formation, South Carolina, and SMOW indicates Standard Mean Ocean Water. $\partial^{13}C_{PDB}$ therefore represents the ∂-value for the $^{13}C/^{12}C$ isotopic ratio relative to the PDB standard. The results obtained from this study in standard notation are given in table A.2.

Table A.2. Isotopic Compositions (C and O) of Sparry Ferroan/Manganoan Calcites Obtained During this Research.

No.	SPECIMEN	∂18O (PDB)	∂13C (PDB)	Sample type.
FRODINGHAM				
1	YAR 6	-8.40	-16.98	Replaced Bioclast
2	YAR 5	-7.18	-8.50	"
3	YAR 4	-8.95	-16.17	"
11	DRAG 31.22	-9.35	-8.52	"
42	DRAG 31.10	-6.03	-4.17	Replaced Bioclast (non-radiaxial calcite)
43	DRAG31.10	-6.17	-3.60	"
46	YAR 7	-7.76	-22.11	"
5	YAR 15	-2.75	1.65	Gryphaea (unreplaced)
8	YAR 16	-1.43	2.91	"
20	YAR 32	-2.21	2.08	"
37	YAR 33	-2.04	2.62	"
38	YAR 14	-3.03	2.30	"
45	YAR 7	-1.52	2.58	"
12	YAR 101	-1.62	2.09	Pinna (unreplaced)
6	YAR 100	-7.05	-5.75	Replaced bioclast (berthierine coated)
7	YAR 8	-7.70	-10.09	"
13	YAR 102	-7.26	-16.77	"
21	YAR 103	-7.81	-13.00	"
35	(coquina)	-7.84	-2.54	Aragonite bioclast from above ironstone
28	YAR 54B	-5.01	-0.85	Ammonite (aragonite)
22	YAR104	-1.05	-0.39	Belemnite from above ironstone
23	YAR 105	0.10	0.41	"
36	YAR 44	-6.68	-11.00	Ammonite void cement
39	YAR 1	-9.43	-9.59	Bioclast void cement
44	YAR 101	-6.58	-10.25	"
48	YAR 22b(i)	-8.17	-17.36	"
BANBURY				
9	HRT(i)	-7.08	-6.03	Cements within brachiopods
10	HRT(i)	-6.66	-4.89	"
14	HRT(ii)	-7.63	-8.67	"
15	HRT(ii)	-7.64	-8.52	"
16	HRT(iii)	-6.53	-8.26	"
17	HRT(iv)	-6.75	-8.74	"
18	HRT(v)	-5.67	-9.47	"
19	HRT(vi)	-7.58	-9.32	"
40	HRT(xi)	-4.58	-10.31	"
41	HRT(xii)	-6.49	-8.93	"
26	HRT 11	-5.86	-7.47	"
27	HRT 11	-6.18	-7.67	"
30	HRT(vii)	-6.12	-8.48	"
31	HRT(viii)	-9.20	-8.67	"
32	HRT(ix)	-5.42	-8.51	"
24	HRT 12	-0.95	1.35	Belemnite from ironstone
25	HRT 26	-0.88	0.29	"
34	HRT20	-0.26	2.33	"
33	HRT(x)	-5.25	-10.15	Vein Calcite

The relationship between the PDB and SMOW scales is given by:

$$\partial^{18}O\ (calcite_{SMOW}) = 1.03086\ \partial^{18}O\ (calcite_{PDB}) + 30.86.$$

(Anderson and Arthur 1983)

A.2.3) X-Ray Diffraction (X.R.D.).

X.R.D. was employed as a standard technique in determining sample mineralogy, but was not used extensively to ascertain mineral compositions as E.P.M.A. facilities were available. A Phillips X.R.D. system with a PW 1730 X-Ray generator using Cukα radiation was used, running at 40KV with a 20mA current. Range and time constants were varied, but typically $4x10^2$ c/s and 4s, scanning at 1°/min gave satisfactory results. Samples were run as 'smear' mounts to accentuate the presence of any clay minerals in the sample, by grinding the sample under acetone, pipetting to a glass slide, and allowing the acetone to evaporate.

A.3) COMPUTERS AND SOFTWARE.

This thesis was produced exclusively using Apple Macintosh Computers and software. The text was written using 'Word' version 4 ©Microsoft Corporation 1987-1989, and tables using 'Excel' version 1.51 ©Microsoft Corporation 1985-1988. All data were entered manually to 'Excel' files, and programs were written within the spreadsheet to recalculate the data as necessary to mineral formulae. Data from these files were transferred to 'TriPlot' version 2.02 (©Gary Carroll 1989), and 'StatView II' ©Abacus Concepts Inc., 1987-1988, for further processing. 'Cricket Graph' version 1.3 ©Cricket Software 1986-1988, was used to transpose data sets, but was not used as the main data processing package due to its limited use in spreadsheet manipulation. This thesis has been printed on an Apple Macintosh LaserWriter II.

APPENDIX B: E.P.M.A. OF URANIUM AND THORIUM IN THE FRODINGHAM IRONSTONE FORMATION.

Concentrations of uranium (U) and thorium (Th) in sediments may be used as diagenetic indicators due to the similar ionic size of these elements, but markedly different geochemical properties. Th is chemically immobile and known to be enriched in deposits such as bauxites and laterites (Adams and Richardson 1960). It is therefore unlikely to be affected by diagenetic processes. Uranium has two common valencies U^{4+} and U^{6+}, the former of which has a similar radius to Th^{4+}, and is similarly incorporated into detrital resistate minerals and absorbed onto clays. However, U^{4+} oxidises readily to U^{6+} and may form the soluble UO_2^{2+} ion, thus becoming chemically mobile. This solubility is enhanced in carbonate bearing solutions where it may also occur as the similarly soluble $UO_2(CO_3)_3^{4-}$ ion (Garrels and Christ 1965). U and Th concentrations in pore waters and minerals precipitated from them, therefore give useful information on the redox potential (i.e. oxidizing/reducing conditions) of the original sediment. Cochran *et al.* (1986) have shown that concentrations of both elements in pore waters may be related to iron-reduction. U^{6+} reduction to U^{4+} occurs at a similar redox potential to iron-reduction, and is hence expected to be removed from pore waters at the same time as Fe^{2+} is being released. Th concentration on the other hand may be increased as the Fe and Mn oxide/hydroxide carriers of the U and Th are reduced and dissolved.

U and Th concentrations can be measured in the field along with potassium (K), by portable gamma-ray spectrometry. The latter is a common component of detrital minerals (felspars, micas, clay minerals). Myers (1989) has used this technique on the Cleveland Ironstone Formation and showed that a higher Th/K ratio occurs in the ironstone seams, consistent with enrichment of Th (and consequent depletion of K) by incorporation of a lateritic derived clay such as (K free) kaolinite. A higher Th/U ratio reflected U leaching under oxidising conditions at the source. Actual measured values were extremely low, in the order of only 45 p.p.m. Th, and 8 p.p.m. U, but it was here postulated that if these elements were concentrated within a specific mineral phase, then these anomalies might also be

detectable by E.P.M.A. Calibration of the probe and files used for this work are described in appendix (A.2.1).

The specific aim of this brief study was to attempt to ascertain the presence and site of U and Th in the Frodingham ironstones, particularly as to their occurrence within ooids or the matrix. The results of this study are shown in table B1 with calculated Th/K and Th/U ratios after Myers (1989). The variation in measured values is often large between single samples and similar occurrences (such as ooids), giving large standard deviations. This suggests that such a pilot study is unfortunately unlikely to yield conclusive results. However, it does show that detectable quantities of U and Th were found, though the precise values are debatable since pure carbonate should contain negligible Th, but was recorded in DRAG. 31.13. To hence avoid misinterpretation, the data is discussed qualitatively only. The variation seen is not random analytical error, as the nuclei of DRAG. 31.28 show a standard deviation of only 0.008 wt% on a mean of 0.115 wt%, for 5 analyses, suggesting precision was good.

Despite the large variation and constraints on this data set, three main conclusions may be tentatively proposed, as predictions for those which would be obtained in a fuller study of this nature:

1) The occurrence of U and Th is not restricted to a single ironstone component.
2) Ooids are enriched in U relative to the muds. This is difficult to interpret, as U would be expected to be more mobile during the oxidising conditions of goethite formation.
3) Analyses of muds in specimens DRAG. 31.1, 13, and 21, and analyses of ooids in specimens DRAG. 31.1, 13, and 28, show an increasing average Th content up the sequence. This is accompanied by a decreasing K content in the muds, and may be tentatively assigned to an increasing lateritic (Th enriched) detrital component, such as kaolinite. This therefore supports the clay mineralogical data of decreasing illitic input to the ironstone during deposition.

Table B.1. Analyses of Th, U, and K, for a Suite of Samples of the Frodingham Ironstone Formation. Obtained by E.P.M.A. (Th(ppm)/K(wt%)) and (Th(ppm)/U(ppm)) ratios are also calculated.

(wt%)	Th	K	U	Th/K	Th/U
DRAG 31.1					
MATRIX	0.000	2.382	0.000	0	
	0.000	2.329	0.000	0	
	0.000	2.646	0.000	0	
	0.009	2.313	0.000	39	
	0.025	2.231	0.000	112	
	0.001	1.924	0.000	5	
	0.012	1.906	0.000	63	
	0.000	2.055	0.000	0	
AVERAGE	0.006	2.223	0.000	27	
STDEV.	0.009	0.251	0.000	42	
OOIDS	0.000	0.254	0.000	0	
	0.079	0.165	0.000	4788	
	0.008	0.096	0.000	833	
	0.018	0.080	0.000	2250	
	0.009	0.090	0.032	1000	0.28
	0.032	0.237	0.042	1350	0.76
	0.172	0.296	0.134	5811	1.28
	0.091	0.138	0.084	6594	1.08
AVERAGE	0.051	0.170	0.037	2828	0.85
STDEV.	0.059	0.083	0.049	2529	0.44
GOETHITE	0.000	0.254	0.000	0	
PARTICLES	0.000	0.070	0.000	0	
	0.000	2.020	0.000	0	
	0.000	0.088	0.000	0	
	0.000	1.927	0.000	0	
AVERAGE	0.000	0.872	0.000	0	
STDEV.	0.000	1.009	0.000	0	
MUSCOVITE	0.024	8.419	0.000	29	
	0.037	1.174	0.000	315	
DRAG 31.13					
BERTHIERINE	0.010	1.478	0.000	68	
MATRIX	0.000	0.469	0.000	0	
	0.008	0.558	0.000	143	
	0.058	0.639	0.000	908	
	0.048	0.510	0.000	941	
AVERAGE	0.025	0.731	0.000	412	
STDEV.	0.026	0.422	0.000	471	
OOIDS	0.087	0.088	0.083	9886	1.05
	0.109	0.094	0.071	11596	1.54
	0.109	0.143	0.045	7622	2.42
	0.089	0.105	0.039	8476	2.28
	0.104	0.101	0.076	10297	1.37
	0.009	0.102	0.000	882	
	0.030	0.072	0.006	4167	5.00
	0.008	0.079	0.014	1013	0.57
AVERAGE	0.068	0.098	0.042	6742	2.03
STDEV.	0.045	0.022	0.033	4203	1.46
CARBONATE	0.019	0.062	0.000	3065	
CEMENT	0.018	0.059	0.000	3051	
AVERAGE	0.019	0.061	0.000	3058	
STDEV.	0.001	0.002	0.000	10	

Table B.1. (Continued).

(wt%)	Th	K	U	Th/K	Th/U
DRAG 31.21					
BERTHIERINE	0.015	0.099	0.015	1515	1.00
MATRIX	0.026	0.168	0.000	1548	
	0.075	0.131	0.003	5725	25.00
	0.028	0.143	0.000	1958	
	0.050	0.148	0.015	3378	3.33
	0.242	0.141	0.036	17163	6.72
	0.015	0.222	0.000	676	
	0.096	0.112	0.007	8571	13.71
	0.057	0.106	0.000	5377	
	0.084	0.305	0.017	2754	4.94
AVERAGE	0.069	0.158	0.009	4867	9.12
STDEV.	0.067	0.063	0.012	4954	8.90
GOETHITE	0.000	0.071	0.008	0	0.00
ONCOID	0.013	0.077	0.030	1688	0.43
	0.094	0.085	0.045	11059	2.09
	0.034	0.078	0.030	4359	1.13
	0.081	0.079	0.131	10253	0.62
	0.076	0.074	0.072	10270	1.06
AVERAGE	0.050	0.077	0.053	6272	0.89
STDEV.	0.039	0.005	0.044	4874	0.72
DRAG 31.28					
AUTHIGENIC	0.000	0.074	0.000	0	
BERTHIERINE	0.067	0.058	0.031	11552	2.16
	0.061	0.082	0.029	7439	2.10
	0.070	0.079	0.084	8861	0.83
	0.105	0.086	0.033	12209	3.18
	0.005	0.067	0.000	746	
	0.000	0.084	0.000	0	
	0.015	0.072	0.000	2083	
	0.000	0.083	0.000	0	
	0.018	0.081	0.000	2222	
AVERAGE	0.034	0.077	0.018	4511	2.07
STDEV.	0.038	0.009	0.028	4974	0.96
OOID(NUCLEI)	0.115	0.095	0.109	12105	1.06
	0.088	0.083	0.110	10602	0.80
	0.142	0.105	0.107	13524	1.33
	0.065	0.084	0.124	7738	0.52
	0.161	0.102	0.124	15784	1.30
AVERAGE	0.114	0.094	0.115	11951	1.00
STDEV.	0.039	0.010	0.008	3031	0.34
OOID(CORTEX)	0.023	0.241	0.000	954	
	0.011	0.257	0.016	428	0.69
	0.013	0.205	0.055	634	0.24
	0.012	0.281	0.008	427	1.50
	0.000	0.165	0.000	0	
AVERAGE	0.012	0.230	0.016	489	0.81
STDEV.	0.008	0.046	0.023	348	0.64

The analyses of the authigenic berthierine cement in DRAG. 31.28 contain the immobile element Th, that was possibly released from detrital oxides during subsequent reduction. The high values of Th in the nuclei of ooids within DRAG. 31.28 is supportive of a lateritic origin, but it is not possible to apply this origin to the ooids themselves on the basis of the data obtained.

APPENDIX C.

Table C.1. Size Data , Shape and Form Parameters Calculated for 50 Measured Iron-Ooids, Sample YAR. 7., Frodingham Ironstone Formation. See Text for Calculation Formulae.

			NOMINAL	WENTWORTH 1922	ZINGG 1935		LUTTIG 1966	
LONG (mm)	INTERM.(mm)	SHORT (mm)	DIAMETER	Flatness Index	I/L	S/I	Elongation	Flatness
0.26	0.23	0.14	0.20	1.78	0.88	0.60	88.24	52.94
0.28	0.25	0.16	0.22	1.63	0.89	0.65	89.09	58.18
0.29	0.26	0.16	0.23	1.69	0.89	0.63	89.47	56.14
0.27	0.25	0.17	0.22	1.55	0.92	0.67	92.45	62.26
0.30	0.28	0.16	0.23	1.85	0.92	0.56	91.67	51.67
0.27	0.27	0.16	0.22	1.71	1.00	0.58	100.00	58.49
0.26	0.24	0.17	0.22	1.51	0.98	0.67	98.08	65.38
0.24	0.21	0.14	0.19	1.63	0.87	0.66	87.23	57.45
0.29	0.25	0.19	0.24	1.41	0.88	0.76	87.72	66.67
0.38	0.26	0.24	0.29	1.36	0.68	0.90	68.42	61.84
0.33	0.31	0.20	0.27	1.64	0.94	0.63	93.94	59.09
0.32	0.29	0.16	0.24	1.88	0.90	0.56	90.48	50.79
0.34	0.27	0.17	0.25	1.83	0.78	0.62	77.94	48.53
0.36	0.29	0.18	0.26	1.83	0.80	0.61	80.28	49.30
0.24	0.19	0.15	0.19	1.48	0.79	0.76	79.17	60.42
0.30	0.24	0.19	0.24	1.46	0.80	0.77	80.00	61.67
0.27	0.27	0.17	0.23	1.59	1.00	0.63	100.00	62.96
0.34	0.25	0.14	0.22	2.15	0.73	0.55	73.13	40.30
0.26	0.25	0.15	0.21	1.68	0.94	0.61	94.23	57.69
0.24	0.23	0.15	0.20	1.60	0.98	0.63	97.87	61.70
0.22	0.19	0.16	0.19	1.32	0.86	0.82	86.36	70.45
0.28	0.23	0.14	0.20	1.85	0.82	0.60	81.82	49.09
0.25	0.23	0.20	0.22	1.19	0.90	0.89	90.00	80.00
0.32	0.30	0.19	0.26	1.65	0.94	0.63	93.65	58.73
0.22	0.15	0.13	0.16	1.48	0.68	0.83	68.18	56.82
0.33	0.29	0.20	0.26	1.53	0.88	0.70	87.69	61.54
0.27	0.27	0.18	0.23	1.53	0.98	0.66	98.15	64.81
0.31	0.29	0.22	0.27	1.36	0.94	0.76	93.55	70.97
0.27	0.25	0.17	0.22	1.50	0.92	0.69	92.45	64.15
0.27	0.22	0.17	0.21	1.47	0.80	0.77	79.63	61.11
0.27	0.25	0.20	0.23	1.32	0.94	0.78	94.34	73.58
0.24	0.23	0.14	0.20	1.68	0.96	0.61	95.83	58.33
0.34	0.31	0.23	0.28	1.42	0.91	0.74	91.04	67.16
0.45	0.36	0.13	0.27	3.08	0.80	0.37	79.78	29.21
0.47	0.40	0.20	0.34	2.18	0.85	0.50	85.11	42.55
0.27	0.20	0.17	0.21	1.37	0.75	0.85	75.47	64.15
0.25	0.24	0.14	0.20	1.80	0.94	0.57	94.00	54.00
0.22	0.21	0.13	0.18	1.63	0.93	0.63	93.18	59.09
0.28	0.24	0.17	0.23	1.53	0.86	0.71	85.71	60.71
0.23	0.18	0.10	0.16	2.13	0.80	0.53	80.00	42.22
0.29	0.27	0.17	0.23	1.68	0.95	0.61	94.74	57.89
0.24	0.21	0.13	0.18	1.80	0.88	0.60	87.50	52.08
0.29	0.25	0.17	0.23	1.57	0.88	0.68	87.72	59.65
0.25	0.22	0.14	0.20	1.74	0.88	0.61	88.00	54.00
0.26	0.23	0.16	0.21	1.58	0.88	0.67	88.46	59.62
0.26	0.23	0.15	0.21	1.62	0.90	0.65	90.20	58.82
0.29	0.26	0.19	0.24	1.45	0.90	0.73	89.66	65.52
0.35	0.30	0.20	0.27	1.61	0.84	0.68	84.29	57.14
0.28	0.23	0.17	0.22	1.49	0.80	0.76	80.36	60.71
0.30	0.26	0.19	0.24	1.45	0.86	0.75	86.44	64.41

Table C.1. (Continued).

SNEED&FOLK		KRUMBEIN	SNEED&FOLK	ASCHENBRENNER	DOBKINS&FOLK	ASCHENBRENNER	WILLIAMS			
1958		1941	1958	1956	1970	1956	1965	Calculations for Sneed-Folk Diagram		
Flatness	Flatness*I	Intercept Sph.	Max.Proj.Sph.	Working Sph.	Obl.Prol.Index	Shape Factor F	Shape Factor	X	Y	Z
0.53	0.25	0.78	0.68	0.90	-4.72	0.68	0.32	52.94	35.29	11.76
0.58	0.26	0.80	0.72	0.92	-4.11	0.73	0.27	58.18	30.91	10.91
0.56	0.24	0.79	0.71	0.91	-4.63	0.70	0.30	56.14	33.33	10.53
0.62	0.20	0.83	0.75	0.92	-4.82	0.73	0.27	62.26	30.19	7.55
0.52	0.17	0.78	0.66	0.90	-6.34	0.61	0.39	51.67	40.00	8.33
0.58	0.00	0.84	0.70	0.91	-8.55	0.58	0.42	58.49	41.51	0.00
0.65	0.06	0.86	0.76	0.93	-6.80	0.68	0.32	65.38	32.69	1.92
0.57	0.30	0.79	0.72	0.91	-3.48	0.75	0.25	57.45	29.79	12.77
0.67	0.37	0.84	0.80	0.93	-1.97	0.87	0.13	66.67	21.05	12.28
0.62	0.83	0.75	0.82	0.92	5.30	1.32	-0.24	61.84	6.58	31.58
0.59	0.15	0.82	0.72	0.92	-5.95	0.67	0.33	59.09	34.85	6.06
0.51	0.19	0.77	0.66	0.89	-6.03	0.62	0.38	50.79	39.68	9.52
0.49	0.43	0.72	0.67	0.89	-1.47	0.80	0.20	48.53	29.41	22.06
0.49	0.39	0.73	0.67	0.89	-2.25	0.76	0.24	49.30	30.99	19.72
0.60	0.53	0.78	0.77	0.92	0.44	0.96	0.04	60.42	18.75	20.83
0.62	0.52	0.79	0.78	0.92	0.35	0.96	0.04	61.67	18.33	20.00
0.63	0.00	0.86	0.73	0.92	-7.94	0.63	0.37	62.96	37.04	0.00
0.40	0.45	0.67	0.61	0.86	-1.24	0.75	0.25	40.30	32.84	26.87
0.58	0.14	0.82	0.71	0.91	-6.30	0.65	0.35	57.69	36.54	5.77
0.62	0.06	0.85	0.73	0.92	-7.20	0.64	0.36	61.70	36.17	2.13
0.70	0.46	0.85	0.83	0.94	-0.55	0.94	0.06	70.45	15.91	13.64
0.49	0.36	0.74	0.67	0.89	-2.91	0.73	0.27	49.09	32.73	18.18
0.80	0.50	0.90	0.89	0.95	0.00	0.99	0.01	80.00	10.00	10.00
0.59	0.15	0.82	0.72	0.91	-5.89	0.67	0.33	58.73	34.92	6.35
0.57	0.74	0.73	0.78	0.91	4.17	1.22	-0.18	56.82	11.36	31.82
0.62	0.32	0.81	0.76	0.92	-2.93	0.80	0.20	61.54	26.15	12.31
0.65	0.05	0.86	0.75	0.93	-6.90	0.67	0.33	64.81	33.33	1.85
0.71	0.22	0.87	0.81	0.94	-3.91	0.81	0.19	70.97	22.58	6.45
0.64	0.21	0.84	0.76	0.93	-4.51	0.75	0.25	64.15	28.30	7.55
0.61	0.52	0.79	0.78	0.92	0.39	0.96	0.04	61.11	18.52	20.37
0.74	0.21	0.89	0.83	0.94	-3.88	0.83	0.17	73.58	20.75	5.66
0.58	0.10	0.82	0.71	0.91	-6.86	0.64	0.36	58.33	37.50	4.17
0.67	0.27	0.85	0.79	0.93	-3.38	0.81	0.19	67.16	23.88	8.96
0.29	0.29	0.62	0.47	0.79	-7.34	0.46	0.54	29.21	50.56	20.22
0.43	0.26	0.71	0.60	0.86	-5.66	0.59	0.41	42.55	42.55	14.89
0.64	0.68	0.79	0.82	0.93	2.87	1.13	-0.11	64.15	11.32	24.53
0.54	0.13	0.80	0.68	0.90	-6.84	0.61	0.39	54.00	40.00	6.00
0.59	0.17	0.82	0.72	0.92	-5.64	0.68	0.32	59.09	34.09	6.82
0.61	0.36	0.80	0.75	0.92	-2.25	0.83	0.17	60.71	25.00	14.29
0.42	0.35	0.70	0.61	0.86	-3.64	0.66	0.34	42.22	37.78	20.00
0.58	0.13	0.82	0.71	0.91	-6.48	0.65	0.35	57.89	36.84	5.26
0.52	0.26	0.77	0.68	0.90	-4.59	0.68	0.32	52.08	35.42	12.50
0.60	0.30	0.81	0.74	0.92	-3.28	0.78	0.22	59.65	28.07	12.28
0.54	0.26	0.78	0.69	0.90	-4.43	0.70	0.30	54.00	34.00	12.00
0.60	0.29	0.81	0.74	0.92	-3.59	0.76	0.24	59.62	28.85	11.54
0.59	0.24	0.81	0.73	0.92	-4.45	0.72	0.28	58.82	31.37	9.80
0.66	0.30	0.84	0.78	0.93	-3.05	0.82	0.18	65.52	24.14	10.34
0.57	0.37	0.78	0.73	0.91	-2.33	0.80	0.20	57.14	27.14	15.71
0.61	0.50	0.79	0.77	0.92	0.00	0.94	0.06	60.71	19.64	19.64
0.64	0.38	0.82	0.78	0.93	-1.85	0.86	0.14	64.41	22.03	13.56

Table C.2. Size Data , Shape and Form Parameters Calculated for 50 Measured Iron-Ooids, Locality 1, Abbotsbury Ironstone. See Text for Calculation Formulae.

			NOMINAL	WENTWORTH 1922	ZINGG 1935		LUTTIG 1966	
LONG (mm)	INTERM.(mm)	SHORT (mm)	DIAMETER	Flatness Index	I/L	S/I	Elongation	Flatness
0.46	0.44	0.19	0.34	2.36	0.97	0.43	96.70	41.76
0.57	0.49	0.18	0.37	2.93	0.87	0.37	86.73	31.86
0.49	0.46	0.26	0.38	1.85	0.93	0.56	92.86	52.04
0.53	0.48	0.18	0.36	2.78	0.90	0.38	90.48	34.29
0.48	0.44	0.18	0.33	2.54	0.91	0.41	90.63	37.50
0.46	0.37	0.18	0.31	2.34	0.80	0.48	80.22	38.46
0.44	0.34	0.26	0.34	1.53	0.77	0.75	77.27	57.95
0.46	0.36	0.15	0.29	2.81	0.77	0.41	77.17	31.52
0.41	0.32	0.17	0.28	2.13	0.77	0.54	76.83	41.46
0.40	0.27	0.20	0.27	1.71	0.66	0.74	66.25	48.75
0.38	0.29	0.19	0.27	1.81	0.76	0.64	76.32	48.68
0.49	0.48	0.20	0.36	2.43	0.98	0.42	97.96	40.82
0.43	0.36	0.17	0.30	2.31	0.83	0.48	82.56	39.53
0.70	0.60	0.58	0.62	1.12	0.86	0.97	86.33	83.45
0.45	0.31	0.21	0.31	1.85	0.69	0.66	68.89	45.56
0.49	0.38	0.22	0.34	2.00	0.77	0.57	77.32	44.33
0.56	0.50	0.27	0.42	1.95	0.90	0.54	90.09	48.65
0.45	0.42	0.19	0.33	2.28	0.94	0.45	94.38	42.70
0.46	0.36	0.16	0.29	2.65	0.78	0.43	78.26	33.70
0.57	0.49	0.21	0.39	2.51	0.87	0.43	86.73	37.17
0.54	0.53	0.25	0.42	2.14	0.98	0.47	98.15	46.30
0.44	0.40	0.23	0.34	1.83	0.91	0.58	90.91	52.27
0.52	0.39	0.24	0.37	1.90	0.75	0.62	75.00	46.15
0.56	0.31	0.30	0.37	1.46	0.55	0.97	54.95	53.15
0.52	0.46	0.20	0.36	2.50	0.88	0.43	87.50	37.50
0.45	0.40	0.17	0.31	2.49	0.90	0.43	89.89	38.20
0.54	0.45	0.18	0.35	2.74	0.84	0.40	84.11	33.64
0.56	0.49	0.21	0.38	2.55	0.87	0.42	86.61	36.61
0.50	0.41	0.12	0.28	3.91	0.82	0.28	81.82	23.23
0.46	0.37	0.21	0.33	2.01	0.81	0.55	81.32	45.05
0.53	0.50	0.19	0.37	2.70	0.93	0.38	93.40	35.85
0.55	0.52	0.19	0.38	2.79	0.94	0.37	94.50	34.86
0.49	0.45	0.22	0.36	2.16	0.92	0.48	91.75	44.33
0.41	0.27	0.20	0.28	1.69	0.65	0.75	64.63	48.78
0.44	0.40	0.13	0.28	3.21	0.90	0.33	89.77	29.55
0.44	0.38	0.17	0.30	2.47	0.87	0.43	87.36	37.93
0.49	0.42	0.18	0.33	2.51	0.87	0.43	86.60	37.11
0.54	0.45	0.20	0.36	2.53	0.84	0.43	84.11	36.45
0.57	0.52	0.25	0.42	2.21	0.92	0.47	92.04	43.36
0.42	0.32	0.24	0.32	1.57	0.76	0.73	76.19	55.95
0.54	0.47	0.21	0.37	2.39	0.86	0.45	86.11	38.89
0.47	0.41	0.21	0.34	2.13	0.86	0.51	86.17	43.62
0.47	0.37	0.20	0.32	2.15	0.79	0.53	78.72	41.49
0.42	0.39	0.21	0.32	1.92	0.94	0.54	93.98	50.60
0.53	0.50	0.35	0.45	1.49	0.95	0.69	95.24	65.71
0.56	0.55	0.29	0.45	1.91	0.99	0.53	99.10	52.25
0.48	0.44	0.17	0.33	2.68	0.92	0.39	91.58	35.79
0.42	0.33	0.27	0.33	1.38	0.80	0.82	79.52	65.06
0.50	0.50	0.24	0.39	2.07	0.99	0.48	99.00	48.00
0.41	0.40	0.17	0.30	2.37	0.99	0.43	98.77	41.98

Table C.2. (Continued).

SNEED&FOLK		KRUMBEIN	SNEED&FOLK	ASCHENBRENNER	DOBKINS&FOLK	ASCHENBRENNER	WILLIAMS			
1958		1941	1958	1956	1970	1956	1965	Calculations for Sneed-Folk Diagram		
Flatness	Flatness^I	Intercept Sph.	Max.Proj.Sph.	Working Sph.	Obl.Prol.Index	Shape Factor F	Shape Factor	X	Y	Z
0.42	0.06	0.74	0.56	0.85	-10.62	0.45	0.55	41.76	54.95	3.30
0.32	0.19	0.65	0.49	0.81	-9.58	0.42	0.58	31.86	54.87	13.27
0.52	0.15	0.78	0.66	0.90	-6.75	0.60	0.40	52.04	40.82	7.14
0.34	0.14	0.68	0.51	0.82	-10.36	0.42	0.58	34.29	56.19	9.52
0.38	0.15	0.70	0.54	0.84	-9.33	0.46	0.54	37.50	53.13	9.38
0.38	0.32	0.68	0.57	0.85	-4.64	0.60	0.40	38.46	41.76	19.78
0.58	0.54	0.77	0.76	0.92	0.70	0.97	0.03	57.95	19.32	22.73
0.32	0.33	0.62	0.50	0.81	-5.29	0.53	0.47	31.52	45.65	22.83
0.41	0.40	0.68	0.61	0.86	-2.51	0.70	0.30	41.46	35.37	23.17
0.49	0.66	0.69	0.71	0.89	3.25	1.11	-0.10	48.75	17.50	33.75
0.49	0.46	0.72	0.68	0.89	-0.79	0.84	0.16	48.68	27.63	23.68
0.41	0.03	0.74	0.55	0.85	-11.41	0.43	0.57	40.82	57.14	2.04
0.40	0.29	0.69	0.57	0.85	-5.35	0.58	0.42	39.53	43.02	17.44
0.83	0.83	0.90	0.93	0.95	3.91	1.12	-0.11	83.45	2.88	13.67
0.46	0.57	0.68	0.67	0.88	1.57	0.96	0.04	45.56	23.33	31.11
0.44	0.41	0.70	0.63	0.87	-2.09	0.74	0.26	44.33	32.99	22.68
0.49	0.19	0.76	0.64	0.89	-6.31	0.60	0.40	48.65	41.44	9.91
0.43	0.10	0.74	0.58	0.86	-9.41	0.48	0.52	42.70	51.69	5.62
0.34	0.33	0.64	0.53	0.82	-5.11	0.55	0.45	33.70	44.57	21.74
0.37	0.21	0.69	0.54	0.84	-7.77	0.49	0.51	37.17	49.56	13.27
0.46	0.03	0.77	0.60	0.87	-10.06	0.48	0.52	46.30	51.85	1.85
0.52	0.19	0.78	0.67	0.90	-5.92	0.63	0.37	52.27	38.64	9.09
0.46	0.46	0.70	0.66	0.88	-0.77	0.82	0.18	46.15	28.85	25.00
0.53	0.96	0.66	0.80	0.88	8.68	1.76	-0.43	53.15	1.80	45.05
0.38	0.20	0.69	0.54	0.84	-8.00	0.49	0.51	37.50	50.00	12.50
0.38	0.16	0.70	0.55	0.84	-8.80	0.47	0.53	38.20	51.69	10.11
0.34	0.24	0.66	0.51	0.82	-7.74	0.48	0.52	33.64	50.47	15.89
0.37	0.21	0.68	0.54	0.83	-7.89	0.49	0.51	36.61	50.00	13.39
0.23	0.24	0.57	0.40	0.74	-11.33	0.35	0.65	23.23	58.59	18.18
0.45	0.34	0.72	0.63	0.88	-3.55	0.68	0.32	45.05	36.26	18.68
0.36	0.10	0.69	0.52	0.82	-11.08	0.41	0.59	35.85	57.55	6.60
0.35	0.08	0.69	0.50	0.82	-11.92	0.39	0.61	34.86	59.63	5.50
0.44	0.15	0.74	0.60	0.87	-7.94	0.53	0.47	44.33	47.42	8.25
0.49	0.69	0.68	0.72	0.88	3.90	1.17	-0.14	48.78	15.85	35.37
0.30	0.15	0.64	0.46	0.79	-12.01	0.37	0.63	29.55	60.23	10.23
0.38	0.20	0.69	0.55	0.84	-7.81	0.50	0.50	37.93	49.43	12.64
0.37	0.21	0.68	0.54	0.84	-7.73	0.49	0.51	37.11	49.48	13.40
0.36	0.25	0.67	0.54	0.83	-6.86	0.52	0.48	36.45	47.66	15.89
0.43	0.14	0.74	0.59	0.86	-8.29	0.51	0.49	43.36	48.67	7.96
0.56	0.54	0.75	0.74	0.91	0.72	0.96	0.04	55.95	20.24	23.81
0.39	0.23	0.69	0.56	0.85	-7.01	0.52	0.48	38.89	47.22	13.89
0.44	0.25	0.72	0.60	0.87	-5.84	0.59	0.41	43.62	42.55	13.83
0.41	0.36	0.69	0.60	0.86	-3.29	0.67	0.33	41.49	37.23	21.28
0.51	0.12	0.78	0.65	0.89	-7.47	0.57	0.43	50.60	43.37	6.02
0.66	0.14	0.86	0.77	0.93	-5.50	0.72	0.28	65.71	29.52	4.76
0.52	0.02	0.80	0.65	0.89	-9.21	0.53	0.47	52.25	46.85	0.90
0.36	0.13	0.69	0.52	0.83	-10.31	0.43	0.57	35.79	55.79	8.42
0.65	0.59	0.80	0.81	0.93	1.33	1.03	-0.03	65.06	14.46	20.48
0.48	0.02	0.78	0.62	0.88	-10.02	0.49	0.51	48.00	51.00	1.00
0.42	0.02	0.75	0.56	0.85	-11.40	0.43	0.57	41.98	56.79	1.23

APPENDIX D: MINERAL COMPOSITIONS OBTAINED BY E.P.M.A.

The following tables contain the full suite of E.P.M.A. analyses presented within the text in an averaged form. A similar order is followed. All analyses are initially expressed as wt% element, with a calculated oxygen percentage assuming oxides with the following valencies; Si(IV), Al(III), Ti(IV), Mg(II), Ca(II), Fe(II), Mn(II), Na(I), K(I), P(V), Sr(II). This is included solely to allow the total wt% oxide to be calculated for comparitive purposes, as a measure of accuracy of the analysis, presence of unanalysed elements in the mineral (especially O, H, and C), porosity, or water content. The data are given in wt% rather than wt% oxide, as the initial concentrations are software corrected to this form, and does not therefore assume the valencies for the elements concerned. The data are therefore presented in the purest and simplest form, from which future workers may make their own assumptions, and calculate to their own needs. Though often accepted as the norm, analyses quoted for clay minerals and carbonates as wt% oxide are false representations, since they do not account for the presence of OH groups and C respectively. Analyses calculated by the methods given in appendix (A.2.1) and described in the text, are given below the original data.

Recalculated data of berthierines and illites are presented to indicate the assumed cation site within the structure, in the tetrahedral, octahedral or interlayer sites respectively. Al is divided between two sites and is expressed as tetrahedral Al(T) and octahedral Al(O). Totals for the octahedral and interlayer sites are given as OCT. and INT. respectively. The assumed number of OH groups in the recalculation is shown.

The following abbreviations and headings have been used in the tables:

BerthCalc. Data recalculated to mineral formulae on the basis of 14 (O, OH).

IlliteCalc. Data recalculated to mineral formulae on the basis of 22 (O, OH).

OoidCalc - Berth (Si[or Mg] normalised). Data recalculated by BerthCalc., with the average Frodingham berthierine composition subtracted, normalised to Si [or Mg].

CarbCalc. Data recalculated to a carbonate of formula XCO_3, where X is the cation species.

PhosphCalc. Data recalculated to mineral formulae on the basis of 26 (O, OH, F, Cl).

Line. Indicates a series of analyses were taken across a mineral phase or particle. For ooids this was always outer to inner.

Nucleus. Used where a line of analyses enters the ooid nucleus.

Inner/Outer. For a cement generation, 'inner' represents the earlier cemented part, i.e.inner-outer represents analyses taken away from the substrate.

Berth. Berthierine.

Gen. Number of the cement generation.

Rep./Unalt. Bio. Replaced or unaltered bioclastic shell fragment.

Ech. Ovgrth. Echinoid overgrowth.

The data given within the text of this thesis presented as AVERAGE and STDEV, represent the calculated mean of the analyses and the sample standard deviation. Note that the computer software used gives the standard deviation calculated by:

$$\frac{n*(\sum(x^2)) - (\sum x)^2}{n*(n-1)}$$

This sample standard deviation gives the best estimate of the population standard deviation based on a sample of the population.

Table D.1. Compositions of Selected Goethitic Iron-Ooids, Analysed by E.P.M.A. in Lines From Outer to Inner Across the Cortex. The Data have been Recalculated as for Berthierines, and the Average Frodingham Berthierine Composition has been Subtracted Relative to Si and Mg (see text).

	YAR 7 (OOID 2)																											
	(LINE 1)											(LINE 2)											(LINE 3)					
	1	2	3	4	5	6	7	8	9	10	11	1	2	3	4	5	6	7	8	9	10	11	1	2	3	4	5	
Si	1.655	2 461	3 843	2 556	3 001	3 870	2 419	2.624	1 809	2.138	2 463	2 784	1 951	3 621	2 235	3 078	3 189	1 953	2 360	1 758	3.045	1 880	4 705	3 322	3 423	2 550	2 125	
Ti	0 071	0 067	0 085	0 084	0 144	0.146	0 093	0.181	0 197	0.100	0 162	0.051	0 012	0 096	0 236	0 133	0 030	0 135	0.038	0 162	0 175	0 124	0 086	0 226	0 168	0 182	0 051	
Al	1 518	2 042	2.493	2 313	2 417	2 855	1 970	2.325	1.734	1 945	2.101	2.321	1 694	2 673	1 989	2 569	2.560	1 978	2 133	1.890	2 477	2.264	3 637	2 802	3 082	2 495	2.045	
Fe	42 200	32 235	17 998	27 371	26 725	23 044	22 766	30 687	30 536	32 614	34 108	32 510	33 693	23 663	30 249	25.732	24.563	33 182	29 780	39.028	29 113	33 733	26 874	33 598	32 707	35 979	36 010	
Mn	0 044	0 000	0.000	0 057	0.079	0 115	0 022	0 097	0 071	0 158	0 102	0 090	0 253	0.031	0 139	0 184	0 037	0.003	0 000	0 179	0 003	0 022	0 184	0 022	0 000	0 032	0 082	
Mg	0 546	0 550	0 725	0 651	0 714	0 948	0 556	0.661	0.391	0 476	0 665	0.642	0 493	0 546	0 530	0 816	0 723	0 558	0 455	0.643	0 648	0 647	1 000	0 699	0 698	0 790	0 402	
Ca	0 717	0 371	0 386	0 397	0 370	0 300	0.277	0 438	0.297	0.330	0.459	0 933	0 515	0.473	0 385	0 400	0 344	0 356	0 361	0 465	0.478	0 363	3 156	0 513	0 509	0 418	0 464	
Na	0 468	0 174	0.324	0.338	0.387	0 143	0 434	0 121	0 213	0 284	0.445	0.185	0 070	0.295	0 284	0 505	0.390	0 189	0.193	0.608	0.087	0.425	0.209	0.074	0 093	0 236	0.079	
K	0 043	0 192	0.106	0 067	0 196	0 224	0 140	0.145	0 121	0.203	0 067	0.166	0 105	0 187	0 170	0 143	0 148	0.154	0 132	0.189	0 200	0 168	0 210	0 126	0.252	0 084	0 174	
P	0 386	0 280	0.063	0.241	0 163	0.162	0.117	0.320	0.310	0.374	0.315	0 251	0.361	0.123	0.269	0 078	0.168	0 354	0.406	0.451	0 266	0 398	0 145	0 213	0 254	0 370	0 400	
S	0.059	0 086	0.014	0 041	0 079	0.000	0.029	0 024	0.047	0.000	0.000	0.051	0.074	0.000	0.090	0 095	0.059	0.000	0.089	0.040	0.051	0.141	0.034	0.006	0 138	0.030	0 024	
O	16 702	14 871	12 656	13 913	14 348	14 730	11.906	15.093	13.378	14 691	15.780	15.828	14 504	14 204	14 163	14 308	13 974	14 646	14.205	16.468	15 163	15.175	18.626	17 050	17 198	16 827	15 644	
TOTAL	64 409	53 329	38 693	48 029	48 623	46 537	40.729	52 716	49 104	53.313	56.667	55 812	53.725	45 912	50 739	48 041	46 185	53.508	50.152	61 881	51 706	55 340	58 866	58 651	58 522	59 993	57 500	
BerthCalc																												
Si	0 832	1 378	2 449	1 523	1 712	2 146	1.656	1.453	1 136	1 228	1.301	1 454	1 135	2 072	1.314	1 739	1 870	1.122	1 414	0 905	1 666	1.050	2.050	1 597	1.643	1 269	1 147	
Al(TOT)	0 795	1 190	1 653	1 434	1 435	1.648	1 404	1.340	1 133	1.163	1.155	1.261	1.026	1 592	1.217	1 510	1.563	1.183	1.330	1 013	1 410	1 316	1 649	1 402	1 539	1 292	1 149	
Ti	0 021	0 022	0 032	0 029	0 048	0 047	0 037	0.059	0.073	0 034	0.050	0.016	0.004	0.032	0 081	0 044	0.010	0 045	0.013	0 049	0.056	0 041	0 022	0 064	0 047	0 053	0 016	
Fe	10.662	9 054	5.764	8 192	7.650	6 427	7.831	8.543	9 631	9.421	9.058	8.525	9.838	6.809	8 923	7.288	7.230	9.586	8 951	10 099	7 998	9 438	5 882	8 121	7 866	9 000	9.769	
Mn	0 011	0 000	0 000	0 017	0 023	0 033	0 008	0.027	0 023	0 046	0.028	0.024	0 075	0 009	0 042	0 053	0 011	0 001	0 000	0 047	0 001	0.006	0 041	0 005	0 000	0 008	0 023	
Mg	0 317	0.356	0 534	0 448	0 471	0 607	0 440	0 423	0 284	0 316	0.406	0.387	0.331	0 361	0 360	0 533	0.490	0.370	0.315	0 383	0 410	0 417	0 503	0.388	0 387	0 454	0 251	
Ca	-0 041	-0 091	0 112	-0 051	0 007	-0 019	0.012	-0 098	-0 163	-0 192	-0 082	0.143	-0 107	0.083	-0 080	0.092	-0 008	-0 164	-0 216	-0 183	-0 037	-0 194	0 868	0 018	-0 013	-0 133	-0 151	
Na	0 287	0 119	0 252	0.246	0 270	0 097	0 363	0 082	0 163	0.199	0 287	0 118	0.050	0 206	0.204	0.348	0 279	0.133	0.141	0 382	0 058	0.290	0 111	0 043	0 055	0 143	0 052	
K	0 016	0 077	0 049	0 029	0 080	0 089	0 069	0 058	0 055	0 084	0 025	0 062	0 044	0 077	0 072	0 058	0 062	0 064	0 057	0.070	0 079	0 067	0 066	0 044	0 087	0 030	0 067	
OH	8 000	8 000	8 000	8 000	8 000	8 000	8.000	8 000	8 000	8 000	8 000	8 000	8 000	8 000	8 000	8 000	8 000	8 000	8.000	8.000	8 000	8 000	8 000	8 000	8 000	8 000	8 000	
OoidCalc - Berth (Si normalised)																												
Si	0 000	0 000	0.000	0 000	0 000	0 000	0.000	0 000	0.000	0 000	0.000	0 000	0 000	0 000	0.000	0.000	0 000	0.000	0.000	0 000	0 000	0.000	0 000	0 000	0 000	0.000	0 000	
Al(TOT)	0 364	0 478	0.388	0 647	0 550	0.539	0 548	0 589	0.546	0 528	0.482	0 510	0 439	0 521	0.538	0 612	0 596	0.603	0.599	0.545	0.549	0.773	0.590	0 576	0 690	0 636	0 556	
Ti	0 020	0 020	0 029	0 027	0 046	0 045	0 035	0 057	0 071	0 032	0.049	0 014	0 003	0 030	0 080	0 042	0 008	0 044	0 012	0.048	0.054	0.039	0 019	0 062	0 045	0 052	0 015	
Fe	9 686	7.439	2 894	6 407	5.643	3 912	5.890	6.839	8.300	7.982	7.534	6.821	8.508	4.381	7.383	5.250	5 038	8.271	7.294	9.038	6.046	8.207	3.479	6.250	5.940	7 512	8.424	
Mn	0.010	-0 002	-0 004	0 015	0.020	0 029	0.005	0.025	0.021	0.045	0 026	0.022	0.074	0.006	0 040	0 051	0.008	-0 001	-0.002	0.046	-0 002	0.005	0.038	0.003	-0 002	0 006	0 021	
Mg	0 097	-0 009	-0 114	0 045	0 018	0 039	0.001	0 038	-0 017	-0.009	0 062	0 003	0 031	-0 187	0 012	0 072	-0.005	0.073	-0.059	0 143	-0.031	0 140	-0 039	-0.034	-0 048	0 118	-0 053	
Ca	-0 059	-0 122	0 057	-0 085	-0 031	-0.067	-0.025	-0 130	-0 189	-0 219	-0 110	0.111	-0 133	0 037	-0.110	0 053	-0 049	-0.189	-0.247	-0.203	-0 074	-0.217	0 822	-0 017	-0 049	-0 161	-0 176	
Na	0 263	0 079	0 181	0 202	0 220	0 035	0.315	0.040	0 131	0 164	0 249	0 076	0 017	0 146	0 166	0 298	0 225	0 100	0 100	0 356	0.010	0.259	0 052	-0 003	0 007	0 107	0 019	
K	0 013	0 073	0 042	0 025	0 076	0 083	0 064	0 054	0.051	0 080	0 022	0 058	0 041	0 071	0 068	0 053	0 057	0 060	0 053	0 067	0 074	0 065	0 060	0 039	0 082	0 027	0 064	
OoidCalc - Berth (Mg normalised)																												
Si	-0 366	0 034	0 432	-0 170	-0 066	-0 149	-0 006	-0.145	0 064	0 034	-0 232	-0 010	-0 117	0.708	-0 046	-0 274	0.019	-0.277	0 224	-0 540	0 118	-0 527	0 148	0 130	0 180	-0 447	0.200	
Al(TOT)	0 175	0 495	0 611	0 559	0 516	0 462	0 545	0.514	0 579	0 546	0 362	0 505	0 378	0.887	0.514	0 470	0 606	0 459	0.715	0.266	0 610	0.500	0.666	0 644	0 784	0 405	0 659	
Ti	0 019	0 020	0 029	0 027	0 046	0 045	0 035	0 057	0 071	0 032	0 048	0 014	0 003	0 031	0 080	0 042	0 008	0 044	0 012	0 047	0 054	0 039	0 020	0 062	0 045	0 051	0 015	
Fe	9 257	7 479	3 400	6 207	5 565	3 737	5 883	6.669	8.375	8 022	7.262	6 810	8 370	5 211	7.328	4.929	5 061	7.946	7.556	8 405	6.184	7 589	3 653	6 402	6 152	6 988	8 658	
Mn	0 009	-0 002	-0 003	0 015	0 020	0 029	0.005	0 025	0 021	0 045	0 025	0 022	0 073	0 007	0 040	0 050	0.008	-0 001	-0.002	0 045	-0 002	0 004	0.038	0.003	-0 002	0 006	0 021	
Mg	0 000	0 000	0 000	0 000	0 000	0.000	0 000	0 000	0 000	0.000	0 000	0 000	0 000	0 000	0.000	0.000	0 000	0 000	0.000	0 000	0 000	0 000	0 000	0 000	0 000	0 000	0 000	
Ca	-0 067	-0 121	0 067	-0 089	-0 032	-0 070	-0 025	-0 133	-0 187	-0 218	-0 116	0.111	-0 135	0 053	-0.111	0 047	-0 049	-0 195	-0.242	-0.215	-0 071	-0 229	0 826	-0 014	-0 045	-0 171	-0 172	
Na	0 253	0 080	0 194	0 197	0 218	0 031	0.315	0 036	0 132	0 165	0 243	0 076	0 014	0 167	0 165	0 290	0 226	0 092	0 107	0 341	0 013	0 244	0 056	0 001	0 012	0 094	0 025	
K	0 012	0 074	0 043	0 024	0 075	0 083	0 064	0 053	0 052	0 081	0 021	0 058	0 040	0 073	0 068	0 053	0 057	0 060	0 054	0 066	0 074	0 063	0 061	0 040	0 083	0 025	0 065	

Table D.1. (Continued).

								YAR 7 (OOID 3)																				
		(LINE 4)						(LINE 1)										(LINE 2)										
	6	1	2	3	4	5	6	1	2	3	4	5	6	7	8	9	10	1	2	3	4	5	6	7	8	9	10
Si	1.669	3.286	2.967	2.863	2.499	2.085	1.783	4.024	4.799	4.829	3.038	2.290	2.689	2.626	1.748	2.051	1.820	5.662	4.865	2.737	2.341	1.762	1.655	1.636	1.692	1.554	1.490
Ti	0.245	0.134	0.148	0.045	0.252	0.164	0.208	0.114	0.024	0.000	0.229	0.115	0.130	0.246	0.249	0.308	0.169	0.077	0.104	0.050	0.115	0.270	0.296	0.230	0.155	0.155	0.183
Al	1.924	2.738	2.569	2.479	2.466	1.967	1.949	2.452	3.341	3.424	2.757	2.500	2.293	2.233	2.118	2.256	2.315	3.682	3.246	2.595	2.030	2.230	2.251	2.362	2.316	2.418	2.194
Fe	37.408	32.503	33.812	33.155	34.545	37.866	39.415	17.061	24.813	22.544	25.489	29.255	20.482	27.906	33.687	31.240	34.693	22.524	22.661	26.677	23.043	33.911	33.046	35.859	37.860	38.865	37.948
Mn	0.197	0.099	0.207	0.145	0.139	0.052	0.110	0.085	0.150	0.177	0.083	0.282	0.141	0.077	0.088	0.086	0.006	0.092	0.013	0.109	0.043	0.000	0.060	0.142	0.053	0.081	0.104
Mg	0.507	0.625	0.568	0.603	0.731	0.497	0.579	0.764	1.324	1.106	0.702	0.748	0.581	0.583	0.553	0.464	0.510	1.130	0.850	0.637	0.442	0.538	0.409	0.553	0.429	0.473	0.314
Ca	0.363	0.616	0.577	0.547	0.491	0.487	0.444	7.847	0.469	0.402	0.351	0.300	0.283	0.360	0.354	0.276	0.292	0.585	0.433	0.357	0.259	0.374	0.399	0.318	0.362	0.330	0.311
Na	0.213	0.155	0.053	0.193	0.658	0.219	0.371	0.314	0.241	0.152	0.388	0.196	0.000	0.239	0.303	0.073	0.222	0.003	0.182	0.170	0.262	0.205	0.333	0.092	0.391	0.263	0.392
K	0.116	0.128	0.163	0.160	0.149	0.193	0.100	0.182	0.149	0.202	0.082	0.137	0.134	0.153	0.126	0.168	0.132	0.106	0.113	0.161	0.170	0.167	0.114	0.175	0.161	0.223	0.079
P	0.380	0.110	0.196	0.211	0.251	0.439	0.517	0.086	0.136	0.164	0.207	0.256	0.174	0.253	0.368	0.382	0.345	0.146	0.132	0.174	0.240	0.375	0.297	0.422	0.476	0.423	0.522
S	0.046	0.083	0.000	0.063	0.088	0.066	0.088	0.046	0.000	0.126	0.056	0.057	0.036	0.128	0.104	0.073	0.042	0.094	0.057	0.025	0.052	0.010	0.010	0.022	0.017	0.014	0.092
O	15.618	16.489	16.420	16.026	16.407	16.302	16.604	15.648	16.956	16.251	14.415	14.412	11.846	14.128	14.831	14.493	15.188	17.445	15.983	14.011	11.994	14.980	14.520	15.536	16.163	16.309	15.830
TOTAL	58.686	56.966	57.680	56.490	58.676	60.337	62.168	48.623	52.402	49.377	47.797	50.548	38.789	48.932	54.529	51.870	55.734	51.546	48.639	47.703	40.991	54.822	53.390	57.347	60.075	61.108	59.459
BerthCalc																											
Si	0.900	1.615	1.479	1.468	1.258	1.084	0.919	2.077	2.297	2.427	1.736	1.319	1.871	1.545	0.995	1.198	1.006	2.640	2.474	1.601	1.629	0.992	0.951	0.892	0.892	0.805	0.809
Al(TOT)	1.080	1.400	1.333	1.323	1.292	1.064	1.046	1.317	1.664	1.791	1.640	1.499	1.660	1.368	1.255	1.372	1.331	1.786	1.718	1.580	1.470	1.306	1.346	1.341	1.270	1.304	1.240
Ti	0.077	0.039	0.043	0.014	0.074	0.050	0.063	0.034	0.007	0.000	0.077	0.039	0.053	0.085	0.083	0.105	0.055	0.021	0.031	0.017	0.047	0.089	0.100	0.074	0.048	0.047	0.058
Fe	10.135	8.014	8.477	8.535	8.725	9.885	10.200	4.419	5.973	5.671	7.312	8.460	7.156	8.226	9.617	9.159	9.629	5.262	5.782	7.843	8.046	9.596	9.547	9.831	10.029	10.122	10.343
Mn	0.054	0.025	0.053	0.038	0.036	0.014	0.029	0.022	0.037	0.045	0.024	0.083	0.050	0.023	0.026	0.026	0.002	0.022	0.003	0.033	0.015	0.000	0.018	0.040	0.014	0.021	0.029
Mg	0.316	0.355	0.327	0.357	0.425	0.299	0.345	0.456	0.732	0.642	0.464	0.498	0.467	0.396	0.364	0.313	0.326	0.609	0.499	0.431	0.355	0.350	0.272	0.348	0.261	0.283	0.197
Ca	-0.172	0.130	0.054	0.033	-0.018	-0.167	-0.242	2.771	0.059	0.017	-0.038	-0.102	-0.045	-0.077	-0.175	-0.224	-0.175	0.088	0.053	-0.007	-0.126	-0.171	-0.097	-0.226	-0.245	-0.211	-0.310
Na	0.140	0.093	0.032	0.121	0.404	0.139	0.234	0.198	0.141	0.093	0.271	0.138	0.000	0.172	0.211	0.052	0.150	0.002	0.113	0.121	0.223	0.141	0.234	0.061	0.252	0.166	0.260
K	0.045	0.045	0.058	0.059	0.054	0.072	0.037	0.068	0.051	0.073	0.034	0.057	0.067	0.065	0.052	0.071	0.052	0.036	0.041	0.068	0.085	0.068	0.047	0.069	0.061	0.083	0.031
OH	8.000	8.000	8.000	8.000	8.000	8.000	8.000	8.000	8.000	8.000	8.000	8.000	8.000	8.000	8.000	8.000	8.000	8.000	8.000	8.000	8.000	8.000	8.000	8.000	8.000	8.000	8.000
OoidCalc - Berth (Si normalised)																											
Si	0.000	0.000	0.000	0.000	0.000	0.000	0.000	0.000	0.000	0.000	0.000	0.000	0.000	0.000	0.000	0.000	0.000	0.000	0.000	0.000	0.000	0.000	0.000	0.000	0.000	0.000	0.000
Al(TOT)	0.615	0.566	0.568	0.564	0.642	0.504	0.571	0.244	0.477	0.537	0.742	0.817	0.693	0.569	0.740	0.752	0.811	0.422	0.439	0.752	0.628	0.794	0.855	0.880	0.809	0.888	0.822
Ti	0.076	0.037	0.041	0.012	0.073	0.049	0.062	0.032	0.004	-0.003	0.075	0.037	0.051	0.083	0.082	0.104	0.054	0.018	0.028	0.015	0.045	0.088	0.099	0.072	0.047	0.046	0.057
Fe	9.080	6.122	6.743	6.814	7.251	8.615	9.123	1.984	3.281	2.826	5.277	6.914	4.963	6.415	8.451	7.755	8.451	2.168	2.883	5.966	6.137	8.434	8.433	8.785	8.984	9.179	9.395
Mn	0.053	0.022	0.051	0.036	0.034	0.012	0.028	0.019	0.033	0.042	0.022	0.081	0.047	0.021	0.024	0.024	0.000	0.018	0.000	0.030	0.013	-0.002	0.016	0.038	0.013	0.020	0.028
Mg	0.078	-0.073	-0.064	-0.031	0.092	0.012	0.102	-0.094	0.124	0.000	0.004	0.149	-0.028	-0.013	0.100	-0.004	0.059	-0.090	-0.155	0.007	-0.076	0.087	0.020	0.112	0.025	0.070	-0.017
Ca	-0.192	0.095	0.021	0.000	-0.046	-0.192	-0.263	2.725	0.008	-0.037	-0.077	-0.131	-0.086	-0.111	-0.197	-0.251	-0.197	0.030	-0.002	-0.043	-0.152	-0.193	-0.118	-0.246	-0.265	-0.229	-0.328
Na	0.114	0.046	-0.010	0.078	0.368	0.108	0.207	0.138	0.075	0.023	0.221	0.100	-0.054	0.127	0.182	0.017	0.121	-0.074	0.042	0.075	0.176	0.112	0.206	0.036	0.226	0.143	0.237
K	0.042	0.041	0.054	0.055	0.050	0.069	0.035	0.062	0.045	0.066	0.029	0.053	0.062	0.060	0.049	0.067	0.050	0.028	0.035	0.063	0.081	0.065	0.044	0.066	0.059	0.081	0.029
OoidCalc - Berth (Mg normalised)																											
Si	-0.294	0.274	0.243	0.118	-0.348	-0.044	-0.384	0.356	-0.470	0.000	-0.015	-0.562	0.106	0.048	-0.379	0.015	-0.225	0.340	0.587	-0.026	0.286	-0.330	-0.075	-0.424	-0.095	-0.265	0.065
Al(TOT)	0.463	0.707	0.694	0.625	0.462	0.481	0.372	0.427	0.234	0.537	0.735	0.526	0.748	0.594	0.544	0.760	0.695	0.598	0.742	0.739	0.776	0.623	0.816	0.660	0.760	0.751	0.855
Ti	0.076	0.037	0.042	0.012	0.072	0.049	0.061	0.032	0.003	-0.003	0.075	0.037	0.051	0.083	0.081	0.104	0.053	0.018	0.029	0.015	0.045	0.087	0.098	0.072	0.047	0.046	0.057
Fe	8.736	6.443	7.028	6.953	6.843	8.563	8.673	2.401	2.730	2.827	5.259	6.256	5.088	6.471	8.007	7.773	8.188	2.566	3.571	5.936	6.473	8.047	8.345	8.287	8.873	8.869	9.471
Mn	0.053	0.023	0.051	0.036	0.033	0.012	0.027	0.020	0.033	0.042	0.022	0.080	0.047	0.021	0.024	0.024	0.000	0.018	0.001	0.030	0.013	-0.002	0.016	0.038	0.013	0.020	0.028
Mg	0.000	0.000	0.000	0.000	0.000	0.000	0.000	0.000	0.000	0.000	0.000	0.000	0.000	0.000	0.000	0.000	0.000	0.000	0.000	0.000	0.000	0.000	0.000	0.000	0.000	0.000	0.000
Ca	-0.199	0.101	0.026	0.003	-0.053	-0.192	-0.271	2.733	-0.002	-0.037	-0.077	-0.143	-0.084	-0.110	-0.206	-0.250	-0.202	0.037	0.011	-0.044	-0.156	-0.201	-0.120	-0.255	-0.267	-0.235	-0.327
Na	0.106	0.054	-0.003	0.082	0.358	0.106	0.196	0.148	0.061	0.023	0.220	0.084	-0.051	0.129	0.171	0.018	0.114	-0.065	0.059	0.074	0.184	0.103	0.204	0.023	0.223	0.136	0.239
K	0.042	0.042	0.055	0.055	0.049	0.069	0.033	0.063	0.044	0.066	0.029	0.052	0.062	0.061	0.048	0.067	0.049	0.029	0.036	0.063	0.081	0.064	0.044	0.065	0.058	0.080	0.029

Table D.1. (Continued).

	YAR. 21 (OOID 7)							YAR. 21 (OOID 8)						YAR. 21 (OOID 9)						YAR. 21 (OOID 10)						YAR. 21 (OOID 11)			
							>nucleus					>nucleus					>nucleus					>nucleus					
	1	2	3	4	5	6	7	8	1	2	3	4	5	1	2	3	4	5	1	2	3	4	5	1	2	3	4	
Si	1 532	1 424	1 604	1 752	1 581	1 907	1 334	1 095	1 659	1 734	3 438	1 570	1 516	1 266	0 760	1 248	1 199	0 718	2 157	1 523	1 418	1 202	1 353	1 256	0 744	1 457	1 611	
Ti	0 090	0 068	0 086	0 183	0 196	0 219	0 134	0 097	0 146	0 145	0 114	0 000	0 010	0 120	0 106	0 084	0 085	0 005	0 113	0 107	0 064	0 096	0 086	0 147	0 000	0 186	0 129	
Al	1 830	1 461	1 943	2 011	1 863	2 310	1 917	2 206	1 744	1 773	3 251	0 963	0 867	1 592	0 631	1 694	1 388	0 483	2 090	1 990	2 005	1 351	1 374	1 889	1 432	2 122	2 131	
Fe	28 845	28 740	37 017	35 048	46 753	43 653	39 600	36 662	32 580	34 561	37 310	51 683	52 994	29 893	10 328	40 946	28 916	35 263	33 562	41 213	36 588	50 795	50 985	40 577	38 023	39 577	43 390	
Mn	0 274	0 269	0 221	0 073	0 264	0 141	0 177	0 271	0 332	0 140	0 090	0 425	0 244	0 157	0 091	0 006	0 250	2 100	0 493	0 074	0 115	0 092	0 227	0 464	0 147	0 253	0 136	
Mg	0 543	0 400	0 570	0 454	0 542	0 464	0 422	0 415	0 529	0 377	0 664	0 702	0 517	0 391	0 078	0 278	0 255	2 518	0 551	0 460	0 519	0 655	0 591	0 262	0 273	0 391	0 422	
Ca	0 496	0 333	0 321	0 314	0 362	0 303	0 285	0 261	0 437	0 309	1 029	0 228	0 254	0 488	0 212	0 363	0 165	3 168	0 597	0 433	0 435	0 241	0 262	0 379	0 205	0 202	0 266	
Na	0 342	0 051	0 480	0 100	0 038	0 058	0 035	0 483	0 256	0 000	0 357	0 097	0 111	0 118	0 006	0 307	0 059	0 520	0 295	0 184	0 136	0 319	0 298	0 053	0 044	0 006	0 437	
K	0 048	0 023	0 120	0 039	0 016	0 172	0 021	0 099	0 150	0 132	0 426	0 032	0 041	0 005	0 040	0 028	0 102	0 009	0 175	0 041	0 208	0 000	0 065	0 085	0 017	0 188	0 077	
P	0 160	0 201	0 329	0 303	0 491	0 411	0 443	0 313	0 296	0 272	0 579	0 739	0 656	0 215	0 130	0 366	0 140	0 000	0 166	0 369	0 388	0 704	0 772	0 244	0 241	0 302	0 400	
S	0 030	0 019	0 064	0 047	0 000	0 062	0 000	0 013	0 000	0 053	0 000	0 000	0 042	0 000	0 111	0 017	0 087	0 038	0 039	0 051	0 048	0 012	0 001	0 000	0 000	0 000	0 000	
O	12 668	11 958	15 401	14 826	18 212	17 934	15 691	14 828	13 993	14 340	19 408	19 125	19 094	12 320	4 798	15 631	11 470	15 069	15 105	16 429	15 064	18 761	19 102	15 644	13 649	15 853	17 356	
TOTAL	46 858	44 947	58 156	55 150	70 318	67 634	60 059	56 743	52 122	53 836	66 666	75 564	76 346	46 565	17 291	60 968	44 116	59 891	55 343	62 874	56 988	74 228	75 116	61 000	54 775	60 537	66 355	
BerthCalc																												
Si	0 992	0 986	0 872	0 987	0 735	0 893	0 722	0 617	0 991	1 006	1 510	0 714	0 684	0 852	1 350	0 671	0 858	0 380	1 167	0 777	0 795	0 556	0 619	0 663	0 452	0 764	0 779	
Al(TOT)	1 233	1 053	1 099	1 179	0 901	1 126	1 080	1 294	1 084	1 071	1 486	0 456	0 407	1 114	1 167	0 948	1 034	0 266	1 177	1 057	1 171	0 650	0 654	1 037	0 905	1 159	1 072	
Ti	0 034	0 028	0 027	0 060	0 053	0 060	0 043	0 032	0 051	0 049	0 029	0 000	0 003	0 047	0 110	0 026	0 036	0 002	0 036	0 032	0 021	0 026	0 023	0 045	0 000	0 057	0 037	
Fe	9 386	10 000	10 100	9 914	10 931	10 267	10 777	10 389	9 783	10 073	8 240	11 823	12 019	10 112	9 140	11 064	10 377	9 383	9 125	10 569	10 311	11 813	11 726	10 765	11 615	10 442	10 551	
Mn	0 091	0 095	0 061	0 021	0 063	0 034	0 049	0 078	0 101	0 042	0 020	0 099	0 056	0 054	0 083	0 002	0 091	0 569	0 136	0 019	0 033	0 022	0 053	0 125	0 046	0 068	0 034	
Mg	0 406	0 320	0 358	0 295	0 291	0 251	0 264	0 270	0 365	0 253	0 337	0 369	0 270	0 304	0 160	0 173	0 211	1 541	0 345	0 271	0 336	0 350	0 312	0 160	0 192	0 237	0 236	
Ca	0 068	-0 049	-0 148	-0 134	-0 227	-0 191	-0 254	-0 164	-0 084	-0 113	-0 068	-0 435	-0 367	0 011	-0 085	-0 161	-0 069	1 175	0 091	-0 130	-0 158	-0 414	-0 449	-0 054	-0 134	-0 165	-0 202	
Na	0 270	0 043	0 319	0 069	0 022	0 033	0 023	0 332	0 187	0 000	0 191	0 054	0 061	0 097	0 013	0 202	0 052	0 336	0 195	0 115	0 093	0 180	0 166	0 034	0 033	0 004	0 258	
K	0 022	0 011	0 047	0 016	0 005	0 058	0 008	0 040	0 064	0 055	0 134	0 010	0 013	0 002	0 051	0 011	0 052	0 003	0 068	0 015	0 084	0 000	0 021	0 032	0 007	0 071	0 027	
OH	8 000	8 000	8 000	8 000	8 000	8 000	8 000	8 000	8 000	8 000	8 000	8 000	8 000	8 000	8 000	8 000	8 000	8 000	8 000	8 000	8 000	8 000	8 000	8 000	8 000	8 000	8 000	
OoidCalc - Berth (Si normalised)																												
Si	0 000	0 000	0 000	0 000	0 000	0 000	0 000	0 000	0 000	0 000	0 000	0 000	0 000	0 000	0 000	0 000	0 000	0 000	0 000	0 000	0 000	0 000	0 000	0 000	0 000	0 000	0 000	
Al(TOT)	0 721	0 543	0 648	0 669	0 521	0 664	0 707	0 975	0 572	0 551	0 706	0 087	0 054	0 674	0 469	0 601	0 590	0 070	0 574	0 655	0 759	0 363	0 334	0 695	0 672	0 764	0 670	
Ti	0 033	0 026	0 026	0 059	0 053	0 059	0 042	0 031	0 050	0 048	0 028	-0 001	0 002	0 046	0 109	0 026	0 035	0 001	0 034	0 031	0 020	0 025	0 022	0 045	-0 001	0 056	0 036	
Fe	8 223	8 845	9 079	8 757	10 069	9 220	9 931	9 666	8 622	8 894	6 471	10 986	11 218	9 114	7 558	10 278	9 372	8 937	7 757	9 658	9 379	11 161	11 001	9 988	11 085	9 546	9 638	
Mn	0 089	0 094	0 060	0 020	0 062	0 032	0 048	0 077	0 100	0 040	0 018	0 098	0 055	0 053	0 081	0 001	0 090	0 568	0 135	0 018	0 032	0 021	0 052	0 124	0 045	0 067	0 032	
Mg	0 144	0 059	0 127	0 034	0 097	0 015	0 073	0 107	0 103	-0 014	-0 063	0 180	0 089	0 078	-0 197	-0 005	-0 016	1 440	0 036	0 066	0 126	0 203	0 149	-0 016	0 072	0 035	0 030	
Ca	0 046	-0 071	-0 167	-0 156	-0 243	-0 211	-0 270	-0 177	-0 106	-0 135	-0 101	-0 451	-0 382	-0 007	-0 115	-0 175	-0 088	1 167	0 065	-0 147	-0 176	-0 426	-0 463	-0 069	-0 144	-0 182	-0 219	
Na	0 242	0 015	0 293	0 040	0 000	0 007	0 002	0 315	0 158	-0 029	0 148	0 033	0 041	0 072	-0 026	0 182	0 027	0 325	0 161	0 092	0 070	0 164	0 149	0 015	0 020	-0 018	0 236	
K	0 020	0 009	0 044	0 013	0 003	0 055	0 006	0 038	0 062	0 052	0 130	0 009	0 011	0 000	0 047	0 009	0 050	0 002	0 065	0 013	0 082	-0 002	0 020	0 030	0 006	0 069	0 025	
OoidCalc - Berth (Mg normalised)																												
Si	-0 543	-0 223	-0 481	-0 130	-0 365	-0 056	-0 275	-0 404	-0 388	0 051	0 237	-0 680	-0 334	-0 297	0 745	0 018	0 061	-5 441	-0 134	-0 248	-0 476	-0 767	-0 561	0 059	-0 272	-0 131	-0 112	
Al(TOT)	0 440	0 428	0 400	0 602	0 333	0 635	0 564	0 766	0 371	0 577	0 828	-0 265	-0 119	0 521	0 854	0 610	0 622	-2 743	0 504	0 527	0 514	-0 033	0 044	0 725	0 531	0 696	0 612	
Ti	0 032	0 026	0 026	0 059	0 052	0 059	0 041	0 031	0 049	0 048	0 028	-0 002	0 001	0 046	0 110	0 026	0 035	-0 006	0 034	0 031	0 020	0 024	0 022	0 045	-0 001	0 056	0 035	
Fe	7 586	8 584	8 515	8 606	9 642	9 155	9 609	9 192	8 167	8 954	6 748	10 189	10 826	8 766	8 431	10 300	9 444	2 560	7 599	9 368	8 821	10 263	10 343	10 058	10 767	9 392	9 507	
Mn	0 088	0 093	0 059	0 019	0 061	0 032	0 047	0 077	0 099	0 040	0 018	0 097	0 055	0 052	0 082	0 001	0 090	0 560	0 134	0 018	0 031	0 020	0 051	0 124	0 045	0 067	0 032	
Mg	0 000	0 000	0 000	0 000	0 000	0 000	0 000	0 000	0 000	0 000	0 000	0 000	0 000	0 000	0 000	0 000	0 000	0 000	0 000	0 000	0 000	0 000	0 000	0 000	0 000	0 000	0 000	
Ca	0 034	-0 076	-0 178	-0 159	-0 251	-0 212	-0 276	-0 186	-0 115	-0 134	-0 096	-0 466	-0 390	-0 014	-0 098	-0 175	-0 086	1 046	0 062	-0 152	-0 186	-0 443	-0 476	-0 068	-0 150	-0 185	-0 222	
Na	0 226	0 008	0 279	0 037	-0 010	0 006	-0 006	0 303	0 147	-0 028	0 155	0 014	0 032	0 064	-0 004	0 183	0 029	0 168	0 157	0 085	0 056	0 142	0 132	0 017	0 012	-0 022	0 232	
K	0 018	0 008	0 043	0 013	0 002	0 055	0 005	0 037	0 061	0 052	0 131	0 007	0 011	-0 001	0 049	0 009	0 050	-0 012	0 064	0 012	0 080	-0 004	0 018	0 031	0 005	0 068	0 024	

Table D.1. (Continued).

	YAR 24 (OOID 12)						YAR 24 (OOID 13)						YAR 24 (OOID 14)						YAR 24 (OOID 15)							YAR 24 (OOID 16)	
										>nucleus	(Broken ooid)						>nucleus							>nucleus			
	1	2	3	4	5	6	1	2	3	4	5	6	1	2	3	4	5	6	1	2	3	4	5	6	7	1	2
Si	1 525	1.561	1 721	1.990	1 356	2.654	1.486	1 277	2 007	1 672	2 122	2 195	1 533	1 797	1 658	1.723	1 349	1 345	1.878	1 312	1 944	2 139	2 992	3 010	2 701	2 463	0 905
Ti	0 028	0.075	0 088	0.094	0 103	0 127	0 015	0.152	0 086	0 184	0 071	0.145	0 079	0 129	0.137	0 007	0 000	0 160	0 080	0.120	0 082	0 063	0 137	0 132	0 053	0 000	0 007
Al	1 720	1.696	2 011	2.599	1 675	2.620	1 654	1.475	1 735	2.194	2.666	2 784	1.523	1.639	1 398	1 758	1.747	1 564	1 347	1 851	1.722	2.001	2.598	2 305	2.362	2.591	0.909
Fe	32.904	34 490	37.227	38.596	36 926	42 317	34 858	33 917	30.353	46 046	45 860	43.987	28.223	27 115	20.663	30.379	45.072	46.148	41 430	30.599	29.926	24 835	25.844	25.672	24 844	32 386	15.984
Mn	0 190	0 215	0 075	0 193	0.722	0.676	0.108	0 332	0.284	0 292	0.324	0.246	0 241	0 274	0 205	0.108	0.407	0.360	0 303	0 213	0 235	0.108	0 315	0 240	0.301	0 198	0.146
Mg	0 529	0.527	0 544	0.747	0.398	0.685	0.316	0.373	0.499	0 603	0 733	0.753	0.441	0.507	0.318	0.332	0.905	0 712	0 639	0.491	0.441	0.592	0.578	0 480	0.610	0 528	0 275
Ca	0.386	0.317	0 315	0.194	0.216	0.308	0.326	0.254	0.260	0.363	0.285	0.255	0.358	0.257	0.189	0.267	0.286	0.229	0 501	0 250	0 270	0.251	0 242	0.350	0.274	0.481	0 280
Na	0.452	0.277	0 167	0.232	0.148	0.350	0.096	0 290	0.261	0 100	0.049	0.669	0.302	0.204	0.359	0.214	0.523	0 224	0.270	0.000	0.390	0.091	0.265	0.084	0.391	0.407	0 039
K	0 057	0.093	0 139	0.144	0.119	0.312	0.154	0.064	0.177	0 111	0.167	0.268	0.143	0.144	0.142	0.110	0 008	0.000	0.073	0.077	0 144	0.161	0.256	0 190	0 045	0 370	0 031
P	0.324	0.382	0.234	0.270	0.209	0.253	0.217	0.243	0 107	0.338	0.328	0.338	0.289	0.159	0.129	0.168	0.399	0.372	0 215	0.189	0.129	0.116	0 040	0.122	0.133	0.193	0 058
S	0.000	0.000	0 083	0.095	0.066	0.027	0.026	0.008	0.000	0 124	0.000	0.020	0.031	0.004	0.032	0.029	0.000	0.000	0 061	0 070	0.098	0.000	0.025	0.074	0 057	0 034	0 022
O	13.859	14 363	15 367	16 782	14 586	18 845	13.875	13 456	13.364	18 292	19.141	19.068	12 250	12 180	9 808	12.906	17 531	17.474	16 356	12.733	13 172	12.109	13.980	13.674	13 246	15 453	6 854
TOTAL	51.974	53.996	57 971	61.936	56.524	69 174	53.131	51 841	49 133	70 319	71.746	70 728	45 413	44.409	35.038	48.001	68 227	68 588	63.153	47.905	48 553	42.466	47.272	46 333	45 017	55 104	25 510
BerthCalc																											
Si	0 924	0.919	0 925	0.981	0 766	1.157	0 884	0 788	1.219	0.761	0 918	0.955	1.052	1 211	1.389	1.096	0 645	0 643	0.943	0 850	1 205	1 438	1 718	1 792	1 664	1 307	1 074
Al(TOT)	1 085	1 040	1 125	1 333	0.985	1 189	1 024	0 947	1.097	1 039	1 200	1.260	1.088	1.149	1.219	1.164	0.870	0 779	0 704	1.248	1.111	1 400	1 553	1 429	1 514	1 431	1 122
Ti	0.010	0.026	0.028	0 027	0.034	0 032	0.005	0 055	0.031	0.049	0 018	0.037	0.032	0.051	0.067	0.003	0.000	0.045	0 024	0 046	0.030	0 025	0.046	0.046	0 019	0.000	0 005
Fe	10.028	10 216	10 040	9 548	10 473	9.273	10.426	10 518	9 270	10 509	9.978	9.618	9.732	9.186	8 691	9.712	10 843	11.101	10 452	9 952	9 299	8 399	7 458	7 669	7 682	8 635	9 524
Mn	0 059	0 065	0 021	0.049	0.208	0 151	0.033	0.105	0.088	0.068	0.072	0.055	0.085	0 094	0.088	0.035	0 100	0.088	0 078	0.071	0.074	0 037	0.092	0 073	0.095	0 054	0 089
Mg	0.370	0 359	0.338	0 425	0.260	0 345	0.217	0 266	0 350	0.317	0.366	0.378	0.350	0.395	0 308	0.244	0 500	0 393	0 371	0 368	0.316	0 460	0 384	0 330	0 434	0 324	0 377
Ca	-0 133	-0 209	-0 071	-0 134	-0 093	-0 073	-0 059	-0 117	0 012	-0 117	-0 128	-0 144	-0 128	-0 041	-0 052	-0 042	-0 193	-0 192	0 013	-0 072	-0 004	0 000	0 063	0 036	-0 006	0 024	0 129
Na	0 335	0 199	0 110	0 140	0 102	0 186	0 070	0 218	0 194	0 056	0 026	0 355	0 253	0 168	0 367	0 166	0 306	0 131	0 166	0 000	0 295	0 075	0 186	0 061	0 294	0 264	0 056
K	0 025	0 039	0 054	0 051	0 048	0 098	0 066	0 028	0 077	0 036	0 052	0 084	0 071	0 070	0 085	0 050	0 003	0 000	0 026	0 036	0 064	0 078	0 106	0 081	0 020	0 141	0 026
OH	8 000	8 000	8 000	8 000	8 000	8 000	8 000	8 000	8 000	8 000	8 000	8 000	8 000	8 000	8 000	8 000	8 000	8 000	8 000	8 000	8 000	8 000	8 000	8 000	8 000	8 000	8 000
OoidCalc - Berth (Si normalised)																											
Si	0 000	0 000	0 000	0 000	0.000	0 000	0.000	0 000	0 000	0 000	0 000	0.000	0.000	0 000	0 000	0 000	0 000	0 000	0.000	0 000	0 000	0 000	0.000	0 000	0 000	0 000	0 000
Al(TOT)	0.607	0.564	0 647	0 826	0 589	0 591	0 567	0 540	0 467	0 646	0.726	0 767	0 544	0 523	0.501	0 597	0 536	0.446	0 217	0 809	0.488	0 657	0 665	0.502	0 654	0 755	0 567
Ti	0.009	0.025	0.027	0.026	0 033	0 031	0 004	0 054	0.029	0 048	0 017	0.036	0 031	0.049	0.066	0 001	-0 001	0 044	0 022	0 045	0.028	0 023	0.044	0 044	0.017	-0 002	0 004
Fe	8.945	9.139	8 956	8.398	9.575	7.917	9.389	9.595	7 842	9.617	8.902	8.499	8.499	7 767	7.064	8.427	10.087	10.347	9.347	8.955	7.887	6.713	5.444	5.568	5 732	7 104	8.266
Mn	0.057	0.063	0.019	0.047	0 207	0 149	0 032	0.103	0 086	0.067	0.070	0.053	0.083	0 093	0.086	0.033	0.099	0 087	0 076	0 069	0.073	0 035	0 090	0 070	0.092	0 052	0 087
Mg	0 126	0 115	0 093	0 166	0 057	0.039	-0 017	0 057	0 028	0 116	0 123	0 126	0 071	0 074	-0 060	-0 046	0 329	0 223	0 121	0 143	-0 003	0 079	-0 071	-0 144	-0 006	-0 022	0 093
Ca	-0 153	-0 230	-0 092	-0 156	-0 110	-0 098	-0 079	-0 134	-0 015	-0 133	-0 148	-0 166	-0 151	-0 067	-0 083	-0 067	-0 207	-0 206	-0 008	-0 090	-0 030	-0 032	0 025	-0 004	-0 042	-0 005	0 105
Na	0 308	0 173	0 083	0 111	0 080	0 153	0 044	0 196	0 158	0 034	-0 001	0 328	0 223	0 133	0 327	0 135	0 287	0 112	0 138	-0 025	0 260	0 033	0 136	0 009	0 246	0 226	0 026
K	0 022	0 037	0 051	0 048	0 046	0 095	0 063	0 026	0 074	0 034	0 049	0 081	0 068	0 066	0 082	0 047	0 001	-0 002	0 024	0 034	0 061	0 074	0 101	0 076	0 015	0 138	0 023
OoidCalc - Berth (Mg normalised)																											
Si	-0 475	-0 436	-0 351	-0 627	-0 215	-0 147	0 063	-0 217	-0 104	-0 437	-0 466	-0 475	-0 269	-0 281	0 226	0 174	-1 245	-0 843	-0 458	-0 539	0 012	-0 300	0 269	0 545	0 023	0 084	-0 351
Al(TOT)	0 361	0 339	0 465	0 502	0 477	0 515	0 600	0 428	0 413	0 420	0 485	0 521	0 405	0 378	0 618	0 687	-0 107	0 010	-0 020	0 530	0 494	0 502	0 804	0 784	0 666	0 799	0 386
Ti	0 008	0 024	0 026	0 025	0 033	0 031	0 004	0 054	0 029	0 048	0 016	0 035	0 030	0 049	0 066	0 001	-0 002	0 043	0 022	0 044	0 028	0 023	0 044	0 045	0 017	-0 001	0 003
Fe	8 388	8 628	8 544	7 664	9 322	7 745	9 463	9 341	7 720	9 105	8 356	7 942	8 183	7 438	7 329	8 631	8 628	9 358	8 810	8 324	7 901	6 362	5 759	6 207	5 759	7 202	7 855
Mn	0 057	0 063	0 019	0 046	0 207	0 149	0 032	0 103	0 086	0 066	0 070	0 053	0 083	0 092	0 086	0 034	0 097	0 086	0 076	0 068	0 073	0 034	0 090	0 071	0 092	0 052	0 086
Mg	0 000	0 000	0 000	0 000	0 000	0 000	0 000	0 000	0 000	0 000	0 000	0 000	0 000	0 000	0 000	0 000	0 000	0 000	0 000	0 000	0 000	0 000	0 000	0 000	0 000	0 000	0 000
Ca	-0 164	-0 239	-0 100	-0 170	-0 115	-0 102	-0 077	-0 139	-0 017	-0 143	-0 159	-0 176	-0 157	-0 074	-0 078	-0 063	-0 234	-0 225	-0 018	-0 102	-0 030	-0 038	0 031	0 009	-0 042	-0 003	0 097
Na	0 294	0 160	0 073	0 093	0 074	0 149	0 046	0 189	0 155	0 021	-0 014	0 314	0 215	0 125	0 334	0 140	0 251	0 088	0 125	-0 040	0 261	0 025	0 144	0 025	0 247	0 228	0 015
K	0 021	0 036	0 050	0 047	0 046	0 094	0 064	0 026	0 074	0 033	0 048	0 080	0 067	0 066	0 082	0 048	-0 002	-0 004	0 023	0 032	0 061	0 073	0 102	0 078	0 015	0 138	0 023

Table D.1. (Continued).

						YAR 24 (OOID 17)							DRAG 31 28 (OOID 21)															
				>nucleus (ooid)							>nucleus(bioclast)		(LINE 1)											(LINE 2)				
	3	4	5	6	7	1	2	3	4	5	6	7	1	2	3	4	5	6	7	8	9	10	1	2	3	4	5
Si	1 199	1 057	1 418	3 166	1 918	1 302	1 428	1 193	1 928	1 751	0.129	0 399	1 212	1 451	1 481	1 288	1 624	1 619	1 617	1 776	2 205	2 327	1 276	1 332	1 571	1 099	1 467
Ti	0 066	0 067	0 058	0 067	0 128	0 132	0 142	0 069	0 107	0 152	0 000	0 014	0 232	0 113	0 146	0 053	0 197	0 197	0 193	0 157	0 165	0 130	0 192	0 205	0 167	0 085	0 192
Al	1 708	1 194	2 142	2 909	2 429	1 533	1 918	1 837	0 211	2 429	0 091	0 515	1 997	2 022	2 103	1 906	2 617	1 860	2 162	2 273	2 541	2 716	1 982	2 006	2 266	1 968	2 535
Fe	29 717	19 347	36 401	29 159	45 329	40 837	33 713	28 917	43 119	30 725	2 365	15 611	36 578	31 088	36 470	26 219	37 763	30 204	35 872	25 843	28 376	35 043	43 646	36 532	35 071	31 472	41 331
Mn	0 231	0 218	0 331	0 165	0 497	0 108	0 111	0 087	0 098	0 171	0 000	0 008	0 198	0 337	0 176	0 235	0 269	0 066	0 295	0 227	0 010	0 134	0 193	0 328	0 424	0 175	0 172
Mg	0 320	0 389	0 444	0 719	0 688	0 516	0 585	0 339	0 671	0 395	0 416	0 281	0 615	0 409	0 427	0 416	0 693	0 492	0 578	0 558	0 574	0 782	0 595	0 505	0 601	0 600	0 672
Ca	0 241	0 164	0 241	0 241	0 395	0 484	0 270	0 201	0 220	0 210	36 368	26 020	0 198	0 273	0 240	0 238	0 201	0 221	0 200	0 095	0 122	0 186	0 173	0 180	0 150	0 248	0 147
Na	0 282	0 000	0 128	0 000	0 434	0 000	0 134	0 159	0 495	0 380	0 372	0 187	0 268	0 269	0 136	0 594	0 606	0 184	0 178	0 173	0 347	0 361	0 390	0 000	0 035	0 390	0 353
K	0 068	0 165	0 111	0 279	0 162	0 000	0 061	0 126	0 115	0 221	0 000	0 000	0 017	0 115	0 109	0 081	0 130	0 165	0 190	0 208	0 215	0 201	0 083	0 143	0 135	0 116	0 094
P	0 226	0 088	0 279	0 183	0 470	0 295	0 229	0 243	0 331	0 159	0 069	0 142	0 178	0 309	0 428	0 227	0 313	0 389	0 308	0 285	0 350	0 255	0 440	0 337	0 263	0 463	0 458
S	0 027	0 034	0 000	0 061	0 136	0 019	0 013	0 056	0 016	0 000	0 107	0 075	0 013	0 118	0 105	0 137	0 037	0 118	0 049	0 101	0 081	0 057	0 000	0 033	0 119	0 098	0 041
O	12 220	8 386	14 900	15 503	18 964	15 580	13 966	12 047	17 679	13 836	15 916	16 217	14 659	13 425	15 153	11 663	16 384	13 315	15 216	12 495	14 059	16 316	17 086	14 868	14 922	13 378	17 180
TOTAL	46 305	31 109	56 453	52 452	71 550	60 806	52 570	45 274	64 990	50 429	55 833	59 469	56 165	49 930	56 974	43 057	60 834	48 830	56 858	44 191	49 045	58 508	66 056	56 469	55 724	50 092	64 642
BerthCalc																											
Si	0 815	1 030	0 791	1.673	0 854	0 695	0 845	0 827	1 007	1.035	0 065	0 200	0.677	0 909	0 831	0.922	0.825	1 037	0 887	1 195	1 324	1 178	0 631	0 752	0 875	0 709	0 723
Al(TOT)	1 209	1 210	1 243	1.600	1 125	0 852	1.182	1 325	0 115	1 494	0 048	0.269	1 161	1 318	1 229	1 420	1 383	1 240	1 234	1 591	1 588	1 431	1 019	1 178	1 313	1 322	1 300
Ti	0 026	0 038	0 019	0.021	0.033	0.041	0.049	0 028	0.033	0 053	0 000	0 004	0 076	0 041	0 048	0 022	0 059	0 074	0 062	0 062	0 058	0 039	0 056	0 068	0 054	0 032	0 055
Fe	10 155	9 462	10 210	7.734	10.120	10 959	10.035	10 060	11 319	9.133	0.579	3 924	10.276	9.762	10 271	9.397	9 638	9 699	9 883	8 712	8 546	8 909	10 847	10.358	9 789	10 188	10 234
Mn	0 080	0 109	0.094	0 045	0 113	0 029	0 034	0 031	0 026	0 052	0 000	0.002	0.057	0 108	0 051	0.086	0 070	0 022	0 083	0 078	0 003	0 035	0 049	0 095	0 121	0 058	0 043
Mg	0 251	0 438	0 286	0 439	0 354	0 318	0 400	0 271	0 405	0 270	0 244	0 163	0 397	0 296	0 277	0 344	0 407	0 364	0 366	0 434	0 398	0 457	0 340	0 329	0 387	0 447	0 383
Ca	-0 117	-0 018	-0 141	-0 057	-0 193	-0 057	-0 093	-0 157	-0 181	-0 055	12 860	9 042	-0 073	-0 173	-0 269	-0 126	-0 169	-0 277	-0 178	-0 245	-0 266	-0 129	-0 269	-0 216	-0 163	-0 339	-0 290
Na	0 234	0 000	0 087	0 000	0 236	0 000	0 097	0 135	0 316	0 274	0 230	0 115	0 183	0 206	0 093	0 519	0 376	0 144	0 119	0 142	0 254	0 223	0 235	0 000	0 024	0 307	0 212
K	0 033	0 115	0 044	0 106	0 052	0 000	0 026	0 063	0 043	0 094	0 000	0 000	0 007	0 052	0 044	0 042	0 047	0 076	0 075	0 101	0 093	0 073	0 029	0 058	0 054	0 054	0 033
OH	8 000	8 000	8 000	8 000	8 000	8 000	8 000	8 000	8 000	8 000	8 000	8 000	8 000	8 000	8 000	8 000	8 000	8 000	8 000	8 000	8 000	8 000	8 000	8 000	8 000	8 000	8 000
OoidCalc - Berth (Si normalised)																											
Si	0 000	0 000	0 000	0 000	0 000	0 000	0 000	0 000	0 000	0 000	0.000	0 000	0 000	0 000	0 000	0 000	0 000	0 000	0 000	0 000	0 000	0.000	0 000	0 000	0 000	0 000	0 000
Al(TOT)	0 787	0 678	0 835	0 735	0 684	0 492	0 745	0 897	-0 406	0 959	0 014	0 165	0 811	0 848	0 799	0 944	0 957	0 704	0 776	0 974	0 903	0 822	0 693	0 789	0 861	0 955	0 926
Ti	0 025	0 037	0 018	0 019	0 032	0 040	0 048	0 027	0 032	0 051	0 000	0 004	0 075	0 040	0 047	0 021	0 058	0 073	0 061	0 060	0 056	0 037	0 055	0 067	0 053	0 031	0 055
Fe	9 200	8 256	9 283	5 773	9 120	10 144	9 044	9 091	10 140	7 920	0 502	3 689	9 482	8 696	9 296	8 316	8 671	8 483	8 844	7 312	6 995	7 529	10 108	9 477	8 764	9 356	9 387
Mn	0 079	0 107	0 093	0 042	0 112	0 028	0 032	0 030	0 025	0 050	0 000	0 002	0 056	0 107	0 049	0 085	0 069	0 020	0 081	0 076	0 001	0 033	0 048	0 093	0 119	0 057	0 042
Mg	0 036	0 165	0 077	-0 004	0 128	0 134	0 176	0 053	0 138	-0 004	0 226	0 110	0 218	0 055	0 057	0 100	0 188	0 090	0 132	0 117	0 048	0 146	0 173	0 130	0 155	0 260	0 191
Ca	-0 135	-0 040	-0 158	-0 094	-0 212	-0 072	-0 112	-0 175	-0 203	-0 078	12 858	9 037	-0 088	-0 193	-0 287	-0 147	-0 187	-0 300	-0 198	-0 271	-0 296	-0 155	-0 283	-0 233	-0 182	-0 355	-0 306
Na	0 211	-0 030	0 064	-0 048	0 211	-0 020	0 072	0 111	0 287	0 244	0 228	0 109	0 163	0 180	0 069	0 493	0 352	0 114	0 094	0 108	0 216	0 189	0 217	-0 022	-0 001	0 287	0 192
K	0 031	0 113	0 042	0 101	0 049	-0 002	0 024	0 060	0 040	0 091	0 000	-0 001	0 005	0 049	0 042	0 039	0 045	0 073	0 072	0 097	0 089	0 070	0 028	0 056	0 052	0 052	0 031
OoidCalc - Berth (Mg normalised)																											
Si	-0 135	-0 625	-0 290	0 014	-0 483	-0.507	-0 667	-0 199	-0.523	0.016	-0 855	-0.415	-0 823	-0 210	-0 215	-0 378	-0.712	-0 339	-0 497	-0 444	-0 181	-0 550	-0 653	-0 492	-0 586	-0 981	-0 723
Al(TOT)	0 718	0 355	0 685	0 742	0.434	0.230	0 400	0.795	-0.676	0 967	-0 428	-0 049	0.386	0 740	0 688	0 748	0 589	0.529	0 519	0 744	0 810	0.538	0.356	0 535	0 558	0 448	0 553
Ti	0 025	0 036	0 018	0 019	0 032	0.040	0 047	0 027	0 031	0 051	-0 001	0.003	0.074	0 040	0 047	0 021	0 057	0.072	0.060	0 060	0 056	0 036	0 054	0 066	0 053	0 030	0 054
Fe	9 042	7 524	8 943	5 790	8.553	9 550	8 263	8.858	9 527	7.939	-0.500	3.202	8.518	8 451	9 044	7 873	7.837	8.086	8.261	6 792	6.783	6 884	9 342	8 900	8 078	8 206	8 540
Mn	0 079	0 106	0 093	0 042	0 111	0.028	0 031	0.029	0 024	0 050	-0 001	0.001	0 054	0.106	0 049	0 084	0 068	0 020	0 081	0 076	0 001	0 032	0 047	0 093	0 118	0 055	0 041
Mg	0 000	0 000	0 000	0 000	0 000	0 000	0.000	0 000	0 000	0 000	0 000	0.000	0.000	0.000	0 000	0 000	0 000	0.000	0 000	0 000	0 000	0 000	0.000	0.000	0 000	0 000	0 000
Ca	-0 138	-0 054	-0 165	-0.094	-0 223	-0 084	-0.126	-0.180	-0.215	-0.078	12 839	9.028	-0 106	-0 197	-0 292	-0 155	-0 203	-0.308	-0 209	-0 281	-0 300	-0 167	-0 297	-0 244	-0 195	-0 377	-0 322
Na	0 207	-0.048	0 056	-0 048	0.197	-0.035	0.053	0.105	0 271	0 245	0.204	0 097	0.140	0.174	0.063	0.482	0.332	0.104	0 079	0 095	0 211	0 173	0 198	-0.036	-0.018	0 259	0 171
K	0 031	0 111	0 042	0 101	0 048	-0.003	0 022	0 060	0 039	0 091	-0 003	-0 002	0 003	0 049	0 041	0 038	0 043	0 072	0 071	0 096	0 089	0 068	0.026	0 055	0 050	0 049	0 029

Table D.1. (Continued).

						(LINE 3)										(LINE 4)										DRAG 31 28 (OO (LINE 1)	
	6	7	8	9	10	1	2	3	4	5	6	7	8	9	10	1	2	3	4	5	6	7	8	9	10	1	2
Si	1 588	1 862	2.012	2 659	1 831	0 881	1 296	1 309	3.620	1 233	1 802	1 521	1 991	2 235	1 571	1 184	1 097	1 291	1 187	1 478	1 561	1 694	2 396	1 896	1 950	1 360	1 470
Ti	0 271	0 142	0 098	0 145	0 136	0 148	0 177	0 141	0 286	0 214	0 222	0 126	0 184	0 153	0 209	0 192	0 250	0 198	0 139	0 170	0 233	0 130	0 188	0 108	0 172	0 099	0 115
Al	2 222	2 304	2.163	2 487	2.287	1 821	2 264	2 104	2.171	2.284	2.317	2.275	2.418	2 599	2 327	1.988	1 896	2 036	1 891	2 314	2.336	2 243	2 737	2 458	2 536	1 716	1.735
Fe	37 034	31 640	24 587	25 967	31.370	36 002	39 866	33 570	32.758	40.721	36 236	33.760	30.760	31.699	36.379	32.378	39 643	35 696	37 512	36.008	39 121	34 776	30.715	34 413	33 715	34 974	27 924
Mn	0 016	0.206	0 003	0.042	0.006	0 202	0.096	0.063	0.181	0.066	0.114	0.198	0 131	0.084	0 177	0.249	0.048	0.264	0.050	0 274	0 290	0 266	0 027	0 180	0 254	0 179	0 094
Mg	0 540	0 623	0.468	0 614	0.508	0 458	0.482	0.515	0.483	0 575	0.580	0.544	0.666	0 692	0.506	0 483	0.534	0.531	0 433	0 461	0 523	0 618	0 627	0 607	0 482	0 677	0 632
Ca	0 155	0 167	0.128	0 268	0.152	0 189	0 182	0 612	0.561	0.200	0.188	0 135	0.162	0.181	0.198	0.395	0.304	0 222	0.326	0 166	0 137	0 150	0 175	0 235	0 097	0 188	0 250
Na	0.349	0.202	0.346	0.169	0 132	0 326	0.000	0.277	0.091	0 049	0.059	0 271	0.295	0.457	0.430	0 196	0.265	0.313	0.382	0.323	0 087	0 194	0 202	0 378	0.200	0 248	0 293
K	0 161	0 095	0 207	0 251	0.175	0.000	0.119	0 149	0.054	0.019	0.163	0.154	0.224	0 263	0.090	0 032	0.038	0.059	0 057	0 174	0 207	0.235	0 232	0 195	0.199	0 000	0 077
P	0.308	0.399	0.386	0.204	0.210	0.302	0 295	0.609	0.333	0.432	0.426	0.252	0 274	0.238	0 247	0.252	0 295	0.307	0.579	0.273	0 442	0 460	0.405	0 280	0 227	0 255	0 198
S	0 000	0 000	0.041	0 097	0 000	0.035	0.015	0 132	0.083	0.011	0 094	0.116	0 100	0.067	0.040	0 073	0 016	0.080	0 016	0 057	0 010	0 106	0 046	0 052	0 048	0 088	0 755
O	15 550	14 473	12 347	13.675	13 948	13 975	15 853	14 590	16 698	16.302	15 738	14 433	14 397	15 113	15.371	13 469	15 429	14 672	15 196	15 121	16 346	15 229	15 221	15 357	15 084	14 149	12 212
TOTAL	58 194	52.113	42 786	46.578	50.755	54 339	60.645	54.071	57.319	62.106	57.939	53.785	51.602	53 781	57 545	50 891	59 815	55 669	57 768	56.819	61.293	56 101	52 971	56 159	54 964	53 933	45 755
BerthCalc																											
Si	0.851	1 091	1.395	1 605	1 082	0 528	0 679	0.788	1.809	0 640	0 971	0.875	1 152	1.222	0 845	0.731	0.592	0.736	0 679	0.812	0 809	0 951	1 333	1.026	1 066	0 799	1 011
Al(TOT)	1 239	1 405	1 560	1 563	1 407	1.135	1.235	1 318	1.129	1.234	1.300	1 362	1.456	1 479	1 302	1 278	1 064	1.208	1 125	1 323	1 260	1 310	1 585	1 384	1 443	1 049	1 242
Ti	0 085	0 049	0 040	0.051	0.047	0 052	0 054	0.050	0.084	0.065	0.070	0 042	0 062	0.049	0.066	0 070	0.079	0.066	0.047	0 055	0 071	0 043	0.061	0 034	0 055	0 034	0 046
Fe	9 977	9 322	8.559	7 858	9 323	10.834	10.506	10.131	8 214	10 625	9.800	9 739	8.926	8 701	9 829	10 040	10.748	10.212	10 785	9 933	10.192	9.788	8.581	9 351	9 261	10.308	9 431
Mn	0 004	0.062	0 001	0 013	0 002	0.062	0.026	0 019	0.046	0 018	0.031	0 058	0 039	0 023	0 049	0 079	0 013	0 077	0 015	0.077	0 077	0 076	0 008	0 050	0 071	0 054	0 033
Mg	0.334	0 422	0 375	0 428	0 347	0 317	0.292	0 358	0.279	0.345	0.361	0 362	0.445	0.437	0 314	0.345	0.333	0.350	0 286	0.293	0.313	0 401	0.403	0 379	0 305	0 459	0 502
Ca	-0.191	-0 285	-0 342	-0 073	-0 125	-0 194	-0 167	-0 296	-0 055	-0 266	-0 276	-0 165	-0.174	-0 127	-0 126	-0.064	-0 126	-0.176	-0 370	-0.163	-0 296	-0 331	-0 272	-0 140	-0 150	-0 149	-0.085
Na	0 228	0.145	0 293	0 125	0 095	0 238	0.000	0.204	0 056	0 031	0 039	0 190	0.208	0 305	0 282	0 148	0 175	0 218	0 267	0 217	0 055	0 133	0 137	0 250	0 134	0 178	0 246
K	0 062	0 040	0 103	0 109	0 074	0 000	0 045	0 064	0 019	0 007	0 063	0 064	0 093	0 103	0 035	0 014	0 015	0 024	0 023	0 069	0 077	0 095	0 093	0 076	0 078	0 000	0 038
OH	8 000	8 000	8 000	8 000	8 000	8 000	8 000	8 000	8 000	8 000	8 000	8 000	8 000	8 000	8 000	8 000	8 000	8 000	8 000	8 000	8 000	8 000	8 000	8 000	8 000	8 000	8 000
OoidCalc - Berth (Si normalised)																											
Si	0 000	0 000	0.000	0.000	0.000	0 000	0 000	0.000	0.000	0 000	0.000	0 000	0 000	0.000	0.000	0 000	0.000	0 000	0.000	0 000	0 000	0 000	0 000	0 000	0 000	0 000	0 000
Al(TOT)	0 799	0 841	0.840	0.733	0.847	0.862	0.884	0.911	0.194	0.903	0 798	0 910	0.861	0.847	0 866	0 900	0.758	0 827	0 775	0 903	0.842	0 819	0.896	0 854	0 892	0 636	0 719
Ti	0 084	0 047	0 038	0.049	0 046	0 051	0.054	0 049	0 082	0.064	0.069	0.041	0.061	0.048	0.065	0.069	0 078	0.065	0 046	0 054	0 070	0.042	0 060	0 033	0 054	0.033	0 045
Fe	8.980	8.044	6 924	5.977	8 055	10.216	9.710	9.207	6 094	9.875	8.662	8.714	7.576	7.269	8.839	9.183	10.054	9.350	9.989	8 982	9.244	8.674	7 019	8 149	8.011	9.372	8 246
Mn	0 003	0 060	-0 001	0 011	0.000	0.061	0.025	0 018	0 043	0 017	0.030	0 057	0 037	0.022	0 047	0.078	0 012	0.076	0.014	0 076	0.076	0 075	0.006	0 048	0.069	0 053	0 032
Mg	0 109	0 133	0 006	0.003	0.060	0 177	0.112	0 150	-0.200	0.175	0.104	0 130	0.140	0 114	0.091	0 151	0.176	0.155	0 106	0 078	0 099	0.149	0 050	0 108	0 022	0 248	0 235
Ca	-0 210	-0 309	-0 373	-0 108	-0 149	-0 206	-0 182	-0.313	-0.095	-0 280	-0.297	-0 184	-0 199	-0.154	-0 145	-0.080	-0 139	-0 192	-0 385	-0 181	-0.314	-0.352	-0 302	-0 163	-0 174	-0 167	-0 108
Na	0 204	0 113	0 253	0 078	0.064	0 223	-0 020	0 181	0 003	0 013	0 011	0 165	0.175	0.270	0 258	0.127	0 157	0 197	0.247	0 193	0 032	0 106	0 099	0 220	0 103	0 155	0 217
K	0 060	0 037	0 099	0 104	0.071	-0.001	0 043	0 062	0.014	0 005	0 060	0 061	0 090	0.100	0 032	0 012	0 013	0 022	0 022	0.066	0 075	0 092	0 089	0 073	0 075	-0.002	0 035
OoidCalc - Berth (Mg normalised)																											
Si	-0 412	-0 503	-0 022	-0 013	-0.229	-0 670	-0 424	-0 566	0 755	-0 663	-0.393	-0 491	-0 530	-0 430	-0 343	-0 571	-0 666	-0.585	-0 402	-0 294	-0 374	-0 563	-0 190	-0 408	-0 084	-0 937	-0 887
Al(TOT)	0 586	0 581	0 828	0.726	0.729	0 516	0.665	0.619	0 584	0 560	0.594	0 656	0.587	0.625	0.688	0 605	0.414	0.525	0.567	0 751	0 648	0 527	0.798	0 643	0 849	0 152	0 261
Ti	0 084	0 047	0 038	0 049	0 046	0 051	0.053	0 048	0 082	0 064	0 068	0 041	0 060	0 047	0 064	0 068	0.078	0 065	0 045	0 053	0 069	0 041	0 059	0 033	0 054	0.032	0 044
Fe	8 497	7 455	6 899	5.961	7.787	9 431	9.214	8 544	6.979	9 098	8.201	8 138	6.954	6.765	8 437	8.514	9.274	8.664	9.518	8.638	8.805	8.014	6 797	7 671	7 912	8.273	7 207
Mn	0.002	0 059	-0 001	0.011	0.000	0 060	0 024	0.017	0 045	0 016	0.029	0.056	0 036	0 021	0 047	0 077	0.011	0 075	0.013	0 075	0.075	0 074	0 005	0 048	0 069	0.051	0 030
Mg	0 000	0 000	0 000	0 000	0 000	0 000	0 000	0.000	0.000	0 000	0.000	0.000	0.000	0.000	0.000	0.000	0.000	0.000	0 000	0.000	0.000	0.000	0 000	0.000	0 000	0 000	0 000
Ca	-0.219	-0 320	-0.374	-0.109	-0 154	-0 221	-0 191	-0.326	-0 078	-0.295	-0 306	-0.195	-0 211	-0.164	-0 152	-0.093	-0.153	-0.205	-0.394	-0.187	-0.323	-0 365	-0.306	-0 172	-0.176	-0 187	-0 127
Na	0.192	0.099	0.252	0 078	0.057	0.204	-0.032	0 165	0.025	-0 007	-0 001	0 151	0 160	0.257	0 248	0.110	0 138	0.180	0.236	0 185	0.021	0 089	0 093	0 208	0.100	0 128	0 191
K	0 059	0 036	0 099	0.104	0 071	-0 003	0 042	0 061	0.017	0 004	0.059	0 060	0 089	0 099	0.032	0.011	0.011	0.021	0.020	0 066	0 074	0 091	0 089	0 072	0 075	-0 005	0 033

Table D.1. (Continued).

D 22)									(LINE 2)										(LINE 3)								(LINE 4)
	3	4	5	6	7	8	9	10	1	2	3	4	5	6	7	8	9	10	1	2	3	4	5	6	7	8	1
Si	1 288	1 374	1 694	1 503	1 599	1 758	1 804	1 733	1 446	1 226	1 404	1 499	1 627	1 880	1 815	2 390	1 642	1 542	5 676	1 212	1 106	1 151	1 250	1 465	1 536	1 925	1 293
Ti	0 152	0 140	0 061	0 144	0 121	0 134	0 201	0 142	0 063	0 242	0 105	0 158	0 106	0 140	0 159	0 095	0 124	0 198	0 002	0 093	0 118	0 195	0 125	0 146	0 199	0 241	0 092
Al	1 922	2 087	2 167	2 110	2 276	2 346	2 496	2 568	1 771	1 972	2 072	2 289	2 215	2 400	2 318	2 917	2 437	2 417	3 503	1 530	1 721	1 996	2 046	2 350	2 373	2 369	1 796
Fe	37 081	29 305	33 124	31 097	35 382	38 485	39 412	42 349	31 911	35 007	33 036	34 371	34 351	35 170	40 491	39 020	40 955	40 490	28 512	28 790	36 896	34 986	40 103	34 148	36 869	39 840	35 540
Mn	0 159	0 117	0 166	0 183	0 350	0 103	0 172	0 095	0 216	0 030	0 132	0 144	0 142	0 209	0 248	0 000	0 283	0 113	0 000	0 229	0 099	0 165	0 083	0 116	0 278	0 097	0 233
Mg	0 454	0 418	0 404	0 496	0 583	0 465	0 551	0 508	0 580	0 412	0 377	0 566	0 459	0 483	0 532	0 610	0 516	0 590	1 515	0 342	0 668	0 505	0 463	0 597	0 552	0 541	0 600
Ca	0 221	0 155	0 138	0 219	0 150	0 156	0 203	0 189	0 135	0 220	0 122	0 122	0 079	0 170	0 227	0 122	0 177	0 209	0 283	4 094	0 102	0 152	0 158	0 137	0 162	0 162	0 210
Na	0 324	0 330	0 257	0 066	0 122	0 216	0 109	0 391	0 229	0 242	0 007	0 076	0 036	0 204	0 000	0 376	0 000	0 436	0 444	0 342	0 780	0 488	0 823	0 391	0 328	0 102	0 207
K	0 093	0 172	0 123	0 180	0 115	0 101	0 201	0 116	0 135	0 093	0 097	0 098	0 142	0 160	0 146	0 265	0 182	0 108	0 095	0 052	0 021	0 089	0 052	0 149	0 130	0 213	0 042
P	0 355	0 170	0 338	0 292	0 207	0 337	0 363	0 347	0 289	0 333	0 324	0 251	0 315	0 266	0 379	0 307	0 272	0 249	0 175	2 119	0 200	0 327	0 379	0 318	0 351	0 375	0 206
S	0 115	0 026	0 105	0 102	0 031	0 071	0 106	0 067	0 095	0 044	0 060	0 064	0 090	0 038	0 016	0 098	0 071	0 031	0 052	0 074	0 000	0 074	0 115	0 094	0 122	0 073	0 103
O	14 924	12 651	14 308	13 498	14 941	16 133	16 741	17 531	13 387	14 242	13 752	14 529	14 559	15 340	16 868	17 591	16 735	16 639	19 262	15 845	14 483	14 292	15 994	14 698	15 659	16 887	14 208
TOTAL	57 088	46 945	52 885	49 890	55 877	60 305	62 359	66 036	50 257	54 063	51 488	54 167	54 121	56 460	63 199	63 791	63 394	63 022	59 519	54 722	56 194	54 420	61 591	54 609	58 559	62 825	54 530
BerthCalc																											
Si	0 727	0 892	0 997	0 933	0 880	0 911	0 903	0 824	0 905	0 723	0 859	0 856	0 936	1 016	0 902	1 127	0 812	0 764	2 399	0 858	0 628	0 677	0 658	0 835	0 824	0 956	0 751
Al(TOT)	1 129	1 411	1 327	1 364	1 304	1 265	1 300	1 271	1 154	1 211	1 319	1 360	1 327	1 350	1 199	1 432	1 254	1 246	1 541	1 127	1 017	1 221	1 121	1 394	1 324	1 224	1 085
Ti	0 050	0 053	0 021	0 052	0 039	0 041	0 059	0 040	0 023	0 084	0 038	0 053	0 036	0 044	0 046	0 026	0 036	0 058	0 000	0 039	0 039	0 067	0 039	0 049	0 063	0 070	0 031
Fe	10 495	9 565	9 775	9 683	9 787	10 013	9 897	10 116	10 020	10 378	10 145	9 850	9 919	9 550	10 116	9 237	10 167	10 083	6 050	10 228	10 531	10 323	10 590	9 766	9 914	9 933	10 350
Mn	0 046	0 039	0 050	0 058	0 098	0 027	0 044	0 023	0 069	0 009	0 041	0 042	0 042	0 058	0 063	0 000	0 072	0 029	0 000	0 083	0 029	0 050	0 022	0 034	0 076	0 025	0 069
Mg	0 296	0 314	0 275	0 356	0 371	0 278	0 319	0 279	0 420	0 281	0 266	0 373	0 305	0 302	0 305	0 332	0 295	0 338	0 740	0 280	0 438	0 343	0 282	0 393	0 342	0 310	0 402
Ca	-0 215	-0 096	-0 244	-0 179	-0 114	-0 207	-0 203	-0 186	-0 214	-0 206	-0 247	-0 168	-0 242	-0 153	-0 206	-0 179	-0 142	-0 114	-0 028	-0 236	-0 131	-0 228	-0 243	-0 219	-0 224	-0 225	-0 095
Na	0 223	0 262	0 185	0 050	0 082	0 137	0 067	0 227	0 175	0 174	0 005	0 053	0 025	0 135	0 000	0 217	0 000	0 264	0 229	0 296	0 541	0 350	0 529	0 272	0 215	0 062	0 147
K	0 038	0 080	0 052	0 080	0 045	0 038	0 072	0 040	0 061	0 039	0 043	0 040	0 059	0 062	0 052	0 090	0 065	0 038	0 029	0 026	0 009	0 038	0 020	0 061	0 050	0 076	0 018
OH	8 000	8 000	8 000	8 000	8 000	8 000	8 000	8 000	8 000	8 000	8 000	8 000	8 000	8 000	8 000	8 000	8 000	8 000	8 000	8 000	8 000	8 000	8 000	8 000	8 000	8 000	8 000
OoidCalc - Berth (Si normalised)																											
Si	0 000	0 000	0 000	0 000	0 000	0 000	0 000	0 000	0 000	0 000	0 000	0 000	0 000	0 000	0 000	0 000	0 000	0 000	0 000	0 000	0 000	0 000	0 000	0 000	0 000	0 000	0 000
Al(TOT)	0 753	0 949	0 812	0 881	0 849	0 794	0 833	0 845	0 686	0 837	0 875	0 917	0 843	0 825	0 733	0 849	0 834	0 852	0 301	0 684	0 692	0 871	0 781	0 963	0 899	0 730	0 697
Ti	0 049	0 052	0 020	0 051	0 038	0 040	0 058	0 039	0 022	0 083	0 037	0 052	0 035	0 043	0 045	0 025	0 035	0 057	-0 002	0 038	0 038	0 066	0 038	0 048	0 062	0 069	0 030
Fe	9 644	8 519	8 606	8 589	8 756	8 946	8 839	9 150	8 959	9 530	9 138	8 847	8 822	8 359	9 059	7 916	9 216	9 188	3 239	9 222	9 795	9 530	9 819	8 788	8 949	8 813	9 470
Mn	0 045	0 037	0 048	0 057	0 097	0 026	0 043	0 022	0 068	0 008	0 040	0 041	0 040	0 056	0 062	-0 002	0 070	0 027	-0 004	0 082	0 028	0 049	0 021	0 033	0 075	0 023	0 068
Mg	0 104	0 077	0 011	0 109	0 138	0 037	0 080	0 061	0 180	0 089	0 039	0 147	0 057	0 033	0 067	0 034	0 080	0 136	0 105	0 053	0 272	0 164	0 107	0 172	0 124	0 057	0 204
Ca	-0 231	-0 116	-0 266	-0 199	-0 134	-0 227	-0 223	-0 205	-0 234	-0 222	-0 266	-0 187	-0 263	-0 175	-0 226	-0 204	-0 160	-0 131	-0 081	-0 255	-0 145	-0 243	-0 258	-0 238	-0 242	-0 246	-0 112
Na	0 202	0 236	0 156	0 023	0 057	0 110	0 041	0 203	0 149	0 154	-0 020	0 028	-0 002	0 105	-0 026	0 184	-0 023	0 242	0 160	0 271	0 522	0 331	0 510	0 248	0 191	0 034	0 125
K	0 036	0 078	0 049	0 078	0 043	0 035	0 070	0 037	0 058	0 037	0 040	0 038	0 056	0 059	0 050	0 087	0 062	0 036	0 022	0 024	0 007	0 036	0 018	0 059	0 048	0 073	0 015
OoidCalc - Berth (Mg normalised)																											
Si	-0 392	-0 293	-0 041	-0 411	-0 521	-0 141	-0 301	-0 231	-0 680	-0 338	-0 148	-0 555	-0 217	-0 124	-0 252	-0 129	-0 302	-0 512	-0 396	-0 199	-1 027	-0 619	-0 406	-0 651	-0 469	-0 217	-0 770
Al(TOT)	0 551	0 798	0 791	0 669	0 580	0 721	0 678	0 726	0 335	0 663	0 799	0 631	0 731	0 761	0 602	0 783	0 678	0 587	0 096	0 581	0 161	0 551	0 571	0 626	0 656	0 618	0 299
Ti	0 049	0 052	0 020	0 051	0 037	0 039	0 058	0 038	0 021	0 082	0 036	0 051	0 034	0 043	0 045	0 025	0 035	0 056	-0 003	0 037	0 037	0 066	0 037	0 047	0 061	0 069	0 029
Fe	9 185	8 176	8 558	8 107	8 145	8 780	8 486	8 880	8 163	9 134	8 965	8 197	8 568	8 214	8 763	7 765	8 862	8 588	2 774	8 989	8 591	8 804	9 343	8 025	8 400	8 558	8 568
Mn	0 044	0 037	0 048	0 056	0 096	0 026	0 042	0 021	0 067	0 007	0 040	0 040	0 040	0 056	0 061	-0 002	0 070	0 027	-0 004	0 081	0 026	0 048	0 021	0 032	0 074	0 023	0 067
Mg	0 000	0 000	0 000	0 000	0 000	0 000	0 000	0 000	0 000	0 000	0 000	0 000	0 000	0 000	0 000	0 000	0 000	0 000	0 000	0 000	0 000	0 000	0 000	0 000	0 000	0 000	0 000
Ca	-0 240	-0 123	-0 267	-0 209	-0 145	-0 231	-0 230	-0 210	-0 249	-0 230	-0 269	-0 199	-0 268	-0 178	-0 231	-0 206	-0 167	-0 142	-0 090	-0 260	-0 168	-0 257	-0 267	-0 252	-0 252	-0 251	-0 129
Na	0 191	0 228	0 155	0 011	0 042	0 106	0 032	0 197	0 129	0 144	-0 024	0 012	-0 008	0 102	-0 033	0 180	-0 032	0 227	0 148	0 265	0 493	0 313	0 498	0 229	0 177	0 028	0 103
K	0 035	0 077	0 049	0 077	0 042	0 035	0 069	0 037	0 056	0 037	0 040	0 036	0 056	0 059	0 049	0 086	0 062	0 035	0 021	0 024	0 004	0 034	0 017	0 057	0 047	0 073	0 013

Table D.1. (Continued).

								Y183.10 (OOID 23) Single Line										Y183.10 (OOID 24) Single Line									
	2	3	4	5	6	7	8	1	2	3	4	5	6	7	8	9	10	1	2	3	4	5	6	7	8	9	10
Si	1 153	1.677	1 200	1 344	1 579	1 616	1 118	3 047	2 591	1 774	3.902	4 659	7 483	7 437	8 297	4 534	7 085	4 645	2 863	2 787	4 839	4.092	6 065	4 624	3 503	4 643	5 488
Ti	0 074	0 144	0 158	0 143	0 141	0 146	0 137	0 103	0 218	0.225	0.212	0 225	0 000	0 082	0 003	0.084	0 107	0 179	0 324	0 144	0 091	0.120	0 042	0.065	0 032	0 113	0 000
Al	1 890	1 986	1 911	2 030	2 284	2 430	2 245	2 153	1 937	1 651	2.751	2 999	4.013	4 203	4 423	2.817	3 852	3.043	2.311	2.258	2.774	2 540	3 462	3.035	2 203	3 023	3 168
Fe	37 644	33 859	38 688	34 909	38 621	41 918	45 697	25 511	30 091	34.042	24.642	24.838	18 987	19.444	18 509	19.210	20.722	25 601	31.840	28 153	17.542	18.579	18.244	19 003	17 979	16 843	16 092
Mn	0 198	0 173	0 201	0 000	0 231	0 000	0 199	0 172	0 160	0 117	0.127	0 102	0.046	0.055	0 000	0 177	0 049	0 136	0 135	0 235	0 163	0 069	0.042	0 088	0 017	0 000	0 004
Mg	0 610	0 302	0 602	0 472	0 540	0 677	0 453	0.716	0 483	0 635	0.715	0.949	1 531	1 599	1 443	1.197	1.444	0 896	0.753	0.793	0.969	1.123	1.333	1 090	0 812	1 189	1 222
Ca	0 084	0 315	0 172	0 343	0 155	0 145	0 178	0 273	0 219	0 179	0 155	0 192	0 173	0 152	0 151	0 075	0 114	0 333	0 268	0 119	0 158	0 164	0 103	0 187	0 207	0 188	0 229
Na	0 421	0 031	0 021	0 270	0 169	0 384	0 190	0 195	0 214	0 221	0 179	0 142	0 141	0 317	0 065	0 117	0 162	0 192	0 000	0 362	0 025	0 181	0 148	0 082	0 064	0 304	0 154
K	0 044	0 181	0 010	0 037	0 089	0 133	0 006	0 249	0 254	0 056	0 293	0 247	0 275	0 341	0 387	0 140	0 115	0 296	0 110	0 157	0 170	0 067	0 200	0 173	0 049	0 152	0 138
P	0 284	0 299	0 361	0 690	0 358	0 303	0 616	0 132	0 194	0 241	0 064	0 159	0 010	0 104	0 043	0 016	0 036	0 129	0 262	0 091	0 029	0 099	0 015	0 106	0 149	0 161	0 079
S	0 059	0 058	0 058	0 075	0 108	0 051	0 116	0 057	0 018	0 064	0 028	0 030	0 004	0 026	0 058	0 000	0 041	0 077	0 072	0 043	0 063	0 076	0 037	0 117	0 102	0 072	0 039
O	14.844	14.283	15 255	14.872	16 013	17 164	17.743	13 683	14 269	14.316	14 868	16.278	18.742	19 279	19 858	14 189	18 643	16 509	15 659	14 258	13 895	13 354	16 286	14 473	11 969	14 080	14 761
TOTAL	57 305	53 308	58.637	55 185	60.288	64.967	68 698	46 291	50.648	53 521	47.936	50 820	51 405	53.039	53.237	42 556	52 370	52 036	54 597	49 400	40 718	40.464	45 977	43.043	37 086	40 768	41.374
BerthCalc.																											
Si	0 647	0.982	0.662	0.802	0 828	0 781	0.544	1.816	1.492	1.027	2.114	2.333	3.188	3 114	3.350	2.554	3.045	2.285	1.515	1 582	2.793	2.487	2 978	2.594	2 404	2 700	3.002
Al(TOT)	1 103	1.210	1 097	1 260	1.246	1.222	1.137	1 335	1.161	0.994	1 551	1.563	1.779	1.831	1 859	1 652	1 723	1 558	1 272	1 334	1 666	1 607	1 769	1.772	1.573	1 829	1.803
Ti	0.024	0 049	0 051	0.050	0.043	0 041	0.039	0 036	0.074	0.076	0.067	0.066	0 000	0.020	0.001	0.028	0 027	0.052	0 100	0 048	0 031	0 043	0.012	0 021	0.013	0 039	0 000
Fe	10.605	9 953	10.715	10 453	10.156	10 179	11 159	7.630	8.711	9 892	6.706	6 248	4 067	4 089	3.748	5.443	4 472	6 317	8.454	8 025	5 076	5 659	4 497	5 333	6 174	4 907	4 417
Mn	0 057	0.052	0.057	0 000	0.062	0 000	0 050	0.052	0.047	0 035	0.035	0.026	0 010	0.012	0 000	0 051	0 011	0 034	0.037	0 068	0 048	0.021	0.011	0.025	0 006	0 000	0 001
Mg	0.395	0.204	0.384	0.325	0.327	0.378	0 255	0.493	0.321	0 425	0.447	0 549	0.754	0.773	0 673	0 779	0 717	0 509	0.460	0 520	0 646	0 789	0 756	0 707	0 644	0 799	0 772
Ca	-0 208	-0.135	-0 234	-0 479	-0 227	-0 172	-0 392	-0 005	-0 080	-0.138	0.006	-0.053	0 045	-0.021	0 016	0 016	0 011	0 019	-0 110	-0 031	0 039	-0 021	0 024	-0 016	-0 055	-0 065	0 022
Na	0 288	0 022	0 014	0 197	0 108	0 227	0 113	0 142	0.151	0 156	0 118	0 087	0 073	0 162	0.032	0 081	0 085	0 115	0.000	0 251	0 018	0 134	0 089	0 056	0 054	0 216	0 103
K	0 018	0 076	0 004	0 016	0 034	0 046	0 002	0 107	0 105	0 023	0 114	0 089	0 084	0 103	0 112	0 057	0 036	0 105	0 042	0 064	0 071	0 029	0 071	0 070	0 024	0 063	0 054
OH	8 000	8 000	8 000	8 000	8 000	8 000	8 000	8 000	8 000	8 000	8 000	8 000	8 000	8 000	8 000	8 000	8 000	8 000	8 000	8 000	8 000	8 000	8 000	8 000	8 000	8 000	8 000
OodCalc - Berth (Si normalised)																											
Si	0.000	0 000	0 000	0.000	0.000	0 000	0.000	0.000	0 000	0.000	0.000	0.000	0.000	0 000	0 000	0.000	0.000	0.000	0 000	0 000	0 000	0.000	0 000	0.000	0 000	0 000	0 000
Al(TOT)	0.769	0 703	0.755	0 846	0 818	0 819	0.856	0.397	0 390	0 464	0 458	0 357	0.132	0.222	0 127	0 331	0 149	0 377	0.490	0.516	0 223	0 321	0.230	0 431	0 331	0.434	0 252
Ti	0 024	0 048	0.050	0 049	0.042	0 040	0 038	0 034	0 072	0.075	0 065	0 063	-0.004	0.016	-0.003	0 025	0.023	0.049	0 099	0.046	0.027	0 040	0.008	0.018	0 010	0 035	-0 004
Fe	9.847	8 803	9.939	9 513	9.186	9.264	10.521	5 502	6.962	8 688	4 229	3.514	0.331	0.440	-0 178	2.449	0.903	3.639	6.679	6.171	1.803	2.744	1.007	2.292	3.357	1.743	0 899
Mn	0 056	0.050	0.056	-0 001	0.061	-0.001	0.049	0 050	0.045	0 033	0 032	0.023	0.005	0.007	-0.005	0.047	0.006	0.031	0 034	0.066	0 044	0.018	0.006	0 021	0 002	-0 004	-0 003
Mg	0.224	-0 056	0 208	0 113	0.108	0.171	0 111	0 012	-0 074	0 153	-0.112	-0 068	-0 090	-0 051	-0 213	0 103	-0 089	-0 095	0.059	0.101	-0 093	0.130	-0 032	0 020	0 008	0 084	-0 022
Ca	-0.222	-0.157	-0.249	-0.496	-0 245	-0 190	-0 404	-0.045	-0 114	-0.161	-0.040	-0.105	-0 026	-0 090	-0 058	-0 041	-0 057	-0 032	-0.144	-0 066	-0.023	-0.076	-0 042	-0 074	-0.108	-0 125	-0 044
Na	0 270	-0 006	-0.005	0.174	0.084	0 204	0 097	0.089	0.107	0 127	0 057	0.019	-0 019	0 072	-0 065	0.007	-0 003	0 049	-0 044	0.205	-0 063	0 063	0.003	-0 019	-0 016	0.138	0 016
K	0 016	0 073	0.002	0 014	0 031	0 044	0 001	0.102	0 101	0.020	0 108	0 082	0 075	0.094	0 103	0.050	0.027	0 098	0 038	0.060	0 063	0 022	0 062	0 063	0.018	0 056	0 046
OodCalc - Berth (Mg normalised)																											
Si	-0.847	0.210	-0 787	-0 427	-0 408	-0 647	-0 418	-0 047	0 278	-0.578	0 423	0.258	0.341	0.191	0.807	-0.390	0.336	0.361	-0 224	-0 383	0 351	-0 493	0.121	-0 075	-0 029	-0 318	0 084
Al(TOT)	0.331	0.811	0 348	0.625	0 607	0 484	0.640	0.372	0 533	0 165	0 677	0.491	0.308	0.321	0.544	0.130	0 323	0.563	0.374	0 318	0.404	0 067	0 292	0.392	0.316	0 269	0 295
Ti	0 023	0.048	0 049	0.049	0.042	0 040	0.038	0.034	0.072	0.074	0 065	0 064	-0.003	0 017	-0.002	0 024	0 024	0 049	0.096	0.046	0 028	0.039	0 009	0.018	0.010	0 035	-0 004
Fe	8.854	9.049	9.016	9.013	8 708	8.505	10 031	5.447	7.288	8.011	4 725	3.817	0 730	0.664	0.767	1.993	1 296	4 062	6.416	5.722	2.214	2 167	1.148	2.204	3 323	1.370	0.997
Mn	0.055	0.051	0 054	-0.002	0 060	-0 002	0 048	0.050	0.045	0.032	0.033	0.023	0 006	0.007	-0 004	0 047	0.007	0.031	0.034	0 065	0 044	0 017	0.006	0.021	0 002	-0 005	-0 003
Mg	0.000	0 000	0 000	0 000	0.000	0 000	0.000	0 000	0.000	0.000	0 000	0 000	0 000	0 000	0 000	0 000	0.000	0 000	0.000	0 000	0 000	0 000	0 000	0 000	0 000	0.000	0 000
Ca	-0.241	-0 152	-0.266	-0 506	-0.254	-0 204	-0.414	-0.046	-0.107	-0.174	-0.031	-0.099	-0 018	-0.086	-0.040	-0.049	-0 049	-0.024	-0.149	-0 074	-0.016	-0 087	-0 039	-0.076	-0.109	-0.132	-0 042
Na	0 245	0.000	-0.028	0.161	0.073	0 185	0.085	0.088	0.115	0.110	0 070	0.027	-0.009	0.078	-0.041	-0.004	0.007	0.060	-0 050	0.194	-0 053	0.048	0.006	-0.021	-0.017	0 129	0 019
K	0 014	0.074	0 000	0 012	0.030	0 042	-0 001	0 102	0.102	0.019	0.109	0 083	0 076	0 095	0 105	0.049	0.028	0.099	0.037	0 059	0.064	0.021	0 063	0 062	0 018	0.055	0 046

Table D.2. Matrix Compositions For DRAG. 31.1 and 7. The Data have been Recalculated to Both Berthierine and Illite Structural Formulae.

	DRAG 31.1									DRAG 31 7									
	1	2	3	4	5	6	7	8	9	1	2	3	4	5	6	7	8	9	10
Si	16.603	17 987	13 597	13 778	21 924	18 620	14 500	14.506	16 026	15.529	17 127	15 053	17 909	11 804	13 336	9 378	8 015	10 685	13.783
Ti	0 303	0 270	0 332	0 124	0 116	0.214	0 272	0 296	0 191	0 105	0 111	0 127	0 148	0 024	0 108	0 000	0 073	0 104	0 203
Al	10 250	10 276	7 822	7 226	8 590	11 259	8 614	8.774	9 569	9 619	9 472	8 128	10 637	6 699	6 354	4 967	5 101	6 825	8 404
Fe	7 568	8 226	7.272	8.021	6 880	7 502	10 260	6.406	7 279	14 295	13 577	13 069	13 882	10 465	10 413	7 479	8 516	11 094	11 983
Mn	0.084	0.000	0 101	0.014	0 000	0 122	0 000	0.018	0.000	0.088	0 080	0 000	0 046	0 155	0 030	0.077	0 111	0 151	0 011
Mg	1.672	1 787	1 594	1 270	1.340	1 498	1 486	1.383	1.523	2.266	2 196	2.141	2 385	1.940	1.793	1 343	1 403	2 022	2.044
Ca	0.201	0 277	0 429	0 224	0 169	0 315	0 127	0 217	0 378	3 594	2.977	6 319	0 868	11 290	12 230	17 012	19 006	11 247	8 459
Na	0 517	0 401	0.992	0 976	0.504	0 406	0 321	0.565	0 489	0 694	0 212	0 292	0 346	0 278	0 239	0 356	0 135	0 382	0 195
K	2.928	2.972	2.030	1 260	2.116	2.031	2 326	1 958	2.736	1 670	2.242	1 546	2 793	1 780	1 216	1 103	1 053	1 407	1 931
P	0 000	0.000	0.000	0 018	0.000	0.000	0.001	0 000	0 009	0.071	0 188	0 000	0 005	0 122	0 044	0 005	0 008	0 070	0 068
S	0.498	0.255	0.799	0.108	0 123	0 210	0 226	0.203	0.305	0.018	0 029	0 003	0 000	0 087	0 042	0 182	0 055	0 008	0 042
O	32.387	34.203	26.762	26 054	36.223	35 223	28.920	27.962	30 877	34.041	35 333	32.557	36 567	28 868	30 360	25 298	24 973	27.867	32 022
TOTAL	73.011	76 654	61 730	59.073	77.985	77 400	67.053	62.288	69.382	81 990	83 544	79 235	85 586	73 512	76 165	67 200	68.449	71 862	79 145
BerthCalc.																			
Si	4.104	4 202	4.082	4 228	4.831	4 222	4 007	4 145	4 152	3 651	3 901	3 688	3 907	3 286	3.513	2 963	2 563	3 071	3 446
Al(T)	-0.104	-0 202	-0.082	-0 228	-0 831	-0 222	-0.007	-0 145	-0 152	0.349	0.099	0 312	0.093	0 714	0 487	1 037	1 437	0 929	0 554
Al(O)	2 741	2 700	2.526	2 536	2 801	2 879	2 484	2.754	2 733	2 005	2 146	1 760	2 322	1 227	1.255	0.596	0 260	1 112	1 633
Ti	0.044	0 037	0.058	0 022	0.015	0 028	0 044	0 050	0 029	0 014	0 015	0 018	0 019	0 004	0 017	0 000	0 014	0 018	0 030
Fe	0.887	0.940	0 993	1 223	0 751	0 835	1 399	0 895	0 914	1 689	1 552	1 610	1.523	1 455	1 375	1 163	1 362	1 603	1 502
Mn	0 011	0.000	0.016	0.002	0 000	0 014	0.000	0 003	0 000	0 011	0 009	0 000	0.005	0 022	0 004	0 012	0 018	0 022	0 001
Mg	0.478	0 482	0 553	0 450	0 341	0 392	0 474	0 457	0 456	0 616	0.578	0.606	0 601	0 624	0 546	0 490	0 518	0 671	0.590
Ca	0 035	0 045	0 090	0 040	0 026	0 050	0 024	0 043	0 065	0 582	0 449	1 085	0 132	2 182	2 250	3 765	4 256	2 253	1 471
Na	0 156	0 114	0.364	0.366	0.136	0 112	0 108	0 197	0 155	0 199	0 059	0 087	0 092	0 095	0 077	0 137	0 053	0 134	0 060
K	0.520	0 499	0 438	0 278	0 335	0 331	0 462	0 402	0 509	0 282	0 367	0 272	0 438	0 356	0 230	0 250	0 242	0 291	0 347
OCT	4 160	4 160	4 146	4 234	3 908	4 149	4 401	4 158	4 131	4 335	4 300	3 994	4 470	3 332	3 196	2 262	2 172	3 426	3 756
INT.	0.711	0.559	0 892	0.683	0 497	0 493	0.594	0 643	0 729	1 063	0.875	1 444	0 562	2 632	2.557	4 152	4 551	2.677	1 878
OH	8.000	8 000	8.000	8 000	8 000	8 000	8 000	8 000	8 000	8 000	8 000	8 000	8 000	8 000	8 000	8 000	8 000	8 000	8 000
IlliteCalc.																			
Si	6 450	6.603	6.415	6.642	7.592	6 635	6.296	6 513	6 524	5 738	6.130	5 795	6.139	5 164	5 520	4 656	4 027	4 826	5.415
Al(T)	1.550	1.397	1.585	1.358	0.408	1.365	1.704	1 487	1 476	2.262	1.870	2.205	1.861	2.836	2.480	3 344	3 973	3.174	2 585
Al(O)	2.594	2.529	2 256	2.267	2 687	2 810	2.189	2.613	2 578	1 437	1 658	1 051	1.934	0 215	0 258	-0 778	-1 306	0 034	0 851
Ti	0 069	0 058	0 092	0 035	0 024	0 045	0 069	0 078	0 046	0 023	0 023	0 029	0.030	0 006	0 026	0 000	0 022	0 028	0 047
Fe	1 394	1.478	1 560	1 922	1 179	1 312	2.198	1 407	1.436	2.653	2 439	2 530	2 393	2 286	2 160	1 828	2 140	2 518	2 360
Mn	0.017	0.000	0.024	0.003	0.000	0 022	0 000	0 004	0.000	0.017	0 015	0 000	0 008	0 035	0 006	0 020	0 029	0 035	0 002
Mg	0 750	0.758	0 869	0.707	0 536	0 617	0 746	0 717	0.716	0 967	0 908	0 952	0 945	0 981	0 858	0 770	0 814	1 055	0.928
Ca	0.055	0 071	0 142	0 070	0 041	0 079	0 038	0 068	0.106	0 915	0 706	1 704	0 207	3 428	3 536	5 916	6 688	3 540	2 312
Na	0 245	0 180	0 572	0 575	0 213	0 177	0 170	0.310	0 243	0 313	0 093	0 137	0 145	0 149	0 121	0 216	0 083	0 211	0 094
K	0 817	0 784	0 688	0 436	0 526	0 520	0 726	0.632	0 800	0.443	0 577	0 428	0 688	0 560	0 362	0 393	0 380	0 457	0 545
OCT	4 878	4 894	4 943	5.005	4.467	4.884	5 240	4 888	4.882	6 012	5.749	6 266	5.517	6 950	6 844	7.756	8.386	7.209	6 501
INT.	1.063	0.964	1.260	1.011	0.740	0.697	0.896	0.942	1.043	0.757	0.669	0.565	0.833	0.708	0.482	0.609	0 463	0 667	0 639
OH	4 000	4 000	4 000	4.000	4.000	4 000	4 000	4 000	4.000	4 000	4 000	4 000	4 000	4 000	4 000	4 000	4 000	4 000	4 000

Table D.3. Matrix Compositions for DRAG. 31.13/14, 21, and YAR. 7, 24. The Data have been Recalculated to Berthierine Structural Formulae Only.

	DRAG. 31.13/14											
	1	2	3	4	5	6	7	8	9	10	11	12
Si	13.031	13.589	13.015	12.364	13.169	12.700	12.883	13.046	13.557	12.588	12.398	12.671
Ti	0.285	0.176	0.235	0.213	0.250	0.236	0.252	0.190	0.204	0.153	0.131	0.128
Al	8.425	8.371	8.511	8.101	8.509	8.285	8.409	8.599	8.037	8.402	7.685	8.044
Fe	24.294	23.740	24.880	23.842	23.498	23.120	23.690	24.119	24.656	24.438	26.864	29.463
Mn	0.132	0.138	0.087	0.603	0.497	0.327	0.104	0.153	0.215	0.307	0.160	0.131
Mg	2.353	2.148	2.227	2.090	2.209	2.200	2.135	2.284	2.567	2.912	2.314	2.079
Ca	0.511	0.371	0.407	0.946	0.709	0.568	0.409	0.459	0.302	0.557	0.319	0.229
Na	0.422	0.244	0.210	0.151	0.072	0.183	0.079	0.286	0.177	0.192	0.408	0.381
K	0.831	1.090	0.625	0.593	0.636	0.786	0.629	0.662	1.318	0.293	0.195	0.048
P	0.000	0.007	0.000	0.000	0.087	0.058	0.000	0.014	0.040	0.000	0.000	0.000
S	0.022	0.000	0.013	0.025	0.010	0.041	0.000	0.072	0.009	0.050	0.055	0.024
O	31.597	31.765	31.535	30.366	31.619	30.689	30.866	31.532	32.047	31.272	30.622	31.757
TOTAL	81.903	81.639	81.745	79.294	81.265	79.193	79.456	81.416	83.129	81.164	81.151	84.955
BerthCalc.												
Si	3.290	3.413	3.292	3.248	3.337	3.312	3.329	3.304	3.381	3.212	3.230	3.183
Al(T)	0.710	0.587	0.708	0.752	0.663	0.688	0.671	0.696	0.619	0.788	0.770	0.817
Al(O)	1.503	1.601	1.532	1.463	1.581	1.560	1.590	1.570	1.467	1.442	1.314	1.286
Ti	0.042	0.026	0.035	0.033	0.037	0.036	0.038	0.028	0.030	0.023	0.020	0.019
Fe	3.082	2.999	3.163	3.147	2.993	3.027	3.078	3.064	3.091	3.130	3.514	3.719
Mn	0.017	0.018	0.011	0.081	0.064	0.044	0.014	0.020	0.027	0.040	0.021	0.017
Mg	0.686	0.623	0.651	0.634	0.647	0.663	0.637	0.668	0.740	0.858	0.697	0.603
Ca	0.090	0.064	0.072	0.174	0.113	0.095	0.074	0.079	0.047	0.100	0.058	0.040
Na	0.130	0.075	0.065	0.048	0.022	0.058	0.025	0.088	0.054	0.060	0.130	0.117
K	0.151	0.197	0.114	0.112	0.116	0.147	0.117	0.120	0.236	0.054	0.037	0.009
OCT.	5.331	5.267	5.392	5.358	5.322	5.330	5.358	5.351	5.355	5.494	5.566	5.644
INT.	0.371	0.336	0.251	0.334	0.251	0.300	0.216	0.288	0.337	0.213	0.225	0.166
CH	8.000	8.000	8.000	8.000	8.000	8.000	8.000	8.000	8.000	8.000	8.000	8.000

Table D.3. (Continued).

	DRAG 31.21									
	1	2	3	4	5	6	7	8	9	10
Si	10.941	11.476	9.337	11.367	11.159	9.908	10.962	9.272	11.357	10.873
Ti	0.110	0.143	0.088	0.134	0.243	0.114	0.215	0.215	0.119	0.166
Al	6.604	6.739	5.676	6.917	6.730	5.884	6.554	5.512	6.793	6.350
Fe	25.023	26.429	22.685	24.807	26.367	26.39	24.150	21.787	26.676	25.754
Mn	1.577	0.592	4.530	0.612	1.364	1.136	1.412	5.767	0.788	1.036
Mg	2.331	2.079	2.369	2.279	2.302	2.071	2.126	2.119	2.270	2.103
Ca	1.101	0.500	2.672	0.513	0.909	0.621	0.869	3.043	0.685	1.031
Na	0.284	0.048	0.244	0.125	0.164	0.349	0.204	0.196	0.089	0.055
K	0.099	0.168	0.131	0.143	0.148	0.141	0.222	0.112	0.106	0.305
P	0.027	0.000	0.000	0.026	0.000	0	0.000	0.000	0.004	0.000
S	0.048	0.052	0.045	0.000	0.079	0.003	0.000	0.017	0.023	0.048
O	not calculated	not calculated	not calculated	not calculated	not calculated	not calculated	not calculated	not calculated	not calculated	not calculated
TOTAL	48.145	48.226	47.777	46.923	49.465	46.617	46.714	48.040	48.910	47.721
BerthCalc.										
Si	3.106	3.210	2.833	3.211	3.095	3.010	3.161	2.820	3.151	3.132
Al(T)	0.894	0.790	1.167	0.789	0.905	0.990	0.839	1.180	0.849	0.868
Al(O)	1.056	1.172	0.625	1.245	1.037	0.871	1.129	0.564	1.113	1.035
Ti	0.018	0.023	0.016	0.022	0.040	0.020	0.036	0.038	0.019	0.028
Fe	3.566	3.711	3.455	3.524	3.668	4.032	3.503	3.330	3.720	3.724
Mn	0.229	0.085	0.703	0.088	0.193	0.176	0.208	0.897	0.112	0.153
Mg	0.764	0.672	0.830	0.744	0.738	0.727	0.708	0.745	0.728	0.700
Ca	0.207	0.098	0.568	0.090	0.177	0.132	0.176	0.648	0.131	0.208
Na	0.098	0.016	0.090	0.043	0.056	0.129	0.072	0.073	0.030	0.019
K	0.020	0.034	0.029	0.029	0.029	0.031	0.046	0.024	0.021	0.063
OCT.	5.634	5.663	5.628	5.623	5.675	5.827	5.584	5.573	5.691	5.640
INT.	0.326	0.148	0.687	0.163	0.262	0.292	0.293	0.746	0.183	0.290
CH	8.000	8.000	8.000	8.000	8.000	8.000	8.000	8.000	8.000	8.000

Table D.3. (Continued).

	YAR. 7						YAR. 24			
	1	2	3	4	5	6	1	2	3	4
Si	5.871	6.892	3.091	5.753	7.061	7.917	0.893	1.085	1.978	2.139
Ti	0.000	0.021	0.045	0.000	0.000	0.024	0.000	0.061	0.035	0.015
Al	3.306	4.245	1.788	3.337	3.926	4.103	0.454	0.495	1.144	1.235
Fe	14.950	10.152	10.961	13.946	17.249	17.985	2.609	2.822	3.950	7.862
Mn	0.000	0.199	0.435	0.145	0.151	0.000	0.355	0.334	0.336	0.349
Mg	1.302	0.866	0.877	1.217	1.481	1.730	0.540	0.583	0.587	0.744
Ca	19.015	17.387	23.599	20.285	10.133	0.454	34.197	33.788	32.109	27.713
Na	0.266	0.148	0.052	0.344	0.043	0.312	0.011	0.164	0.032	0.313
K	0.054	0.821	0.248	0.254	0.097	0.077	0.088	0.100	0.327	0.000
P	0.000	0.684	0.256	0.049	0.378	0.000	0.180	0.296	0.013	0.024
S	0.073	0.112	0.059	0.331	0.093	0.037	0.000	0.058	0.000	0.055
O	22.463	23.222	18.807	22.692	22.065	19.281	16.534	16.954	17.823	17.592
TOTAL	67.300	64.749	60.218	68.353	62.677	51.920	55.861	56.740	58.334	58.041
BerthCalc.										
Si	2.086	2.490	1.342	2.037	2.629	3.276	0.439	0.526	0.886	0.973
Al(T)	1.914	1.510	2.658	1.963	1.371	0.724	3.561	3.474	3.114	3.027
Al(O)	-0.691	0.086	-1.850	-0.734	0.150	1.043	-3.329	-3.224	-2.580	-2.443
Ti	0.000	0.004	0.011	0.000	0.000	0.006	0.000	0.017	0.009	0.004
Fe	2.660	1.827	2.382	2.432	3.214	3.736	0.645	0.676	0.890	1.787
Mn	0.000	0.037	0.097	0.026	0.029	0.000	0.089	0.083	0.077	0.081
Mg	0.535	0.362	0.440	0.498	0.637	0.827	0.306	0.327	0.304	0.391
Ca	4.734	4.252	7.111	5.021	2.558	0.132	11.716	11.388	10.076	8.823
Na	0.115	0.065	0.028	0.149	0.020	0.158	0.007	0.097	0.018	0.174
K	0.014	0.213	0.077	0.065	0.026	0.023	0.031	0.035	0.105	0.000
OCT.	2.504	2.316	1.080	2.222	4.030	5.613	-2.289	-2.122	-1.300	-0.179
INT.	4.863	4.530	7.216	5.234	2.603	0.312	11.753	11.520	10.199	8.997
CH	8.000	8.000	8.000	8.000	8.000	8.000	8.000	8.000	8.000	8.000

Table D.4. Compositions of Berthierine Cements. The Data have been Recalculated to Berthierine Structural Formulae.

	DRAG. 31.19										DRAG. 31.28			
	One end of the slide					Other end of the slide					GEN. 1 (Pore-lining)			
	1	2	3	4	5	1	2	3	4	5	1	2	3	4
Si	10.958	9.946	9.480	8.936	9.828	10.001	10.028	11.013	10.764	9.714	8.608	8.288	8.721	8.842
Ti	0.010	0.019	0.000	0.019	0.000	0.000	0.000	0.036	0.000	0.000	0.034	0.000	0.000	0.028
Al	6.976	6.089	5.549	5.286	5.846	6.198	6.336	6.919	6.666	6.137	3.721	3.765	3.799	4.016
Fe	30.240	25.732	24.451	23.232	26.150	26.234	26.247	30.130	29.838	25.408	18.656	18.019	18.689	19.510
Mn	0.000	0.109	0.137	0.000	0.001	0.058	0.000	0.123	0.000	0.000	0.005	0.014	0.000	0.045
Mg	1.610	1.859	1.433	1.605	1.597	1.636	1.912	1.431	1.568	1.724	1.962	2.303	2.323	2.266
Ca	0.106	0.713	0.277	0.206	0.250	0.259	0.304	0.096	0.040	0.234	0.108	0.223	0.201	0.233
Na	0.155	0.205	0.165	0.292	0.016	0.259	0.309	0.168	0.198	0.340	0.140	0.112	0.330	0.225
K	0.000	0.000	0.089	0.000	0.015	0.045	0.000	0.000	0.019	0.000	0.023	0.016	0.000	0.052
P	0.000	0.000	0.000	0.000	0.000	0.000	0.000	0.000	0.000	0.000	0.000	0.000	0.000	0.000
S	0.009	0.039	0.004	0.028	0.019	0.000	0.000	0.002	0.002	0.000	0.000	0.000	0.026	0.030
O	28.515	25.742	23.909	22.791	25.048	25.719	26.066	28.432	27.862	25.150	19.873	19.604	20.391	20.940
TOTAL	78.579	70.453	65.494	62.395	68.770	70.409	71.202	78.350	76.957	68.707	53.130	52.344	54.480	56.187
BerthCalc.														
Si	3.065	3.083	3.162	3.128	3.130	3.101	3.068	3.089	3.081	3.080	3.454	3.372	3.412	3.369
Al(T)	0.935	0.917	0.838	0.872	0.870	0.899	0.932	0.911	0.919	0.920	0.546	0.628	0.588	0.631
Al(O)	1.096	1.047	1.089	1.054	1.067	1.102	1.086	1.109	1.067	1.106	1.009	0.966	0.958	0.961
Ti	0.002	0.003	0.000	0.004	0.000	0.000	0.000	0.006	0.000	0.000	0.008	0.000	0.000	0.006
Fe	4.253	4.005	4.101	4.086	4.186	4.091	4.039	4.250	4.295	4.052	3.765	3.687	3.672	3.733
Mn	0.000	0.017	0.023	0.000	0.000	0.009	0.000	0.018	0.000	0.000	0.001	0.003	0.000	0.009
Mg	0.520	0.666	0.552	0.649	0.588	0.586	0.676	0.464	0.519	0.632	0.910	1.082	1.050	0.998
Ca	0.021	0.155	0.065	0.051	0.056	0.056	0.065	0.019	0.008	0.052	0.030	0.064	0.055	0.062
Na	0.053	0.078	0.067	0.125	0.006	0.098	0.115	0.058	0.069	0.132	0.069	0.056	0.158	0.105
K	0.000	0.000	0.021	0.000	0.003	0.010	0.000	0.000	0.004	0.000	0.007	0.005	0.000	0.014
OCT.	5.871	5.738	5.766	5.792	5.841	5.788	5.800	5.847	5.881	5.789	5.693	5.738	5.681	5.707
INT.	0.074	0.232	0.153	0.175	0.065	0.164	0.181	0.076	0.081	0.184	0.106	0.124	0.213	0.181
OH	8.000	8.000	8.000	8.000	8.000	8.000	8.000	8.000	8.000	8.000	8.000	8.000	8.000	8.000

Table D.4. (Continued).

	DRAG. 31.28													
	GEN. 1 (Cont.)												GEN.2 (Pore-filling)	
	5	6	7	8	9	10	11	12	13	14	15	16	1	2
Si	8.566	7.657	8.360	7.989	10.011	9.884	8.236	9.925	9.460	9.110	6.854	9.934	8.550	9.838
Ti	0.023	0.000	0.000	0.051	0.000	0.014	0.002	0.008	0.016	0.025	0.031	0.044	0.000	0.000
Al	3.851	3.625	3.735	3.709	4.862	4.845	3.654	4.876	4.361	3.957	3.648	4.959	3.954	4.491
Fe	18.913	15.790	18.025	16.467	23.096	23.177	17.208	23.728	21.570	19.742	13.694	24.996	17.842	22.365
Mn	0.000	0.014	0.056	0.025	0.000	0.010	0.052	0.000	0.000	0.013	0.000	0.000	0.053	0.040
Mg	2.241	1.988	2.288	2.269	2.289	2.384	2.190	2.167	2.234	2.283	1.990	2.258	2.332	2.447
Ca	0.095	0.137	0.138	0.175	0.157	0.191	0.192	0.236	0.220	0.219	0.100	0.208	0.190	0.233
Na	0.271	0.121	0.122	0.234	0.374	0.459	0.000	0.344	0.283	0.149	0.135	0.137	0.320	0.138
K	0.028	0.007	0.000	0.030	0.080	0.053	0.000	0.034	0.059	0.029	0.000	0.000	0.023	0.027
P	0.000	0.000	0.000	0.000	0.047	0.000	0.000	0.000	0.000	0.000	0.000	0.000	0.000	0.021
S	0.082	0.044	0.134	0.051	0.065	0.070	0.000	0.037	0.036	0.078	0.000	0.070	0.000	0.115
O	20.231	17.882	19.629	18.809	24.122	24.038	19.097	24.094	22.514	21.222	16.393	24.536	20.111	23.405
TOTAL	54.301	47.265	52.487	49.809	65.103	65.125	50.631	65.449	60.753	56.827	42.845	67.142	53.375	63.120
BerthCalc.														
Si	3.380	3.417	3.402	3.390	3.323	3.282	3.439	3.286	3.352	3.427	3.334	3.231	3.391	3.361
Al(T)	0.620	0.583	0.598	0.610	0.677	0.718	0.561	0.714	0.648	0.573	0.666	0.769	0.609	0.639
Al(O)	0.962	1.101	0.984	1.027	1.002	0.956	1.028	0.967	0.961	0.976	1.181	0.910	1.022	0.958
Ti	0.005	0.000	0.000	0.013	0.000	0.003	0.000	0.002	0.003	0.006	0.009	0.008	0.000	0.000
Fe	3.739	3.535	3.665	3.504	3.846	3.860	3.614	3.946	3.838	3.722	3.350	4.079	3.558	3.826
Mn	0.000	0.003	0.012	0.005	0.000	0.002	0.011	0.000	0.000	0.003	0.000	0.000	0.011	0.007
Mg	1.022	1.025	1.076	1.112	0.878	0.915	1.057	0.829	0.915	0.992	1.119	0.849	1.068	0.966
Ca	0.026	0.043	0.039	0.052	0.027	0.044	0.056	0.055	0.055	0.058	0.034	0.047	0.053	0.051
Na	0.131	0.066	0.061	0.121	0.152	0.186	0.000	0.139	0.122	0.068	0.080	0.054	0.155	0.058
K	0.008	0.002	0.000	0.009	0.019	0.013	0.000	0.008	0.015	0.008	0.000	0.000	0.007	0.007
OCT.	5.728	5.664	5.737	5.662	5.725	5.735	5.710	5.743	5.717	5.697	5.659	5.846	5.660	5.757
INT.	0.165	0.111	0.100	0.182	0.198	0.243	0.056	0.202	0.192	0.134	0.114	0.102	0.214	0.116
CH	8.000	8.000	8.000	8.000	8.000	8.000	8.000	8.000	8.000	8.000	8.000	8.000	8.000	8.000

Table D.4. (Continued).

	GEN . 2 (Cont.)						GEN. 2 (Where Berthierine is replaced by siderite/pyrite)							
	3	4	5	6	7	8	1	2	3	4	5	6	7	8
Si	8.887	7.950	7.278	7.163	7.059	7.482	8.810	9.554	8.165	8.117	8.323	8.850	8.977	8.480
Ti	0.058	0.001	0.036	0.000	0.062	0.000	0.040	0.000	0.000	0.000	0.000	0.000	0.000	0.026
Al	4.022	3.793	3.454	3.579	3.657	3.656	3.989	4.605	3.613	3.788	3.749	4.035	4.135	3.815
Fe	19.596	16.224	14.384	14.484	14.227	14.993	19.144	22.215	17.600	17.062	16.796	19.776	19.962	18.129
Mn	0.032	0.039	0.000	0.078	0.000	0.000	0.027	0.025	0.039	0.038	0.003	0.019	0.135	0.000
Mg	2.331	2.372	1.949	1.986	2.076	1.975	2.320	2.309	2.145	2.395	2.153	2.264	2.342	2.276
Ca	0.223	0.184	0.143	0.160	0.108	0.194	0.078	0.191	0.132	0.203	0.229	0.179	0.234	0.157
Na	0.211	0.297	0.150	0.271	0.410	0.000	0.163	0.451	0.119	0.289	0.247	0.212	0.102	0.281
K	0.041	0.039	0.002	0.036	0.005	0.023	0.030	0.033	0.017	0.007	0.023	0.020	0.000	0.004
P	0.000	0.000	0.000	0.000	0.000	0.000	0.003	0.000	0.000	0.000	0.000	0.000	0.038	0.000
S	0.063	0.086	0.091	0.000	0.007	0.073	0.087	0.112	0.109	0.002	0.039	0.124	0.198	0.090
O	21.070	18.836	16.901	16.989	16.964	17.452	20.729	23.112	19.077	19.275	19.229	20.982	21.382	19.924
TOTAL	56.534	49.821	44.388	44.746	44.575	45.848	55.420	62.607	51.016	51.176	50.791	56.461	57.505	53.182
BerthCalc.														
Si	3.366	3.370	3.439	3.363	3.319	3.422	3.394	3.301	3.418	3.359	3.454	3.369	3.366	3.398
Al(T)	0.634	0.630	0.561	0.637	0.681	0.578	0.606	0.699	0.582	0.641	0.546	0.631	0.634	0.602
Al(O)	0.952	1.043	1.138	1.111	1.108	1.163	0.993	0.957	0.992	0.990	1.073	0.967	0.979	0.989
Ti	0.013	0.000	0.010	0.000	0.017	0.000	0.009	0.000	0.000	0.000	0.000	0.000	0.000	0.006
Fe	3.723	3.443	3.399	3.420	3.362	3.434	3.694	3.843	3.685	3.550	3.498	3.765	3.732	3.638
Mn	0.006	0.008	0.000	0.019	0.000	0.000	0.005	0.004	0.008	0.008	0.001	0.004	0.026	0.000
Mg	1.020	1.162	1.064	1.077	1.128	1.044	1.033	0.922	1.037	1.145	1.032	0.996	1.015	1.054
Ca	0.059	0.055	0.047	0.053	0.036	0.062	0.020	0.046	0.039	0.059	0.067	0.048	0.053	0.044
Na	0.098	0.154	0.087	0.155	0.235	0.000	0.077	0.190	0.061	0.146	0.125	0.099	0.047	0.138
K	0.011	0.012	0.001	0.012	0.002	0.008	0.008	0.008	0.005	0.002	0.007	0.005	0.000	0.001
OCT.	5.714	5.656	5.611	5.627	5.615	5.641	5.735	5.726	5.723	5.693	5.604	5.732	5.751	5.687
INT.	0.168	0.220	0.135	0.220	0.273	0.070	0.105	0.245	0.105	0.207	0.199	0.152	0.100	0.183
CH	8.000	8.000	8.000	8.000	8.000	8.000	8.000	8.000	8.000	8.000	8.000	8.000	8.000	8.000

Table D.4. (Continued).

	GEN. 2 (Cont.)			Filling Fractures Within Ooids						Darker berthierine				
	9	10	11	1	2	3	4	5	6	1	2	3	4	5
Si	9.897	9.267	8.721	9.363	9.699	9.509	8.873	9.898	9.923	8.636	10.264	10.334	8.658	8.615
Ti	0.000	0.037	0.059	0.000	0.044	0.000	0.000	0.007	0.016	0.000	0.000	0.000	0.032	0.000
Al	4.755	4.272	4.017	4.371	4.743	4.608	4.615	4.811	4.809	4.355	5.031	4.798	4.134	3.945
Fe	22.253	20.605	18.426	22.234	23.108	23.547	20.714	23.435	23.989	27.835	25.155	23.234	18.189	18.218
Mn	0.039	0.072	0.000	0.094	0.146	0.000	0.000	0.066	0.000	0.523	0.000	0.024	0.080	0.000
Mg	2.445	2.293	2.509	2.430	2.276	2.449	2.207	2.241	2.235	2.829	2.505	2.575	2.532	2.444
Ca	0.179	0.177	0.262	0.137	0.196	0.084	0.156	0.099	0.185	0.569	0.163	0.166	0.168	0.221
Na	0.319	0.000	0.268	0.094	0.214	0.199	0.029	0.338	0.245	0.000	0.346	0.000	0.338	0.428
K	0.026	0.047	0.014	0.000	0.042	0.082	0.008	0.031	0.023	0.000	0.000	0.000	0.112	0.000
P	0.000	0.051	0.000	0.000	0.000	0.000	0.018	0.000	0.000	0.000	0.000	0.000	0.000	0.000
S	0.039	0.110	0.101	0.055	0.047	0.020	0.033	0.014	0.090	0.038	0.044	0.000	0.000	0.022
O	23.688	21.960	20.678	22.638	23.585	23.408	21.698	23.931	24.100	23.927	25.209	24.465	20.670	20.388
TOTAL	63.640	58.891	55.055	61.416	64.100	63.906	58.351	64.871	65.615	68.712	68.717	65.596	54.913	54.281
BerthCalc.														
Si	3.333	3.382	3.368	3.300	3.277	3.240	3.267	3.299	3.287	2.880	3.249	3.369	3.341	3.371
Al(T)	0.667	0.618	0.632	0.700	0.723	0.760	0.733	0.701	0.713	1.120	0.751	0.631	0.659	0.629
Al(O)	1.000	1.005	0.982	0.904	0.944	0.875	1.036	0.968	0.945	0.391	0.906	0.997	1.001	0.977
Ti	0.000	0.008	0.013	0.000	0.009	0.000	0.000	0.001	0.003	0.000	0.000	0.000	0.007	0.000
Fe	3.764	3.765	3.561	3.933	3.919	4.032	3.830	3.926	3.983	4.662	3.998	3.809	3.529	3.581
Mn	0.007	0.013	0.000	0.017	0.025	0.000	0.000	0.011	0.000	0.089	0.000	0.004	0.016	0.000
Mg	0.951	0.967	1.119	0.990	0.888	0.964	0.939	0.863	0.855	1.090	0.916	0.970	1.129	1.105
Ca	0.042	0.034	0.071	0.034	0.046	0.020	0.036	0.023	0.043	0.133	0.036	0.038	0.045	0.061
Na	0.131	0.000	0.126	0.040	0.088	0.083	0.013	0.138	0.099	0.000	0.134	0.000	0.159	0.205
K	0.006	0.012	0.004	0.000	0.010	0.020	0.002	0.007	0.005	0.000	0.000	0.000	0.031	0.000
OCT.	5.722	5.758	5.676	5.844	5.785	5.871	5.805	5.770	5.786	6.232	5.820	5.779	5.682	5.663
INT.	0.180	0.046	0.201	0.074	0.145	0.123	0.051	0.168	0.148	0.133	0.170	0.038	0.236	0.265
OH	8.000	8.000	8.000	8.000	8.000	8.000	8.000	8.000	8.000	8.000	8.000	8.000	8.000	8.000

Table D.4. (Continued).

								DRAG. 31.33						
	Darker berthierine (Continued)							Berthierine cement						
	6	7	8	9	10	11	12	1	2	3	4	5	6	7
Si	11.061	10.095	11.186	11.362	6.661	9.573	10.446	8.340	8.728	10.773	9.689	8.693	8.969	9.022
Ti	0.091	0.039	0.000	0.014	0.054	0.000	0.071	0.015	0.056	0.073	0.056	0.020	0.010	0.031
Al	4.839	4.695	5.107	4.857	3.684	4.316	4.561	3.939	4.315	5.186	4.464	4.148	4.391	4.249
Fe	25.388	21.666	24.891	25.796	13.367	21.802	23.930	19.857	21.323	27.854	24.433	20.927	22.386	22.216
Mn	0.004	0.049	0.026	0.000	0.000	0.010	0.078	0.100	0.003	0.001	0.051	0.000	0.026	0.000
Mg	2.710	2.769	3.100	2.639	1.736	2.396	2.562	1.826	2.040	2.342	1.919	2.063	1.966	1.963
Ca	0.221	0.264	0.220	0.120	0.100	0.221	0.272	0.229	0.191	0.205	0.119	0.173	0.144	0.180
Na	0.191	0.195	0.323	0.193	0.075	0.032	0.015	0.229	0.100	0.000	0.234	0.293	0.000	0.211
K	0.060	0.060	0.000	0.086	0.000	0.035	0.000	0.000	0.000	0.000	0.073	0.000	0.037	0.000
P	0.000	0.000	0.017	0.000	0.000	0.000	0.000	0.000	0.000	0.002	0.000	0.000	0.000	0.000
S	0.023	0.070	0.000	0.000	0.027	0.000	0.000	0.052	0.024	0.054	0.000	0.051	0.018	0.000
O	26.191	23.931	26.686	26.533	15.938	22.678	24.684	20.106	21.383	26.540	23.468	21.130	21.911	21.880
TOTAL	70.779	63.833	71.556	71.600	41.642	61.063	66.619	54.693	58.163	73.030	64.506	57.498	59.858	59.752
BerthCalc.														
Si	3.369	3.367	3.346	3.415	3.334	3.367	3.375	3.310	3.256	3.239	3.293	3.283	3.265	3.288
Al(T)	0.631	0.633	0.654	0.585	0.666	0.633	0.625	0.690	0.744	0.761	0.707	0.717	0.735	0.712
Al(O)	0.903	0.996	0.936	0.934	1.253	0.946	0.909	0.937	0.932	0.862	0.872	0.913	0.929	0.900
Ti	0.016	0.008	0.000	0.002	0.016	0.000	0.013	0.003	0.012	0.013	0.011	0.004	0.002	0.007
Fe	3.886	3.623	3.745	3.899	3.359	3.856	3.888	3.955	3.997	4.205	4.176	3.966	4.096	4.072
Mn	0.001	0.008	0.004	0.000	0.000	0.002	0.013	0.020	0.001	0.000	0.009	0.000	0.005	0.000
Mg	0.954	1.067	1.071	0.916	1.004	0.974	0.956	0.837	0.879	0.814	0.753	0.900	0.827	0.827
Ca	0.047	0.062	0.043	0.025	0.035	0.054	0.062	0.064	0.050	0.042	0.028	0.046	0.037	0.046
Na	0.071	0.079	0.118	0.071	0.046	0.014	0.006	0.111	0.046	0.000	0.097	0.135	0.000	0.094
K	0.013	0.014	0.000	0.019	0.000	0.009	0.000	0.000	0.000	0.000	0.018	0.000	0.010	0.000
OCT.	5.759	5.702	5.757	5.753	5.632	5.778	5.780	5.753	5.821	5.894	5.821	5.784	5.859	5.806
INT.	0.131	0.155	0.161	0.115	0.081	0.077	0.067	0.175	0.095	0.042	0.143	0.181	0.046	0.140
CH	8.000	8.000	8.000	8.000	8.000	8.000	8.000	8.000	8.000	8.000	8.000	8.000	8.000	8.000

Table D.4. (Continued).

										Y183. 3				
		Darker berthierine												
	8	1	2	3	4	5	6	7	8	1	2	3	4	5
Si	8.550	8.818	8.520	9.033	9.676	8.468	8.713	9.280	9.451	8.888	8.346	8.261	9.951	10.571
Ti	0.026	0.040	0.032	0.053	0.000	0.000	0.000	0.000	0.000	0.055	0.000	0.057	0.028	0.000
Al	3.953	4.116	3.964	4.267	4.575	4.048	4.145	4.162	4.440	4.410	4.019	3.877	5.274	6.444
Fe	20.372	22.107	20.302	22.426	21.724	19.402	21.620	22.540	22.040	21.595	19.232	19.243	24.958	27.035
Mn	0.000	0.057	0.036	0.000	0.000	0.020	0.000	0.070	0.000	0.000	0.126	0.000	0.000	0.000
Mg	1.846	1.978	1.930	1.997	2.480	2.054	2.003	2.021	2.480	1.934	1.806	1.818	2.115	2.052
Ca	0.223	0.155	0.121	0.207	0.174	0.164	0.096	0.211	0.173	0.169	0.093	0.180	0.215	0.232
Na	0.161	0.355	0.332	0.429	0.256	0.200	0.318	0.331	0.375	0.228	0.251	0.207	0.120	0.181
K	0.004	0.005	0.000	-0.000	0.004	0.039	0.000	0.066	0.006	0.035	0.000	0.000	0.000	0.032
P	0.034	0.000	0.000	0.000	0.032	0.000	0.000	0.000	0.000	0.000	0.038	0.031	0.036	0.000
S	0.027	0.008	0.025	0.059	0.008	0.000	0.000	0.000	0.065	0.000	0.041	0.092	0.073	0.010
O	20.515	21.572	20.514	22.093	23.149	20.307	21.274	22.295	22.863	21.699	19.993	19.790	24.762	27.032
TOTAL	55.711	59.211	55.776	60.564	62.078	54.702	58.169	60.976	61.893	59.013	53.945	53.556	67.532	73.589
BerthCalc.														
Si	3.337	3.260	3.313	3.263	3.344	3.326	3.266	3.320	3.299	3.267	3.345	3.344	3.217	3.119
Al(T)	0.663	0.740	0.687	0.737	0.656	0.674	0.734	0.680	0.701	0.733	0.655	0.656	0.783	0.881
Al(O)	0.942	0.844	0.918	0.867	0.989	0.980	0.883	0.869	0.912	0.954	1.021	0.977	0.992	1.098
Ti	0.006	0.009	0.007	0.011	0.000	0.000	0.000	0.000	0.000	0.012	0.000	0.014	0.005	0.000
Fe	3.994	4.109	3.966	4.065	3.774	3.832	4.076	4.055	3.859	3.992	3.869	3.901	4.048	4.010
Mn	0.000	0.011	0.007	0.000	0.000	0.004	0.000	0.013	0.000	0.000	0.026	0.000	0.000	0.000
Mg	0.832	0.845	0.867	0.833	0.990	0.932	0.868	0.835	1.000	0.821	0.836	0.850	0.790	0.700
Ca	0.041	0.040	0.033	0.052	0.025	0.045	0.025	0.053	0.042	0.044	0.003	0.032	0.031	0.048
Na	0.077	0.160	0.158	0.189	0.108	0.096	0.146	0.145	0.160	0.102	0.123	0.102	0.047	0.065
K	0.001	0.001	0.000	0.000	0.001	0.011	0.000	0.017	0.002	0.009	0.000	0.000	0.000	0.007
OCT.	5.775	5.818	5.765	5.777	5.754	5.748	5.827	5.772	5.771	5.779	5.752	5.742	5.835	5.808
INT.	0.119	0.202	0.191	0.242	0.134	0.152	0.171	0.214	0.204	0.155	0.126	0.134	0.078	0.120
CH	8.000	8.000	8.000	8.000	8.000	8.000	8.000	8.000	8.000	8.000	8.000	8.000	8.000	8.000

Table D.4. (Continued).

	Y183. 3 (Cont.)			YAR. 7					
	6	7	8	1	2	3	4	5	6
Si	9.358	10.102	10.005	8.668	8.064	8.516	9.249	9.095	8.900
Ti	0.036	0.000	0.000	0.000	0.000	0.088	0.000	0.001	0.080
Al	4.775	5.230	5.246	4.428	4.055	7.171	4.535	4.371	4.495
Fe	23.013	24.747	26.002	20.033	17.492	18.472	20.924	20.448	20.201
Mn	0.054	0.081	0.000	0.070	0.000	0.068	0.105	0.000	0.082
Mg	2.052	2.031	2.158	1.982	1.718	1.967	2.051	1.930	2.071
Ca	0.235	0.156	0.192	0.364	0.375	0.356	0.435	0.517	0.396
Na	0.105	0.349	0.295	0.016	0.000	0.186	0.283	0.202	0.219
K	0.000	0.085	0.000	0.105	0.000	0.051	0.012	0.000	0.019
P	0.000	0.000	0.000	0.000	0.065	0.000	0.000	0.000	0.000
S	0.003	0.000	0.000	0.000	0.024	0.039	0.000	0.051	0.000
O	23.022	24.813	25.113	21.050	19.170	20.294	22.221	21.655	21.603
TOTAL	62.653	67.594	69.011	56.716	50.963	57.208	59.815	58.270	58.066
BerthCalc.									
Si	3.242	3.247	3.177	3.284	3.375	2.959	3.320	3.352	3.286
Al(T)	0.758	0.753	0.823	0.716	0.625	1.041	0.680	0.648	0.714
Al(O)	0.964	0.997	0.911	1.030	1.141	1.552	1.014	1.028	1.013
Ti	0.007	0.000	0.000	0.000	0.000	0.018	0.000	0.000	0.017
Fe	4.009	4.000	4.153	3.817	3.677	3.222	3.777	3.781	3.751
Mn	0.010	0.013	0.000	0.014	0.000	0.012	0.019	0.000	0.015
Mg	0.821	0.754	0.792	0.868	0.831	0.790	0.851	0.822	0.883
Ca	0.057	0.035	0.043	0.097	0.094	0.087	0.109	0.133	0.102
Na	0.044	0.137	0.114	0.007	0.000	0.079	0.124	0.091	0.099
K	0.000	0.020	0.000	0.029	0.000	0.013	0.003	0.000	0.005
OCT.	5.811	5.765	5.856	5.728	5.649	5.594	5.660	5.631	5.679
INT.	0.101	0.192	0.157	0.133	0.094	0.178	0.237	0.224	0.206
OH	8.000	8.000	8.000	8.000	8.000	8.000	8.000	8.000	8.000

Table D.5. Compositions of Berthierine Cements Replacing Shell Fragments. The Data have been Recalculated to Berthierine Structural Formulae.

	YAR. 7										YAR. 21		YAR. 24						
	1	2	3	4	5	6	7	8	9	10	1	2	1	2	3	4	5	6	7
Si	10.343	10.183	12.178	9.513	8.611	8.776	9.361	9.648	11.038	12.148	11.796	11.176	11.570	11.065	11.546	11.266	10.386	4.989	8.936
Ti	0.008	0.083	0.000	0.000	0.000	0.000	0.031	0.011	0.000	0.075	0.078	0.000	0.000	0.000	0.025	0.036	0.000	0.000	0.000
Al	4.947	4.977	5.966	4.615	4.074	4.340	4.596	4.745	5.335	6.089	6.319	6.146	6.598	6.267	5.904	5.600	5.314	2.892	4.588
Fe	24.449	24.642	28.568	21.165	19.282	19.947	22.348	22.323	28.607	30.081	28.888	26.566	28.294	27.866	28.967	28.601	24.249	10.735	20.333
Mn	0.000	0.000	0.000	0.000	0.000	0.000	0.165	0.060	0.000	0.000	0.040	0.063	0.031	0.000	0.000	0.021	0.000	0.269	0.000
Mg	2.177	2.162	2.412	2.122	1.841	1.937	2.059	2.033	2.336	2.667	2.673	2.403	2.103	2.083	2.445	2.199	2.082	1.294	1.967
Ca	0.523	0.619	0.504	0.539	0.523	0.326	0.299	0.342	2.641	0.485	0.825	0.697	2.943	3.481	0.506	0.851	0.485	4.703	0.592
Na	0.329	0.023	0.263	0.393	0.153	0.216	0.195	0.249	0.503	0.000	0.480	0.328	0.203	0.232	0.318	0.000	0.000	0.137	0.054
K	0.041	0.074	0.175	0.010	0.030	0.022	0.078	0.070	0.195	0.145	0.160	0.263	0.259	0.227	0.087	0.147	0.000	0.000	0.133
P	0.000	0.000	0.050	0.000	0.000	0.011	0.000	0.000	1.008	0.000	0.000	0.000	0.984	1.398	0.001	0.049	0.000	0.000	0.000
S	0.022	0.000	0.122	0.033	0.085	0.012	0.000	0.038	0.063	0.040	0.094	0.130	0.057	0.117	0.075	0.041	0.010	0.000	0.039
O	24.958	24.836	29.345	22.756	20.438	21.072	22.782	23.206	29.625	29.901	29.688	27.856	31.118	30.856	28.662	27.921	25.069	14.187	21.662
TOTAL	67.797	67.599	79.583	61.146	55.037	56.659	61.914	62.725	81.351	81.631	81.041	75.628	84.160	83.592	78.536	76.732	67.595	39.206	58.304
BerthCalc.																			
Si	3.306	3.270	3.322	3.335	3.364	3.325	3.277	3.317	3.149	3.241	3.171	3.203	3.129	3.092	3.215	3.229	3.304	2.805	3.291
Al(T)	0.694	0.730	0.678	0.665	0.636	0.675	0.723	0.683	0.851	0.759	0.829	0.797	0.871	0.908	0.785	0.771	0.696	1.195	0.709
Al(O)	0.951	0.933	1.016	1.019	1.020	1.036	0.951	1.015	0.732	0.932	0.940	1.037	0.985	0.915	0.926	0.899	1.064	0.497	1.050
Ti	0.001	0.016	0.000	0.000	0.000	0.000	0.006	0.002	0.000	0.012	0.012	0.000	0.000	0.000	0.004	0.006	0.000	0.000	0.000
Fe	3.927	3.980	3.905	3.727	3.773	3.799	3.934	3.854	4.096	4.032	3.895	3.813	3.841	3.902	4.047	4.117	3.879	3.035	3.760
Mn	0.000	0.000	0.000	0.000	0.000	0.000	0.030	0.011	0.000	0.000	0.005	0.009	0.004	0.000	0.000	0.003	0.000	0.077	0.000
Mg	0.804	0.802	0.760	0.860	0.831	0.848	0.833	0.808	0.770	0.822	0.830	0.796	0.657	0.673	0.787	0.728	0.765	0.841	0.837
Ca	0.117	0.139	0.088	0.132	0.143	0.084	0.073	0.082	0.354	0.091	0.155	0.140	0.397	0.445	0.099	0.162	0.108	1.852	0.153
Na	0.128	0.009	0.088	0.168	0.073	0.100	0.083	0.105	0.175	0.000	0.158	0.115	0.067	0.079	0.108	0.000	0.000	0.094	0.024
K	0.009	0.017	0.034	0.003	0.008	0.006	0.020	0.017	0.040	0.028	0.031	0.054	0.050	0.046	0.017	0.030	0.000	0.000	0.035
OCT.	5.684	5.731	5.682	5.605	5.624	5.683	5.755	5.689	5.598	5.797	5.683	5.655	5.488	5.489	5.764	5.753	5.708	4.450	5.647
INT.	0.255	0.165	0.210	0.303	0.225	0.190	0.176	0.204	0.569	0.118	0.344	0.309	0.514	0.570	0.224	0.193	0.108	1.946	0.212
OH	8.000	8.000	8.000	8.000	8.000	8.000	8.000	8.000	8.000	8.000	8.000	8.000	8.000	8.000	8.000	8.000	8.000	8.000	8.000

Table D.6. Compositions of Berthierine Ooids. The Data have been Recalculated to Berthierine Structural Formulae.

	YAR. 30												
	BERTH OOID 1 (LINE)											BERTH OOID 2 (LINE)	
	1	2	3	4	5	6	7	8	9	10	11	1	2
Si	12.605	9.935	9.282	9.980	8.761	8.841	8.909	9.705	9.221	9.851	10.289	9.038	8.612
Ti	0.202	0.124	0.066	0.069	0.065	0.105	0.038	0.134	0.132	0.159	0.376	0.125	0.106
Al	7.325	5.875	5.539	6.106	5.055	5.049	5.102	5.172	4.487	4.709	5.258	5.381	5.274
Fe	16.474	16.585	16.566	17.867	15.780	14.738	15.775	17.424	15.277	15.251	15.769	18.618	15.877
Mn	0.040	0.031	0.019	0.000	0.000	0.104	0.000	0.098	0.000	0.007	0.018	0.000	0.141
Mg	1.892	1.982	1.807	2.087	1.675	1.652	1.718	2.015	1.770	1.648	2.081	1.772	1.759
Ca	0.622	0.574	0.375	0.400	0.469	0.434	0.596	0.321	0.336	0.396	0.350	0.259	0.285
Na	0.026	0.138	0.382	0.278	0.125	0.056	0.226	0.168	0.153	0.154	0.355	0.160	0.168
K	1.191	0.578	0.371	0.435	0.432	0.433	0.379	0.410	0.646	0.671	0.784	0.163	0.251
P	0.208	0.250	0.000	0.074	0.132	0.170	0.234	0.074	0.028	0.000	0.000	0.000	0.000
S	0.041	0.076	0.018	0.055	0.032	0.007	0.000	0.031	0.120	0.084	0.063	0.077	0.036
O	27.756	23.410	21.844	23.781	20.632	20.474	21.058	22.459	20.482	21.323	22.965	21.859	20.545
TOTAL	68.382	59.558	56.269	61.132	53.158	52.063	54.035	58.011	52.652	54.253	58.308	57.452	53.054
BerthCalc.													
Si	3.683	3.467	3.389	3.372	3.435	3.507	3.457	3.472	3.606	3.688	3.575	3.300	3.345
Al(T)	0.317	0.533	0.611	0.628	0.565	0.493	0.543	0.528	0.394	0.312	0.425	0.700	0.655
Al(O)	1.910	1.601	1.495	1.518	1.498	1.591	1.517	1.398	1.433	1.523	1.477	1.346	1.476
Ti	0.035	0.025	0.014	0.014	0.015	0.024	0.009	0.028	0.030	0.035	0.077	0.027	0.024
Fe	2.415	2.899	3.039	3.028	3.106	2.939	3.078	3.130	2.984	2.858	2.746	3.407	3.095
Mn	0.006	0.006	0.004	0.000	0.000	0.021	0.000	0.018	0.000	0.001	0.003	0.000	0.028
Mg	0.639	0.799	0.762	0.815	0.759	0.757	0.770	0.833	0.800	0.713	0.836	0.748	0.789
Ca	0.035	0.009	0.096	0.057	0.051	0.019	0.025	0.040	0.076	0.104	0.085	0.066	0.078
Na	0.009	0.059	0.170	0.115	0.060	0.027	0.107	0.073	0.073	0.070	0.151	0.071	0.080
K	0.250	0.145	0.097	0.106	0.122	0.123	0.106	0.105	0.182	0.181	0.196	0.043	0.070
OCT.	5.004	5.330	5.314	5.374	5.377	5.333	5.374	5.407	5.247	5.130	5.139	5.527	5.413
INT.	0.295	0.212	0.364	0.277	0.232	0.169	0.238	0.219	0.330	0.355	0.432	0.180	0.227
OH	8.000	8.000	8.000	8.000	8.000	8.000	8.000	8.000	8.000	8.000	8.000	8.000	8.000

Table D.6. (Continued).

	BERTH OOID 1 (LINE CONTINUED)				>nucleus		BERTH OOID 3 (LINE)						
	3	4	5	6	7	8	1	2	3	4	5	6	7
Si	9.408	7.250	8.671	7.519	7.940	7.049	8.334	6.924	7.775	7.323	7.981	8.560	7.429
Ti	0.152	0.011	0.123	0.195	0.083	0.102	0.068	0.103	0.150	0.105	0.091	0.061	0.020
Al	5.736	4.438	5.148	3.633	4.902	4.396	4.949	4.433	4.736	4.552	4.949	5.008	4.617
Fe	16.937	12.093	16.081	9.327	12.685	13.039	13.205	12.678	13.153	12.024	13.478	16.028	11.294
Mn	0.046	0.143	0.026	0.000	0.050	0.000	0.000	0.039	0.101	0.000	0.003	0.093	0.107
Mg	1.807	1.342	1.730	0.839	1.374	1.516	1.425	1.583	1.564	1.463	1.672	1.741	1.161
Ca	0.332	0.288	0.250	11.274	0.259	0.218	0.395	0.232	0.205	0.197	0.209	0.244	0.220
Na	0.165	0.270	0.355	0.457	0.192	0.301	0.018	0.345	0.221	0.000	0.162	0.228	0.146
K	0.484	0.342	0.310	0.396	0.376	0.199	0.553	0.258	0.339	0.313	0.417	0.311	0.557
P	0.048	0.000	0.000	0.007	0.013	0.013	0.254	0.022	0.003	0.034	0.026	0.031	0.025
S	0.100	0.094	0.051	0.115	0.060	0.044	0.053	0.043	0.036	0.000	0.003	0.106	0.094
O	22.328	16.882	20.579	19.902	18.279	16.991	19.269	16.878	18.229	17.057	18.777	20.293	16.899
TOTAL	57.543	43.153	53.324	53.664	46.213	43.868	48.523	43.538	46.512	43.068	47.768	52.704	42.569
BerthCalc.													
Si	3.380	3.430	3.362	3.020	3.473	3.316	3.553	3.283	3.404	3.439	3.400	3.380	3.522
Al(T)	0.620	0.570	0.638	0.980	0.527	0.684	0.447	0.717	0.596	0.561	0.600	0.620	0.478
Al(O)	1.525	1.615	1.440	0.539	1.704	1.469	1.749	1.470	1.563	1.664	1.595	1.438	1.800
Ti	0.032	0.003	0.028	0.046	0.021	0.028	0.017	0.029	0.039	0.029	0.023	0.014	0.006
Fe	3.044	2.858	3.127	1.864	2.779	3.076	2.821	3.014	2.890	2.840	2.887	3.164	2.673
Mn	0.008	0.035	0.005	0.000	0.011	0.000	0.000	0.009	0.023	0.000	0.001	0.019	0.026
Mg	0.750	0.733	0.775	0.389	0.694	0.824	0.702	0.867	0.791	0.794	0.823	0.794	0.636
Ca	0.058	0.095	0.068	3.168	0.071	0.063	-0.046	0.061	0.061	0.041	0.046	0.049	0.055
Na	0.072	0.156	0.168	0.224	0.103	0.173	0.009	0.200	0.118	0.000	0.084	0.110	0.085
K	0.125	0.116	0.086	0.114	0.118	0.067	0.169	0.088	0.107	0.106	0.128	0.088	0.190
OCT.	5.360	5.243	5.376	2.837	5.209	5.397	5.289	5.390	5.305	5.326	5.328	5.429	5.141
INT.	0.255	0.368	0.322	3.507	0.291	0.303	0.133	0.349	0.286	0.146	0.258	0.247	0.329
CH	8.000	8.000	8.000	8.000	8.000	8.000	8.000	8.000	8.000	8.000	8.000	8.000	8.000

Table D.6. (Continued).

				Y183. 8									
		>nucleus		BERTH OOIDS (10 in TOTAL)									
	8	9	10	1	2	3	4	5	6	7	8	9	10
Si	9.049	11.084	10.048	11.829	10.292	12.376	10.548	14.420	10.862	11.759	12.498	11.233	11.189
Ti	0.128	0.058	0.000	0.221	0.142	0.269	1.066	0.758	0.174	0.198	0.120	0.291	0.339
Al	4.876	5.734	5.487	7.465	6.493	8.039	6.766	8.556	7.087	7.601	8.281	7.369	7.347
Fe	15.065	25.966	23.109	19.851	25.033	19.851	15.225	15.830	20.977	16.988	25.705	19.882	19.309
Mn	0.085	0.000	0.033	0.100	0.000	0.000	0.164	0.000	0.000	0.065	0.117	0.004	0.000
Mg	1.754	2.193	2.222	1.792	1.752	1.875	1.466	1.866	1.782	1.775	1.867	1.844	1.841
Ca	0.253	0.291	0.257	0.328	0.212	0.319	0.377	0.518	0.325	0.257	0.365	0.300	0.365
Na	0.191	0.000	0.120	0.359	0.261	0.423	0.577	0.471	0.268	0.382	0.043	0.352	0.289
K	0.488	0.005	0.032	0.735	0.065	0.880	0.713	1.648	0.493	1.066	0.404	0.575	0.555
P	0.063	0.000	0.000	0.000	0.000	0.031	0.042	0.073	0.000	0.046	0.000	0.028	0.003
S	0.019	0.029	0.047	0.000	0.056	0.001	0.112	0.046	0.009	0.073	0.003	0.000	0.043
O	20.575	26.765	24.570	27.566	26.109	28.845	24.673	31.110	26.300	26.856	30.555	26.853	26.615
TOTAL	52.546	72.125	65.925	70.246	70.415	72.909	61.729	75.296	68.277	67.066	79.958	68.731	67.895
BerthCalc.													
Si	3.532	3.304	3.263	3.422	3.146	3.430	3.426	3.717	3.294	3.507	3.262	3.344	3.355
Al(T)	0.468	0.696	0.737	0.578	0.854	0.570	0.574	0.283	0.706	0.493	0.738	0.656	0.645
Al(O)	1.512	1.082	1.117	1.670	1.211	1.748	1.713	2.012	1.531	1.867	1.512	1.627	1.648
Ti	0.029	0.010	0.000	0.037	0.025	0.044	0.203	0.115	0.031	0.035	0.018	0.051	0.060
Fe	2.954	3.888	3.767	2.888	3.840	2.767	2.471	2.047	3.198	2.539	3.374	2.976	2.906
Mn	0.017	0.000	0.005	0.015	0.000	0.000	0.027	0.000	0.000	0.010	0.016	0.001	0.000
Mg	0.791	0.755	0.834	0.599	0.619	0.600	0.550	0.556	0.624	0.612	0.563	0.634	0.638
Ca	0.032	0.061	0.058	0.066	0.045	0.049	0.065	0.065	0.069	0.033	0.067	0.050	0.075
Na	0.091	0.000	0.048	0.127	0.097	0.143	0.229	0.148	0.099	0.139	0.014	0.128	0.106
K	0.137	0.001	0.007	0.153	0.014	0.175	0.166	0.305	0.107	0.228	0.076	0.123	0.120
OCT.	5.303	5.736	5.724	5.210	5.695	5.159	4.965	4.729	5.384	5.062	5.483	5.289	5.251
INT.	0.260	0.062	0.114	0.346	0.157	0.367	0.460	0.519	0.276	0.401	0.156	0.301	0.301
CH	8.000	8.000	8.000	8.000	8.000	8.000	8.000	8.000	8.000	8.000	8.000	8.000	8.000

Table D.7. Compositions of Berthierine Peloids in Y183.8, and Flakes in YAR.2. The Data have been Recalculated to Berthierine Structural Formulae.

	Y183. 8				YAR. 2						
	BERTH. PELOIDS				BERTH. FLAKES						
	1	2	3	4	1	2	3	4	5	6	7
Si	3.986	3.383	3.378	2.485	3.698	2.908	3.203	3.703	3.361	3.542	3.135
Ti	0.000	0.020	0.000	0.003	0.043	0.349	0.011	0.084	0.000	0.000	0.019
Al	2.398	2.015	2.101	1.547	1.938	1.570	1.725	2.377	1.785	2.080	1.646
Fe	8.976	7.732	7.558	5.494	8.823	6.530	8.940	6.029	8.945	9.406	8.110
Mn	0.000	0.044	0.000	0.069	0.557	0.847	0.556	0.524	0.730	0.443	0.602
Mg	0.462	0.485	0.591	0.515	0.949	0.693	0.811	0.847	0.850	1.078	0.923
Ca	25.066	26.500	26.282	30.384	22.777	26.222	22.863	23.981	23.557	24.054	22.965
Na	0.651	0.888	0.908	0.893	0.180	0.267	0.072	0.208	0.050	0.217	0.077
K	0.216	0.174	0.204	0.126	0.174	0.129	0.000	0.371	0.087	0.064	0.000
P	10.032	10.362	10.131	11.390	0.106	0.334	1.555	0.569	0.000	0.420	0.473
S	0.163	0.183	0.202	0.254	0.001	0.000	0.017	0.017	0.022	0.009	0.007
O	32.785	32.513	32.206	33.318	18.608	18.535	19.608	19.282	18.191	19.652	17.958
TOTAL	84.735	84.299	83.561	86.478	57.854	58.384	59.361	57.992	57.578	60.965	55.915
BerthCalc.											
Si	2.851	2.655	2.604	2.268	1.605	1.302	1.572	1.636	1.474	1.507	1.476
Al(T)	1.149	1.345	1.396	1.732	2.395	2.698	2.428	2.364	2.526	2.493	2.524
Al(O)	0.637	0.300	0.289	-0.262	-1.520	-1.967	-1.548	-1.271	-1.711	-1.572	-1.717
Ti	0.000	0.009	0.000	0.002	0.011	0.092	0.003	0.022	0.000	0.000	0.005
Fe	3.178	2.989	2.861	2.420	1.925	1.470	2.202	1.336	1.969	2.011	1.919
Mn	0.000	0.018	0.000	0.032	0.124	0.194	0.139	0.118	0.164	0.096	0.145
Mg	0.382	0.440	0.526	0.543	0.476	0.358	0.460	0.432	0.431	0.530	0.502
Ca	1.719	2.283	2.394	3.721	6.856	7.999	6.706	7.043	7.239	6.901	7.239
Na	0.569	0.851	0.855	0.995	0.095	0.146	0.043	0.112	0.027	0.113	0.044
K	0.111	0.098	0.113	0.083	0.054	0.041	0.000	0.118	0.027	0.020	0.000
OCT.	4.197	3.756	3.676	2.735	1.016	0.148	1.257	0.638	0.852	1.066	0.854
INT.	2.399	3.232	3.361	4.800	7.005	8.187	6.749	7.273	7.293	7.033	7.283
CH	8.000	8.000	8.000	8.000	8.000	8.000	8.000	8.000	8.000	8.000	8.000

Table D.8. Compositions of Authigenic Calcites, Various Thin-sections. The Data have been Recalculated to Calcite Formulae.

	DRAG. 31.1										DRAG. 31.2				
	Rep. Bio.										Rep. Bio.				
	1	2	3	4	5	6	7	8	9	10	1	2	3	4	5
Ca	37.111	37.900	38.321	35.315	38.993	36.070	36.816	35.827	36.504	35.890	36.617	37.107	36.544	36.546	36.415
P	0.000	0.000	0.040	0.000	0.020	0.000	0.000	0.000	0.000	0.000	0.000	0.004	0.012	0.000	0.039
Sr	0.154	0.106	0.067	0.023	0.085	0.060	0.027	0.041	0.037	0.046	0.055	0.038	0.042	0.056	0.052
Si	0.043	0.060	0.024	0.000	0.022	0.044	0.027	0.012	0.012	0.110	0.015	0.019	0.086	0.014	0.019
Al	0.014	0.020	0.000	0.002	0.000	0.019	0.006	0.000	0.000	0.079	0.005	0.005	0.051	0.003	0.002
Mg	0.268	0.158	0.138	0.377	0.269	0.304	0.367	0.368	0.344	0.351	0.360	0.282	0.367	0.317	0.376
Na	0.213	0.267	0.215	0.037	0.257	0.092	0.041	0.017	0.024	0.044	0.005	0.022	0.008	0.011	0.019
Fe	0.143	0.243	0.118	1.493	0.110	1.514	1.668	1.688	1.714	1.600	1.701	1.199	1.596	1.240	1.619
Mn	0.019	0.073	0.025	0.710	0.012	0.719	0.714	0.917	0.826	0.683	0.410	0.449	0.289	0.419	0.294
O	15.201	15.523	15.595	15.000	15.935	15.353	15.692	15.322	15.559	15.435	15.494	15.519	15.541	15.308	15.423
TOTAL	53.166	54.350	54.543	52.957	55.703	54.175	55.378	54.192	55.020	54.238	54.662	54.644	54.536	53.914	54.258
CarbCalc.															
Ca	0.979	0.980	0.986	0.940	0.980	0.942	0.939	0.934	0.937	0.940	0.945	0.956	0.948	0.954	0.947
Fe	0.003	0.005	0.002	0.029	0.002	0.028	0.031	0.032	0.032	0.030	0.032	0.022	0.030	0.023	0.030
Mn	0.000	0.001	0.000	0.014	0.000	0.014	0.013	0.017	0.015	0.013	0.008	0.008	0.005	0.008	0.006
Mg	0.012	0.007	0.006	0.017	0.011	0.013	0.016	0.016	0.015	0.015	0.015	0.012	0.016	0.014	0.016
Sr	0.002	0.001	0.001	0.000	0.001	0.001	0.000	0.000	0.000	0.001	0.001	0.000	0.000	0.001	0.001
Na	0.010	0.012	0.010	0.002	0.011	0.004	0.002	0.001	0.001	0.002	0.000	0.001	0.000	0.001	0.001

	DRAG. 31.7					DRAG. 31.10											
	Rep. Bio.					GEN. 1 (Scalenohedral)			GEN. 2 (Pore-fill)				Ech. Overth.		GEN. 1 (Fibrous)		
	1	2	3	4	5	1	2	3	1	2	3	4	1	2	1	2	3
Ca	37.589	38.535	37.267	37.139	38.159	37.632	37.816	37.357	37.320	37.115	37.313	36.788	37.301	37.400	37.265	37.615	37.762
P	0.000	0.000	0.002	0.000	0.000	0.000	0.011	0.000	0.000	0.000	0.000	0.000	0.000	0.000	0.000	0.033	0.000
Sr	0.009	0.038	0.055	0.065	0.040	0.032	0.041	0.036	0.045	0.030	0.032	0.055	0.040	0.032	0.039	0.044	0.036
Si	0.007	0.011	0.032	0.011	0.005	0.012	0.016	0.007	0.007	0.012	0.003	0.008	0.008	0.006	0.009	0.012	0.016
Al	0.004	0.006	0.013	0.000	0.000	0.007	0.000	0.000	0.003	0.005	0.024	0.000	0.000	0.001	0.000	0.000	0.000
Mg	0.122	0.539	0.319	0.363	0.151	0.157	0.152	0.130	0.101	0.118	0.113	0.115	0.128	0.149	0.172	0.136	0.160
Na	0.000	0.000	0.000	0.000	0.000	0.043	0.000	0.002	0.004	0.011	0.000	0.011	0.017	0.006	0.023	0.014	0.027
Fe	0.528	1.618	1.543	1.428	0.838	0.679	0.746	0.619	0.512	0.603	0.648	0.700	0.513	0.705	0.818	0.759	0.820
Mn	1.953	0.530	0.399	0.530	0.700	1.421	1.032	1.067	1.474	1.677	1.623	1.673	1.545	1.444	0.917	1.214	0.874
O	15.820	16.381	15.705	15.653	15.790	15.775	15.751	15.502	15.560	15.583	15.659	15.473	15.595	15.667	15.516	15.746	15.704
TOTAL	56.032	57.658	55.335	55.189	55.683	55.758	55.565	54.720	55.026	55.154	55.415	54.823	55.147	55.410	54.759	55.573	55.399
CarbCalc.																	
Ca	0.949	0.940	0.950	0.948	0.965	0.953	0.960	0.962	0.958	0.952	0.953	0.950	0.955	0.953	0.959	0.957	0.961
Fe	0.010	0.028	0.028	0.026	0.015	0.012	0.014	0.011	0.009	0.011	0.012	0.013	0.009	0.013	0.015	0.014	0.015
Mn	0.036	0.009	0.007	0.010	0.013	0.026	0.019	0.020	0.028	0.031	0.030	0.032	0.029	0.027	0.017	0.023	0.016
Mg	0.005	0.022	0.013	0.015	0.006	0.007	0.006	0.006	0.004	0.005	0.005	0.005	0.005	0.006	0.007	0.006	0.007
Sr	0.000	0.000	0.001	0.001	0.000	0.000	0.000	0.000	0.001	0.000	0.000	0.001	0.000	0.000	0.000	0.001	0.000
Na	0.000	0.000	0.000	0.000	0.000	0.002	0.000	0.000	0.000	0.000	0.000	0.000	0.001	0.000	0.001	0.001	0.001

Table D.8. (Continued).

	DRAG. 31.10 (Cont.)												DRAG. 31.23					
	GEN. 2 (Pore-fill)							Line into Large Bioclast.					GEN. 1 (Rep. Bio.)			GEN. 2 (Rep.Bio.)		
	1	2	3	4	5	6	7	1	2	3	4	5	1	2	3	1	2	3
Ca	37.633	37.598	37.661	37.385	36.993	36.667	37.374	37.480	37.315	37.145	36.317	36.653	41.636	37.842	37.473	38.355	37.612	38.659
P	0.000	0.000	0.000	0.000	0.000	0.049	0.000	0.000	0.039	0.048	0.014	0.014	0.000	0.000	0.000	0.000	0.001	0.000
Sr	0.028	0.051	0.042	0.031	0.050	0.048	0.051	0.048	0.050	0.059	0.019	0.032	0.132	0.127	0.102	0.068	0.068	0.073
Si	0.005	0.013	0.012	0.016	0.011	0.017	0.006	0.012	0.046	0.018	0.011	0.010	0.001	0.000	0.000	0.001	0.007	0.001
Al	0.002	0.001	0.004	0.000	0.000	0.003	0.000	0.000	0.001	0.000	0.000	0.000	0.005	0.000	0.000	0.004	0.000	0.001
Mg	0.121	0.225	0.295	0.139	0.400	0.173	0.164	0.223	0.208	0.141	0.099	0.138	0.440	0.442	0.327	0.142	0.132	0.117
Na	0.019	0.007	0.015	0.000	0.021	0.014	0.013	0.001	0.007	0.011	0.020	0.006	0.024	0.020	0.032	0.014	0.006	0.008
Fe	0.865	1.063	1.192	0.685	1.152	1.138	1.032	0.847	0.908	0.787	0.564	0.596	0.906	0.869	0.743	0.960	0.840	0.809
Mn	0.859	1.197	0.799	0.786	0.584	1.041	0.986	1.043	1.104	1.641	1.551	1.705	0.944	0.810	0.917	1.655	1.441	1.533
O	15.620	15.838	15.833	15.464	15.560	15.479	15.631	15.678	15.729	15.721	15.218	15.428	17.483	15.913	15.684	16.184	15.785	16.206
TOTAL	55.152	55.993	55.853	54.506	54.771	54.629	55.257	55.332	55.407	55.571	53.813	54.582	61.571	56.023	55.278	57.383	55.892	57.407
CarbCalc.																		
Ca	0.962	0.949	0.951	0.966	0.950	0.951	0.955	0.955	0.953	0.948	0.955	0.950	0.951	0.949	0.954	0.946	0.952	0.952
Fe	0.016	0.019	0.022	0.013	0.021	0.021	0.019	0.015	0.017	0.014	0.011	0.011	0.015	0.016	0.014	0.017	0.015	0.014
Mn	0.016	0.022	0.015	0.015	0.011	0.020	0.018	0.019	0.021	0.031	0.030	0.032	0.016	0.015	0.017	0.030	0.027	0.028
Mg	0.005	0.009	0.012	0.006	0.017	0.007	0.007	0.009	0.009	0.006	0.004	0.006	0.017	0.018	0.014	0.006	0.006	0.005
Sr	0.000	0.001	0.000	0.000	0.001	0.001	0.001	0.001	0.001	0.001	0.000	0.000	0.001	0.001	0.001	0.001	0.001	0.001
Na	0.001	0.000	0.001	0.000	0.001	0.001	0.001	0.000	0.000	0.000	0.001	0.000	0.001	0.001	0.001	0.001	0.000	0.000

	DRAG. 31.23 (Cont.)			Y183. 10									Y183. 13			
	Cementing Ooids			Cements					Rep. Bio.				Ferroan Calcite			
	1	2	3	1	2	3	4	5	1	2	3	4	1	2	3	4
Ca	37.069	38.312	36.744	36.883	35.733	36.320	37.637	31.601	36.210	35.481	36.178	35.574	35.712	37.614	37.863	39.050
P	0.000	0.000	0.019	0.003	0.020	0.000	0.006	0.000	0.000	0.000	0.011	0.021	0.000	0.000	0.057	0.082
Sr	0.045	0.068	0.063	0.027	0.043	0.045	0.032	0.034	0.035	0.000	0.031	0.034	0.042	0.037	0.044	0.070
Si	0.009	0.002	0.000	0.361	0.370	0.485	0.114	2.124	0.013	0.000	0.605	0.004	0.435	0.240	0.052	0.001
Al	0.005	0.005	0.001	0.223	0.252	0.228	0.073	1.399	0.007	0.000	0.382	0.014	0.230	0.135	0.034	0.000
Mg	0.077	0.097	0.471	0.208	0.196	0.197	0.224	0.703	0.252	0.294	0.203	0.250	0.204	0.178	0.159	0.118
Na	0.024	0.015	0.009	0.064	0.003	0.020	0.010	0.049	0.000	0.000	0.022	0.020	0.057	0.030	0.013	0.000
Fe	0.759	0.770	0.913	1.383	1.526	1.261	1.231	4.028	1.574	1.717	1.604	1.556	1.443	1.246	0.892	1.096
Mn	1.570	1.575	1.023	0.615	0.421	0.567	0.358	0.333	0.248	0.252	0.480	0.223	0.540	0.704	0.813	0.173
O	15.554	16.061	15.578	16.076	15.634	15.925	15.841	18.017	15.172	14.923	16.231	14.934	15.690	16.107	15.887	16.151
TOTAL	55.112	56.905	54.821	55.843	54.198	55.048	55.526	58.288	53.511	52.667	55.747	52.630	54.353	56.291	55.814	56.741
CarbCalc.																
Ca	0.952	0.953	0.943	0.952	0.953	0.956	0.961	0.879	0.954	0.949	0.951	0.954	0.951	0.956	0.961	0.972
Fe	0.014	0.014	0.017	0.026	0.029	0.024	0.023	0.080	0.030	0.033	0.030	0.030	0.028	0.023	0.016	0.020
Mn	0.029	0.029	0.019	0.012	0.008	0.011	0.007	0.007	0.005	0.005	0.009	0.004	0.010	0.013	0.015	0.003
Mg	0.003	0.004	0.020	0.009	0.009	0.009	0.009	0.032	0.011	0.013	0.009	0.011	0.009	0.007	0.007	0.005
Sr	0.001	0.001	0.001	0.000	0.001	0.001	0.000	0.000	0.000	0.000	0.000	0.000	0.001	0.000	0.001	0.001
Na	0.001	0.001	0.000	0.003	0.000	0.001	0.000	0.002	0.000	0.000	0.001	0.001	0.003	0.001	0.001	0.000

Table D.8. (Continued).

	Y183. 13 (Cont.)										YAR. 2					
	Non-Ferroan										Line Across Replaced Bioclast (Radiaxial)					
	1	2	3	4	5	6	7	8	9	10	1	2	3	4	5	6
Ca	37.413	38.038	36.758	36.965	36.906	37.233	38.164	38.757	37.118	38.215	38.622	38.289	38.260	41.224	40.446	39.382
P	0.000	0.036	0.000	0.014	0.003	0.000	0.016	0.000	0.000	0.000	0.000	0.000	0.000	0.000	0.000	0.033
Sr	0.069	0.098	0.029	0.034	0.056	0.073	0.055	0.078	0.071	0.083	0.040	0.059	0.044	0.020	0.033	0.049
Si	0.008	0.024	0.099	0.010	0.004	0.017	0.006	0.001	0.002	0.008	0.008	0.006	0.009	0.000	0.003	0.003
Al	0.004	0.006	0.026	0.004	0.000	0.018	0.007	0.001	0.000	0.004	0.000	0.000	0.000	0.000	0.023	0.000
Mg	0.297	0.209	0.261	0.445	0.378	0.206	0.115	0.324	0.220	0.254	0.410	0.268	0.234	0.080	0.153	0.466
Na	0.014	0.227	0.022	0.019	0.015	0.014	0.000	0.000	0.003	0.000	0.003	0.002	0.017	0.006	0.000	0.008
Fe	0.000	0.000	0.000	0.000	0.000	0.000	0.006	0.017	0.012	0.003	1.398	1.427	1.315	0.769	0.872	1.832
Mn	0.000	0.000	0.000	0.000	0.000	0.000	0.003	0.002	0.000	0.010	0.809	2.584	2.470	1.141	1.264	0.216
O	15.161	15.449	14.995	15.095	15.006	15.053	15.357	15.706	14.982	15.454	16.341	16.642	16.548	17.068	16.894	16.675
TOTAL	52.966	54.087	52.190	52.586	52.368	52.614	53.729	54.886	52.408	54.031	57.631	59.277	58.897	60.308	59.688	58.664
CarbCalc.																
Ca	0.986	0.985	0.988	0.980	0.982	0.990	0.994	0.985	0.989	0.988	0.944	0.919	0.924	0.964	0.957	0.945
Fe	0.000	0.000	0.000	0.000	0.000	0.000	0.000	0.000	0.000	0.000	0.025	0.025	0.023	0.013	0.015	0.032
Mn	0.000	0.000	0.000	0.000	0.000	0.000	0.000	0.000	0.000	0.000	0.014	0.045	0.044	0.019	0.022	0.004
Mg	0.013	0.009	0.012	0.019	0.017	0.009	0.005	0.014	0.010	0.011	0.017	0.011	0.009	0.003	0.006	0.018
Sr	0.001	0.001	0.000	0.000	0.001	0.001	0.001	0.001	0.001	0.001	0.000	0.001	0.000	0.000	0.000	0.001
Na	0.001	0.010	0.001	0.001	0.001	0.001	0.000	0.000	0.000	0.000	0.000	0.000	0.001	0.000	0.000	0.000

	YAR. 2 (Cont.)										YAR. 21					
	GEN. 1 (Fibrous)			GEN. 2 (Line, Pore-filling Calcite)				Cementing Ooids			Line between ooids. 1					
	1	2	3	1	2	3	4	1	2	3	1	2	3	4	5	6
Ca	39.270	39.051	39.517	39.857	39.250	39.650	40.697	37.800	38.385	38.930	37.228	37.892	38.222	36.073	37.311	37.865
P	0.000	0.000	0.000	0.000	0.000	0.000	0.000	0.015	0.000	0.000	0.000	0.000	0.000	0.000	0.027	0.009
Sr	0.044	0.052	0.052	0.057	0.052	0.052	0.005	0.064	0.074	0.063	0.062	0.129	0.066	0.049	0.054	0.051
Si	0.002	0.004	0.005	0.003	0.002	0.001	0.000	0.000	0.011	0.007	0.001	0.006	0.002	0.282	0.000	0.002
Al	0.000	0.000	0.000	0.000	0.000	0.000	0.000	0.000	0.000	0.000	0.000	0.000	0.000	0.164	0.000	0.000
Mg	0.181	0.141	0.151	0.299	0.152	0.107	0.131	0.327	0.215	0.308	0.480	0.329	0.380	0.324	0.475	0.524
Na	0.013	0.022	0.003	0.000	0.004	0.008	0.018	0.008	0.003	0.032	0.011	0.014	0.000	0.009	0.003	0.000
Fe	1.078	0.972	0.997	1.274	0.774	0.735	0.808	1.039	1.291	1.468	1.704	1.224	1.458	1.736	1.650	1.586
Mn	1.153	1.016	1.161	0.779	1.889	1.651	0.838	0.506	2.472	0.632	0.381	0.350	0.686	0.569	0.544	0.427
O	16.455	16.278	16.515	16.714	16.554	16.603	16.816	15.784	16.582	16.379	15.793	15.830	16.140	15.756	15.884	16.063
TOTAL	58.196	57.536	58.401	58.983	58.677	58.807	59.313	55.543	59.033	57.819	55.660	55.774	56.954	54.962	55.948	56.527
CarbCalc.																
Ca	0.953	0.958	0.956	0.952	0.947	0.953	0.966	0.957	0.925	0.949	0.941	0.956	0.945	0.942	0.940	0.942
Fe	0.019	0.017	0.017	0.022	0.013	0.013	0.014	0.019	0.022	0.026	0.031	0.022	0.026	0.033	0.030	0.028
Mn	0.020	0.018	0.020	0.014	0.033	0.029	0.015	0.009	0.043	0.011	0.007	0.006	0.012	0.011	0.010	0.008
Mg	0.007	0.006	0.006	0.012	0.006	0.004	0.005	0.014	0.009	0.012	0.020	0.014	0.016	0.014	0.020	0.022
Sr	0.000	0.001	0.001	0.001	0.001	0.001	0.000	0.001	0.001	0.001	0.001	0.001	0.001	0.001	0.001	0.001
Na	0.001	0.001	0.000	0.000	0.000	0.000	0.001	0.000	0.000	0.001	0.000	0.001	0.000	0.000	0.000	0.000

Table D.8. (Continued).

	YAR. 21 (Cont.)															
	Line between ooids. 2						Line between ooids. 3					Line between ooids. 4				
	1	2	3	4	5	6	1	2	3	4	5	1	2	3	4	5
Ca	38.306	38.004	38.084	37.757	38.767	38.288	37.345	37.875	37.979	37.799	38.284	36.655	37.664	37.339	36.742	36.016
P	0.000	0.053	0.000	0.047	0.000	0.091	0.030	0.009	0.065	0.043	0.020	0.001	0.006	0.091	0.000	0.026
Sr	0.042	0.051	0.078	0.051	0.064	0.078	0.035	0.042	0.052	0.036	0.054	0.039	0.017	0.042	0.034	0.026
Si	0.000	0.000	0.001	0.005	0.000	0.020	0.000	0.000	0.000	0.000	0.000	0.000	0.001	0.000	0.000	0.012
Al	0.000	0.000	0.000	0.002	0.000	0.014	0.000	0.000	0.000	0.000	0.000	0.000	0.001	0.000	0.000	0.000
Mg	0.409	0.440	0.221	0.398	0.399	0.353	0.460	0.437	0.438	0.475	0.413	0.496	0.446	0.449	0.441	0.361
Na	0.000	0.000	0.005	0.000	0.005	0.013	0.016	0.004	0.008	0.016	0.014	0.029	0.016	0.020	0.015	0.118
Fe	1.507	1.471	1.306	1.237	1.173	1.381	1.695	1.600	1.670	1.711	1.541	1.734	1.529	1.558	1.591	1.604
Mn	0.470	0.370	0.789	0.528	0.691	0.259	0.554	0.448	0.503	0.533	0.503	0.242	0.324	0.296	0.407	0.528
O	16.137	16.068	15.970	15.920	16.289	16.160	15.909	16.016	16.170	16.116	16.184	15.544	15.880	15.865	15.543	15.321
TOTAL	56.871	56.457	56.454	55.945	57.388	56.657	56.044	56.431	56.885	56.729	57.013	54.740	55.884	55.660	54.773	54.012
CarbCalc.																
Ca	0.948	0.948	0.952	0.951	0.950	0.955	0.939	0.945	0.942	0.939	0.946	0.941	0.947	0.946	0.944	0.941
Fe	0.027	0.026	0.023	0.022	0.021	0.025	0.031	0.029	0.030	0.031	0.027	0.032	0.028	0.028	0.029	0.030
Mn	0.008	0.007	0.014	0.010	0.012	0.005	0.010	0.008	0.009	0.010	0.009	0.005	0.006	0.006	0.008	0.010
Mg	0.017	0.018	0.009	0.017	0.016	0.015	0.019	0.018	0.018	0.020	0.017	0.021	0.019	0.019	0.019	0.016
Sr	0.000	0.001	0.001	0.001	0.001	0.001	0.000	0.000	0.001	0.000	0.001	0.000	0.000	0.000	0.000	0.000
Na	0.000	0.000	0.000	0.000	0.000	0.001	0.001	0.000	0.000	0.001	0.001	0.001	0.001	0.001	0.001	0.005

Table D.9. Compositions of Calcite Cements Within Specimen AMM. 2. The Data have been Recalculated to Calcite Formulae.

	GEN. 1									GEN. 2								
	INNER			MIDDLE			OUTER											
	1	2	3	1	2	3	1	2	3	1	2	3	4	5	6	7	8	9
Ca	37.271	38.320	38.858	38.686	38.085	37.901	36.182	37.118	38.401	37.273	39.034	39.054	39.172	37.944	40.331	39.349	36.218	38.721
P	0.036	0.000	0.000	0.000	0.000	0.000	0.028	0.000	0.042	0.000	0.000	0.000	0.049	0.020	0.000	0.000	0.000	0.000
Sr	0.051	0.047	0.047	0.068	0.062	0.051	0.041	0.038	0.039	0.059	0.030	0.094	0.037	0.040	0.036	0.035	0.034	0.037
Si	0.000	0.000	0.000	0.000	0.000	0.000	0.000	0.010	0.000	0.000	0.000	0.000	0.000	0.000	0.000	0.000	0.000	0.000
Al	0.000	0.000	0.000	0.000	0.000	0.000	0.000	0.000	0.000	0.000	0.000	0.000	0.000	0.000	0.000	0.000	0.000	0.002
Mg	0.165	0.128	0.135	0.103	0.151	0.136	0.089	0.083	0.104	0.069	0.082	0.097	0.078	0.103	0.075	0.069	0.083	0.111
Na	0.008	0.022	0.010	0.018	0.007	0.018	0.012	0.009	0.007	0.001	0.014	0.000	0.007	0.007	0.010	0.005	0.002	0.010
Fe	0.742	0.759	0.752	0.656	0.819	0.781	0.575	0.572	0.618	0.541	0.469	0.721	0.594	0.644	0.508	0.597	0.592	0.728
Mn	0.750	0.742	0.699	0.641	0.712	0.788	0.772	0.748	0.641	0.736	0.723	0.500	0.619	0.625	0.641	0.851	0.758	0.670
O	15.477	15.831	16.032	15.904	15.759	15.689	14.940	15.275	15.825	15.306	15.992	16.024	16.112	15.617	16.492	16.181	14.910	15.946
TOTAL	54.500	55.849	56.533	56.076	55.595	55.364	52.639	53.853	55.677	53.985	56.344	56.490	56.668	55.000	58.093	57.087	52.597	56.225
CarbCalc.																		
Ca	0.964	0.966	0.968	0.971	0.965	0.964	0.969	0.971	0.972	0.972	0.974	0.973	0.974	0.971	0.976	0.971	0.970	0.969
Fe	0.014	0.014	0.013	0.012	0.015	0.014	0.011	0.011	0.011	0.010	0.008	0.013	0.011	0.012	0.009	0.011	0.011	0.013
Mn	0.014	0.014	0.013	0.012	0.013	0.015	0.015	0.014	0.012	0.014	0.013	0.009	0.011	0.012	0.011	0.015	0.015	0.012
Mg	0.007	0.005	0.006	0.004	0.006	0.006	0.004	0.004	0.004	0.003	0.003	0.004	0.003	0.004	0.003	0.003	0.004	0.005
Sr	0.001	0.001	0.001	0.001	0.001	0.001	0.001	0.000	0.000	0.001	0.000	0.001	0.000	0.000	0.000	0.000	0.000	0.000
Na	0.000	0.001	0.000	0.001	0.000	0.001	0.001	0.000	0.000	0.000	0.001	0.000	0.000	0.000	0.000	0.000	0.000	0.000

	GEN. 3									GEN. 4								
	INNER			MIDDLE			OUTER											
	1	2	3	1	2	3	1	2	3	1	2	3	4	5	6	7	8	9
Ca	37.201	38.316	36.205	38.838	34.960	38.633	36.229	38.586	37.183	39.922	38.100	38.789	38.691	38.361	40.599	40.122	38.993	40.343
P	0.000	0.019	0.000	0.000	0.000	0.000	0.027	0.000	0.000	0.000	0.013	0.000	0.000	0.017	0.004	0.000	0.000	0.000
Sr	0.051	0.078	0.068	0.093	0.067	0.053	0.086	0.090	0.047	0.070	0.040	0.050	0.055	0.086	0.051	0.049	0.035	0.028
Si	0.000	0.000	0.000	0.000	0.000	0.000	0.000	0.000	0.000	0.000	0.000	0.000	0.000	0.000	0.000	0.000	0.000	0.000
Al	0.000	0.000	0.000	0.000	0.000	0.000	0.000	0.000	0.000	0.000	0.000	0.000	0.000	0.000	0.000	0.000	0.000	0.000
Mg	0.214	0.224	0.203	0.193	0.207	0.160	0.168	0.160	0.162	0.174	0.191	0.215	0.185	0.125	0.080	0.194	0.065	0.060
Na	0.002	0.002	0.001	0.000	0.002	0.016	0.003	0.005	0.010	0.000	0.000	0.017	0.012	0.011	0.014	0.005	0.004	0.005
Fe	1.089	1.304	1.141	1.224	1.179	0.898	0.928	1.018	0.878	1.101	1.120	1.121	1.022	0.802	0.574	1.106	0.474	0.468
Mn	0.575	0.588	0.588	0.632	0.625	0.542	0.527	0.533	0.569	0.572	0.644	0.544	0.555	1.094	0.932	0.639	0.948	0.766
O	15.481	16.028	15.098	16.183	14.625	15.958	15.044	15.974	15.379	16.546	15.868	16.121	16.036	15.985	16.715	16.658	16.029	16.509
TOTAL	54.613	56.559	53.304	57.163	51.665	56.260	53.012	56.366	54.228	58.385	55.976	56.857	56.556	56.481	58.969	58.773	56.548	58.179
CARB CALC																		
Ca	0.959	0.956	0.957	0.958	0.954	0.966	0.964	0.964	0.965	0.963	0.959	0.961	0.963	0.959	0.970	0.961	0.971	0.976
Fe	0.020	0.023	0.022	0.022	0.023	0.016	0.018	0.018	0.016	0.019	0.020	0.020	0.018	0.014	0.010	0.019	0.008	0.008
Mn	0.011	0.011	0.011	0.011	0.012	0.010	0.010	0.010	0.011	0.010	0.012	0.010	0.010	0.020	0.016	0.011	0.017	0.014
Mg	0.009	0.009	0.009	0.008	0.009	0.007	0.007	0.007	0.007	0.007	0.008	0.009	0.008	0.005	0.003	0.008	0.003	0.002
Sr	0.001	0.001	0.001	0.001	0.001	0.001	0.001	0.001	0.001	0.001	0.000	0.001	0.001	0.001	0.001	0.001	0.000	0.000
Na	0.000	0.000	0.000	0.000	0.000	0.001	0.000	0.000	0.000	0.000	0.000	0.001	0.001	0.000	0.001	0.000	0.000	0.000

Table D.10. Compositions of Unreplaced Bioclasts and Echinoid Fragments. The Data have been Recalculated to Calcite Formulae.

	Echinoid Fragments													Unalt. Bio.	
	DRAG. 31.2					DRAG. 31. 7					DRAG. 31.22			DRAG31.1	
	1	2	3	4	5	1	2	3	4	5	1	2	3	1	2
Ca	36.232	36.633	37.477	35.376	36.903	35.096	37.775	32.426	36.925	31.900	36.966	37.558	36.613	37.704	38.773
P	0.007	0.000	0.011	0.075	0.000	0.028	0.000	0.000	0.044	0.023	0.000	0.000	0.015	0.053	0.015
Sr	0.079	0.043	0.057	0.043	0.090	0.024	0.057	0.049	0.055	0.028	0.089	0.027	0.074	0.080	0.060
Si	0.038	0.189	0.339	0.353	0.211	0.619	0.019	1.661	0.295	0.124	0.024	0.014	0.025	0.028	0.017
Al	0.007	0.094	0.186	0.182	0.120	0.388	0.000	1.033	0.164	0.032	0.007	0.000	0.002	0.002	0.006
Mg	0.309	0.211	0.255	0.344	0.603	0.337	0.297	0.560	0.299	1.222	0.301	0.114	0.731	0.127	0.091
Na	0.013	0.021	0.019	0.017	0.063	0.000	0.020	0.000	0.000	0.067	0.090	0.000	0.031	0.240	0.207
Fe	0.799	0.943	1.142	1.283	0.706	1.533	0.809	3.054	1.168	3.274	0.524	0.829	0.472	0.017	0.000
Mn	1.539	1.463	1.195	1.136	1.077	1.041	1.067	0.611	0.906	2.070	1.208	1.413	0.773	0.005	0.000
O	15.422	15.775	16.387	15.722	16.030	16.065	15.858	17.186	16.085	15.307	15.538	15.738	15.531	15.341	15.666
TOTAL	54.445	55.372	57.068	54.531	55.803	55.131	55.902	56.580	55.941	54.047	54.747	55.693	54.267	53.597	54.835
CarbCalc.															
Ca	0.941	0.945	0.946	0.937	0.939	0.935	0.952	0.900	0.948	0.843	0.952	0.954	0.944	0.988	0.991
Fe	0.015	0.017	0.021	0.025	0.013	0.029	0.015	0.061	0.022	0.062	0.010	0.015	0.009	0.000	0.000
Mn	0.029	0.028	0.022	0.022	0.020	0.020	0.020	0.012	0.017	0.040	0.023	0.026	0.015	0.000	0.000
Mg	0.013	0.009	0.011	0.015	0.025	0.015	0.012	0.026	0.013	0.053	0.013	0.005	0.031	0.006	0.004
Sr	0.001	0.001	0.001	0.001	0.001	0.000	0.001	0.001	0.001	0.000	0.001	0.000	0.001	0.001	0.001
Na	0.001	0.001	0.001	0.001	0.003	0.000	0.001	0.000	0.000	0.003	0.004	0.000	0.001	0.011	0.009

Table D.11. Compositions of the Carbonates Within Specimen YAR.22. The Data have been Recalculated to Carbonates of the Calcite Group.

	UNALT. BIO.			GEN. 1 Calcite										GEN. 2 Arboraceous Siderite									
	1	2	3	1	2	3	4	5	6	7	8	9	10	1	2	3	4	5	6	7	8	9	10
Ca	39.458	39.713	39.188	38.284	38.370	38.254	37.116	37.437	38.635	38.044	37.212	37.430	38.008	4.521	3.812	3.946	3.952	4.139	3.881	3.757	3.975	3.549	4.118
P	0.000	0.022	0.011	0.000	0.000	0.000	0.001	0.006	0.000	0.041	0.018	0.000	0.042	0.000	0.000	0.044	0.008	0.000	0.000	0.000	0.000	0.000	0.000
Sr	0.054	0.060	0.071	0.028	0.065	0.025	0.041	0.050	0.064	0.038	0.027	0.020	0.019	0.003	0.016	0.000	0.006	0.029	0.000	0.000	0.004	0.004	0.001
Si	0.000	0.000	0.000	0.001	0.000	0.000	0.000	0.000	0.000	0.000	0.000	0.000	0.000	0.000	0.008	1.412	0.000	0.000	0.000	0.001	0.000	0.000	0.000
Al	0.003	0.003	0.000	0.007	0.001	0.006	0.001	0.001	0.002	0.002	0.002	0.007	0.004	0.000	0.005	0.000	0.002	0.004	0.003	0.000	0.003	0.005	0.000
Mg	0.073	0.084	0.078	0.194	0.176	0.194	0.186	0.173	0.200	0.228	0.200	0.181	0.247	3.673	3.969	3.732	3.806	3.807	4.426	4.382	4.653	4.525	4.197
Na	0.185	0.137	0.199	0.005	0.084	0.000	0.004	0.000	0.009	0.002	0.000	0.008	0.013	0.060	0.068	0.050	0.078	0.075	0.276	0.063	0.045	0.013	0.040
Fe	0.027	0.001	0.028	1.089	1.142	1.078	1.091	1.011	1.187	1.236	1.141	0.985	1.007	32.903	33.622	33.131	32.426	33.667	31.720	32.180	32.381	31.895	32.708
Mn	0.013	0.000	0.001	0.661	0.611	0.582	0.622	0.556	0.579	0.630	0.661	0.620	0.653	1.083	1.332	2.138	2.579	1.202	2.170	2.250	2.194	2.797	1.677
O	15.888	15.998	15.800	15.929	15.980	15.888	15.444	15.528	16.081	15.938	15.536	15.537	15.880	13.985	14.195	15.829	14.164	14.188	14.280	14.280	14.584	14.357	14.279
TOTAL	55.701	56.018	55.376	56.198	56.429	56.027	54.506	54.762	56.757	56.159	54.797	54.788	55.873	51.707	53.215	56.336	53.069	52.972	52.875	53.156	53.864	53.596	52.902
CarbCalc.																							
Ca	0.992	0.993	0.991	0.960	0.959	0.962	0.960	0.963	0.959	0.956	0.958	0.962	0.959	0.129	0.107	0.109	0.111	0.116	0.108	0.105	0.109	0.099	0.115
Fe	0.000	0.000	0.001	0.020	0.020	0.019	0.020	0.019	0.021	0.022	0.021	0.018	0.018	0.674	0.679	0.672	0.657	0.680	0.636	0.646	0.636	0.637	0.656
Mn	0.000	0.000	0.000	0.012	0.011	0.011	0.012	0.010	0.010	0.012	0.012	0.012	0.012	0.023	0.027	0.044	0.053	0.025	0.044	0.046	0.044	0.057	0.034
Mg	0.003	0.003	0.003	0.008	0.007	0.008	0.008	0.007	0.008	0.009	0.008	0.008	0.010	0.173	0.184	0.174	0.177	0.177	0.204	0.202	0.210	0.208	0.193
Sr	0.001	0.001	0.001	0.000	0.001	0.000	0.000	0.001	0.001	0.000	0.000	0.000	0.000	0.000	0.000	0.000	0.000	0.000	0.000	0.000	0.000	0.000	0.000
Na	0.008	0.006	0.009	0.000	0.004	0.000	0.000	0.000	0.000	0.000	0.000	0.000	0.001	0.003	0.003	0.002	0.004	0.004	0.013	0.003	0.002	0.001	0.002

	GEN. 3 Calcite (inner)					Calcite (outer)					SIDERITE CEMENTING OOIDS						
	1	2	3	4	5	1	2	3	4	5	1	2	3	4	5	6	7
Ca	37.839	37.927	38.457	38.417	38.654	36.031	36.238	36.214	36.707	37.041	3.032	3.822	4.189	4.084	4.001	3.362	3.694
P	0.000	0.004	0.000	0.000	0.032	0.000	0.000	0.000	0.000	0.030	0.000	0.015	0.044	0.000	0.005	0.000	0.008
Sr	0.012	0.026	0.022	0.040	0.033	0.030	0.058	0.042	0.054	0.052	0.011	0.015	0.024	0.015	0.012	0.032	0.023
Si	0.003	0.000	0.005	0.003	0.005	0.000	0.000	0.000	0.008	0.004	0.000	0.005	0.024	0.000	0.002	0.005	0.009
Al	0.000	0.001	0.000	0.000	0.000	0.000	0.000	0.000	0.000	0.004	0.001	0.005	0.010	0.000	0.000	0.000	0.006
Mg	0.071	0.121	0.141	0.180	0.222	0.244	0.239	0.251	0.242	0.225	4.360	4.303	4.039	4.121	4.335	3.826	4.614
Na	0.003	0.000	0.009	0.012	0.000	0.001	0.000	0.001	0.000	0.008	0.013	0.002	0.004	0.021	0.031	0.000	0.000
Fe	0.789	1.002	1.056	1.492	1.668	1.850	1.813	1.895	1.821	1.682	33.155	32.824	32.833	32.844	32.233	33.482	32.331
Mn	0.597	0.733	0.808	0.729	0.744	0.762	0.781	0.743	0.736	0.753	2.977	2.032	1.886	2.016	2.080	1.958	2.730
O	15.559	15.732	15.996	16.109	16.324	15.302	15.381	15.389	15.568	15.695	14.453	14.387	14.385	14.349	14.312	14.034	14.600
TOTAL	54.873	55.546	56.494	56.982	57.682	54.220	54.510	54.535	55.136	55.494	54.970	53.588	53.249	53.366	53.010	53.337	54.321
Ca	0.971	0.963	0.960	0.952	0.948	0.940	0.941	0.939	0.942	0.945	0.084	0.105	0.115	0.114	0.111	0.096	0.101
Fe	0.015	0.018	0.019	0.027	0.029	0.035	0.034	0.035	0.034	0.031	0.657	0.656	0.660	0.656	0.646	0.684	0.636
Mn	0.011	0.014	0.015	0.013	0.013	0.015	0.015	0.014	0.014	0.014	0.060	0.041	0.039	0.041	0.042	0.041	0.055
Mg	0.003	0.005	0.006	0.007	0.009	0.010	0.010	0.011	0.010	0.009	0.199	0.197	0.187	0.189	0.200	0.180	0.208
Sr	0.000	0.000	0.000	0.000	0.000	0.000	0.001	0.000	0.001	0.001	0.000	0.000	0.000	0.000	0.000	0.000	0.000
Na	0.000	0.000	0.000	0.001	0.000	0.000	0.000	0.000	0.000	0.000	0.001	0.000	0.000	0.001	0.002	0.000	0.000

Table D.12. Compositions of Carbonate and Phosphatic Cements Within Specimen DRAG. 31.22. The Carbonate Data have been Recalculated to Carbonates of the Calcite Group.

	REP. BIO.			GEN. 1						GEN. 2						GEN. 3a			GEN. 3b		
	Calcite			Calcite						Calcite						Ankerite			Siderite		
	1	2	3	1	2	3	4	5	6	1	2	3	4	5	6	1	2	3	1	2	3
Ca	36.827	36.376	36.377	36.929	35.500	35.768	36.813	36.778	36.081	37.705	36.595	36.149	36.587	36.694	36.254	12.822	9.181	9.965	4.827	6.519	4.780
P	0.000	0.038	0.012	0.014	0.000	0.034	0.000	0.011	0.000	0.000	0.009	1.014	0.000	0.000	0.000	0.000	0.000	0.055	0.014	0.000	0.000
Sr	0.053	0.058	0.080	0.050	0.032	0.072	0.059	0.075	0.065	0.039	0.028	0.085	0.066	0.077	0.076	0.035	0.002	0.000	0.010	0.026	0.006
Si	0.004	0.001	0.000	0.015	0.005	0.015	0.011	0.010	0.000	0.002	0.001	0.000	0.020	0.001	0.010	0.047	0.037	0.089	0.005	0.005	0.012
Al	0.010	0.000	0.000	0.000	0.000	0.006	0.000	0.000	0.000	0.000	0.000	0.000	0.010	0.006	0.005	0.008	0.000	0.015	0.000	0.000	0.001
Mg	0.244	0.284	0.167	0.257	0.161	0.297	0.148	0.218	0.213	0.136	0.136	0.287	0.124	0.147	0.146	2.583	1.903	2.071	3.115	3.313	3.161
Na	0.001	0.001	0.000	0.018	0.005	0.021	0.013	0.004	0.012	0.000	0.007	0.044	0.000	0.000	0.000	0.053	0.070	0.087	0.011	0.012	0.000
Fe	1.004	0.913	0.571	0.807	0.782	0.764	0.819	0.687	0.767	0.935	0.845	0.710	0.968	1.000	1.048	6.196	4.454	4.802	30.982	29.693	31.354
Mn	1.600	1.882	1.528	1.366	1.139	1.639	1.200	1.812	1.453	1.086	1.447	1.639	1.547	1.508	1.659	1.512	1.126	1.158	3.853	3.194	3.197
O	15.639	15.579	15.270	15.591	14.847	15.257	15.404	15.590	15.203	15.735	15.383	16.641	15.458	15.491	15.382	9.120	6.588	7.270	14.004	14.235	13.918
TOTAL	55.382	55.132	54.005	55.047	52.471	53.873	54.467	55.185	53.794	55.638	54.451	56.569	54.780	54.924	54.580	32.376	23.361	25.512	56.821	56.997	56.429
CarbCalc.																					
Ca	0.941	0.935	0.952	0.948	0.955	0.940	0.955	0.943	0.947	0.957	0.950	0.938	0.947	0.946	0.942	0.565	0.560	0.559	0.137	0.183	0.137
Fe	0.018	0.017	0.011	0.015	0.015	0.014	0.015	0.013	0.014	0.017	0.016	0.014	0.018	0.019	0.020	0.196	0.195	0.196	0.635	0.598	0.646
Mn	0.030	0.035	0.029	0.026	0.022	0.031	0.023	0.034	0.028	0.020	0.027	0.033	0.029	0.028	0.031	0.049	0.050	0.048	0.080	0.065	0.067
Mg	0.010	0.012	0.007	0.011	0.007	0.013	0.006	0.009	0.009	0.006	0.006	0.013	0.005	0.006	0.006	0.188	0.191	0.194	0.147	0.153	0.150
Sr	0.001	0.001	0.001	0.001	0.000	0.001	0.001	0.001	0.001	0.000	0.000	0.001	0.001	0.001	0.001	0.001	0.000	0.000	0.000	0.000	0.000
Na	0.000	0.000	0.000	0.001	0.000	0.001	0.001	0.000	0.001	0.000	0.000	0.002	0.000	0.000	0.000	0.004	0.007	0.009	0.001	0.001	0.000

	GEN. 3c			GEN. 4						GEN. 5a			GEN. 5b		GEN. 6			GEN. 7				
	Phosphate			Ankerite						Siderite			Calcite		Calcite			Calcite				
	1	2	3	1	2	3	4	5	6	1	2	3	1	2	1	2	3	1	2	3	4	5
Ca	34.775	35.608	32.302	21.449	21.346	22.982	21.265	20.277	21.632	5.260	4.063	7.501	38.042	33.765	34.751	37.055	36.711	37.256	36.969	37.221	35.632	36.238
P	13.352	12.781	11.129	0.000	0.000	2.392	0.001	0.026	0.000	0.000	0.016	0.000	0.000	0.010	0.081	0.032	0.029	0.000	0.020	0.000	0.000	0.014
Sr	0.234	0.251	0.207	0.043	0.040	0.088	0.040	0.053	0.046	0.028	0.017	0.027	0.059	0.030	0.069	0.022	0.058	0.041	0.021	0.040	0.059	0.032
Si	0.005	0.003	0.005	0.006	0.003	0.012	0.005	0.013	0.004	0.003	0.000	0.007	0.008	0.007	0.000	0.000	0.000	0.007	0.006	0.003	0.011	0.011
Al	0.006	0.001	0.008	0.000	0.000	0.001	0.000	0.000	0.009	0.000	0.000	0.004	0.000	0.001	0.010	0.004	0.006	0.004	0.007	0.000	0.005	0.005
Mg	0.708	0.783	1.245	4.535	4.565	3.813	4.646	4.191	4.532	3.136	3.155	3.433	0.129	0.118	0.289	0.126	0.323	0.175	0.138	0.178	0.140	0.235
Na	0.544	0.592	0.458	0.030	0.027	0.197	0.024	0.000	0.027	0.009	0.018	0.018	0.014	0.021	0.000	0.000	0.000	0.000	0.000	0.004	0.000	0.000
Fe	2.352	2.650	3.864	10.618	10.477	9.331	10.736	10.184	10.637	31.122	32.863	27.676	0.962	0.809	0.884	0.862	0.922	0.891	0.903	1.006	0.821	0.763
Mn	0.653	0.696	0.933	2.845	2.910	2.501	2.758	2.586	3.031	3.479	3.100	3.515	0.800	1.443	1.175	1.418	1.192	1.447	1.399	1.572	1.299	1.635
O	32.701	32.456	29.676	15.443	15.395	18.273	15.449	14.582	15.578	14.105	14.047	14.229	15.805	14.244	14.785	15.585	15.533	15.684	15.558	15.734	14.958	15.357
TOTAL	85.330	85.821	79.827	54.969	54.763	59.590	54.924	51.912	55.496	57.142	57.279	56.410	55.819	50.448	52.044	55.104	54.774	55.505	55.021	55.758	52.925	54.290
CarbCalc.																						
Ca	0.604	0.650	0.580	0.555	0.554	0.543	0.550	0.556	0.555	0.149	0.115	0.211	0.961	0.948	0.945	0.952	0.946	0.949	0.951	0.945	0.952	0.944
Fe	0.171	0.154	0.194	0.197	0.195	0.204	0.199	0.201	0.196	0.632	0.672	0.558	0.017	0.016	0.017	0.016	0.017	0.016	0.017	0.018	0.016	0.014
Mn	0.048	0.041	0.048	0.054	0.055	0.056	0.052	0.052	0.057	0.072	0.064	0.072	0.015	0.030	0.023	0.027	0.022	0.027	0.026	0.029	0.025	0.031
Mg	0.118	0.104	0.144	0.193	0.195	0.191	0.198	0.190	0.192	0.146	0.148	0.159	0.005	0.005	0.013	0.005	0.014	0.007	0.006	0.007	0.006	0.010
Sr	0.011	0.009	0.007	0.001	0.000	0.001	0.000	0.001	0.001	0.000	0.000	0.000	0.001	0.000	0.001	0.000	0.001	0.000	0.000	0.000	0.001	0.000
Na	0.096	0.083	0.056	0.001	0.001	0.010	0.001	0.000	0.001	0.000	0.001	0.001	0.001	0.001	0.000	0.000	0.000	0.000	0.000	0.000	0.000	0.000

Table D.13. Compositions of Carbonate Cements Within Specimen DRAG. 31.36a. The Data have been Recalculated to Carbonates of the Calcite Group.

	GEN. 1					GEN. 2												GEN. 3			GEN. 4	
	Cementing Oolds					Inner			Middle			Outer			Outer-Most Rounded Part				Siderite			Siderite	
	1	2	3	4	5	1	2	3	1	2	3	1	2	3	1	2	3	4	1	2	3	1	2
Ca	24.520	24.842	16.112	23.707	24.330	34.819	32.713	35.615	35.624	34.979	34.495	35.151	31.334	37.780	34.201	34.079	34.497	37.441	4.989	4.324	4.106	4.485	4.272
P	0.037	0.008	0.023	0.000	0.000	0.001	0.028	0.057	0.000	0.000	0.000	0.066	0.047	0.000	0.000	0.053	0.001	0.000	0.000	0.022	0.000	0.057	0.004
Sr	0.035	0.034	0.000	0.031	0.032	0.137	0.096	0.073	0.133	0.155	0.107	0.065	0.065	0.108	0.050	0.047	0.078	0.064	0.000	0.042	0.022	0.018	0.015
Si	0.000	0.000	0.000	0.000	0.002	0.005	0.004	0.006	0.072	0.000	0.000	0.000	0.034	0.003	0.015	0.004	0.010	0.020	0.031	0.014	0.011	0.083	0.020
Al	0.005	0.010	0.000	0.012	0.010	0.001	0.000	0.000	0.051	0.000	0.000	0.008	0.006	0.006	0.006	0.000	0.000	0.016	0.000	0.000	0.000	0.002	0.000
Mg	1.577	1.629	1.116	1.499	1.672	0.397	0.248	0.202	0.255	0.266	0.359	0.422	1.204	0.256	0.752	0.709	0.529	0.371	4.183	4.403	4.382	3.414	3.766
Na	0.063	0.047	0.096	0.051	0.049	0.049	0.057	0.016	0.025	0.035	0.016	0.029	0.033	0.014	0.020	0.028	0.049	0.035	0.084	0.337	0.132	0.038	0.590
Fe	0.050	0.032	0.081	0.000	0.031	0.745	0.761	0.869	0.876	0.931	0.771	1.119	1.995	1.104	2.073	1.275	1.302	1.446	30.469	31.027	31.213	32.211	30.985
Mn	13.679	12.913	9.320	14.309	13.522	3.987	2.587	2.179	1.980	2.222	2.299	2.162	4.423	0.493	1.743	3.249	1.945	0.943	1.922	1.833	2.147	2.094	2.720
O	14.905	14.800	9.967	14.951	14.793	15.586	14.272	15.333	15.376	15.093	14.922	15.375	15.288	15.743	15.288	15.473	15.103	15.941	14.098	14.216	14.153	14.061	14.088
TOTAL	54.871	54.315	36.715	54.560	54.441	55.727	50.766	54.350	54.392	53.681	52.969	54.397	54.429	55.507	54.148	54.917	53.514	56.277	55.776	56.218	56.166	56.463	56.460
CarbCalc.																							
Ca	0.658	0.671	0.646	0.646	0.657	0.892	0.917	0.932	0.933	0.925	0.923	0.918	0.823	0.958	0.894	0.883	0.913	0.940	0.142	0.121	0.116	0.126	0.121
Fe	0.001	0.001	0.002	0.000	0.001	0.014	0.015	0.016	0.016	0.018	0.015	0.021	0.038	0.020	0.039	0.024	0.025	0.026	0.621	0.628	0.632	0.667	0.631
Mn	0.269	0.255	0.274	0.285	0.266	0.075	0.053	0.042	0.038	0.043	0.045	0.041	0.085	0.009	0.033	0.062	0.038	0.017	0.040	0.038	0.044	0.044	0.056
Mg	0.070	0.073	0.074	0.067	0.074	0.017	0.011	0.009	0.011	0.012	0.016	0.018	0.052	0.011	0.032	0.030	0.023	0.015	0.196	0.205	0.204	0.162	0.176
Sr	0.000	0.000	0.000	0.000	0.000	0.002	0.001	0.001	0.002	0.002	0.001	0.001	0.001	0.001	0.001	0.001	0.001	0.001	0.000	0.001	0.000	0.000	0.000
Na	0.003	0.002	0.007	0.002	0.002	0.002	0.003	0.001	0.001	0.002	0.001	0.001	0.002	0.001	0.001	0.001	0.002	0.002	0.004	0.017	0.006	0.002	0.029

	GEN. 4 (Cont.)				GEN. 5					REP. BIO.			REP. BIO.			SIDERITES				
	Siderite				Pore-filing Calcite					Siderite			Calcite			Replacing Calcite		Nucleating on Crystals.		
	3	4	5	6	1	2	3	4	5	1	2	3	1	2	3	1	2	1	2	3
Ca	4.848	5.143	4.108	4.860	35.355	35.443	36.166	37.451	36.650	4.098	3.879	3.488	37.117	37.807	37.921	4.265	3.998	3.798	3.997	4.107
P	0.017	0.000	0.023	0.000	0.040	0.000	0.000	0.023	0.000	0.000	0.012	0.065	0.000	0.000	0.000	0.000	0.006	0.000	0.000	0.000
Sr	0.014	0.027	0.004	0.008	0.064	0.055	0.043	0.049	0.034	0.026	0.000	0.023	0.054	0.087	0.087	0.041	0.014	0.015	0.000	0.002
Si	0.008	0.000	0.014	0.002	0.003	0.012	0.036	0.000	0.000	0.008	0.026	0.007	0.000	0.006	0.002	0.008	0.021	0.070	0.002	0.003
Al	0.000	0.000	0.000	0.000	0.004	0.004	0.004	0.000	0.002	0.000	0.012	0.000	0.000	0.005	0.000	0.000	0.000	0.047	0.010	0.003
Mg	3.332	4.018	4.027	3.916	0.346	0.332	0.358	0.309	0.348	3.232	2.803	3.491	0.266	0.359	0.265	3.874	3.813	3.807	4.157	4.261
Na	0.025	0.058	0.055	0.051	0.015	0.056	0.046	0.011	0.029	0.066	0.065	0.133	0.018	0.046	0.018	0.046	0.029	0.072	0.052	0.050
Fe	32.433	31.308	30.330	31.577	1.988	1.804	1.896	1.872	1.755	33.397	32.511	33.567	1.151	1.520	1.194	30.468	32.552	31.800	31.405	31.422
Mn	2.045	1.921	2.713	2.040	0.712	0.635	0.697	0.645	0.661	2.013	1.969	1.949	0.516	0.522	0.456	3.257	1.941	1.955	1.934	1.810
O	14.058	14.251	13.835	14.179	15.193	15.115	15.488	15.921	15.574	13.953	13.359	14.015	15.489	15.960	15.812	13.962	14.041	13.851	13.921	13.996
TOTAL	56.780	56.726	55.109	56.633	53.720	53.456	54.734	56.281	55.053	56.793	54.636	56.738	54.611	56.312	55.755	55.921	56.415	55.415	55.478	55.654
CarbCalc.																				
Ca	0.137	0.144	0.118	0.137	0.932	0.937	0.935	0.941	0.940	0.116	0.096	0.110	0.957	0.946	0.958	0.122	0.114	0.110	0.115	0.117
Fe	0.663	0.629	0.631	0.638	0.038	0.034	0.035	0.034	0.032	0.701	0.693	0.693	0.021	0.027	0.022	0.626	0.666	0.664	0.647	0.643
Mn	0.043	0.039	0.057	0.042	0.014	0.012	0.013	0.012	0.012	0.043	0.041	0.042	0.010	0.010	0.008	0.068	0.040	0.041	0.040	0.038
Mg	0.157	0.186	0.192	0.182	0.015	0.014	0.015	0.013	0.015	0.139	0.166	0.153	0.011	0.015	0.011	0.183	0.179	0.183	0.197	0.200
Sr	0.000	0.000	0.000	0.000	0.001	0.001	0.001	0.001	0.000	0.000	0.000	0.000	0.001	0.001	0.001	0.001	0.000	0.000	0.000	0.000
Na	0.001	0.003	0.003	0.003	0.001	0.003	0.002	0.000	0.001	0.003	0.007	0.004	0.001	0.002	0.001	0.002	0.001	0.004	0.003	0.002

Table D.14. Compositions of Carbonate Cements Associated with Authigenic Berthierine Precipitation. The Data have been Recalculated to Carbonates of the Calcite Group.

	DRAG. 31.19			DRAG. 31.19						DRAG. 31.28					
	Calcite Cements			Siderite Cements						Siderite Cements/Replacements					
	1	2	3	1	2	3	4	5	6	1	2	3	4	5	6
Ca	36.957	38.048	39.640	4.103	4.310	3.827	3.698	3.849	4.161	3.523	3.121	3.489	2.906	3.382	3.389
P	0.000	0.012	0.000	0.000	0.088	0.000	0.006	0.000	0.000	0.013	0.117	0.000	0.000	0.105	0.076
Sr	0.048	0.053	0.074	0.017	0.038	0.047	0.039	0.032	0.021	0.033	0.033	0.018	0.039	0.056	0.029
Si	0.000	0.000	0.009	0.000	0.004	0.000	0.013	0.000	0.011	0.037	0.018	0.177	0.109	0.015	0.001
Al	0.000	0.000	0.000	0.000	0.000	0.000	0.000	0.000	0.000	0.007	0.009	0.094	0.053	0.041	0.005
Mg	0.110	0.116	0.149	2.824	2.779	2.723	2.696	2.772	2.418	3.093	3.044	4.031	3.354	2.969	3.118
Na	0.000	0.000	0.003	0.010	0.000	0.000	0.000	0.010	0.018	0.062	0.067	0.014	0.052	0.008	0.039
Fe	0.772	0.762	1.341	33.768	33.955	34.211	33.938	34.039	32.929	32.404	33.890	32.604	34.016	33.506	33.595
Mn	2.002	1.679	1.288	2.658	2.274	2.410	2.592	2.346	2.035	3.420	3.373	2.858	3.426	3.638	3.657
O	15.638	15.999	16.706	13.951	14.064	13.831	13.758	13.806	13.302	13.814	14.150	14.512	14.307	14.165	14.217
TOTAL	55.527	56.669	59.210	57.331	57.512	57.049	56.740	56.854	54.895	52.883	54.701	54.308	55.356	54.503	54.737
CarbCalc.															
Ca	0.943	0.950	0.948	0.117	0.119	0.110	0.107	0.111	0.125	0.102	0.083	0.098	0.082	0.091	0.092
Fe	0.014	0.014	0.023	0.693	0.701	0.709	0.708	0.706	0.710	0.676	0.700	0.657	0.689	0.691	0.685
Mn	0.037	0.031	0.022	0.055	0.048	0.051	0.055	0.049	0.045	0.073	0.071	0.059	0.071	0.076	0.076
Mg	0.005	0.005	0.006	0.133	0.132	0.130	0.129	0.132	0.120	0.148	0.144	0.186	0.156	0.141	0.146
Sr	0.001	0.001	0.001	0.000	0.001	0.001	0.001	0.000	0.000	0.000	0.000	0.000	0.001	0.001	0.000
Na	0.000	0.000	0.000	0.000	0.000	0.000	0.000	0.001	0.001	0.003	0.003	0.001	0.003	0.000	0.002

	DRAG. 31.28 (Cont.)							
	Siderite Surrounding Ooids							
	1	2	3	4	5	6	7	8
Ca	3.370	4.531	2.482	3.840	3.620	3.255	3.494	1.346
P	0.075	0.000	0.000	0.000	0.106	0.144	0.000	0.004
Sr	0.053	0.050	0.055	0.036	0.049	0.031	0.035	0.109
Si	0.022	0.484	1.232	0.008	0.006	0.015	0.459	6.251
Al	0.012	0.259	0.609	0.003	0.003	0.004	0.240	4.222
Mg	3.169	3.120	3.192	3.594	3.318	3.057	3.210	2.446
Na	0.045	0.065	0.064	0.015	0.022	0.025	0.092	0.165
Fe	33.501	29.248	33.146	32.810	33.418	33.648	31.672	30.222
Mn	3.586	6.393	3.263	3.641	3.456	3.713	4.896	2.073
O	14.230	14.917	15.516	14.381	14.373	14.254	14.781	22.368
TOTAL	54.693	54.536	57.077	54.488	54.751	54.891	55.385	67.860
CarbCalc.								
Ca	0.091	0.128	0.073	0.107	0.096	0.084	0.099	0.046
Fe	0.684	0.593	0.700	0.654	0.677	0.692	0.646	0.754
Mn	0.074	0.132	0.070	0.074	0.071	0.078	0.102	0.053
Mg	0.149	0.145	0.155	0.165	0.155	0.145	0.150	0.140
Sr	0.001	0.001	0.001	0.000	0.001	0.000	0.000	0.002
Na	0.002	0.003	0.003	0.001	0.001	0.001	0.005	0.010

Table D.15. Phosphate Compositions in the Frodingham Ironstone Formation. The Data have been Recalculated to Phosphate Formulae (26 (O, OH, Cl, F)).

	Echinoid Debris Replaced By Phosphate							
	1	2	3	4	5	6	7	8
Si	0.675	0.609	0.376	0.306	0.627	0.433	0.397	0.306
Ti	0.012	0.000	0.000	0.054	0.124	0.060	0.001	0.360
Al	0.516	0.404	0.292	0.296	0.400	0.338	0.291	0.259
Fe	1.212	0.740	1.043	0.558	0.850	0.919	3.843	1.185
Mn	0.092	0.112	0.000	0.000	0.093	0.193	0.624	0.032
Mg	0.368	0.176	0.184	0.112	0.093	0.205	0.405	0.033
Ca	37.415	37.422	37.054	37.451	37.379	37.076	33.751	36.930
Na	0.533	0.731	0.619	0.603	0.396	0.522	0.616	0.495
K	0.101	0.091	0.094	0.124	0.101	0.057	0.164	0.032
P	14.106	14.688	14.555	14.527	14.508	13.349	13.250	14.381
S	0.322	0.221	0.150	0.231	0.238	0.118	0.156	0.313
Cl	0.000	0.000	0.000	0.034	0.014	0.000	0.000	0.000
O	35.214	35.596	34.934	34.830	35.303	33.525	33.097	34.685
TOTAL	90.566	90.790	89.301	89.126	90.126	86.795	86.595	89.011
PhosphCalc.								
Si	0.284	0.253	0.159	0.130	0.263	0.191	0.178	0.131
Ti	0.003	0.000	0.000	0.013	0.031	0.016	0.000	0.090
Al	0.226	0.175	0.129	0.131	0.175	0.155	0.136	0.115
Fe	0.256	0.155	0.222	0.119	0.179	0.204	0.865	0.254
Mn	0.020	0.024	0.000	0.000	0.020	0.044	0.143	0.007
Mg	0.179	0.085	0.090	0.055	0.045	0.105	0.209	0.016
Ca	11.029	10.912	11.010	11.161	10.990	11.480	10.586	11.052
Na	0.274	0.372	0.321	0.313	0.203	0.282	0.337	0.258
K	0.031	0.027	0.029	0.038	0.030	0.018	0.053	0.010
P	5.380	5.542	5.596	5.602	5.520	5.348	5.377	5.569

Table D.16. Compositions of Berthierine in the Cleveland Ironstone Formation. The Data have been Recalculated to Berthierine Structural Formulae.

	STH. 26									STH. 32				
	MATRIX						FLAKES			MATRIX				
	1	2	3	4	5	6	1	2	3	1	2	3	4	5
Si	13.349	14.286	14.673	13.654	13.450	14.745	12.437	11.933	11.331	5.964	5.763	5.912	4.921	5.786
Ti	0.123	0.305	0.489	0.222	0.081	0.178	0.263	0.185	0.427	0.138	0.034	0.057	0.132	0.021
Al	10.836	11.018	11.238	10.867	11.087	11.993	10.467	10.198	9.521	4.533	4.468	4.864	3.956	4.225
Fe	21.789	20.109	19.280	21.162	22.785	19.402	25.896	27.006	27.043	6.456	8.199	9.514	7.337	7.279
Mn	0.052	0.000	0.090	0.020	0.000	0.000	0.016	0.053	0.055	0.000	0.009	0.074	0.000	0.000
Mg	1.825	1.728	1.960	1.869	2.020	2.010	3.306	3.201	2.886	0.772	0.586	0.837	0.569	0.728
Ca	0.098	0.125	0.110	0.131	0.136	0.213	0.061	0.000	0.052	18.401	17.427	14.695	19.734	19.141
Na	0.193	0.365	0.373	0.351	0.313	0.145	0.370	0.291	0.365	0.429	0.117	0.226	0.085	0.321
K	1.302	1.845	1.701	1.381	1.196	1.284	0.461	0.460	0.167	1.021	0.753	0.676	0.405	0.652
P	0.000	0.000	0.000	0.000	0.000	0.000	0.017	0.000	0.000	8:228	7.740	6.636	8.645	8.697
S	0.111	0.116	0.000	0.082	0.131	0.015	0.071	0.068	0.045	0.000	0.021	0.000	0.000	0.017
O	32.760	33.732	34.400	33.125	33.504	34.864	33.523	32.845	31.507	31.607	30.448	29.051	30.846	32.047
TOTAL	82.438	83.629	84.314	82.864	84.703	84.849	86.888	86.240	83.399	77.549	75.565	72.542	76.630	78.914
BerthCalc.														
Si	3.253	3.381	3.402	3.289	3.205	3.373	2.964	2.899	2.869	3.423	3.335	3.193	3.207	3.464
Al(T)	0.747	0.619	0.598	0.711	0.795	0.627	1.036	1.101	1.131	0.577	0.665	0.807	0.793	0.536
Al(O)	2.000	2.094	2.113	2.014	1.954	2.229	1.559	1.478	1.378	2.130	2.026	1.927	1.891	2.096
Ti	0.018	0.042	0.066	0.031	0.011	0.024	0.037	0.026	0.063	0.046	0.012	0.018	0.050	0.007
Fe	2.658	2.381	2.248	2.555	2.717	2.231	3.096	3.293	3.439	1.863	2.381	2.584	2.405	2.187
Mn	0.006	0.000	0.011	0.002	0.000	0.000	0.002	0.007	0.007	0.000	0.003	0.020	0.000	0.000
Mg	0.514	0.472	0.525	0.520	0.556	0.531	0.910	0.899	0.844	0.512	0.392	0.522	0.428	0.504
Ca	0.017	0.021	0.018	0.022	0.023	0.034	0.004	0.000	0.009	0.264	0.298	0.145	0.498	0.161
Na	0.057	0.105	0.106	0.103	0.091	0.041	0.108	0.086	0.113	0.301	0.083	0.149	0.068	0.235
K	0.228	0.314	0.283	0.239	0.205	0.211	0.079	0.080	0.030	0.421	0.313	0.262	0.190	0.280
OCT.	5.196	4.990	4.964	5.124	5.238	5.015	5.604	5.702	5.732	4.552	4.813	5.071	4.774	4.794
INT.	0.302	0.440	0.407	0.364	0.319	0.286	0.191	0.167	0.152	0.985	0.694	0.556	0.755	0.676
CH	8.000	8.000	8.000	8.000	8.000	8.000	8.000	8.000	8.000	8.000	8.000	8.000	8.000	8.000

Table D.16. (Continued).

	STH. 36												
	MATRIX					OOIDS (BERTHIERINE)							
	1	2	3	4	5	1	2	3	4	5	6	7	8
Si	13.183	10.074	12.281	11.520	13.140	11.674	11.231	10.343	12.657	14.951	13.924	13.326	10.681
Ti	0.080	0.053	0.094	0.000	0.198	0.072	0.024	0.015	0.098	0.254	0.118	0.099	0.050
Al	11.576	9.631	10.147	10.667	10.296	10.380	10.57	9.716	10.924	12.183	11.269	11.127	9.522
Fe	21.540	22.164	17.798	22.206	18.787	28.569	26.064	25.269	25.517	20.458	23.786	23.943	22.930
Mn	0.036	0.000	0.000	0.000	0.031	0.084	0.046	0.000	0.000	0.012	0.003	0.052	0.000
Mg	1.629	1.733	1.578	1.859	1.554	2.232	1.655	1.511	2.260	2.322	2.119	1.960	1.716
Ca	0.086	0.052	0.090	0.065	0.095	0.090	0.048	0.096	0.133	0.096	0.055	0.105	0.028
Na	0.186	0.100	0.384	0.483	0.165	0.259	0.207	0.053	0.503	0.321	0.293	0.355	0.302
K	1.345	0.295	0.843	0.475	1.615	0.267	0.154	0.205	0.798	1.260	1.125	0.811	0.371
P	0.000	0.000	0.000	0.000	0.000	0.000	0.043	0.000	0.000	0.000	0.000	0.000	0.000
S	0.080	0.126	0.046	0.049	0.134	0.099	0.118	0.098	0.113	0.111	0.026	0.096	0.063
O	32.997	27.685	29.559	30.489	31.099	32.440	30.962	28.768	33.391	35.840	34.528	33.641	28.562
TOTAL	82.738	71.913	72.820	77.813	77.114	86.166	81.122	76.074	86.394	87.808	87.246	85.515	74.225
BerthCalc.													
Si	3.188	2.905	3.315	3.015	3.373	2.872	2.905	2.870	3.026	3.330	3.217	3.162	2.984
Al(T)	0.812	1.095	0.685	0.985	0.627	1.128	1.095	1.130	0.974	0.670	0.783	0.838	1.016
Al(O)	2.102	1.796	2.165	1.920	2.124	1.530	1.750	1.676	1.744	2.153	1.926	1.909	1.753
Ti	0.011	0.009	0.015	0.000	0.030	0.010	0.004	0.002	0.014	0.033	0.016	0.014	0.008
Fe	2.611	3.199	2.411	2.917	2.410	3.524	3.377	3.514	3.056	2.280	2.761	2.847	3.214
Mn	0.004	0.000	0.000	0.000	0.004	0.011	0.006	0.000	0.000	0.001	0.000	0.006	0.000
Mg	0.455	0.577	0.492	0.562	0.461	0.635	0.495	0.484	0.624	0.597	0.566	0.537	0.554
Ca	0.015	0.011	0.017	0.012	0.017	0.016	-0.008	0.019	0.022	0.015	0.009	0.017	0.005
Na	0.055	0.035	0.127	0.154	0.052	0.078	0.065	0.018	0.147	0.087	0.083	0.103	0.103
K	0.234	0.061	0.163	0.089	0.298	0.047	0.029	0.041	0.137	0.202	0.187	0.138	0.074
OCT.	5.185	5.582	5.083	5.399	5.030	5.710	5.630	5.677	5.437	5.066	5.269	5.313	5.529
INT.	0.303	0.107	0.307	0.256	0.367	0.141	0.086	0.077	0.306	0.304	0.278	0.259	0.183
CH	8.000	8.000	8.000	8.000	8.000	8.000	8.000	8.000	8.000	8.000	8.000	8.000	8.000

Table D.17. Compositions of Carbonates Within the Cleveland Ironstone Formation. The Data have been Recalculated to Carbonates of the Calcite Group.

	STH. 25				STH. 25					STH. 26				
	CALCITES REPLACING OOIDS				SIDERITES REPLACING THE MATRIX					SIDERITES REPLACING THE MATRIX				
	1	2	3	4	1	2	3	4	5	1	2	3	4	5
Ca	35.383	35.412	26.367	24.630	3.098	2.427	3.143	3.073	3.279	2.347	2.707	3.068	2.744	2.091
P	0.000	0.000	0.000	0.000	0.170	0.135	0.000	0.230	0.149	0.000	0.116	0.268	0.096	0.000
Sr	0.045	0.082	0.058	0.084	0.062	0.047	0.037	0.050	0.050	0.030	0.034	0.019	0.019	0.000
Si	0.925	0.966	3.948	5.079	0.006	0.164	0.099	0.256	0.009	0.012	0.095	0.055	0.153	0.140
Al	0.771	0.633	2.017	3.454	0.020	0.121	0.067	0.186	0.006	0.011	0.067	0.049	0.107	0.114
Mg	0.417	0.370	0.578	0.742	3.725	2.286	2.695	2.214	2.109	3.496	2.298	2.206	2.249	2.865
Na	0.037	0.066	0.037	0.066	0.125	0.054	0.026	0.069	0.048	0.047	0.085	0.108	0.070	0.045
Fe	2.468	1.977	4.011	4.769	34.663	37.308	36.439	36.813	36.731	35.516	36.716	35.906	36.267	36.673
Mn	0.233	0.169	0.250	0.198	0.158	0.571	0.800	0.385	0.724	0.479	0.478	0.494	0.920	0.536
O	16.935	16.697	18.443	20.642	13.963	13.824	13.889	14.130	13.664	13.598	13.604	13.600	13.655	13.659
TOTAL	57.214	56.372	55.709	59.664	52.892	54.510	54.052	54.333	53.490	55.536	56.200	55.773	56.280	56.123
CarbCalc.														
Ca	0.930	0.940	0.866	0.834	0.080	0.064	0.091	0.078	0.089	0.069	0.074	0.077	0.077	0.062
Fe	0.047	0.038	0.095	0.116	0.732	0.807	0.761	0.800	0.790	0.750	0.798	0.796	0.788	0.784
Mn	0.004	0.003	0.006	0.005	0.003	0.013	0.017	0.009	0.016	0.010	0.011	0.011	0.020	0.012
Mg	0.018	0.016	0.031	0.041	0.181	0.114	0.129	0.111	0.104	0.170	0.115	0.112	0.112	0.141
Sr	0.001	0.001	0.001	0.001	0.001	0.001	0.000	0.001	0.001	0.000	0.000	0.000	0.000	0.000
Na	0.002	0.003	0.002	0.004	0.006	0.003	0.001	0.004	0.003	0.002	0.004	0.006	0.004	0.002

	STH. 26		STH. 32								
	SIDERITES (CONT.)		SIDERITES REPLACING THE MATRIX					SIDERITES REPLACING OOIDS			
	6	7	1	2	3	4	5	1	2	3	4
Ca	1.406	3.555	3.375	6.159	3.820	4.414	7.531	3.242	3.239	3.549	4.081
P	0.011	0.440	0.429	1.550	0.426	0.010	2.721	0.327	0.368	0.504	0.405
Sr	0.072	0.035	0.036	0.030	0.035	0.050	0.109	0.019	0.152	0	0
Si	3.794	0.054	0.233	0.082	0.009	0.156	0.045	0.326	0.243	0.112	0
Al	3.196	0.042	0.146	0.070	0.012	0.134	0.031	0.280	0.276	0.141	0.001
Mg	3.472	2.461	2.144	1.739	2.240	3.176	1.621	2.085	2.311	1.958	2.041
Na	0.079	0.118	0.076	0.114	0.108	0.056	0.132	0.141	0.087	0.071	0.088
Fe	30.143	35.451	35.216	34.266	35.460	33.608	31.962	35.544	35.003	36.147	35.311
Mn	0.248	0.311	0.316	0.744	0.262	0.644	0.700	0.340	0.33	0.333	0.344
O	18.773	14.000	13.922	15.839	13.850	14.006	17.092	14.045	13.994	14.087	13.743
TOTAL	61.194	56.467	55.893	60.593	56.222	56.254	61.944	53.107	52.764	53.353	51.933
CarbCalc.											
Ca	0.048	0.080	0.078	0.091	0.090	0.128	0.059	0.080	0.077	0.077	0.099
Fe	0.745	0.784	0.801	0.795	0.787	0.703	0.821	0.801	0.791	0.812	0.786
Mn	0.006	0.007	0.007	0.018	0.006	0.014	0.018	0.008	0.008	0.008	0.008
Mg	0.197	0.125	0.112	0.093	0.114	0.153	0.096	0.108	0.120	0.101	0.104
Sr	0.001	0.000	0.001	0.000	0.000	0.001	0.002	0.000	0.002	0.000	0.000
Na	0.005	0.006	0.004	0.006	0.006	0.003	0.008	0.008	0.005	0.004	0.005

Table D.18. Compositions of Calcites Cementing Brachiopods in the Banbury Ironstone. The Data have been Recalculated to Calcite Formulae.

HRT. C	BRACHIOPOD 1							BRACHIOPOD 2						
	GEN. 1 (Fibrous)			GEN. 2 (Line into Pore)				GEN. 1 (Fibrous)			GEN. 2 (Line into Pore)			Unrep.Bio.
	1	2	3	1	2	3	4	1	2	3	1	2	3	1
Ca	33.524	36.384	36.419	35.742	36.824	36.482	36.531	35.299	33.299	34.531	36.466	36.208	36.569	38.023
P	0.027	0.000	0.006	0.001	0.000	0.000	0.000	0.000	0.000	0.000	0.000	0.000	0.000	0.000
Sr	0.037	0.051	0.033	0.018	0.028	0.035	0.012	0.093	0.052	0.045	0.036	0.047	0.031	0.110
Si	0.019	0.052	0.036	0.005	0.006	0.014	0.014	0.228	0.557	0.156	0.012	0.013	0.001	0.010
Al	0.000	0.015	0.000	0.000	0.000	0.000	0.000	0.170	0.422	0.113	0.000	0.000	0.000	0.001
Mg	0.094	0.108	0.112	0.096	0.072	0.041	0.032	0.121	0.166	0.108	0.090	0.081	0.053	0.142
Na	0.039	0.034	0.036	0.035	0.026	0.037	0.026	0.030	0.062	0.028	0.031	0.034	0.027	0.206
Fe	0.755	1.002	0.786	0.655	0.530	0.550	0.379	1.165	1.832	0.961	0.598	0.573	0.452	0.027
Mn	0.176	0.170	0.151	0.125	0.104	0.197	0.202	0.102	0.106	0.105	0.121	0.125	0.124	0.006
O	13.789	15.026	14.948	14.579	14.951	14.841	14.799	14.973	14.998	14.458	14.853	14.743	14.815	15.385
TOTAL	48.460	52.842	52.527	51.256	52.541	52.197	51.995	52.181	51.494	50.505	52.207	51.824	52.072	53.910
CarbCalc.														
Ca	0.974	0.971	0.976	0.979	0.984	0.982	0.986	0.968	0.950	0.972	0.981	0.981	0.985	0.987
Fe	0.016	0.019	0.015	0.013	0.010	0.011	0.007	0.023	0.038	0.019	0.012	0.011	0.009	0.001
Mn	0.004	0.003	0.003	0.002	0.002	0.004	0.004	0.002	0.002	0.002	0.002	0.002	0.002	0.000
Mg	0.005	0.005	0.005	0.004	0.003	0.002	0.001	0.005	0.008	0.005	0.004	0.004	0.002	0.006
Sr	0.000	0.001	0.000	0.000	0.000	0.000	0.000	0.001	0.001	0.001	0.000	0.001	0.000	0.001
Na	0.002	0.002	0.002	0.002	0.001	0.002	0.001	0.001	0.003	0.001	0.001	0.002	0.001	0.009

	BRACHIOPOD 3														
	GEN. 1 (Fibrous)			GEN. 2 (Line into Pore)					GEN. 3 (Pore-filling, may be GEN. 2)			Unrep. Bio.	Cementing Ooids		
	1	2	3	1	2	3	4	5	1	2	3	1	1	2	3
Ca	36.835	35.441	35.247	36.212	36.279	35.453	37.489	35.946	37.771	39.334	37.301	37.100	37.944	38.201	39.105
P	0.048	0.000	0.000	0.032	0.059	0.036	0.000	0.022	0.000	0.000	0.035	0.000	0.017	0.000	0.000
Sr	0.042	0.027	0.121	0.066	0.027	0.031	0.023	0.019	0.039	0.042	0.068	0.097	0.026	0.033	0.026
Si	0.029	0.033	0.022	0.009	0.005	0.013	0.010	0.007	0.007	0.006	0.010	0.005	0.000	0.000	0.000
Al	0.011	0.000	0.000	0.000	0.001	0.000	0.000	0.000	0.000	0.000	0.000	0.000	0.000	0.000	0.000
Mg	0.140	0.147	0.110	0.100	0.100	0.057	0.020	0.091	0.121	0.128	0.181	0.286	0.112	0.163	0.060
Na	0.029	0.037	0.036	0.036	0.035	0.032	0.043	0.029	0.011	0.016	0.034	0.160	0.011	0.012	0.007
Fe	0.691	0.865	0.850	0.372	0.893	0.639	0.012	0.022	0.885	1.127	1.228	0.158	0.721	0.835	0.484
Mn	0.074	0.120	0.116	0.457	0.141	0.201	0.000	0.011	0.183	0.157	0.207	0.020	0.103	0.128	0.105
O	15.139	14.583	14.481	14.837	14.945	14.511	15.012	14.469	15.484	16.175	15.503	15.129	15.488	15.644	15.827
TOTAL	53.038	51.253	50.983	52.121	52.485	50.973	52.609	50.616	54.501	56.985	54.567	52.955	54.422	55.016	55.614
CarbCalc.															
Ca	0.978	0.973	0.973	0.978	0.974	0.979	0.998	0.994	0.974	0.971	0.964	0.979	0.979	0.975	0.986
Fe	0.013	0.017	0.017	0.007	0.017	0.013	0.000	0.000	0.016	0.020	0.023	0.003	0.013	0.015	0.009
Mn	0.001	0.002	0.002	0.009	0.003	0.004	0.000	0.000	0.003	0.003	0.004	0.000	0.002	0.002	0.002
Mg	0.006	0.007	0.005	0.004	0.004	0.003	0.001	0.004	0.005	0.005	0.008	0.012	0.005	0.007	0.002
Sr	0.001	0.000	0.002	0.001	0.000	0.000	0.000	0.000	0.000	0.000	0.001	0.001	0.000	0.000	0.000
Na	0.001	0.002	0.002	0.002	0.002	0.002	0.002	0.001	0.000	0.001	0.002	0.007	0.000	0.001	0.000

Table D.18. (Continued).

HRT. A	BRACHIOPOD 4						BRACHIOPOD 5													
	GEN. 1 (Fibrous)			GEN. 2 (Line into Pore)			GEN. 1 (Fibrous)			GEN. 2 (Line into Pore)			GEN. 3 (Pore-filling)			Cementing Ooids				
	1	2	3	1	2	3	1	2	3	1	2	3	1	2	3	1	2	3	4	5
Ca	37.550	39.829	36.413	39.074	39.375	38.886	36.478	39.828	38.488	37.357	38.795	37.323	39.126	37.749	38.342	39.218	39.312	38.768	38.183	37.919
P	0.014	0.000	0.030	0.000	0.000	0.000	0.000	0.045	0.000	0.000	0.000	0.000	0.000	0.000	0.000	0.016	0.071	0.024	0.000	0.069
Sr	0.031	0.026	0.028	0.052	0.029	0.053	0.053	0.033	0.037	0.041	0.049	0.021	0.030	0.024	0.040	0.028	0.060	0.079	0.040	0.485
Si	0.000	0.000	0.000	0.000	0.000	0.000	0.000	0.000	0.000	0.000	0.000	0.000	0.000	0.000	0.000	0.005	0.003	0.021	0.012	0.008
Al	0.001	0.001	0.001	0.000	0.002	0.000	0.002	0.003	0.006	0.005	0.000	0.003	0.006	0.007	0.000	0.004	0.000	0.051	0.004	0.033
Mg	0.087	0.081	0.087	0.115	0.085	0.138	0.186	0.153	0.130	0.091	0.155	0.119	0.086	0.075	0.117	0.125	0.105	0.155	0.130	0.135
Na	0.000	0.000	0.000	0.003	0.011	0.008	0.009	0.000	0.000	0.000	0.000	0.000	0.000	0.000	0.000	0.000	0.000	0.003	0.002	0.000
Fe	0.835	0.333	0.753	0.709	0.557	0.817	0.953	0.175	0.206	0.623	0.846	0.924	0.571	0.526	0.924	0.901	0.928	0.931	0.926	1.754
Mn	0.361	0.065	0.255	0.111	0.131	0.135	0.119	0.030	0.048	0.117	0.140	0.178	0.137	0.140	0.181	0.156	0.078	0.151	0.152	0.148
O	15.417	16.072	14.928	15.920	15.983	15.900	15.007	16.125	15.535	15.198	15.881	15.301	15.889	15.321	15.708	16.076	16.157	16.004	15.664	15.998
TOTAL	54.296	56.407	52.495	55.984	56.173	55.937	52.807	56.392	54.450	53.432	55.866	53.869	55.845	53.842	55.312	56.529	56.714	56.187	55.113	56.549
CarbCalc.																				
Ca	0.974	0.989	0.976	0.980	0.984	0.976	0.970	0.990	0.989	0.982	0.975	0.974	0.983	0.984	0.974	0.976	0.977	0.973	0.974	0.954
Fe	0.016	0.006	0.015	0.013	0.010	0.015	0.018	0.003	0.004	0.012	0.015	0.017	0.010	0.010	0.017	0.016	0.017	0.017	0.017	0.032
Mn	0.007	0.001	0.005	0.002	0.002	0.002	0.002	0.001	0.001	0.002	0.003	0.003	0.003	0.003	0.003	0.003	0.001	0.003	0.003	0.003
Mg	0.004	0.003	0.004	0.005	0.004	0.006	0.008	0.006	0.006	0.004	0.006	0.005	0.004	0.003	0.005	0.005	0.004	0.006	0.005	0.006
Sr	0.000	0.000	0.000	0.001	0.000	0.001	0.001	0.000	0.000	0.000	0.001	0.000	0.000	0.000	0.000	0.000	0.001	0.001	0.000	0.006
Na	0.000	0.000	0.000	0.000	0.000	0.000	0.000	0.000	0.000	0.000	0.000	0.000	0.000	0.000	0.000	0.000	0.000	0.000	0.000	0.000

Table D.19. Compositions of Berthierines and the Surface Oxidation Layer Within Specimen HRT. OX of the Banbury Ironstone. The Data have all been Recalculated to Berthierine Structural Formulae.

	HRT.OX											
	MATRIX						OOIDS (BERTHIERINE/GOETHITE)					
	1	2	3	4	5	6	1	2	3	4	5	6
Si	9.984	10.353	10.075	7.760	10.780	10.846	7.099	5.796	9.079	6.991	5.364	7.090
Ti	0.066	0.073	0.000	0.028	0.000	0.000	0.163	0.161	0.062	0.509	0.759	0.483
Al	7.188	7.488	7.318	5.527	7.625	7.916	5.357	3.919	6.362	5.561	4.459	5.134
Fe	26.902	25.431	26.238	22.992	29.992	29.376	27.256	15.677	30.837	21.529	24.055	22.308
Mn	0.000	0.000	0.045	0.047	0.027	0.000	0.105	0.003	0.074	0.037	0.063	0.034
Mg	1.368	1.496	1.312	0.988	1.263	1.580	1.484	0.673	1.103	1.056	0.868	1.647
Ca	0.272	0.325	0.346	0.370	0.229	0.221	0.641	0.651	0.427	0.364	0.260	0.162
Na	0.194	0.251	0.198	0.346	0.043	0.279	0.393	0.111	0.186	0.133	0.000	0.514
K	0.082	0.000	0.000	0.096	0.122	0.035	0.026	0.072	0.000	0.008	0.127	0.288
P	0.000	0.069	0.130	0.136	0.021	0.000	0.042	0.248	0.070	0.063	0.130	0.040
S	0.079	0.059	0.066	0.121	0.000	0.000	0.073	0.110	0.036	0.016	0.098	0.051
O	26.613	27.081	26.755	21.490	28.654	29.046	22.229	15.765	25.950	20.400	18.363	20.805
TOTAL	72.748	72.626	72.483	59.901	78.756	79.299	64.868	43.186	74.186	56.667	54.546	58.556
BerthCalc.												
Si	2.994	3.063	3.029	2.914	3.004	2.978	2.557	3.015	2.804	2.748	2.360	2.728
Al(T)	1.006	0.937	0.971	1.086	0.996	1.022	1.443	0.985	1.196	1.252	1.640	1.272
Al(O)	1.238	1.369	1.319	1.074	1.216	1.240	0.565	1.137	0.848	1.022	0.402	0.784
Ti	0.012	0.013	0.000	0.006	0.000	0.000	0.034	0.049	0.011	0.117	0.196	0.109
Fe	4.047	3.777	3.959	4.322	4.203	4.057	4.926	4.076	4.784	4.253	5.304	4.308
Mn	0.000	0.000	0.007	0.009	0.004	0.000	0.019	0.001	0.012	0.007	0.014	0.007
Mg	0.474	0.511	0.456	0.429	0.407	0.501	0.618	0.404	0.394	0.480	0.441	0.732
Ca	0.057	0.055	0.049	0.066	0.041	0.043	0.153	0.159	0.079	0.085	0.046	0.034
Na	0.071	0.091	0.073	0.159	0.015	0.094	0.173	0.071	0.070	0.064	0.000	0.242
K	0.018	0.000	0.000	0.026	0.024	0.007	0.007	0.027	0.000	0.002	0.040	0.080
OCT.	5.771	5.670	5.740	5.841	5.829	5.798	6.162	5.667	6.049	5.879	6.357	5.940
INT.	0.146	0.146	0.122	0.251	0.080	0.143	0.332	0.257	0.149	0.151	0.086	0.356
OH	8.000	8.000	8.000	8.000	8.000	8.000	8.000	8.000	8.000	8.000	8.000	8.000

Table D.19. (Continued).

	GOETHITE OXIDATION LAYER (INNER)							GOETHITE OXIDATION LAYER (OUTER)							
	1	2	3	4	5	6	7	1	2	3	4	5	6	7	8
Si	1.541	7.411	2.893	2.879	3.247	7.538	7.674	8.465	10.984	2.323	7.888	2.711	5.181	2.397	2.098
Ti	0.000	0.063	0.000	0.034	0.000	0.068	0.049	0.238	0.000	0.087	0.069	0.000	0.027	0.052	0.000
Al	0.377	4.951	1.266	0.617	1.457	5.297	5.381	6.614	7.480	2.012	5.337	1.102	3.252	2.042	1.041
Fe	26.841	41.095	46.154	51.614	49.843	27.695	40.508	34.023	30.044	43.112	39.060	43.257	40.709	39.749	41.389
Mn	0.202	0.070	0.185	0.144	0.165	0.000	0.264	0.153	0.089	0.239	0.139	0.546	0.184	0.258	0.393
Mg	0.076	1.107	0.735	0.095	0.058	0.941	0.939	0.867	0.973	0.602	0.745	0.684	0.651	0.664	0.387
Ca	0.329	0.341	0.379	0.244	0.176	0.203	0.322	0.850	0.966	0.524	0.757	0.544	0.686	0.599	0.441
Na	0.320	0.298	0.437	0.450	0.331	0.253	0.409	0.340	0.012	0.112	0.083	0.458	0.248	0.367	0.406
K	0.000	0.041	0.005	0.035	0.042	0.023	0.082	0.135	0.000	0.031	0.058	0.001	0.004	0.000	0.004
P	0.010	0.000	0.000	0.000	0.059	0.125	0.000	0.096	0.039	0.010	0.015	0.158	0.016	0.000	0.008
S	0.018	0.000	0.127	0.000	0.066	0.164	0.057	0.029	0.000	0.000	0.000	0.074	0.014	0.072	0.064
O	10.145	25.659	18.486	19.004	19.631	22.232	26.149	26.657	28.881	17.579	25.863	17.653	21.339	16.849	15.870
TOTAL	39.859	81.036	70.667	75.116	75.075	64.539	81.834	78.467	79.468	66.631	80.014	67.188	72.311	63.049	62.101
BerthCalc.															
Si	1.214	2.303	1.250	1.208	1.327	2.734	2.342	2.548	3.040	1.055	2.435	1.244	1.939	1.136	1.056
Al(T)	2.786	1.697	2.750	2.792	2.673	1.266	1.658	1.452	0.960	2.945	1.565	2.756	2.061	2.864	2.944
Al(O)	-2.477	-0.095	-2.180	-2.522	-2.054	0.734	0.051	0.620	1.194	-1.994	0.149	-2.229	-0.794	-1.857	-2.398
Ti	0.000	0.011	0.000	0.008	0.000	0.014	0.009	0.042	0.000	0.023	0.012	0.000	0.006	0.014	0.000
Fe	10.627	6.424	10.007	10.893	10.231	5.026	6.209	5.147	4.182	9.846	6.063	9.971	7.660	9.458	10.465
Mn	0.081	0.011	0.041	0.031	0.034	0.000	0.041	0.024	0.013	0.055	0.022	0.128	0.035	0.063	0.101
Mg	0.069	0.398	0.367	0.046	0.027	0.394	0.331	0.302	0.311	0.316	0.266	0.363	0.282	0.364	0.225
Ca	0.177	0.074	0.115	0.072	0.036	0.024	0.069	0.162	0.181	0.164	0.161	0.131	0.176	0.199	0.153
Na	0.308	0.113	0.231	0.231	0.165	0.112	0.152	0.125	0.004	0.062	0.031	0.257	0.113	0.212	0.250
K	0.000	0.009	0.002	0.011	0.012	0.006	0.018	0.029	0.000	0.010	0.013	0.000	0.001	0.000	0.001
OCT.	8.301	6.749	8.234	8.456	8.239	6.168	6.641	6.135	5.700	8.246	6.513	8.233	7.188	8.041	8.392
INT.	0.485	0.197	0.347	0.313	0.213	0.142	0.239	0.316	0.185	0.236	0.205	0.388	0.291	0.411	0.404
OH	8.000	8.000	8.000	8.000	8.000	8.000	8.000	8.000	8.000	8.000	8.000	8.000	8.000	8.000	8.000

Table D.20. Compositions of Berthierines in the Raasay Ironstone. The Data have been Recalculated to Berthierine Structural Formulae.

	RSY. 4														
	BERTHIERINE OOIDS							SPHERULITIC BERTHIERINE							
	1	2	3	4	5	6	7	1	2	3	4	6	7	8	9
Si	7.346	9.179	9.175	9.077	7.937	7.832	8.935	9.254	9.115	8.380	9.254	8.976	9.212	9.051	9.059
Ti	0.062	0.052	0.093	0.180	0.112	0.081	0.038	0.058	0.094	0.130	0.000	0.015	0.028	0.082	0.000
Al	7.189	8.896	8.862	8.744	7.650	8.350	9.599	11.499	10.554	10.205	10.194	11.256	11.045	10.898	10.482
Fe	22.727	29.280	30.067	29.424	25.571	28.860	29.730	34.489	34.108	33.565	34.115	34.257	34.063	34.841	34.763
Mn	0.146	0.067	0.000	0.127	0.012	0.000	0.027	0.000	0.000	0.093	0.000	0.000	0.229	0.000	0.000
Mg	1.044	1.188	1.100	1.349	0.892	0.846	1.167	0.887	1.100	1.034	1.001	1.054	0.904	1.123	0.957
Ca	2.310	0.117	0.816	0.451	2.016	2.447	0.589	0.100	0.018	0.109	0.034	0.000	0.047	0.014	0.083
Na	0.210	0.000	0.350	0.442	0.000	0.067	0.049	0.202	0.386	0.178	0.061	0.056	0.092	0.100	0.312
K	0.000	0.108	0.000	0.018	0.096	0.000	0.120	0.000	0.000	0.000	0.000	0.000	0.000	0.000	0.003
P	1.099	0.000	0.305	0.082	0.904	1.262	0.298	0.426	0.296	0.195	0.288	0.453	0.508	0.566	0.400
S	0.015	0.064	0.000	0.000	0.026	0.029	0.125	0.000	0.007	0.027	0.039	0.000	0.000	0.062	0.000
O	24.461	27.663	28.576	28.037	25.830	27.859	28.698	31.934	30.854	29.392	30.449	31.361	31.466	31.552	30.892
TOTAL	66.609	76.614	79.344	77.931	71.046	77.633	79.375	88.849	86.532	83.308	85.435	87.428	87.594	88.289	86.951
BerthCalc.															
Si	2.543	2.648	2.596	2.592	2.567	2.382	2.520	2.352	2.386	2.294	2.455	2.326	2.385	2.343	2.379
Al(T)	1.457	1.352	1.404	1.408	1.433	1.618	1.480	1.648	1.614	1.706	1.545	1.674	1.615	1.657	1.621
Al(O)	1.134	1.319	1.207	1.190	1.143	1.025	1.337	1.393	1.261	1.202	1.269	1.362	1.360	1.280	1.243
Ti	0.013	0.009	0.015	0.030	0.021	0.014	0.006	0.009	0.014	0.021	0.000	0.002	0.004	0.012	0.000
Fe	3.955	4.240	4.279	4.225	4.156	4.411	4.201	4.408	4.489	4.618	4.546	4.465	4.435	4.529	4.590
Mn	0.026	0.010	0.000	0.019	0.002	0.000	0.004	0.000	0.000	0.013	0.000	0.000	0.030	0.000	0.000
Mg	0.418	0.396	0.360	0.445	0.333	0.297	0.380	0.260	0.333	0.327	0.307	0.316	0.270	0.336	0.290
Ca	0.560	0.024	0.162	0.090	0.457	0.521	0.116	0.018	0.003	0.021	0.006	0.000	0.009	0.003	0.015
Na	0.089	0.000	0.121	0.154	0.000	0.025	0.017	0.063	0.123	0.060	0.020	0.018	0.029	0.032	0.100
K	0.000	0.022	0.000	0.004	0.022	0.000	0.024	0.000	0.000	0.000	0.000	0.000	0.000	0.000	0.001
OCT.	5.544	5.973	5.861	5.910	5.656	5.748	5.928	6.070	6.097	6.181	6.122	6.145	6.100	6.158	6.124
INT.	0.649	0.046	0.283	0.248	0.479	0.546	0.158	0.080	0.127	0.080	0.026	0.018	0.038	0.034	0.116
CH	8.000	8.000	8.000	8.000	8.000	8.000	8.000	8.000	8.000	8.000	8.000	8.000	8.000	8.000	8.000

APPENDIX E: PUBLISHED BERTHIERINE ANALYSES.

The following list, and tables of berthierine compositions, are compiled from published berthierine analyses, recalculated if necessary on the basis of 14 oxygens to be of a similar format to those of this thesis. The analyses were obtained from the papers quoted, some of which are themselves compilations, and the reader is referred to these papers for the original references therein. It is these analyses that are implied to, when reference is made in the text to published berthierine compositions. The following list gives the location of each sample:

Hughes (1989), A.T.E.M. Analysis. Values quoted are averages.

1) Cleveland Ironstone, Main Seam, Staithes, Yorkshire, England.
2) Frodingham Ironstone, Scunthorpe, England.
3) (As above).
4) Wasia Formation ironstone, Arabia.

Garzanti et al. (1989), E.P.M.A. Values quoted are averages.

5) Ferruginous Oolite Formation, Zangla section, Zanskar, N. India.
6) (as above).
7) (as above).

Brindley (1982). Wet Chemical Analyses. Single analyses from various sources.

8) Belgorod District, Kursk, U.S.S.R.
9) (as above).
10) (as above).
11) Wabana, Newfoundland, Canada.
12) Voronezh anticline, Kursk, U.S.S.R.
13) (as above).
14) (as above).
15) Ayrshire, Scotland.
16) Weald Clay, Sussex, England.
17) Stanion Lane Pit, Corby, England.
18) Pegnitz, Germany.
19) Gunflint Iron Formation, U.S.A.-Canada.
20) Sainte-Barbe, France.
21) Kank, Kutna Hora, Czechoslovakia.
22) Chamozente, Switzerland.
23) Windgalle, Switzerland.
24) Schmiderfeld, Germany.
25) Gledic, Yugoslavia.
26) Raasay, Scotland.
27) Frodingham, Scunthorpe, England.
28) Loch Etive, Scotland.

Iijima and Matsumoto (1982), E.P.M.A. Values quoted are averages.

29) Hiramatsu, Utatsu, Japan. K-Type.
30) (as above) S-Type.
31) (as above) V-Type.

Maynard (1986). E.P.M.A. Values quoted are averages.

32) Frodingham Ironstone, Scunthorpe, England.
33) Northampton Sand Ironstone, Corby, England.
34) Mines a Poix, Hayange, France.
35) Ardnish Ironstone, Broadford, Skye, Scotland.
36) Cleveland Ironstone, Staithes, Yorkshire, England.
37) Raasay Ironstone, Straithard, Skye, Scotland.

Table E.1. Analyses of Berthierine From the Literature. Data has been Recalculated Where Necessary, to be Quoted in a Similar Format to This Thesis.

	Hughes (1989)				Garzanti et al. (1989)			Brindley (1982)					
	1	2	3	4	5	6	7	8	9	10	11	12	13
Si	2.820	3.080	3.140	2.580	2.633	2.619	2.756	2.292	2.194	2.548	2.448	2.552	2.414
Al(T)	1.180	0.920	0.860	1.420	1.367	1.381	1.244	1.708	1.806	1.452	1.552	1.448	1.586
Al(O)	1.040	0.740	0.780	1.140	1.431	1.423	1.248	1.922	1.838	2.05	1.872	1.636	1.574
Ti	0.040	0.000	0.000	0.000	0.004	0.017	0.012	n.d.	n.d.	n.d.	n.d.	n.d.	n.d.
Fe(II)	3.720	3.980	3.840	3.460	3.653	3.616	3.523	2.97	3.322	3.002	3.580	2.668	3.288
Fe(III)	0.420	0.440	0.420	0.220	n.d.	n.d.	n.d.	0.446	0.372	0.322	0.022	0.304	0.432
Mn	0.020	0.000	0.000	0.000	0.002	0.000	0.001	n.d.	n.d.	n.d.	0.004	n.d.	n.d.
Mg	0.300	0.580	0.720	0.960	0.827	0.826	1.152	0.33	0.266	0.162	0.348	1.144	0.494
Ca	0.120	0.100	0.060	0.000	0.045	0.072	0.029	n.d.	n.d.	n.d.	n.d.	n.d.	n.d.
Na	0.000	0.000	0.000	0.000	0.002	0.016	0.009	n.d.	n.d.	n.d.	n.d.	n.d.	n.d.
K	0.300	0.060	0.020	0.000	0.000	0.000	0.030	n.d.	n.d.	n.d.	n.d.	n.d.	n.d.
OCT.	5.540	5.740	5.760	5.940	5.917	5.882	5.937	5.668	5.798	5.536	5.826	5.752	5.788
INT.	0.420	0.160	0.080	0.000	0.047	0.088	0.068	n.d.	n.d.	n.d.	n.d.	n.d.	n.d.
CH	8.000	8.000	8.000	8.000	8.000	8.000	8.000	7.856	8.000	7.800	8.000	7.904	8.000
	n=7	n=12	n=20	n=12	n=8	n=3	n=8						

Table E.1. (Continued).

									Bhattacharyya (1983)				
	14	15	16	17	18	19	20	21	22	23	24	25	26
Si	2.574	2.854	2.650	2.670	2.714	2.914	3.070	3.034	3.274	2.616	2.992	2.568	3.050
Al(T)	1.426	1.146	1.350	1.330	1.286	1.086	0.930	0.966	0.726	1.384	1.008	1.432	0.950
Al(O)	1.794	1.696	1.682	1.474	1.460	1.262	1.184	0.730	1.482	0.574	1.122	1.396	1.132
Ti	n.d.	n.d.	n.d.	n.d.	n.d.	n.d.	n.d.	n.d.	n.d.	n.d.	n.d.	n.d.	n.d.
Fe(II)	3.610	2.960	3.672	3.386	3.320	3.334	3.584	3.616	3.412	3.658	3.220	2.178	3.204
Fe(III)	0.042	0.542	0.020	0.360	0.468	0.000	0.000	0.466	0.300	1.048	0.564	1.332	0.568
Mn	0.004	0.004	n.d.	n.d.	n.d.	n.d.	0.102	0.004	0.002	0.002	n.d.	0.100	0.036
Mg	0.344	0.256	0.452	0.530	0.430	1.316	1.006	1.066	0.274	0.598	0.754	0.344	0.686
Ca	n.d.	n.d.	n.d.	n.d.	n.d.	n.d.	n.d.	n.d.	n.d.	n.d.	n.d.	n.d.	n.d.
Na	n.d.	n.d.	n.d.	n.d.	n.d.	n.d.	n.d.	n.d.	n.d.	n.d.	n.d.	n.d.	n.d.
K	n.d.	n.d.	n.d.	n.d.	n.d.	n.d.	n.d.	n.d.	n.d.	n.d.	n.d.	n.d.	n.d.
OCT.	5.794	5.458	5.826	5.750	5.678	5.912	5.876	5.882	5.470	5.880	5.660	5.350	5.626
INT.	n.d.	n.d.	n.d.	n.d.	n.d.	n.d.	n.d.	n.d.	n.d.	n.d.	n.d.	n.d.	n.d.
OH	8.000	7.848	7.928	7.984	8.000	6.928	8.000	8.000	8.000	8.000	8.000	8.000	8.000

Table E.1. (Continued).

			Iijima & Matsumoto (1982)			Maynard (1986)							
	27	28	29	30	31	32	33	34	35	36	37	AVERAGE	STDEV
Si	2.862	3.366	2.600	2.660	2.595	3.400	3.180	2.940	2.920	2.840	2.760	2.789	0.286
Al(T)	1.138	0.634	1.400	1.340	1.405	0.600	0.820	1.060	1.080	1.160	1.240	1.211	0.286
Al(O)	1.692	0.610	1.715	1.675	1.550	1.740	1.500	0.960	1.300	1.780	1.400	1.395	0.384
Ti	n.d.	n.d.	n.d.	n.d.	n.d.	n.d.	n.d.	n.d.	n.d.	n.d.	n.d.	0.011	0.015
Fe(II)	3.350	n.d.	3.815	3.830	4.155	3.100	3.560	4.340	4.060	3.280	4.300	3.488	0.435
Fe(III)	0.620	3.006	n.d.	n.d.	n.d.	n.d.	n.d.	n.d.	n.d.	n.d.	n.d.	0.509	0.603
Mn	0.038	0.076	n.d.	n.d.	n.d.	n.d.	n.d.	n.d.	n.d.	n.d.	n.d.	0.022	0.035
Mg	0.792	0.742	0.295	0.315	0.220	0.540	0.580	0.500	0.620	0.660	0.240	0.586	0.300
Ca	n.d.	n.d.	0.010	0.005	0.010	n.d.	n.d.	n.d.	n.d.	n.d.	n.d.	0.045	0.042
Na	n.d.	n.d.	n.d.	n.d.	n.d.	n.d.	n.d.	n.d.	n.d.	n.d.	n.d.	0.004	0.006
K	n.d.	n.d.	n.d.	n.d.	n.d.	n.d.	n.d.	n.d.	n.d.	n.d.	n.d.	0.059	0.109
OCT.	6.492	4.434	5.825	5.820	5.925	5.380	5.640	5.800	5.980	5.720	5.940	5.735	0.299
INT.	n.d.	n.d.	n.d.	n.d.	n.d.	n.d.	n.d.	n.d.	n.d.	n.d.	n.d.	n.d.	n.d.
CH	8.000	8.000	8.000	8.000	8.000	8.000	8.000	8.000	8.000	8.000	8.000		
			n=10	n=9	n=6								

REFERENCES.

ADAMS, J. A. S., & RICHARDSON, R. 1960. Thorium, uranium and zirconium concentrations in bauxite. *Economic Geology*, **55**, 1653-1675.

ADELEYE, D. R. 1973. Origin of ironstones, an example from the Middle Niger Valley, Nigeria. *Journal of Sedimentary Petrology*, **43**, 709-727.

----------. 1975. Derivation of fragmentary oolites and pisolites from dessication cracks. *Journal of Sedimentary Petrology*, **45**, 794-798.

----------. 1980. Origin of oolitic iron formations - discussion. *Journal of Sedimentary Petrology*, **50**, 1001-1003.

AGER, D. V. 1956. The geographical distribution of brachiopods in the British Lias. *Quarterly Journal of the Geological Society of London*, **112**, 157-182.

ALEXANDERSSON, T. 1972. Intragranular growth of marine aragonite and Mg-calcite: evidence of precipitation from supersaturated seawater. *Journal of Sedimentary Petrology*, **42**, 441-460.

ALLER, R. C., MACKIN, J. E., & COX, R.T. 1986. Diagenesis of iron and sulphur in Amazon inner-shelf muds - apparent dominance of iron-reduction and implications for the genesis of ironstones. *Continental Shelf*, **61**, 263-289.

ALLING, H. L. 1947. Diagenesis of the Clinton hematite ores of New York. *Geological Society of America Bulletin*, **58**, 991-1018.

ANDERSON, F. W., & DUNHAM, K. C. 1966. *The geology of northern Skye*. Memoir of the Geological Survey of Scotland.

ANDERSON, T.F. & ARTHUR, M. A. 1983. Stable isotopes of oxygen and carbon and their application to sedimentologic and palaeoenvironmental problems. *In:*. ARTHUR, M. A., ANDERSON, T. F., KAPLAN, I. R., VEIZER, J., & LAND, L. S. *Stable isotopes in sedimentary geology*. Society of Economic Pal eontologists and Mineralogists Short Course Notes, **10**, 1.1-1.151.

ANDREWS-SPEED, C. P., OXBURGH, E. R., & COOPER, B. A. 1984. Temperature and depth dependent heat flow in the Western North Sea. *American Association of Petroleum Geologists Bulletin*, **68**, 1764-1781.

ARKELL, W. J. 1933. *The Jurassic System in Great Britain*. Clarenden Press.

---------- 1936. The Corallian rocks of Dorset. Pt 1. The coast..*Proceedings of the Dorset Archaeological and Natural History Society*, **57**, 59-93.

ASCHENBRENNER, B. C. 1956. A new method of expressing particle sphericity. *Journal of Sedimentary Petrology*, **26**, 15-31.

BAAS-BECKING, L. G. M., KAPLAN, I. R. & MOORE, D. 1960. Limit of the natural environment in terms of pH and oxidation-reduction potentials. *Journal of Geology*, **68**, 243-284.

BARRETT, P. J. 1980. The shape of rock particles, a critical review. *Sedimentology*, **27**, 291-303.

BATHURST, R. G. C. 1959. The cavernous structure of some Mississippian "Stromatactis" reefs in Lancashire, England. *Journal of Geology*, **67**, 506-521.

----------. 1966. Boring algae, micrite envelopes, and lithification of molluscan biosparites. *Geological Journal*, **5**, 15-32.

----------. 1975. *Carbonate sediments and their diagenesis*. Elsevier.

----------. 1982. Genesis of stromatactis cavities between submarine crusts in Palaeozoic carbonate mud buildups. *Journal of the Geological Society of London*, **139**, 165-181.

BERNER, R. A. 1970. Sedimentary pyrite formation. *American Journal of Science*, **268**, 1-23.

----------. 1975. The role of magnesium in the crystal growth of calcite and aragonite from seawater. *Geochimica et Cosmochimica Acta*, **39**, 489-504.

----------. 1980. *Early diagenesis: a theoretical approach*. Princetown University Press.

----------. 1981. A new geochemical classification of sedimentary environments. *Journal of Sedimentary Petrology*, **51**, 359-365.

----------. 1984. Sedimentary pyrite formation: an update. *Geochimica et Cosmochimica Acta*, **48**, 605-615.

BHATTACHARYYA, D. P. 1983. Origin of berthierine in ironstones. *Clays and Clay Minerals*, **31**, 173-182.

----------. 1989. Concentrated and lean oolites: examples from the Nubia Formation at Aswan, Egypt, and significance of the oolite types in ironstone genesis. *In:* YOUNG, T. P., & TAYLOR, W. E. G. (eds.) *Phanerozoic Ironstones*. Geological Society of London, Special Publication, **46**, 93-103.

BHATTACHARYYA, D. P., & KAKIMOTO, P.K. 1982. Origin of ferriferous ooids; an S.E.M. study of ironstone ooids and bauxite pisoids. *Journal of Sedimentary Petrology*, **52**, 849-857.

BINDER, G., & TROLL, G. 1989. Coupled anion substitution in natural carbon-bearing apatites. *Contributions to Mineralogy and Petrology*, **101**, 394-401.

BINDA, P. L., & MOLTZER, J. G. 1979. Origin of oolitic iron formations - discussion. *Journal of Sedimentary Petrology*, **49**, 1351-1352.

BISCHOFF, J. L., & FYFE, W. S. 1968. Catalysis, inhibition, and the aragonite problem. 1. The aragonite - calcite transformation. *American Journal of Science*, **266**, 65-79.

BJØRLYKKE, K., & BRENDSDAL, A. 1986. Diagenesis of the Brent Sandstone in the Statflord Field, North Sea. *In:* GAUTIER, D. (ed.) *Roles of organic matter in sediment diagenesis*. Society of Economic Palaeontologists and Mineralogists Special Publication, **38**, 157-167.

BOLES, J. R. 1978. Active ankerite cementation in the subsurface Eocene of southwest Texas. *Contributions to Mineralogy and Petrology*, **68**, 13-22.

BOLES, J. R., LANDIS, C. A., & DALE, P. 1985. The Moeraki boulders - anatomy of some septarian concretions. *Journal of Sedimentary Petrology*, **55**, 398-406.

BOLES, J. R., & RAMSEYER, K. 1987. Diagenetic carbonate in Miocene sandstone reservoir, San Joaquin Basin, California. *American Association of Petroleum Geologists Bulletin*, **71**, 1475-1487.

BRADSHAW, M. J., JAMES, S. J. & TURNER, P. 1980. Origin of oolitic ironstones - discussion. *Journal of Sedimentary Petrology*, **50**, 295-304.

BRADSHAW, M. J. & PENNEY, S. R. 1982. A cored Jurassic sequence from North Lincolnshire, England: Stratigraphy, facies analysis and regional context. *Geological Magazine*, **119**, 113-228.

BRAITHWAITE, C. J. R. 1979. Crystal textures of recent fluvial pisolites and laminated crystalline crusts in Dyfed, South Wales. *Journal of Sedimentary Petrology*, **49**, 181-194.

BRINDLEY, G. W. 1982. Chemical composition of berthierines - a review. *Clays and Clay Minerals*, **30**, 153-155.

BRINDLEY, G. W., & BROWN, G. (eds.) 1980. *Crystal structures of clay minerals and their X-Ray identification*. Mineralogical Society Monograph Number 5.

BROCKAMP, B. 1942. Die palaogeographisce Stellung der Eisenablagerungen. *In:* BROCKAMP, B. (ed.) *Zur Entstehung deutscher Eisenerzlagerstatten*. Archiv, fur Lagerstattenforschung, **75**, 181-6.

BROOKFIELD, M. 1971. An alternative to the "clastic trap" interpretation of oolitic ironstone facies. *Geological Magazine*, **108**, 137-143.

----------. 1973. The palaeoenvironment of the Abbotsbury Ironstone (U. Jurassic) of Dorset. *Palaeontology*, **16**, 261-274.

BROWN, G. 1980. Associated minerals. *In:* BRINDLEY, G. W., & BROWN, G. 1980.(eds.) *Crystal structures of clay minerals and their X-Ray identification*. Mineralogical Society Monograph No. 5.

BUBENICEK, L. 1967. Diagenesis of iron-rich rocks (illustrated by the role of diagenesis in oolitic iron ores). *In:* LARSEN, G., & CHILINGAR, G. V. (eds.) *Diagenesis in sediments*. Developments in Sedimentology. Volume 6. Elsevier.

BUDD, D. A., & PERKINS, R. D. 1980. Bathymetric zonation and palaeoecological significance of microborings in Puerto Rican shelf and slope sediments. *Journal of Sedimentary Petrology*, **50**, 881-904.

BURLEY, S. D., & WAUGH, B. KANTOROWICZ, J. D., 1985. Clastic diagenesis. *In:* BRENCHLEY, P. J., & WILLIAMS, B. P. J. (eds.) *Sedimentology, recent developments and applied aspects*. Geological Society Special Publication. Blackwell.

BUSENBERG, E., & PLUMMER, N. L. 1985. Kinetic and thermodynamic factors controlling the distribution of SO_4^{2-} and Na in calcites and selected aragonites. *Geochimica et Cosmochimica Acta*, **49**, 713-726.

CAILLERE, S., & KRAUT, F. 1953. Considerations sur la genese des minerais de fer oolithiques Lorrains. *In:* BLONDEL, F. (ed.) *La genese des gites de fer*. Proceedings of the 19th International Geological Congress, Section 10, 101-117.

CAROZZI, A. V. 1961. Distorted oolites and pseudo-oolites. *Journal of Sedimentary Petrology*, **31**, 262-274.

CARPENTER, S. J., ERICKSON, J. M., LOHMANN, K. C., & OWEN, M. R. 1988. Diagenesis of the fossiliferous concretions from the Upper Cretaceous Fox Hills Formation, North Dakota. *Journal of Sedimentary Petrology*, **58**, 706-723.

CATT, J. A., GAD, M. A., LeRICHE, H. H., & LORD, A. R. 1971. Geochemistry, micropalaeontology and origin of the Middle Lias ironstones in northeast Yorkshire. *Chemical Geology*, **8**, 61-76.

CAYEUX, L. 1922. *Les minerais de fer oolithique de France, fasc. II. Minerais de fer secondaires*. Ministere des Travaux publics, Paris, Imprimerie National.

CHAFETZ, H. S., WILKINSON, B. H. , & LOVE, K. M. 1985. Morphology and composition of non-marine carbonate cements in near-surface settings. *In:* SCHNEIDERMANN, N., & HARRIS, P. M. (eds.) *Carbonate Cements*. Society of Economic Pal eontologists and Mineralogists Special Publication, **36**, 337-347.

CHAMPETIER, Y., HAMDADOU, E., & HAMDADOU, M. 1987. Examples of biogenic support of mineralisation in two oolitic iron ores - Lorraine (France) and Gara Djebilet (Algeria). *Sedimentary Geology*, **51**, 249-255.

CHAUVEL, J-J., & DIMROTH, E. 1974. Facies types and depositional environments of the Sokoman Iron Formation, Labrador Trough, Quebec, Canada. *Journal of Sedimentary Petrology*, **44**, 229-327.

CHAUVEL, J-J., & GUERRAK, S. 1989. Oolitization processes in Palaeozoic ironstones of France, Algeria and Libya. *In:* YOUNG, T. P., & TAYLOR, W. E. G. (eds.) *Phanerozoic Ironstones*. Geological Society of London, Special Publication, **46**, 165-173.

CHAVE, K. E. 1954. Aspects of the biogeochemistry of magnesium. 1. Calcareous marine organisms. *Journal of Geology*, **62**, 266-283.

CHOWNS, T. M. 1968. *Environmental and diagenetic studies of the Cleveland Ironstone Formation of north-east Yorkshire*. PhD Thesis, University of Newcastle Upon Tyne.

----------. 1986. Petrology of Lower Jurassic chamosite-siderite ironstones from northeast England. *American Association of Petroleum Geologists Bulletin*, **70**, 573.

CLAYPOOL, G. E., & KAPLAN, I. R. 1974. The origin and distribution of methane in marine sediments. *In:* KAPLAN, I. R. (ed.) *Natural gases in marine sediments*. 99-139. Plenum Press.

COCHRAN, J. K., CAREY, A. E., SHOLKOVITZ, E. R., & SURPRENANT, L. D. 1986. The geochemistry of uranium and thorium in coastal marine sediments and sediment pore waters. *Geochimica et Cosmochimica Acta*, **50**, 663-680.

COLEMAN, M. L. 1985. Geochemistry of diagenetic non-silicate minerals: Kinetic considerations. *Philosophical Transactions of the Royal Society*, **A315**, 39-56.

COLLEY, H. & DAVIES, P. J. 1969. Ferroan and non-ferroan calcite cements in Pleistocene - Recent carbonates from the New Hebrides. *Journal of Sedimentary Petrology*, **39**, 554-558.

CONLEY, C. D. 1977. Origin of distorted ooliths and pisoliths. *Journal of Sedimentary Petrology*, **47**, 554-564.

COPE, J. C. W. 1971. Abbotsbury iron ore at Litton Cheney. *Proceedings of the Dorset Archaeological and Natural History Society*, **92**, 42.

COPE, J. C. W., GETTY, T. A., HOWARTH, M. K., MORTON, N., & TORRENS, H. S. 1980. *A correlation of Jurassic rocks in the British Isles. Part one. Introduction and Lower Jurassic*. Geological Society of London. Special Report Number 14.

COX, B. M., & GALLOIS, R. W. 1981. The stratigraphy of the Kimmeridge Clay of the Dorset type area and its correlation with some other Kimmeridgian sequences. *Institute of Geological Sciences Report*. **80/4**.

CRAIG, H. 1965. The measurement of oxygen isotope palaeotemperatures. *In:* TONGIORGI, E. (ed.) *Stable isotopes in oceanographic studies and palaeotemperatures*. Consiglio Nazionale delle Richerche, Laboratorio di Geologia Nucleare, Pisa. 161-182.

CROSS, J. E. 1875. The geology of north-west Lincolnshire. *Quarterly Journal of the Geological Society of London*, **31**, 115-129.

CURTIS, C. D. 1977. Sedimentary geochemistry: Environments and processes dominated by involvement of an aqueous phase. *Philosophical Transactions of the Royal Society*, **A286**, 353-372.

----------. 1983. Geochemistry of porosity enhancement and reduction in clastic sediments. *In:* BROOKS, J. (ed.) *Petroleum geochemistry and exploration of Europe*. 113-125. Blackwell Scientific Publications.

----------. 1985. Some mineral precipitation and transformations during burial diagenesis. *Philosophical Transactions of the Royal Society*, **A315**, 91-105.

----------. 1987a. Inorganic geochemistry and petroleum exploration. *In: Advances in petroleum geochemistry*. Academic Press.

----------. 1987b. Mineral consequences of organic matter degradation in sediments, inorganic/organic diagenesis. *In:* LEGGETT, J. K., & ZUFFA, G. G. (eds.) *Marine clastic sedimentology*. 108-123. Graham and Trottman.

CURTIS, C. D., & COLEMAN, M. L. 1986. Controls on the precipitation of early diagenetic calcite, dolomite, and siderite concretions in complex depositional sequences. *In:* GAUTIER, D. (ed.) *Roles of organic matter in sediment diagenesis*. Society of Economic Pal eontologists and Mineralogists Special Publication, **38**, 23-33.

CURTIS, C. D., COLEMAN, M. L., & LOVE, L. G. 1986. Pore water evolution during sediment burial from isotopic and mineral chemistry of calcite, colomite and siderite concretions. *Geochimica et Cosmochimica Acta*, **50**, 2321-2334.

CURTIS, C. D., HUGHES, C. R., WHITEMAN, J. A., & WHITTLE, C. K. 1985. Compositional variation within some sedimentary chlorites and some comments on their origin. *Mineralogical Magazine*, **49**, 375-386.

CURTIS, C. D., IRELAND, B. J., WHITEMAN, J. A., MULVANEY, R., & WHITTLE, C. K. 1984. Authigenic chlorites: Problems with chemical analysis and structural formula calculation. *Clay Minerals*, **19**, 471-481.

CURTIS, C. D., & SPEARS, D. A. 1968. The formation of sedimentary iron minerals. *Economic Geology*, **63**, 257-270.

DAHANAYAKE, K., & KRUMBEIN, W. 1986. Microbial structures in oolitic iron-formations. *Mineralium Deposita*, **21**, 85-94.

DAVIDSON, C. F. 1961. Oolitic ironstones of fresh-water origin. *Mining Magazine*, **104**, 158-159.

DAVIES, P. J., BUBELA, B., & FERGUSON, J. 1978. The formation of ooids. *Sedimentology*, **25**, 703-730.

DAVIES, W., & DIXIE, R. J. M. 1951. Recent work on the Frodingham Ironstone. *Proceedings of the Yorkshire Geological Society*, **28**, 85-96.

DEELMAN, J. C. 1978. Experimental ooids and grapestones: Carbonate aggregates and their origin. *Journal of Sedimentary Petrology*, **48**, 503-512.

DEER, W. A., HOWIE, R. A., & ZUSSMAN, J. 1962. *Rock forming minerals. Volume 5. Non-silicates.* Longmans.

DEVOL, A. H., & AHMED, S. I. 1981. Are high rates of sulphate reduction associated with anaerobic oxidation of methane?. *Nature*, **291**, 407-408.

DICKSON, J. A. D. 1965. A modified staining technique for carbonates in thin-section. *Nature*, **205**, 587.

----------. 1966. Carbonate identification and genesis revealed by staining. *Journal of Sedimentary Petrology*, **36**, 491-505.

DICKSON, J. A. D., & BARBER, C. 1976. Petrography, chemistry and origin of early diagenetic concretions in the Lower Carboniferous of the Isle of Man. *Sedimentology*, **23**, 189-211.

DOBKINS, J. E., & FOLK, R. L. 1970. Shape development on Tahiti-nui. *Journal of Sedimentary Petrology*, **40**, 1167-1203.

DOTT, R. H. Jnr, & BOURGEOUIS, J. 1981. *Hummocky cross stratification.* Yearbook of Science and Technology 349-351. McGraw Hill.

----------. 1982. Hummocky stratification: significance of its variable bedding sequences. *Geological Society of America Bulletin*, **93**, 663-680.

DRAVIS, J. J., & YUREWICZ, D. A. 1985. Enhanced carbonate petrography using fluorescence microscopy. *Journal of Sedimentary Petrology*, **55**, 795-804.

DREESEN, R. 1989. Oolitic ironstones as event-stratigraphical marker beds within the Upper Devonian of the Ardenno-Rhenish Massif. *In:* YOUNG, T. P., & TAYLOR, W. E. G. (eds.) *Phanerozoic Ironstones*. Geological Society of London, Special Publication, **46**, 65-78.

DUNHAM, K. C. 1960. Syngenetic and diagenetic mineralization in Yorkshire. *Proceedings of the Yorkshire Geological Society*, **32**, 229-284.

DUNHAM, R. J. 1962. Classification of carbonate rocks according to depositional texture. *In:* HAM, W. E. (ed.) *Classification of carbonate rocks*. Memoir of the American Association of Petroleum Geologists. **1**. 108-121.

EDMONDS, E.A., POOLE, E.G., & WILSON, V. 1965. *Geology of the country around Banbury and Edge Hill*. Memoir of the Geological Survey.

EMERY, D., HUDSON, J. D., MARSHALL, J. D., & DICKSON, J. A. D. 1988. The origin of late spar cements in the Lincolnshire Limestone, Jurassic of central England. *Journal of the Geological Society of London*, **145**, 621-633.

EPSTEIN, S., BUCHSBAUM, R., LOWENSTAM, H. A., & UREY, H. C. 1953. Revised carbonate-water isotopic temperature scale. *Bulletin of the Geological Society of America*, **64**, 1315-1326.

FERGUSON, J., BURNE, R. V., & CHAMBERS, L. A. 1983. Iron mineralization by continental groundwaters, Fisherman Bay, South Australia. *Sedimentary Geology*, **34**, 41-57.

FOLK, R. L. 1959. Practical petrographic classification of limestones. *American Association of Petroleum Geologists Bulletin*, **43**, 1-38.

----------. 1962. Spectral subdivision of limestone types. *In:* HAM, W. E. (ed.) *Classification of carbonate rocks*. Memoir of the American Association of Petroleum Geologists, **1**, 62-84.

----------. 1965. Some aspects of recrystallization in limestones. *In:* PRAY, L. C., & MURRAY, R. C. (eds.) *Dolomitisation and limestone diagenesis: a symposium*. Society of Economic Pal eontologists and Mineralogists, Special Publication, **13**, 14-48.

----------. 1974. The natural history of crystalline calcium carbonate: effect of magnesium content and salinity. *Journal of Sedimentary Petrology*, **44**, 40-53.

FOLK, R. L., CHAFETZ, H. S., & TIEZZI, P. A. 1985. Bizarre forms of depositional and diagenetic calcite in hot-spring travertines, central Italy. *In:* SCHNEIDERMANN, N., & HARRIS, P. M. (eds.) *Carbonate Cements*. Society of Economic Pal eontologists and Mineralogists Special Publication, **36**, 349-369.

FREEMAN, T. 1962. Quiet water oolites from Laguna Madre, Texas. *Journal of Sedimentary Petrology*, **32**, 475-483.

FREY, R. W. 1975. (ed.) *The study of trace fossils*. Springer Verlag.

FRIEDMAN, G.M. 1959. Identification of carbonate minerals by staining methods. *Journal of Sedimentary Petrology*, **29**, 87-97.

----------. 1964. Early diagenesis and lithification in carbonate sediments. *Journal of Sedimentary Petrology*, **34**, 777-813.

FROELICH, P. N., KLINKHAMMER, G. P., BENDER, M. L., LEUDTKE, N. A., HEATH, G. R., CULLEN, D., DAUPHIN, P., HAMMOND, D., HARTMAN, B., & MAYNARD, V. 1979. Early oxidation of organic matter in pelagic sediments

of the eastern equatorial Atlantic: Suboxic diagenesis. *Geochimica et Cosmochimica Acta*, **43**, 1075-1090.

FRONDEL, G. M., & BAUER, L. H. 1955. Kutnohorite: A manganese dolomite, $CaMn(CO_3)_2$. *American Mineralogist*, **40**, 748.

GAD, M. A., CATT, J. A., & LeRICHE, H. H. 1969. Geochemistry of the Whitbian (U. Lias) sediments of the Yorkshire coast. *Proceedings of the Yorkshire Geological Society*, **37**, 105-139.

GARRELS, R. M., & CHRIST, C. L. 1965. *Solutions minerals and equilibria*. Harper Row.

GARZANTI, E., HAAS, R., & JADOUL, F.1989. Ironstones in the Mesozoic passive margin sequence of the Tethys Himalaya (Zanskar, northern India): sedimentology and metamorphism. *In:* YOUNG, T. P., & TAYLOR, W. E. G. (eds.) *Phanerozoic Ironstones*. Geological Society of London, Special Publication, **46**, 229-244.

GATRALL, M., JENKYNS, H. C., & PARSONS, C. F. 1972. Limonitic concretions from the European Jurassic, with particular reference to the "Snuff Boxes" of southern England. *Sedimentology*, **18**, 79-103.

GAUNT, G. D., IVEMEY-COOK, H. C., PENN, I. E., & COX, B. M. 1980. *Mesozoic rocks proved by I.G.S. boreholes in the Humber and Acklam areas*. Institute of Geological Sciences Report. **79/13.**

GAUTIER, D. L. 1982. Siderite concretions: Indicators of early diagenesis in the Gammon Shale (Cretaceous). *Journal of Sedimentary Petrology*, **52**, 859-871.

----------. 1985. Interpretation of early diagenesis in ancient marine sediments. *In:* GAUTIER, D. L., & SURDAM, R. C. (eds.) *Relationship of organic matter and mineral diagenesis*. Society of Economic Pal .eontologists and Mineralogists Short Course Notes, **17**, 6-78.

GEHRING, A. U. 1989. The formation of goethitic ooids in condensed Jurassic deposits in northern Switzerland.*In:* YOUNG, T. P., & TAYLOR, W. E. G. (eds.) *Phanerozoic Ironstones*. Geological Society of London, Special Publication, **46**, 133-139.

----------. 1990. Diagenesis of ferriferous phases in the Northampton Ironstone in the Cowthick quarry near Corby (England). *Geological Magazine*, **127**, 169-176.

GIRESSE, P. & ODIN, G. S. 1973. Nature mineralogique et origine des glauconies du plateau continental du Gabon et du Congo. *Sedimentology*, **20**, 457-488.

GIRESSE, P., WIEWIORA, A., & LACKE, B. 1988. Mineral phases and processes within green peloids from two recent deposits near the Congo River mouth. *Clay Minerals*, **23**, 447-458.

GIVEN, R. K., & WILKINSON, B. H. 1985. Kinetic control of morphology, composition, and mineralogy of abiotic sedimentary carbonates. *Journal of Sedimentary Petrology*, **55**, 109-119.

GOLDHABER, M. B., ALLER, R. C., COCHRAN, J. K., ROSENFIELD, J. K., MARTENS, C. S., & BERNER, R. A. 1977. Sulphate reduction, diffusion and

bioturbation in Long Island Sound sediments: report of the FOAM group. *American Journal of Science*, **277**, 193-237.

GOLDSMITH, J. R. 1983. Phase relations of rhombohedral carbonates. *In:* REEDER, R. J. (ed.) *Carbonates, mineralogy and chemistry*. Mineralogical Society of America, Reviews in Mineralogy, **11**, 49-96.

GOLUBIC, S., PERKINS, R. D. & LUKAS, K. J. 1975. Boring microorganisms and microborings in carbonate substrates. *In:* FREY, R. W. (ed.) *The study of trace fossils*. Springer -Verlag, 229-259.

GREENSMITH, J. T., RAWSON, P. F., SHALABY, S. E. 1980. An association of minor fining-upward cycles and aligned gutter marks in the Middle Lias (Lower Jurassic) of the Yorkshire coast. *Proceedings of the Yorkshire Geological Society*, **42**, 525-538.

GROSS, G. A. 1965. Geology of iron deposits in Canada. Vol. 1. General geology and evaluation of ore deposits. *Canadian Geological Survey, Economic Geology Report.* **22**.

GUERRAK, S. 1987. Paleozoic oolitic ironstones of the Algerian Sahara: A review. *Journal of African Earth Sciences*, **6**, 1-8.

----------. 1989. Time and space distribution of Palaeozoic oolitic ironstones in the Tindouf Basin, Algerian Sahara. *In:* YOUNG, T. P., & TAYLOR, W. E. G. (eds.) *Phanerozoic Ironstones*. Geological Society of London, Special Publication, **46**, 197-212.

GUERRAK, S., & CHAUVEL, J. J. 1985. Ferriferous mineralizations in the Algerian Sahara: Mecheri Abdelaziz oolitic iron deposit (Tindouf Basin). *Mineralium Deposita*, **20**, 249-259.

GYGI, R.A. 1981. Oolitic iron formations: Marine or not marine?. *Eclogae Geologicae Helvetiae*, **74**, 223-254.

HAGNI, R.D. 1986. Importance of cathodoluminescence microscopy of sedimentary ironstones. *American Association of Petroleum Geologists Bulletin*, **70**, 598.

HALLAM, A. 1963. Observations on the palaeoecology and ammonite sequence of the Frodingham Ironstone (Lower Jurassic). *Palaeontology*, **6**, 554-574.

----------. 1967. Siderite and calcite-bearing concretionary nodules in the Lias of Yorkshire. *Geological Magazine*, **104**, 222-227.

----------. 1975. *Jurassic environments*, Cambridge University Press.

HALLAM, A., & BRADSHAW, M. J. 1979. Bituninous shales and oolitic ironstones as indicators of transgressions and regressions. *Journal of the Geological Society of London*, **136**, 157-164.

HALLAM, A., & SELLWOOD, B. W. 1976. Middle Mesozoic sedimentation in relation to tectonics in the British area. *Journal of Geology*, **84**, 301-321.

HALLIMOND, A. F. 1925. *Iron ores - Bedded ores of England and Wales - Petrography and chemistry*. Special Report on the Mineral Resources of Great Britain. Memoir of the Geological Survey, **29**.

----------. 1951. Problems of sedimentary iron ores. *Proceedings of the Yorkshire Geological Society*, **28**, 61-66.

HARDER, H. 1978. Synthesis of iron layer silicate minerals under natural conditions. *Clays and Clay Minerals*, **26**, 65-72.

----------. 1980. Synthesis of glauconite at surface temperatures. *Clays and Clay Minerals*, **28**, 217-222.

----------. 1989. Mineral genesis in ironstones: A model based upon laboratory experiments and petrographic observations. *In:* YOUNG, T. P., & TAYLOR, W. E. G. (eds.) *Phanerozoic Ironstones*. Geological Society of London, Special Publication, **46**, 9-18.

HARMS, J. C., SOUTHARD, J. B., SPEARING, D. R., & WALKER, R. G. 1975. *Depositional environments as interpreted from primary sedimentary structures and stratification sequences*. Society of Economic Pal eontologists and Mineralogists Short Course Notes **2**.

HARRIS, R. C., & PILKEY, O. H. 1966. Temperature and salinity control of the concentration of skeletal Na, Mn, and Fe in *Dendraster excentricus*. *Pacific Science*, **20**, 235-238.

HARRISON, R. K., HOWARTH, M. K., STYLES, M. T., & YOUNG, B. R. 1983. *Ooids with goyazite-crandalite rims from the top of the Marlstone Rock Bed (Toarcian, Lower Jurassic) near Harston Leicestershire*. Institute of Geological Sciences Report. **83/1**. 16-23.

HAYES, J. B. 1970. Polytypism of chlorite in sedimentary rocks. *Clays and Clay Minerals*, **18**, 285-306.

HEMINGWAY, J. E. 1951. Cyclic sedimentation and the deposition of ironstone in the Yorkshire Lias. *Proceedings of the Yorkshire Geological Society*, **28**, 67-74.

----------. 1974. The Jurassic. *In:* RAYNER, D. H. & HEMINGWAY, J. E. (eds.) *The geology and mineral resources of Yorkshire*. Yorkshire Geological Society, 161-223.

HO, C., & COLEMAN, J. M. 1969. Consolidation and cementation of recent sediments in the Atchafalaya Basin. *Geological Society of America Bulletin*, **80**, 183-192.

HOEFS, J. 1980. *Stable isotope geochemistry*. Springer-Verlag.

HORTON, A., IVEMEY-COOK, H.C., HARRISON, R. K., & YOUNG, B. R. 1980. Phosphatic ooids in the Upper Lias (Lower Jurassic) of central England. *Journal of the Geological Society of London*, **137**, 731-740.

HOWARD, A. S. 1985. Lithostratigraphy of the Staithes Sandstone and Cleveland Ironstone Formations (Lower Jurassic) of northeast Yorkshire. *Proceedings of the Yorkshire Geological Society*, **45**, 261-275.

HOWARTH, M. K. 1955. Domerian of the Yorkshire coast. *Proceedings of the Yorkshire Geological Society*, **30**, 147-175.

----------. 1980. The Toarcian age of the upper part of the Marlstone Rock Bed of England. *Palaeontology*, **23**, 637-656.

HUBER, N. K. & GARRELS, R. M. 1953. Relation of pH and oxidation potential to sedimentary iron mineral formation. *Economic Geology*, **48**, 337-357.

HUDSON, J. D. 1977. Stable isotopes and limestone lithification. *Quarterly Journal of the Geological Society of London*, **133**, 637-660.

----------. 1978. Concretions, isotopes, and the diagenetic history of the Oxford Clay (Jurassic) of central England. *Sedimentology*, **25**, 339-370.

HUGHES, C. R. 1987. *The composition and origin of layer silicates in iron-formations and ironstones: A preliminary Analytical Transmission Electron Microscopial Study*. PhD Thesis, University of Sheffield.

----------. 1989. The application of Analytical Transmission Electron Microscopy to the study of oolitic ironstones: A preliminary study. *In:* YOUNG, T. P., & TAYLOR, W. E. G. (eds.) *Phanerozoic Ironstones*. Geological Society of London, Special Publication, **46**, 121-131.

HUMPHREYS, B., SMITH, S. A., & STRONG, G. E. 1989. Authigenic chlorite in late Triassic sandstones from the central Graben, North Sea. *Clay Minerals*, **24**, 427-444.

IIJIMA, A. & MATSUMOTO, R. 1982. Berthierine and chamosite in coal measures of Japan. *Clays and Clay Minerals*, **30**, 264-274.

IRWIN, H., CURTIS, C. D., & COLEMAN, M. 1977. Isotopic evidence for source of diagenetic carbonates formed during burial of organic-rich sediments. *Nature*, **269**, 209-213.

JAHREN, J. S., & AAGAARD, P. 1989. Compositional variations in diagenetic chlorites and illites, and relationships with formation-water chemistry. *Clay Minerals*, **24**, 157-170.

JAMES, H. E., & VAN HOUTEN, F. W. 1979. Miocene goethitic and chamosite oolites, northern Columbia. *Sedimentology*, **26**, 125-133.

JAMES, H. L. 1954. Sedimentary facies of iron formation. *Economic Geology*, **49**, 235-293.

----------. 1966. *Chemistry of the iron-rich sedimentary rocks*. United States Geological Survey Professional Paper, **113**.

JONES, H. A. 1965. Ferruginous oolites and pisolites. *Journal of Sedimentary Petrology*, **35**, 838-845.

JØRGENSEN, B. B. 1983. The microbial sulphur cycle. *In:* KRUMBEIN, W. E. (ed.) *Microbial geochemistry*. 91-124. Blackwell.

KANTOROWICZ, J. D. 1985. The origin of authigenic ankerite from the Ninian Field, U.K. North Sea. *Nature*, **315**, 214-216.

KEARSLEY, A. T. 1989. Iron-rich ooids, their mineralogy and microfabric: clues to their origin and evolution. *In:* YOUNG, T. P., & TAYLOR, W. E. G. (eds.) *Phanerozoic Ironstones*. Geological Society of London, Special Publication, **46**, 141-164.

KENDALL, A. C. 1977. Fascicular-optic calcite: A replacement of bundled acicular carbonate cements. *Journal of Sedimentary Petrology*, **47**, 1056-1062.

----------. 1985. Radiaxial fibrous calcite: A reappraisal. *In:* SCHNEIDERMANN, N., & HARRIS, P. M. (eds.) *Carbonate cements*, Society of Econonomic Palaeontologists and Mineralogists Special Publication, **36**, 59-77.

KENDALL, A. C., & TUCKER, M. E. 1973. Radiaxial fibrous calcite: A replacement after acicular carbonate. *Sedimentology*, **20**, 365-389.

KENT, P. E. 1953. Shallow borings in the Jurassic rocks near Hibaldstow, north Lincolnshire. *Transactions of the Lincolnshire Naturalists Union*, **13**, 30-32.

----------. 1980. Subsidence and uplift in east Yorkshire and Lincolnshire: A double inversion. *Proceedings of the Yorkshire Geological Society*, **42**, 505-524.

KETTENBRINK, E. C., & MANGER, W. L. 1971. A deformed marine pisolite from the Plattsburg Limestone (Upper Pennsylvanian) of southeastern Kansas. *Journal of Sedimentary Petrology*, **41**, 435-443.

KIMBERLEY, M. M. 1974. Origin of oolitic iron ore by diagenetic replacement of calcareous oolite. *Nature*, **250**, 319-320.

----------. 1975. Proposal of iron formation origin by cycles of aragonite sedimentation, cover by volcanic ash or terrigenous mud, acid-base aragonite replacement, and mud erosion: A Quaternary analogue (abstract). *Geological Society of America Abstracts with Programs*, **7**, 1146-1147.

----------. 1978. Palaeoenvironmental classification of iron formations. *Economic Geology*, **73**, 215-229.

----------. 1979a. Geochemical distinctions among environmental types of iron formations. *Chemical Geology*, **25**, 185-212.

----------. 1979b. Origin of oolitic iron formations. *Journal of Sedimentary Petrology*, **49**, 111-132.

----------. 1980. The Paz De Rio oolitic inland-sea iron formation. *Economic Geology*, **75**, 97-106.

----------. 1983. Ferriferous ooids. *In:* PERYT, P. (ed.) *Coated grains*. Springer-Verlag.

KNELL, S. J., & KNELL, M. P. 1988. *The natural history of the Frodingham Ironstone.* Scunthorpe Museum Publication.

KNOX, R. W. O'B. 1970. Chamosite oolites from the Winter Gill ironstone (Jurassic) of Yorkshire, England. *Journal of Sedimentary Petrology*, **40**, 1216-1225.

----------. 1971. An alternative to the "Clastic trap" interpretation of oolitic ironstone facies - Discussion. *Geological Magazine*, **108**, 544-545.

KNOX, R. W. O'B., & FLETCHER, T. P. 1987a *Genesis of a mixed silicate-oxide oolitic ironstone: The Frodingham Ironstone (Sinemurian) of eastern England.*[abstract]. Phanerozoic Ironstones Symposium, Sheffield.

----------. 1987b. Unpublished fieldguide to the Frodingham Ironstone. Phanerozoic Ironstones Symposium, Sheffield.

KRAUSKOPF, K. B. 1957. Separation of manganese from iron in sedimentary processes. *Geochimica et Cosmochimica Acta*, **12**, 61-68.

----------. 1979. *Introduction to geochemistry*. McGraw Hill.

KRUMBEIN, W. C. 1941. Measurement and geological significance of shape and roundness of sedimentary particles. *Journal of Sedimentary Petrology*, **11**, 64-72.

LAMPLUGH, G. W., WEDD, C. B., & PRINGLE, J. 1920. *Iron ores (continued). Bedded ores of the Lias, oolites and later Formations in England*. Special Report on the Mineral Resources of Great Britain Volume 12. Memoir of the Geological Survey.

LAND, L. S. 1967. Diagenesis of skeletal carbonates. *Journal of Sedimentary Petrology*, **37**, 914-930.

LAWRENCE, J. R., & TAYLOR, H. P. Jnr. 1971. Deuterium and oxygen-18 correlation: Clay minerals and hydroxides in Quaternary soils compared to meteoric waters. *Geochimica et Cosmochimica Acta*, **35**, 993-1003.

LEE, G. W. 1920. *The Mesozoic rocks of Applecross, Raasay and north-east Skye*. Memoir of the Geological Survey vii.

LEEDER, M. R. 1982. *Sedimentology, process and product*. Allen and Unwin.

LEMOALLE, J. & DUPONT, B. 1973. Iron-bearing oolites and the present conditions of sedimentation in Lake Chad (Africa). *In:* AMSTUTZ, G. C., & BERNARD, A. J. (eds.) *Ores in sediments*. Springer-Verlag.

LINDHOLM, R. C. & FINKELMAN, R. B. 1972. Calcite staining: Semiquantitative determination of ferrous iron. *Journal of Sedimentary Petrology*, **42**, 239-242.

LIVINGSTONE, D. A. 1963. *Chemical composition of rivers and lakes*. United States Geological Survey Professional Paper, **440-G**.

LOHMANN, K. C. 1988. Geochemical patterns of meteoric systems and their applications to studies of paleokarst. *In:* JAMES, N. P., & CHOQUETTE (eds.) *Paleokarst*. Springer-Verlag.

LOHMANN, K. C. & MEYERS, W. J. 1977. Microdolomite inclusions in cloudy prismatic calcites: A proposed criterion for former high-magnesium calcites. *Journal of Sedimentary Petrology*, **47**, 1078-1088.

LONGMAN, M. W. 1980. Carbonate diagenetic textures from near surface diagenetic environments. *American Association of Petroleum Geologists Bulletin*, **64**, 461-487.

MACGREGOR, M., LEE, G. W., & WILSON, G. V. 1920. *The iron ores of Scotland*. Memoir of the Geological Survey, **11**.

MANHEIM, F. T., & GULBRANDSEN, R. A. 1979. Marine Phosphorites. *In:* BURNS, R. G. (ed.) *Marine Minerals*. Mineralogical Society of America, Short Course Notes, **6**, 151-173.

MARSHALL, J. D. 1981. Zoned calcites in Jurassic ammonite chambers: Trace elements, isotopes, and neomorphic origin. *Sedimentology*, **28**, 867-887.

MARSHALL, J. D., & ASHTON, M. 1980. Isotopic and trace element evidence for submarine lithification of hardgrounds in the Jurassic of eastern England. *Sedimentology*, **27**, 271-289.

MATSUMOTO, R., & IIJIMA, A. 1981. Origin and diagenetic evolution of Ca - Mg - Fe carbonates in some coalfields of Japan. *Sedimentology*, **28**, 239-259.

MATTHEWS, R. K. 1966. Genesis of recent lime mud in southern British Honduras. *Journal of Sedimentary Petrology*, **36**, 428-454.

MAYNARD, J. B. 1982. Extension of Berners "New geochemical classification of sedimentary environments" to ancient sediments. *Journal of Sedimentary Petrology*, **52**, 1325-1331.

----------. 1983. *Geochemistry of sedimentary ore deposits*, Springer-Verlag.

----------. 1986. Geochemistry of oolitic iron ores, an electron microprobe study. *Economic Geology*, **81**, 1473-1483.

MAZZULLO, S. J. 1980. Calcite pseudospar replacive of marine acicular aragonite, and implications for aragonite cement diagenesis. *Journal of Sedimentary Petrology*, **50**, 409-422.

MAZZULLO, S. J., BISCHOFF, W. D., & LOBITZER, H. 1990. Diagenesis of radiaxial fibrous calcites in a subconformity, shallow-burial setting: Upper Triassic and Liassic, northern Calcareous Alps, Austria. *Sedimentology*, **37**,407-425.

McCLELLAN, G. M. 1980. Mineralogy of carbonate fluorapatites. *Journal of the Geological Society of London*, **137**, 675-681.

McFARLANE, M. J. 1976. *Laterite and landscape*, Academic press.

McKERROW, W. S. 1978. *The ecology of Fossils*. Gerald Duckworth & Co. Ltd.

MEYERS, W. J. 1974. Carbonate cement stratigraphy of the Lake Valley Formation (Mississippian), Sacramento Mountains, New Mexico. *Journal of Sedimentary Petrology*, **44**, 837-861.

MITTERER, R. M., & CUNNINGHAM, R. Jnr. 1985. The interaction of natural organic matter with grain surfaces: implications for calcium carbonate precipitation. *In:* SCHNEIDERMANN, N., & HARRIS, P. M. (eds.) *Carbonate Cements*. Society of Economic Palaeontologists and Mineralogists Special Publication, **36**, 17-31.

MOORE, C. H. 1989. *Carbonate diagenesis and porosity*. Developments in Sedimentology. Volume 46. Elsevier.

MOZLEY, P. S. 1989. Complex compositional zonation in concretionary siderite: implications for geochemical studies. *Journal of Sedimentary Petrology*, **59**, 815-818.

MULLER, G., & FORSTNER, U. 1973. Recent iron ore formation in Lake Malawi, Africa. *Mineralium Deposita*, **8**, 278-290.

MULLER, G., IRION, G., & FORSTNER, U. 1972. Formation of inorganic Ca-Mg carbonates in the lacustrine environment. *Naturwissenschaften*, **59**, 158-164.

MUROWCHICK, J. B., & BARNES, H. L. 1986. Marcasite precipitation from hydrothermal solutions. *Geochimica et Cosmochimica Acta*, **50**, 2615-2629.

MYERS, K. J. 1989. The origin of the Lower Jurassic Cleveland Ironstone Formation of north-east England: evidence from portable Gamma-Ray spectrometry. *In:* YOUNG, T. P., & TAYLOR, W. E. G. (eds.) *Phanerozoic Ironstones*. Geological Society of London, Special Publication, **46**, 221-228.

NAHON, D., CAROZZI, A. V., & PARRON, C. 1980. Lateritic weathering as a mechanism for the generation of ferruginous ooids. *Journal of Sedimentary Petrology*, **50**, 1287-1298.

NASH, A. J., & PITTMAN, E. D. 1975. Ferro-magnesian calcite cement in sandstones. *Journal of Sedimentary Petrology*, **45**, 258-265.

NELSON, B. W., & ROY, R. 1958. Synthesis of the chlorites and their structural and chemical constitution. *The American Mineralogist*, **43**, 707-725.

NISSENBAUM, A., & KAPLAN, I. R. 1972. Chemical and isotopic evidence for the *in situ* origin of marine humic substances. *Limnology and Oceanography*, **17**, 570.

NISSENBAUM, A., PRESLEY, B. J., & KAPLAN, I. R. 1972. Early diagenesis in a reducing fjord, Saanich Inlet, British Columbia-1. Chemical and isotopic changes in major components of interstitial water. *Geochimica et Cosmochimica Acta*, **36**, 1007-1027.

ODIN, G. S. 1988. *Green marine clays*. Developments in Sedimentology. Volume 45. Elsevier.

OLDERSHAW, A. E., & SCOFFIN, T. P. 1967. The source of ferroan and non-ferroan calcite cements in the Halkin and Wenlock Limestones: *Geological Journal*, **50**, 309-320.

PALMER, T. J., & WILSON, M. A. 1990. Growth of ferruginous oncoliths in the Bajocian (Middle Jurassic) of Europe. *Terra Nova*, **2**, 142-147.

PARK, R. G. 1983. *Foundations of structural geology*. Blackie.

PEARSON, M. J. 1974. Sideritic concretions from the Westphalian of Yorkshire: A chemical investigation of the carbonate phase. *Mineralogical Magazine*, **39**, 696-699.

PEDRO, G., CARMOUZE, J. P., & VELDE, B. 1978. Peloidal nontronite formation in recent sediments in Lake Chad. *Chemical Geology*, **23**, 139-149.

PERYT, T. 1983. (ed.) *Coated Grains*. Springer Verlag.

PORRENGA, D. H. 1965. Chamosite in recent sediments of the Higer and Orinoco deltas. *Geologie en Mijnbouw*, **44**, 400-403.

----------. 1967. Glauconite and chamosite as depth indicators in the marine environment. *Marine Geology*, **5**, 495-501.

POSTMA, D. 1977. The occurrence and chemical composition of recent Fe-rich mixed carbonates in a river bog. *Journal of Sedimentary Petrology*, **47**, 1089-1098.

----------. 1982. Pyrite and siderite formation in brackish and freshwater swamp sediments. *American Journal of Science*, **282**, 1151-1183.

PRESLEY, B. J., & KAPLAN, I. R. 1968. Changes in dissolved sulphate, calcium and carbonate from interstitial water of near-shore sediments. *Geochimica et Cosmochimica Acta*, **32**, 1037-1048.

PREZBINDOWSKI, D. R. 1985. Burial cementation. *In:* SCHNEIDERMANN, N., & HARRIS, P. M. (eds.) *Carbonate Cements*. Society of Economic Pal eontologists and Mineralogists Special Publication, **36**, 241-264.

PULFREY, W. 1933 The iron ore oolites and pisolites of North Wales. *Quarterly Journal of the Geological Society of London*, **356**, 401-430.

PYE, K. 1981. Marshrock formed by iron sulphide and siderite cementation in saltmarsh sediments. *Nature*, **294**, 650-652.

----------. 1984. S.E.M. analysis of siderite cements in intertidal marsh sediments, Norfolk, England. *Marine Geology*, **56**, 1-12.

PYE, K., DICKSON, J. A. D., SCHIAVON, N., COLEMAN, M. L., & COX, M. 1990. Formation of siderite - Mg calcite - iron sulphide concretions in intertidal marsh and sandflat sediments, north Norfolk, England. *Sedimentology*, **37**, 325-343.

RAISWELL, R. 1971. The growth of Cambrian and Liassic concretions. *Sedimentology*, **17**, 145-146.

----------. 1988. Evidence for surface reaction-controlled growth of carbonate concretions in shales. *Sedimentology*, **35**, 571-575.

RASTALL, R. H., & HEMINGWAY, J. E. 1940. The Yorkshire Dogger I-The coastal region. *Geological Magazine*, **76**, 177-197 & 257-275.

----------. 1949. The Yorkshire Dogger IV-Rosedale and Farndale. *Geological Magazine*, **86**, 201-225 & 265-278.

RAWSON, P. F., GREENSMITH, J. T., & SHALABY, S. E. 1982. Coarsening upward cycles in the uppermost Staithes and Cleveland Ironstone Formations (Lower Jurassic) of the Yorkshire coast, England. *Proceedings of the Geologists' Association*, **94**, 91-93.

READING, H. G. 1986. *Sedimentary environments and facies*. Blackwell.

REDFIELD, A. C. 1958. The biological control of chemical factors in the environment. *American Journal of Science*, **46**, 206-226.

RICHTER, D. K. 1983. Calcareous ooids: a synopsis. *In:* PERYT, T. M. (ed.) *Coated Grains*. Springer Verlag.

RICHTER, D. K., & FUCHTBAUER, H. 1978. Ferroan calcite replacement indicates former magnesian calcite skeletons. *Sedimentology*, **25**, 843-860.

ROHRLICH, V. 1974. Microstructure and microchemistry of iron ooliths. *Mineralium Deposita*, **9**, 133-142.

ROHRLICH, V., PRICE, N. B., & CALVERT, S. E. 1969. Chamosite in the recent sediments of Loch Etive, Scotland. *Journal of Sedimentary Petrology*, **39**, 624-631.

ROUSE, J. E., & SHIRLEY, S. S. 1988. *Calculation scheme and computer program for the correction of carbon and oxygen isotopic data*. British Petroleum Sunbury Internal Report, GCB/55/88.

SALLER, A. H. 1986. Radiaxial calcite in Lower Miocene strata, subsurface Enewetak Atoll. *Journal of Sedimentary Petrology*, **56**, 743-762.

SAMES, C. W. 1966. Morphometric data of some recent pebble associations and their application to ancient sediments. *Journal of Sedimentary Petrology*, **36**, 126-142.

SCHNEIDERMANN, N., & HARRIS, P. M. 1985. *Carbonate cements*. Society of Economic Pal eontologists and Mineralogists Special Publication, **36**.

SCHOLLE, P. A., & HALLEY, R. B. 1985. Burial diagenesis: out of sight, out of mind!. *In:* SCHNEIDERMANN, N., & HARRIS, P. M. (eds.) *Carbonate Cements*. Society of Economic Pal eontologists and Mineralogists Special Publication, **36**, 309-334.

SCHROEDER, J. H., DWORNIK, E. J., & PAPIKE, J. J. 1969. Primary protodolomite in echinoid skeletons. *Bulletin of the Geological Society of America*, **80**, 1613-1616.

SHACKLETON, N. J., & KENNETT, J. P. 1975. Palaeotemperature history of the Cenozoic and the initiation of the Antarctic glaciation: oxygen and carbon isotope analysis in D.S.D.P. sites 277, 279, and 281. *In: Initial reports of the Deep Sea Drilling Project 24*. United States Government Printing Office.

SIEHL, A., & THIEN, J. 1986. Origin of Minette typre ironstones. *American Association of Petroleum Geologists Bulletin*, **70**, 648.

----------. 1989. Minette-type ironstones. *In:* YOUNG, T. P., & TAYLOR, W. E. G. (eds.) *Phanerozoic Ironstones*. Geological Society of London, Special Publication, **46**, 175-193.

SNEED, E.D., & FOLK, R.L. 1958. Pebbles in the lower Colorado River, Texas. A study in particle morphogenesis. *Journal of Geology*, **66**, 114-150.

SORBY, H.C. 1857. On the origin of the Cleveland Hill Ironstone. *Proceedings of the Polytechnic Society of the West Riding of Yorkshire*, **3**, 457-461.

----------. 1906. The origin of the Cleveland Ironstone. *The Naturalist*, Oct. 1906. 354-357.

STRAKHOV, N. M. 1967. *Principles of lithogenesis -1*. Oliver and Boyd.

SUESS, E. 1973. Interaction of organic compounds with calcium carbonate - II. Organic - carbonate association in recent sediments. *Geochimica et Cosmochimica Acta*, **37**, 2435-2448.

TAN, F. C., & HUDSON, J. D. 1974. Isotopic studies of the palaeoecology and diagenesis of the Great Estuarine Series (Jurassic) of Scotland. *Scottish Journal of Geology*, **10**, 91-128.

TALBOT, M.R. 1971. Calcite cements in the Corallian Beds (Upper Oxfordian) of southern England. *Journal of Sedimentary Petrology*, **41**, 261-273.

----------. 1974. Ironstones in the Upper Oxfordian of southern England. *Sedimentology*, **21**, 433-450.

TAYLOR, R. M. 1987. Non-silicate oxides and hydroxides. *In:* NEWMAN, A. C. D. (ed) *Chemistry of clays and clay minerals*. Mineralogical Society Monograph No. 6.

TAYLOR, J.H. 1949. *Petrology of the Northampton Sand Ironstone Formation*. Memoir of the Geological Survey.

----------. 1951. Sedimentation problems of the Northampton Sand Ironstone. *Proceedings of the Yorkshire Geological Society*, **28**, 74-84.

TEYSSEN, T.A.L. 1984. Sedimentology of the Minette oolitic ironstones of Luxembourg and Lorraine: A Jurassic subtidal sandwave complex. *Sedimentology*, **31**, 195-211.

----------. 1989. A depositional model for the Liassic Minette ironstones (Luxemburg and France), in comparison with other Phanerozoic oolitic ironstones. *In:* YOUNG, T. P., & TAYLOR, W. E. G. (eds.) *Phanerozoic Ironstones*. Geological Society of London, Special Publication, **46**, 79-92.

TUCKER, M. E. 1981. *Sedimentary petrology, an introduction*. Geoscience Texts Volume 3. Blackwell Scientific Publications.

TUCKER, M.E., & WRIGHT, P.V. 1990. *Carbonate sedimentology*. Blackwell Scientific Publications.

UMEORAH, E.M. 1987 Depositional environment and facies relationships of the Cretaceous ironstone of the Agbaja Plateau, Nigeria. *Journal of African Earth Sciences*, **6**, 385-390.

USSHER, W.A.E. 1890. *The geology of parts of north Lincolnshire and south Yorkshire*. Memoir of the Geological Survey, **8**.

UWADIALE, G.G.O.O., & HALL, A.J. 1985. Mineralogy of ironstone from Agbaja Deposit, Nigeria, in relation to beneficiation. *Transactions of the Intitute of Mining and Metallurgy*. Section B, *Applied Earth Science*, **94**, 161-165.

VAN HOUTEN, F.B. 1985. Oolitic ironstones and contrasting Ordovician and Jurassic Palaeogeography. *Geology*, **13**, 722-724.

----------. 1986a. Search for Milankovich patterns among oolitic ironstones. *Palaeoceanography*, **4**, 459-466.

----------. 1986b. Stratigraphic patterns among Phanerozoic oolitic ironstone. *American Association of Petroleum Geologists Bulletin*, **70**, 659.

VAN HOUTEN, F. B., & ARTHUR, M. A. 1989. Temporal patterns among Phanerozoic oolitic ironstones and oceanic anoxia. *In:* YOUNG, T. P., & TAYLOR, W. E. G. (eds.) *Phanerozoic Ironstones*. Geological Society of London, Special Publication, **46**, 33-49.

VAN HOUTEN, F.B., & BHATTACHARYYA, D.P. 1982. Phanerozoic ironstones - Geological record and facies. *Earth and Planetary Science Letters*, **10**, 441-458.

VAN HOUTEN, F.B., & KARASEK, R.M. 1981. Sedimentologic framework of late Devonian oolitic iron formation, Shatti Valley, west-central Libya. *Journal of Sedimentary Petrology*, **51**, 415-427.

VAN HOUTEN, F.B., & PURUCKER, M.E. 1984. Glauconitic peloids and chamositic ooids - Favourable factors, constraints, and problems. *Earth Science Review*, **20**, 211-243.

VEIZER, J. 1983. Chemical diagenesis of carbonates: theory and application of trace element technique. *In:* ARTHUR, M. A., ANDERSON, T. F., KAPLAN, I. R.,

VEIZER, J., & LAND, L. S *Stable isotopes in sedimentary geology*. Society of Economic Palaeontologists and Mineralogists Short Course Notes, **10**, 3.1-3.100.

VELDE, B. 1977. A proposed phase diagram for illite, expanding chlorite, corrensite and illite-montmorillonite mixed layered minerals. *Clays and Clay Minerals*, **25**, 264-270.

VON GAERTNER, H. R., & SCHELLMAN, W. 1965. Recente sedimente in kuestenbereich des Halbinsel Kaloum, Guinea. *Min. Petr. Mitt.*, **10**, 349-367.

WADELL, H. 1932. Volume, shape and roundness of rock particles. *Journal of Geology*, **40**, 443-451.

WALTHER, L. M. 1985. Relative reactivity of skeletal carbonates during dissolution: implications for diagenesis. *In:* SCHNEIDERMANN, N., & HARRIS, P. M. (eds.) *Carbonate Cements*. Society of Economic Palaeontologists and Mineralogists Special Publication, **36**, 3-16.

----------. 1986. Relative efficiency of carbonate dissolution and precipitation during diagenesis: a progress report on the role of solution chemistry. *In:* GAUTIER, D. (ed.) *Roles of organic matter in sediment diagenesis*. Society of Economic Pal eontologists and Mineralogists Special Publication, **38**, 1-11.

WALTHER, L. M., & MORSE, J. W. 1984. A re-evaluation of magnesian calcite stabilities. *Geochimica et Cosmochimica Acta*, **48**, 1059-1069.

WARREN, E. A., & CURTIS, C. D. 1989. The chemical composition of authigenic illite within two sandstone reservoirs as analysed by A.T.E.M. *Clay Minerals*, **24**, 137-156.

WATKINS, P. 1972. *The geochemistry and mineralogy of the Frodingham Ironstone*. Unpublished PhD Thesis. University of Sheffield.

WEBER, J.N. 1969. The incorporation of magnesium into the skeletal calcites of echinoderms. *American Journal of Science*, **267**, 537-566.

WENTWORTH, C. K. 1922. *The shapes of beach pebbles*. United States Geological Survey Professional Paper, **131-C**, 75-83.

WHITEHEAD, T.H., ANDERSON, W., WILSON, V., & WRAY, D.A. 1952. *The Mesozoic ironstones of England. The Liassic ironstones*. Memoir of the Geological Survey.

WIEWIORA, A. 1990. Crystallochemical classifications of phyllosilicates based on the unified system of projection of chemical composition: III The serpentine - kaolin group. *Clay Minerals*, **25**, 93-98.

WILKINSON, B. H., & LANDING, E. 1978. "Eggshell diagenesis" and primary radial fabric in calcite ooids. *Journal of Sedimentary Petrology*, **48**, 1129-1138.

WILLIAMS, E. M. 1965. A method of indicating particle shape with one parameter. *Journal of Sedimentary Petrology*, **35**, 993-996.

WILSON, V. 1948. *British regional geology: East Yorkshire and Lincolnshire*. Memoir of the Geological Survey.

WOODWARD, H.B. 1893. *Jurassic rocks of Britain 3, the Lias of England and Wales (Yorkshire excepted).* Memoir of the Geological Survey.

WORONICK, R. E., & LAND, L. S. 1985. Late burial diagenesis, Lower Cretaceous Pearsall and Lower Glen Rose Formations, South Texas. *In:* SCHNEIDERMANN, N., & HARRIS, P. M. (eds.) *Carbonate Cements.* Society of Economic Pal eontologists and Mineralogists Special Publication, **36**, 265-275.

YANITSKY, A. L. 1960. Oligotzenovye oolitovye zheleznye rudy severnogo Turgaya i ikh genezis [Oligocene oolitic iron ores of the northern Turgai and their genesis]. *Trudy Instituta Geologicheskikh Rudnykh Mestorozhdenii, Moscow*, **37**.

YOUNG, T.P. 1989a Phanerozoic Ironstones: an introduction and review. *In:* YOUNG, T. P., & TAYLOR, W. E. G. (eds.) *Phanerozoic Ironstones.* Geological Society of London, Special Publication, **46**, ix-xxv.

----------. 1989b. Eustatically controlled ooidal ironstone deposition: facies relationships of the Ordovician open shelf ironstones of Western Europe. *In:* YOUNG, T. P., & TAYLOR, W. E. G. (eds.) *Phanerozoic Ironstones.* Geological Society of London, Special Publication, **46**, 51-63.

YOUNG, T. P., AGGETT, J. R., PARSONS, D., & HOWARD, A. S. 1990. *Jurassic and Ordovician ironstones.* Unpublished fieldguide for the International Association of Sedimentologists Congress, Nottingham. [Copy enclosed at back of thesis, subject to modification prior to publication].

YURTSEVER, Y. 1975. *Worldwide survey of stable isotopes in precipitation.* Report Section of Isotope Hydrology I.A.E.A. Nov. 1975.

ZINGG, T. 1935. Beitrage zur Schotteranalyse. *Schweiz. miner. Petrog. Mitt.*, **15**, 38-140.

Copy of:

Jurassic and Ordovician Ooidal Ironstones.

T. P. Young, J. R. Aggett, D. Parsons, A. S. Howard.

Unpublished Fieldguide for the
International Association of Sedimentologists Congress,
Nottingham, August 1990.

The enclosed fieldguide was originally presented as a double-sided document. The guide is presently being modified for publication, so the authors request that any portions of this work that other authors may wish to cite, be checked with them, in order to avoid discrepancies between the enclosed, and the final published document.

This copy to be placed in the folder at the back of the thesis.

Jurassic and Ordovician Ooidal Ironstones

T.P. Young[1], J.R. Aggett[2], D. Parsons[3], A.S. Howard[4]

This fieldtrip will examine ooidal ironstones and their sequence-stratigraphic settings in the Jurassic of the western margin of the North Sea Basin and in the Ordovician of the northern part of the Welsh Basin. The ironstone deposits have all been of economic significance, but none of them is now worked.

The Cleveland Ironstone (Pliensbachian) contains ironstones developed on flooding surfaces bounding progradational parasequences of distal storm-dominated fine-grained clastic sediments. Siltstones and fine sandstones in the upper parts of the progradational units may contain early diagenetic siderite nodules. The subsequent flooding surface may involve sufficient winnowing of the top of the underlying sediments to exhume these nodules into the basal shell lags of the ironstones. The ironstones themselves originally consisted of berthierine-rich ooidal mud- or wacke-ironstones, but during early diagenesis these often became strongly sideritized. Many of the ironstones show very high phosphate contents, partly in association with phosphatized lag material, but largely reflecting the widespread development of francolite cements. In the upper part of the formation in the north of the area the ironstone beds of successive cycles became amalgamated because of the very low rate of subsidence. Here the primary stratigraphy is largely overprinted by the development of rhythmic siderite cementation.

The Frodingham Ironstone (Sinemurian) was developed near the northern limit of the Midlands Platform. The local palaeogeography remains unclear, but the ironstone probably represents the largely *in-situ* development of iron-rich minerals in a shallow-water storm-influenced condensed deposit. Subsidence and sedimentation rates were very low; there is little facies change between the base and top of the formation suggesting a rate as low as 1mm/300years, which was maintained for between 2 and 4Ma. The Frodingham Ironstone is strongly bioclastic in its coarser-grained lithologies. These high-porosity rocks have been cemented by a complicated sequence of berthierine, siderite and calcite cements.

Detailed analysis of the palaeoecology provides important information on how the ironstone accumulated and on the nature of the substrate.

The northern part of the Welsh Basin contains ooidal ironstones at several levels within the Ordovician succession. These ironstones are associated with major transgressive events during the Arenig, the early Llanvirn and during the *Nemagraptus gracilis* Biozone. The Ordovician ironstones are similar to the Jurassic examples in many respects, but there are prominent differences. The ironstones contain little benthic fauna apart from sponges and inarticulate brachiopods. This assemblage resembles those of some of the contemporary basinal mudstones. The ironstones are often rich in the phosphatic oncoids known as *"Bolopora undosa"*, and there appears to be a gradation between large chloritic pisoids and the oncoids.

The Arenig/Llanvirn boundary ironstone coincides approximately with the onset of volcanism in the western Llŷn, and post-dates a major phase of subsidence in Anglesey, Llŷn and the Harlech Dome. This tectonic activity resulted in the reworking of the ironstone deposits by a variety of mass-flow processes.

1 Dept. of Geology, UWCC, PO Box 914, Cardiff, CF1 3YE.
2 Dept. of Geology, The University, Manchester, M13 9PL.
3 Somerset County Museum, Taunton Castle, Taunton.
4 British Geological Survey, Keyworth, Nottingham.

The Cleveland Ironstone Formation

T.P.. Young, J.R. Aggett and A.S. Howard

i. Background

The Cleveland ironstones were first worked in 1836, when the first exploitation of the Avicula Seam by the Whitby Stone Company began at Grosmont, although ironstone had been known from the Yorkshire Lias from at least as early as 1790. Later the Pecten Seam was worked in the same area. In 1838 mining started on the coastal exposures, but the exploitation was short-lived because of the difficulty in shipping the ore. In 1850 the Main Seam was discovered at Eston and workings commenced along the northern outcrop, with the annual output exceeding 5 million tons by 1873 (WHITEHEAD *et al.* 1952). The Main Seam became the dominant source of ore from the field, and for the latter part of the exploitation it was the only seam worked. In all some 350,000,000 tons were extracted from the Main Seam. As the southern limit of the ore-grade material was reached production declined, and by 1920 the Frodingham Ironstone became the major source of iron ore in Britain. The last mining of the Cleveland Ironstone took place at the North Skelton mine, which finally closed in 1964.

The Cleveland Ironstone Formation outcrops along the escarpment which bounds the North York Moors to the north and west. It is also seen in some of the deeply incised dales which cut the moors and at Eston as a faulted outlier to the north of the main escarpment. On the coast the formation is exposed around Staithes and reappears farther south at Runswick and in the area of Robin Hood's Bay.

ii. Stratigraphic Overview

The stratigraphy of the Pliensbachian rocks of the Cleveland area has been the subject of several recent studies (CHOWNS 1968; HOWARD 1984, 1985; POWELL 1984; SHALABY 1980). The Cleveland Ironstone Formation lies within the upper part of the Pliensbachian (*margaritatus* and *spinatum* Biozones). The sequence stratigraphy of the formation can be viewed as a succession of genetic stratigraphic sequences (*sensu* GALLOWAY 1989) bounded by drowning surfaces. These sequences comprise Cycles I-V in the Penny Nab Member and Cycles i-vi in the Kettleness Member. The coarsening-up cycles of the Penny Nab Member were first recorded by Chowns (1968) for

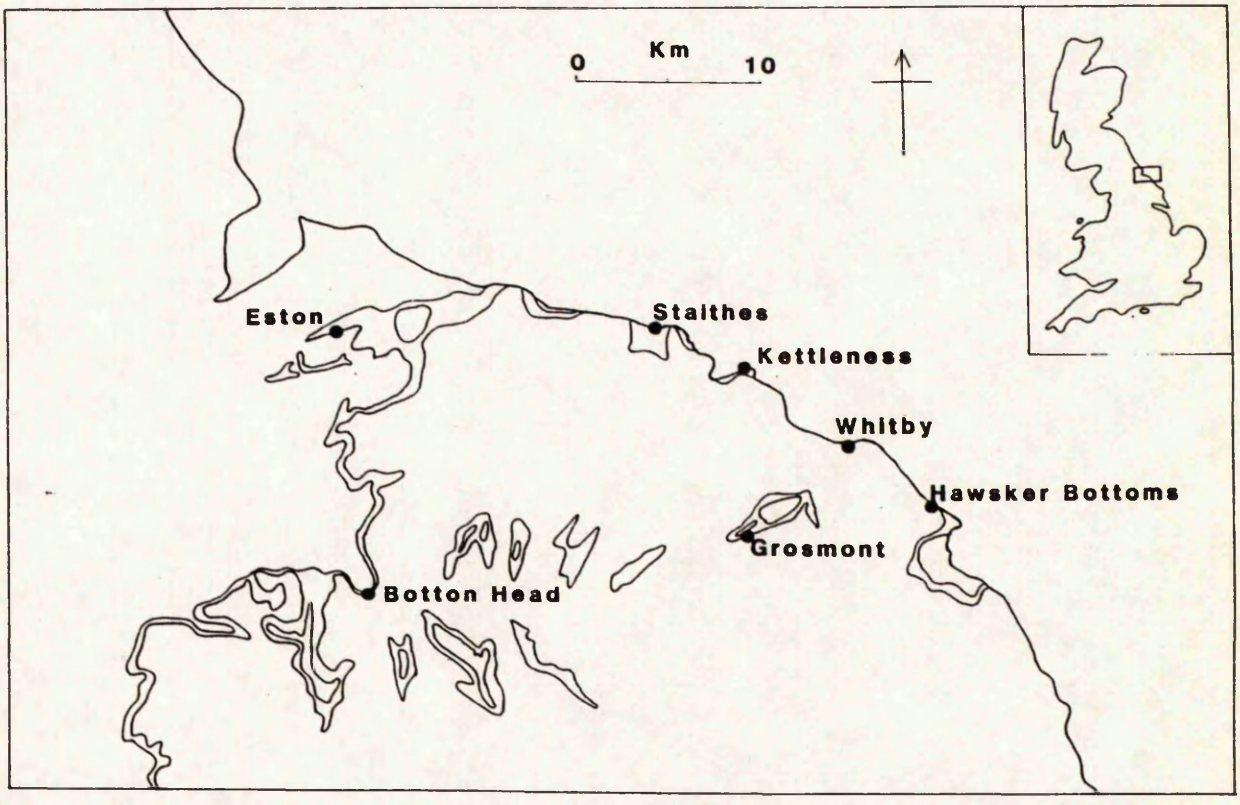

Figure 1. Outcrop of the Pliensbachian sediments of the Cleveland Basin, showing localities mentioned in the text, and those described in the guide.

the beds below the Avicula and Raisdale Seams. Subsequently Shalaby (1980), Rawson *et al.* (1982) and Howard (1984, 1985) have further discussed the cyclic nature of the sediments within the formation.

In this paper the cycles nomenclature is redefined so that the cycles as named coincide with the parasequences. The base of each cycle is therefore drawn at the base of the appropriate ooidal ironstone rather than its top. On facies with sideritic doggers (e.g. the classic type 2 cycles) the boundaries still coincide with the top of the doggers.

The Cleveland Ironstone Formation comprises two members, both bearing ooidal ironstones, but which exhibit rather different sedimentary facies:

a The Penny Nab Member (*Amaltheus stokesi* to *Amaltheus gibbosus* Subzones) consists of coarsening-upward cycles of fine-grained clastic sediments; the Type 1 cycles of Howard (1985) (designated I-V in upper case Roman numerals). These cycles are bounded by ironstones. In the more condensed developments of the formation these are developed as ooidal ironstones, often with conglomeratic material, whereas in the more expanded developments the Type 1 cycles are capped by siderite nodule horizons.

A typical Type 1 cycle, as defined by Howard (1984, 1985) with the base redefined as above, is 2-5m thick, commences with dark silty mudstone, which becomes progressively lighter in colour up sequence, and discrete silt or fine sand grade ripple cross-laminated beds become more common. The uppermost parts of some cycles exhibit significant erosional features, sometimes associated with the event beds as gutter casts. The upper levels of some cycles are particularly rich in horizons of siderite concretions. These siderite concretions may be reworked into the overlying ironstone, thus demonstrating the very early diagenetic origin of the concretions. Each cycle is capped by an ooidal ironstone with an erosional base. The presence of the strong basal erosion surface, which sometimes forms an angular unconformity, and the lack of clastic material within the ironstones, all strongly suggest, however, that the ironstones would be better regarded as the basal unit of each cycle. The unconformable or disconformable base of each ironstone can be regarded as transgressive surface, the maximum flooding surface (*sensu* GALLOWAY 1989) may be represented by the top of an ironstone bed. In contrast to Galloway's analysis of shallow marine sediments, therefore, the unconformities bounding the parasequences are the transgressive surfaces, not the maximum flooding surfaces.

The Penny Nab Member lies on the Staithes Sandstone Formation, a storm-influenced sand-dominated unit, which itself shows a cyclic stratigraphy.

b The upper part of the formation, the Kettleness Member (*Pleuroceras apyrenum* to *Pleuroceras hawskerense* Subzones) shows a similar cyclic arrangement in the more expanded succession in the southeastern part of the area (Type 2 cycles of Howard 1985; designated i-vi in lower case Roman numerals). In the condensed development seen in other areas, however, the member may be present largely in an ooidal ironstone facies without obvious cyclicity. Chowns (1968) recognised the existence of an important unconformity below the Kettleness Member, as well as a significant unconformity within the member in the upper part of the Main Seam.

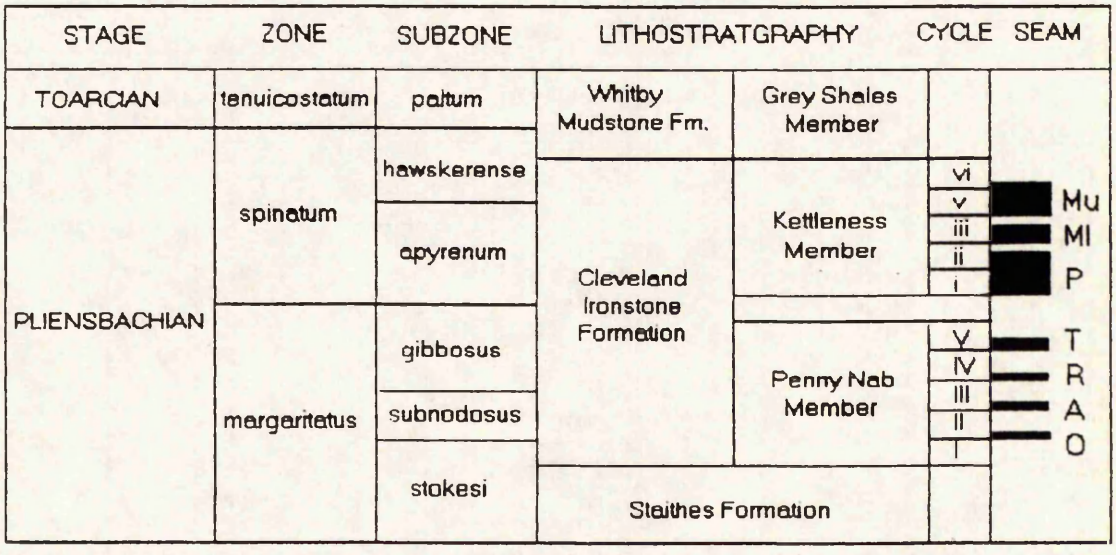

Figure 2. Stratigraphic framework of the Cleveland Ironstone Formation. Age of top of Cleveland Ironstone Fm. and ironstone seams based on Staithes section. Ironstone Seams: Mu Main Seam upper block, Ml Main Seam lower block, P Pecten Seam, T Two Foot Seam, R Raisdale Seam, A Avicula Seam, O Osmotherley Seam.

iii. Sedimentology

Type 1 Cycles

The sedimentology of the Penny Nab Member has been studied by several workers (CHOWNS 1968; GREENSMITH *et al.* 1980; HOWARD 1984), and the sediments have been interpreted as representing progradational, or aggradational, storm-generated successions (fig. 10). The cycles coarsen-upwards, with the upper part of each cycle composed of fining-up storm generated siltstone and/or sandstone beds. The occurrence of gutter-casts in the higher beds of two of the cycles has been described (GREENSMITH *et al.* 1980). The deposits bearing the gutter-casts appear to be the most "proximal" facies preserved, but probably represents a relatively offshore environment of deposition. The gutter casts of Staithes bed 34 (upper part of Cycle III) run approximately E-W.

Immediately below the Osmotherley Seam at Staithes and 50cm above the base of Cycle II at Staithes and Hawsker are siderite nodules with an abundant shelly fauna preserved with their original aragonitic shells.

Cycles I and II are rather similar to one another, as are Cycles III, IV and V. Cycles I and II may show a very thin fining-up sequence at their base. There is a transgressive surface with *Entolium lunare* 0.3m below the base of the Avicula Seam at the top of Cycle II. Cycle II is rather variable in thickness, mainly because of different amounts of sub-Avicula Seam erosion.

Cycle II has laminated siltstones in its upper levels. These are the host sediment to the sideritic concretions seen just below the Avicula Seam. Cycle III shows well developed graded siltstone beds with significant scour structures, including gutter casts, in its upper part. Similar coarser-grained clastic deposits can be inferred to have existed at the top of Cycle IV for laminated siltstone clasts occur reworked in the Two Foot Seam. The upper parts of Cycle V appear to have been removed by erosion between the deposition of the Penny Nab and Kettleness Members.

Cycle I thickens slightly eastwards, Cycle II is variable because of subsequent erosion, Cycle III shows only slight thickness variation, while Cycle IV increases slightly to the south and east. Chowns claimed an inverse thickness relationship between Cycles III and IV, but Howard (1984) suggested that this was more true for Cycles IV and V. Howard suggested that this might be explained by sea-floor topography existing after the deposition of the Two Foot Seam.

The Penny Nab Member Ironstones

1. The Osmotherley Seam

This is best developed in north and west Cleveland. It consists of a single block of grain-poor ooidal ironstone. There is no lag at the base. Farther east it is patchy in its distribution; sideritic nodules with rare ooids are seen at Staithes, and at Hawsker the seam is just 2 cm of sideritic berthierine mud-ironstone sandwiched between 2 layers of nodular sideritic mud-ironstone (HOWARD 1984).

2. The Avicula Seam

This seam exhibits complicated lateral variability. It is at maximum thickness at Grosmont. Here it has an upper block of berthierine ooidal sideritic mud-ironstone and a lower block of berthierine ooidal sideritic wacke-ironstone, separated by a thin layer of clastic mudstones.

Cobbles in the conglomeratic shelly lag at the base of the seam (e.g. at Staithes) are reworked early diagenetic siderite concretions. On exhumation the outer rinds became oxidised, and on reburial they underwent sulphidic diagenesis to give a pyrite rim. Some of the examples are bored (HOWARD 1984). The outer rinds are also strongly phosphatic (approximately 30% francolite). In the order of 1m of erosion can be determined below the Avicula Seam (HOWARD 1984).

At Staithes the top block of the seam is represented only by a thin bed of worn and fragmented shell debris, with pebbles of ooidal sideritic ironstone. There seems to have been a patchy distribution of ironstone with shell pavements between the accumulations at this level.

3. The Raisdale Seam

This seam thins gradually to the south and east, passing from grain rich to grain poor facies. The grain rich facies of the Raisdale does not go as far east as that of the Two Foot Seam.

Both seams show basal erosion surfaces, and both seams bear oolitic grain-ironstone nodules. Chowns (1968) demonstrated that some of the calcite cement represents pseudomorphs after aragonite. In the Two Foot Seam there are borings in these nodules. They represent early nodular cementation of storm-generated (?) grainstone beds, with subsequent erosion and biological reworking of the less cemented parts.

4. The Two Foot Seam

The Two Foot Seam is very similar in lithology and facies development to the Raisdale Seam. There are small gutter casts in the middle of the Two Foot seam at Staithes, together with reworked sideritic clasts and a shell hash. This forms a prominent

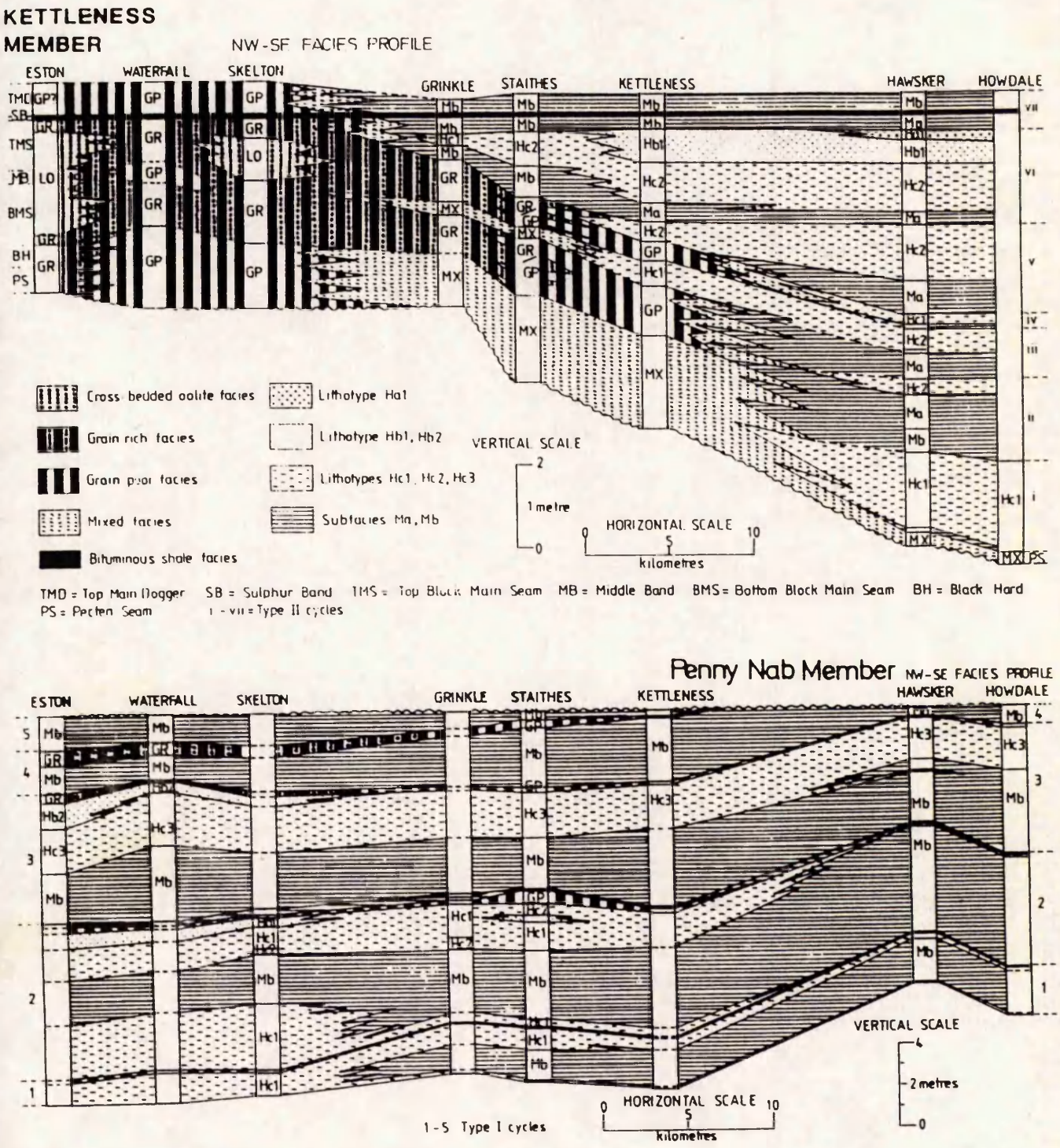

Figure 3. Lateral variation in the Cleveland Ironstone Formation.

division of the seam into upper and lower blocks at outcrop. The upper block of the seam is strongly phosphatic, reaching over 20% francolite in its upper levels.

Type 2 cycles

There are six type 2 cycles. Cycle vi is the only one to persist as far as Staithes in clastic facies. They coarsen-upwards from silty mudstones to siltstones or fine-grained sandstones. The cycles as described by Howard (1984, 1985) are capped by nodular sideritic mud-ironstones, forming sheets or nodules (doggers). The cycles thicken and coarsen towards the southeast, and to the southeast of Kettleness and Grosmont Cycle vi coarsens up into argillaceous sandstones, suggesting a sand source towards the southeast in *hawskerense* Subzone times.

Siderite formed in the cycle tops, where there was reduced sedimentation. These levels tend to have large concentrations of infaunal bivalves *in situ*.

Howard (1984) suggested that the overlying shales may have trapped upward moving pore fluids, but it seems likely that the siderite developed, at least in part, before the overlying unit was deposited.

According to Howard (1984) Type 2 cycles differ from the Type 1 cycles because "they did not produce recognisable effects across the entire basin, since they cannot be correlated with any vertical facies change within the laterally equivalent ironstone facies of west and north Cleveland.... They are not associated with a major widespread sedimentation break, although there was probably a brief period of reduced sedimentation rate at the cycle tops". He argued, therefore, that the cycles must be subsidence-generated. Such a view can now be modified, with the identification of probably correlative cycles within the ooidal ironstone facies.

The Kettleness Member at Staithes contains evidence for deposition during repeated flooding events. There are a similar number of these events to the number of Type 2 cycles. The position of these cycles within the succession at Staithes is comparable to that of the Type 2 cycles in neighbouring sections. The Type 2 cycles are therefore here tentatively correlated through to the Staithes area (Fig. 4).

In this correlation, the ooidal ironstones of a parasequence lie on top of the flooding surface, whereas the sideritic doggers of Howard's typical Type 2 cycles underlie the surface. In this respect the Type 2 cycles resemble the Type 1, with generation of siderite within the tops of the progradational parasequences, followed by the generation of ooidal ironstones on the sediment-starved flooding surfaces (Fig. 6). The ooidal ironstones may, in turn, become sideritized during early diagenesis. Type 2 cycles differ from the type 1 cycles in the relatively abrupt lateral transition from parasequences in clastic facies to parasequences in ooidal ironstone facies. The zone of interbedding of clastic progradational units with transgressive ooidal ironstones is very narrow.

Two of the type 2 cycles (cycles i and v) lie on major erosion surfaces. In the south of the area cycle v lies directly on the Penny Nab Member and eventually the Staithes Fm.

The Kettleness Member Ironstones

1. The ooidal ironstones:

Pecten Seam: This is the most laterally persistent of the ironstone units within the Kettleness Member. It grades from a facies with grainstone units in the northwest, through wackestone facies with variable siderite cementation (e.g. Staithes), to an ironstone with strong clastic component at some horizons (e.g. Grosmont). The top of the seam is diachronous. In the north the seam probably consists of amalgamated ironstone facies from at least two Type 2 cycles (cycles i and ii), whereas in the south it is only the product of the transgressive phase of the earlier cycle. It is possible that the lower part of the Pecten Seam at Grosmont represents a still earlier cycle not seen in the area to the north. Such a three fold division of the Pecten Seam was also proposed by Chowns (1968) (and in a modified form as a two-fold division by Howarth 1980). He named three units, the Grosmont Unit, the Eston Shell Beds and the Top Unit, within the Pecten Seam. In the division proposed here the Top Unit is the basal part of cycle ii, the Eston Shell Beds are largely equivalent to cycle i at Staithes, with the Grosmont unit either being a complex transgressive base to cycle i or the poorly preserved remnants of a still earlier cycle.

The base of the Pecten Seam represents one of the most erosional parasequence boundaries seen, and coincides with the observed *margaritatus/spinatum* Biozonal boundary. This is marked by an unconformity over much of the UK below the Marlstone Rock (COPE *et al.* 1980).

The sideritized horizons (60-70% siderite) of the Pecten Seam at Staithes appear to be more heavily bioturbated than the interbeds (20-25% siderite). The sideritized beds have gradational bases and tops, and are laterally impersistent (they cannot be correlated in even neighbouring sections at a single outcrop). The sideritization is discussed further below.

Black Hard: This unit is an ooidal mudstone bed lying above the Pecten Seam *sensu stricto*, with close lithological similarity to the Pecten Seam, but there are no sideritic hard bands. It appears to represent the upper part of cycle ii. The SiO_2:Al_2O_3 ratio is slightly higher in this bed than in most of the Pecten Seam, suggesting a slightly elevated clastic component, compatible with its position high in cycle ii.

Main Seam, Lower Block: The alternation of lithologies with different degrees of sideritization is similar to the Pecten Seam, but does not exhibit so extreme a range of siderite contents (typically 45-70% siderite). This ironstone forms the condensed facies of cycle iii.

Main Seam, Middle Band: At Staithes the unit clearly shows an elevated clastic content, together with an increased level of sulphides. The unit lies in the upper part of cycle iii. The appearance of clastic sediments in the upper part of cycle iii forms an important facies change across the region, known as the "Shale Line". The appearance of this clastic division within the main seam formed the southeastern limit of economic mining.

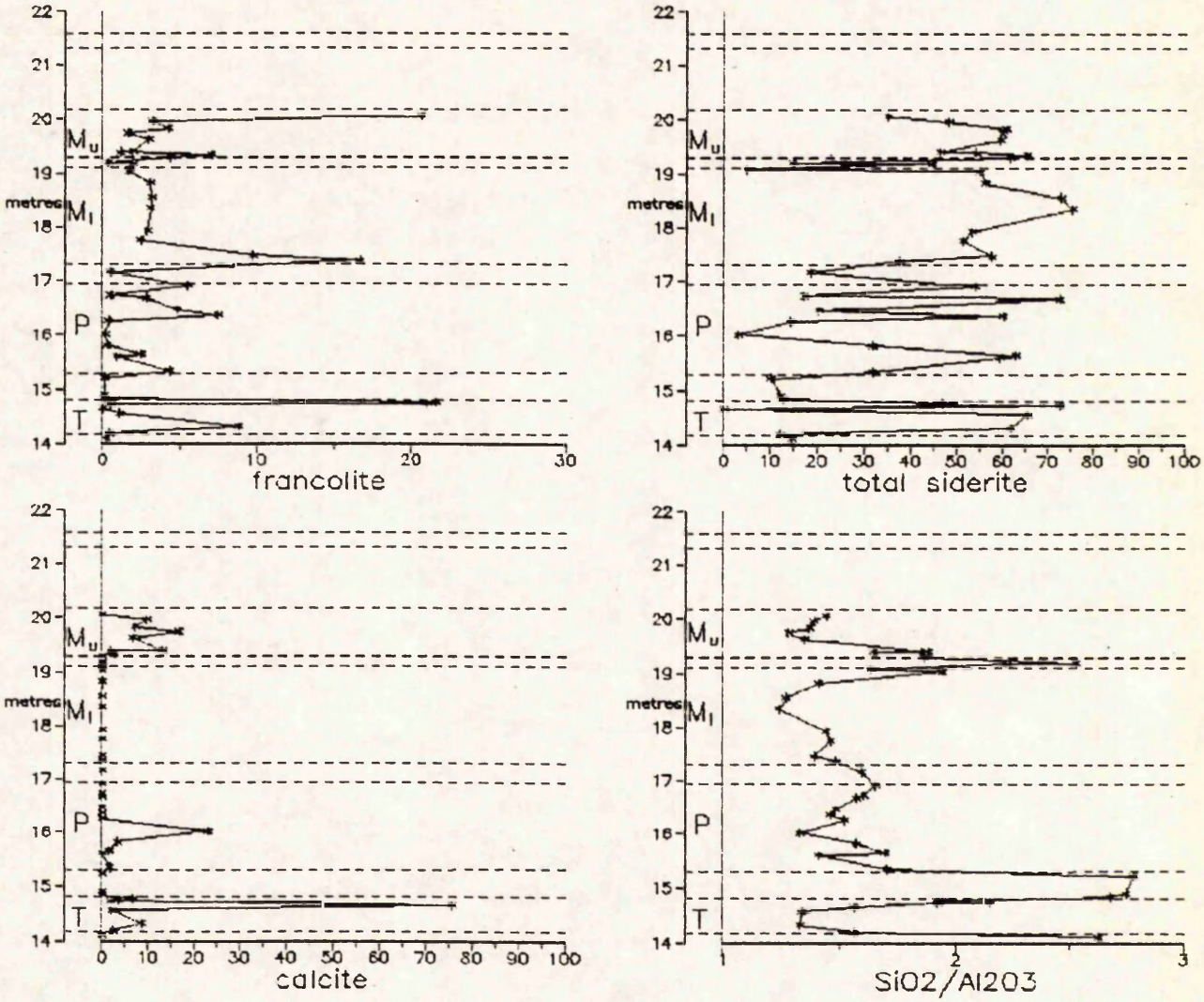

Figure 4. Chemical variation through the upper part of the Cleveland Ironstone Formation at Staithes. T: Two Foot Seam, P: Pecten Seam, ML: Main Seam lower block, MU: Main Seam upper block.

Main Seam, Top Block: The phosphate bed at the base of cycle v in the upper block of the Main Seam at Staithes is equivalent to a slight angular unconformity in west Cleveland, with the lower beds of the Member being cut out southwards (HOWARD 1985). The upper block of the main seam represents the condensed facies of cycle v. Cycle v saw widespread development of ooidal ironstones on the flooding surface; the base of cycle v at Grosmont is marked by ooidal ironstones.

The dating of cycle v is somewhat problematical, as its clastic facies has been assigned to the *hawskerense* subzone and what is here interpreted as the ironstone facies of the same cycle (Main Seam, upper block) to the earlier *apyrenum* subzone.
The actual ammonites discussed by Howarth (1955), however, do not allow the unambiguous assignation of the subzonal boundary in either facies.

Cycle vi: Cycle vi is developed solely in ironstone facies in the far north of the area, but at Staithes it is represented by the coarsening-up clastic unit (the "hawskerense shales") above the Main Seam. The base of the cycle is not clearly marked, but probably lies close to the top of the Main Seam, where there is a slight shelly lag.

2. The siderite "doggers"

The tops of the type 2 cycles in the clastic facies are of silt, or even sand grade, often quite strongly bioturbated. They contain assemblages of *in-situ* infaunal bivalves. These beds are generally cemented by siderite, forming distinctive concretionary horizons known as doggers.

iv. Ironstone Petrology

The Cleveland Ironstone Formation ooidal ironstones contain more or less altered berthierine ooids in a more or less strongly sideritized muddy matrix. There are reworked horizons with ooidal grainstones, which become a more important lithology towards the north and west. In the sections to be visited grainstones are restricted to the Raisdale and Two Foot Seams (as early lithified beds) and to the Avicula Seam (as burrow fills: "tubular tempestites"). Packstone horizons are seen at Staithes in the upper block of the Main Seam, and these probably represent similar winnowing or transport events.

Most of the ooidal ironstones are ooidal mud-ironstones or ooidal wacke-ironstones. These are probably not entirely primary textures, but the result of biological remixing of winnowed/reworked grainstone/mudstone interbeds. The texture of the sediment in which the ooids grew is not known, but they may well have been generated concurrently with the reworking, in a matrix similar to that seen today. The texture of the sediment has been further modified by compaction. The early generation of siderite has preserved original textures, so that the sideritized ironstones are texturally original, whereas the compacted mud-ironstones may be more compositionally unaltered.

The ooids are oblate ellipsoids 0.3-0.5mm long, with an elongation ratio of 2:1 to 3:1. The nuclei are almost entirely berthierine stacks. These have often been described in the past as flakes, crystals, crust fragments and pisoid fragments. A concretionary horizon in cycle V has yielded authigenic berthierine stacks in the early stages of becoming coated with a cortex.

Replacement of the ooids by phosphates, siderite, calcite and kaolinite are all seen. Structure may be maintained during phosphatisation (probably because the fine-grained francolite grows initially within porosity), but is lost in the other replacements. Siderite replacement of ooids is rare at the localities to be visited. Kaolinite replacement is very common, particularly in the lower block of the Main Seam. Kaolinite typically replaces the inner parts of an ooid first. A similar feature occurs in ferroan calcite replacement, which also starts at the centre of the ooid. In some examples it can be seen that it is the stack forming the nucleus which is preferentially replaced. Stacks occurring in concretionary mudstones in cycle V also show replacement by ferroan calcite.

The major cement phase is siderite. This usually occurs as 5-30µm crystals ("microspar"). The crystals are sometimes euhedral rhombs, but are more commonly subrounded. Many samples of the larger grained siderite show dark "cores" to the crystals. These appear however to be holes, and is uncertain what material was originally at the cores of the siderite crystals.

Most of the ironstones, and indeed the intervening clastic rocks are rather devoid of bioclasts. There are some shelly lags present, but the ironstones contain few dispersed shells.

v. Palaeontology

Penny Nab Member

Ichnofauna: The mudstone facies in the lower part of the Type I cycles has a low-diversity ichnofauna with *Chondrites*, *Planolites* and faecal pellet-packed burrows. This assemblage belongs to the *Zoophycus* ichnofacies. The overlying sediments have *Siphonites* or *Teichichnus* instead of the pellet-filled burrows. *Rhizocorallium* and *Thalassinoides* occur towards the tops of the Type I cycles at Staithes.

The lower part of the Avicula Seam has an ichnofauna similar to that of the middle part of the coarsening-up clastic sediments, but with fewer *Chondrites* and more *Planolites* & *Siphonites*. In the Raisdale and Two Foot Seams there is a Cruziana ichnofacies assemblage with *Planolites*, *Siphonites*, and occasional *Rhizocorallium*, *Thalassinoides* and *Teichichnus*. Oblique dwelling burrows and meniscus packed J shaped burrows are common in the Two Foot Seam at many localities.

Macrofauna: The Penny Nab Member yields a macrofauna dominated by bivalves including *Entolium lunare*, *Pseudolimea acuticostata*, *Pseudopecten aequivalvis*, *Gryphaea* sp., *Camptonectes lohbergensis*, *Meleagrinella papyria*, *M. substriata*, *Plicatula spinosa*, *Parainoceramus* sp., *Chlamys* sp., *Palmoxytoma cygnipes*, *Oxytoma inequivalvis*, *Liostrea* sp., *Protocardia truncata*, *Tutcheria submulticostata*, *Goniomya hybrida*, *Hippopodium ponderosum*, *Gresslya intermedia*, *Modiolus scalprum*, *Grammatodon inson*, *Mesosacella galathea*, and *Ryderia graphicus*. Brachiopods are represented by *Rhynchonelloidea lineata*. Nektonic elements include belemnites and ammonites. The ammonites are relatively abundant and have enable the detailed description of the biostratigraphy of the Cleveland Ironstone Formation (HOWARTH 1955; HOWARD 1985).

Palaeoecology: The mudstones of the lower part of the cycles have a "disturbed neighbourhood assemblage". Transported assemblages occur towards the tops of the cycles. There is no significant difference between the fauna of the bulk of the sediment and that of the nodules.

In cycles I and II the faunas were assigned by Howard (1984) to the *Tutcheria*, *Entolium-Pseudolimea* and *Entolium-Protocardia* Associations in ascending

order.

The *Tutcheria* Association is very similar in composition to the *Protocardia* Association seen elsewhere in the succession, except for the replacement of *Protocardia* by *Tutcheria*. *Entolium* is also very common in this association. Howard (1984) speculates that the low sedimentation rate at the base of the Type 1 cycles may be responsible, and that the *Tutcheria* Association may have been dependent on the growth of seaweed. The ichnofauna is dominated by *Chondrites* and *Planolites* although faecal pellet-filled burrows also occur. Other shelly fossils include *Pseudolimea*, *Grammatodon*, *Mesosacella*, *Gresslya* and *Protocardia*.

The *Entolium-Pseudolimea* Association has a shelly fauna dominated by the two eponymous bivalves and ichnofauna with *Chondrites* and *Planolites*. Additional taxa include *Mesosacella* and *Grammatodon*.

The uppermost silty shales bear the *Entolium-Protocardia* Association. The bivalves *Entolium*, *Protocardia* and *Pseudolimea* are all common, with *Gresslya* and *Pseudopecten* as accessory species. The ichnofauna is dominate by *Chondrites* and *Planolites*, although *Teichichnus* and faecal pellet-packed burrows occur.

In cycles III-V the fine-grained clastic sediments have disturbed neighbourhood assemblages, but are often poorly fossiliferous. Many juvenile and/or stunted forms are present. Since the preservation is often excellent then this must reflect a primary ecological phenomenon. The coarser grained sediments in the upper part of cycle III have entirely transported assemblages, present only as lags on the base of storm sand beds and gutter casts. The fauna of the clastic sediments of these cycles was referred to the *Pseudolimea* Association by Howard (1984). This association has the ichnofossils *Chondrites*, *Planolites* and faecal pellet-packed burrows. The shelly fossils have *Pseudolimea* and small *Protocardia* as common elements, but *Mesosacella*, *Grammatodon*, *Meleagrinella* and *Procerithium* also occur.

The Avicula, Raisdale and Two Foot Seams bear a *Pseudopecten* Association fauna. This occurs as a heavily reworked transported and mixed assemblage. *Planolites* is abundant, and the shelly fauna is dominated by *Pseudopecten*, *Palaoxytoma* and *Rhynchonelloidea*. Other taxa include *Chlamys*, *Gresslya*, *Cardinia*, *Plicatula*, *Oxytoma* and *Pseudolimea*, together with the ichnotaxa *Siphonites*, *Chondrites*, *Skolithos* and *Rhizocorallium*. The upper part of the Two Foot Seam bears a *Protocardia* Association consisting entirely of juvenile or stunted individuals. In the Raisdale Seam deep burrowing pholadomyids are preserved in life position with a packstone infill.

The Kettleness Member

Ichnofauna: Because of the high bioturbation the deeper, larger burrows are preferentially preserved (*Planolites, Rhizocorallium*). In the ooidal mud- and wacke-ironstone facies *Planolites, Siphonites, Chondrites* and occasional *Rhizocorallium*. In the more ooid-rich lithologies *Rhizocorallium* is more abundant, together with some *Thalassinoides*. This is similar to the assemblage in the stratigraphically equivalent coarser grained clastic sediments in the upper parts of the Type 2 cycles. All these are referable to the *Cruziana* ichnofacies.

The trace fossils of the clastic rocks of the member are broadly similar to those of the Penny Nab Member cycles.

Macrofauna: The lower part of the Pecten Seam and the upper block of the Main Seam are the only parts of the member at Staithes to contain much macrofauna. There is a tendency for the shells to be broken and worn. Frequently only *Gresslya* sp. and "nests" of *Rhynchonelloidea lineata* are seen. The latter preserved because of the higher preservation potential of the brachiopods' calcite shell, the former possibly because of the depth of its burrowing. The dissolution of shell material seems the most likely explanation for the lack of shelly macrofauna in the member.

Palaeoecology: The interpretation of the palaeoecology of the Kettleness Member is hampered by the poor preservation of the macrofauna, and the complication of the ichnofauna by the differential cementation and compaction. It is still unclear whether the apparent preferential occurrence of *Rhizocorallium* in the sideritic bands of the Pecten Seam is real, or a preservational artefact. It seems likely that the siderite bands are preferentially burrowed by *Rhizocorallium*, and that there may be a causal relationship. Where sideritization is incomplete the burrows are the preferential sites of siderite generation. This could be due to the enhanced organic content of the burrows, or due to preferential fluid-flow through the burrow fills during early diagenesis.

vi. Diagenesis

The diagenetic history of the ironstones is still not completely understood, but new data have substantially improved the situation. The discussion presented here is based largely on the unpublished studies of Young (wholerock analyses) and Aggett (electron microprobe analyses).

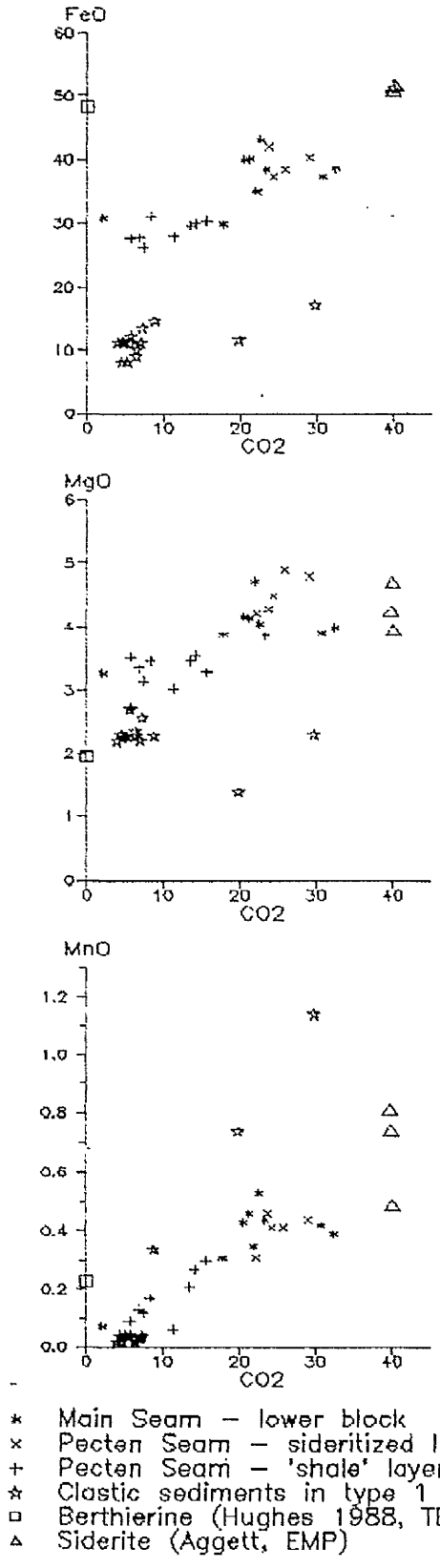

Figure 5. Comparison of wholerock variation in iron, magnesium, manganese oxides and CO_2 content with EMP analyses of siderite and TEM analyses of berthierine, Cleveland Ironstone Formation, Staithes.

Siderite cementation in the Kettleness Member: The variable siderite cementation of the Kettleness Member is largely responsible for the nature of the bedding visible at outcrop at Staithes. Some, but not all, of this variation in cementation is controlled by original sediment composition (the more clastic-rich parts of the member have not generally been subject to such intense cementation). The original sediment variation is not clearly visible because of this overprinting, and much of the study of the early diagenesis has been aimed at attempting to "see through" the sideritization to examine the original ironstone itself.

Whole rock analyses (Fig. 5) of the Kettleness Member demonstrate a good correlation between the bulk composition of the sideritized rocks and the composition of individual siderite rhombs.

Phosphatization: Phosphatization of the ironstones in the Cleveland Ironstone Formation is very frequent. The upper parts of each of the Penny Nab Member ironstones is phosphatized. In the Two Foot Seam the francolite forms over 20% of the upper levels. Phosphate cements are also seen in the Kettleness Member ironstones. The phosphate content of some of the minor concretionary beds in the Penny Nab Member (e.g. in the middle of cycle IV) is also high, particularly around the edges of the concretions.

Phosphatized pebbles have been recorded from the Kettleness Member (HOWARD 1985), and in the Penny Nab Member phosphatization of reworked siderite nodules has been observed (pers. obs.). The relative importance of included phosphatized intraclasts and of *in-situ* early diagenetic authigenic phosphates has not yet been determined.

The pattern of phosphate occurrence in the Penny Nab Member ironstones associated with the basal lag deposits and as a cement in the higher parts of the ironstone bed resembles that recorded from an Ordovician ironstone in the Kermeur Formation of Brittany (YOUNG 1989b, and unpublished data). In the Kermeur Formation ironstone phosphate is particularly abundant as a cement in the uppermost levels of the sediment below the ironstone, as intraclastic material in the basal part of the ironstone, and in the upper part of the ironstone in diagenetic concretions.

In the Kettleness Member peaks of phosphate concentration (figure 4) occur (1) in the base of Pecten Seam (15.35m), (2) 1m above the base of the Pecten Seam (16.35m), (3) at the top of the Pecten Seam (16.90m), (4) the base of the Main Seam (17.35m), (5) the base of the upper block of the Main Seam (19.40m), and (6) at the top of the Main Seam (20.05m). This distribution reflects the succession of otherwise cryptic drowning surfaces within the Kettleness Member, equivalent to those bounding the Type 2 cycles described by Howard (1985)

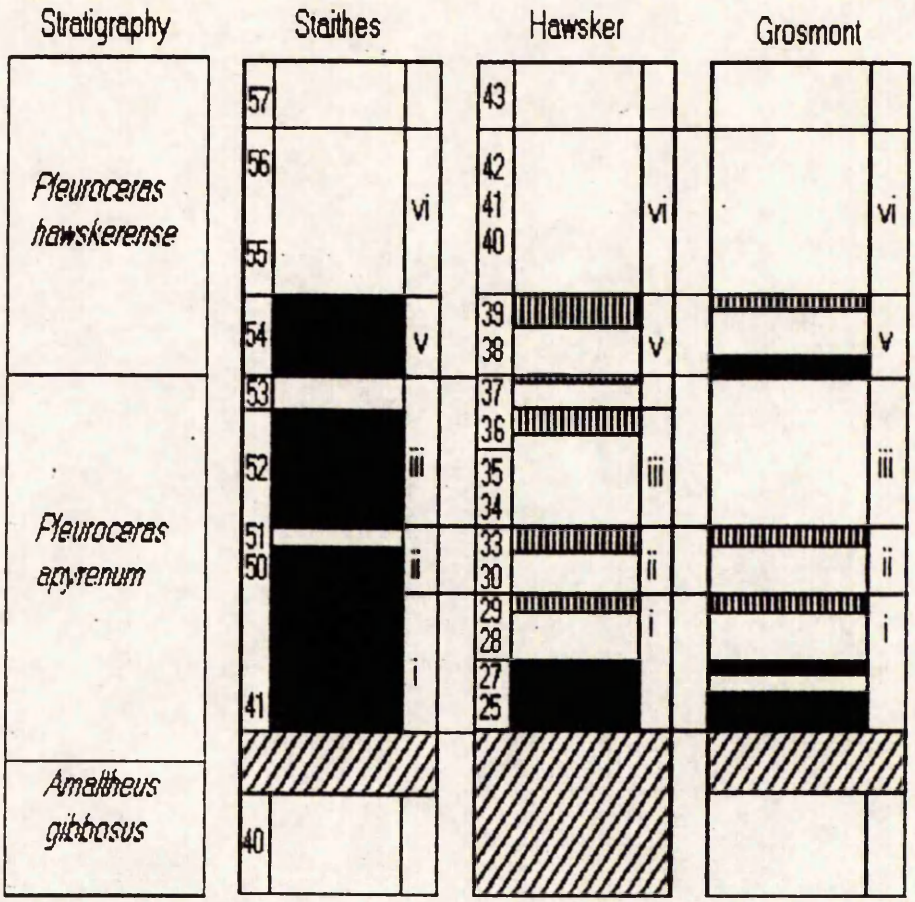

Figure 6. Stratigraphy of the upper part of the Cleveland Ironstone Formation, showing the tentative correlation of the type 2 cycles seen at Hawsker Bottoms and Grosmont with the Kettleness Mbr. sequence of Staithes. Bed numbers after Howarth (1955), cycle numbers after Howard (1985). Cross-hatch: absent, vertical ornament: sideritic doggers, solid ornament: ooidal ironstones.

from the more expanded facies of Hawsker Bottoms.

Chowns (1968) subdivided the Pecten Seam into three units defined largely by their faunal content. These subdivisions of the Pecten Seam were rejected by Howard (1985) on the basis that the faunas had no stratigraphic significance, and that there was no field evidence for the proposed intra-Pecten Seam unconformity proposed by Chowns. However, the phosphate data suggests that the Pecten Seam does contain at least one break (level 2 above), with a possible second break at the base of the Black Hard (level 3 above).

Distribution of Thorium: The distribution and significance of thorium in the ironstones was discussed by Myers (1989) using data from portable gamma ray spectrometry. This data has now been augmented by XRF analyses.

The ironstones are enriched in thorium, and are interpreted (Fig. 7) as originally containing approximately 60 ppm thorium, although some individual siderite-rich ironstone samples have thorium contents of up to 100 ppm.. This level was subsequently diluted by the addition of early

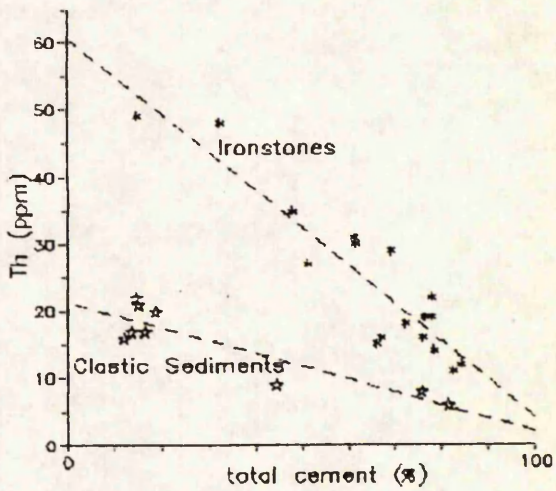

Figure 7. Thorium content as determined by XRF plotted against estimate of total cement (total siderite + total calcite + total francolite)

The thorium content of the background clastic sediments is about 20ppm, which was interpreted by Myers as partly reflecting the high proportion of thorium-bearing kaolinite (CATT *et al.* 1980) in the mudstones.

The composition of the original sediment: The chemical composition of the non-cement fraction has been calculated by subtraction of francolite, siderite (of composition determined by EMP) and calcite from the measured wholerock composition. Francolite was subtracted on the basis of the phosphate content, and assumes a $CaO:P_2O_5$ ratio of 1.39. Allowance was made for slight variation in the siderite composition, first subtracting siderite based on the composition observed by Aggett (unpub. data) using manganese as control. If excess iron, magnesium and carbonate is left, then further siderite is subtracted by taking iron, magnesium, calcium and carbonate in the same ratio. Excess carbonate and calcium were then subtracted as calcite.

The calculated composition of the non-carbonate material was analysed for variation with progressive sideritization. The results indicate that iron is stripped progressively from the original sediment, and that the initial $SiO_2:Al_2O_3$ ratio is maintained. If SiO_2 and Al_2O_3 have not been lost from the system then the original sediment did not contain enough iron or manganese to produce the observed siderite. These materials have been added to the sediment during the sideritization process.

The preservation of the original SiO_2 and Al_2O_3 during sideritization is supported by the maintenance of constant $SiO_2:TiO_2$ and $Th:SiO_2$ ratios during sideritization.

The estimate of the original composition is hampered by the lack of wholerock samples with very low siderite compositions. The best estimates currently available are compatible with material of approximately 25% kaolinite and 75% berthierine.

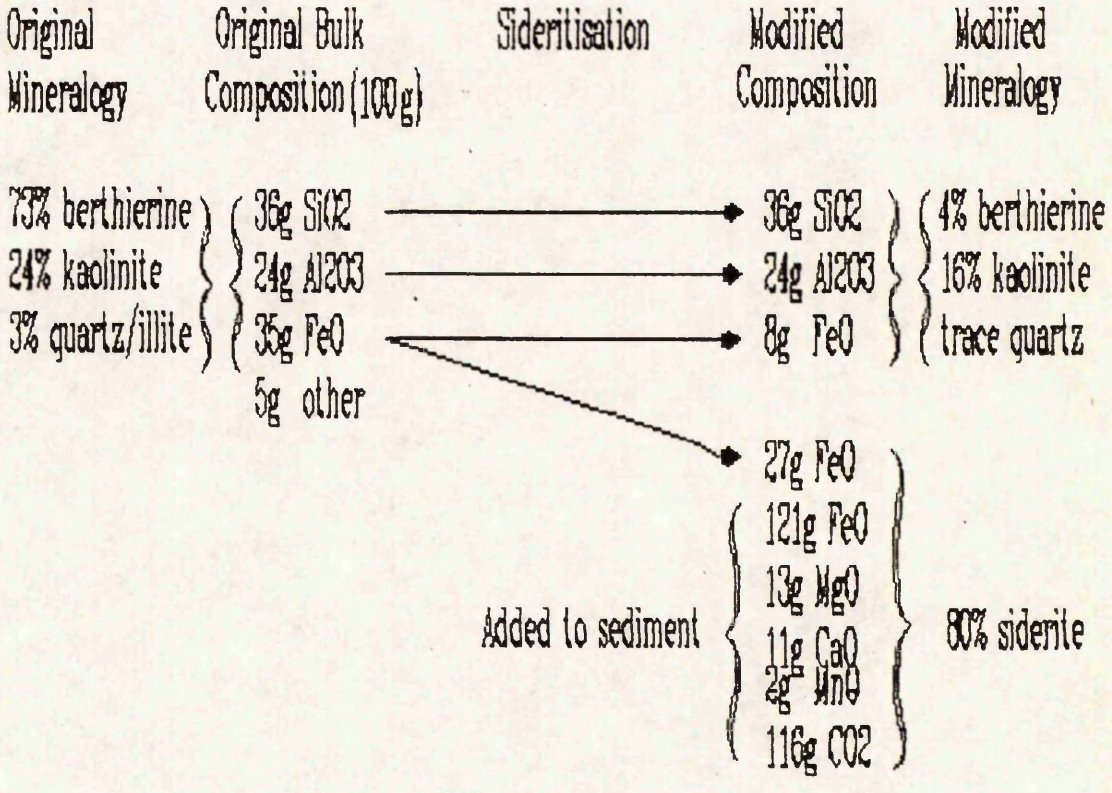

Figure 8. A model for the evolution of Cleveland Ironstone Formation ferruginous sediment composition and mineralogy during early diagenesis. 100g of original sediment (excluding hydoxyl) of 73% berthierine and 24 % kaolinite with 80% porosity, generates a fully indurated rock of approximately 4% berthierine, 16% kaolinite and 80% siderite.

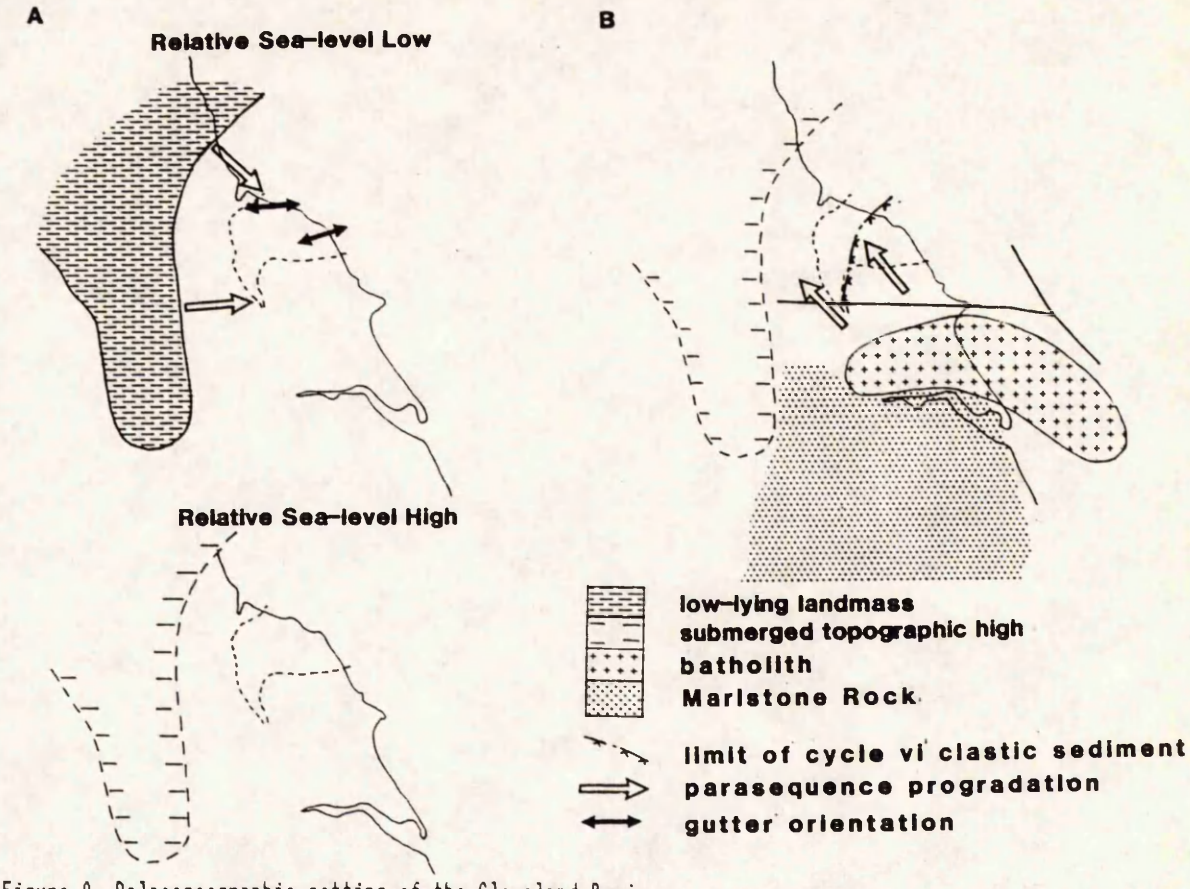

Figure 9. Palaeogeographic setting of the Cleveland Basin.
A. Palaeogeography during Penny Nab Member deposition.
B. Palaeogeography during Kettleness Member deposition.

vii. A Model for Sedimentation

Any model for the sedimentation of the Cleveland Ironstone Formation must account for the difference in facies relationships between the two members of the formation. Howard (1984) proposed a model for the Penny Nab Member which involved repeated flooding of a depositional system not unlike that of the earlier Staithes Formation; a barrier system with offshore sediment transport during storm events (Fig. 9).

The repeated progradation of the fine-grained clastic units from the north and west suggests that sediment was derived from those directions during Penny Nab Member times. The exact nature of the source cannot be ascertained, because of subsequent removal of the Jurassic rocks from the Pennine area. The ooidal ironstones lie on the flooding surfaces. They appear to be particularly developed towards the north and west - the areas of low subsidence rates bounding the Cleveland basin. Howard proposed a relatively small land area to the west of the basin as a source for the Staithes Fm., and it seems likely that the drowning events producing the ironstones may have flooded the landmass entirely.

During Kettleness Member times clastic progradation appears to be from the southeast. The north and west of the depositional area are characterized by reworked grain-ironstones, with an almost total absence of clastic material. This suggests that the postulated sediment source to the northwest remained flooded, although shallowly and with low subsidence, throughout Kettleness Member times. The sediment supply from the southeast may reflect either sediment transport paths by-passing the Pennine high, or, perhaps more likely, the relative uplift of a new source (e.g. part of the Market Weighton structure).

A major difference between the facies relationships in the two members is that in the Penny Nab Member the ironstones are separated by continuous clastic units. The Kettleness Member ironstones, however, amalgamate towards the northwest (the area of maximum condensation). This area is interpreted as being relatively shallow water. This suggests that the Kettleness Member ironstones may be due, at least in part, to a topographic rise "clastic trap" system (e.g. HALLAM, 1975). The Penny Nab Member ironstones may rather be due to the sediment starvation produced distally on a shelf during relative sea-level rise (e.g. YOUNG 1989b) (fig. 6).

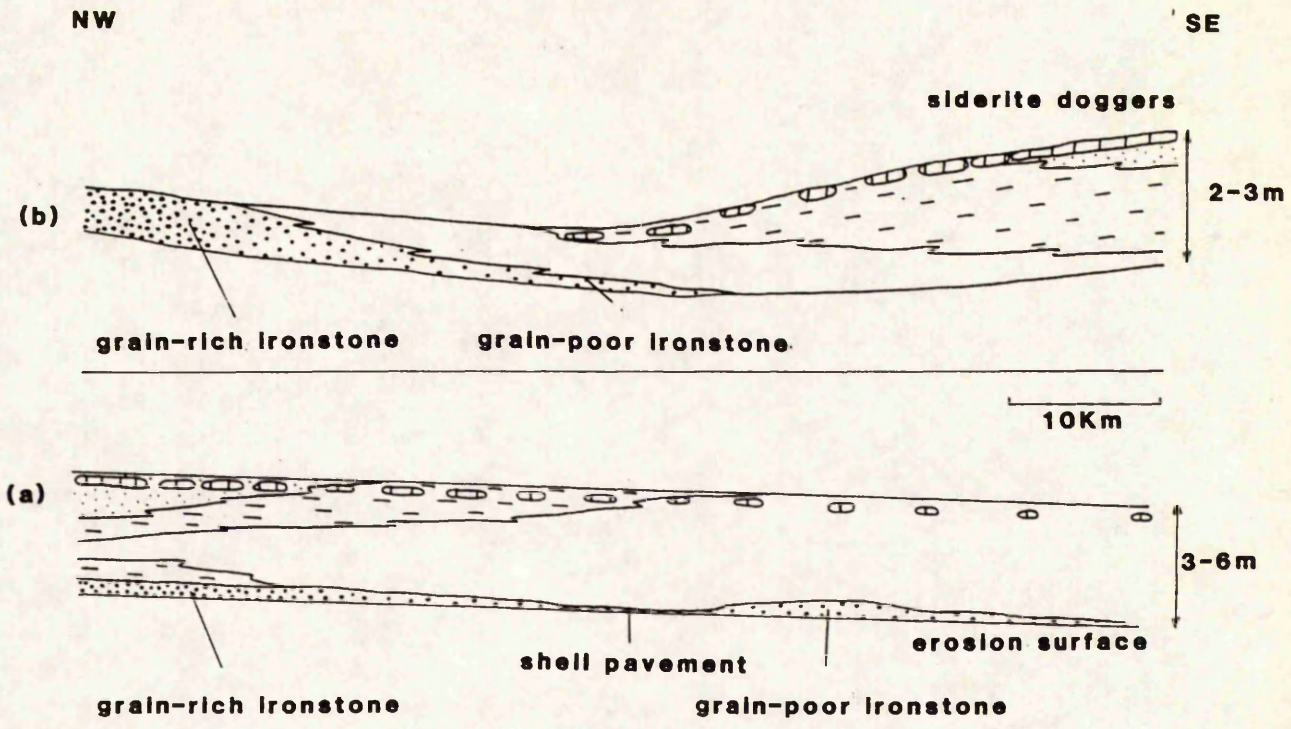

Figure 10. NW/SE profile showing facies relationships of parasequences of (a) Penny Nab and (b) Kettleness Members.

viii. Origin of the Ooidal Ironstones

The ironstones occur on the drowning surfaces of the depositional sequences. They represent deposits formed during rising sea-level. Estimates of depth of deposition are hard to derive, but Howard (1984) suggested that the entire formation was deposited in water depths of less than 50m.

Estimates of deposition rates are also difficult because of the poor control on the time involved. Estimates for the duration of an average Jurassic ammonite subzone are typically approximately 400,000 years (TORRENS *in* COPE *et al.* 1980), giving an overall sedimentation rate of 1mm/70 years. Haq *et al.* (1988) allow 2.5Ma for the *margaritatus* and *spinatum* Biozones, giving a rate of 1mm/100 years. Where the Kettleness Member is developed purely as ironstone there is about 4m of ooidal ironstone representing 2 subzones (i.e. overall accumulation rate of 1mm/300years). In the Penny Nab Member at Staithes there is a total of 1.5m of ironstone and 13.8m of clastic sediment. It is uncertain, however, how to partition the time involved between the formation of the two facies, and the periods of non-deposition/erosion. The cycles themselves number 5 in 2 subzones in the Penny Nab Member and 5 in 2 subzones in the Kettleness Member giving an average cycle duration of 165-250,000 years depending on the timescale used. Cycles of a similar nature are known from the Pliensbachian of Gloucestershire and Dorset, and it seems plausible that they were eustatically driven.

The source of the iron for the ironstones has been much debated (e.g. CATT *et al.* 1980; CHOWNS 1966, 1968; HOWARD 1984) but the problem may not be real. The background clastic sediment contains around 10wt% FeO while the primary ironstone sediment was probably around 25 wt% FeO (see below). Given the long time period during which it is believed that the ironstones developed this is not a great enrichment. Similarly the thorium content of the clastic mudstones is about 20ppm and that of the original ironstones is interpreted to have been about 60ppm. These materials were probably transported to the site of deposition associated with clay minerals, particularly kaolinite. There would be no problem in supplying sufficient thorium to the sediment, without needing a highly enriched transporting phase.

The transported clay minerals were largely unstable in the prolonged oxic and sub-oxic environment of the ironstone sediment, and degradation of the clastic minerals occurred. The released immobile elements became enriched in the authigenic phases (particularly berthierine or its precursor) developing in the sediment, in a process closely analogous to the development of lateritic soils. The development of ooids in this environment is not understood, but presumably their development

is analogous to the development of pedogenic pisoids. The formation of berthierine stacks, and their utilisation as ooid nuclei may hint that degradation of clastic micas might have been important in nucleating berthierine.

The sediment veneer on the transgressive surfaces was subject to prolonged physical and biological reworking. The original site of ooid generation was presumably intermediate between the shallow water cross-bedded deposits of reworked ooids and the distal ooid-free areas with siderite cementation of the pre-existing sediment (CHOWNS 1968; HOWARD 1984).

ix. Fieldguide

Locality 1: Staithes

The Staithes section is the best-known exposure of the Cleveland Ironstone Formation. It has figured prominently in previous discussions of the formation, and has been the subject of much of the recent research in the area. A complete section of the formation is exposed between Penny Nab (Grid Ref. NZ788189) and Brackenberry Wyke (NZ794183). The coastal exposure of the formation, both in the cliff and in the wave-cut platform is magnificent. It should be noted however that the section requires care in access, as the tide reaches the foot of the cliff, reaching first at a point near Staithes itself. The exposure should only be visited on a falling tide. In bad weather, particularly with strong east winds the fall of the tide may be difficult to predict, and great care should be taken. Storm waves may reach the foot of the cliff even at low tide! A further hazard is provided by the frequent fall of material from the cliffs. Hard hats should be worn.

Locality 1a: The Staithes Sandstone Formation is well-exposed around Staithes village and harbour, as well as in the cliffs between the village and Penny Nab. Howard (1984) has demonstrated that the sedimentological processes responsible for this formation were very similar to those acting during the deposition of the siliciclastic parts of the Cleveland Ironstone Formation.

The sediments of the Staithes Sandstone Formation are arranged in two coarsening-upwards cycles. These cycles are interpreted as being of similar nature to those of the overlying Cleveland Ironstone Formation. The contact between the two cycles is seen on the coast about 100m west of Penny Nab. The top of the lower coarsening-upward cycle is highly sideritized, and includes silty sandstones. This is ovelain by a transgressive sheet sandstone. Above this sheet the entire upper cycle is preserved. Storm generated sedimentary structures are well exhibited. Trace fossils are abundant and diverse (including (*Chondrites, Siphonites, Helminthoidea, Teichichnus, Thalassinoides, Rhizocorallium, Phoebichnus*). A diverse benthic macrofauna is also present, with most of the shelly material preserved as storm lags and coquinoid lenses.

Locality 1b: The Osmotherley Seam is exposed on the foreshore of the point of Penny Nab. It is developed at Staithes as a nodular sideritic horizon. In thin section this is seen as a sideritized siltstone with *Chondrites*. The texture is often pelletal. Rare ooids are occasionally found in burrow fills. The ironstone is interpreted as a level of sideritization developed below the flooding surface. Some ooids were developed on, or transported across, this surface and were trapped by burrows.

The Osmotherley Seam caps the lowest of the Cleveland Ironstone Formation Type 1 cycles, and lies 2.65m above the base of cycle (the top of the Staithes Sandstone Formation).

Locality 1c: The cliffs and foreshore in Jet Wyke expose a section through the upper part of the Cleveland Ironstone Formation. In particular the Type 1 cycles II and III are easily examined here. The Avicula Seam records a complex series of events around the top of cycle II. This horizon is rather variable along the outcrop but includes a regressive unit of storm generated siltstones with gutter casts near the top of cycle II. This is overlain by a shell hash with an erosional base and reworked siderite nodules. Further storm generated siltstones in similar facies overlie this bed, and include *in-situ* siderite concretions. The uppermost level of these silts (some 60cm above the base of the shell hash) contain further large sideritic concretions, and is overlain erosionally by the conglomeratic base to the Avicula Seam proper. The ironstone seam is often in two blocks separated by a shell layer.

Cycle III is the most spectacular example of the coarsening-upwards cycles, and it was the "striped beds" at the top of this cycle which were described by Greensmith *et al.* (1980).

The Raisdale Seam, above the "striped beds" is a 30cm sideritized ooidal ironstone. It often shows remnants of an ooidal grain-ironstone lithology half-way up. The Raisdale Seam contains abundant *in-situ* burrowing bivalves.

Locality 1d: The point at Old Nab exposes good sections through the Kettleness Member, including some collapsed adits. The Two Foot Seam, together with the Type 1 cycles IV and V, is also well seen

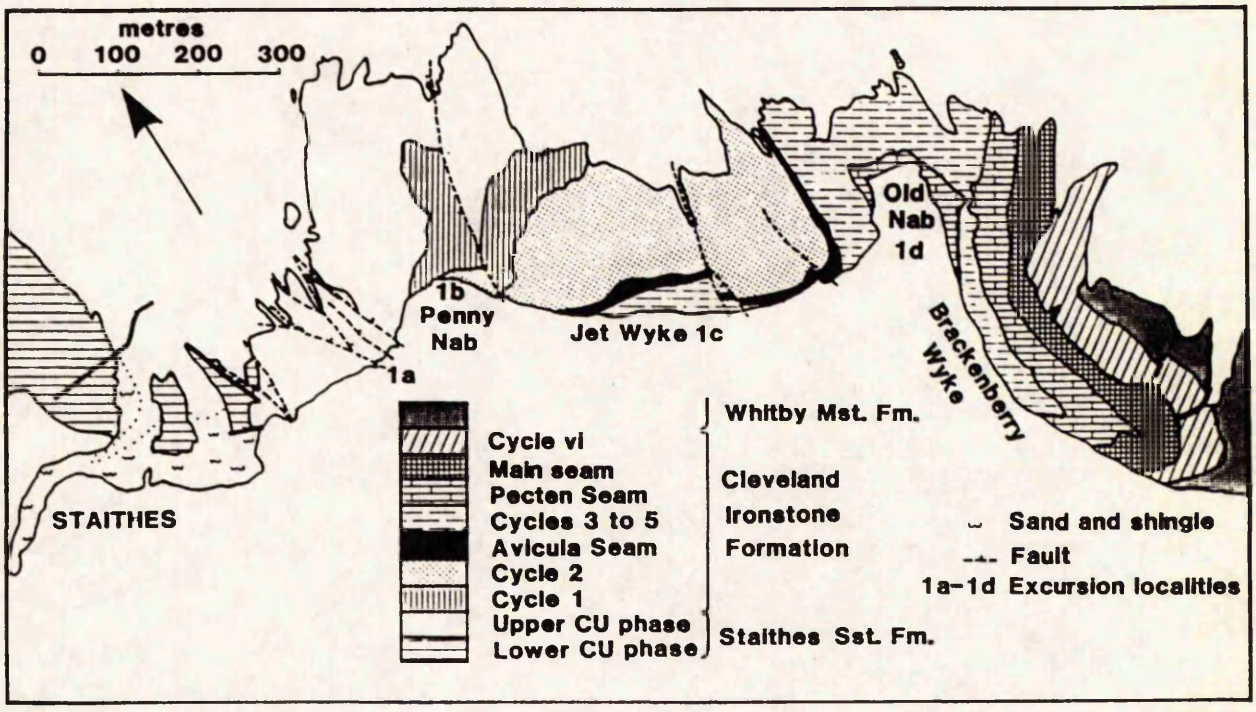

Figure 11. Plan of the Staithes section showing localities described in the text. Outcrop after Howarth (1955).

on this point.

The Two Foot Seam is very similar to the Raisdale Seam, with a partly reworked ooidal grain-ironstone layer, *in-situ* deep burrowing bivalves, and strongly phosphatic upper levels.

The Pecten Seam has a shell lag at the base, but the actual unconformity between the Kettleness and Penny Nab members is not obvious. The differential generation of siderite is well demonstrated here. The boundary between cycles i and ii is placed at the change from rather bioclastic ironstone up into bioclast-poor ironstone. The upper part of cycle ii is formed by the "black hard" an ooidal mud- or wacke-ironstone with a low siderite content, and a small amount of clastic material.

The base of the Main Seam lower block approximately coincides with the base of cycle iii. There are spectacular trace fossils formed through the preferential sideritisation of *Rhizocorallium*, both within the base of cycle iii and penetrating down into the top of cycle ii. The base of cycle iii at this locality also contained a partially articulated plesiosaur skeleton, now largely removed.

The upper part of cycle iii is believed to be represented by the middle band of the Main Seam. This is a clastic siltstone with some reworked ironstone material. At the base of the middle band there is an interesting horizon formed from a compacted spastolithic ooidal pack- or grain-ironstone, in which the ooids, although intensely deformed, are preserved as berthierine.

The significance of cycle iv is uncertain. It is very thin at the localities in the clastic facies where it has been identified, and it has not been recognised to date at Staithes. The base of cycle v is marked by the base of the upper block of the Main Seam, but as with the base of cycle iii the actual contact has been much disturbed by bioturbation. The base of the upper block is actually the sideritized top to the clastic sediments of the middle band. The base of cycle v is marked by both intraclastic and bioclastic lag material

Cycle vi is represented largely by the coarsening up clastic sediments, capped by a sideritized siltstone, seen above the Main Seam. The base of the cycle is tentatively placed at the top of the Main Seam upper block, where there is a slight bioclastic lag, but it is possible that the base lies lower within the block at an as yet unrecognised level.

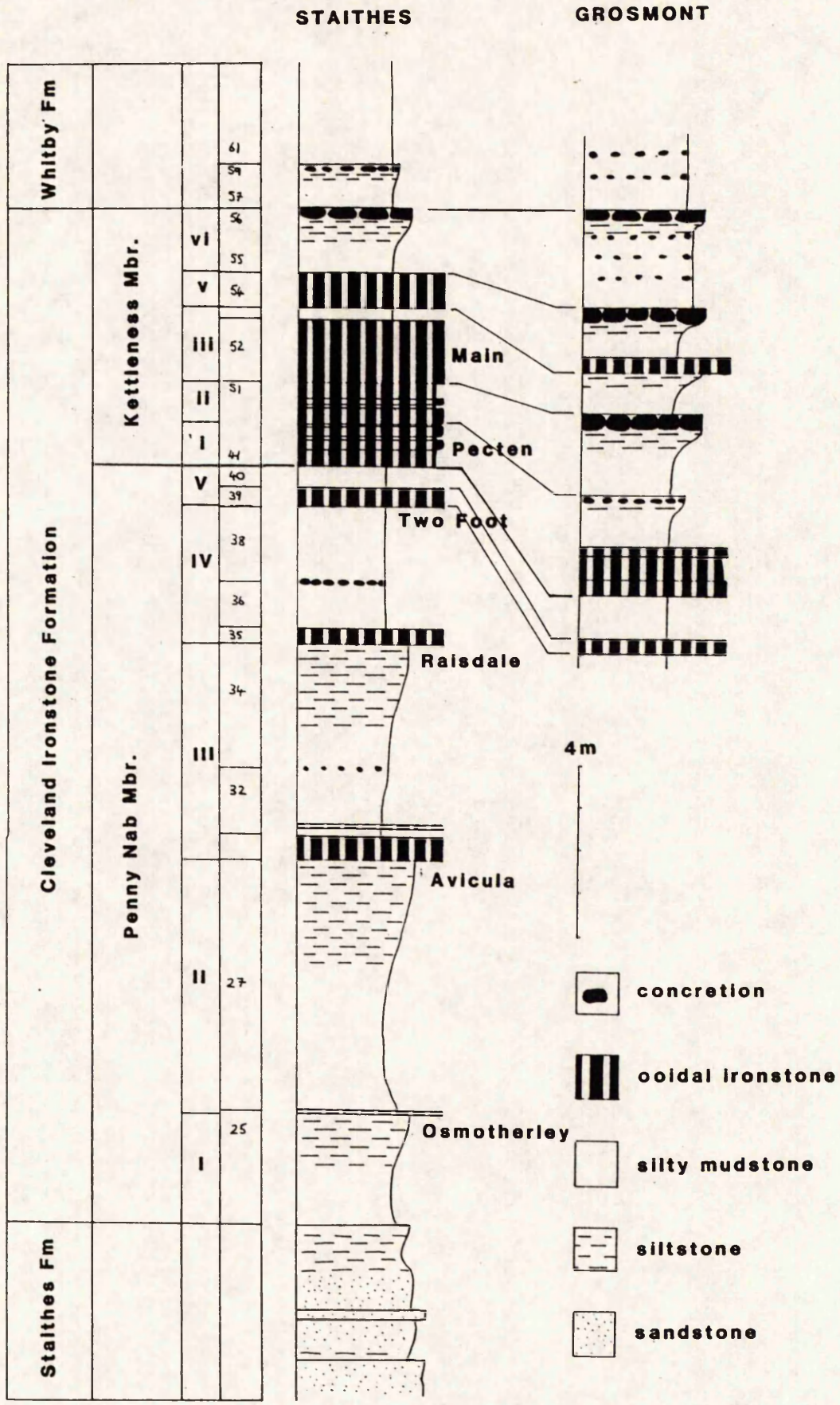

Figure 12. Logs of the Staithes and Grosmont sections. Staithes bed numbers after Howarth (1955).

Locality 2: Grosmont

The section of the upper part of the Cleveland Ironstone Formation seen in the river cliffs of the Murk Esk at Grosmont (NZ 830052) provides one of the best inland exposures of the formation. The locality is approached down a small track leading from the road just above the level crossing. Access to the section can be difficult when the river is high, and at all times great care should be taken of the extremely unstable cliff. Hard hats must be worn!

The Kettleness Member here is very different from Staithes. It is developed as a succession of coarsening-upwards cycles, each with a sideritic ironstone. These are classic Type 2 cycles (*sensu* HOWARD 1985). The sequence forms a good comparison with that at Staithes for the unconformity below the Pecten Seam lies at approximately the same level as at Staithes (1.13m above the Two Foot Seam).

The Two Foot Seam is visible in the river bank at ground level midway along the section. It is thinner than at Staithes, but is rather similar in character, with life position deep burrowing bivalves and burrows with ooidal grain-ironstone fills (tubular tempestites).

The Pecten Seam is well seen in the lower part of the face at the eastern end of the section. It consists of a sideritized ironstone, with *Rhizocorallium* in its lower part and life position infaunal bivalves in its upper part, resting directly on the unconformity. This is overlain by the highly fossiliferous beds bearing the spectacular assemblages of pectinids seen in fallen blocks. This lithology has a high clastic component and may represent the regressive part of a very thin cycle below cycle i. The top of the Pecten Seam is formed by a hard block of sideritized wacke-ironstone. This block may represent the transgressive base to cycle i. The Pecten Seam of Grosmont is, therefore, only equivalent to the lowest part of the Pecten Seam of Staithes, and indeed most of the seam may be earlier than the oldest Pecten Seam at Staithes. The bulk of cycle i is formed by a coarsening-upwards mudstone/siltstone unit capped by sideritized siltstones 1.3m above the top of the Pecten Seam.

Cycle ii is formed by a similar siltstone unit capped by the sideritic nodules 1.8m higher. Cycle iii is truncated 1m above its base by a marked shell lag overlain by a sideritized ooidal ironstone at the base of cycle v. As with the Staithes section cycle iv has not been recognised at Grosmont. Cycle vi is rather similar in character at Grosmont to Staithes.

The Frodingham Ironstone Formation

T.P. Young, D. Parsons and J.R. Aggett

i. Background

The Sinemurian Frodingham Ironstone Formation was exploited until 1989. The exposure of the formation is within the workings, and many of these are now threatened with becoming land-fill sites. There is some evidence that the Liassic ironstones of the Scunthorpe area were worked on a small scale during the Roman occupation, but subsequently the potential of the field was forgotten until the middle of the last century. The first record of exploitation is of 2000 tons raised in 1859. Production rose steadily and in 1940 annual output was around 4,500,000 tons. By 1952 the increasing depth of overburden as the faces were worked eastwards had forced the start of underground working. The peak of production was reached in the late 1960s, since when the decline of field has been rapid. During the 1980s the quarries were producing just a tiny fraction of their output previously, and by the end of the decade even this had finished. The steelworks now entirely utilise imported ore.

The outcrop of the formation was very limited and exposure is now confined to the workings. These extend for some 12km along strike. Access to the remaining pits is becoming difficult as backfilling operations are underway. Permission to visit, and details of current accessibility of faces should be sought from British Steel.

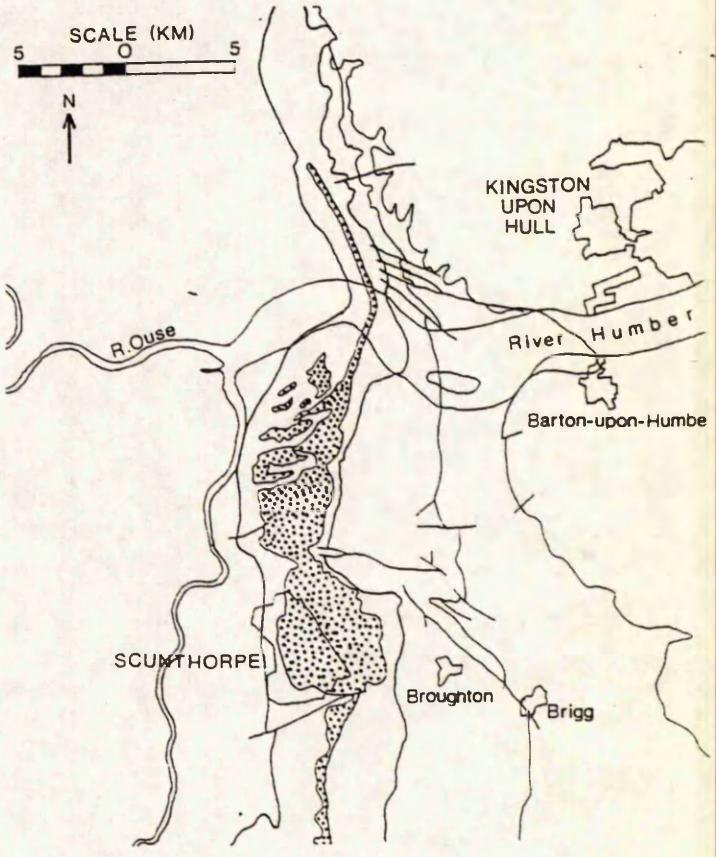

Figure 13. Location of the Frodingham Ironstone

ii. Stratigraphic Overview

The Frodingham Ironstone is the most important of the several ironstones within the lower part of the Lias in the East Midlands. The Frodingham Ironstone ranges in age from probably late in the *Arnioceras semicostatum* Biozone (*Euagassiceras sauzeanum* Subzone) to early in the *Oxynoticeras oxynotum* Biozone (*Oxynoticeras simpsoni* Subzone). Cope *et al.* (1980) indicated that the youngest ages are only recorded from the north of the outcrop, and that mixed ammonite assemblages from the upper part of the ironstone suggested condensation. The detailed biostratigraphic subdivision of the ironstone is not possible, partly because of poor localisation of old, but biostratigraphically significant, specimens in museum collections.

The ironstone is a condensed deposit. It varies between 6 and 10m in thickness within its outcrop, whereas the equivalent clastic sediments farther south and to the north in N. Yorkshire are up to 40m thick. This condensation reflects the development of the ironstone on the southern side of the Market Weighton structure (fig. 14). In the same area an ironstone, the Pecten Ironstone (not to be confused with the entirely different Pecten Seam of the Cleveland Ironstone), was developed in the early Pliensbachian (*Uptonia jamesoni* to *Tragophylloceras ibex Biozones*). Much of the higher Pliensbachian is cut out by the unconformity below the Marlstone Rock Bed (the equivalent of the Kettleness Member of the Cleveland Ironstone). The Marlstone Rock and the Pecten Ironstone are seen in the overburden in some of the deeper workings of the Frodingham Ironstone.

iii. Sedimentology

Within the Frodingham Ironstone, grading, bioturbation, sedimentary structures and shell-rich coquinoid biofabrics indicate that stratification consists of alternating storm- and fair-weather layers. These form a characteristic tripartite structure - a storm couplet below, overlain by background sediments. Typical pseudocycles are structurally multiple-event deposits (AIGNER 1979), modified to various degrees by subsequent lower energy events.

All pseudocycles have sharp, scoured, planar to undulating lower contacts. These may have become "blurred" as a result of further storm-event reworking, especially where there was no bioclast input to form a definite shell-rich base.

The Frodingham Ironstone was deposited during approximately 6 ammonite subzones (estimated at between 2 and 4Ma). The 8m thickness of ironstone was therefore accumulated at a rate of 1m in 250-500,000yrs; 1mm in 250-500 years. A 50cm storm unit thus might be expected to be a less than 1 in 150,000 year event. The depth of scouring is of a similar magnitude to the bed thickness, which in turn suggests that the residence time of the sediment in the mobile superficial layer was also in the order of 10^5 years. Such a long residence time is supported by the faunal mixing indicated by the occurrence of ammonites belonging to different subzones at the same horizon.

iv. Ironstone Petrology

There are bulk variations in the lithology of the ironstone, with differences in the proportions of the ironstone lithotypes. The base of the ironstone grades downwards into the ferruginous limestones and shales of the clays beneath.

There is great variation in lithology on a small scale. Davies and Dixie (1952) erected four lithotypes to describe the ironstone body. Watkins later added a fifth lithotype based on the gradational lithologies at the base of the ironstone body, and Parsons has subdivided one of the lithotypes. These lithotypes have proved quite useful in subsequent field studies:

Type A: Calcitic bioclasts and goethite/berthierine ooids, more or less replaced by siderite, all covered with a thin berthierine grain coating and siderite cement. In hand specimen a spongy mass of berthierine bearing shiny ooids. Bioclastic ooidal grain-ironstone.

Type B: Small rhombs of siderite amongst parallel oriented berthierine flakes. Ooids and bioclasts absent. In hand specimen a tough indurated blue/grey mudstone. Sideritic mud-ironstone.

Type C: Goethite\berthierine ooids, more or less replaced by siderite, within a fine grained berthierine/siderite "matrix". Goethite ooidal wacke-ironstone.

Type D: Goethite\berthierine ooids and calcareous bioclasts, more or less replaced by siderite, in a coarse sparry calcite cement. Ferruginous bioclastic limestone. (Subsequently divided by Parsons into D1 - dominantly bioclastic and D2 - dominantly ooidal)

Type E: Berthierine-bearing silty ooidal mudstone. siderite absent, clastic material prominent.

The ooids are dominantly of goethite. They are oblate, non-perfect ellipsoids. The long axis is usually 0.40-0.50mm, the intermediate 0.30-0.45 and the short 0.15-0.25. Ooid growth occurs through a three stage process. The early growth on the nucleus increases roundness, secondly preferential accretion in one plane leads to the generation of the oblate ellipsoid. A third period of growth, may act to increase sphericity.

Ooid nuclei are usually unstructured goethite or an ooid fragment, but bioclasts also, uncommonly, act as nuclei.

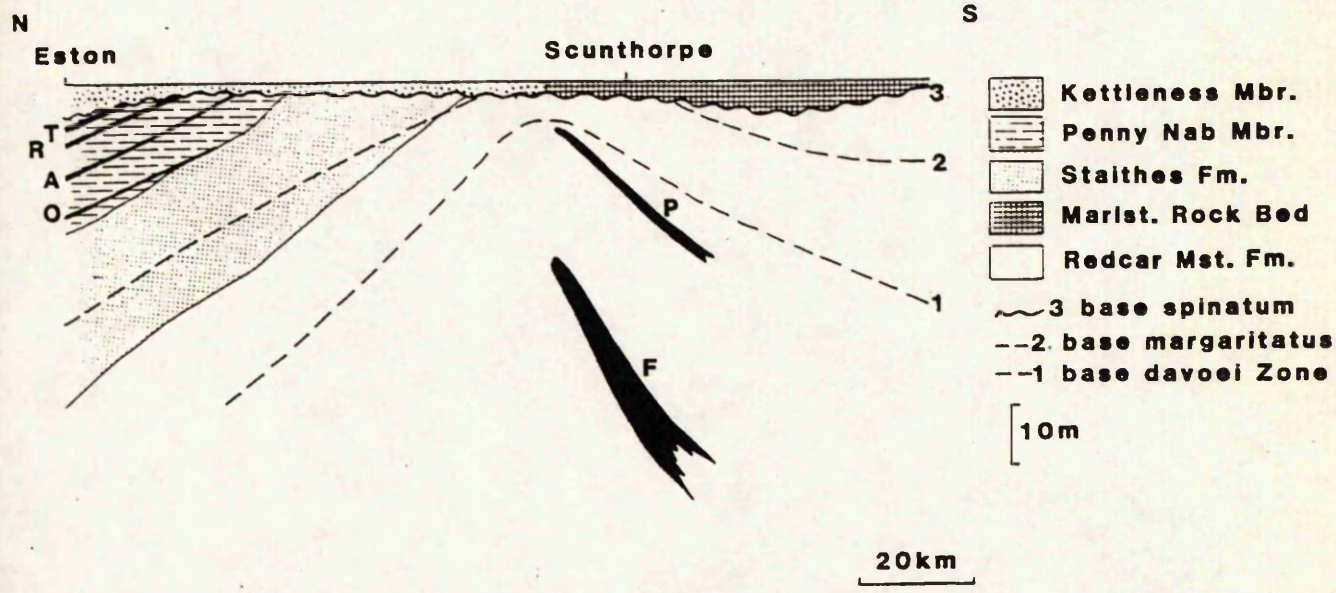

Figure 14. Section across the Cleveland Basin and Market Weighton Axis (After HOWARD 1985) showing the relationship of the Early Jurassic ironstones of the eastern UK to the structure.

Cortical layering reflects varying proportions of goethite and berthierine, and possibly differing porosity (HUGHES 1989). Ooids with dominantly berthierine cortices are rare, only being found in lithologies with a high mud content. They are usually strongly deformed (spastoliths). High sphericity examples are only found where there was an early carbonate cement, or edge replacement by siderite.

Larger concentrically zoned pisoids of goethite or berthierine also occur, usually in discrete laminae or beds. The cortical sheaths of these larger bodies is less distinct than in the ooids and is often wavy. A biogenic origin is favoured for these pisoids.

Bioclasts are often well preserved (calcitic shells), but aragonitic shells, and some calcitic ones, are replaced in the bioclastic ironstones. In the muddier lithologies aragonitic shells may be entirely removed, with compaction giving rise to compound moulds.

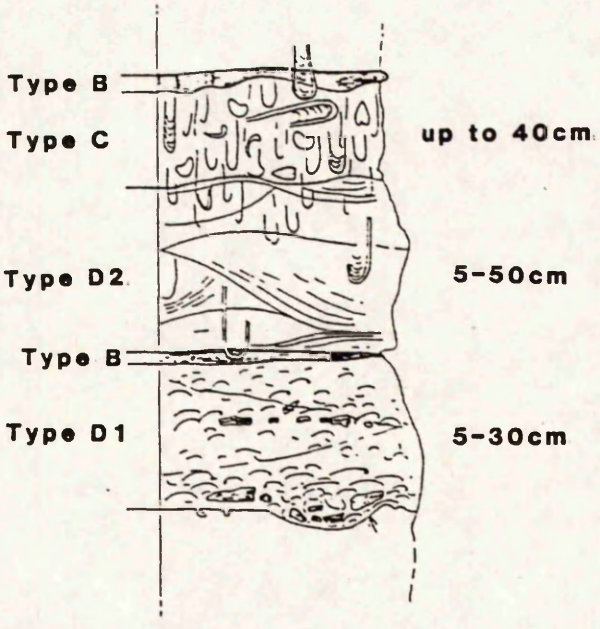

Figure 15. Log of an idealised pseudocycle from the Frodingham Ironstone.

v. Palaeoecology

The faunas of the storm-produced layers of the Frodingham Ironstone have suffered considerable taphonomic distortion. The alteration of the original spatial and temporal ecological patterns was the result of biostratinomic processes which were largely storm-controlled. All skeletal remains have suffered *in-situ* reworking, repeated within-habitat *post-mortem* lateral transport and diagenetic distortion.

The observed biofabric types result from storm-events or fair-weather episodes of reworking over long periods of time. The species recovered from the storm-produced units are essentially the same as those preserved in the interstratified fair-weather deposits. Relative abundances have been altered, often drastically, and in many cases species occurrences are "obscured".

Within an ideal pseudocycle biotic change involves an upward increase in diversity and differential changes in abundance and packing. There is always an upward increase in the density (area, or spatial distribution of living populations) and superimposition of burrows. This indicates decreasing turbidity and water content of the substrate. Within any well-preserved pseudocycle (one relatively unaffected by episodes of reworking), there is an upward decrease in grain (particle) size, with a concomitant upward increase in mud, silt and organic content.

a) Background ("fair-weather") sediments - Type C ironstones

These fossil-rich units have biofabrics which show the interplay between physical processes and biological responses. The Type C ironstones possess a biologically dominated fabric and represent the closest approximation of a preserved host substrate. Freshly deposited sediment was finely cross-laminated mud and ooids. In most cases, however, all traces of these structures has been lost through intense figurative bioturbation.

A large percentage of the observed preserved body fossil fauna consists of benthonic elements. Bivalves dominate overall, but are usurped by brachiopods at certain levels. Forty-two bivalve species have been positively identified (PARSONS unpub. studies). Most morphological groups of bivalves are represented:

- low activity medium and deep burrowers
- vagile shallow burrowers
- semi-infaunal nestlers - byssally attached
- semi-infaunal sedentary forms - byssally

attached
- epifaunal recliners (free living)
- epifaunal cemented and byssally attached forms
- free swimming/living forms

The ecological spectrum within the background sediments does not necessarily indicate very shallow water, but rather, quiet conditions combined with very low rates of sedimentation.

Low activity, medium to deep infaunal bivalves: The following are most frequently preserved in life orientation: *Pholadomya* cf. *ambigua*, *P.* cf. *corrugata*, *Pleuromya* cf. *oxynoti*, *P.* cf. *striatula*, possibly *P.* cf. *glabra*, *Arcomya* cf. *vetusa* and *Gresslya* sp. All are thought to have been incapable of reburrowing after exposure by scour and are generally regarded as slow burrowers unable to respond quickly enough to survive anastrophic burial or deep scour. They are all considered to have been low-level suspension feeders.

Low activity, shallow infaunal bivalves: *Ryderia* cf. *renevieri* or *R.* cf. *textura* (poor preservation precludes identification).

Ryderia was a low activity, shallow infaunal, sedentary form: a non-siphonate, low-level suspension feeder and/or deposit feeder. All extant nuculoids are known to ingest mud as part of their diet using their palp proboscides. In *Ryderia* a long rostrum has been substituted for the siphonal tubes, and this would suggest mainly suspension feeding, but minor deposit feeding cannot be ruled out. Some non-rostrate forms extant forms posses a fairly large foot by which means rapid locomotion is presumed possible. The general morphology of *Ryderia*, however, suggests minimal locomotory capability.

Vagile (active) medium to shallow infaunal bivalves: These include: *Astarte* cf. *obsoleta*, *Hettangia* cf. *ferrea*, *Cardinia gigantea*, *C. crassiuscula*, *C. concinna*, *C. hybrida*, *C. listeri*, and *Mactromya cardioides*.

Astarte is more commonly found in the Type D_2 ironstones where it is preserved preferentially. It had short siphons and was a shallow fairly active vagile burrower. Fossil forms are considered similar to extant species as low-level suspension feeders. As shallow burrowers they were easily exposed by storm scour and presumably killed by exposure and transport within the bed load.

Hettangia also is commonly found in D_2 ironstones. Although the morphological features of the shell are contradictory, this genus was probably a vagile intermediate depth burrower. It is considered to have been a low-level siphonate suspension feeder. Possession of a fairly strong hinge, and overall morphology suggest that rapid movement was possible.

Five species of *Cardinia* are found in abundance at all levels in the ironstone. They would have occupied different niches and common occurrence in Type D_2 ironstones suggests that they were among the few species suited to a shifting substrate. They are considered to be shallow, vagile burrowers and low-level non-siphonate suspension feeders. All species could easily reburrow after exposure by scour and were probably killed by factors resulting from transport within the bed load.

Mactromya is considered to have been a shallow to medium depth vagile burrower. Although a low-level suspension feeder it is doubted whether true siphons were present. More likely it constructed mucous-lined tubes by a puncturing action of its foot. It has occasionally been found preserved in background sediments, but rarely occurs in Type D ironstones, as it did not usually withstand reworking.

Semi-infaunal nestlers (byssally attached) and semi-infaunal sedentary byssally attached bivalves: These include *Modiolus hillanus*, *M.* cf. *scalprum*, *Hippopodium ponderosum*, *H. ferri* and *Pinna folium*.

Modiolus hillanus is considered to have been either epifaunal and byssally attached or semi-infaunal and either byssally attached or free living. Epifaunal forms would have colonised dead-shell substrates (micro-hardgrounds), but no life-orientation specimens have been recovered.

Modiolus cf. *scalprum* was byssally attached and semi-infaunal. Some authorities consider it infaunal and possibly even a shallow burrower. It occurs only in the top few metres of the ironstone in Type C lithologies, often in life orientation. Both of these species of *Modiolus* would have been low-level suspension feeders.

Hippopodium was probably a semi-infaunal, byssally attached genus, sedentary throughout life. It possesses a well defined pallial sinus and, therefore, probably had large powerful siphons. It is doubtful whether *Hippopodium* ever moved after its larval stage except to reposition its byssus. The species here were low-level suspension feeders. *H. ponderosum* has been recovered in life orientation from Type C ironstones.

Epifaunal reclining (free living) bivalves: These include *Oxytoma inequivalvis*, *Meleagrinella papyria* and three species of the oyster *Gryphaea*.

Oxytoma inequivalvis is a good example of an epifaunal, free-living, low level suspension feeder. Seilacher (1984) has described this form-type an "outriggered recliner". *Oxytoma* was byssally attached during its early stages of growth. Some authorities believe that the ability to use its byssus was retained in the adult, others consider it became

redundant and that the animal was free-living. It is possible that a byssus was employed depending on environmental conditions.

Meleagrinella papyria is a form-type of similar life position and trophic level to *Oxytoma*. Both genera are believed to have inhabited stable Type C substrates. Generally they are degraded out of highly reworked levels and would not have survived repeated lateral transport.

The oyster *Gryphaea* occurs extensively throughout the ironstone. Although attached during early life, the adult was a free-living, low-level suspension feeder, ideally adapted for life on Type C substrates. Three species are reported to occur (*Gryphaea (G.) arcuata incurva, G. (G.) mccullochii mccullochii* and *G. (G.) mccullochii arcuatiform*. Their calcite construction and robust nature enabled them to survive repeated reworking. Together with *Cardinia* spp. they are the commonest faunal element and by far the most easily observed.

Epifaunal cemented and byssally attached bivalves: Cemented forms such as *Placunopsis* cf. *alpina*, *Plicatula* cf. *spinosa*, *Liostrea hissingeri*, *Ctenostreon tuberculatum* and *Terquemia arietis* can be found encrusting the surfaces of most other fossil types. They were all epifaunal low-level suspension feeders. Some forms were important as opportunistic pioneers, re-colonising after storm events. However, they are known from all ironstone types. Their populations developed primarily on the exposed dead-shell component of Type C substrates during prolonged periods of stability.

Epifaunal byssally attached forms are common to abundant and include: *Plagiostoma gigantea*, *Antiquilima succincta, Camptonectes lohbergensis, Chlamys* cf. *textoria* and *C. subulata*.

Plagiostoma was probably attached by a byssus. *Antiquilima* certainly had a byssus as an adult. Both *Chlamys* and *Camptonectes* were byssally attached. Modern forms rely on byssal attachment into adult life, but are known to sever this attachment to partake in locomotion during times of stress: a very useful strategy for survival. In living populations their numbers would be limited to the availability of suitable sites for attachment. All were non-siphonate, low-level suspension feeders.

Free living or swimming epifaunal bivalves: These forms are abundant in the ironstone and include *Pseudopecten priscus*, possibly *P. aequivalvis*, *Entolium lunare* and *E. hehli*.

Extant *Pseudopecten* favour a shell-rich substrate with little mud; they also nestle slightly. *Entolium* is very abundant and has long been recognised as a typical bivalve form-type for ooidal substrates. Its lack of a byssal notch at the adult stage means a change to a free-living and swimming mode of life. This form-type was, therefore, ideally adapted for life in the ironstone environment. *Entolium* and *Pseudopecten* were non-siphonate, probably low-level suspension feeders.

No epifaunal species have been found in life orientation. However, more articulated specimens occur in Type C substrates than were observed in Type D. The disarticulated valve-pairs of epifaunal and semi-infaunal bivalves frequently occur next to one another. This signifies rapid burial with little or no *post-mortem* disturbance prior to internment. Such valve pairs have not been observed in Type D ironstones.

b) Tempestite sediments - Types D_1 and D_2 ironstones

The storm sediments have an extensively modified sedimentary fabric. Taphonomic studies suggest that the ironstone faunal assemblages have suffered *in-situ* reworking and within-habitat transport, forming parautochthonous coquinas. Physically induced losses have produced assemblages of lower diversity. The bivalves exhibit low articulation ratios and their skeletons show all stages of fragmentation. Most storm-produced layers exhibit a dominant convex-up orientation of valves.

The wide-scale production of coquinas at the base of each tempestite sequence has generated "reference horizons" (AIGNER 1982). These are typified by the so-called "*Cardinia* beds", composed principally of *Cardinia* spp., entoliform and *Pecten* group bivalves. They are indicative of storm concentration combined with lateral transport and re-suspension of "fines". Although generally a multiple event product and therefore diachronous, they prove very useful for local correlation where developed on a deeply scoured extensive surface.

No medium to deep burrowing bivalves have been observed within Type D ironstones, with the exception of the bivalve *Goniomya* which occurs in Type D_2 substrates. Recorded specimens are extremely rare: none has been found in life orientation. It is the only mya present uniquely adapted as a vagile burrower of shallow to medium depth. *Goniomya* was a low level, siphonate suspension feeder, capable of reburrowing after exposure by scour and surviving limited anastrophic burial.

The presence of a highly active ichnofauna, principally *Diplocraterion*, together with the sedimentary structures in the upper part of the D_2 ironstones, suggests that the substrate was too unstable for many burrowers.

Palaeosynecological deductions concerning the ironstone biotic association are possible only by detailed analysis of Type C biofabrics, together with analysis of the contacts between all ironstone types and overlying Type B mudstone drapes. This approach has enabled the recognition of the following stages

of palaeoecological development:

a. Production of a basal scour surface, or scoured re-exposure of such a surface, without storm sediment deposition: surface probably available for short-term colonisation by epifaunal suspension feeders (opportunistic pioneers).

b. Production or re-exposure of a surface plated with a closely-packed shell armour without storm sediment deposition: surface probably available for short period colonisation by epifaunal suspension feeders - free-living, byssally attached forms and high numbers of cemented encrusters (opportunistic pioneers).

On wave or current swept shell grounds (giving an extended colonisation period) forms such as *Placunopsis, Plagiostoma* and *Antiquilima* may have been more numerous.

c. Production, re-exposure and/or addition to a Type O1 substrate, followed by rapid deposition of ooidal fines: production of a loose, unconsolidated Type O2 ooid sand substrate. Substrate available for vagile (active) shallow infaunal and free-living, epifaunal suspension feeding bivalves.

Subsequent physical modification (cross-bedding) continually interfered with ecological spatial relationships, maintaining a low degree of association development. The shifting ooidal facies was dominated by epifaunal, free-living *Entolium* and rapid response, shallow burrowing *Cardinia*. The *Cardinia* were well adapted to life within such a substrate and probably occurred in large populations. Deposit feeders are lacking because the substrate was unattractive as a food-source.

d. Stabilisation of the ooid sands as a result of biological action and/or lessening physical control led to a firmer substrate: frequency of preserved bioturbation structures increases. This is the best possible indication of the development of a firm ground and explains the marked contact between Type O2 and the overlying Type C sediments.

Once the critical point of substrate stability has been reached, wave action is insufficient under normal circumstances to maintain a well-washed, shifting oolite. Consequently, ooids and mud accumulate together and exhibit fine scale cross lamination. Where the sedimentation continued for long periods of time, unhindered by physical events, Type C sediments accumulated. It is possible that the ooids grew largely in this sort of substrate.

e. The upper few centimetres of background sediments were probably rather soft due to high pore fluid content. Lower down however an excellent firmground developed. Syn-sedimentary cementation does not appear to have taken place, possibly because of the intensive bioturbation. True hardgrounds never developed, even through scour re-exposure.

Ecologically, the formation of firmgrounds was important as they permitted an increases in faunal diversity. However, only with the net incorporation of a mud/silt fraction did diversity alter markedly. For this reason the mya group in particular could not colonise until muddy firmgrounds became established. An exception, however, appears to be *Goniomya*, which was presumably adapted for life in more unstable substrates.

The biotic association of the deposit was dominated by suspension feeders, suggesting an active physical environment. Presumably direct sediment feeding, if it occurred, only prevailed where a nutrient-enriched mud substrate became established and the sere attained its climax. Local turbulence or larger scale catastrophic events would prevent build up of such a substrate and/or eradicate any deposit feeding component. *Ryderia* was a fragile form of rare occurrence: it did not survive the rigours of biostratinomic degradation. *Ryderia* has not been found outside the Type C ironstone and is one of the rarest bivalves from the Frodingham ironstone.

The occurrence together of abundant myas in life orientation and *Diplocraterion* shows that fair-weather sedimentation within this storm-generated sequence represents net accumulation over a very long period. However, the predominance of protrusive spreiten bears witness to the extensive fine scale negative sedimentation that has also occurred. The internal moulds of myas are commonly truncated by surfaces of scouring, giving clear evidence for scour of at least 60cm.

Appreciation of biotic association complexity and successional development can only be obtained by studying Type C ironstones: it is here that the most diverse biological elements of the shoal and their relationships are preserved. The level of sere climax attained is that represented by maximum niche use and diversity.

The following trace fossils have been recorded from the type C ironstones: *Chondrites* spp. (possibly two types), *Rhizocorallium jenense, Diplocraterion parallelum, Thalassinoides* sp., large straight burrows indet., *Planolites* sp., *Kulindrichnus* sp. (two types), large borings (seen particularly in *Cardinia* and *Gryphaea* shells), sponge borings, *Zapfella* (acrothoracian barnacle borings).

vi. Diagenesis

The diagenetic history of the Frodingham Ironstone is very complex, because of the prolonged history of reworking. The depositional events following the storm-induced scouring produced graded

beds, with good sorting. The coarser parts of these beds are the bioclastic type O ironstones. These are generally well sorted, and consequently of high porosity and permeability; a complex succession of cement phases was generated in these lithologies. Berthierine occurs abundantly as the initial isopachous pore lining cement, and in the replacement of many bioclasts. It also occurs in ooids, but these are largely altered to goethite (or goethite/berthierine mixtures). The berthierine composition varies little from:

$(Ca_{0.5}Na_{0.10}K_{0.01})_{0.16}(Fe_{3.69}Mn_{0.01}Mg_{1.00}Al_{1.01})_{5.71}(Si_{3.37}Al_{0.63})_4O_{10}(OH)_8$

Siderite occurs, particularly where berthierine is abundant, as a replacement of berthierine and as an early cement. It is always calcian, manganoan and magnesian (up to 14% $CaCO_3$, 8% $MnCO_3$ and 20% $MgCO_3$). The siderite generally predates the last phase of ferroan calcite cementation. Ferroan calcite is the most abundant carbonate cement. It is typically 1-4% $FeCO_3$+$MnCO_3$, and may occur as more than one generation. Highly manganoan (up to 27% $MnCO_3$) calcites have also been recorded replacing berthierine. Calcites have $\delta^{13}C_{PDB}$ from -3.26 to -22.1‰ consistent with mixing of marine and organically derived HCO_3^- in meteoric waters. $\delta^{18}O_{PDB}$ values of -6.0 to -9.43‰ are more problematical, suggesting a possible late meteoric influence.

The fines from the storm events are believed to have formed the type B ironstones. These are formed from reworked berthierine flakes, presumably the product of earlier diagenetic activity. These mud drapes seem to become lithified very quickly for they are often seen as angular rip-up clasts in subsequent storm deposits.

The muddier type C ironstones are interpreted as forming the "fair-weather" background sediment. They are clearly greatly influenced by small scale reworking and winnowing events. Biological mixing of the sediments means that "fair-weather" depositional fabrics are rarely, if ever, preserved. It is within the Type C ironstones that evidence for the nature of the early diagenetic processes generating the berthierine and the ooids should be sought.

In type C ironstones the early dissolution of aragonitic bioclasts was commonly not accompanied by calcite precipitation. Bioclasts are often compacted forming compound moulds. Most life-position *Pholadomya* are preserved as moulds. Ammonites are often similarly preserved, and if buried at an angle to bedding they are compacted to elliptical outlines.

Sulphides are common only in the muddier sediments where pyrite is the dominant phase. In the "Snap Band" pyrite is abundant, often occurring together with ferroan calcites in the replacements of bivalve shells. The increased role of sulphate reduction in the diagenesis of the Snap Band is interpreted as a short period of higher sedimentation rate, which allowed sufficient organic matter to be buried below the oxic zone.

vii. Model for sedimentation

The intense and prolonged reworking of the sediments of the Frodingham Ironstone is remarkable. The age span of the ironstone of 2-4Ma implies maintenance of these conditions over a time span much greater than that involved in the generation of most of the Liassic ironstones. The role of relative sea level change in the formation of the ironstone is unclear, but would not, therefore, appear to have been major. Fluctuations in the sedimentation rate suggested by the "Snap Band" indicate that what appears to have been a relatively minor change could allow sulphidic diagenesis to start. This serves to emphasis the remarkable stability of the environment during the remainder of the time of deposition of the formation.

The environment of deposition of the ironstone was a submerged part of the Market Weighton high. Previous models (KNOX & FLETCHER unpublished fieldguide, Phanerozoic Ironstones Symposium, Sheffield, 1987) invoking a lagoonal origin for the ferruginous allochems of the Frodingham Ironstone Formation seems unnecessary, given the widespread development of berthierine as an early diagenetic cement in the ironstone. The model of Hallam (1975) proposing development of the ironstone on a submerged shoal isolated from any sediment supply seems quite adequate. The supply of iron to the system is envisaged as being in colloidal material or clay minerals, or material adsorped onto clay minerals which are subsequently degraded during prolonged oxic/post-oxic diagenesis. The ironstone accumulated very slowly and the rate of iron incorporation into the sediment is less than half that of the lateral equivalent clastic mudrock facies.

viii. Origin of the Ooidal Ironstones

Direct evidence for the origin of the ferruginous allochems of the Frodingham ironstone is difficult to find because of their prolonged reworking history. The nuclei of the ooids might be expected to provide evidence for the site of ooid generation, but significant amounts of goethite particles are not encountered in the sediment except as ooid nuclei. The ooids might therefore be interpreted as being allochthonous, or it is possible that broken ooids and other goethite grains **usually** became further coated.

The large pore spaces of the coquinoid beds, and the secondary porosity formed through dissolution of aragonitic bioclasts, allowed the generation of

significant volumes of cements. These allow the examination of berthierine cements, which are commonly not preserved, or not easily seen, in the muddier ironstones. There is no doubt that large volumes of berthierine were generated in these settings during very early diagenesis. It seems highly likely therefore that the berthierine ooids were also generated under similar diagenetic conditions. It would appear erroneous therefore to demand any more "special" or unusual environment for the genesis of the ooids.

Once berthierine had been generated in the sediment it could quickly be leached to goethite under oxidising conditions. The ooids in the sediment are generally strongly goethitic, reflecting more or less complete penecontemporaneous oxidation and leaching. Similar oxidation is also seen as oxidised halos around burrows. The preferential preservation of berthierine in the cements rather than the ooids reflects the fact that the cement has not been reworked and reoxidised.

ix. Fieldguide

Locality 3: Scunthorpe, Yarborough Pit

This pit was the last to be worked, and consequently retains some relatively fresh faces. The pit is currently being clay-lined for use for waste disposal.

The lowest part of the ironstone is not easily examined here, although it has been visible occasionally in drainage sumps. This part of the ironstone was left *in-situ* to provide a firm base for the movement of heavy plant. The overburden was removed by dragline. The ironstone was quarried along a long face, with the pit being filled in continuously behind with the overburden and slag from the steel making process.

The lower part of the worked face consists of pseudocycles with a dominance of the basal cross-bedded bioclastic lag deposits (Type D_1).

The middle part of the face is dominated by Type D_2 ironstones.

The upper part of the face is dominated by the Type C ironstones. These often show very clearly the succession of biological activity. Contacts between units are usually scoured, and examples of *Pholadomya* in life position truncated by the scour surfaces can be seen.

Towards the top of the face the "Snap Band" forms an obvious, darker, horizon.

The top of the ironstone can not easily be seen here, because the scraped top is used as a platform for the draglines.

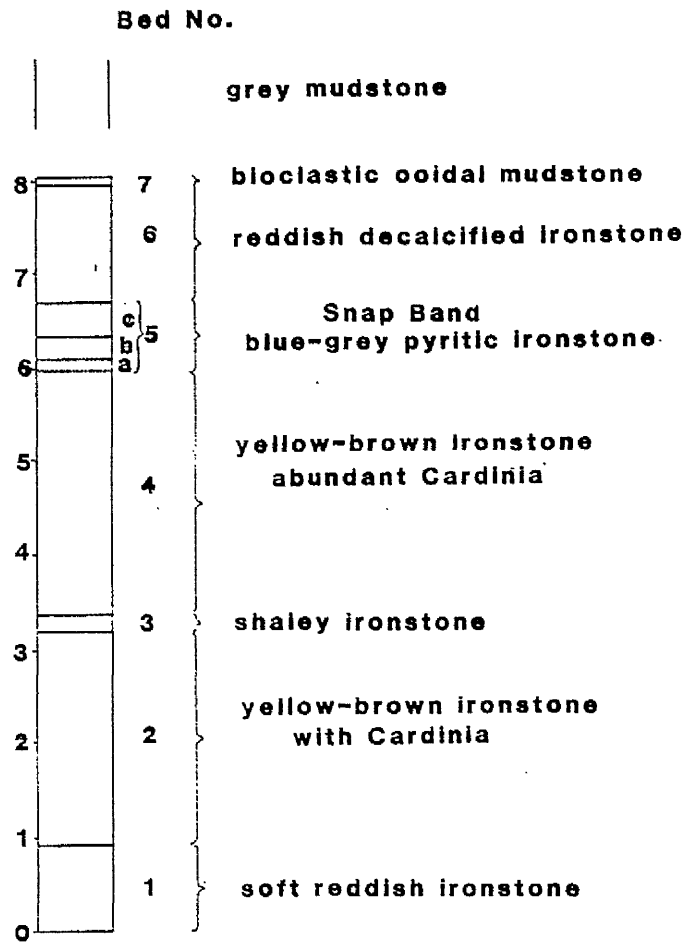

Figure 16. Log of the Frodingham Ironstone as seen in Yarborough Pit.

The Ordovician Ironstones of North Wales

T.P. Young

i. Background

Ooidal ironstones have long been an object of study in the northern part of the Welsh Basin. They have been exploited at various times in the past, particularly between about 1840 and 1920. The deposits are typically rather small, tectonically complicated, geographically isolated and often yield a very hard ore. These factors combined to make the industry very marginal, and only a handful of quarries (including Llandegai, Betws Garmon and Hendy-Capel) were exploited to any significant degree.

ii. Stratigraphic Overview

The Ordovician ooidal ironstones of the Welsh Basin occur at three main stratigraphic horizons. These correspond to major transgressions. The earliest of these horizons is the basal Arenig transgression. This major transgression marks a drastic change in the palaeogeography of the Welsh Basin, and the onset of the deposition of the second of the supergroups of the basin infill, the Gwynedd Supergroup (WOODCOCK 1990). The localities recognised as containing ooidal ironstones within the transgressive deposits are restricted to the western Llŷn at present. In this area the transgression is of Moridunian age (BECKLY 1988; GIBBONS & MCCARROLL in press). The lateral extent of ironstone development is not known. Ironstones of this age will not be visited during this excursion.

The second major phase of ironstone formation occurs in the early Llanvirn or latest Arenig. The Llanvirn-Arenig boundary has been interpreted as a time of major sea-level rise (FORTEY 1984; YOUNG 1989b). This period also saw a phase of extensional tectonics in the Welsh Basin. In many areas there are debris-flow deposits of late Arenig age (BECKLY 1987) deposited in front of active fault scarps. The presence of large amounts of "basement" material in the debris-flows in western Llŷn and Anglesey shows that considerable vertical displacements of the extensional faults were involved. The rapid deepening of some parts of the basin during this event does not appear to have produced ironstones (although sufficiently fine-scale biostratigraphic control does not exist in many areas), but the subsequent eustatic event produced ironstones over a wide area. Indeed ooidal ironstones were deposited during the transgression over most of the Gondwanan shelf in the region (Morocco, Algeria, Spain, Portugal, France, Germany, Czechoslovakia as well as the northern Welsh Basin: YOUNG 1989b).

The synsedimentary faulting did affect the nature of the ironstones produced. In many regions the ironstones are largely themselves debris-flows and the associated volcanicity led to the development of manganese rich ironstones at some localities.

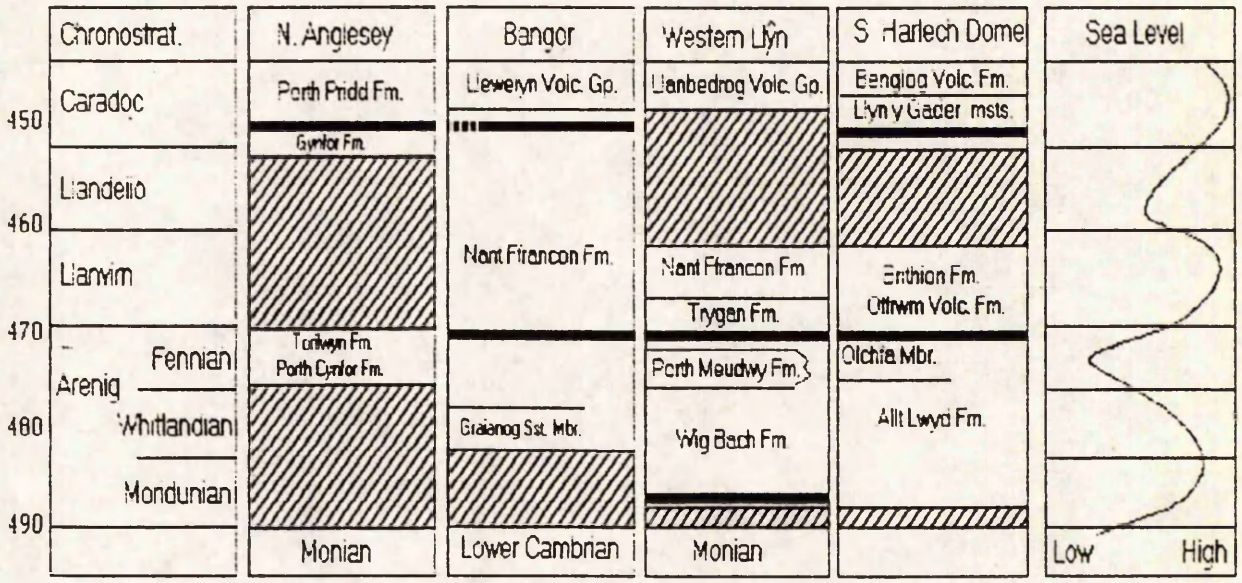

Figure 17. Simplified lithostratigraphy of areas within the northern part of the Welsh Basin. Solid lines represent ooidal ironstone horizons. N. Anglesey after Bates (1972), Bangor after Howells *et al* 1983, Llŷn after Gibbons and McCarroll (in press) and pers. obs., Harlech Dome modified after BGS (1982), sea level after Fortey (1984), dates after McKerrow (1988).

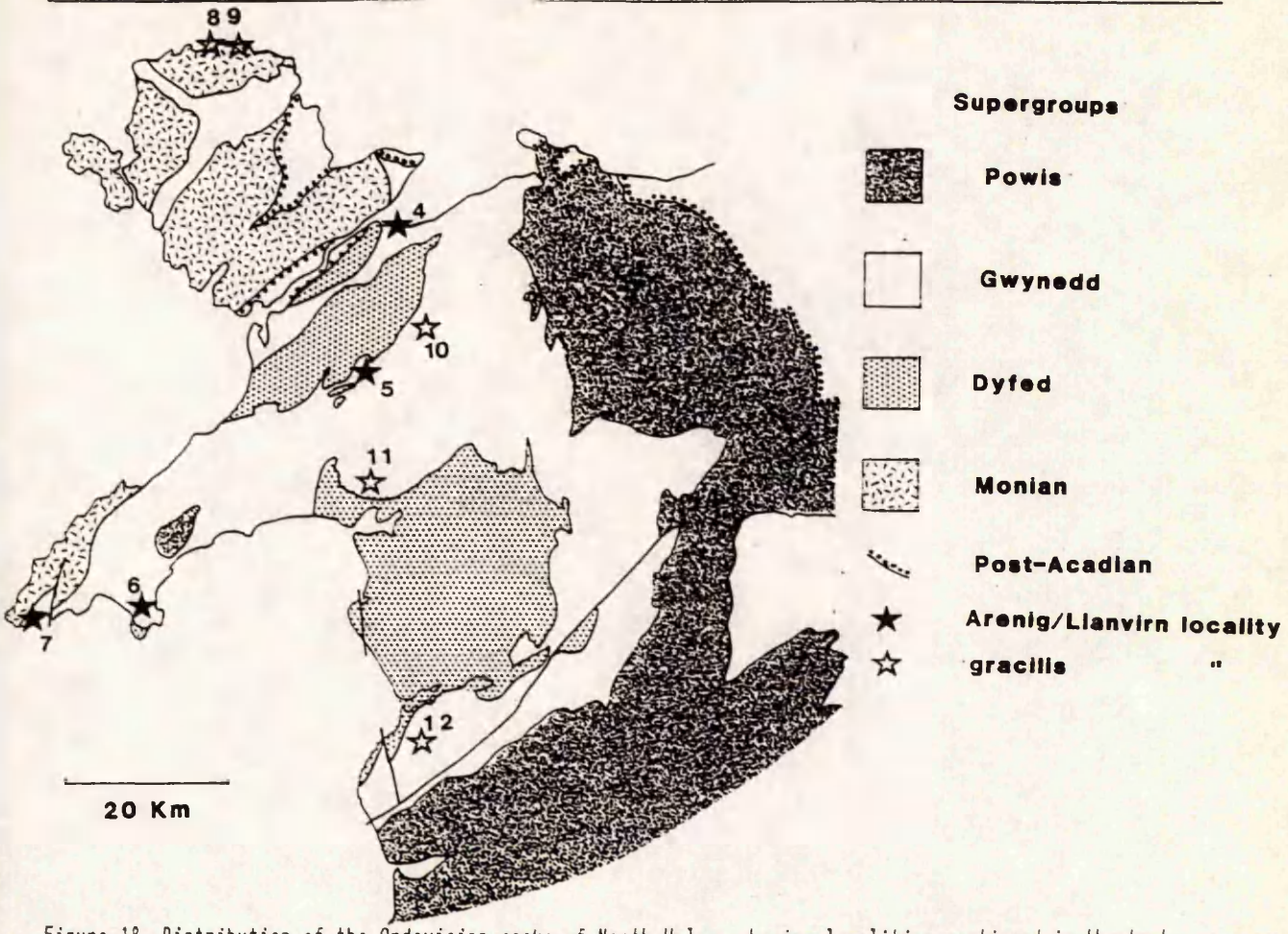

Figure 18. Distribution of the Ordovician rocks of North Wales, showing localities mentioned in the text.

The deposits close to the Arenig/Llanvirn boundary around the Harlech Dome, the Olchfa Member of the Allt Lŵyd Formation, often contain ooidal ironstones. These ironstones have been described recently as being of Fennian age (TRAYNOR 1990), although the biostratigraphic control is poor and Beckly (1987) placed the ironstones on, or close to, the Arenig/Llanvirn boundary.

The third ironstone-producing event was the transgression during the *Nemagraptus gracilis* Biozone. This event produced the Penterfyn Ironstone Formation in N. Anglesey, the Fferam-uchaf Ironstone in central Anglesey, an ironstone near the top of the Nant Ffrancon Formation in N. Snowdonia and the Tremadoc Ironstone south of Snowdonia. The age of the "Crossed Foxes" ironstone in the Cadair Idris area and similar ironstones near Arenig has not been revised, although studies by the BGS are currently in progress in the region. A *Glyptograptus teretiusculus* Biozone age was ascribed to these ironstones by Cox (1925), but the validity of this age must await the new research; a *gracilis* Biozone age for these too does not seem unlikely. The younger age for this ironstone is indicated in figure 17.

The age of the *gracilis* Biozone ironstone in terms of the international series and stages remains uncertain, and indeed it is not certain that all the occurrences in North Wales are contemporaneous. In the Llanbabo Formation of central Anglesey the Fferam-uchaf ironstone is overlain by the Fferam shales with a *gracilis* Biozone graptolite fauna, 18m thick (BATES 1972). These shales are overlain by the Llanbabo Church grits which yield a Costonian (earliest Caradoc) shelly fauna (BATES 1972) and a graptolite fauna "high up in the zone of *Nem. gracilis*" (ELLES, *in* GREENLY 1919). In central Anglesey the Fferam-uchaf ironstone could therefore be of earliest Caradoc or Llandeilo age. In Snowdonia the ironstone lies upon a thick Llanvirn-?Llandeilo mudstone sequence (the bulk of the Nant Ffrancon Formation) and is overlain by beds yielding faunas as old as Harnagian. The study of the microflora of the ironstone at Tremadoc suggested (TRYTHALL *et al.* 1987) that it was not earlier than Caradoc, and the ironstone is overlain by a shale with a graptolite fauna of *gracilis* Biozone, or just possibly younger, age.

iii. Sedimentology

a. The Arenig/Llanvirn boundary ironstone: The ironstone close to the Arenig/Llanvirn boundary is very variable in its sedimentary facies. On the south side of the Harlech Dome the ironstone is generally very thin (less than a metre). Here it may represent a considerable condensed sequence, or may rest on a

disconformity since the thin Olchfa Member containing the ironstone is of Fennian age, but lies on Moridunian strata (TRAYNOR 1990). However, it is not yet clear whether the time gap is at the horizon of the ironstone, or at the base of the Olchfa Member.

On the north-east of the Harlech Dome at Nant yr Olchfa itself the ironstone is interbedded with graptolitic clastic siltstones, and the ironstone may be reworked.

On the Llŷn, the ironstone is seen apparently *in-situ* to the SW of Aberdaron (Porth Meudwy, see below). At this locality it is very thin and lies gradationally on some organic-rich siltstones. Farther east on the Llŷn the ironstones are largely reworked. On the St. Tudwal's Peninsula (Pen y gaer and Hen dy Capel) the ironstone is largely formed of debris flows. The ironstone is mixed with clastic material, including some reworked volcanic material. At Sarn Meillteryn the "Trygarn Formation" (the "Trygarn Formation" is the unpublished provisional name for the lower Llanvirn strata of the Sarn area; field mapping in progress) overlies a thin ironstone horizon, but itself includes numerous beds (?turbidites or debris flows) with reworked ironstone material. Only 2km south of the outcrop of the ironstone at the base of the formation, the same horizon has been penetrated by a borehole and 3m of well-sorted grain-ironstone seen (BROWN & EVANS 1989).

Localities in the northern part of Llŷn are highly tectonised (e.g. Trevor; TRYTHALL *et al.* 1987), but may be *in-situ* deposits.

Farther east on the northern side of Snowdonia there are some thick developments of ironstones at this horizon, but the sedimentology of the deposits has not been studied. Trythall (1989a) described the ironstone at Betws Garmon as including well sorted ooidal pack-ironstones. This may indicate that the thick lenses of ironstones represent reworked ooid shoals.

In the Menai Straits area at Bangor the ironstone is represented by reworked ferruginous and phosphatic material within the transgressive sequence (BECKLY 1985).

b. The *Nemagraptus gracilis* Biozone ironstone: The sedimentology of the ironstones of this age is even more poorly known than the earlier ironstones.

On the southern side of the Harlech Dome the ironstones attributed to this age (Ffordd Ddu, Crossed Foxes) is clearly bedded. The beds are alternations of allochem-rich and allochem-poor lithologies. There does not appear to be evidence for extensive reworking, but at some localities in the area Trythall (1989a) reported up to 7m of ooidal pack-ironstone. This suggests that there may have been some reworking into shoals, as tentatively suggested for the earlier ironstones in Snowdonia.

The Tremadoc locality has been the subject of much debate on the role of soft-sediment deformation (TRYTHALL 1989a; SMITH 1987). The ironstone sediment does not show significant evidence for being other than an *in-situ* deposit, but the sedimentology is difficult to interpret in such a highly deformed locality.

Similarly the ironstones of this age in northern Snowdonia may well be *in-situ*. They are thin, appear not to be well bedded and do not contain significant intraclastic material.

On Anglesey the ironstones are rather variable, but are generally closely associated with sandstones and appear to have been current reworked, with consequent admixing of clastic material.

iv. Ironstone Petrology

Recent studies of the petrology of the North Wales ironstones are largely unpublished (TRYTHALL 1989b). Older accounts include the study by Pulfrey (1933b) and Weinberg (1973).

The ironstones are mainly very similar to the Jurassic examples described above, but there are significant differences. The first of these is that there is little or no calcareous bioclastic material in the ironstones. Bioclasts are restricted to sponge spicules, inarticulate brachiopods and other phosphatic material. The lack of bioclastic material may be partly responsible for the lack of extensive carbonate cements in many of the ironstones. A second major difference is the range of grainsize in the allochems of the unsorted examples. Although ironstones do exist with small ooids as the dominant allochems (as in the Jurassic examples) it is more normal to see a range of grain size.

The ironstone at Porth Meudwy (YOUNG *in* GIBBONS & MCCARROLL in press) is believed to have had little reworking, and represents a typical ironstone from N. Wales. The ooids in this ironstone are generally about 400µm diameter, but may be as much as 1000µm. There are also larger coated intraclasts of up to 6mm diameter, which are probably oncoids. Other exposures in the same area have phosphatic oncoids several centimetres in diameter.

These phosphatic oncoids were previously known as *Bolopora undosa* (LEWIS 1926; HOFMANN 1975) and were once thought to be bryozoans. These structures are a common feature of condensed or transgressive deposits in the Ordovician of the Welsh Basin. They are seen in the Arenig/Llanvirn and *gracilis* Biozone ironstones, as well as the transgressive lags at the base of the Arenig sequences. Probably identical structures have recently been described as grain coatings on pebbles in the basal Arenig deposits of the St. Tudwal's Peninsula (NIEDERMEYER & LANGBEIN 1989).

v. Palaeontology

The Ordovician ironstones of North Wales are remarkably poor in macrofauna. Several ironstone localities yield graptolites, but these are generally in interbedded clastic rocks rather than in primary ironstones. Inarticulate brachiopods are locally relatively abundant.

Two important biological agents to contribute to the ironstones are sponges and bacteria. Bacteria are interpreted to be the producers of the phosphatic oncoids described above (NIEDERMEYER & LANGBEIN 1989).

Sponge spicules occur frequently in the Ordovician ironstones (PULFREY 1933a), although they are not a particularly abundant part of the benthic fauna of the associated sediments. It is likely that this is a reflection of the firmer substrates associated with the condensed ironstone deposits.

The infauna of the ironstones is restricted. Small burrows are present in most of the ironstones, but the degree of biological reworking of the sediment is much less than the Jurassic ironstones.

vi. Diagenesis

Little detailed work on the diagenesis of the North Wales ironstones has been published. The low grade regional metamorphism of the region has affected the mineralogy and geochemistry of the sediments.

One aspect of the early diagenesis which is, however, particularly clearly visible is the widespread development of phosphatic concretions and cements. The pale-weathering phosphatic nodules are often prominent in the field, and preserve high sphericity ooids against compaction and cleavage.

Hughes (1989) has described the composition of the chlorite forming ooids from Betws Garmon and Tremadoc. The principal iron-bearing phase at these localities is chamosite. There are several localities which have their mineralogy dominated by the occurrence of magnetite. Stilpnomelane is another feature of the low-grade metamorphism of the sediments which can be clearly seen in the ironstones (PULFREY 1933b).

v. Fieldguide

The Arenig/Llanvirn boundary ironstone

Locality 4: Bangor Foreshore (SH 603731)

This locality has been described by Beckly (1985), but there is no published account of this important section.

Access to the section is from Port Penrhyn, Bangor, and entails a walk of approximately 1km eastwards along the foreshore. Care must be taken in visiting the locality at high tide, and the route must be expected to be extremely muddy.

The section is faulted, but an incomplete section across the Arenig-Llanvirn boundary exists. The section yields abundant fauna allowing good biostratigraphic control.

The locality lies just to the south of the Bangor Fault, one of the major fault lines of the Menai Straits region. In the past the palaeogeographic relationship of Anglesey with the N. Wales mainland has been much disputed, but current opinion is that the two regions are in more or less their Ordovician relative position (e.g. BECKLY 1989).

The lower part of the sequence exhibits 5cm thick bioturbated pale siltstone beds in a dark background sediment. These overlie gradationally the laminated siltstones of the bulk of the lower part of the Nant Ffrancon Formation. The coarser grained sediment packet yields a fauna (BECKLY 1985) of Fennian age. The details of the upward sequence from this unit are unclear, but across a small fault dark mudstones yield Llanvirn pendent didymograptids. These mudstones contain lenses of very coarse, basement-derived sandstone. This coarse clastic material becomes more prominent across a second small fault as approximately 80cm of coarse sandstone with phosphatic clasts and ferruginous ooids, overlying the mudstones.

The coarse sandstones are themselves overlain by further dark mudstones.

The contact between the transgressive dark mudstones and the underlying bioturbated bedded siltstones is seen 35cm below the lowest coarse sandstone lens, and is marked by pyrite concretions. A similar horizon of pyrite concretions lies in the upper part of the sequence seen at the west end of the outcrop; Beckly (1985) recorded a Fennian fauna with *Pseudoisograptus* from just above these concretions. It is not certain at present whether these two concretion horizons are the same.

The earliest transgression above the bioturbated siltstones is within the Fennian, and it is not known whether there is a discrete second transgressive surface below the dark mudstones with coarse sandstones of Llanvirn age.

Locality 5: Betws Garmon (SH 542578)

The old iron mines at Betws Garmon present an excellent section through a major ooidal ironstone deposit. Details of the mines and their exploitation are given by Cantrill and Sherlock (1922). The ore was worked as three separate concessions; Gareg-fawr, Ystrad and Tyddyn-bâch. Ystrad Mine extended from the

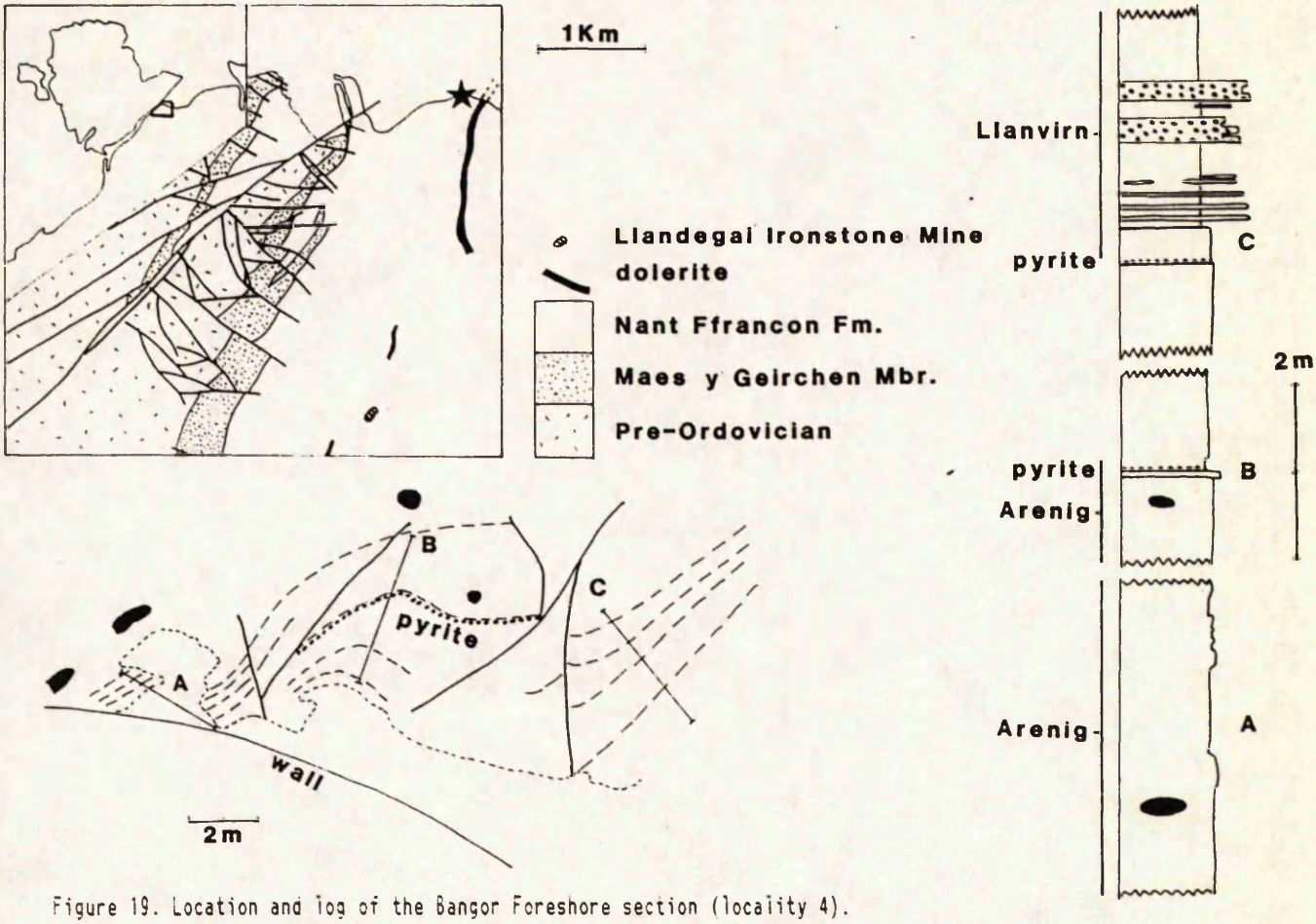

Figure 19. Location and log of the Bangor Foreshore section (locality 4).

main road (A4085) eastwards up the hill to the wall forming the parish boundary of Betws Garmon, beyond which was the concession of Gareg-fawr in the parish of Waunfawr. Tyddyn-bâch Mine lay to the west of the road.

The earliest workings were at Gareg-Fawr, and were in existence before 1841. The output from Ystrad was first recorded in 1911, shortly before the closure of Gareg-fawr in 1913. Ore was shipped from Ystrad via the adjacent narrow gauge railway, and in 1917 output reached 300 tons a week. The higher Gareg-fawr mine had its ore carried, at least in its later workings, by aerial ropeway some 4km across the mountain to the NE to Llanberis. Tyddyn-bâch was a short-lived mine worked towards the end of the First World War. Mining ceased in area during the 1920s. There were apparently earlier workings at Tyddyn-bâch for the Mining Journal dated 8th April 1854 offers a copper mine for sale there (reference quoted in FOSTER-SMITH undated).

The relationship of the ironstone to the enclosing sediments is only poorly known, and the stratigraphic attribution of the ironstone has been the subject of much debate. Cattermole and Jones (1970) placed the locality within the Cambrian, but remapping of the area demonstrated its Ordovician age, and position within the Nant Ffrancon Formation (HOWELLS *et al.* 1983).

There is little local biostratigraphic data, but the apparent position in the lower part of the Nant Ffrancon Formation would suggest an Arenig-early Llanvirn age. Trythall *et al.* (1987) described a microflora from this locality which they described as being similar to that from the Llandegai, Trefor and Pen y Gaer localities. They ascribed an early *gracilis* Biozone age to this microflora which appears to be incorrect (see Pen y Gaer below), and an early Llanvirn age for all these localities seems much more likely.

The ironstones of this locality have been described by Trythall *et al.* (1987) and Trythall (1989). The ironstone appears to lie at about 100-150m above the Graianog Sandstone Member at the base of Nant Ffrancon Formation. The description by Trythall and coworkers indicates that the ironstone has a laterally persistent lower division of oncoidal ooidal wacke-ironstones, overlain by an eastward thickening ooidal grain-ironstone. This grain-ironstone has ooids largely replaced by magnetite, and forms the exploited ore-body. The top of the ironstone appears to be relatively sharp, with an abrupt transition to the overlying fine-grained pyritic mudstones. At some localities a few oncoids can be seen in the base of these mudstones.

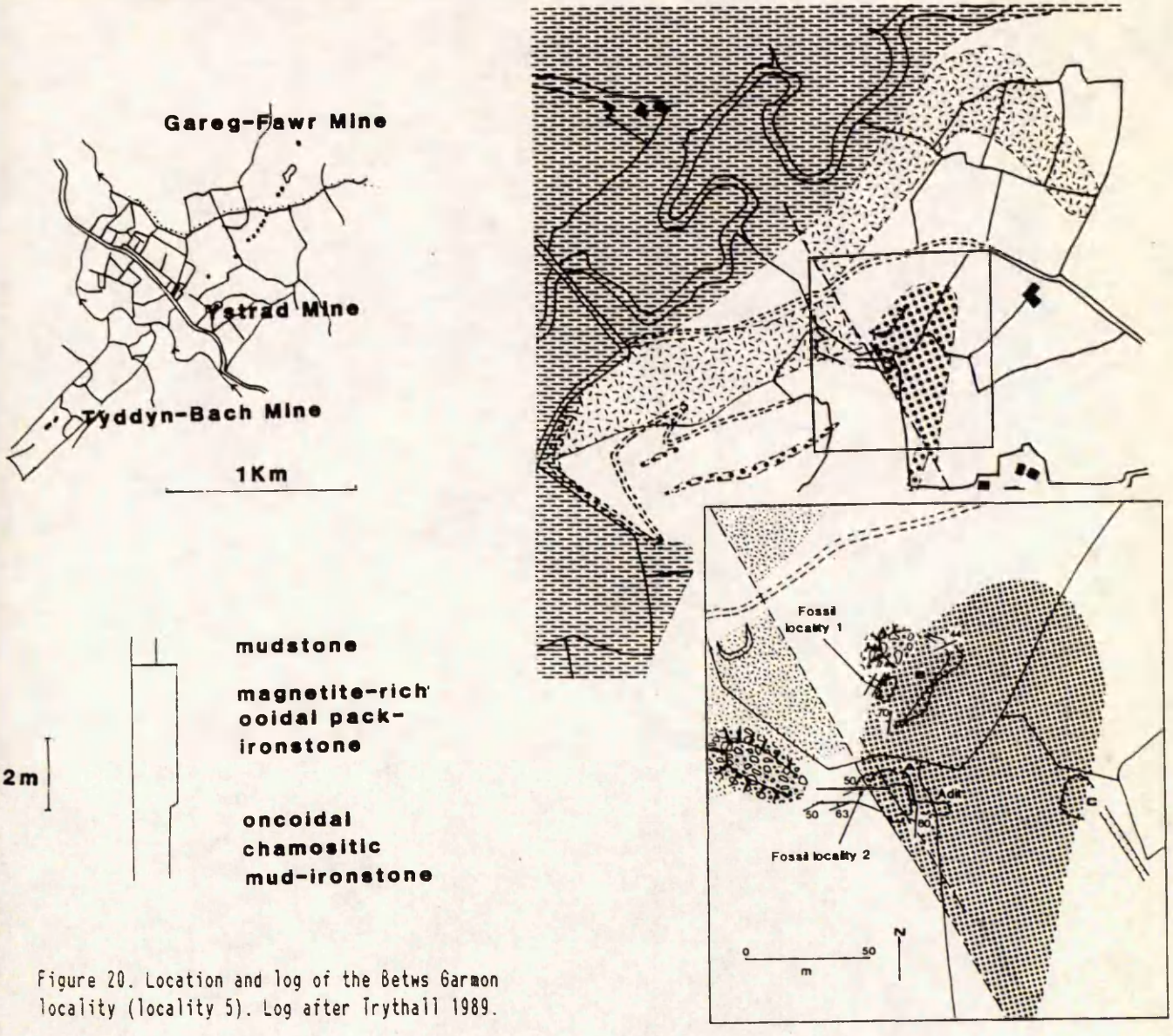

Figure 20. Location and log of the Betws Garmon locality (locality 5). Log after Trythall 1989.

Locality 6: Pen-y-Gaer

This locality lies in the northern part of the St. Tudwal's Peninsula near the southern Llyn coast. The hill has three separate workings, which appear to have been little more than trials.

The locality forms the most northerly exposure of the ironstone above the Llanengan mudstones which is visible in several places between Pen y Gaer and Penrhyn Ddu. The exploitation of iron in the St. Tudwal's area dates to at least 1830. The main quarry was at Hen-dy-Capel, 1.5 km south of Pen-y-Gaer. Hen-dy-Capel quarry was named after the adjacent chapel which had to be replaced in 1828 after the persistent damage to its roof during blasting at the quarry. This quarry was linked to the coast by a railway, built by the Llanengan Ironstone Company in 1842. It seems likely that the Pen y Gaer trials were undertaken by the same mining company, but structural complications prohibited exploitation. The Hen-dy-Capel Quarry is partially infilled, but provides good sections through the ironstone and the overlying

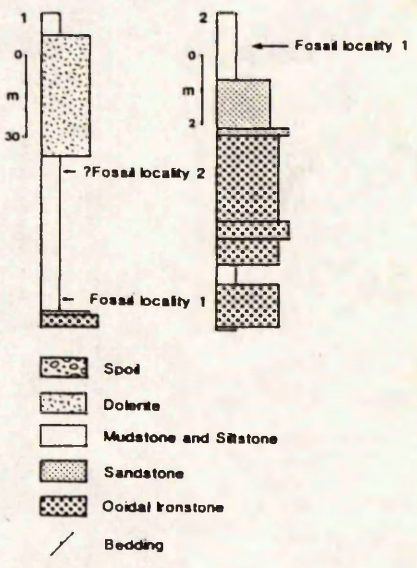

Figure 21. Locality map and log for Pen y gaer (locality 6)

clastic sediments.

A guide to the Hen-dy-Capel locality was given by Trythall (1989a). For this excursion however the trials of Pen-y-gaer will be visited for they have provided new evidence on the age of the deposits, as well as clearly illustrating the reworked nature of the ironstones here.

Work in progress (author's unpublished studies) has demonstrated the presence of Llanvirn graptolites in mudstones overlying the ironstone at Pen y Gaer previously attributed to the *gracilis* Biozone (NICHOLAS 1915; TRYTHALL *et al.* 1987; TRYTHALL 1989a).

The ironstone here is interpreted as forming part of the early Llanvirn deposits. The sediments are apparently debris-flows, containing ironstone material (ooids, pisoids and phosphatic oncoids) in a siltstone matrix, with occasional large clasts of volcanic rocks. Such sediments are rather reminiscent of the "Trygarn Formation" of the Sarn area 6km northwest.

In other localities in the are the ironstone is seen to lie on the Fennian "Llanengan mudstones".

Locality 7: Porth Meudwy

The Aberdaron area has recently been remapped by Gibbons and McCarroll (in press), and the opportunity arose for a reinvestigation of the Arenig and Llanvirn sedimentary sequence. The stratigraphy of the area was revised by Beckly (1985, 1989). The recently recognised ironstone lies just above the Porth Meudwy Formation, and lies within a sequence recording the onset of major faulting and volcanism in the area.

Biostratigraphic control on the sequence still remains sparse, but the studies of Beckly, supplemented by some recent work, have allowed tentative correlation of the sediments here. The Porth Meudwy Formation represents a localised coarse-grained deposit, probably a submarine fan derived from an active fault to the northwest. Clasts in the formation include much material consistent with derivation from the local Gwna Melange (late Proterozoic or just possibly earliest Cambrian). The formation is interpreted as being of Fennian age, but could possibly be early Llanvirn.

The sediments below the Porth Meudwy Formation were deposited in a relatively stable clastic shelf setting, and the onset of the fan deposits represents a major change in environment. The sedimentary rocks above the Porth Meudwy Formation contain a large amount of fine-grained volcanoclastic material and probably represent part of the volcanic complex seen farther east around Rhiw and Sarn, where the "Trygarn Formation" (Young unpub. data) includes both volcanoclastic sediments and a thin welded tuff. A thin ironstone lies within the volcanoclastic succession at Porth Meudwy, and in the correlative "Trygarn Formation" farther east reworked ironstones are common.

At Pen y Cil 2km south of Porth Meudwy the uppermost levels of the Porth Meudwy Formation include beds rich in phosphatic oncoids.

Siltstone horizons a few metres above the ironstone yield graptolites which are probably of early Llanvirn age.

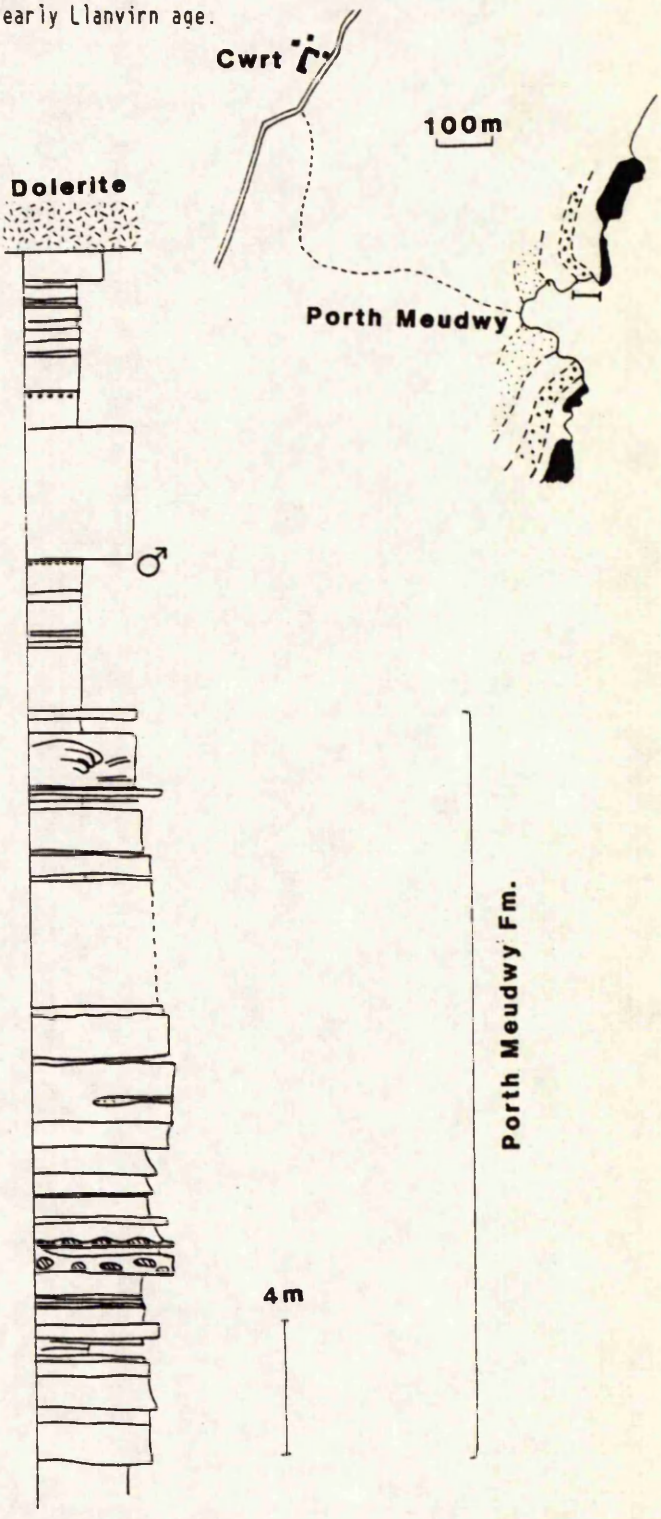

Figure 22. Locality map and log for Porth Meudwy (locality 7)

The *Nemagraptus gracilis* Biozone ironstones

Locality 8: Llanbadrig - Ogof Gynfor

The Llanbadrig area with the Ordovician rocks of the "Gynfor Outliers" is classic area for geology in northern Anglesey. The Gwna Melange (probably late Proterozoic) is well seen in area, including localities with olistoliths of stromatolitic limestones bearing microfloras which have been referred to the Lower Cambrian. The Gwna Melange is unconformably overlain by the Porth Wen Group (Arenig, Fennian). The conglomeratic Porth Wen Group is divided into the localised Porth Cynfor Formation below and the Torllwyn Formation above (BATES 1972). The Torllwyn Formation is unconformably overlain by *gracilis* Biozone sediments of the Llanbadrig Group.

At Ogof Gynfor the Torllwyn Formation is 25m thick and yields a diverse brachiopod fauna from its finer-grained beds (*Ahtiella quadrata*, *Antigonambonites* sp., *Estlandia* (?) sp., *Hespernomiella* (?) sp., *Lenorthis* sp., *Monorthis* sp., *Panderina* sp., *Pleurorthis* sp., *Reinversella* (?) sp., *Rhynchorthis rotundatus*, *Skenidioides* sp. and *Tritoechia* sp.). This conglomerate is of approximately the same age as the Porth Meudwy Formation at Aberdaron (see Porth Meudwy above) and probably reflects the same tectonic event. The shelly fauna from the Torllwyn Formation is important for it is one of the faunas ascribed by Neuman (1984) to the "Celtic Province", and interpreted as indicating a palaeogeographic position for Anglesey as an "island" within the Iapetus Ocean separated from the Welsh Basin. Such a view is now no longer widely held (e.g. BECKLY 1989) and the "diagnostic" elements of the "Celtic Province" (e.g. *Rhynchorthis*) have now been widely recorded in other parts of the Welsh Basin, and some of them from other parts of the Gondwanan margin.

The basal *gracilis* Biozone sediments are simply a reworking of the upper part of the Torllwyn Fm. and comprise a reworked conglomeratic bed with some red chert. This bed forms the base of the Gynfor Shale Formation, a unit of shales, sometimes sandy, and cherts. The Penterfyn Ironstone Formation abruptly overlies these shales. Only about 1.25m of the ironstone is exposed in a tight anticline near low-water mark (WEINBERG 1973).

Locality 9: Porth Pridd (SH 408945)

This locality was described by Weinberg (1973). The 2m thick ironstone is bedded in 30cm units, fining upwards from ooidal siltstone to silty mudstone. The underlying sandstones are strongly sideritized. The ooids are replaced variably by phosphates, quartz, siderite and kaolinite. The ironstone is very similar here to its development at Porth Padrig (see above) some 3km to the west. The context of the ironstone is better seen at this locality, where the underlying Gynfor Shale Formation consists of at least 45m of shales, fine grained sandstones and cherts, overlain by 15m of sandstones.

Locality 10: Nant Ffrancon (SH64056120)

The ironstone exposed in Nant Ffrancon has been correlated with other localities just below the base of the Caradoc volcanics, and appears to be part of continuous bed at this horizon. The ironstone is intensely deformed, and at this locality is strongly folded. The ironstone has some trial workings within it, but these were probably not for iron (Nant Ffrancon was exploited for its rich sulphide mineralisation, particularly for arsenic, a smelter for which was located 3.5km down the valley).

Locality 11: Tremadog (SH 553403)

The ironstone at Tremadog has been the subject of considerable debate, and a focus of the study of N. Welsh ironstones since the pioneering studies of Fearnsides (1910). Fearnsides considered that the ironstones were not sedimentary deposits but were formed during contact metamorphism and subsequently deformed by thrusting to give the appearance of being bedded. This view was obviously strongly influenced by the Tremadoc ironstone.

The Tremadog ironstone is indeed strongly deformed into lensoid pods (described by Fearnsides as ranging in size from that of beans to 100 ton schooners). The nature of deformation is controversial. Fearnsides (1910) interpreted the structure as a major thrust bringing the Caradoc sequence (with the ironstone at its base) over the lower Ordovician rocks to the south. Smith (1987) has reinterpreted the structure as an early, pre-lithification, slump. The similar structure to the north of the St. Tudwal's Peninsula to the west has been interpreted as a thrust (pers. obs.) and the interpretation of the Tremadog structure must remain open.

The ironstone lies in the lower part of the Tyddyn-dicwm beds, most of which comprise dark mudstones with a *gracilis* Biozone graptolite fauna. The lateral equivalents of the volcanics overlying the Tyddyn-dicwm beds have elsewhere yielded a shelly fauna of Costonian age (BATES *in* BROMLEY 1965).

Locality 12: Ffordd Ddu (SH 64771283)

The Ffordd Ddu locality is difficult to interpret, for the local succession is repeated by faulting. The locality displays excellent pisoidal and oncoidal wacke-ironstones. The allochems are often picked out on weathered surfaces because of

their silicification.

The locality is a small quarry in the ironstone which runs the length of the Cadair Idris escarpment, at a horizon within the Llyn y Gadair mudstones. The ironstone occurs at a level close to that interpreted to be the local base of the *gracilis* Biozone succession.

Acknowledgements

This fieldguide forms a contribution to IGCP Project 277 "Phanerozoic Ironstones". The authors acknowledge the cooperation of all the owners of localities visited during the fieldtrip.

References

AIGNER, T. 1979. Schill-Tempestite im Oberen Muschelkalk (Trias, SW-Deutschland). *Neues Jahrbuch fur Geologie und Palaontologie, Abhandlungen*, **157**, 362-343

AIGNER, T. 1982. Event-stratification in nummulite accumulations and in shell beds from the Eocene of Egypt. *In:* EINSELE, E. & SEILACHER, A. (eds) *Cyclic and Event Stratification*. Springer, 248-262.

BATES, D.E.B. 1972. The stratigraphy of the Ordovician rocks of Anglesey. *Geological Journal*, **8**, 29-56.

BATES, D.E.B. & DAVIES, J.R. 1981. *Anglesey*, Geologists' Association Guide No. 40. Geologists' Association, London.

BECKLY, A.J. 1985. *The Arenig Series in North Wales*. Unpublished PhD thesis, University of London.

BECKLY, A.J. 1987. Basin development in North Wales during the Arenig. *Geological Journal*, **22**, 19-30.

BECKLY, A.J. 1988. The stratigraphy of the Arenig Series in the Aberdaron to Sarn area, western Llyn, North Wales. *Geological Journal*, **23**, 321-337.

BECKLY, A.J. 1989. A new Arenig trilobite fauna from the Bangor area, North Wales. *Bulletin of the British Museum (Natural History), Geology*, **45**, 1-20.

BGS, 1982. *1:50000 Series Geological Survey of England and Wales. Sheet 135: Harlech.*

BROMLEY, A.V. 1965. Intrusive quartz latites in the Blaenau Festiniog area, Merioneth. *Geological Journal*, **4**, 247-257.

BROWN, M.J. & EVANS, A.D. 1989. Geophysical and geochemical investigations of the manganese deposits of Rhiw, western Llŷn, North Wales. British Geological Survey Technical Report WF/89/14 (BGS Mineral Reconnaissance Programme Report 102)

CATTERMOLE, P. & JONES, A. 1970. The geology of the area around Mynydd Mawr, Nantlle, Caernarvonshire. *Geological Journal*, **7**, 111-128.

CATT, J.A., GAD, M.A., LERICHE, H.H. & LORD, A.R. 1971. Geochemistry, micropalaeontology and origin of the Middle Lias ironstones in Northeast Yorkshire (Great Britain). *Chemical Geology*, **8**, 61-76.

CHOWNS, T.M. 1966. Depositional environment of the Cleveland ironstone Series. *Nature (London)*, **211**, 1286-1287.

CHOWNS, T.M. 1968. *Environmental and diagenetic studies of the Cleveland Ironstone Formation of north-east Yorkshire*. Unpublished PhD thesis, University of Newcastle upon Tyne.

COPE, J.C.W., GETTY, T.A., HOWARTH, M.K., MORTON, N. & TORRENS, H.S. 1980. *A correlation of Jurassic rocks in the British Isles; Part One: Introduction and Lower Jurassic*. Geological Society of London Special Report No. 14, 48-52.

COX, A.H. 1925. The geology of the Cader Idris range (Merioneth). *Quarterly Journal of the Geological Society of London*, **81**, 539-594.

DAVIES, W. & DIXIE, R.J.M. 1951. Recent work on the Frodingham Ironstone. *Proceedings of the Yorkshire Geological Society*, **28**, 85-96.

DONATO, J.A. & MEGSON, J. 1990. A buried granite batholith beneath the East Midland Shelf of the Southern North Sea Basin. *Journal of the Geological Society of London*, **147**, 133-140.

FORTEY, R.A. 1984. Global earlier Ordovician transgressions and regressions and their biological implications. *In:* BRUTON, D.L. (ed.), *Aspects of the Ordovician System. Palaeontological contributions from the University of Oslo*, **295**, 37-50.

FOSTER-SMITH, J.R. undated. *The Mines of Anglesey and Caernarvonshire*. British Mining, **4**.

GIBBONS, W. & MCCARROLL, D. in press. The Geology of the country around Bardsey, Sheet 133, British Geological Survey 1:50000 Series, Memoir of the British Geological Survey.

GREENLY, E. 1919. *The geology of Anglesey*, 2 volumes, Memoirs of the Geological Survey of Great Britain, London.

GREENSMITH, J.T., RAWSON, P.F. & SHALABY, S.E. 1980. An association of minor fining-upward cycles and aligned gutter marks in the Middle Lias (Lower Jurassic) of the Yorkshire coast. *Proceedings of the Yorkshire Geological Society*, **42**, 525-538.

HALLAM, A. 1963. Observations on the palaeoecology and ammonite sequence of the Frodingham ironstone (Lower Jurassic). *Palaeontology*, **6**, 554-574.

HEMINGWAY, J.E. 1974. Jurassic. In: RAYNER, D. & HEMINGWAY, J.E. (eds), *The Geology and mineral resources of Yorkshire*, Yorkshire Geological Society Occasional Publication No. 2, 161-223.

HOFMANN, H.J. 1975. *Bolopora* not a bryozoan, but an Ordovician phosphatic oncolitic accretion. *Geological Magazine*, 112, 523-526.

HOWARD, A.S. 1984. *Palaeoecology, sedimentology and depositional environments of the Middle Lias of North Yorkshire*. Unpublished PhD thesis, University of London.

HOWARD, A.S. 1985. Lithostratigraphy of the Staithes Sandstone and Cleveland Ironstone formations (Lower Jurassic) of north-east Yorkshire. *Proceedings of the Yorkshire Geological Society*, **45**, 261-275.

HOWARTH, M.K. 1955. The Domerian of the Yorkshire Coast. *Proceedings of the Yorkshire Geological Society*, **30**, 147-175.

HOWARTH, M.K. 1980. Pliensbachian correlation chart. In: COPE, J.C.W. *et al.* (eds), *A correlation of Jurassic rocks in the British Isles. Part One: Introduction and Lower Jurassic.* Geological Society of London Special Report No. 14, 48-52.

HOWELLS, M.F., LEVERIDGE, B.E., ADDISON, R., & REEDMAN, A.J. 1983. The lithostratigraphic subdivision of the underlying the Snowdon and Crafnant Volcanic Groups, North Wales. *Report of the Institute of Geological Sciences*, **83/1**, 11-15.

HUGHES, C.R. 1989. The application of analytical transmission electron microscopy to the study of oolitic ironstones: a preliminary study. *In*: YOUNG, T.P. & TAYLOR, W.E.G. (eds), *Phanerozoic Ironstones*, Geological Society Special Publication No. 46, 121-131.

KEARSLEY, A.T. 1989. Iron-rich ooids, their mineralogy and microfabric: clues to their origin and evolution. *In*: YOUNG, T.P. & TAYLOR, W.E.G. (eds), *Phanerozoic Ironstones*, Geological Society Special Publication No. 46, 141-164.

KOKELAAR, P. 1988. Tectonic controls of Ordovician arc and marginal basin volcanism in Wales. *Journal of the Geological Society of London*, **145**, 759-775.

LEWIS, H.P. 1926. *Bolopora undosa* gen. et sp. nov. *Quarterly Journal of the Geological Society of London*, **82**, 411-427.

MAYNARD, J.B. 1986. Geochemistry of Oolitic Iron ores: an electron microprobe study. *Economic Geology*, **81**, 1473-1483.

MYERS, K.J. 1989. The origin of the Lower Jurassic Cleveland Ironstone Formation of North-East England: evidence from portable gamma-ray spectrometry. *In*: YOUNG, T.P. & TAYLOR, W.E.G. (eds), *Phanerozoic Ironstones*, Geological Society Special Publication No. 46, 221-228.

NEUMAN, R.B. 1984. Geology and palaeobiology of islands in the Ordovician Iapetus Ocean: Review and implications. *Bulletin of the Geological Society of America*, **95**, 1188-1201.

NEUMAN, R.B. & BATES, D.E.B. 1978. Reassessment of Arenig and Llanvirn age (Early Ordovician) brachiopods from Anglesey, north-west Wales. *Palaeontology*, **21**, 571-613.

NICHOLAS, T.C. 1915. Geology of the St. Tudwal's Peninsula. *Quarterly Journal of the Geological Society of London*, **71**, 83-143.

NIEDERMEYER, R.-O. & LANGBEIN, R. 1989. Probable microbial origin of Ordovician (Arenig) phosphatic pebble coats ('*Bolopora*') from North Wales, U.K. *Geological Magazine*, **126**, 691-698.

POWELL, J.H. 1984. Lithostratigraphic nomenclature for the Lias Group in the Yorkshire Basin. *Proceedings of the Yorkshire Geological Society*, **45**, 51-58.

PULFREY, W. 1933a. Note on the occurrence of Sponge-Spicules, associated with the Iron-ores of North Wales. *Annual Magazine of Natural History*, **11**, 67-76.

PULFREY, W. 1933b. The iron ore oolites and pisolites of North Wales. *Quarterly Journal of the Geological Society of London*, **89**, 401-430.

RAWSON, P.F., GREENSMITH, J.T. & SHALABY, S.E. 1982. Coarsening upward cycles in the uppermost Staithes and Cleveland Ironstone Formations (Lower Jurassic) of the Yorkshire coast, England. *Proceedings of the Geologists' Association*, **94**, 91-93.

REEDMAN, A.J., WEBB, B.C., ADDISON, R., LYNAS, B.D.T., LEVERIDGE, B.E. & HOWELLS, M.F. 1983. The Cambrian-Ordovician boundary between Aber and Betws Garmon, Gwynedd, North Wales. *Report of the Institute of Geological Sciences*, **83/1**, 7-10.

SEILACHER, A. 1984. Constructional morphology of bivalves: evolutionary pathways in primary versus secondary soft-bottom dwellers, *Palaeontology*, **27**, 207-237.

SHALABY, S.E. 1980. *The Middle Lias sedimentary rocks of the coastal zone of north-east Yorkshire: their petrology and sedimentation.* Unpublished PhD thesis, University of London.

SMITH, M. 1987. The Tremadoc "thrust" zone in southern central Snowdonia. *Geological Journal*, **22**, 119-129.

TRAYNOR, J.-J. 1990. Arenig sedimentation and basin tectonics in the Harlech Dome area (Dolgellau Basin), North Wales. *Geological Magazine*, **127**, 13-30.

TRYTHALL, R.J.B. 1989a. The mid-Ordovician oolitic ironstones of North Wales: a field guide. *In*: YOUNG, T.P. & TAYLOR, W.E.G. (eds), *Phanerozoic Ironstones*, Geological Society Special Publication No. 46, 213-220.

TRYTHALL R.J.B. 1989b. *The Mid-Ordovician oolitic ironstones of North Wales.* Unpublished PhD thesis, CNAA, Luton CHE.

TRYTHALL, R.J.B., ECCLES, C., MOLYNEUX, S.G. & TAYLOR, W.E.G. 1987. Age and controls of ironstone deposition (Ordovician) North Wales. *Geological Journal*, **22**, 31-43.

WEINBERG, R.M. 1973. *The petrology and geochemistry of the Cambro-Ordovician ironstones of North Wales.* Unpublished D.Phil. thesis, University of Oxford.

WHITEHEAD, T.H., ANDERSON, W., WILSON, V. & WRAY D.A. 1952. *The Mesozoic Ironstones of England, The Liassic Ironstones, with contributions on the petrography by K.C. Dunham.* Memoirs of the Geological Survey of Great Britain.

WOODCOCK, N.H. 1990. Sequence stratigraphy of the Palaeozoic Welsh Basin. *Journal of the Geological Society of London*, 147, 537-547.

YOUNG, T.P. 1988. The lithostratigraphy of the upper Ordovician of central Portugal. *Journal of the Geological Society of London*, **145**, 377-392.

YOUNG, T.P. 1989a. Phanerozoic Ironstones: an introduction and review. *In*: YOUNG, T.P. & TAYLOR, W.E.G. (eds) *Phanerozoic Ironstones*, Geological Society Special Publication No. 46, ix-xxv.

YOUNG, T.P. 1989b. Eustatically controlled ooidal ironstone deposition: facies relationships of the Ordovician open-shelf ironstones of western Europe. *In*: YOUNG, T.P. & TAYLOR, W.E.G. (eds) *Phanerozoic Ironstones*, Geological Society Special Publication No. 46, 51-63.

YOUNG, T.P. 1990. Ordovician sedimentary facies and faunas of Southwest Europe: palaeogeographic and tectonic implications. *In*: MCKERROW, W.S. & SCOTESE, C.R. (eds), *Palaeozoic Palaeogeography and Biogeography*, Geological Society Memoir No. 12, 419-428.